THESIS FOR THE DEGREE OF DOCTOR OF PHILOSOPHY

Impact strength optimization with cohesive zone elements of multi-material bonded structures used in the automotive industry

by

José Joaquim da Mota Machado

Supervisor:

Eduardo André de Sousa Marques (INEGI)

Co-supervisors:

Lucas Filipe Martins da Silva (FEUP)

Benjamin Desai (Aston Martin Lagonda Limited®)

DEMec, Faculdade de Engenharia da Universidade do Porto, Rua Dr. Roberto Frias, 4200-465 Porto, Portugal

Porto, June 2019

© José Joaquim da Mota Machado

Departamento de Engenharia Mecânica

Faculdade de Engenharia da Universidade do Porto

Rua Dr. Roberto Frias, s/n

4200-465 Porto

Portugal

Abstract

The transport sector is currently a key sector for the European Union (EU) climate and energy policy. The EU has adopted a target of improving energy efficiency by 20% and to reduce the CO_2 emissions to 95 g/km until 2020, which requires significant reductions of the structural weight of vehicles. The increasingly larger use of driving safety aids as well as the shift to electric propulsion also created the need to constantly lower the weight of an automotive structure. However, such approach requires the use of light multi-material structures (e.g. joints using composite plus aluminium materials) which are quite difficult to assemble using traditional methods of joining such as welding or fastening. As an alternative, adhesive bonding techniques are appropriate for these structures, being suitable for bonding different materials and at the same time providing vehicle strength, stiffness, being inexpensive and, most importantly allowing to design safe structures under impact conditions.

To guarantee that these parameters are achieved, analysis and testing of adhesive joints and structures are needed. Most of the existent analysis and testing of structural adhesive joints focus on quasi-static strength at room temperature and short-term durability. However, this information is of limited use for automotive manufacturers, who are currently searching for the most effective method to design and predict the strength of vehicle structures under impact, varying the temperature and in terms of durability (subjected to an aging process) which are the key issues for the automotive industry.

The probability of the occurrence of an impact loads is very high during the life time of a vehicle, therefore, to predict the impact strength of bonded structures, it is important to understand if the strength is affected by high rates of loading and temperature, and if the bonded structure can absorb large amounts of energy under impact conditions. The impact performance of bonded joints must first be understood so that suitable predictions can be made. However, modern multi-material structures in vehicles also incorporate composite materials and the impact behaviour of adhesive joints with these materials is different than with metals and still not fully understood. The adhesive must retain strength so that the substrate can dissipate the energy through plastic deformation, being therefore ductile and not brittle. Multi-material structures in vehicles incorporate not only metals but also composite materials. The impact behaviour of adhesive joints made with composite substrates is distinct from joints made with metal substrates, and not well

documented in literature. In addition, thermal effects are also often ignored but the automotive industry must ensure that vehicles perform adequately from -30 to 80 ºC. Besides the behaviour of structures under impact condition, understanding the durability of joints after aging and drying processes, as well under fatigue conditions present during its life cycles is to be explored, as limited research is published in this field.

The presented research work aimed firstly to develop a procedure to mechanically characterize adhesives subjected to the single or joint effect of strain rate and temperature, followed by the full investigation of the influence of impact behaviour of adhesive joints, using both similar and dissimilar (multi-materials) substrates combinations, from -30 to 80 ºC, proposing new methods and design changes to improve impact strength, as well as to assess the joints behaviour after aging and drying subsequent to aging as well as under fatigue loads. The experiments were numerically simulated using damage mechanics. The mechanical properties of the adhesive were first be determined as a function of strain rate and testing temperature with simple fracture mechanics specimens and later validated with single lap joints which have a more complex stress state. Finally, a more advanced model was built, representing a joint typical of the automotive industry. This model is based on an actual bonded component provided by Aston Martin Lagonda®, tested under quasi-static and impact loads.

The duration of this research was of three years in the Adhesive´s group at FEUP, being performed in association with the Japanese company Nagase ChemteX®, which provided a prototype crash resistant epoxy adhesive specifically developed for the automotive industry, as well the British automobile manufacturer Aston Martin Lagonda® participating as a consultant, therefore ensuring proper and valid transfer of technology to the industry. The research developed demonstrated that using modern test procedures and simulation tools it was possible to design strong and durable similar and dissimilar (multi-material) substrates joints using a crash resistant adhesive that ensure high performance under a wide range of strain rates and temperatures of real application.

Keywords: Adhesive bonding; Crash resistant adhesive; Strain rate; Impact; Temperature; Composites; Mixed adhesive joints; Hygrothermal aging; Fatigue; Cohesive elements; Automotive industry.

Resumo

O sector dos transportes representa um sector chave na política climática e energética da União Europeia (UE). A UE estabeleceu como objetivo de, até 2020, melhorar a eficiência energética 20% e reduzir as emissões médias de CO2 para 95 g/km em veículos de passageiros, sendo que o cumprimento deste objetivo implica uma redução significativa do peso estrutural. O aumento da segurança na condução, bem como a transformação do automóvel num veículo de propulsão elétrica, também cria a necessidade de reduzir constantemente o peso de um automóvel. No entanto, esta abordagem exige o uso de estruturas leves e multimateriais, difíceis de construir recorrendo a métodos tradicionais de união estrutural. Como alternativa surgem as técnicas de ligação adesiva, capazes de unir com sucesso uma grande diversidade de materiais, possibilitando estruturas leves, resistentes e económicas, nunca descurando a necessidade de garantir máxima segurança para os ocupantes do veículo.

Para garantir que esses parâmetros sejam alcançados, são necessárias análises e testes de juntas e estruturas adesivas. A maioria das análises e testes existentes de juntas adesivas estruturais concentra-se na resistência quase estática à temperatura ambiente e na durabilidade a curto prazo. No entanto, esta informação é de uso limitado para os fabricantes de automóveis, que procuram implementar métodos eficazes para projetar e prever a resistência das estruturas de veículos sob impacto, sob condições variadas de temperatura e quando submetidas a um processo de envelhecimento. Para prever a resistência ao impacto de estruturas coladas, é importante entender se a resistência é afetada por altas taxas de deformação e temperatura, e se a estrutura metálica pode absorver grandes quantidades de energia sob condições de impacto. O desempenho de impacto das juntas coladas deve primeiro ser entendido para que previsões adequadas possam ser feitas. No entanto, as estruturas modernas de veículos também incorporam materiais compostos e o comportamento de impacto das juntas adesivas com estes materiais é diferente do que com metais e ainda não totalmente compreendido. O adesivo deve reter a resistência de modo que o substrato possa dissipar a energia através de deformação plástica, sendo, portanto, dúctil e não quebradiço. Além disso, os efeitos da temperatura também são frequentemente ignorados, mas a indústria automóvel deve garantir que os veículos apresentem um desempenho adequado de -30 a 80 ºC. Além do comportamento de estruturas sob condição de impacto, o conhecimento da durabilidade das juntas após o envelhecimento e secagem após o processo de envelhecimento, bem

como sob condições de fadiga presentes durante seus ciclos de vida, deve ser explorado, pois pouca pesquisa foi realizada neste campo.

O trabalho apresentado visa primeiramente desenvolver um procedimento para caracterizar mecanicamente os adesivos submetidos ao efeito único ou conjunto de taxa de deformação e temperatura, seguido da investigação completa da influência do comportamento de impacto das juntas adesivas, usando tanto similar como dissimilar (multimateriais) combinações de substratos, de -30 a 80 ºC, propondo novos métodos e modificações de projeto para melhorar a resistência ao impacto, bem como avaliar o comportamento das juntas após o envelhecimento e secagem subsequente ao envelhecimento, assim como sob cargas de fadiga. O trabalho experimental foi simulado numericamente usando uma abordagem baseada na mecânica de danos. As propriedades mecânicas do adesivo serão primeiramente determinadas como uma função da taxa de deformação e temperatura de teste com espécimes mecânicos de fratura e serão validadas posteriormente com juntas mais complexas, sendo mais tarde usadas para criar um modelo mais avançado. representando uma junta típica da indústria automóvel. Este modelo permitirá a definição de uma geometria de junta, baseada em elementos fornecidos pela Aston Martin Lagonda®, que será testada sob cargas quase estáticas e de impacto.

A duração desta pesquisa foi de três anos, sendo realizada em associação com a empresa japonesa Nagase ChemteX®, que forneceu um adesivo epóxi protótipo resistente à colisão, desenvolvido especificamente para a indústria automóvel, bem como o fabricante de automóveis britânico Aston Martin Lagonda® como consultor, garantindo assim a transferência adequada e válida de tecnologia para a indústria. A pesquisa desenvolvida demonstrou que usando modernos procedimentos de teste e ferramentas de simulação é possível projetar juntas de substratos fortes e duráveis similares e diferentes (multimaterial) usando um adesivo resistente a colisão que garante alto desempenho sob uma ampla faixa de taxas de deformação e temperaturas reais. aplicação.

Palavras chave: Ligação adesiva; Adesivo resistente ao impacto; Taxa de deformação; Impacto; Temperatura; Compósitos; Juntas adesivas mistas; Envelhecimento higrotérmico; Fadiga; Elementos coesivos; Indústria automóvel.

Acknowledgements

I would like to start by expressing my sincere gratitude to my supervisor Professor Lucas da Silva for his intellectual and academic inspiration and constant support through the course of this work. Also, to thank him for giving me the opportunity to work under his supervision.

A special thanks to my Co-supervisor Doctor Eduardo Marques for providing groundwork upon which this thesis was based, for his valuable advices, willingness to help me whenever I needed and most of all friendship and support. I also must highlight Professor Raul Campilho, whose help was fundamental in the experimental component relative to the composite characterization, as well for the numerical sections under impact.

I would like to thank all the members of the adhesive team (Guilherme Viana, Ana Queirós, Ana Loureiro, Marcelo Costa and Ricardo Carbas) for their support and friendship. I also want to thank all the master students (Hélder Araújo, Pablo Gamarra, Paulo Nunes and Nelson Silva) who worked closely with me during their master thesis, and who made an important contribution to this work.

The extraordinary support provided by Professor Chiaki Sato must also be acknowledged, who not only made his laboratory available for conducting my research but was also extremely kind and generous to allow me to do an internship in his laboratory in Tokyo Institute of Technology (Japan). To his team (Asuka Hayashi, Yu Sekiguchi, Noriaki Okada, Minori Makanouchi, Shunsuke Watanabe, Kazuhiro Sensui, He Ning, Runa Okumba, Yu-to Imaeda and Ryo Sakakibara), I also would to like to thank them for receiving and helping me as a member of the team.

I would also like to refer those who work in the laboratories and workshops of FEUP and that helped me immensely through my work, namely, Professor José Esteves, Mr. Miguel Figueiredo, Mr. Rui Silva, Ms. Emília Soares, Ms. Rosa Siva, Mr. José Almeida, Mr. Albino Calisto, Mr. Pedro Falcão, Mr. André Alves and Mr. Domingos Carvalho. Also, I would like to thank all the people that made my time at the Faculty of Engineering of the University of Porto for all the support: friends, colleagues, members of staff and secretariat and apologies that I could not mention personally one by one.

I would like to thank Nagase ChemteX® (Japan) for providing the adhesive XNR6852 E-3, for all the technical, for the financial support and for inviting me to visit their facilities in Hyogo, Japan.

To Aston Martin Lagonda® (United Kingdom), especially to Mr. Benjamin Desai, for providing the aluminium specimens and real automotive joints, as for all the technical knowledge and guidance through the final process of validation of this work.

Also, to gratefully acknowledge the funding of Project NORTE-01-0145-FEDER-000022 – SciTech – Science and Technology for Competitive and Sustainable Industries, co-financed by Programa Operacional Regional do Norte (NORTE2020), through Fundo Europeu de Desenvolvimento Regional (FEDER), and to the Portuguese Foundation of Technology (FCT) for the funding provided by the PhD grant SFRH/BD/139341/2018 "Impact strength optimization with cohesive zone elements of multi-material bonded structures used in the automotive industry".

A warm thanks to my dear friends (Helena Martins, Joana Moreira, Maria Moutinho, Bruno Rodrigues, Pedro Teixeira, Armanda Teixeira, João Dias da Silva, Marta Campos Ferreira, Thiago Sobral, Sérgio Duarte and Catarina Pinto) who have always supported and encouraged me during this period.

A special thanks to my colleague and dear friend Professor José Almacinha, who has always motivated and supported me during all my academic path and greatly influenced my career.

Lastly, I would like to express my profound gratitude to my family for the constant encouragement, motivation and support, without which I would never be able to achieve this goal.

Contents

Abstract i

Resumo iii

Acknowledgements v

List of Acronyms xi

List of Notations xiii

List of publications xv

Summary of thesis 1

1. Introduction 1

1.1. Background and motivation 1

1.2. Problem definition 4

1.3. Objectives 6

1.4. Research methodology 8

1.5. Outline of the thesis 16

2. Adhesives and substrates 35

2.1. Crash resistant adhesive 35

2.2. Adhesives used in mixed adhesive joints configurations 36

2.3. Substrates 39

3. Specimen manufacturing 43

3.1. XNR6852 E-3 adhesive 44

3.1.1. Tensile bulk specimens 44

3.1.2. DCB 46

3.1.3. Torsion specimens 48

3.2. CFRP 49

3.2.1. CFRP plates 49

3.2.2. DCB 51

3.2.3. ENF 52

3.3. Glass transition temperature (*Tg*) 55
3.4. Single lap joints (SLJs) 55
3.5. Mixed adhesive single lap joints (SLJs) 59
3.6. Hygrothermal aging 61
3.6.1. CFRP plates 61
3.6.2. XNR6852 E-3 adhesive bulk plates 62
3.6.3. Hygrothermal aging and desorption process 62
3.6.4. Gravimetric analysis 63
3.6.5. Diffusion analysis 64
3.7. Automotive joint ("roof frame header") from Aston Martin Lagonda® 66
4. Test methods 71
4.1. Glass transition temperature (T_g) 72
4.2. Definition of strain rate 73
4.3. Quasi-static tests 74
4.3.1. Tensile bulk of XNR6852 E-3 adhesive 75
4.3.2. Torsion tests of XNR6852 E-3 adhesive 76
4.3.3. SLJs 78
4.4. Fracture tests 79
4.4.1. Mode I 79
4.4.2. Mode II 88
4.5. Impact tests 90
4.5.1. Tensile bulk of XNR6852 E-3 adhesive 90
4.5.2. SLJs 91
4.6. Fatigue tests 94
4.7. Automotive joint from Aston Martin Lagonda® 94
5. Numerical modelling 97
5.1. Cohesive zone models 97

5.2. Quasi-static model 99

5.3. Impact model 103

6. Conclusions 107

7. Future work 113

References 117

Paper 1 129

Paper 2 163

Paper 3 181

Paper 4 195

Paper 5 205

Paper 6 215

Paper 7 231

Paper 8 249

Paper 9 267

Paper 10 283

Paper 11 297

Paper 12 309

Paper 13 321

Paper 14 331

Paper 15 363

Paper 16 377

Paper 17 407

Paper 18 425

Paper 19 455

List of Acronyms

2D	Two-Dimensional
3D	Three-Dimensional
ASTM	American Society for Testing and Materials
BS	British Standard
CBBM	Compliance Based Beam Method
CBT	Compliance Beam Theory
CCM	Compliance Calibration Method
CFRP	Carbon Fibre Reinforced Polymer
COH2D4	4-Node-Two-Dimensional Cohesive Element
CPS4R	4-Node Bilinear Please Stress Quadrilateral, Reduced Integration
CZM	Cohesive Zone Modelling
DCB	Double Cantilever Beam
DIN	Deutsches Institut für Normung
DLJ	Double Lap Joint
ELS	End Loaded Split
ENF	End Notched Flexure
FE	Finite Element
FEA	Finite Element Analysis
FEM	Finite Element Method
FPZ	Fracture Process Zone
HT	High Temperature
IMP	Impact
ISO	International Organization for Standardization
LEFM	Linear Elastic Fracture Mechanics
LT	Low Temperature
NF	French Standard
QS	Quasi-static
RT	Room Temperature
RTV	Room Temperature Vulcanizing

SDEG	Scalar Stiffness Degradation
SHPB	Split Hopkinson Pressure Bar
SLJ	Single Lap Joint
TAST	Thick Adherend Shear Test
TDCB	Tapered Double Cantilever Beam

List of Notations

a	Crack length
a_e	Equivalent crack´s length
a_0	Initial crack length
c	Critical damping
C	Compliance
E	Young's modulus
E_x	Longitudinal normal modulus
E_b	Equivalent bending modulus
E_P	Potential energy
E_K	Kinetic energy
g	Gravitational acceleration
G	Shear modulus
G_c	Critical fracture toughness
G_I / G_n	Energy release rate in mode I
G_{II} / G_s	Energy release rate in mode II
G_{IC} / G_n^c	Critical energy release rate or fracture toughness in mode I
G_{IIC} / G_s^c	Critical energy release rate or fracture toughness in mode II
k	Bending moment factor
K	Stress intensity factor
$\boldsymbol{K}$	Elastic constitutive matrix
K_c	Critical stress intensity factor
l	Overlap length
L	Mid length of ENF specimen
L_o	Original length

M_b	Bending moment
m	Equivalent mass
P	Applied load
T_g	Glass transition temperature
t	Thickness
t_n^0	Tensile/normal strength
t_n	Cohesive tensile/normal stress
t_s^0	Shear strength
t_s	Cohesive shear stress
$v(t)$	Test velocity
w	Width of the specimen
δ	Displacement
δ_n^0	Initial tensile/normal displacement
δ_s^0	Initial shear displacement
δ_n^f	Final tensile/normal displacement
δ_s^f	Final shear displacement
Δ	Correction factor of crack´s length
ε_n	Tensile/normal strain
ε_s	Shear strain
$\dot{\varepsilon}$	Strain rate
$\dot{x}$	Displacement rate
v	Poisson’s ratio

List of publications

This work is composed of several research papers, being each chapter structured using one or more papers in sequence. The main goal of such method was the validation of each experimental and numerical contribute being presented. Special care and effort were taken to provide the readers with the necessary experimental and numerical details, as well as avoiding the repetition of information from a paper to another.

The following list comprehends a total of eighteen papers integrating this thesis:

[1] Machado, J. J. M., Marques, E. A. S., da Silva, L. F. M., "**Adhesives and adhesive joints under impact loadings: An overview.**", *The Journal of Adhesion*, Vol. 94(6): pp. 421-452. (2018), DOI: 10.1080/00218464.2017.1282349.

[2] Machado, J. J. M., Hayashi, A., Nunes, P. D. P., Marques, E. A. S., Carbas, R. J. C., Sato, C., da Silva, L. F. M., "**Strain rate dependence of a crash resistant adhesive for the automotive industry.**", *Proceedings of the Institution of Mechanical Engineers, Part L: Journal of Materials: Design and Application*, (2019), DOI: 10.1177/1464420719836914.

[3] Machado, J. J. M., Marques, E. A. S., Campilho, R. D.S., da Silva, L. F. M., "**Mode I fracture toughness of CFRP under impact as a function of temperature.**", *Journal of Composite Materials*, Vol. 51(23): pp. 3315-3326. (2017), DOI: 10.1177/0021998316682309.

[4] Machado, J. J. M., Campilho, R. D.S., Marques, E. A. S., da Silva, L. F. M., "**Mode II fracture toughness of CFRP as a function of temperature and strain rate.**", *Composites Part B: Engineering*, Vol. 114: pp. 331-318. (2017), DOI: 10.1016/j.compositesb.2017.02.013.

[5] Machado, J. J. M., Hayashi, A., Sekigushi, Y., Marques, E. A. S., Campilho, R. D.S., Sato, C., da Silva, L. F. M., "**Dynamic behaviour in mode I fracture toughness of CFRP as a function of temperature.**", *Theoretical and Applied Fracture Mechanics*, Vol. 103, (2019), DOI: 10.1016/j.tafmec.2019.102257.

[6] Araújo, H. A. M., Machado, J. J. M., Marques, E. A. S., da Silva, L. F. M., "**Dynamic behaviour of composite adhesive joints for the automotive industry.**", *Composite Structures*, Vol. 171: pp. 549-561. (2017), DOI: 10.1016/j.compstruct.2017.03.071.

[7] Machado, J. J. M., Marques, Nunes, P.D.P., E. A. S., da Silva, L. F. M., "**Mechanical behaviour of adhesively bonded composite single lap joints under quasi-static and impact conditions with variation of temperature and overlap.**", *Journal of Composite Materials*, Vol. 52.26: pp. 3621-3635. (2018), DOI: 10.1177/0021998318766641.

[8] Machado, J. J. M., Nunes, P., Marques, E. A. S., da Silva, L. F. M., "**Adhesive joints using aluminium and CFRP substrates tested at low and high temperatures under quasi-static and impact conditions for the automotive industry.**", *Composites Part B: Engineering*, Vol. 158: pp. 102-112. (2019), DOI: 10.1016/j.compositesb.2018.09.067.

[9] Machado, J. J. M., Gamarra, P.M-R., Marques, E. A. S., da Silva, L. F. M., "**Improvement in impact strength of composite joints for the automotive industry.**", *Composites Part B: Engineering*, Vol. 138: pp. 243-255. (2018), DOI: 10.016j/compositesb.2017.11.038.

[10] Machado, J. J. M., Marques, E. A. S., da Silva, L. F. M., "**Influence of low and high temperature on mixed adhesive joints under quasi-static and impact conditions.**", *Composite Structures*, Vol. 194: pp. 68-79. (2018), DOI: 10.1016/j.compstruct.2018.03.093.

[11] Machado, J. J. M., Nunes, P.D.P., Campilho, R.D.S.G., Marques, E. A. S., da Silva, L. F. M., "**Numerical study of mode I fracture toughness of CFRP under an impact load.**", *Proceedings of the Institution of Mechanical Engineers, Part L: Journal of Materials: Design and Application,* (2019), (**Submitted on May 2019 – under review**).

[12] Machado, J. J. M., Silva, M.R.G., Marques, E. A. S., da Silva, L. F. M., "**Numerical study of the impact behaviour of mixed adhesive single lap joints for the automotive industry.**", *International Journal of Adhesion and Adhesives*, Vol. 94: pp. 92-100. (2018), DOI: 10.1016/j.ijadhadh.2018.02.036.

[13] Machado, J. J. M., Gamarra, P.M-R., Marques, E. A. S., da Silva, L. F. M., "**Numerical study of the behaviour of composite mixed adhesive joints under impact strength for the automotive industry.**", *Composite Structures*, Vol. 185: pp. 373-380. (2018), DOI: 10.1016/j.compstruct.2017.11.045.

[14] Machado, J. J. M., Nunes, P.D.P., Marques, E. A. S., da Silva, L. F. M., "**Numerical study of similar and dissimilar single lap joints under quasi-static and impact**

conditions as a function of temperature.", *International Journal of Adhesion and Adhesives,* (2019), (**Submitted on May 2019 – under review**).

[15] Machado, J. J. M., Barbosa, A. Q., Marques, E. A. S., da Silva, L. F. M., **"Effect of hygrothermal aging on the quasi-static behaviour of CFRP joints varying the overlap length."**, *Composite Structures*, Vol. 214: pp. 451-462. (2019), DOI: 10.1016/j.compstruct.2019.02.035.

[16] Machado, J. J. M., Barbosa, A. Q., Marques, E. A. S., da Silva, L. F. M., **"Influence of hygrothermal aging on the quasi-static and impact behaviour of single lap joints using CFRP and aluminium substrates."**, *Mechanics of Advanced Materials and Structures,* (2019), (**Submitted on February 2019 – under review**).

[17] Machado, J. J. M., Barbosa, A. Q., Marques, E. A. S., da Silva, L. F. M., **"Performance under fatigue loads of single lap joint using CFRP and aluminium substrates prior and after hygrothermal aging."**, *Fatigue and Fracture Engineering Materials and Structures*, (2019).

[18] Silva, N. D. D., Machado, J. J. M., Marques, E. A. S., Parente, M., da Silva, L. F. M., **"Experimental and numerical study of the quasi-static response of an adhesively bonded automotive structure."**, *Engineering Failure Analysis,* (2019), (**Submitted on July 2019 – under review**).

[19] Silva, N. D. D., Machado, J. J. M., Marques, E. A. S., Moreira, O. M. G. P., da Silva, L. F. M., **"Experimental and numerical study of the dynamic response of an adhesively bonded automotive structure."**, *Mechanics of Materials,* (2019), (**Submitted on July 2019 – under review**).

1. Introduction

1.1. Background and motivation

A bonded joint is a type of permanent material union, using an adhesive to join two or more substrates/adherends [1]. Traditional fastening methods such as bolts, pins, nuts, screws and welding create variable stress distributions with a considerable stress concentration and are prone to cause fatigue cracking and corrosion problems in metallic components [2]. Adhesive bonding can solve those problems, as well as providing engineers with the freedom to design complex geometries, which would be impossible to produce using other joining methods [3]. Some of the main advantages of this method are: a significant reduction of structures weight; the possibility to bond both similar and dissimilar materials; excellent stress distribution along the overlap length; the possibility to be applied in association with other joining methods; and the fact that it is an excellent method to join composite materials. As for the main disadvantages, it can be pointed the need to understand how the adhesives behave under diverse environmental conditions such as temperature and humidity, behaviour under fatigue loads, requirement for surface treatment and the necessity to implement stringent quality control procedures [4].

The automotive industry has significantly increased the use of adhesives for joining load-bearing components with the aim of reducing vehicle weight, to improve fuel economy and reduce pollutant emissions. However, the design process of a bonded structure can be complex, as the properties of adhesives vary significantly, from brittle (like epoxides) to highly deformable (like polyurethanes) behaviour [5, 6]. Adhesives are viscoelastic, and their properties greatly depend on several factors such as temperature, loading rate and other factors as humidity. While some design criteria consider these effects [7], there is still limited information regarding the impact behaviour of bonded joints [8], especially when used with composite substrates [9, 10]. The behaviour of composites is anisotropic in respect to stiffness and strength. In the fibre direction, unidirectional composites can be very strong and stiff whereas the transverse and shear properties are much lower. Composite bonded joints experience peel loading so the composite may fail in transverse tension before the adhesive fails [11].

da Silva et al. [12-14] studied the problem of peel stresses in adhesive joints with composites and proposed designs to reduce them, such as an internal taper and adhesive fillet to reduce the peel stresses. Another possibility is to reduce the stiffness at the ends of the overlap by applying locally a flexible and ductile adhesive, producing a mixed adhesive joint [12]. This creates a uniform stress distribution which leads to joint strength improvements [15]. Several authors [12, 15-21] have performed extensive research on the use of mixed adhesive joints with excellent results. This technique creates a more uniform stress distribution, leading to improvements in joint performance in comparison to a single adhesive [15].

The design process of adhesively bonded joints subjected to impact loads includes experimental investigation of material properties and failure criteria, stress analysis, and strength prediction by applying failure criteria to applied stresses [22]. The main difference between impact and quasi-static cases is the need for a stress analysis considering stress wave propagations, the dependency stress-strain relations, and the strength of materials.

To perform impact strength prediction, automotive designers require the strain rate dependent mechanical properties of the adhesives, including their fracture properties [23]. Information regarding the mechanical behaviour under high strain rates is very limited as it is difficult to obtain experimentally [24] and few applicable standards exist. da Silva et al. [25] have developed methods to assess the strain rate dependency of the tensile and shear properties of materials, as well as the fracture energy.

Impact tests as a function of temperature are also rare. However, temperature has a significant effect on adhesives, introducing residual stresses (when bonding multi-material joints), and some experimental work has been performed in the assessment of the thermal behaviour of adhesive and adhesive joints under quasi-static conditions [19, 26, 27].

The effect of water ingress on long term joint durability is also an important factor to consider in design of structural joints, the effect being intensified with high strain rates and temperature [28]. Water (either as liquid or vapour) is absorbed by the adhesives and alters their properties, but a potentially greater problem is the effect on interfaces [29], although it can be minimised by use the of an adequate surface pre-treatment. Several studies have been performed on the effect of moisture on adhesive properties and strength

of adhesive joints under quasi-static loading, even in combination with temperature effects [30-35]. However, there is very limited data regarding the combined effect of aging and impact loadings. The only known work published in this field was by Zhang et al. [36] in 2015, where it suggested that the aging effects and the strain rate are independent, and their interaction effect is insignificant. Due to limited data, considerable scientific value exists in further exploring these phenomena.

Another important condition which can greatly affect the joint durability and resistance are the fatigue loads, and generally, in most applications, the presence of such loads should be addressed in the project phase. The influence of hygrothermal aging in combination with the occurrence of fatigue loads is generally known as causing a significant decrease of the number of cycles that a joint can withstand (as it affects the interface between the adhesive and the substrates), and also decreasing the threshold fracture toughness value, leading to the earlier initiation of crack propagation, although exceptions to such behaviour have been reported [33, 34].

Numerical modelling of the impact behaviour of adhesive joints is currently a very active research topic with direct industrial application. The evaluation of new designs for crashworthy structures may be streamlined using finite element analysis (FEA), reducing the large costs inherent in building or testing prototypes. The literature suggests a variety of models of differing complexity to solve this problem, which can include inertial effects and strain rate dependent properties (derived from experimental data or constitutive models). Dynamic models are available in some commercial or custom designed FEA packages [37-40] and can perform strain-rate dependent stress analysis.

Recently, numerical models have been developed where the strength of materials and fracture mechanics approaches have been combined, creating cohesive zone models (CZM). The CZMs attempt to minimize the limitations of the strength of materials and fracture mechanics approaches [41, 42]. These models can be successfully employed for thin planes of materials, making them especially well-suited for adhesive joints [43, 44]. These models employ traction-separation laws, which model stiffness and degradation of the element. These laws can be constructed with several different shapes, the most common being the triangular and the trapezoidal laws.

The use of CZM's coupled to conventional FEA is a modern method for predicting static strength of adhesive joint [45]. Most of CZM studies relate to static applications

[46] and many focus on the simulation of fracture toughness tests, such as Double Cantilever Beam (DCB) and End Notched Flexure (ENF) [47, 48].

Few studies include damage as a function of temperature [49, 50]. More recently, other authors have demonstrated the validity of using this type of approach to predict impact joint strength [50-55], and have shown that modern commercial software packages support the prediction accurate failure load predictions using complex dynamical cohesive models with strain rate dependent data.

1.2. Problem definition

The automotive industry is currently adopting lighter, multi-material structures that enable the reduction of vehicle weight and lead to reduced fuel consumption and emissions, at the same time providing more dynamic and safer vehicles. Also, the drive for increased vehicle electrification has the inherent problem of the increasing the weight of the vehicle due to the large batteries required, which intensifies the need for structural weight reduction. These structures rely heavily on adhesive bonding (Figure 1), but the prediction of their behaviour under the influence of several combined working conditions (such as: high strain rates, temperature, humidity and fatigue) is not trivial and represents a challenge for vehicle designers.

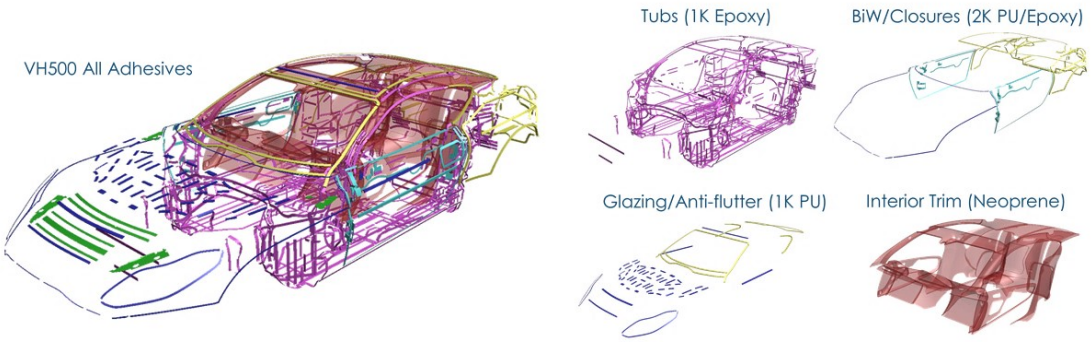

Figure 1 – Schematic representation of the different types of adhesives used, as well the specific locations in an Aston Martin DB11 (image provided by Aston Martin Lagonda®).

The automotive industry has recently recognised the advantages of using adhesives and is nowadays introducing this technology not only in limited series of sport cars but

also in large productions, especially in the construction of electric cars that require very light structures to overcome the weight increase.

The impact behaviour of joints of metallic substrates is reasonably well understood, where the adhesive is supposed to keep the metal together so it can absorb all the plastic deformation. In the case of composite or composite/metal joints, the information available is more limited. One of the main goals of this work is therefore also to provide experimental data for composites and multi-material joints to understand the joints mechanic behaviour when subject impact loads and under the influence of a wide range of temperatures, which an automotive structure should be designed to operate at. The low transverse strength of the composites and the temperature variations are the major challenges to solve.

Another aspect of great importance that needs to be investigated is the residual impact strength after a period of hygrothermal aging. The average life expectancy of an automotive is currently of 10-15 years, and during that life expectancy period, an automotive structure can be subjected to humidity and to temperatures ranging from -30 to 80 ºC. These conditions will degrade the adhesive and the interface and it's important to assess if the residual impact strength is acceptable.

By developing highly advanced joining techniques, innovative, durable, and efficient vehicles can be achieved. Vehicles with multi-material structures designed with durability in mind can be in service for longer. Durable adhesive bonding technique can be an integral of a paradigm shift serving as a tool to faster innovation. Vehicle manufacture can be partially replaced by a continuous upgrade process, where a single structure can be made to last decades safely, with a powerful influence in resource and energy consumption.

This work focused on the answer to the mentioned problems by creating a cooperation between three host institutions (main: FEUP, INEGI and secondary: TokyoTech) and two industrial companies (Nagase ChemteX® and Aston Martin Lagonda®) (Figure 2). The acquired knowledge will then be transferred to the industry to solve manufacturing problems and help in the development of new products.

Figure 2 – Representation of the designation and local of the institution and companies involved.

1.3. Objectives

The main objective of this thesis is the complete development of a design methodology for adhesively bonded joints for the automotive industry. A defined methodology for this purpose does not currently exist at this moment and manufacturers are searching for a validated procedure that will enable them to minimize experimentation and associated costs. To develop this methodology, it is essential to understand, and address four important challenges currently faced by the automotive industry.

The first of these challenges is the accurate determination of the mechanical and cohesive properties of structural adhesives and composites used by the automotive industry, for a wide range of temperatures and strain rates. By carefully selecting advanced characterization tests in conjunction with appropriate data reduction techniques, it should be possible to understand how the material properties change as a function of these variables. This is an important step as no standard process is currently defined for the characterization of adhesive mechanical properties under large strain rates and this work would allow the establishment of such procedure.

For the second challenge, this work focuses on the development of alternative joint configurations, such as mixed adhesive joints. These types of configuration are expected to reduce the fundamental problems associated to composite bonded joints, such as premature delamination and susceptibility to thermally induced stresses, enabling automotive designers to dramatically improve joint strength with no weight or cost penalties. The automotive industry has shown interest in this technology, especially for joints with dissimilar materials and, consequently, large residual stresses. However, to date there is still no practical implementation of this technique.

The third main challenge is the development of a numerical models able to efficiently and quickly model the impact behaviour of adhesive joints, reducing the need to perform costly experimental tests. Strain rate sensitive cohesive zone models of adhesively bonded structures will be created in this project and validated with experimental data.

Lastly, the work will study the influence of aging on the impact strength of adhesive joints. Such information is extremely limited in the literature but also of high importance, as it is fundamental to guarantee that the impact strength of the bonded vehicle structure does not suffer significant changes during the vehicle lifetime. The influence of aging conditions will also be assessed under fatigue, as it is another important variable which can greatly condition the lifetime and the integrity of an automotive structure, and a case where there is limited information for supporting the design of adhesive joints.

All the previously mentioned challenges are be crucial to achieve the main goal, which consists in acquiring data that will allow to perform numerical analysis, able to predict the behaviour of an automotive structures provided by Aston Martin Lagonda®, subjected to quasi-static (1 mm/min) and impact (3 m/s) conditions at 24 ºC. Such data will then be compared with the experimental results obtained by testing the automotive structure under those conditions, culminating in a direct comparison between the capability of the numerical models to predict the behaviour of a structures under quasi-static (1 mm/min) and impact (3 m/s) loading conditions.

To provide answers to these four challenges, **five main tasks** were defined, in an incremental effort to improve the processes that enable the prediction of joint strength under impact (3 m/s) conditions. In **Section 1.4.** each one of the five main tasks will be scrutinised in terms of objectives as well as the description of methodology.

1.4. Research methodology

A schematic representation of the research methodology considered in this work is presented in Figure 3, in terms of the tasks previously stated, which will be detailed in this section in terms of experimental (type of tests and equipment required) and numerical sequence.

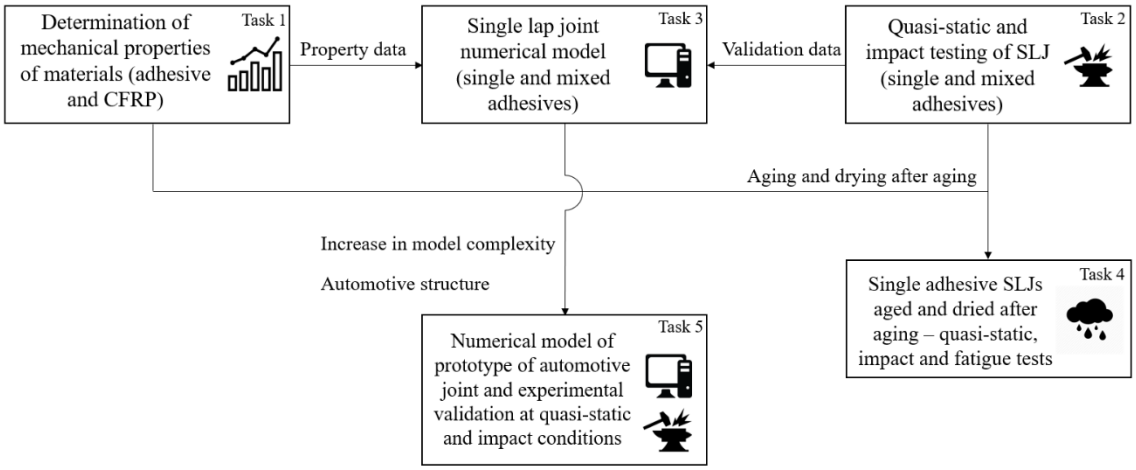

Figure 3 – Schematic representation of the workflow of the tasks performed in this work.

As stated in **Section 1.3.**, a total of **five distinct tasks** were considered, being the detailed description of each one subsequently performed.

Task 1 – Determination of the mechanical properties of a crash resistant adhesive and substrate, as a function of loading rate and testing temperature (-30, 24 and 80 ºC):

The objective of this task was to determine the crash resistant adhesive and substrate mechanical properties under quasi-static (1 mm/min) and impact (3 m/s) conditions from low to high temperatures separately. A crash resistant adhesive typically used in the automotive industry for the manufacture of the body in white was used. Two high strength aluminium alloys (used by Aston Martin Lagonda®), and carbon fibre reinforced polymer (CFRP) were selected as substrates, and as it is known that for the case of aluminium alloys there are no changes in its mechanical properties as a function of strain rate and testing temperatures (identified in this work by experimental tests), therefore only the CFRP substrate was characterized. Each material (adhesive and substrate) was tested individually to assess its influence on the joint behaviour.

Failure strength tests and fracture energy tests were carried out. For the failure strength tests, bulk specimens were tested to obtain the stress-strain behaviour. For the fracture energy tests, double cantilever beam (DCB) specimens for mode I and end notch flexure (ENF) for mode II were used to assess the fracture energy of the adhesive and the interlaminar strength of the composite. The failure strength tests, and fracture energy tests were carried out from quasi-static (1 mm/min) conditions to high strain rates/impact (3 m/s) at -30, 24 and 80 ºC testing temperatures. The use of very high strain rates for testing fracture mechanics specimens was an innovative approach, with limited work described in the literature. This required the development of new testing jigs, modification of specimen geometries and the implementation of adequate data reduction schemes to deduce the fracture energies. If this approach was found to be unsuitable for a given material, tests were performed at lower strain rates and an extrapolation process which was employed to predict the properties at higher strain rates.

A tensile testing machine was available for quasi-static tests. The machine was fitted with a climatic chamber that enables it to perform tests at low and high temperatures. The impact tests were performed in a instrumented falling weight impact tester. For low and high temperature testing, localised cooling with nitrogen and heating with an induction coil was used. As for testing automotive structures from Aston Martin Lagonda®, a drop-weight impact testing machine was developed in-house for testing adhesive joints and was available for the high strain rate tests.

The tests allowed the determination of the cohesive laws of both the adhesive and the CFRP as a function of strain rate and temperature. The stiffness and strength of the cohesive law were determined by the stress-strain results and the toughness from the fracture energy tests. The cohesive properties determined in this task were used to model in **Task 3** the single lap joints (SLJs) tested in **Task 2**, being also of extreme importance for the execution of **Task 5**.

Milestone 1: Crash resistant adhesive and CFRP mechanical properties under quasi-static (1 mm/min) and impact (3 m/s) conditions. Cohesive law properties (stiffness, strength and toughness) as a function of strain rate and test temperature.

Task 2 – Quasi-static (1 mm/min) and impact (3 m/s) testing of SLJs (single and mixed adhesives) from low to high temperatures:

The objective of this task was to test various SLJs configurations with two aluminium alloys and CFRP substrates (similar and dissimilar combinations), as well as single and mixed adhesives, under quasi-static (1 mm/min) and impact (3 m/s) conditions from low to high temperatures. Load-displacement (P-δ) curves were recorded to enable to determine the joint strength and energy absorbed for each testing condition.

SLJs with aluminium alloys and CFRP substrates were manufactured in a mould to control rigorously all the geometrical parameters. Multi-material joints (e.g. aluminium-CFRP) were also manufactured as they match the bonds found in modern automotive structures. To increase the impact energy absorption of the SLJs, the mixed adhesive technique, consisting in the use of SLJs with two adhesives (one ductile at the ends of the overlap and one brittle in the middle of the overlap) was explored (Figure 4). This approach will reduce stresses at the ends of the overlap length, reducing the possibility of interlaminar failure in the case of CFRP, and counteract undesirable unbalanced stresses when bonding dissimilar materials. In this case, only the best combination of adhesives was tested experimentally under the influence of the testing temperature.

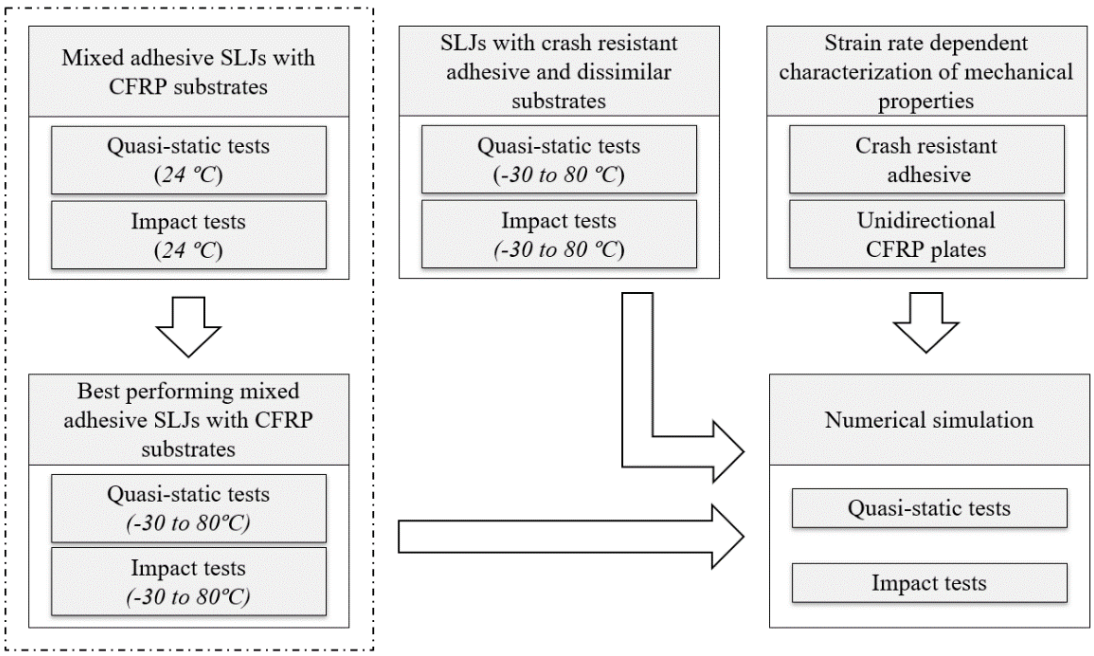

Figure 4 – Schematic representation of the detailed of the workflow of Task 2.

Different surface treatments were applied to the substrates to avoid an interface failure, being the aluminium alloys anodized (process performed by the manufacturing company).

SLJs were tested under quasi-static (1 mm/min) conditions in a tensile machine for reference purposes. A climatic chamber was used for low and high temperature testing at -30, 24 and 80 ºC. *P-δ* curves were recorded for each test. In-plane impact (3 m/s) tests were carried out in the drop weight machine described in **Task 1**. This machine does not currently possess a climatic chamber and cooling and heating were locally applied to the specimen. Liquid nitrogen under pressure was used for the -30 ºC tests and induction heating with a suitable coil was applied to obtain 80 ºC. The resultant *P-δ* curves were used to assess joint strength and energy absorption.

The quasi-static (1 mm/min) and impact (3 m/s) results obtained in this task were modelled in **Task 3** using the cohesive laws determined in **Task 1**.

Milestone 2: Determination of the quasi-static (1 mm/min) and impact (3 m/s) behaviour of SLJs as a function of strain rate and test temperature.

Task 3 – Numerical simulation of the quasi-static (1 mm/min) and impact (3 m/s) behaviour of SLJs (single and mixed adhesives):

The objective of this task was to develop a numerical procedure able to accurately model the SLJs (single and mixed adhesives) quasi-static (1 mm/min) and impact (3 m/s) results obtained experimentally in the previous task. The damage simulation model was able to consider the influence of thermal effects and strain rates.

The cohesive zone model properties determined in **Task 1** were used to simulate the crack initiation and propagation in the SLJs. Several parameters were assessed, namely, the strain rate, the test temperature and the type of substrate (aluminium alloys and CFRP). In addition, two distinct types of joints were modelled: simple SLJs (both similar and dissimilar substrates combinations) and mixed adhesive SLJs (as previously mentioned, only the best combination of adhesives was tested experimentally under the influence of the testing temperature) (Figure 4). The numerical *P-δ* curves were compared with the experimental results for validation of the cohesive law properties.

All the modelling was carried out in the finite element software Abaqus®. A triangular law was assumed for the cohesive zone model shape. The cohesive properties determined in **Task 1** were used to model the SLJs experimentally tested in **Task 2**. Two equations for each cohesive parameter (stiffness, strength and toughness) were determined and introduced in the model as a function of strain rate and testing temperature.

Milestone 3: Validation of the cohesive law properties as a function of strain rate and test temperature determined in **Task 1** for simple joint geometries.

Task 4 – Quasi-static (1 mm/min), impact (3 m/s) and fatigue testing of unaged, aged and dried after aging SLJs (single adhesive and in similar and dissimilar substrates combination):

The objective of this task was to test SLJs (using a single adhesive and in similar and dissimilar substrates combination) in the following conditions: unaged, hygrothermally aged (subjected to moisture and temperature, being immersed in deionised water) and dried after hygrothermal aging in quasi-static (1 mm/min), impact (3 m/s) and fatigue conditions.

The SLJs were manufactured and aged immersed in distilled water at 50 ºC for 2000 hours, being also posteriorly dried at 50 ºC with the purpose of assessing the degree of recovery from the aging process. Simple bulk specimens of both the crash resistant adhesive and CFRP were used for moisture uptake and desorption water measurement by a gravimetric analysis to determine the diffusion coefficient and, therefore, understand how the water ingresses and desorption occurs during the same period. The specimens were aged in an MMM climatic chamber and weighted by a precision scale (KERN machine). Fick's law and other more sophisticated diffusion models were tested to approximate the experimental data and get the most realistic diffusion model in the adhesive.

This task was limited to experimental tests to verify the durability of SLJs performed in **Task 3**, and to allow for a comparison and evolution of the behaviour of the SLJs under those conditions in terms of failure load and energy absorption. Although not one of the main goals of this task, a numerical analysis was also completed to predict the water

ingress in the adhesive layer of SLJs, as well the behaviour of the SLJs under quasi-static (1 mm/min) conditions.

The residual quasi-static (1 mm/min) and impact (3 m/s) strength testing at -30, 24 and 80 ºC of SLJs after being hygrothermally aged, as well dried after hygrothermal aging was executed. The residual joint strength and energy absorbed was assessed and compared with the values obtained for the unaged condition. Fatigue tests were performed considering three ranges of load (60, 40 and 20%) and two distinct combinations of substrates.

Milestone 4: Evolution of fatigue behaviour, as well as residual failure load and energy absorbed of SLJs tested under quasi-static (1 mm/min) and impact (3 m/s), following aging and drying after aging.

Task 5 – Validation of the numerical quasi-static (1 mm/min) and impact (3 m/s) models of an automotive structure by performing experimental tests:

This task necessitated a more complex numerical model and it can be divided into two main steps, the first was regarding a numerical simulation, being the second to its validation by experimental tests. Initially, a prediction of the behaviour of a real component from an automotive (provided by Aston Martin Lagonda®) being solicited under a quasi-static (1 mm/min) and impact (3 m/s) loads at room temperature was performed, by creating a detailed finite element model. The model was based on the techniques developed and validated in **Task 3**. All the modelling was carried out in the finite element software Abaqus®, although the mesh of the geometry was constructed using HyperMesh® software (as commonly used in the automotive industry). A triangular law was assumed for the cohesive zone model shape, using the properties identified in **Task 1** as an input. The model supported quasi-static and dynamical simulations by using strain rate dependent material properties and by considering inertial effect. Thermal effects were also considered due to the inclusion of temperature dependent material properties (also determined in **Task 1**). The numerically modelled automotive joint was assessed in terms of joint strength and impact energy absorption capabilities, enabling the validation of strength prediction techniques developed during this work after experimental tests.

The experimental setup configuration considered loads representative of those existing on a vehicle structure. To ensure repeatability, these joints were manufactured by rigorously controlling all the geometrical parameters. The automotive joint was manufactured using materials supplied by Aston Martin Lagonda® (the selected section of an automotive was the "roof frame header", which is also internally designated as "front header assembly" by Aston Martin Lagonda®), with the objective of being fully representative of a joint employed in automotive structures (Figure 5). The prototype joints were tested under testing conditions fully matching those used in **Task 2**. For this purpose, this task required the development of a new testing jig, compatible with the in-house developed drop weight impact testing machine.

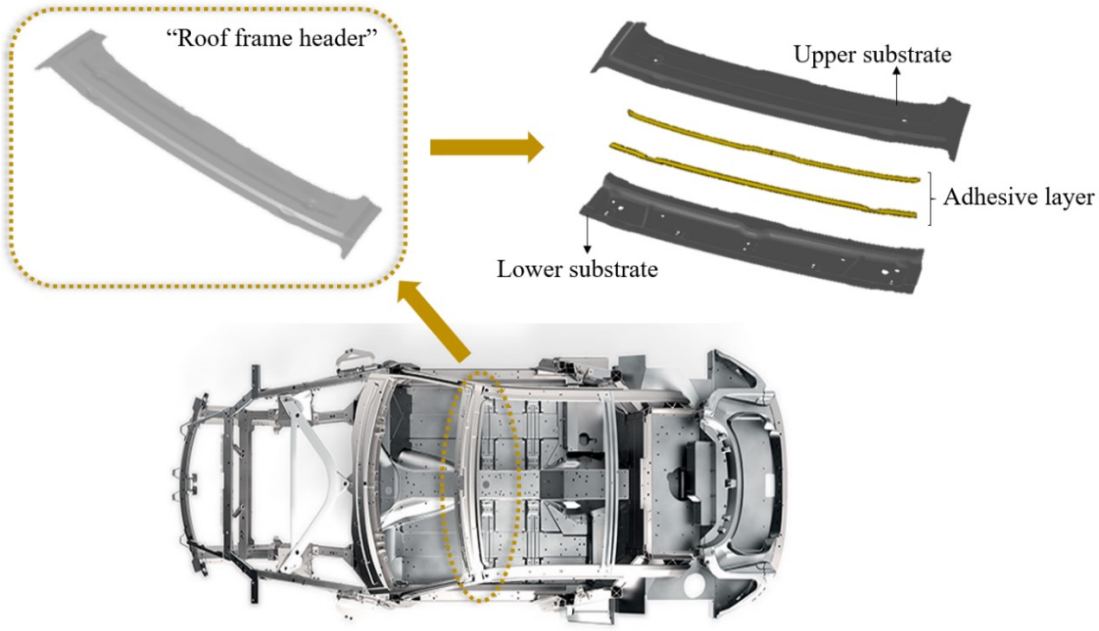

Figure 5 – Automotive section ("roof frame header") experimentally studied under quasi-static (1 mm/min) and impact (3 m/s) conditions – Aston Martin DB11 (provided by Aston Martin Lagonda®).

Aston Martin Lagonda® fully supported this phase by precisely describing the forces acting upon joints used in automotive structures and by providing advice regarding the configurations that are more adequate for industrial implementation. The outcome of this task was the complete validation through experimental tests of a numerical model able to predict the behaviour of an adhesive joint subjected to both quasi-static (1 mm/min) and impact (3 m/s) loads. The comparative data generated during this testing procedure was expected to make a strong contribution for the improvement of the structural design process at Aston Martin Lagonda®.

Milestone 5: Development of a more complex numerical model, representative of an automotive joint provided by Aston Martin Lagonda®, after experimental validation.

As previously mentioned, the structure of this thesis comprehends one or several papers supporting each task. The scrutinized list of these papers is therefore presented in Figure 6, and it serves to guide the reader in the analysis and understanding of the complete research process and its associated workflow.

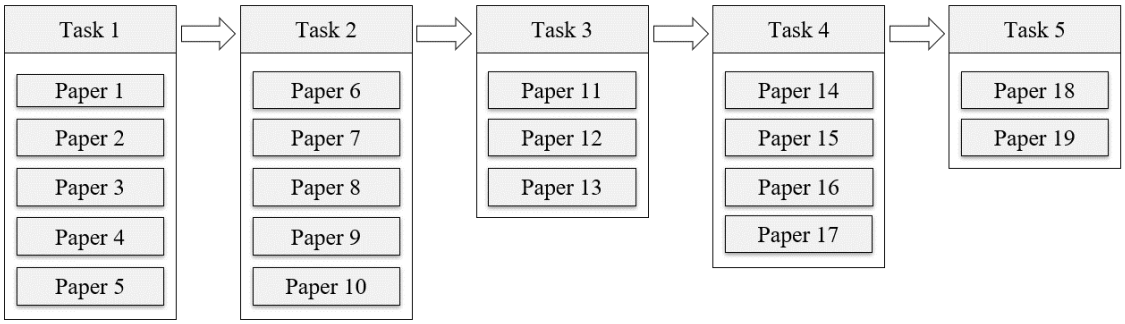

Figure 6 – List of papers assigned for each task performed.

1.5. Outline of the thesis

This thesis consists on nineteen papers and a summary, being each section of the work described by a single or several papers. The introduction of each paper details and abstract is performed in this section.

Paper 1 – Machado, J. J. M., Marques, E. A. S., da Silva, L. F. M., "**Adhesives and adhesive joints under impact loadings: An overview.**", *The Journal of Adhesion*, Vol. 94(6): pp. 421-452. (2018), DOI: 10.1080/00218464.2017.1282349.

Abstract of Paper 1: The study of the behaviour of adhesive joints under impact loading is a very active field of research, driven by significant industrial interest. Many industries, such as the automotive industry, are currently employing adhesive joints extensively, making use of the inherent properties of adhesive joints to improve the mechanical behaviour, reduce weight and simplify manufacturing. Reduced structural weight is achieved by combining multiple lightweight materials, which is made possible by using adhesive joints. Impact strength is also a major factor, as vehicles must be able to provide adequate safety levels for their occupants during collisions. Another example of industrial application is the defence industry, which uses bonded structures to withstand ballistic impacts, with extremely high impact velocities. Understanding the behaviour of adhesive joints under impact is, therefore, crucial for designing stronger and safer structures. This document aims to review the research that has been previously undertaken in this field. Discussed research topics include high strain rate property determination, adhesive joint testing, effects of coupling environmental conditions with impact loads, and sections on numerical and constitutive modelling procedures. The final sections describe some practical applications of adhesive joints under large strain rates and relate them with the fundamental concepts previously discussed.

Paper 2 – Machado, J. J. M., Hayashi, A., Nunes, P. D. P., Marques, E. A. S., Carbas, R. J. C., Sato, C., da Silva, L. F. M., "**Strain rate dependence of a crash resistant adhesive for the automotive industry.**" *Proceedings of the Institution of Mechanical Engineers, Part L: Journal of Materials: Design and Application*, (2019), DOI: 10.1177/1464420719836914.

Abstract of Paper 2: The wide and diverse application of adhesives in the automotive industry has increased over the last decades, driven by the need to produce efficient yet strong vehicles, able to meet both fuel economy and safety standards. This method allows to bond a variety of dissimilar materials used for structural parts, as well to achieve lighter structures, and higher failure loads over other traditional methods such as fastening or welding. It is therefore important to understand the behaviour of adhesives under a wide range of strain rates and temperatures. These data are fundamental to ensure vehicle safety, as adhesives must be able to sustain impact conditions, deforming but at the same time keeping the integrity of the structure and transmitting the loads without damaging the joint. The aim and novelty of this work is the complete mechanical characterization of a high-performance crash resistant adhesive under varied strain rate and temperature conditions, necessary for the validation of structures used in the automotive industry. The mechanical behaviour of these materials is still poorly understood and described in the literature. The results showed a change in the mechanical properties of the adhesive with the variation of strain rate (quasi-static and impact of 3 m/s) and temperature (-30, 24 and 80 °C). With the mechanical properties determined it was possible to define cohesive laws for implementation in finite element simulation, as a function of strain rate and temperature.

Paper 3 – Machado, J. J. M., Marques, E. A. S., Campilho, R. D.S., da Silva, L. F. M., "**Mode I fracture toughness of CFRP as a function of temperature and strain rate.**", *Journal of Composite Materials*, Vol. 51(23): pp. 3315-3326. (2017), DOI: 10.1177/0021998316682309.

Abstract of Paper 3: Composite structures currently used in the automotive industry must meet strict requirements for safety reasons. They need to maintain strength under varied temperatures and strain rates, including impact. It is therefore critical to fully understand the impact behaviour of composites. This work presents experimental results regarding the influence of a range of temperature and strain rates on the fracture energy in mode I, G_{IC}, of carbon fibre reinforced plastic plates. To determine G_{IC} as a function of temperature and strain rate, double cantilever beam specimens were tested at 20, 80 and -30 ºC, with strain rates of 0.2 and 11 s^{-1}. A complementary numerical study was performed with the aim of predicting strength using the measured values. This work has demonstrated a significant influence of the strain rate and temperature on G_{IC} of the composite materials, with higher strain rates and lower temperatures causing a decrease in the G_{IC} values.

Paper 4 – Machado, J. J. M., Marques, E. A. S., Campilho, R. D.S., da Silva, L. F. M., "**Mode II fracture toughness of CFRP as a function of temperature and strain rate.**", *Composites Part B: Engineering*, Vol. 114: pp. 331-318. (2017), DOI: 10.1016/j.compositesb.2017.02.013.

Abstract of Paper 4: Knowledge of the fracture properties of composite materials is fundamental to predict the impact behaviour of the lightweight structures currently used in the automotive industry. Although there is substantial research on mode I fracture behaviour of composites, limited information exists on mode II behaviour. This work aims to fulfil this gap, presenting experimental data regarding the influence of temperature and strain rate on the fracture energy in mode II, G_{IIC}, of composite plates. Significant influence of the strain rate and temperature on G_{IIC} of the composite materials was found. Higher strain rates led to a decrease of G_{IIC} up to 17%. An increase of temperature corresponded to an increase of G_{IIC} up to 15% and a decrease of temperature originated a decrease of G_{IIC} up to 7%.

Paper 5 – Machado, J. J. M., Hayashi, A., Sekigushi, Y., Campilho, R. D. S., Marques, E. A. S., Sato, C., da Silva, L. F. M., "**Dynamic behaviour in mode I fracture toughness of CFRP as a function of temperature.**", *Theoretical and Applied Fracture Mechanics*, Vol. 103, (2019), DOI: 10.1016/j.tafmec.2019.102257.

Abstract of Paper 5: The aim of this work is to assess the influence of high strain rates and testing temperature on the fracture energy in mode I, G_{IC}, of carbon fibre reinforced plastic (CFRP) plates. Double cantilever beam (DCB) specimens were tested to determine G_{IC} as a function of temperature (24 and 80 °C) under an impact load of 4.7 m/s (using a falling-wedge impact test machine), with the results being compared with the values previously determined by the authors under quasi-static loads. This work has demonstrated a significant influence of the testing temperature on the G_{IC} of composite materials, as this value greatly increased for higher temperatures. On the other hand, a less significant influence of the strain rate on G_{IC} was found, which slightly decreased by increasing the strain rate.

Paper 6 – Araújo, H. A. M., Machado, J. J. M., Marques, E. A. S., da Silva, L. F. M., "**Dynamic behaviour of composite adhesive joints for the automotive industry.**", *Composite Structures*, Vol. 171: pp. 549-561. (2017), DOI: 10.1016/j.compstruct.2017.03.071.

Abstract of Paper 6: The automotive industry has significantly increased the use of adhesive joints in vehicle construction, which can be explained in part by the widespread adoption of composite materials and structures. The combined use of composites and bonding allows the manufacture of structures with high mechanical strength and reduced weight. However, to ensure vehicle safety, these adhesive joints must be able to sustain large impact loads, transmitting the load to the structure without damaging the joint. This work aims to study the impact behaviour of composite adhesive joints bonded with a ductile epoxy adhesive, comparing different overlap lengths. For this purpose, a characterization of the behaviour of single lap joints was performed under quasi-static and impact conditions. Dynamic tests were also performed using vibration analysis to assess the damping capabilities of the studied joints. Numerical models were developed with cohesive elements in ABAQUS® software, including both quasi-static and dynamic models. It was demonstrated that joints manufactured with this type of adhesives and substrates can exhibit excellent impact strength and damping capabilities. It was also shown that the behaviour of these joints can be successfully modelled using static and dynamic finite element analysis.

Paper 7 – Machado, J. J. M., Marques, E. A. S., da Silva, L. F. M., "**Mechanical behaviour of adhesively bonded composite single lap joints under quasi-static and impact conditions with variation of temperature and overlap.**", *Journal of Composite Materials*, Vol. 52(26): pp. 3621-3635. (2018), DOI: 10.1177/0021998318766641.

Abstract of Paper 7: The use of adhesively bonded joints in structural components for the automotive industry has significantly increased over the last years, supported by the widespread integration of composite materials. This synergy allows vehicle manufacturers to offer a significant weight reduction of the vehicle allowing for fuel and emissions reduction and, at the same time, providing high mechanical strength. However, to ensure vehicle safety, the crashworthiness of these adhesive joints must be assessed, to evaluate if the structures can sustain large impact loads, transmitting the load and absorbing the energy, without damaging the joint. The novelty of this work is the study of the strain rate dependent behaviour of unidirectional composite adhesive joints bonded with a ductile epoxy crash resistant adhesive, subjected to low and high testing temperatures and using different overlap lengths. It was demonstrated that joints manufactured with this type of adhesive and composite substrates can exhibit excellent quasi-static and impact performance for the full range of temperatures tested. Increasing the overlap length, and independently of the testing temperature, it was observed an increase of energy absorbed for both quasi-static and impact loads, this is of considerable importance for the automotive industry, demonstrating that composite joints exhibit higher performance under impact.

Paper 8 – Machado, J. J. M., Nunes, P. D. P., Marques, E. A. S., da Silva, L. F. M., "**Adhesive joints using aluminium and CFRP substrates tested at low and high temperatures under quasi-static and impact conditions for the automotive industry.**", *Composites Part B: Engineering*, Vol. 158: pp. 102-116. (2018), DOI: 10.1016/j.compositesb.2018.09.067.

Abstract of Paper 8: The use of adhesives to bond metallic and composite structural components has increased substantially over the last decades. The aim of this work is to understand and predict the behaviour of dissimilar adhesive joints, using composite and aluminium substrates, under quasi-static and impact loads. Several testing temperatures (-30 to 80 ºC) were considered, following the requirements for the automotive industry. It was possible to conclude that dissimilar adhesive joints, if used in conjunction with modern crash resistant adhesives, can effectively be used for the construction of automotive structures, without significant sacrifices in joint performance, with good energy absorption capabilities under impact.

Paper 9 – Machado, J. J. M., Gamarra, P. M-R., Marques, E. A. S., da Silva, L. F. M., "**Improvement in impact strength of composite joints for the automotive industry.**", *Composites Part B: Engineering*, Vol. 138: pp. 243-255. (2018), DOI: 10.016j.compositesb.2017.11.038.

Abstract of Paper 9: The use of composite structures in the automotive industry aims to produce vehicles able to meet both fuel economy and safety standards. This work focused on the improvement of static and impact strength of composite adhesive joints, avoiding early delamination of the composite. The techniques applied are mixed adhesive combinations (use of two adhesives in one overlap) and the use of crash resistant adhesives. Experimental results demonstrated that a crash resistant adhesive provides the best mechanical performance under quasi-static and impact loads. A mixed adhesive configuration provided good results and improvements over single adhesives.

Paper 10 – Machado, J. J. M., Marques, E. A. S., da Silva, L. F. M., "**Influence of low and high temperature on mixed adhesive joints under quasi-static and impact conditions.**", *Composite Structures*, Vol. 194: pp. 68-79. (2018), DOI: 10.1016/j.compstruct.2018.03.093.

Abstract of Paper 10: The increasing use of composite structures in the automotive industry is due to strict regulations regarding fuel efficiency and safety standards. The main advantage of the use of adhesives is the possibility of joining dissimilar materials, particularly composites. The technique studied was the mixed adhesive joints, as two or more adhesives can be used in a single lap joint combining the properties of those adhesives to attain mechanical performance superior to that obtained using those adhesives individually. The main goal was to assess if a previously validated combination of mixed adhesives in a composite joint, tested under quasi-static and impact conditions, offers the same advantage over the use of a single adhesive when subjected to low (−30 °C) and high (80 °C) temperatures. The influence of temperature on the behaviour of the composite joints was assessed in quasi-static and impact conditions allowing to infer the effect on each adhesive. Another important aspect of the use of this type of technique is to avoid the early delamination of the composite substrates. This method was found to improve the performance under quasi-static and impact conditions although its behaviour under the wide range of temperature tested was found to vary significantly.

Paper 11 – Machado, J. J. M., Nunes, P. D. P., Marques, E. A. S., Campilho, R. D. S., da Silva, L. F. M., "**Numerical study of mode I fracture toughness of CFRP under an impact load as a function of temperature.**", *Proceedings of the Institution of Mechanical Engineers, Part L: Journal of Materials: Design and Application*, (**Submitted on May 2019 – under review**).

Abstract of Paper 11: The main objective of this work is, by using cohesive zone modelling (CZM), to compute the fracture toughness behaviour in mode I of unidirectional carbon-fibre reinforced plastic (CFRP) subjected to an impact load at 4.7 m/s. To perform this task, Double-Cantilever Beam (DCB) specimens were simulated, being assessed its opening displacement and crack propagation, as well as the evolution of strain rate through the test. Therefore, by plotting the crack propagation, it was possible to calculate the fracture toughness in mode I (G_{IC}). A comparison of the numerical results with experimental tests previously performed by using a drop weight falling-wedge impact test equipment was made, allowing to infer that the numerical approach, based on a triangular CZM, is capable to predict the behaviour of such specimens under impact, accurately obtain G_{IC}, and to determine the value of strain rate achieved through the test.

Paper 12 – Machado, J. J. M., Marques, E. A. S., Silva, M. R. G., da Silva, L. F. M., "**Numerical study of impact behaviour of mixed adhesive single lap joints for the automotive industry.**", *International Journal of Adhesion and Adhesives*, Vol. 84: pp. 92-100. (2018), DOI: 10.1016/j.ijadhadh.2018.02.036.

Abstract of Paper 12: The automotive industry is now extensively using multi-material structures to reduce vehicle weight. Joining these dissimilar materials effectively in a single structure demands the use of adhesive bonding, but the presence of stress concentrations leads to low mechanical performance. Mixed adhesive joints have been proposed as a solution for this issue, using two adhesives in the same joint, combining stiffness and flexibility on the same overlap, improving performance. This work focuses on the numerical modelling of the mechanical behaviour of these joints, using previously published experimental data for validation. The proposed models use cohesive laws with strain rate dependent data to simulate quasi-static and impact loads on several configurations of mixed adhesive joints, using four different adhesives. The models were able to predict the behaviour of most configurations under study, especially for the stiffer adhesives. The model was found to be less effective for modelling high ductility adhesives under impact.

Paper 13 – Machado, J. J. M., Gamarra, P. M-R., Marques, E. A. S., da Silva, L. F. M., "**Numerical study of the behaviour of composite mixed adhesive joints under impact strength for the automotive industry.**", *Composite Structures*, Vol. 185: pp. 373-380. (2018), DOI: 10.1016/j.compstruct.2017.11.045.

Abstract of Paper 13: The increasing use of composite structures in the automotive industry is due to strict regulations regarding both fuel efficiency and safety standards, since this kind of structures allow to produce strong yet light vehicles. The main advantage of the use of adhesives is the possibility of joining dissimilar materials, particularly composite materials, representing an optimal method in comparison with more traditional ones such as fastening or welding. This work focused on the development and validation of numerical models able to simulate the performance of previously experimentally tested joints. The experimental tests were performed to assess the improvement of quasi-static and impact strength of composite adhesive joints, and with the focus of avoiding early delamination of the composite substrates. The technique selected for this purpose was the use of mixed adhesive joints. Mixed adhesive joints combine two or more adhesives in a single lap joint and combine these properties to attain mechanical performance superior to that obtained using those adhesives individually. The numerical results demonstrated to be able to simulate the experimental results with reasonable accuracy.

Paper 14 – Machado, J. J. M., Nunes, P.D.P., Marques, E. A. S., da Silva, L. F. M., "**Numerical study of similar and dissimilar single lap joints under quasi-static and impact conditions as a function of temperature.**", *International Journal of Adhesion and Adhesives*, (**Submitted on May 2019 – under review**).

Abstract of Paper 14: Aiming to achieve the targets of reduction of fuel consumption and emissions, automotive manufacturers are increasingly using lightweight materials in the vehicle structures, namely, carbon fibre composites and aluminium alloys. The construction techniques for vehicle structures using this type of materials differ greatly from the techniques used for the most commonly used steel bodies, with adhesive bonding being extensively used due to its capability to bond dissimilar materials. Nevertheless, the application of adhesive bonding poses several challenges to the automotive industry, as dissimilar bonded joints must be designed to perform well under impact. In this work, numerical models were created and validated against previously determined experimental data in both quasi-static and impact conditions of similar and dissimilar (CFRP and aluminium as substrates) single lap joints bonded using a crash resistant adhesive. Cohesive zone models were used to simulate adhesive failure and composite delamination while damage models were used to simulate plastic deformation and failure of the aluminium alloy.

Paper 15 – Machado, J. J. M., Marques, E. A. S., Barbosa, A. Q., da Silva, L. F. M., **"Effect of hygrothermal aging on the quasi-static behaviour of CFRP joints varying the overlap length."**, *Composite Structures*, Vol. 214: pp. 451-462. (2019), DOI: 10.1016/j.compstruct.2019.02.035.

Abstract of Paper 15: Adhesively bonded joints with composite substrates are crucial for the manufacture of lightweight structural components for the automotive industry. However, the safety of the vehicles must still be ensured after hygrothermal aging of both composite substrates and adhesive, as adverse conditions such as moisture and temperature will be a constant during a vehicle lifecycle. This work studies the influence of hygrothermal aging and temperature on the quasi-static behaviour of adhesive joints made with unidirectional composite substrates and a crash resistant adhesive using different overlap lengths. A complementary numerical simulation was performed to model both the water uptake processes and the failure process of moisture affected materials. Both the simulation and the experimental data showed increased susceptibility to delamination failure induced by water absorption in the composite and changes in the adhesive properties.

Paper 16 – Machado, J. J. M., Marques, E. A. S., Barbosa, A. Q., da Silva, L. F. M., **"Influence of hygrothermal aging on the quasi-static and impact behaviour of single lap joints using CFRP and aluminium substrates."**, *Mechanics of Advanced Materials and Structures*, (**Submitted on February 2019 – under review**).

Abstract of Paper 16: The use of adhesive to bond composites in vehicles continues to increase. Due to hygrothermal conditions, both adhesive and composite properties can be altered, making the mechanical behaviour of a joint unpredictable. The novelty of this work is the assessment of the behaviour of joints manufactured using composite and aluminium substrates tested under quasi-static and impact conditions in the following states: unaged, hygrothermally aged, and dried after hygrothermal aging. A significant reduction of failure load was registered for composite joints (quasi-static and impact) after hygrothermal aging. Joints dried after aging achieved a recovery in the failure load of quasi-static tests.

Paper 17 – Machado, J. J. M., Marques, E. A. S., Barbosa, A. Q., da Silva, L. F. M., **"Performance under fatigue loads of single lap joint using CFRP and aluminium substrates prior and after hygrothermal aging."**, *Fatigue and Fracture Engineering Materials and Structures,* (2019).

Abstract of Paper 17: Adhesive bonding has been used to join composites and aluminium alloys over the last decades in the automotive industry, requiring deep understanding of its fatigue behaviour. The novelty of this work is the evaluation of the combined performance of joints manufactured with CFRP and aluminium substrates subjected to fatigue loads in the unaged, hygrothermally aged and dried after hygrothermal aging states. The experimental results allowed to conclude the fatigue performance of joints can be alternated by changes induced by the drying process or losses in the interface strength, and that dissimilar combination of substrates sustain higher number of cycles to failure.

Paper 18 – Silva, N. D. D., Machado, J. J. M., Marques, E. A. S., Parente, M., da Silva, L. F. M., **"Experimental and numerical study of the quasi-static response of an adhesively bonded automotive structure."**, *Engineering Failure Analysis,* (2019), (**Submitted on July 2019 – under review**).

Abstract of Paper 18: The constant demand for fuel saving in the automotive industry requires the design of lighter structures, which encourage the application of low-density materials together with structural adhesives to bond the automotive frames. Still, it is fundamental to ensure that weight reduction does not compromise mechanical resistance, making it possible to obtain lighter yet strong structures, able to fulfil the requirements of this sector. The aim of this work is to analyse the quasi-static behaviour of a component-scale automotive frame bonded with a crash-resistant epoxy adhesive, representative of the use of adhesives in real-life automotive structures. The tests were performed at room temperature (24 ºC), characteristic of normal service conditions. A numerical simulation of the structure was also conducted, allowing the comparison of the finite element model predictions with the experimental data. The results showed that the adhesive did not compromise the integrity of the automotive structure, as the failure was caused by fracture in the lower aluminium substrate. The numerical analysis revealed good accuracy in the failure load prediction of the joint. Considering the experimental observations, a more flexible polyurethane adhesive was considered to join the component, avoiding the previous fracture.

Paper 19 – Silva, N. D. D., Machado, J. J. M., Marques, E. A. S., Moreira, O. M. G. P., da Silva, L. F. M., **"Experimental and numerical study of the dynamic response of an adhesively bonded automotive structure."**, *Mechanics of Materials,* (2019), (**Submitted on July 2019 – under review**).

Abstract of Paper 19: Based on economic and environmental factors related to energy efficiency, the automotive industry is being increasingly encouraged to design lighter structures, making use of adhesive bonding in vehicle body frames. To meet the standards of the automotive sector, adhesive joints must provide high strength and stiffness, low cost and good energy absorption at a component level, therefore ensuring good impact strength and passenger safety. This work aims to study, at room temperature (24 ºC), the impact response of a real scale automotive structure bonded with a crash-resistant epoxy, allowing to access the suitability of adhesives for automotive structural purposes. The same component was also analysed through a finite element model, so that the numerical predictions could be compared with experimental data. The epoxy adhesive was found to successfully transfer the loads to the substrates and not to compromise the integrity of the structure, as its failure was dominated by the behaviour of the aluminium. Furthermore, the simulation showed good accordance with the experimental failure load, revealing that numerical analysis can be a viable tool to predict structure's behaviour. Additionally, a polyurethane was used as an alternative to the epoxy system to bond the structure, proving that the joint behaves better in the presence of a more flexible adhesive.

2. Adhesives and substrates

Adhesively bonded joints are composed of one or more adhesives, used to join similar or dissimilar substrates. In this section, a brief description of all the adhesives and substrates used will be made, accompanied by the reasoning behind their selection.

2.1. Crash resistant adhesive

The main adhesive used in this work is a crash resistant epoxy-based material with the designation of XNR6852 E-3, supplied by the company Nagase ChemteX® (Osaka, Japan). This adhesive is a prototype under development, aiming for application in the automotive industry (more precisely, in structures that must sustain impact loads), and being especially designed for Aston Martin Lagonda®.

The general properties of XNR6852 E-3 adhesive are presented in Table 1.

Table 1 – General properties of XNR6852 E-3 adhesive.

Adhesive	XNR6852 E-3
Type	Epoxy (Crash-resistant)
Physical form	One-part system
Cure cycle	4 hours at 165 °C
T_g (°C)	132 ± 4.5 °C (measured)

XNR6852 E-3 adhesive is currently in its forth version, being one of the goals of this work its mechanical characterization under the combined effect of high strain rate and temperature (**Paper 2**), therefore, providing enough data and allow the validation of several parameters mandatory to meet the automotive application requirements. The data obtained from this work will also be of extreme importance for the improvement and evolution of the adhesive chemical formulation, aiming to improve its mechanical performance for the automotive industry, as well as allowing for better and easier application and handling characteristics, which will determine its capability to be used in an industrial environment. This data will also be useful to establish the adhesive cohesive laws to input in the numerical models.

The adhesive is provided in a paste form with a light-yellow colour. Other key adhesive properties are its insolubility in water, the fact that it is not hazardous in terms

of combustion/explosion, a flash point above 120 °C, relative density of 1.16, and a viscosity is 515 Pa.s.

This adhesive was used in the manufacture of all different types of joints and its configurations tested in this work. As XNR6852 E-3 adhesive was formulated for the automotive industry, it was considered as the base line reference for comparison with the results from the mixed adhesive joints configurations, as its high strength and ductility represent one of the best characteristics for the application being considered in this work.

2.2. Adhesives used in mixed adhesive joints configurations

An issue that should be addressed in adhesively bonded joints is the stress concentration at the overlap ends of the bonding area, which can lead to premature failure of the joints (or a significant decrease of its resistance) due to the introduction of peel stresses, as the adhesives are best suitable to withstand shear loads.

A possible solution to the mentioned problem will be addressed in this work, as a form of mixed adhesive configuration (**Paper 8** to **Paper 10**) and validated by performing tests on SLJs with CFRP substrates. The concept of mixed adhesive joints consists in using a flexible adhesive at the end of the overlap length and a stiffer adhesive in the centre (Figure 7).

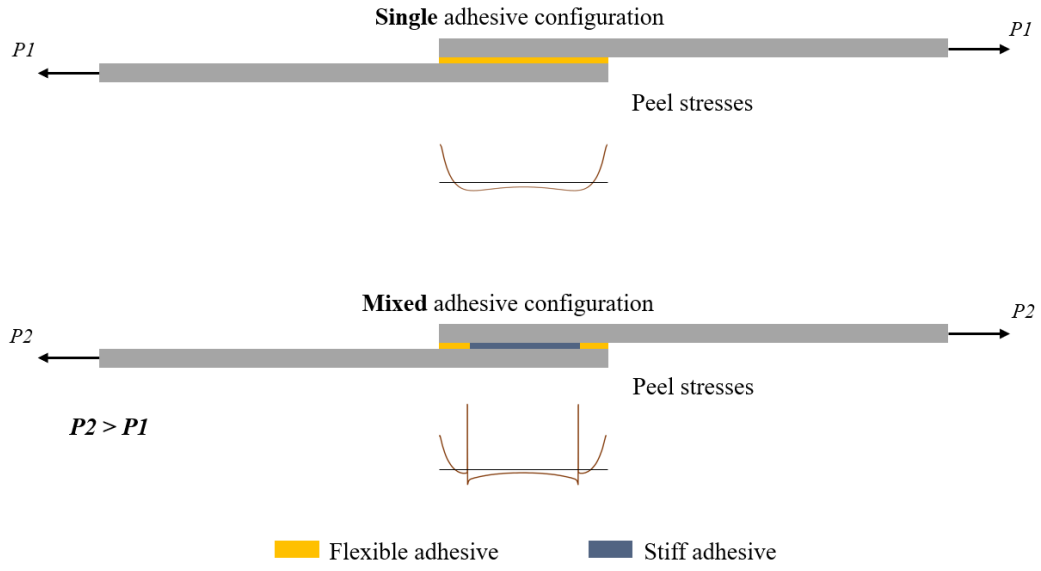

Figure 7 – Schematic representation of SLJs made with single and mixed adhesive configuration, with representation of the peel stress distribution along the overlap length (P_1 and P_2 are the applied loads to test the SLJs).

In this work, **five** distinct **adhesives** were selected for use in mixed adhesive joints (**Paper 8** to **Paper 10**). It is important to refer that although this method is not new, no results of this type of joints tested using CFRP substrates (the only substrate used to perform experimental tests) or even as a function of strain rate and temperature are found in the literature.

The selected adhesives were previously tested and mechanically characterized in the Adhesive´s group at FEUP, being part of the reason why they were used in this work. The following list presents the five adhesives and contains detailed information regarding its applicability in SLJs:

1. Araldite® **AV 138** (Salt Lake City, UT, USA): an epoxy adhesive with very stiff and brittle mechanical behaviour. When used alone in adhesive joints, it normally leads to low strength due to the large stress concentration it creates. It is therefore a good candidate for showing improvements when combined with a second, less stiff adhesive. Used as a **stiff adhesive**.
2. Nagase ChemteX® **XNR6852 E-3** (Osaka, Japan): a one-part system epoxy adhesive, formulated for use in automotive structures. It was selected due to its high strength and ductility, which provide excellent impact behaviour to this adhesive. It is commonly known as a crash resistant adhesive and was selected for this work as the main adhesive, also representing an actual adhesive employed by the automotive industry. Used as a **stiff adhesive**.
3. 3M® **DP 8005** (Maplewood, Minnesota, USA): It is a two-component structural acrylic adhesive specially formulated to bond polymers such as PVC, PVE or PP. This adhesive owns good resistance to water, humidity and chemical substances. It has already been tested in mixed adhesive joints, demonstrating good results. Used as a **flexible adhesive**.
4. SikaFast® **5211 NT** (Baar, Switzerland): a two-component structural acrylic adhesive with a very fast curing time and good ductility. This adhesive was selected for use in the mixed adhesive joints due to its ductile behaviour. Used as a **flexible adhesive**.
5. Momentive® **RTV 106** (Albany, NY, USA): a silicone rubber acetoxy type adhesive. It is a very ductile adhesive, excellent for insulating. It has low mechanical strength but very high ductility which provides good impact performance. This adhesive was selected for this work as it has already been tested

in mixed adhesive joints research with promising results. Used as a **flexible adhesive**.

The adhesives can be divided in two distinct types, namely, as stiff or flexible, and can ordered from the highest to the lowest in terms of Young´s Modulus value (Figure 8), once stiffness is the mechanical properties which allow the correct selection of each adhesive to for valid mixed adhesive joint.

	Stiff adhesives		**Flexible adhesives**		
	AV 138 (epoxy)	**XNR6852 E-3** (crash resistant adhesive)	**DP 8005** (acrylic)	**5211 NT** (acrylic)	**RTV 106** (RTV silicone)
E [MPa]	4890	1675	632	260	1.6

Decrease in stiffness

Figure 8 – List of adhesives used to manufacture mixed adhesive SLJs, divided in stiff and flexible type and ordered considering the higher to the lower values of Young´s Modulus (decrease in stiffness).

Due to manufacturing problems such as, mixing between the adhesives (fluidity of one adhesive could cause its passage to the correspondent section of the other adhesive, causing the contamination of the adhesive area), and distinct curing cycle (can greatly change the mechanical properties of one of the adhesives), not all combinations could be manufactured in practice. Another issue addressed was related to the achieved joint strength, since some mixed adhesive configurations presented the same values in strength as a single adhesive, or even lower values. Those combinations were dismissed.

In Table 2 all the considered single and mixed adhesives configurations manufactured and analysed in this work are shown, specifying the type of adhesives that should be placed at the centre of the overlap length (stiff) and at the end of the overlap ends (flexible).

Table 2 – List of configurations of mixed adhesives SLJs possible to perform with the five selected adhesives (n/a – not applicable, since no data was found in the literature and no experimental tests could be performed to determine this mechanical property).

		Adhesive at the **centre of overlap**				
		XNR6852 E-3	AV 138	DP 8005	5211 NT	RTV 106
Adhesive at the **overlap ends**	XNR6852 E-3	Single adhesive joint	n/a	n/a	n/a	n/a
	AV 138	n/a	Single adhesive joint	n/a	n/a	n/a
	DP 8005	n/a	Mixed adhesive joint	Single adhesive joint	n/a	n/a
	5211 NT	Mixed adhesive joint	Mixed adhesive joint	n/a	Single adhesive joint	n/a
	RTV 106	Mixed adhesive joint	Mixed adhesive joint	n/a	n/a	Single adhesive joint

2.3. Substrates

The selection of the materials used as substrates in this work is of great importance since these materials should be as close as possible to those used in the automotive industry, allowing to obtain representative results in terms of mechanical characterization and joint behaviour, leading to an increase in the capabilities of the numerical models and achieving reliable predictions of structural behaviour under the joint effect of strain rate and temperature.

Considering the concerns mentioned above, four of the most representative materials of the current automotive industry (settled after an initial contact with Aston Martin Lagonda®) were selected as substrates for this work (Table 3), namely, a carbon fibre reinforced epoxy (CFRP) and three high strength aluminium alloys (namely, the Al 5754-H22, Al 6060-T6 and Al 6016-T4).

Table 3 – List and description of the materials selected as substrates for the similar and dissimilar SLJs.

Substrates	Description
CFRP	Unidirectional (0°) plies; Thickness of 2.1 mm; Made of 14 plies of carbon/epoxy pre-preg SEAL® Texipreg HS 160 RM.
Al 5754-H22	Aluminium alloy 5754-H22; Thickness of 1.5 mm; Used to manufacture SLJs (single and multi-material combinations); Designation in this work will be Al 1.5.
Al 6060-T6	Aluminium alloy 6060-T6; Thickness of 2.0 mm; Used to manufacture SLJs (single and multi-material combinations); Designation in this work will be Al 2.0.
Al 6016-T4	Aluminium alloy 6016-T4; Thickness of 2.0 mm; Used to manufacture SLJs (single combination); Provided as a section of an automotive: top part connecting the roof and the windshield.

In Table 3 it is possible to observe the values of thickness used for each substrate, those values corresponding to thicknesses typically used by the automotive industry is structural construction (as indicated by Aston Martin Lagonda®). Consequently, in this work it was assumed that the most representative condition in terms of joints validation was the use of such values.

Examples of curves representing the yield stress *versus* plastic strain, of the aluminium alloys: 5754-H22, 6060-T6 and 6016-T4 are presented in Figure 9.

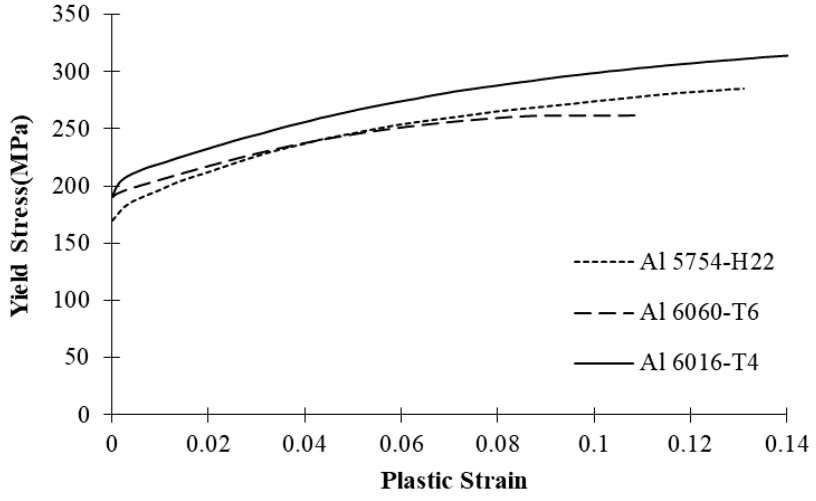

Figure 9 – Examples of Yield stress versus plastic strain of the aluminium alloys: 5754-H22 and 6060-T6.

The unidirectional (0°) CFRP used in this work, although not suitable for a direct application in the automotive industry (generally other more complex layups are used), was considered for two reasons: the first was that this material was already partially mechanically characterized within the Adhesive´s group from FEUP, and secondly due to the higher mechanical properties offered by this configuration in a single directions, it simplifies failure mode analysis and enables better scrutinization of the delamination process (using images recorded during the tests was easier to observe the evolution of such phenomena). This specific CFRP laminate presents a carbon fibre volume ratio of 60% after curing. The mechanical properties of the CFRP are presented in terms of quasi-static (**Paper 3** and **Paper 4**) and impact conditions (**Paper 5**), as a function of the testing temperature.

The three aluminium alloys (Al 5754-H22, Al 6060-T6 and Al 6016-T4) were provided by Aston Martin Lagonda® in an anodized state. These aluminium alloys are currently being used in the latest automotive models commercialized (such as, the Aston Martin DB11 model), as well as prototypes being developed by this car manufacturer.

A distinct separation between the supplied aluminium alloys should be made. The 5754-H22 and 6060-T6 aluminium alloys were analysed in both single and multi-material SLJs (also identified in this work as similar and dissimilar joints), allowing to infer the behaviour of the joints in quasi-static and impact conditions varying the testing temperature (**Paper 8**), under the influence of aging and drying after aging (**Paper 15**), as well under fatigue loads (**Paper 16**). As for the 6016-T4 aluminium alloy, it was provided in the shape of SLJs substrates as well of a section of an automotive (Table 3), to be tested at room temperature under quasi-static (**Paper 18**) and impact loads (**Paper 19**).

3. Specimen manufacturing

Experimental testing is a task of great importance during research in the field of adhesive joints. Due to the large variety in adhesive types and their properties as well as the large amount of different possible substrates, surface preparations and curing procedures, there is the need to validate experimentally any new bonding procedure. Doing so will ensure that each part of the joint is working correctly, and that its potential is fully exploited, avoiding costly failures further on. For such reason, distinct manufacturing processes were extensively performed during this work, being of extreme importance to determine the cohesive properties necessary to perform accurate simulations.

Aiming to perform a thorough mechanical characterization of XNR6852 E-3 adhesive (**Paper 2**), several distinct specimens were manufactured, namely specimens for: T_g, tensile bulk, DCB, and torsion.

The following tests were performed to characterize the CFRP substrate: T_g (**Paper 3**), and fracture toughness, namely, DCB (**Paper 3 and Paper 5**) and ENF (**Paper 4**).

To evaluate the maximum strength, deformation and energy absorbed, several SLJs were manufactured, comprised of different adhesives and substrates. The different SLJs manufactured can be divided in:

- SLJs made with CFRP substrates (**Paper 6** and **Paper 7**);
- SLJs made with similar and dissimilar substrates (CFRP, Al 5754-H22 and Al 6060-T6) combinations (**Paper 8**);
- SLJs made using mixed adhesives combination (**Paper 9** and **Paper 10**); influence of aging and drying after aging on the quasi-static (1 mm/min), impact (3 m/s) and fatigue behaviour of SLJs (**Paper 15**, **Paper 16** and **Paper 17**);
- and an automotive joint ("roof frame header" made of Al 6016-T4) tested under quasi-static (1 mm/min) (**Paper 18**) and impact (3 m/s) (**Paper 19**) conditions.

The main manufacturing procedures are described in detail in the following sections, where the problems/difficulties and solutions considered during the manufacturing process are also discussed.

3.1. XNR6852 E-3 adhesive

3.1.1. Tensile bulk specimens

Tensile bulk specimens were obtained from a cured sheet plate of adhesive. These specimens have a specific geometry (informally designated as “dogbone”), in accordance with the BS 2782 standard [56] (Figure 10).

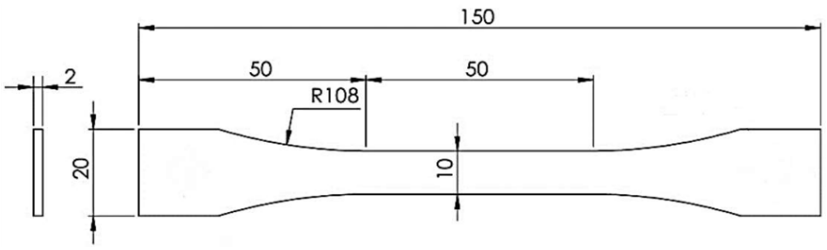

Figure 10 – Geometry of bulk specimens according to BS 2782 standard [56](dimensions in mm).

The manufacture process of such specimens is complex, mainly due to the difficulty in obtaining a specimen that is not only geometrically accurate but also devoid of defects. Any void, crack or section with incomplete cure leads to erroneous and unreliable results. For such reason, to manufacture high quality bulk sheet plates, an in-house designed steel mould was used (Figure 11), a design based on French NF T 76-142 standard [57].

To prepare for use, the mould was manually abraded with sandpaper to remove remnants of previous use and then degreased with acetone. The last step in the preparation of the mould was the application of three layers of mould release agent (Loctite® Frekote 770-NC). This step was performed to promote easier removal of the cured adhesive plate from the mould. A silicone rubber frame (Figure 11) was used to both ensure the required thickness of the adhesive plate and to provide hydrostatic pressure necessary to avoid any defect during the manufacturing process.

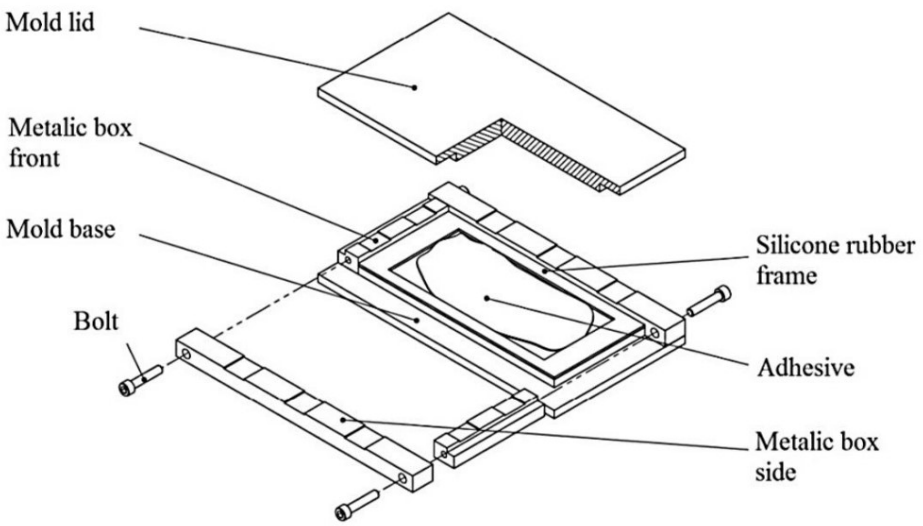

Figure 11 – Mould for producing the bulk specimens with steel plates and silicone rubber frame [58].

Once the mould was prepared, a high-speed centrifugal mixing machine (SpeedMixer® DAC 150.1 FVZ-K) was used (3 minutes at 2000 rpm) to increase the temperature of the adhesive (making it more fluid). XNR6852 E-3 adhesive was placed in a small cylindrical container, and several tests were performed to set the right quantity of adhesive to introduce for each bulk plate (35 grams), the correct rotation speed (2000 rpm) and time (3 minutes), aiming not to degrade the adhesive, compromising its mechanical properties. The adhesive requires this heating process as it is extremely viscous, and an amount of pre-heating promotes easier application. As higher temperature can cause degradation of an adhesive, therefore changing its mechanical properties, several tests were conducted using XNR6852 E-3 adhesive to ensure that undergoing the initial high temperature there was no compromise of the mechanical properties, and a comparison with some results provided by the manufactures was performed. The adhesive was applied on the mould cavity using a spatula. A generous amount of adhesive was used to prevent the appearance of voids, being necessary to use a wide spatula to spread the adhesive in several direction until all the air trapped inside was removed. After the adhesive has been applied and spread, the mould is closed and placed in a hot plate press for the cure schedule of 165 °C for 4 hours, simultaneously applying the curing temperature and pressure on the mould, according to the specific cure cycle of XNR6852 E-3 adhesive. The manufacturer indicates a cure cycle of 180 °C for 1.5 hours, but since CFRP substrates were used, it was necessary to find other cure cycle which required lower cure temperature, but at the same time did not comprise the mechanical properties of

XNR685 E-3 adhesive (test results allowed to determine that the difference between the two cure cycles was of -2% when using the lower cure temperature).

Once the cure cycle was completed, the bulk sheet plates were machined with the required dogbone shape (Figure 10) by using a milling machine. By manufacturing an adhesive bulk plate to be machine into the final shape of the specimens, the presence of defects in the specimens was drastically achieved.

3.1.2. DCB

The DCB specimen is of quite simple construction, consisting of two parallel beams (substrates) bonded lengthwise by an adhesive layer (Figure 12). High strength steel (DIN 40 CrMnMo 8-6-4) substrates were used to avoid plastic deformations of the DCB specimens, once XNR6852 E-3 adhesive is very tough. It is important to mention that due to the necessity to perform tests under different temperatures (using a climatic chamber) the total length of the substrates was reduced from 290 mm (as indicated in the ASTM D3433 standard [59]) to 155 mm.

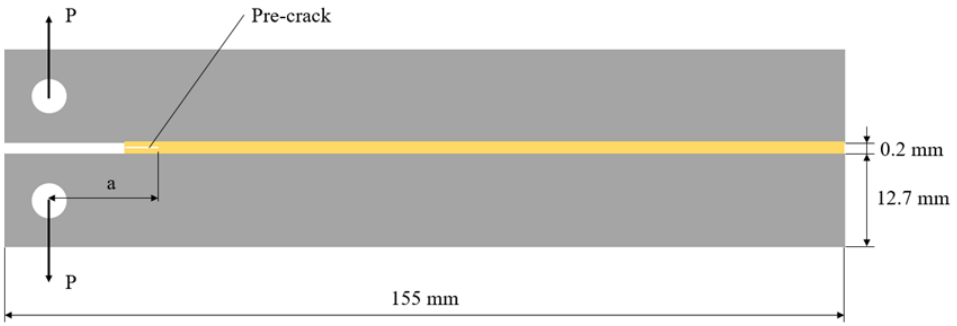

Figure 12 – Schematic representation of the geometry of the DCB specimens and loads applied (P is the load and a is the pre-crack length (a_0 = 30 mm)).

The preparation of the DCB specimens was the first step taken. Since the substrates are reusable, cleaning was required to remove any remaining adhesive particles from the bonding surface. For that purpose, the area where the adhesive is applied was sandblasted. Aluminium oxide particles were projected onto the substrates surface using compressed air, at 4 bar of pressure, until the surface presented a clean and rough finish, free of any previous contamination and at the same time providing the surface roughness necessary

to enhance interface strength. Finally, to clean and degrease the surface, acetone was used. This step fully cleans the bonding surface from any contaminants.

The adhesive was spread in excess quantity to guarantee that no air bubbles stay trapped in the adhesive, after undergoing 3 minutes at 2000 rpm in a high-speed centrifugal mixing machine to increase the temperature of the adhesive (making it more fluid). The adhesive thickness was ensured using spacers and razor blades (Figure 13). Calibrated tape of 0.2 mm was used for the spacers. On each blade, 0.05 mm thick calibrated tape was glued in each side of the blade, reaching a total of 0.2 mm thickness. While the blades have the same function of the spacers to control the adhesive thickness, they are also used to introduce a pre-crack in the adhesive, to ensure stable crack propagation from the beginning of the test.

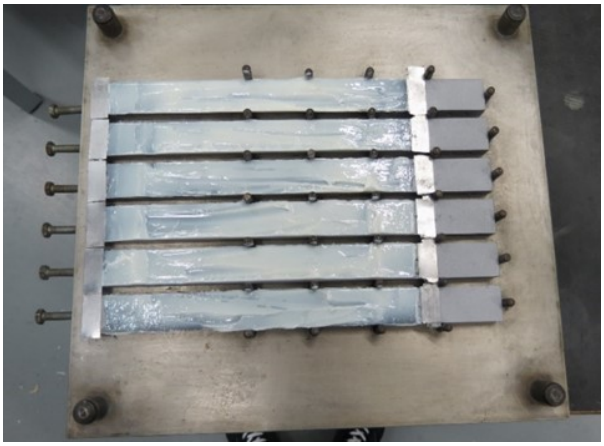

Figure 13 – Adhesive applied in the open substrates.

The substrates were then assembled in the mould and aligned by the mould pins. Small plates of silicon rubber were added between each specimen to avoid the excess adhesive from joining two neighbour specimens.

The mould was closed and placed on a hot plate hydraulic press. XNR6852 E-3 adhesive was cured accordingly to the cure cycle (165 °C for 4 hours). The pressure applied was of 2 MPa. Once the cure cycle was finished, the mould was removed from the hot press, and then, the specimens were removed from the mould. During the cure cycle excessive adhesive flowed out from the bondline.

To enable clear measurement of the pre-crack length and to avoid incorrect test results, the excess of adhesive was removed from the sides of the specimens with sandpaper and a milling machine.

3.1.3. Torsion specimens

The geometry of the torsion specimens is shown in Figure 14. The adhesive was applied on the tops of each section of the specimens. The adhesion surface was treated by using sandpaper, being therefore degreased using acetone.

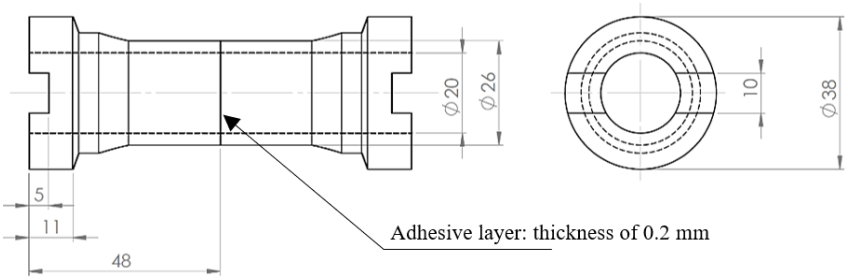

Figure 14 – Schematic representation of the torsion specimens (adapted from [60, 61]).

After applying XNR6852 E-3 adhesive on both section of the specimens, they were positioned in a jig (Figure 15). A micrometre was installed at the upper part of the jig that was temporally fixed to the upper substrate with adhesive tape. The spindle of the micrometre met the lower part of the jig so that proper thickness of the gap between the substrates could be obtained.

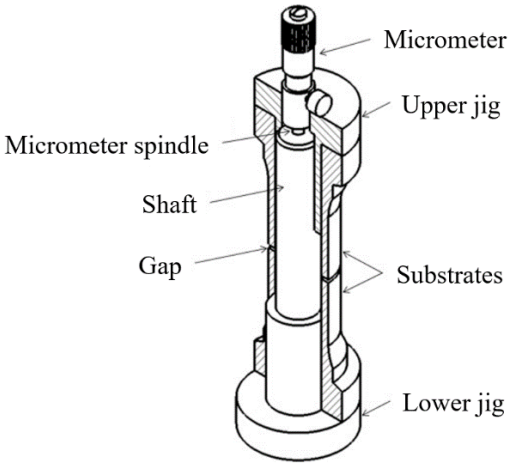

Figure 15 – Schematic representation of the torsion jig used to control the adhesive thickness (cut model) (adapted from [62]).

The mechanism enabled the control of the adhesive layer thickness at an objective value of 0.2 mm, to match the adhesive thickness values used for all the manufactured specimens employed to characterize XNR6852 E-3 adhesive. The jig was then placed inside a chamber with the temperature suitable to cure the adhesive (165 °C for 4 hours).

Both the substrates and the jig of the torsion specimens were made of S45C steel, aiming to avoid any differences of bonding space between the substrates during the curing process. Spew fillets around the specimens were removed with an ultrasonic knife to control the stress concentration.

3.2. CFRP

Unidirectional (0° lay-ups) laminates of CFRP were used to manufacture the DCB and ENF specimens, as well as the required substrates for SLJs and hygrothermal aging specimens.

3.2.1. CFRP plates

The CFRP plates were produced by hand lay-up and then cured in a hot plate press. Each plate, 300x300 mm in size, was fabricated by stacking of 0° plies, allowing it to exhibit excellent properties in the fibre direction. Each ply of carbon/epoxy pre-preg (SEAL® Texipreg HS 160 RM) had 0.15 mm of thickness. For each experiment different plate thicknesses were manufactured.

The manufacturing process of CFRP plates is descried in the following steps:

1) The carbon/epoxy pre-preg roll was removed from the freezer and left until it reached ambient temperature;

2) The pre-preg roll was cut into 300 mm squares using a blade (Figure 16);

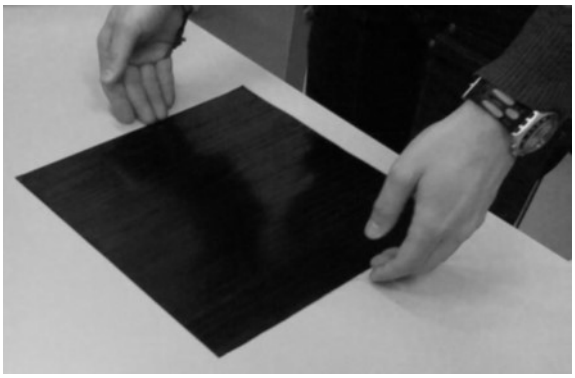

Figure 16 – Squares of pre-preg CFRP.

3) Two different plies were disposed side by side (Figure 17a);

4) Both plies were uniformly heated, promoting an easier adhesion (Figure 17a);

5) The laminates were stacked by hand lay-up, maintaining the 0° orientation between plies. A small hand tool was used to apply some pressure on the stacked plies and remove any air bubbles (Figure 17b);

Figure 17 – (a) Heating the plies and (b) applying pressure.

6) The metal mould was sanded and cleaned with acetone to remove any contaminant;

7) Three layers of mould release agent were applied, with the aim of preventing the CFRP plate from sticking to the mould;

8) Calibrated metal tape was used to regulate the mould height and therefore the final plate thickness;

9) The plates were then cured in a hot press according to the cure cycle (135 °C for 1.5 hours);

10) After the cure cycle was completed, the plates were cut according to specimens' geometry. The machine used was a diamond disc cutting was the model DV 25 Batisti Meccanica.

3.2.2. DCB

The geometry of the CFRP DCB specimens was based on the ISO 15024 [63] standard from 2001, which is used to determine, in mode I, the interlaminar fracture toughness, G_{IC}, for unidirectional reinforced fibre-reinforced plastic composites.

Each DCB specimen was manufactured by stacking twenty layers of CFRP, each one being 0.15 mm thick. Following the indications from the standard ISO 15024 [63] the dimensions (Figure 18) of each DCB specimen were the following: length of 125 mm, width of 25 mm and thickness of 3 mm. A pre-crack (a_0) of 45 mm was introduced, using a layer of Teflon® with a thickness of 0.03 mm (as it was the thinnest material available) while manufacturing the CFRP plate. During the curing process (135 °C for 1.5 hours) the Teflon layer did not change its properties with the temperature. This layer of Teflon was introduced with the aim of inducing stable crack-propagation, and its thickness was a very important parameter as it cannot be close to the thickness of each CFRP layer, to avoid interference with the type failure and therefore originate an intralaminar failure mode with different values in terms of fracture energy.

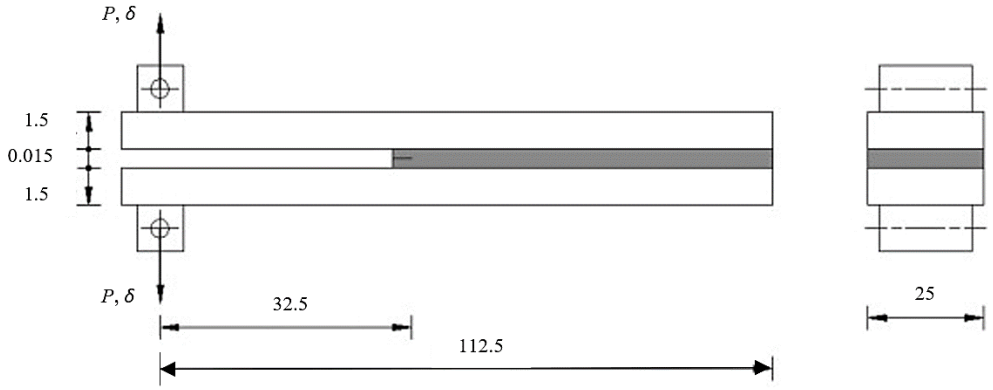

Figure 18 – Schematic representation of the geometry of CFRP DCB specimen (dimensions in mm).

The ISO 15024 standard [63] also indicates that the crack-opening mode due to a load applied perpendicularly to the plane of delamination using the DCB specimen can be achieved with the use of hinges or load blocks. In this work it was decided to use load blocks, which were bonded to the carbon plates using Araldite® 420 A/B adhesive. The bonded blocks were left to cure at room temperature for a week and under several weights to obtain the lowest adhesive thickness, with the objective of obtaining the highest bonding resistance and ensuring correct alignment between both blocks and the specimen (Figure 19).

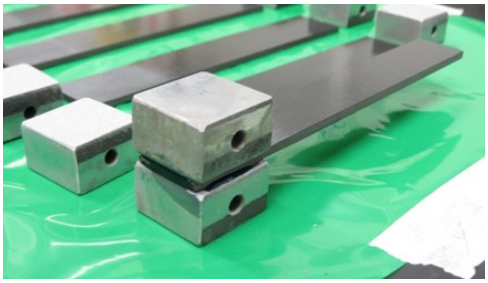

Figure 19 – DCB CFRP specimen with steel blocks.

With the aim to correctly measure the crack propagation, the side of the specimen was painted using a white spray paint. All specimens were pre-cracked (opened until it was possible to hear the fibre separation) and the correspondent value of crack length (a_0) was been obtained and registered, and the Teflon® layer has been removed before the specimens being unloaded. The specimens were thereafter ready to be tested.

3.2.3. ENF

The geometry of the CFRP ENF specimens is presented in Figure 20. It is important to refer that no standard was directly followed for this test and that the validation of the dimensions was executed through FEM simulations based on the work of de Moura *et al.* [64]. The manufacturing process was the same as indicated in previous section.

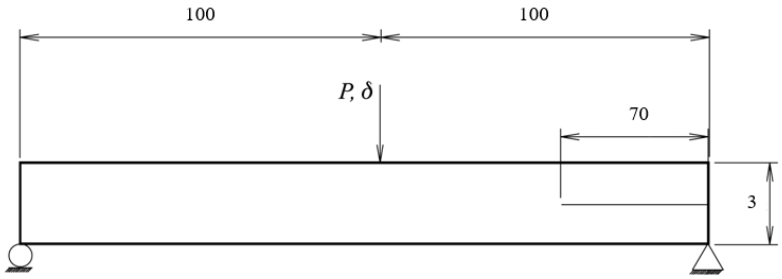

Figure 20 – Schematic representation of the effective dimensions of ENF CFRP specimen (mm).

The validation of dimensions of the ENF CFRP were performed using the Abaqus® (explicit) finite element. The simulation results were obtained using a triangular cohesive law based on the mechanical and cohesive properties of the CFRP (Table 4), based on the mechanical properties determined in the work of Campilho [65] using the same material.

Table 4 – Mechanical properties of CFRP (both material and cohesive – which were used in the software Abaqus®).

Properties	***Value***
CFRP Material	
E1	109340
E2	8819
E3	8819
Nu12	0.342
Nu13	0.342
Nu23	0.38
G12	4315
G13	4315
G23	3200
CFRP Cohesive	
Nominal stress (normal)	21.63
Nominal stress (first direction)	17.9
Nominal stress (second direction)	17.9
Normal mode fracture energy	0.3
Shear mode fracture energy (first direction)	0.9
Shear mode fracture energy (second direction)	0.9

The middle section of the specimen was considered to comprehend a layer of 0.015 mm thickness with cohesive properties and elastic properties were considered for the rest of the remaining area of the specimen. In this model, the mesh has been refined in the sections corresponding to the supports and loading regions (Figure 21).

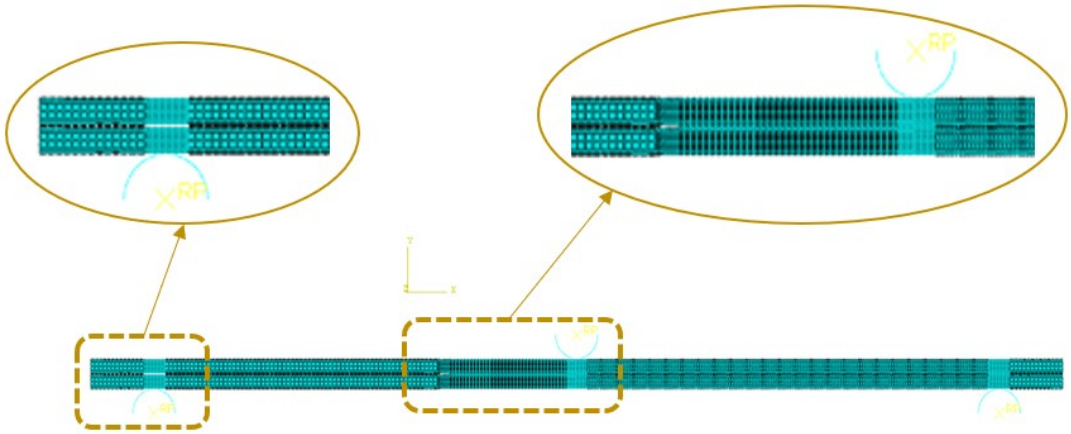

Figure 21 – Mesh section of the model of ENF specimen made of CFRP.

The analysis performed considered the von Mises stresses due to the normal and shear tension being applied to the specimen (Figure 22). With the type of analysis, it was possible to observe if the specimen dimensions allow the crack to propagate and if the thickness is enough to tolerate bending without delaminating or breaking, allowing to avoid extreme displacements.

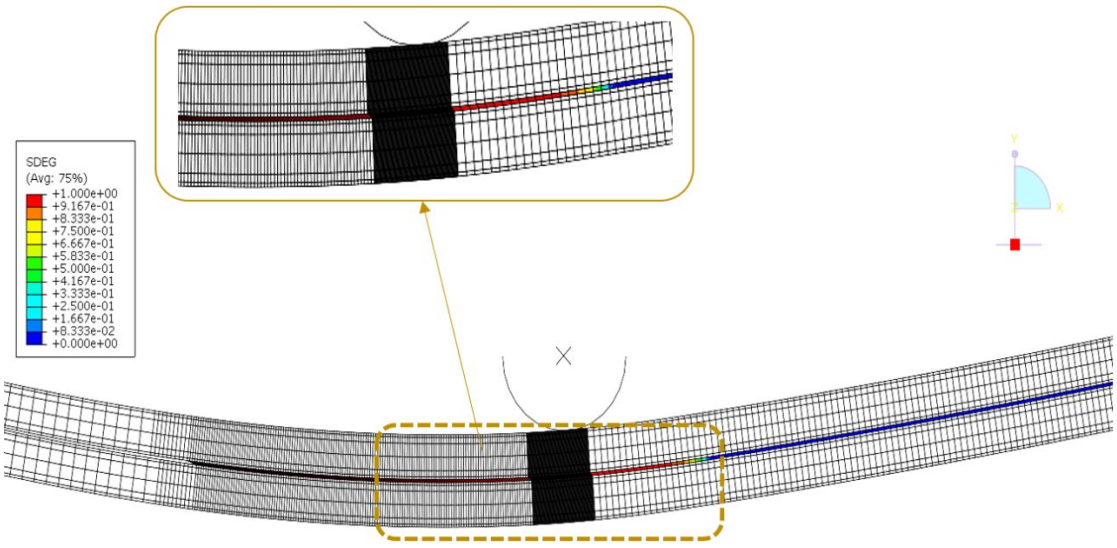

Figure 22 – Finite element analysis of SDEG of the ENF specimen made of CFRP.

Each ENF specimen was made by stacking twenty layers of CFRP having each one 0.15 mm of thickness. The width of the specimen was 25 mm.

Each ENF specimen was made by stacking twenty layers of CFRP having each one 0.15 mm of thickness. The width of the specimen was 25 mm.

A pre-crack of a_0 = 85 mm was introduced, using a layer of Teflon® with thickness of 0.075 mm with the aim to induce stable crack-propagation.

To enable direct measurement of the crack propagation, the sides of the specimen were painted using a white spray paint.

3.3. Glass transition temperature (*Tg*)

The bulk T_g specimens have the following dimensions: 10x25x2 mm, with a hole with Ø=3.5 mm in the centre of each specimen. A schematic representation of the T_g specimens for both XNR6852 E-3 and CFRP materials is represented in Figure 23.

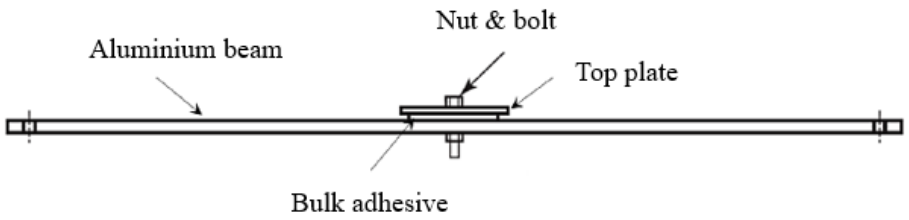

Figure 23 – Schematic representation of the specimen for T_g measurement.

For XNR6852 E-3 adhesive, the bulk specimen was machined from a bulk plate (as described in **Section 3.2.1.**). For the case of CFRP, only the resin component was used to produce T_g specimens, as the presence of fibres was not providing valid results (due to the damping properties of the fibres). To obtain only the resin of the CFRP, during the curing process of the plates, the excess of resin which came out of the mould, when manufacturing the CFRP plates, was collected and machined in the shape of the required specimen.

3.4. Single lap joints (SLJs)

The SLJs specimens followed the standards ASTM D1002-99 [66] and ISO 4587:1995 [67] standards. The geometry of the manufactured SLJs is show in Figure 24. Holes with 6 mm diameter were drilled, located near the end of each substrate, to allow a

correct alignment of the specimens when mounted in the testing tools, as well to improve joint resistance by avoiding its slippage during testing. One hole was drilled for quasi-static tests and two for impact tests.

Several distinct types of SLJs were manufactured, considering similar and dissimilar combinations of substrates and using different overlap lengths (12.5, 25 and 50 mm).

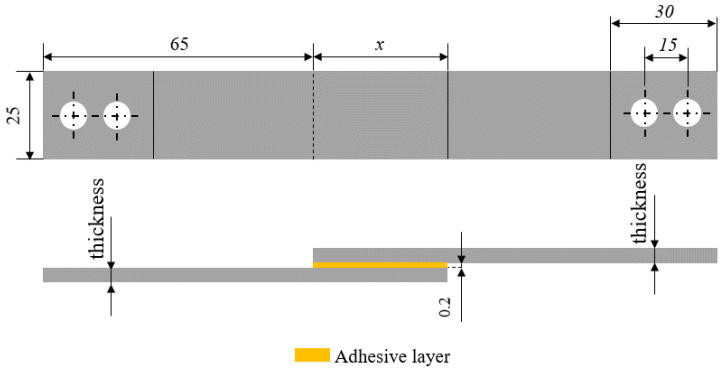

x corresponds to the different SLJs overlap length used: 12.5, 25 and 50 mm.

Thickness of each substrate varying accordingly to its type: CFRP – 2.1 mm; Al 5754-H22 – 1.5 mm and Al 6060-T6 – 2.0 mm.

Figure 24 – Schematic representation of SLJs geometry (dimensions in mm).

As mentioned in **Section 2.3.**, substrates of three different materials were used to manufacture SLJs: CFRP (thickness of 2.1 mm), Al 5754-H22 (thickness of 1.5 mm) and Al 6060-T6 (thickness of 2.0 mm).

This type of specimens was manufactured and tested through all this work since it allows to perform a more complex analysis of the adhesive and substrates behaviour, and to compare the results when subjecting the specimens to the variation of strain rate, temperature, aging and fatigue conditions.

A steel mould was used to manufacture the SLJs (Figure 25). The mould ensures that the substrates' alignment is correct, restricts their movement, controls the overlap length and defines the adhesive thickness, due to its specially designed alignment pins, shims and positioner blocks.

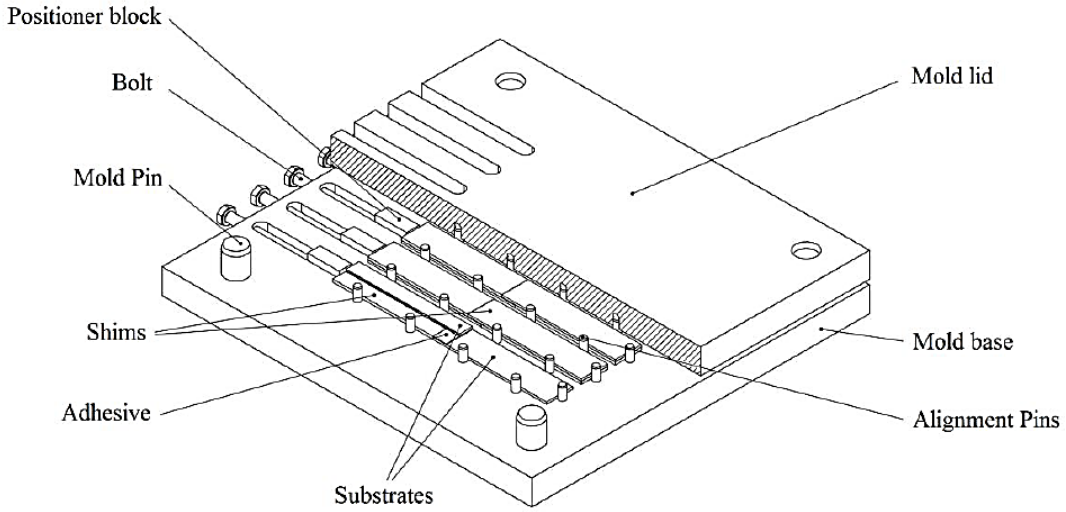

Figure 25 – Schematic representation the mould used to manufacture the SLJs.

First the mould was cleaned with acetone and all the remaining particles of adhesive were removed using sandpaper, and three layers of mould release agent were applied on the surface. Spacers and thin metal stripes were used to ensure the correct position and adhesive thickness.

Several surface treatments can be performed to ensure or improve the correct adhesion. For the case of CFRP substrates, the bonding area was sanded using two types of sandpaper (with two different grit sizes); initially with a rougher grit, followed by a passage with a less aggressive grit to obtain a more uniform surface topography.

A comparison between the initial state and the state after sanding is presented in Figure 26. The experimental results revealed that the best results were obtained when sanding the surface of CFRP, therefore this process was included in the SLJs preparation. It was also stated (by testing SLJs and observing the failure surface – recurring to Scanning Electron Microscope (SEM)) that cleaning the CFRP surface with acetone did not cause any detectable changes in its surface state or its chemical composition.

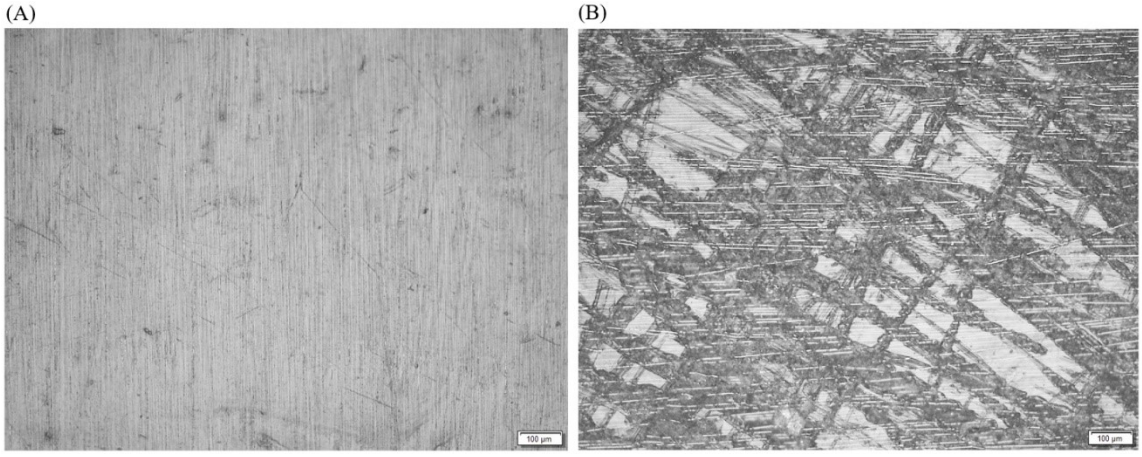

Figure 26 – Image of the surface of CFRP substrates: (A) obtained from manufacturing process, and (B) after being sanded (magnification of 100 µm).

The CFRP substrates were sanded (at 45° in two directions to avoid the presence of a preferable pattern) before being degreased with acetone to remove any surface contaminate and to ensure adhesion. The aluminium substrates were cleaned with isopropanol, followed of an hour on a stove at 190º C and then cleaned again with isopropanol to ensure that all the grease was removed (Vickers hardness tests were performed during all stages and consistent results were registered, ensuring that the materials strength was not affected by this procedure).

After the mould preparation, the adhesive was spread in abundance to guarantee that air bubbles are expelled with the adhesive flow out. Before application, the adhesive undergoes 3 minutes at 2000 rpm in a high-speed centrifugal mixing machine to increase its temperature (making it more fluid). Once the adhesive was applied, the substrates were joined, and the mould was closed. It was then placed in the hot plate press and heated following the adhesive cure cycle stated above.

As soon as the cure cycle was completed (165 °C for 4 hours), the mould was removed from the hot press and the excess adhesive on the sides of the SLJ was removed. Holes were drilled on each end of the specimens (as shown in Figure 24), to allow the assembly of the specimen on the machine holding device. For the quasi-static tests, steel square tabs were added to the SLJs, having only one hole drilled. For the impact tests two holes were drilled in each substrate, two tabs were added on each end of the specimens: on side used 1 mm thick steel tabs and the other side used 3 mm tabs aluminium tabs.

These tabs are used to enhance the grip during testing, avoiding slippage of the specimen in the clamps during testing. Additionally, they also reinforce the clamped area and prevent hole failure during impact testing. In both cases, Araldite® 420 A/B was used to join the tabs to the specimens, let to cure for one week at room temperature.

3.5. Mixed adhesive single lap joints (SLJs)

The mixed adhesive SLJs were manufactured with a single overlap length of 25 mm. The overall dimensions of the joints and general geometry is identical to that previously described (**Section 3.4.**). Only CFRP substrates were used to manufacture this type of SLJs. Each mixed SLJ used two adhesives, one stiffer in the centre and another more flexible at the end of the overlap length, providing an adhesive thickness of 0.2 mm (Figure 27).

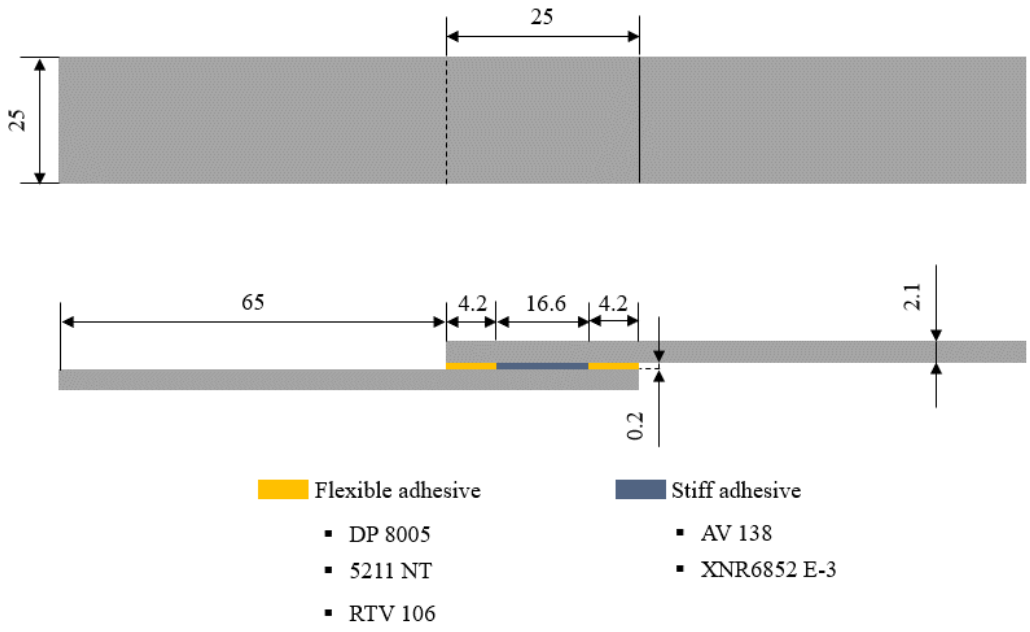

Figure 27 – Schematic representation of mixed adhesive SLJs geometry – stiff adhesive in the centre and a more flexible at the end of the overlap length (dimensions in mm).

The five different adhesives (described in **Section 2.2.**) were used in ten different configurations listed below:

- RTV 106 (full overlap);
- AV 138 (full overlap);
- SikaFast 5211 NT (full overlap);
- DP 8005 (full overlap);
- XNR6852 E-3 (full overlap);
- RTV 106 (edges) + XNR6852 E-3 (centre);
- RTV 106 (edges) + AV 138 (centre);
- SikaFast 5211 NT (edges) + XNR6852 E-3 (centre);
- SikaFast 5211 NT (edges) + AV 138 (centre);
- DP 8005 (edges) + AV 138 (centre).

The adhesive ratio (Figure 27) was selected as it has been previously studied [68] with good results in a similar using metallic substrates. Also, some other ratios were studied without better results being achieved.

The manufacturing process was to the one explained for the SLJs (**Section 3.4.**). The only difference in the process of manufacturing SLJ using mixed adhesives is the use of a nylon wire bonded to the substrates which serves to physically separate the overlap length in three different areas (Figure 28). It was observed that this method was the least invasive and with less influence on the joint mechanical properties.

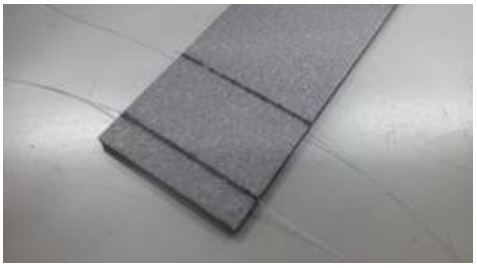

Figure 28 – Example of nylon wire setup used to separate the adhesives in the overlap length of the mixed adhesive SLJs (the nylon wire was bonded to the substrate surface with a small amount of cyanoacrylate adhesive).

The CFRP substrates preparation sequence is the following:

- It was first necessary to abrade with sandpaper the section where the adhesive was to be applied;
- After that, all the pieces were marked in the sanded face by a permanent pen in order to create a visual mark where to glue the nylon wire;
- The fishing wire was glued to the adherends mark with the help of a cyanoacrylate glue, applied directly over the nylon wire.

After the completion of these steps, the CFRP pieces were ready to be assembled in the mould (Figure 29).

Figure 29 – Example of the application of a flexible adhesive in a mixed adhesive SLJ (application of the flexible adhesive RTV 106 at the end of the overlap length – colour red).

3.6. Hygrothermal aging

3.6.1. CFRP plates

CFRP plates with a thickness of 2.1 mm (a total of 14 prepreg plies) were used for the SLJs substrates and 1 mm thick plates (a total of 7 plies) were produced to suit the specimens used in the assessment of hygrothermal aging (dimensions of 60x60 mm, based on ISO/DIS 294-3 [69]). This material was cured following a one-hour and half stage at 130 °C. After curing, the laminates were cut into the final dimensions using a diamond bladed rotary cutter.

The exposed surfaces of the hygrothermal aging specimens were lightly sanded manually using 90-grit sandpaper. This was performed with the objective of removing any silicone film or release agent that might have been picked up from the surface of the mould used, as well as improving the surface roughness. This surface treatment also allows for better water absorption rate through the removal of the glossy resin on the surface of the hygrothermal aging specimens.

3.6.2. XNR6852 E-3 adhesive bulk plates

Bulk plates of XNR6852 E-3 adhesive were manufactured for the assessment of the hygrothermal aging and drying processes, as well as determining the influence of those processes in the mechanical properties of the material. Following the French NF T 76-142 standard [57]. XNR6852 E-3 adhesive plates with a thickness of 1 mm were manufactured in a steel mould lined with a silicone rubber frame in a hot plate press. The curing process was performed under pressure at a temperature of 165 ºC for 4 hours. A hydrostatic pressure condition is generated on the uncured adhesive by the confinement of the silicone rubber frame, which is critical for obtaining good surface finish and avoiding internal defects in the adhesive plates.

The 1 mm thick adhesive plates (for hygrothermal aging) were then machined to the final dimensions of 60x60 mm (based on ISO/DIS 294-3 [69]) and the 2 mm thick plates (for determination of tensile properties) were machined according the “dogbone” geometry presented in Figure 10, which follows the BS 2782 standard [56]. These specimens were manufactured to be tested under quasi-static (1 mm/min) conditions.

3.6.3. Hygrothermal aging and desorption process

The determination of the moisture diffusion was performed using the bulk plate specimens of XNR6852 E-3 adhesive and the CFRP. A total of six plates were considered for the absorption study for each material being studied. Using the same value of thickness (1 mm) allows to compare the absorption rate between both materials and ensures that the diffusion is one dimensional.

After being manufactured, all specimens were kept in a container with silica desiccant, to remove any moisture that might have been absorbed from the environment during their preparation. In addition, prior to the initiation of the absorption tests, the specimens were placed in an oven and dried at 50 ºC and 10% of moisture. Measurements were carried out until a constant mass was attained.

The specimens were weighed using a microbalance with 1 mg of accuracy (Kern-Toledo, Balingen, Germany). After weight stabilization, the specimens were immersed in deionized water (in a closed glass container, each specimen being positioned in the middle of the liquid medium using a nylon wire, exposing the entire surfaces) and kept at a constant temperature of 50 ± 2 °C, selected according to the standard ISO 62:2008 [70] standard, typically used to perform this type of tests and allowing comparisons to be performed [71]. The period of immersion was 2000 hours. The selected temperature is significantly lower than the T_g of the materials under study, ensuring that only physical processes ensue, and no chemical changes on both materials would occur [31, 72].

All the specimens were kept immersed in deionized water until the moisture absorption mass stabilized (designated as infinite mass (M_∞)). In the case of XNR6852 E-3 adhesive a constant value of the maximum moisture absorption was observed. In the case of the CFRP it was not possible to fully saturate this material, and the maximum water uptake considered corresponds to the last measurement.

After a time period of 2000 hours immersed in deionized water was completed, the specimens were manually dried (water removed from the surface using paper), and thereafter stored inside a glass container full of silica desiccant in the same climatic chamber at 50 ºC. The drying process was performed until no water was present in the adhesive, assessed by regular mass measurements performed as previously described for the absorption process.

3.6.4. Gravimetric analysis

All XNR6852 E-3 adhesive plate specimens had their weight regularly measured until saturation was achieved. The maximum aging period was set to 2000 hours to reduce the probability of interfacial failure of the SLJs. In the case of the CFRP plates, this aging period of 2000 hours was not enough to reach saturation. The process of weighing the

specimens started with the removal of the water of the surface with a dry cloth, the specimens being handled with gloves to prevent the contamination of the surface. Special care was taken to avoid drying the specimens during the weighing process, which has a significant impact on the absorbed moisture measurements.

The moisture uptake M_t was determined using the following equation:

$$M_t = \frac{w_t - w_0}{w_0} \times 100\% \qquad \text{Eq. (1)}$$

Where, w_t corresponds to the mass of the specimen while immersed in deionised water, and w_0 is the initial constant mass. The saturation of the mass uptake in considered to occur when the overall weight gain increases less than 1% after three consecutive measurements.

The effect of swelling was also assessed by measuring the specimens periodically (three times a day) with an outside micrometre (Mitutoyo, Mizonokuchi Japan), with the volumetric increase being determined by using Equation 2.

$$\frac{\Delta V}{V_0} = \frac{V_f - V_0}{V_0} \qquad \text{Eq. (2)}$$

Being, V_f the volume of XNR6852 E-3 adhesive or CFRP plates after aging, and V_0 the initial volume of XNR6852 E-3 adhesive or CFRP plates in the final stage of considered aging.

3.6.5. Diffusion analysis

Using the diffusion coefficient (D) it is possible to quantify the absorption behaviour of XNR6852 E-3 adhesive and the CFRP. The most common approach to model moisture sorption is the Fick´s law, which can forecast the mass of water absorbed. The simple Fickian diffusion assumes that the moisture flux is directly proportional to the concentration gradient in a material. When moisture uptake occurs, the absorbed mass of water follows a linear increase with the square root of time, thereafter, slowly decreasing until equilibrium is achieved (M_∞). In general, the moisture absorption of adhesives and

some composite materials (accordingly to the resin properties and environmental conditions, as experimentally assessed by some authors [73-75]) under hygrothermal conditions can be described by Fick´s law [76] and presented by Equation 3.

$$\frac{\partial c}{\partial t} = D\frac{\partial^2 c}{\partial x^2} \qquad \text{Eq. (3)}$$

Where, D is the coefficient of diffusion, c is the concentration of water and t is time of the process. Crank [77] suggests a simplification of Equation 1, stating that for the initial stage of the process, where $\frac{M_t}{M_\infty} < 6$, the resulting relationship can be applied as follows:

$$\frac{M_t}{M_\infty} = \frac{4}{\sqrt{\pi h}}\sqrt{Dt} \qquad \text{Eq. (4)}$$

For several materials, due to their chemical properties, it is necessary to consider the dual Fickian models [78], and two distinct diffusion mechanisms working simultaneous occur, where the fractional mass uptake increases continuously until M_∞ is reached. Such models are commonly designated as “parallel dual Fickian” (PDF). By assuming a pseudo-equilibrium state at intermediate exposure times prior to reaching the final saturation, Ameli et al. [79] developed the “sequential dual Fickian” (SDF) model (Equation 5), specifically for highly toughened epoxy adhesives, as in the case of XNR6852 E-3 adhesive being used in this work.

$$\begin{aligned} M_t = &\left(1 - \frac{8}{\pi^2}\sum_{n=0}^{\infty}\frac{1}{(2n+1)^2}exp\left(\frac{-D_1(2n+1)^2\pi^2 t}{4h^2}\right)\right) \times M_{1\infty} \\ &+ \emptyset(t - t_d) \\ &\times\left(1 - \frac{8}{\pi^2}\sum_{n=0}^{\infty}\frac{1}{(2n+1)^2}exp\left(\frac{-D_2(2n+1)^2\pi^2 t}{4h^2}\right)\right) \times M_{2\infty} \end{aligned} \qquad \text{Eq. (5)}$$

Being $M_{1\infty}$ and $M_{2\infty}$ the first and second uptakes, and $M_{1\infty} + M_{2\infty} = M_\infty$.

Rearranging both Equation 4 and Equation 5, the relationship for D is given by:

$$D = \pi\left(\frac{h}{4M_\infty}\right)^2\left(\frac{M_t}{\sqrt{t}}\right)^2 \qquad \text{Eq. (6)}$$

3.7. Automotive joint ("roof frame header") from Aston Martin Lagonda®

The automotive joint provided by the automotive company Aston Martin Lagonda® consisted on a "roof frame header" from the model DB11 (in a pre-production stage).

The "roof frame header" was manufactured using the aluminium alloy 6016-T6 and it consists in a cross frame connection which supports the roof and the windshield of the car (as previously shown in Figure 5), being composed of two distinct parts, namely, an upper and a lower substrate, bonded together by two parallel layers of a structural adhesive, as indicated in Figure 30. Such structural component is of great importance as it should guarantee the passengers safety in the event of an impact or in a situation of rollover of the automotive. This component under impact should deform, absorbing the impact energy but keeping the integrity of the structure. The general dimensions of the automotive section are presented in Figure 30, and it is important to mention that the thickness of the upper and lower substrates are correspondently of 1.7 and 1.2 mm.

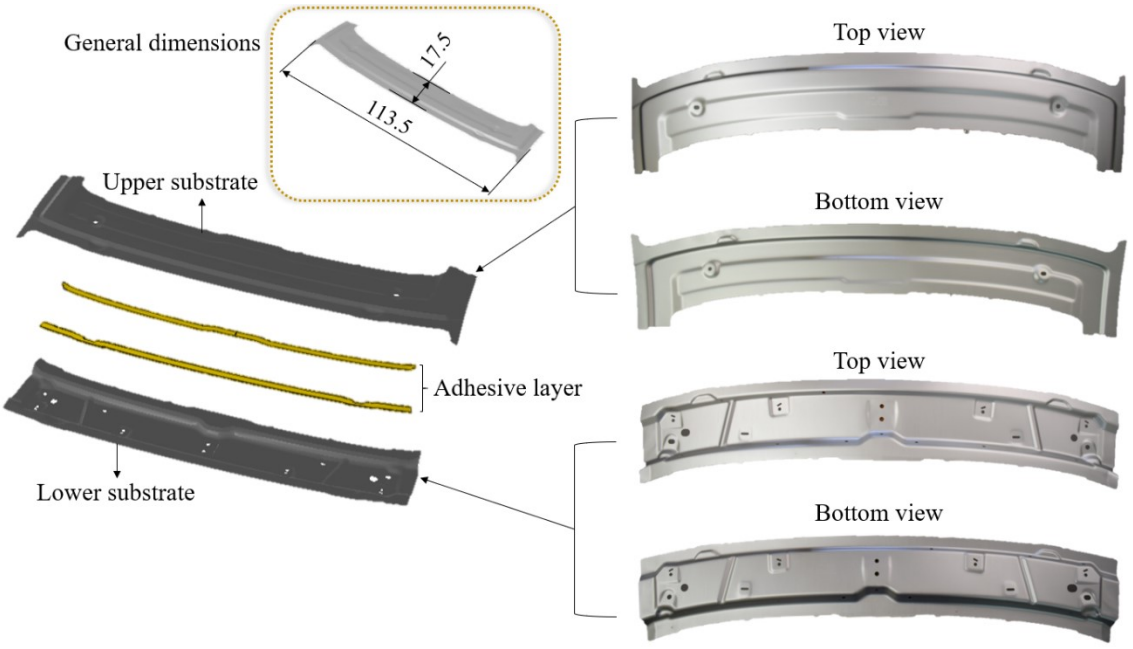

Figure 30 – Automotive section ("roof frame header" – composed by two parts, a lower and a upper) experimentally studied under quasi-static (1 mm/min) and impact (3 m/s) conditions – Aston Martin DB11 (provided by Aston Martin Lagonda®), with general dimensions in cm, (thickness of the upper substrate: 1.7 mm and thickness of the lower substrate: 1.2 mm).

The XNR6852 E-3 adhesive was used to bond the two substrates, with a layer thickness of 1.6 mm and an average layer width of 17 mm (as specified by Aston Martin Lagonda® in their design). To ensure that is values are obtained in practice, an initial assessment of the nozzle diameter of the adhesive applicator was executed to assess the required spread of the adhesive after pressure is applied to the adhesive bead. An adhesive bead was positioned between two acrylic plates, two spacers were used to set the desired layer thickness (1.6 mm) and by applying controlled pressure with an universal testing machine it was possible to assess that by using a nozzle with the diameter of 6 mm, the adhesive layer met the required width (17 mm) (Figure 31). Using this bead configuration, 70 g of XNR6852 E-3 adhesive were used on average to produce the two adhesive bondlines.

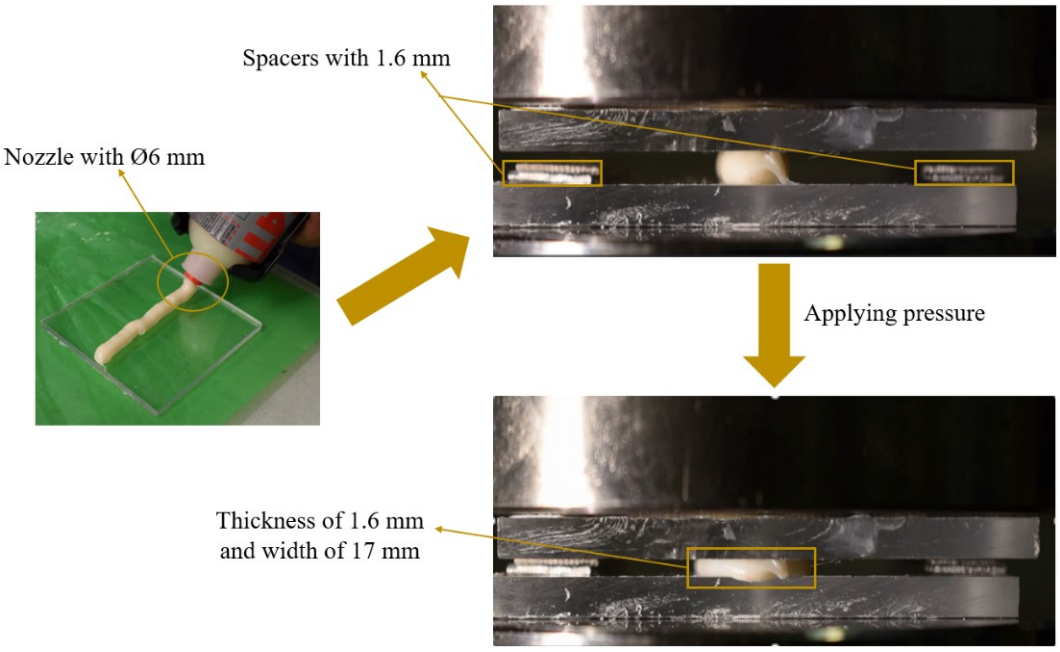

Figure 31 – Sequence of the test performed to analyse the correct application of the adhesive layer to apply in the "roof frame header" (thickness of 1.6 mm and width of 17 mm), using polycarbonate substrates.

The substrates are supplied in an already anodized state. The first step of the manufacturing process was to clean both parts using isopropanol alcohol, to remove any contaminant at the surface. Figure 32 represents the manufacturing sequence designed to obtain the "roof frame header" joints.

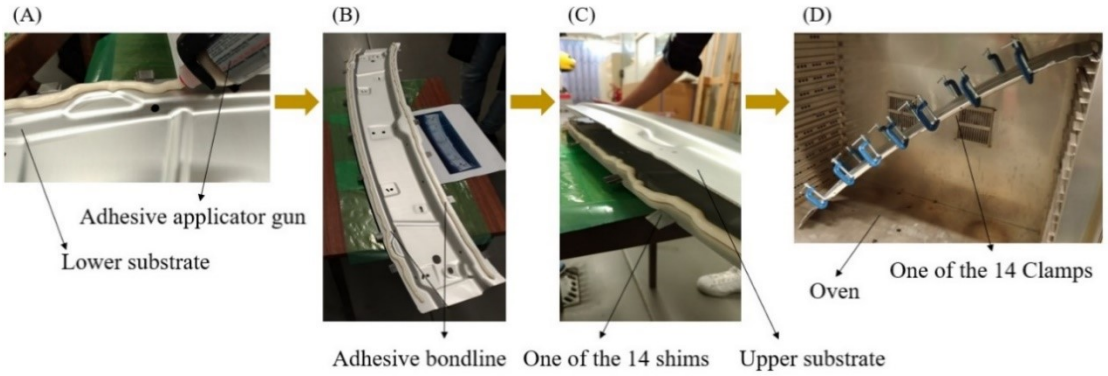

Figure 32 – Representation of the manufacturing sequence of the "roof frame header" joints: (A) adhesive applicator gun starting the application of the adhesive; (B) adhesive beads applied to the lower substrate; (C) introduction of 14 spacers with the thickness of the adhesive layer with assembly of the upper substrate; and (D) positioning of 14 clamps (on top of each spacer) followed by the introduction of the joint in a oven to be subjected to the cure cycle.

A total of 14 shims were positioned along the lower substrate (seven in each side), to ensure the adhesive layer thickness, positioned in the "brims" present on both substrates edges (Figure 33). The application of XNR682 E-3 adhesive beads was performed on the lower substrate using an adhesive applicator gun along two distinct and parallel bondlines; thereafter, the upper substrate was carefully positioned on top of the lower substrate, ensuring perfect alignment between the outer edges of both substrates.

As some of the provided substrates presented a slight bending distortion (assumed to have occurred due during the stamping process), therefore, to ensure the correct alignment of both the upper and lower substrates, a total of 14 clamps were positioned along the overlap length and adjusted accordingly (Figure 33). These clamps also ensure that an accurate adhesive layer thickness is reached and restrain the substrates movement during the cure process.

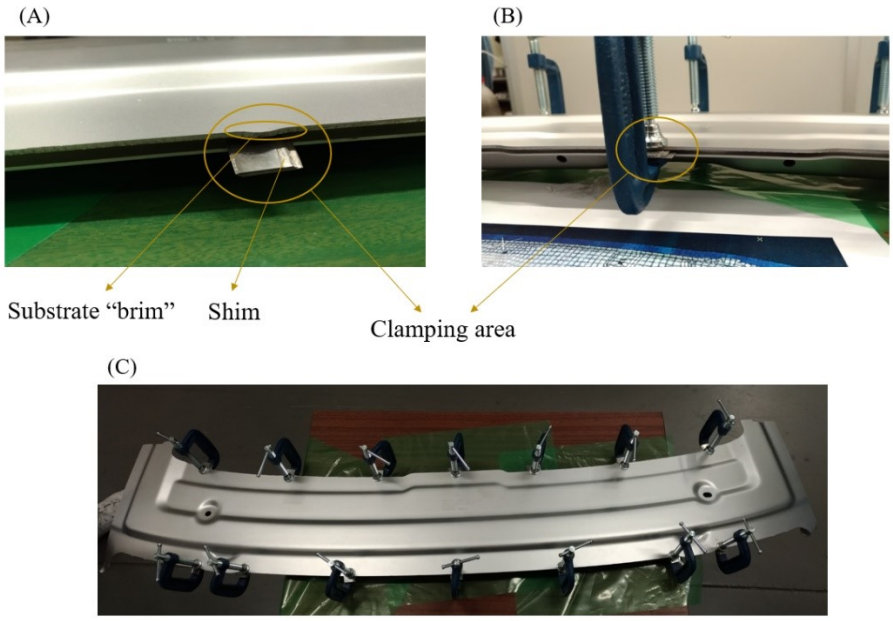

Figure 33 – Manufacturing details of the "roof frame header": (A) example location of a "brim" of the substrates, and positioning of a shim, (B) application of pressure on the shim area using a metallic clamp, and (C) finalization of the assembly with all the shims and metallic clamps to hold the two parts together.

The final step consisted on clamping both substrates by positioning clamps on the areas where the shims were previously positioned, to allow a homogenous application of pressure long the overlap area. The specimens were kept in an oven at the curing temperature, and to finalize the manufacture of the joints, excess adhesive was trimmed from the edges.

4. Test methods

As previously stated, experimental testing is a task of great importance during research in the field of adhesive joints as, when performed correctly, enables to determine and compare adhesive and joint performance, validate numerical models and identify areas for improvement. This section describes thoroughly the experimental procedures performed to test both XNR6852 E-3 adhesive, CFRP substrates, SLJs and real automotive joint under quasi-static (1 mm/min) and impact (3 m/s) conditions (and as a function of temperature when possible).

These experimental tests can be divided into four main sets:

- Determination of the tensile and shear properties of XNR6852 E-3 adhesive in bulk;
- Evaluation of the fracture energy properties of CFRP;
- Assessment of the strength of complete joints (single and mixed adhesive combination, as well similar and dissimilar substrates) under quasi-static (1 mm/min) and impact (3 m/s) conditions as a function of temperature;
- Testing under quasi-static (1 mm/min) and impact (3 m/s) at the room temperature of the real automotive joint provided by Aston-Martin Lagonda® ("roof frame header").

A comprehensive mechanical characterization of XNR6852 E-3 adhesive (**Paper 2**), as a function of strain rate and temperature was made by performing: T_g, bulk tests, DCB, and torsion tests.

In the case of CFRP substrates, T_g and fracture energy as a function of strain rate and testing temperature tests were performed, namely, DCB (**Paper 3 and Paper 5**) and ENF (**Paper 4**).

The SLJs manufactured were used for the evaluation of the maximum strength, deformation and energy absorbed, considering both the effect of substrates and adhesives, allowing comparative studies between joints with different designs and materials.

These tests can be divided in:

- SLJs manufactured with CFRP substrates (**Paper 6** and **Paper 7**);

- SLJs manufactured with similar and dissimilar substrates (CFRP, Al 5754-H22 and Al 6060-T6) combinations (**Paper 8**);
- SLJs manufactured using mixed adhesives combination (**Paper 9** and **Paper 10**);
- Influence of aging and drying after aging on the quasi-static (1 mm/min), impact (3 m/s) and fatigue behaviour of SLJs (**Paper 15**, **Paper 16** and **Paper 17**);
- Automotive joint ("roof frame header") (**Paper 18** and **Paper 19**) tested under quasi-static (1 mm/min) and impact (3 m/s) conditions at room temperature.

The strength of adhesive joints was predicted using cohesive damage models (triangular law), and in order to create these models it is important to measure the fracture properties of XNR6852 E-3 adhesive, namely the tensile strength, Young´s modulus and fracture toughness in mode I and II.

4.1. Glass transition temperature (T_g)

The T_g of an adhesive is an extremely important parameter to understand its behaviour when subjected to large temperature gradients. This property allows to determine if the adhesive is going to have a brittle or flexible behaviour at a given temperature and therefore, if it's prone to failure or flexible enough to handle any deformation.

The apparatus used is an in-house development equipment which is based on the work by Zhang *et al*. [80] and allows the determination of the T_g by measuring changes in the damping properties of the adhesive. When reaching the T_g there is a significant increase in the damping of the material. The apparatus works by keeping a beam containing an adhesive sample vibrating at the resonance frequency and gradually varying the temperature. When the T_g is reached, the damping of the adhesive sample rises significantly, and the amplitude of the beam's vibration is almost reduced to zero (this test takes less than 10 minutes, therefore avoiding post cure of the adhesive). Figure 34 shows the main components of this device.

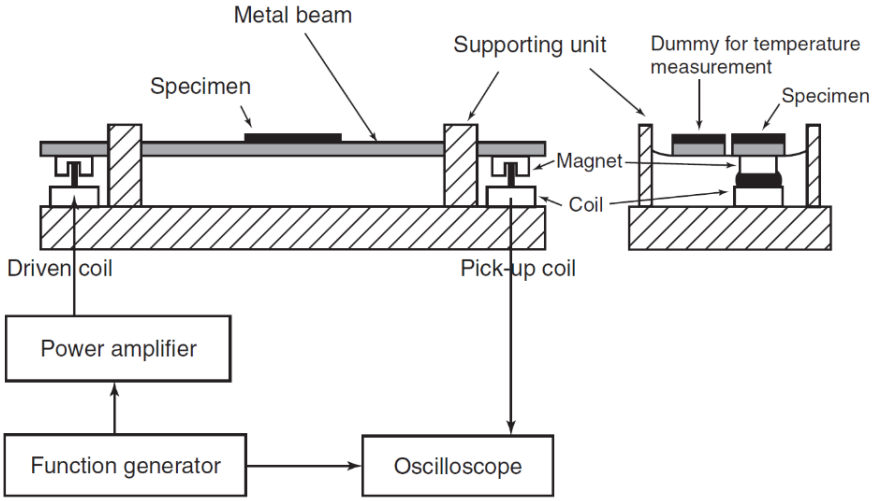

Figure 34 – Schematic representation of the T_g measurement apparatus.

4.2. Definition of strain rate

From each testing machine it is possible to select different values of testing velocity, by controlling the cross-head displacement for the cases of tests performed under quasi-static conditions (which have mm/min as units), and in terms of initial impact velocity for tests performed under high strain rates (units in m/s). The analysis being performed is regarded the influence of strain rate and temperature int terms of mechanical properties of materials (adhesive and substrates) and SLJs, so, therefore it is required to proceed to the conversion (which has s^{-1} as units).

The concept of strain rate [81] is characterized as being the change in strain (deformation) of a specific material with respect to time. The equation which can be used to determine the strain rate is the following:

$$\dot{\varepsilon}(t) = \left(\frac{L(t) - L_0}{L_0}\right) = \frac{v(t)}{L_0} \qquad \text{Eq. (7)}$$

Where, L_0 is the original length, L(t) corresponds to the length at each time t, and v(t) corresponds to the speed at which the ends are moving away from each other. For each paper presented, an analysis in terms of strain rate will be always presented.

The determination of the strain rate is a complex subject, especially when considering adhesives and CFRP. It was possible to observe that for each type of test being performed,

there is a significant difference of the effective strain rate being achieved, which requires several different testing velocities to equally match the mechanical behaviour of a joint under a specific strain rate.

For every test description, the value of strain rate achieved for each condition will be indicated.

4.3. Quasi-static tests

The quasi-static tests were performed at 1 and 100 mm/min (for some types of tests, which will be mentioned along this section) of crosshead displacement, allowing to obtain distinct strain rates due to the type of test being performed.

All the quasi-static tests were performed using a universal testing machine, of the type Instron® 3367 (Norwood, Massachusetts, USA) with a load cell capacity of 30 kN.

For room temperature tests (24 °C), air conditioning in the testing room was used to stabilize the temperature. In tests performed under low temperature (-30 °C) and high temperature (80 °C), a heated climatic chamber was integrated in the testing machine. In the case of low temperature, the same chamber was used, with nitrogen being injected in a controlled manner to achieve the lower temperature. With the use of a thermocouple positioned in contact with each specimen the temperature was measured, to ensure a homogeneous temperature distribution. Each test was only performed after a stage of 10 minutes at the intended temperature. While the tests were being performed the specimens remained enclosed in the chamber under a constant temperature. Prior to the start of tests, the climatic chamber was kept at the desired testing temperature for 45 minutes, in order to ensure a homogenous temperature inside the chamber and on the testing tools.

To obtain the average representative values of the mechanical properties being assessed, a total of six specimens were tested for each type of specimen and temperature condition.

4.3.1. Tensile bulk of XNR6852 E-3 adhesive

From testing XNR6852 E-3 tensile bulk specimens, it was possible to record load and displacement values, which allowed to obtain *P-δ* curves, aiming to determine the elastic moduli, tensile strength and assess ductility.

The specimens were mounted on the machine using two wedge grips (Figure 35). This test consists on applying a load on the longitudinal direction of the specimen until failure. An optical method was used to record the displacement of the specimen, with a digital camera taking pictures of the gauge length between the two lines during the test, allowing to record all the stages until failure. An image processing and analysing software was used to obtain the strain for each specimen. The width and thickness of each specimen were measured to calculate the stress of each strain stage.

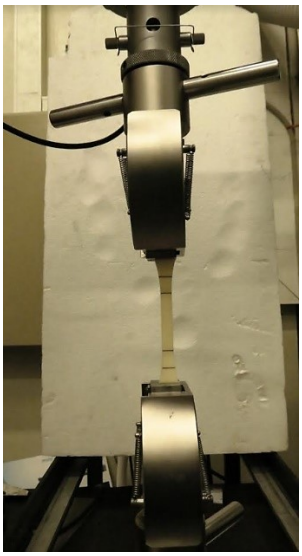

Figure 35 – Setup used for XNR6852 E-3 adhesive bulk tensile specimens under quasi-static conditions.

The properties obtained from this test were: Young's modulus, tensile strength and strain at failure (%). Young's modulus was determined considering the slope of the stress-strain curve between 0.05 % and 0.25 % strain, which is usually in the elastic behaviour of structural adhesives, and the tensile strength was obtained directly from the stress-strain curve [1].

Three distinct testing temperatures were used, namely, -30, 24 and 80 °C. Two cross-head displacements were used for quasi-static tests, respectively, 1 and 100 mm/min.

Considering the value of L_0 the distance between each grip of 120 mm, the achieved values in terms of strain rate are of 0.00014 and 0.014 s^{-1}.

4.3.2. Torsion tests of XNR6852 E-3 adhesive

A torsion equipment (consisting in a hydraulic machine) was used in Tokyo Institute of Technology to perform torsion tests of XNR6852 E-3 adhesive (Figure 36).

The hydraulic actuator has two chambers, for tensile and shear loading, being controlled by a couple of closed-loop feedback systems, containing: a load cell, displacement sensors, strain amplifiers, electric circuits, and servo valves. For quasi-static tests, a feedback control system since displacement control was possible to be obtained when considering the response time, as for high-loading rates, an open-loop control was selected due to low response of control systems. With the aim of identifying the stress increment rate, preliminary tests were performed to determine the required increments to perform with the actuator. The fact of both oil chambers in the actuator start simultaneously loading as soon as one of the loads exceeds the quasi-static friction represents one of the main advantages of the equipment design, therefore resulting on the synchronization of both tensile and torsional loading, specifically for high strain rates.

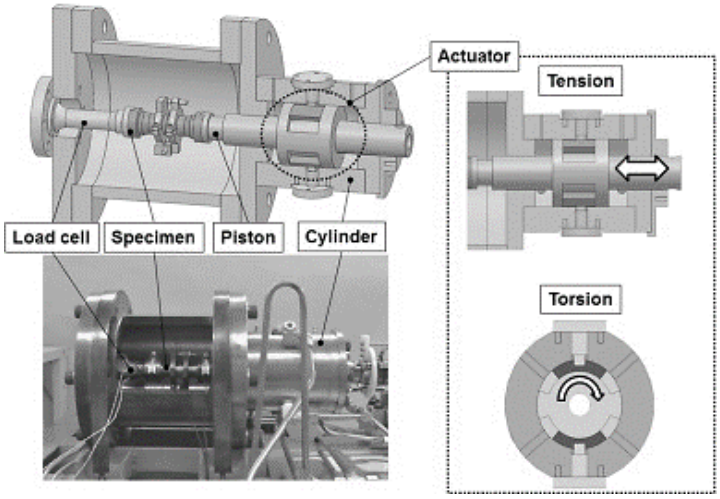

Figure 36 – Setup used to test XNR6852 E-3 adhesive under torsion (hydraulic testing machine) (adapted from [61]).

A specially designed load cell was used to measure the applied loads, allowing to assess tensile and torsion loads. The adhesive layer deformation of each specimen was

measured using a biaxial extensometer (Figure 37), containing two eddy current gap sensors positioned in the axial and circumferential directions.

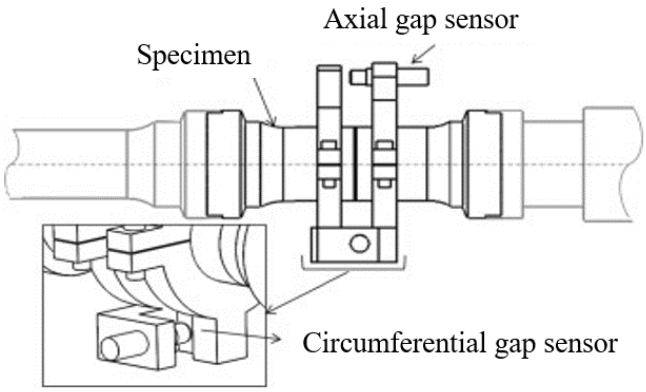

Figure 37 – Schematic representation of the setup of the biaxial extensometer (adapted from [61]).

Three distinct strain rates were selected to test XNR6852 E-3 adhesive, categorized as: low (0.0014 s^{-1}), intermediate (0.7 s^{-1}) and high (11.4 s^{-1}), with six specimens being used for each stage.

The tensile stress, σ, and shear stress, τ, within the adhesive layer can be determined by using the following equations:

$$\sigma = \frac{F}{\frac{\pi}{4}(d_o^2 - d_i^2)} \quad \text{Eq. (8)}$$

$$\tau = \frac{T}{\frac{\pi}{16}\frac{(d_o^2 - d_i^2)}{d_o}} \quad \text{Eq. (9)}$$

Being F the tensile load applied, T corresponds to the torque, d_o to the outer diameter (26 mm) and d_i to the inner diameter (20 mm) of the torsion specimen.

The tensile strain, ε, and the shear strain, γ, were determined from the measured displacements with biaxial extensometer, being calculated by using the following set of equations:

$$\varepsilon = \frac{l_1}{t} \quad \text{Eq. (10)}$$

$$\gamma = \frac{l_2}{t} \quad \text{Eq. (11)}$$

Where l_1 is the axial displacement, l_2 corresponds to the circumferential displacement at the outer diameter of the torsion specimen, and t is the adhesive thickness.

4.3.3. SLJs

To better study the behaviour of the adhesive and substrates in a joint, SLJ specimens were tested. All tests were performed at a constant crosshead displacement of 1 mm/min, which corresponds to an average strain rate of 0.08 s^{-1} in the adhesive layer, since the considered value of l_0 was the adhesive thickness of 0.2 mm.

An example of the setup used to test the SLJs is shown in Figure 38. It is possible to observe that the SLJs were positioned and held vertically by using two grips (pressure being created by using four screws on each one, using the dynamometric key to set 30 Nm of torque for each screw). Metallic tabs were positioned bellow one side of each section of the SLJs to ensure horizontality of the specimens when griped. Also, two centre pins were used during the tests (on each substrate) to ensure the correct alignment of the specimens as well as to provide more grip for the tests where higher loads are attained, minimizing or avoiding sliding of the specimens.

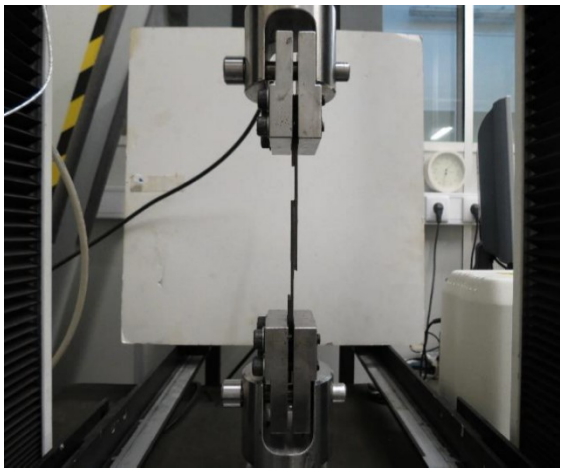

Figure 38 – Setup used to test SLJs under quasi-static conditions.

Three distinct testing temperatures were used, namely, -30, 24 and 80 °C. A total of six specimens were tested for each overlap and temperature condition, and *P-δ* curves were obtained for all SLJs tested, enabling the determination of the tensile strength. The area below the *P-δ* curves was also used to provide information regarding the energy absorbed during each test.

4.4. Fracture tests

The fracture toughness is dependent on the type of loading (mode I, mode II, mode III or mixed mode). While there are many alternative methods for its determination, the fracture toughness is usually measured under mode I by performing DCB tests and under mode II by performing ENF tests.

4.4.1. Mode I

Several methods have been developed to obtain the fracture energy value from the DCB test data. Most require the constant monitoring of the crack tip position, to correlate the crack advance with the load level. This, however, poses significant problems as it is very hard to measure the actual crack tip location and does not consider the presence of a fracture process zone (FPZ) immediately ahead of the crack tip. Additionally, if a DCB test is done inside a thermally controlled chamber, it becomes especially difficult to measure the crack progression. Therefore, a method that does not require crack length

measurement was employed in this work, the Compliance-Based Beam Method (CBBM). This method was proposed by de Moura et al. [82, 83] in 2008 and does not require information regarding the crack tip location. Instead it uses the crack equivalent concept, which is dependent only on the specimen's compliance, obtained directly from the testing data. The G_{IC} equation uses an estimated crack tip location calculated from the Castigliano beam deflection theorem, with a correction needed due to the initial crack length. By using the experimental data and the measured initial compliance of the DCB specimen, this formula considers the experimental compliance and the FPZ at the crack tip, removing any variability introduced from crack measurement procedures.

DCB tests were performed to obtain the critical strain energy release rate in mode I of XNR6852 E-3 adhesive and CFRP substrates. A vertical load is applied at the ends of the beams, forcing their separation and creating a crack that gradually progresses through the adhesive layer. If stable crack propagation exists, the P-δ curve obtained can be processed to obtain the fracture energy of the adhesive layer in mode I.

The tests were performed according to the ASTM D3433 standard [59]. The setup used to test the DCB specimens is shown on Figure 39.

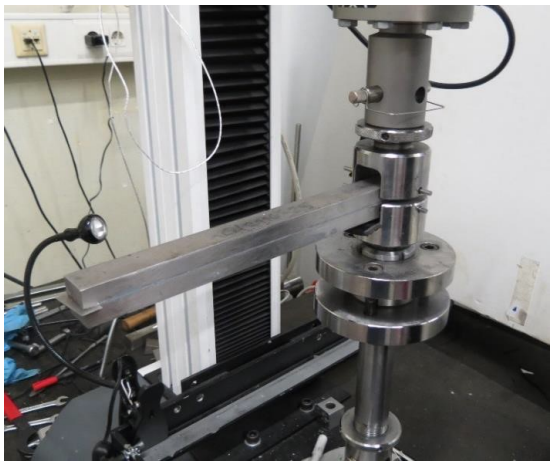

Figure 39 – Setup used to test DCBs under quasi-static conditions.

In this test, the load is applied perpendicularly to the adhesive layer (Figure 40). Three distinct testing temperatures were used for XNR6852 E-3 adhesive, namely, -30, 24 and 80 °C. Two crosshead displacements were used for quasi-static tests, respectively, 1 and 100 mm/min. For each testing temperature, three distinct cross displacements were

used, namely, 1, 10 and 100 mm/min, corresponding to strain rates of 0.08, 0.83 and 8.33 s^{-1}, respectively, since the considered value of l_0 was the adhesive thickness of 0.2 mm.

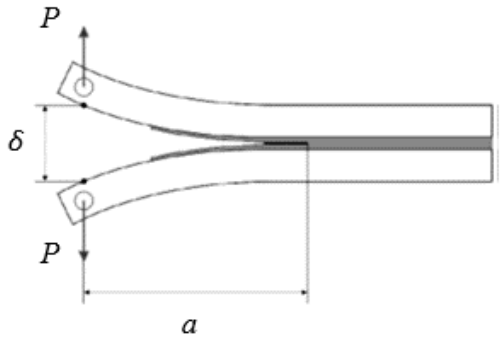

Figure 40 – Measurement of the crack length (a), being P the load and δ the displacement.

Several data reduction schemes for fracture energy determination can be considered and will be therefore presented.

The compliance calibration method (CCM) is based on Irwin-Kies equation and it also uses the load displacement data and the real crack's length [84, 85]. Equation 12 gives the failure energy derives from Irwin-Kies theory.

$$G_{Ic} = \frac{P^2}{2w}\frac{dC}{da} \qquad \text{(Eq. 12)}$$

Where G_{IC}, is the energy available for an increment of the crack propagation, P is the applied load, w is the width of the specimen, C is the compliance and, a is the crack length:

$$C = \frac{\delta}{P} \qquad \text{(Eq. 13)}$$

The partial derivative of compliance is calculated using the displacement (δ) and the applied load (P). The compliance, based on the flexibility of the substrate, is given by a polynomial function of third degree which is a function of the crack length:

$$C = C_3a^3 + C_2a^2 + C_1a + C_0 \qquad \text{(Eq. 14)}$$

The corrected beam theory (CBT), as in the previous method, requires load-displacement data and also the real crack's length, which it also derives from the Irwin-Kies theory [85]. The failure energy is given by,

$$G_{Ic} = \frac{3P\delta}{2B(a + |\Delta|)} \quad \text{(Eq. 15)}$$

The crack tip rotation and deflection were considered in this method. In order to take into account such effect, a correction factor of crack's length is used, Δ, which was proposed by Wang and Williams [86] in 1992 and is given by,

$$\Delta = t\sqrt{\frac{1}{13k}\left(\frac{E_x}{G_{xy}}\right)\left(3 - 2\left(\frac{\Gamma}{1+\Gamma}\right)^2\right)} \quad \text{(Eq. 16)}$$

Where E_x and G_{xy} correspond to the longitudinal normal and shear modulus of the substrate, t is the thickness of the substrate and k is the shear stress distribution constant for correcting the deflection caused by shear force, which is 0.85 for DCB specimens.

$$\Gamma = \frac{\sqrt{E_x E_y}}{kG_{xy}} \quad \text{(Eq. 17)}$$

And, E_y is the Young's modulus of the substrates on the thickness direction [87].

The crack's length correction factor is set by a linear regression $C=f(a)$, which can be obtained experimentally, loading the specimen with three different loads, obtaining three different cracks' lengths Figure 41) [65].

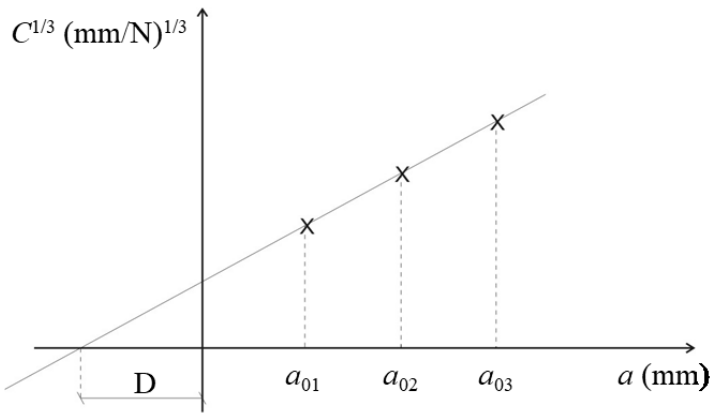

Figure 41 – Representation of linear regression of the correction crack length factor [88].

The compliance-based beam method (CBBM) is based on the beam theory, which allows to express the crack location by considering the compliance of adherends. Since this theory does not take in consideration the stress concentration and rotation of the adherends near the crack, equivalent bending modulus is used [82].

The failure energy is given by Equation 18.

$$G_{Ic} = \frac{6P^2}{B^2 h}\left(\frac{2a_e^2}{h^2 E_f} + \frac{1}{5G_{13}}\right) \quad \text{(Eq. 18)}$$

Where P is the applied load, B is the specimen's width, h is the specimen´s thickness, E_f is the equivalent bending modulus, a_e is the equivalent crack´s length, and G_{13} is the shear modulus.

Contrarily to the previous methods, as it can be seen in Equation 18, instead of the use of real crack's length, this method has its own definition of equivalent crack length (a_e). This measurement depends only of the specimen's compliance during the test. Equivalent crack's length is measured until half of the Fracture Process Zone (FPZ) (Figure 42), which is defined by the existence of multiple micro-cracks and plasticization's ahead the major crack that absorb some of the energy. For ductile adhesives, the energy dissipated in the FPZ is higher. This method is based on the beam theory of Timoshenko [82, 83, 89].

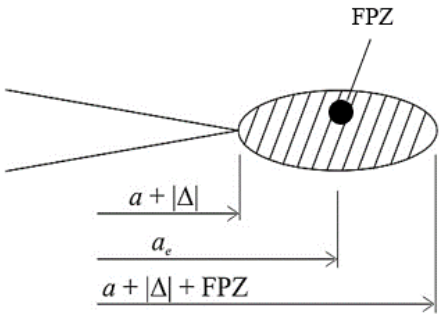

Figure 42 – Schematic representation of the FPZ and crack equivalent concept (adapted from [84]).

The energy of deformation of the adherends, due to its rotation at the tip of the crack and consideration of the shear stress, is given by:

$$U = 2\left[\int_0^a \frac{M_f^2}{2E_I I}dx + \int_0^a \int_{-\frac{h}{2}}^{\frac{h}{2}} \frac{\tau^2}{2G_{13}} B dz dx\right] \quad \text{(Eq. 19)}$$

Being M_f the bending moment, I the second moment of area of the straight section of a substrate, E_I and G_{13} are respectively the Young modulus and the shear modulus. The shear stress throughout the thickness of each substrate is given by:

$$\tau = \frac{3}{2}\frac{V}{Bh}\left(1 - \frac{z^2}{c^2}\right) \quad \text{(Eq. 20)}$$

Where c is half of each substrate thickness, V is the shear load in each substrate, comprehended between 0 and a, and z is the distance in z axis.

Using the Castigliano´s method, the displacement δ is obtained from the following equation:

$$\delta = \frac{\partial U}{\partial P} = \frac{8Pa^3}{E_1 Bh^3} + \frac{12Pa}{5BhG_{13}} \quad \text{(Eq. 21)}$$

The Equation 10 is based on the beam theory and allows to define the flexibility ($C = \delta/P$) of the substrates. However, the beam theory does not consider the concentration of stresses and the rotation of the substrates at the tip of the crack.

Applying the CBBM method it´s possible to determine G_{IC} using the Equation 22 [82, 85, 88, 90].

$$G_{IC} = \frac{6P^2}{B^2 h}\left(\frac{2a_{eq}^2}{h^2 E_f} + \frac{1}{5G_{13}}\right) \quad \text{(Eq. 22)}$$

Where a_{eq} is an equivalent crack length obtained from the experimental compliance and accounting for the fracture pressure zone (FPZ) that is a region where a progressive softening occurs [84], at the crack tip, E_f is a corrected flexural modulus to account for

all phenomena affecting the *P*-δ curve, such as a stress concentration at the crack tip and stiffness variability between specimens, and *G* is the shear modulus of the adherends [91].

One can obtain E_f by using the following equation:

$$E_f = \left(C_0 - \frac{12(a_0 + |\Delta|)}{5BhG_{13}} \right)^{-1} \frac{8(a_0 + |\Delta|)^3}{Bh^3} \quad \text{(Eq. 23)}$$

The crack equivalent concept can be determined by, which appears from solving Equation 21 in order to a:

$$a_{eq} = \frac{1}{6\alpha} A - \frac{2\beta}{A} \quad \text{(Eq. 24)}$$

Where the coefficients can be obtained by the following equation:

$$\alpha = \frac{8}{Bh^3 E_f}; \beta = \frac{12}{5BhG_{13}}; \gamma = -C \quad \text{(Eq. 25)}$$

$$A = \left(\left(1 - 108\gamma + 12\sqrt{3\frac{(4\beta^3 + 27\gamma^2\alpha)}{\alpha}} \right) \alpha^2 \right)^{1/3} \quad \text{(Eq. 26)}$$

The use of CBBM allowed to obtain the resistance curve (R-curve) of each experiment. The values were obtained from the plateau in the R-curve of each experiment, that occurred when the crack propagation stabilized. A representative R-curve of XNR6852 E-3 adhesive tested at 1 mm/min is shown in Figure 43.

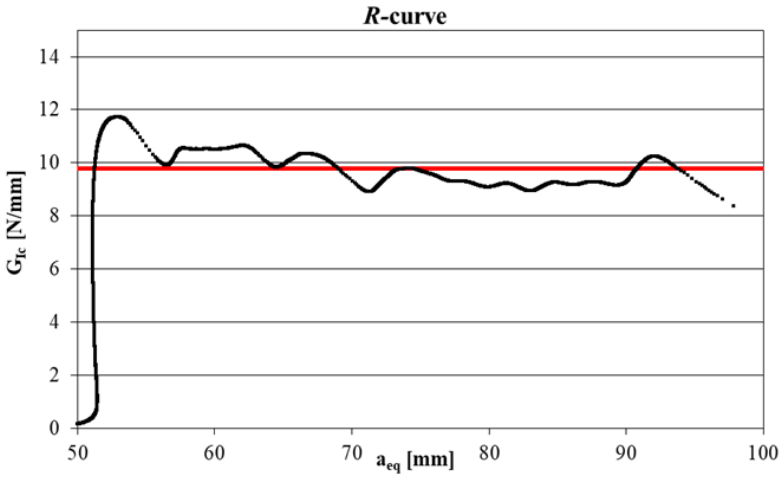

Figure 43 – Example of R-curve from the DCB test.

An inspection on the fracture surfaces allow to conclude that mixed failure in the adhesive layer occurred, with a combination of adhesive and cohesive failure for all temperatures and strain rates. Is also perceived that the adhesive, regarding the mixed mode of failure, is plasticized trough all since presents a whitish colour, whereas its colour before the test its beige (Figure 44).

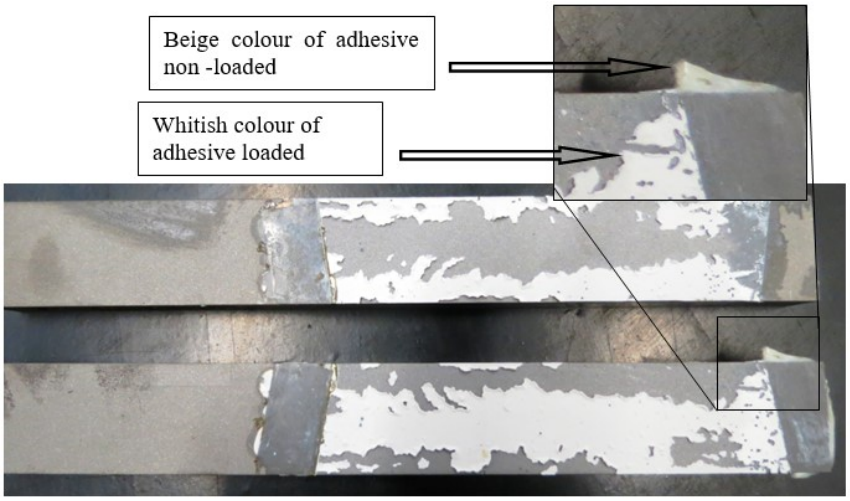

Figure 44 – Example of failure surface of a DCB.

For the case of CFRP substrates, for each testing stage of strain rate and temperature analysed five specimens per configuration were tested, accordingly the specification of ISO 15024 [63]. All tests were performed at a constant crosshead displacement of 2 and

100 mm/min, which corresponds to an average strain rate of 0.2 and 11 s^{-1}, since the considered value of l_0 was of a single ply thickness of 0.15 mm.

All the specimens have been pre-cracked using a pre-testing procedure. In this procedure, the specimen was loaded until the crack starts to propagate away from the Teflon insert. As soon this natural crack growth was detected, the specimen was unloaded. The length of initial pre-crack is then registered, and a paper scale glued to the specimen starting from the tip of the pre-crack. This scale allows the measurement of crack growth while the test being performed (Figure 45).

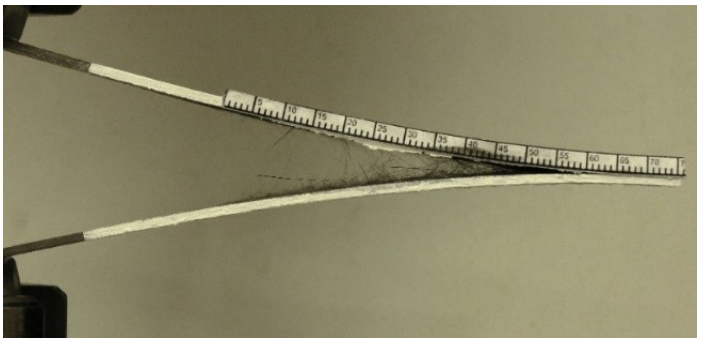

Figure 45 – DCB CFRP testing (occurrence of fibre bridging).

During the test, the onset of stable delamination growth is monitored, and the delamination initiation and propagation readings are recorded. The crack length of tests performed at room temperature and for the case of cross-head speed displacement of 2 mm/min was recorded by taking pictures every 5 seconds while for those tests with a strain rate of 100 mm/min a video was logged instead.

4.4.2. Mode II

Testing the fracture toughness (Figure 46) of adhesives in mode II is considerably more complex than in mode I. The most popular tests used to determine the fracture energy in mode II, G_{IIC}, are the End Notched Flexure (ENF) and End Loaded Split (ELS) [72].

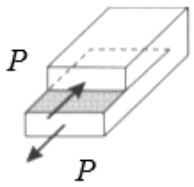

Figure 46 – Schematic representation of mode II applied load (P) [65].

Regarding XNR6852 E-3 adhesive, only DCB could be performed, as the high values of stiffness of the adhesive revealed not be possible to be determined by ENF tests, as there was a significant plastic deformation of the steel substrates prior crack propagation. Only CFRP substrates were used to perform such tests.

The ENF test is used to determine the mode II fracture toughness of an adhesive, the G_{IIC}. Nevertheless, these tests are based on interlaminar fracture of composites in mode II, G_{IIC}, which can be adopted to the study the behaviour of adhesives [92].

The test consists of a simply supported beam loaded at mid-length and supported at both ends, with a pre-crack at one of the edges (Figure 47). The shear mode loading in the adhesive layer is therefore promoted. The instability of the crack propagation may be a disadvantage of this method if Equation 27 is not taken into consideration [62, 93, 94].

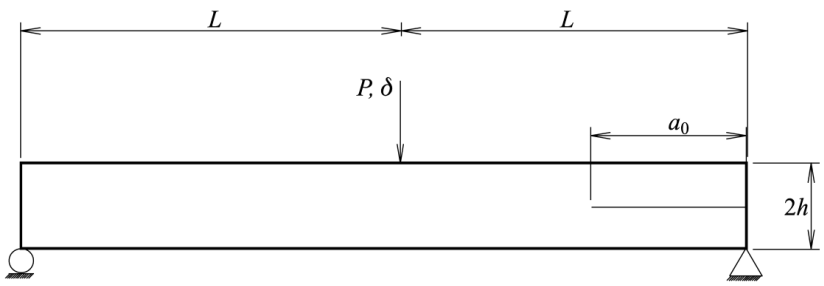

Figure 47 – Schematic representation of the End Notched Flexure (ENF) specimen [95].

The plasticization of substrates must be avoided, as it has direct influence on the results. Without the separation of substrates, as it takes place in DCB tests, the measurement of the real crack length becomes difficult, which sometimes does not allow the use of measurement methods of fracture energy requiring the real crack´s length [62].

In the case of testing composite materials, in order to avoid unstable crack propagation, the following relation stated in Equation 27, should be taken into consideration [96].

$$\frac{a_0}{L} > 0.7 \qquad \text{Eq. (27)}$$

Being a_0 the initial crack length, and L the mid-length of the specimen.

The strain energy release rate can be derived from an experimental load-displacement curve, using a data reduction scheme such as the compliance-based beam method (CBBM). Unlike other methods, this technique allows the determination of the compliance curve (R-curve), without constant measurement of the crack-length. Instead of this measured value, the concept of equivalent elastic crack length (a_{eq}) is used [94, 97, 98].

The same procedure has been used for the experimental ENF tests of CFRP, and the setup is shown in Figure 48.

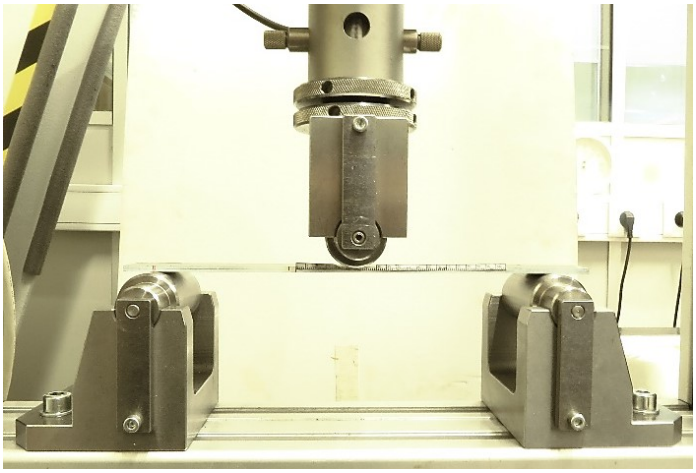

Figure 48 – Setup used to test the ENF specimen at 20 °C and strain rate of 0.2 and 11 s^{-1}.

For the case of CFRP substrates, for each testing stage of strain rate and temperature analysed five specimens per configuration were tested. All tests were performed at a constant crosshead displacement of 2 and 100 mm/min, which corresponds to an average strain rate of 0.2 and 11 s^{-1}, since the considered value of l_0 was of a single ply thickness of 0.15 mm.

4.5. Impact tests

4.5.1. Tensile bulk of XNR6852 E-3 adhesive

A tensile testing machine (Shimadzu Hydroshot HITS-T10), with a maximum impact force of 10 kN and an impact speed of 20 m/s (allowing a maximum displacement of 300 mm), was used to test XNR6852 E-3 adhesive bulk at an initial impact velocity of 3 m/s at -30, 24 and 80 ºC (Figure 49).

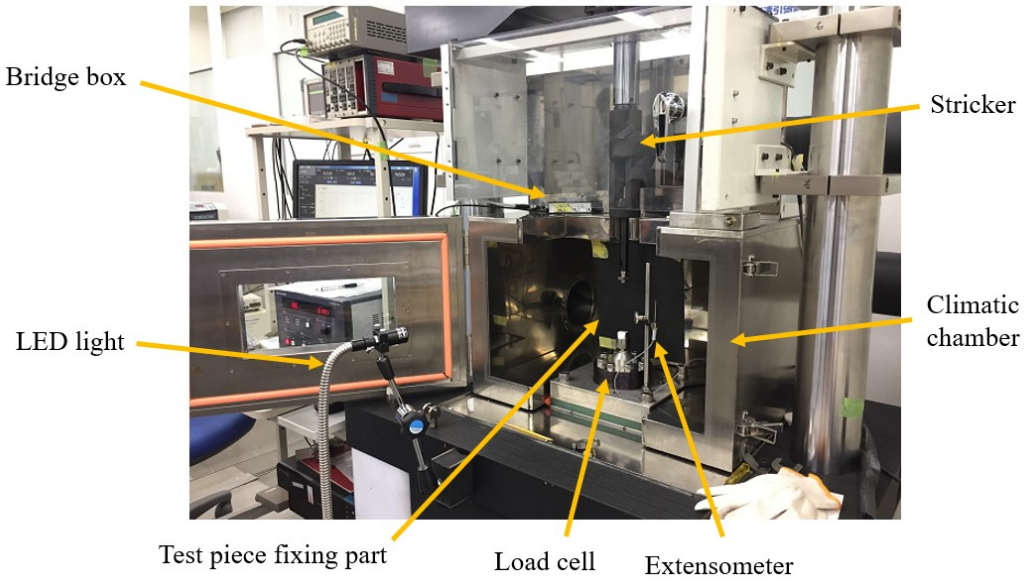

Figure 49 – Setup used to test XNR6852 E-3 bulk adhesive under impact.

A jig was used to hold the specimens (similar to the setup used in **Section 4.3.1.**), and a striker hits the upper section of the mentioned jig with the defined impact velocity. A high-speed camera was used to record the tests, which were performed at low and high temperatures

4.5.2. SLJs

The impact tests were performed in a Rosand® Instrumented Falling weight impact tester, type 5 H.V. (Stourbridge, West Midlands, U.K.) coupled with a load cell of 60 kN. This equipment operates by having a mass being dropped from a certain height, until it impacts the specimen. The specimen is mounted and kept vertically with the use of a specially designed fixture. The impactor strikes the lower section of the fixture, accelerating the test assembly so that the specimen is loaded in tension-shear. A total maximum impactor weight of 26 kg was available for the setup of the testing machine.

The mass and the height of the impactor assembly establish the energy and the speed, respectively, that is applied on the specimen during the impact test. The energy and speed can be calculated using Equation 14 and Equation 15.

$$E_P = mgh \quad \text{(Eq. 28)}$$

$$E_K = \frac{1}{2}mv^2 \quad \text{(Eq. 29)}$$

The load is fully transmitted to the SLJ by the vertical guide (Figure 50). A load cell attached to the impactor is used to measure the load and time.

The fixture system that was initially available in the machine was found to work unsatisfactorily, causing failure in the SLJ specimens in the clamping area and/or slippage of the specimen. To correct this, four new tools were designed and manufactured. These tools were designed to provide and increase in the contact area and use stronger screws to permit the use of higher clamping forces. For the impact tests, metallic tabs were added to the ends of the SLJ specimens. This was performed in order to align the load, improve the grip, as well as preventing hole failure by reinforcing the clamped area. Araldite® 420 A/B adhesive was used for bonding the tabs.

The load is fully transmitted to the SLJ through the vertical specimen holder. To avoid failures in the clamped area, a holder tool was devised to ensure a proper fixation, providing an increase to the contact area, and using stronger screws to allow higher clamping forces. It is also important to apply a correct preload to the screw to avoid slippage. A load cell in the top of the impactor measures the load which is combined with

the time data. The testing machine can use this information and provide plots of loads, velocity and energy curves.

During the setup of the testing machine, the mass was set to the maximum value of 26 kg. The height was adjusted to a speed test of 2 m/s, for the case of 12.5 mm overlap length, providing an impact energy of 50 J. For the 25 mm overlap length the mass was set to 26 kg, and the speed test was slightly increased to 3 m/s, in order to provide a higher impact energy of 117 J.

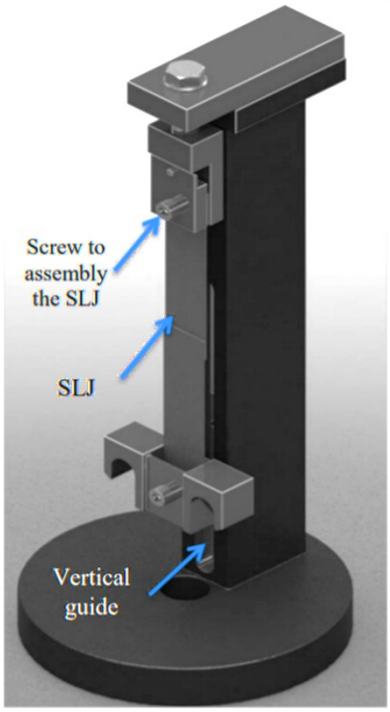

Figure 50 – 3D representation of the setup for impact testing of SLJs.

For each adhesive configuration, six specimens were tested.

The full procedure for testing the specimens under impact is described below:

- The specimen was fixed to the bottom support, with a dynamometric wrench, tightened with 30 Nm of torque (Figure 50);
- Grease was applied to the clamping tool guide, in order to reduce the friction as much as possible;
- Once the bottom piece was fixed (using two screws on top and another two at the bottom), the opposite side of the specimen was also fastened, using the dynamometric wrench, adjusted to apply 30 Nm of tightening torque (Figure 51);

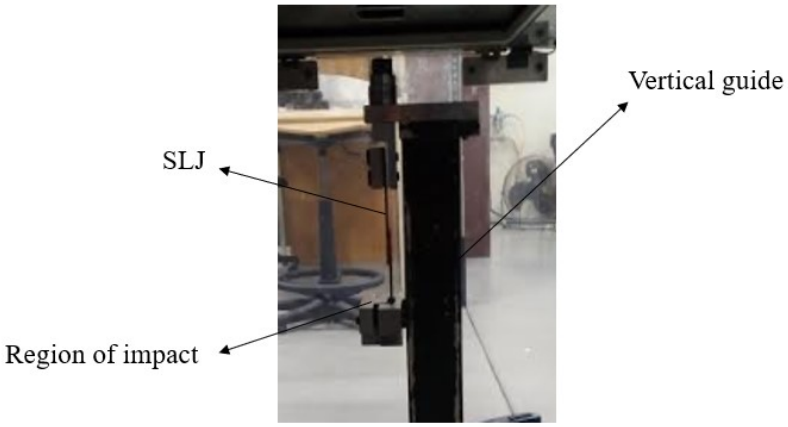

Figure 51 – Specimen assembled in the impact machine (improved design, using two screws to apply clamping force to the SLJ specimens).

- The necessary parameters were inserted in the computer, such as velocity, weight or energy;
- The impactor was lowered slowly until it contacted the specimen and the machine. It was then was automatically zeroed;
- The impactor was then moved up to the desired height and the machine was armed;
- The machine was fired, releasing the impactor to complete the impact test;
- After the test was completed the data was extracted from the testing machine.

The average strain rate in the adhesive layer, was of 15000 s^{-1} (corresponding to a displacement speed of 3 m/s).

For tests performed at LT, gaseous nitrogen was applied directly to the SLJs. In the case of HT, an induction coil was used to heat-up the SLJs. In both temperature levels, a thermocouple was attached in the overlap length area to measure and control the temperature of the specimen. Each test occurred when the adhesive layer temperature was found to be stabilized at the desired value.

4.6. Fatigue tests

The fatigue behaviour of SLJs was determined by testing the specimens in force control with a sinusoidal waveform, load ratio (minimum to maximum load) of R=0.1 and frequency of 5 Hz. The fatigue tests were performed considering three distinct ranges of load values, namely, 20, 40 and 60% of the quasi-static (1 mm/min) load of SLJs being analysed.

A servo-hydraulic MTS 810 testing machine was used to test SLJs under fatigue. The testing setup was the same as described in **Section 4.3.3.**, being thermocouples placed at various points on the surface of the SLJs to investigate any thermal effects, such as the increase of temperature causing mechanical changes in the properties of XNR6852 E-3 adhesive layer of CFRP substrates. It was concluded that during testing no significant changes were found.

The fatigue experiments were conducted up to failure of the specimens or to a maximum of one million load cycles (runout). Specimens which achieved the runout cycles were thereafter tested under quasi-static (1 mm/min) conditions to assess the residual strength

4.7. Automotive joint from Aston Martin Lagonda®

A custom designed structure was manufactured to hold the “roof frame header” specimen in place during the quasi-static (1 mm/min) and impact (3 m/s) tests, as shown in Figure 52. This structure was designed considering the impact load being applied, but at the same time presenting a low weight to allow its transportation and assembly on the testing equipment. A total of two “roof frame header” were tested for each testing condition, respectively, quasi-static (1 mm/min) and impact (3 m/s).

The test setup was assumed to be similar to a three-point bending but with the edges restrained in terms of movement, and the distant between the encastred areas was of 82 cm (four screws were used on each side to clamp the specimens).

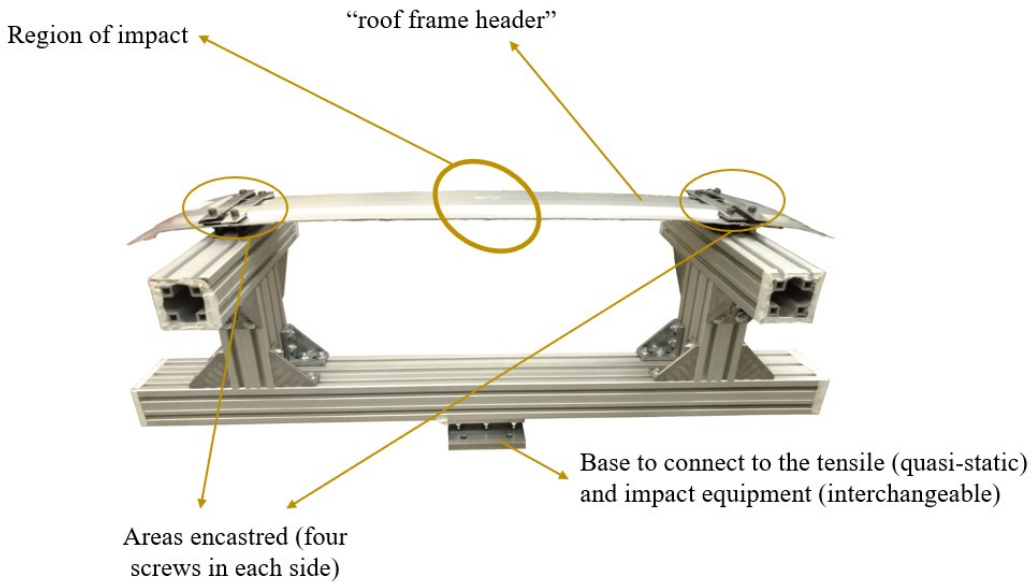

Figure 52 – Structure designed to hold the "roof frame header".

In Figure 53 it is possible observe the tool manufactured to perform quasi-static (1 mm/min) and impact (3 m/s) tests, the design of which was adjusted to enable it to be assembled on both setups.

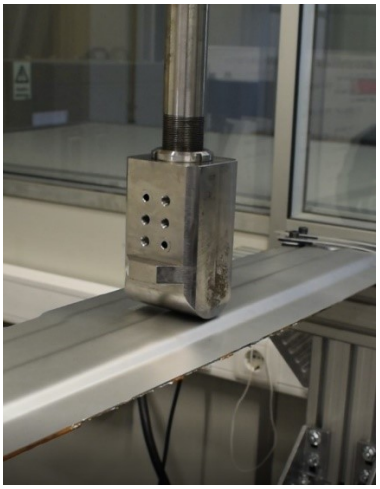

Figure 53 – Impactor designed to test the "roof frame header".

The quasi-static tests (1 mm/min) were performed in a servo-hydraulic testing machine, of the Instron® 8801 model, with a load cell of 100 kN. During the test load is applied to the centre of the specimens, as specified in Figure 52, a configuration generally similar to a 3-point bending test, differing only by not allowing free movement of the specimen outer edges. The acquired data from this test was the load and the displacement.

As for impact (3 m/s) tests, an in-house impact equipment (drop weight type) was developed to meet the Adhesive´s Group testing requirements in terms of impact and energy capability (Figure 54). The drop weight machine consists of several mechanisms and hardware components that allow it to have the desired functions, such as lifting, velocity acquisition, anti-rebound system, anvil impactor, and the data acquisition sub-system.

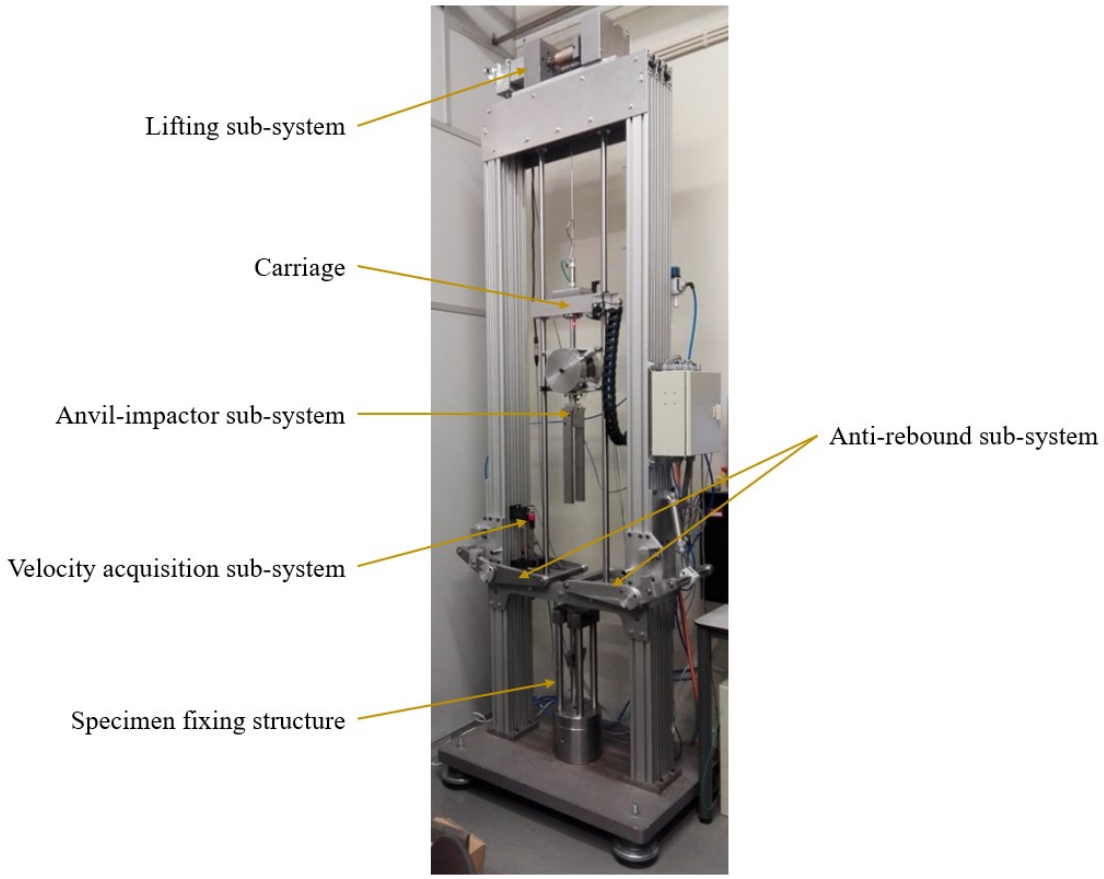

Figure 54 – In-house developed drop weight machine to test under impact conditions.

The drop weight machine allows a drop mass of 56 kg to be released from a 1.27 m height, reaching an impact a maximum initial velocity of 5 m/s, which corresponds to a maximum energy of 700 J. In this specific case, the required initial impact velocity was of 3 m/s, being a mass of 30 kg used, and representing a maximum energy of 135 J. As per indicated in Figure 52, the region of impact was in the centre of the specimens, being the load and the displacement at the centre recorded.

5. Numerical modelling

Numerical models were created to predict the SLJ strength under quasi-static (1 mm/min) and impact (3 m/s) conditions. For this purpose, Abaqus® (Dassault Systèmes, Suresnes, France) was the Finite Element Method (FEM) software used. Simulations were only carried out for room temperature because of the limited information available regarding shear properties for the adhesive at low and high temperature.

P-δ curves were determined and the prediction of the failure load was recorded. The software also allows to extracted information regarding crack initiation and propagation and state of plasticity from cohesive elements.

The data obtained from the previously performed characterization of the cohesive zone model parameters is used to predict the behaviour of SLJs. Concerning the following mechanical properties: Young's modulus (E) and normal cohesive stress (t_n^0) were obtained from bulk tensile tests; shear modulus (G) and shear cohesive stress (t_s^0) were obtained from torsion tests, and fracture toughness's in pure modes I and II (G_n^0 and G_s^0) were obtained from DCB an ENF (only of CFRP substrates) experiments, respectively.

5.1. Cohesive zone models

The CZM natively integrated in Abaqus® and used in this work makes use of triangular traction separation laws. This type of law can be modelled with three main parameters for each type of loading mode which are then combined internally by the software according to a user specified mixed mode law [99]. Using a triangular traction separation law, the three properties required for each mode (mode I and mode II) are the elastic modulus, the yield stress and the fracture energy.

The triangular CZM was used due to its simplicity and common use in previous studies. This model is available in the Abaqus® and enables the use of mixed mode loading (Figure 55). The adhesive layer was modelled with 0.2 mm thick cohesive elements, the same thickness of the adhesive layer to control the zone of crack initiation.

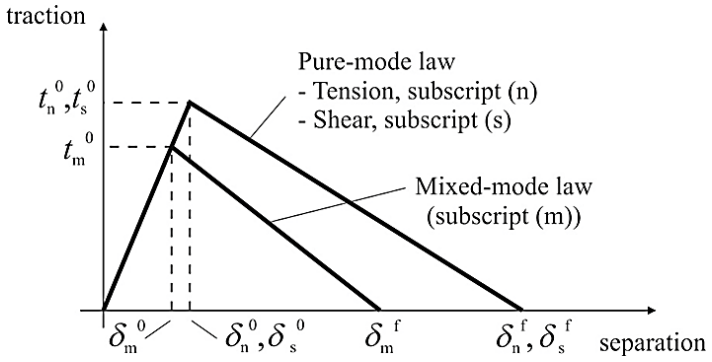

Figure 55 – Traction-separation mixed-mode law available in Abaqus® [100].

Regarding the mathematical approach, as the initial behaviour of the law is elastic it can be modelled by the elastic constitutive matrix, K (Equation 30) [100].

$$t = \begin{Bmatrix} t_n \\ t_{s2} \end{Bmatrix} = \begin{bmatrix} K_{nn} & K_{ns} \\ K_{ns} & K_{ss} \end{bmatrix} \begin{Bmatrix} \varepsilon_n \\ \varepsilon_s \end{Bmatrix} = K\varepsilon \quad \text{(Eq. 30)}$$

For thin adhesive layers, several considerations can be made: K_{nn}=E, K_{ss}=G and K_{ns}=0, where E and G are the Young's modulus and shear modulus, respectively.

The complete separation and mixed-mode failure displacement are predicted by the following linear power law form equation of the required energies for failure in the pure modes (Equation 31) [100].

$$\frac{G_n}{G_n^c} + \frac{G_{s1}}{G_{s1}^c} = 1 \quad \text{(Eq. 31)}$$

To implement this method, varied property data of the adherends and the adhesives is required, such as the Young´s modulus (E) and shear modulus (G), cohesive strength in tension and shear (t_n and t_s, respectively), the tensile (G_{Ic}) and shear toughness (G_{IIc}), that can be obtained experimentally.

5.2. Quasi-static model

To correctly simulate the failure mode and failure loads of the experimental joints, the finite element models were developed making use of cohesive type elements. These elements use a cohesive zone model (CZM). This type of models is increasingly being used to improve the failure load prediction of finite element models (FEM). Needleman [101], Tvergaard et al. [45] and Camacho et al. [102] have proven the suitability of this technique for use in modelling adhesive joints. A CZM can represent the fracture process and location, advancing beyond the typical continuum mechanics modelling. It does this by including in the model a series of discontinuities modelled by cohesive elements, which use both strength and energy parameters to simulate the nucleation and advance of a fracture crack [103, 104]. Cohesive models use fracture mechanic concepts, combining strength and energy parameters to simulate a crack progression on the material.

For the numerical simulation a few conditions were considered with the objective of making the models as reliable as possible. Since three distinct types of materials were used during this work, the elements used to simulate them need to be chosen according to their physical behaviour. Figure 56 shows the model of a dissimilar joint with aluminium and CFRP adherends were all the different types of elements used in all the possible configurations are presented. As mentioned before, for the adhesive a 0.2 mm layer was modelled with cohesive elements. For CFRP adherends, elastic orthotropic properties (engineering constants) were used but it was also needed to resort to cohesive elements to predict a possible failure by delamination. To simulate this, a 0.15 mm thick layer was added at a distance of 0.15 mm from the interface between adhesive and CFRP. The thickness of 0.15mm corresponds to one ply of the prepreg used to manufacture the CFRF adherend. Aluminium substrates were simulated with elastic isotropic and plastic properties.

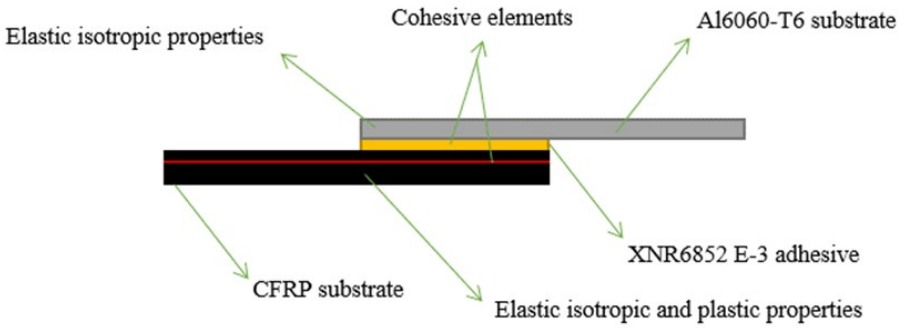

Figure 56 – Elements introduced in FE software for the quasi-static (1 mm/min) analysis (example of SLJs made with dissimilar substrates combination of CFRP and aluminium 6060-T6).

The curves of Yield Stress- Plastic Strain for the aluminium alloys have already been presented in Figure 9. The data related with the aluminium alloys was provided by Aston Martin Lagonda®.

Triangular laws for XNR6852 E-3 adhesive (Figure 57) and for cohesive layer of CFRP (Figure 58) were created for both loading modes. The adhesive tensile properties, Young's modulus (E) and normal cohesive stress (t_{n0}), were obtained from bulk tensile tests. Fracture toughness in pure mode I (G_{n0}) was obtained from DCB tests. The other properties, shear modulus (G), shear cohesive stress (t_{s0}) and fracture toughness in pure mode II (G_{s0}), needed to complete the triangular law were obtained from a previous works [105-107], as well the cohesive and elastic properties for the CFRP.

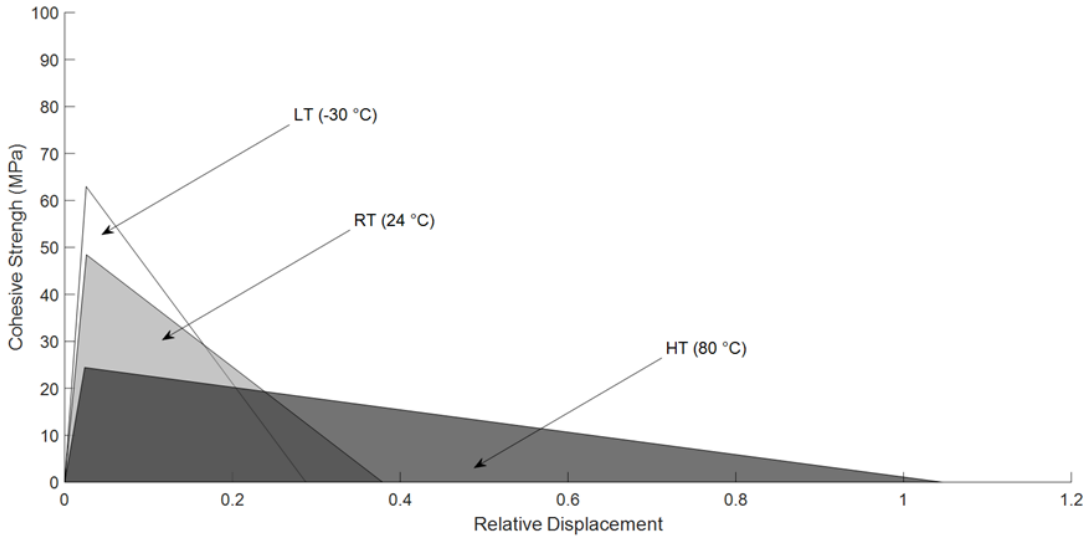

Figure 57 – Triangular law for XNR6852E-3 adhesive at quasi-static (1 mm/min) conditions and as a function of temperature.

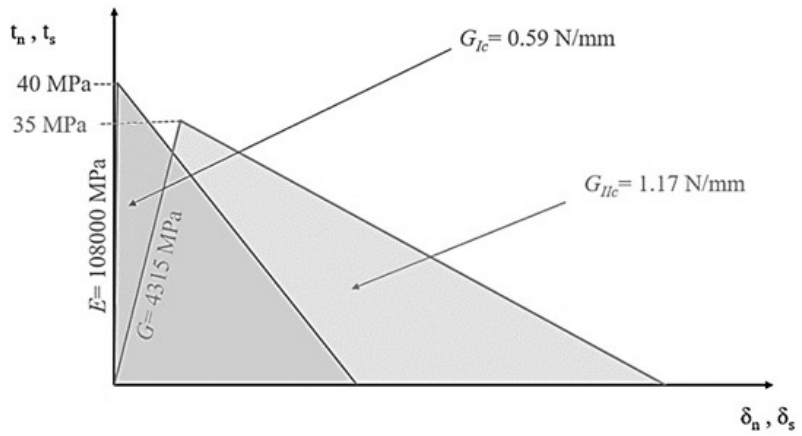

Figure 58 – Triangular law for CFRP at quasi-static (1 mm/min) conditions at room temperature.

The boundary conditions were defined as indicated in Figure 59. At one end of the specimen, a clamped condition was added in order to simulate the static grip of tensile machine while in the other end a longitudinal displacement was applied, restrained in the perpendicular direction of the displacement, simulating the grip that applies the force during the test.

Figure 59 – Boundary conditions applied for the quasi-static model.

The mesh design was constructed with elements of different sizes, resorting to biasing (Figure 60). Cohesive elements with 0.15 mm and 0.2 mm length were used, respectively, for the CFRP adherends and for the adhesive layer. The size of elements increased as they move away from the ends of the overlap zone, as the stresses gradients are less pronounced.

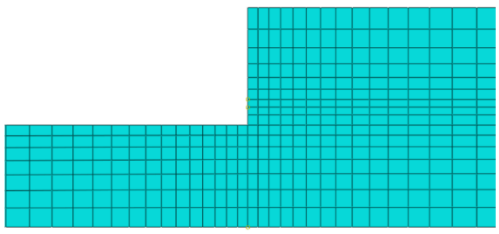

Figure 60 – Representative mesh in the overlap area.

For the visualization of the CZM degradation, scalar stiffness degradation (SDEG) was requested in the field outputs. This also enables the monitoring of the crack propagation.

Regarding to the element types, the bondline area was defined as a 4-node-two-dimensional cohesive element (COH2D4 in Abaqus®) and substrates were defined as a 4-node bilinear plane stress quadrilateral, reduced integration, hourglass control (CPS4R in Abaqus®).

As for the "roof frame header", a 3-D model (including the upper and lower substrates and the adhesive layer) was provided by Aston Martin Lagonda®, and the model mesh was imported into Abaqus CAE from the Hypermesh® software (Figure 61).

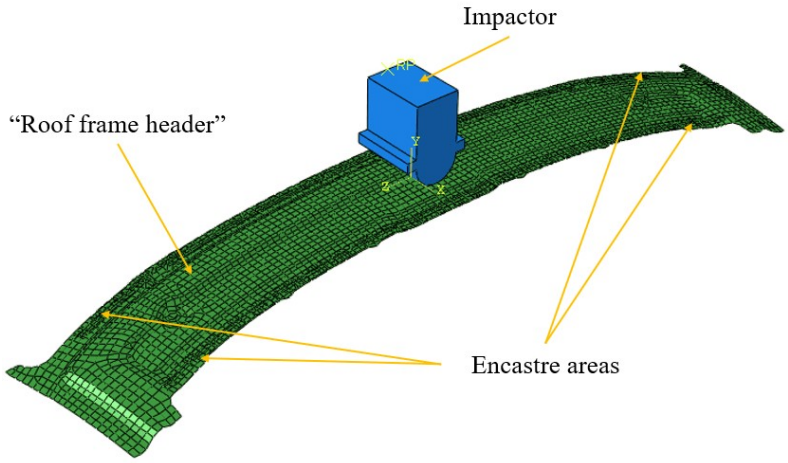

Figure 61 – Representation of the boundary conditions applied to numerically simulated the "roof frame header", for both quasi-static (1 mm/min) and impact (3 m/s) conditions.

Shell elements with thicknesses of 1.7 and 1.2 mm were used, respectively, to model the upper and lower aluminium substrates. The majority of the elements were defined as explicit, linear quadrilateral elements (designated by S4 in Abaqus®), but linear triangular elements (S3R in Abaqus®) were also applied in sections of the joint with more complex geometry, such as: holes, centre region of loading, and in areas with drastic change of geometry. The two adhesive bondlines were determined as a single layer of explicit, 8-node three dimensional cohesive elements (COH3D8 in Abaqus®), based on the mechanical properties presented in Figure 57. Regarding the impactor, since its deformation and stress states did not represent a significant influence for the numerical

results, it was modelled as a rigid body. To avoid the direct passage of the impactor through the "roof frame header", an interaction between surfaces was defined, with a normal behaviour of the "hard contact" type and a tangential behaviour with a friction coefficient of 0.61 (a typical value for modelling relative movement between steel and aluminium).

As boundary conditions, the ends of the "roof frame header" were defined as being encastred on both sides, simulating the service conditions (matching the locations where the joints are rigidly connected to the rest of the automotive structure), and the impactor was allowed to move only in the vertical direction, with a maximum displacement of 160 mm (Figure 61). A dynamic, explicit step was used to simulate the testing process and the SDEG parameter, the reaction forces at the encastred areas and the displacement of the impactor were the requested outputs.

5.3. Impact model

To recreate the impact conditions of the drop weight test, a 2-D model was created resorting to Abaqus/Explicit. The model was similar to the one used for quasi-static simulations with one modification, the addition of a mass to the non-clamped edge that represents the impact block in the experimental tests. The boundary conditions were similar to those used in the quasi-static model with the difference being the application of a velocity field of 3 m/s to a mass that was added to the model (Figure 62), instead of a longitudinal displacement in the non-clamped end of the joint. In order to simulate the 117 Joules of impact energy with a 3 m/s velocity of the mass, the density was adjusted in order to guarantee that the mass was 26 kg. The mesh geometry used was the same was the quasi-static model and SDEG field output was also requested.

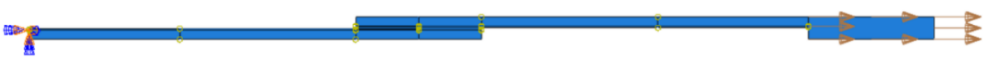

Figure 62 – Boundary conditions applied for the impact model.

For XNR6852 E-3 adhesive properties, Young's modulus (E), normal cohesive stress (t_{n0}) and fracture toughness in pure mode I (G_{n0}) were extrapolated from experimental results resorting to a logarithmic trend line as described in the results chapter. Shear

modulus (G), shear cohesive stress (t_{s0}) and fracture toughness in pure mode II (G_{s0}) were obtained from a previous work [105-107]. Again, a new triangular cohesive law was made for the adhesive at impact (Figure 63)

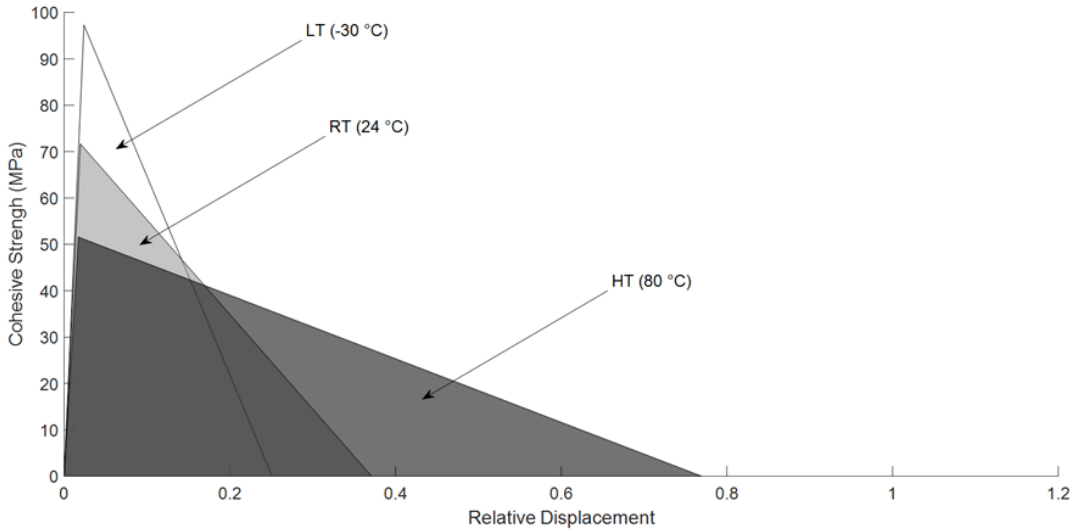

Figure 63 – Triangular law for XNR6852 E-3 adhesive at impact (3 m/s) conditions.

As stated in the literature review chapter, the aluminium alloys are insensitive to the strain rate (Al 6060-T6), or at least slightly sensitive (Al 5754-H22) and the properties used for the quasi-static model could be used for the dynamic as well. The CFRP behaves in a different manner, while strain rate insensitive in the tensile direction the same does not occurs in the other directions. For simulation purposes, and because CFRP properties, namely the same specific material used in this study, were determined in previous works, the properties from the elastic domain were kept as constant and those from the plastic domain were considered as a function of the strain rate. New triangular cohesive law was made for CFRP at impact (Figure 64).

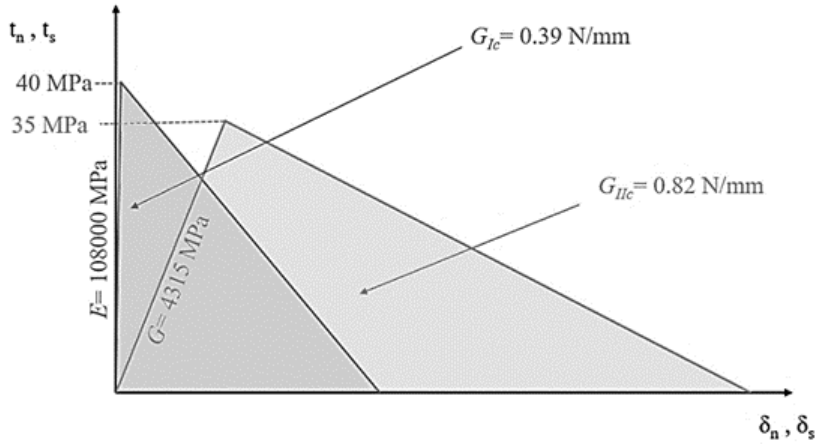

Figure 64 – Triangular law for CFRP at impact (3 m/s) conditions at room temperature.

Similarly, to what was previously stated for the quasi-static (1 mm/min) load, the model mesh was imported from the software Hypermesh® (Figure 61). The structure of the model used for impact was similar to the one of quasi-static conditions, the only differences being the properties of the adhesive (Figure 63) and the boundary conditions (namely, mass and velocity). As the total mass and impact velocity of the dropping structure in the experimental tests are 26 kg and 3 m/s, respectively, these parameters were applied to the impactor. As verified in the quasi-static model, the ends of the automotive structure, at both sides, were simulated as an encastre.

6. Conclusions

The introduction of adhesives in the manufacturing process of automotive structures has constantly increased in the last years, creating the need to evaluate and predict various aspects during its project and development stages, namely how structures will behave under the variation of strain rate, temperature, aging and fatigue conditions. An in-depth analysis mainly focused on the impact behaviour of composite and aluminium adhesive joints was performed during this work, comprehending all the mentioned aspects.

A list of the main conclusions drawn from this work in terms of each task investigated is therefore presented.

Task 1 – Determination of the adhesive and CFRP mechanical properties as a function of loading rate and testing temperature:

- **XNR6852 E-3 adhesive:**
  - The tensile stress-strain response of the adhesive at high strain rates exhibited the non-linear characteristics including the obvious yielding and strain softening. The tension behaviour is strongly dependent on the strain rate and temperature.
  - For all the displacement rates tested, with the increase of the testing temperature, a decrease of the tensile strength was observed, and that with the increase of the strain rate values there was an increase of the values of the tensile strength.
  - A decrease of the Young´s modulus values was found to occur with the increase of temperature, regardless of the displacement rate, being more pronounced between 24 to 80 °C.
  - The value of G_{IC} increased with the increase of both strain rate and temperature, once the temperature approaches T_g the adhesive becomes more ductile and tough. Such behaviour is due to the increased viscoelastic and viscoplastic effects that become as the material operates closer to T_g. With the increase of the value of strain rate there was an increase of the shear strength.

- **CFRP:**
  - The behaviour of fracture toughness in both mode I and mode II revealed to be similar, when varying the testing displacement rate and temperature. For tests performed at 80 °C, the value of fracture toughness has a larger increase in

comparison with the values obtained when testing at -30 and 24 ºC. With the increase of temperature, it was observed an increase of the fracture energy, which can be supported by the brittle behaviour of the resin of the CFRP matrix.

The mechanical characterization process developed in this work is of great important as it will allow other materials (both substrates and adhesives) to be characterized with these methods. It is possible to conclude that XNR6852 E-3 prototype adhesive is well suitable for the automotive application due high strength and stiffness properties.

Task 2 – Quasi-static (1 mm/min) and impact (3 m/s) testing of SLJs (single and mixed adhesives) from low to high temperatures:

- **Single adhesive:**
  - The CFFR-CFRP SLJs configuration exhibited the highest failure load for all conditions except for the impact test at -30°C, where the performance of all SLJs under study was similar.
  - The performance of the dissimilar SLJs performance (maximum load) was found to be limited by the aluminium deformation at all conditions tested.
  - At quasi-static (1 mm/min) conditions the aluminium-aluminium similar joints absorbed the most energy for all temperatures tested.
  - At impact (3 m/s) conditions the CFRP-CFRP joints were those that absorbed more energy, except for tests performed at the temperature of -30ºC.
  - A significant difference in absorbed energy from quasi-static (1 mm/min) and impact (3 m/s) was found when testing the aluminium-aluminium joints. This is since failure occurred in the clamped section during impact testing.

As a final remark, it is possible to conclude that dissimilar adhesive joints can effectively be used for the construction of automotive structures, without significant sacrifices in joint performance, including energy absorption under impact, if used in conjunction with modern crash resistant adhesives (such as the adhesive XNR6852 E-3), and increased the failure loads over the use of single adhesives. Moreover, their performance can also be simulated using advanced cohesive zone models minimizing the need to perform extensive experimental testing.

- **Mixed adhesive joints:**

A new technique for the manufacture of mixed adhesive joints using composite specimens has been successfully developed. Further improvements are still needed for some adhesives, which have managed to escape the containment created by the nylon wire.

- The effectiveness of the mixed adhesives in composites has been demonstrated in quasi-static (1 mm/min) and impact (3 m/s) tests, with the combination between SikaFast 5211 NT + AV 138, exhibiting significant improvements in both cases.
- Failure loads under impact (3 m/s) conditions were found to be much higher, due to the strain-rate dependence of the adhesives.
- XNR6852 E-3 adhesive exhibits very high strength under quasi-static (1 mm/min) and impact (3 m/s) conditions, very far from those reached by another single adhesive or mixed adhesive combination. Moreover, the flexible adhesives combined with XNR6852 E-3 were not found to be useful. This adhesive was therefore shown to be a valid crash resistant adhesive for use in composite structures.
- SikaFast 5211 NT and DP 8005 were also found to be able to join CFRP substrates, with good failure loads and a totally cohesive failure in the adhesive.
- RTV106 exhibited significant adhesion problems with the CFRP, and all the specimens using this adhesive suffered adhesive failure.

Finally, the use of mixed adhesive joints with CFRP substrates can reduce the effect of peel loads and increased the failure loads over the use of single adhesives. However, it is important to note that modern crash resistant adhesives can already achieve this effect and provide extremely high adhesive joint strengths, ductility and, consequentially, energy absorption. More research is necessary to determine if improvements can be made to crash resistant adhesives using the mixed adhesive joint technique.

Task 3 – Numerical simulation of the quasi-static (1 mm/min) and impact (3 m/s) behaviour of SLJs (single and mixed adhesives):

- **Single adhesive:**
  - The quasi-static (1 mm/min) models using cohesive zone modelling were able to simulate reasonably well the mechanical behaviour of most of the configurations under study, especially when predicting the failure of CFRP substrates. However, given the limited property data, proper modelling of the aluminium failure process was not possible.
  - The impact (3 m/s) models developed during this work were also able to simulate reasonably well the mechanical behaviour of most of the configurations under study. Again, the failure process of CFRP materials was found to be more accurately modelled that then the failure process of aluminium.
- **Mixed adhesive joints:**
  - The quasi-static (1 mm/min) models developed were able to simulate reasonably well most of the configurations under study. However, models of the single adhesive joints with very flexible adhesives (DP 8005 and RTV 106) exhibited poor results, mainly due to triangular cohesive zone model inability to model very flexible adhesives effectively.
  - The numerical models for the impact (3 m/s) tests were also able to model most of the experimental results. Again, the most inaccurate models were those containing the flexible DP 8005 and RTV 106 adhesives. In this case, not only the use of a triangular cohesive zone law contributes to the poor results but also the difficulty in establishing the correct strain rate dependent properties.

Task 4 – Quasi-static (1 mm/min), impact (3 m/s) and fatigue testing of age and dried after hygrothermal aging SLJs (single adhesive an in similar and dissimilar substrates combination):

- The aging process of XNR6852 E-3 adhesive and CFRP substrates was assessed for a period of 2000 hours at 50 ºC. Thereafter, drying after hygrothermal aging was performed by keeping the specimens at 50 ºC. It was observed a small decrease of T_g for both materials, supported by plasticization of the polymer network with the moisture absorption; and an increase of this parameter value was obtained after drying the specimens, once this process might have created an increase in crosslinking between some polymeric chains, therefore affecting the materials properties by inducing a post-cure effect.
- For joints manufactured with CFRP substrates, a significant decrease of the failure load was observed for both quasi-static (1 mm/min) and impact (3 m/s) conditions after hygrothermal aging, even though a recovery in the failure load value was obtained for joints dried only under quasi-static (1 mm/min) conditions. Plasticization of the CFRP substrates was the cause for this behaviour.
- The experimental results have shown that in the case of joints manufactured using CFRP + Al 5754-H22 substrates, for both quasi-static (1 mm/min) and impact (3 m/s) conditions there was no significant change of the failure load, although a decrease on the energy absorbed by the joints was observed. The behaviour of these joints was controlled by the plastic deformation of the aluminium substrate.

Task 5 – Validation of the numerical quasi-static (1 mm/min) and impact (3 m/s) models of an automotive structure by performing experimental tests:

- The experimental results have shown that the “roof frame header” under both quasi-static (1 mm/min) and impact (3 m/s) conditions presented a deformation and subsequent rupture of the aluminium lower substrate, but the XNR6852 E-3 adhesive was able to undergo both loading conditions keeping the integrity of the structure, which was the main goal.

- The quasi-static (1 mm/min) and impact (3 m/s) experimental results revealed to be similar in terms of the failure load, although slightly higher in the case of the impact (3 m/s) conditions, which might be due to impact wave propagation. In terms of strain at failure, under quasi-static (1 mm/min) it was registered a higher value of deformation of the specimens in comparison with the impact (3 m/s) conditions.
- Numerical simulations based on a 3-D model were able to correctly infer the behaviour of the "roof frame header" under the different loading conditions, revealing to be an important tool to predict the mechanical behaviour of adhesively bonded structures.

The **main conclusions** which can be **drawn for this work are the following**:

- Development of an experimental methodology to mechanically characterize a crash resistant epoxy adhesive.
- Alternative SLJs manufacturing process using the mixed adhesive concept, allowing to reduce the peel forces and therefore improve joint strength while achieving a more controlled failure of the CFRP by delamination.
- Numerical simulation of SLJs based on cohesive elements using the determined mechanical properties.
- Assessment of the effect of hygrothermal aging and fatigue of SLJs made with aluminium and CFRP substrates bonded with a crash resistant adhesive.
- Experimental testing of an automotive structure, followed by numerical simulations, based on the experimentally determined mechanical properties of the adhesive, allowed to predict the joint behaviour.

7. Future work

The experimental work presented focused on the development of a methodology which allows the determination of the mechanical properties of adhesives, substrates and its combination in SLJs, aiming to infer the behaviour of a structure under the influence of both strain rate and temperature.

Due to the complexity of the impact phenomena, many additional experimental procedures can be suggested to further the knowledge on the impact behaviour of adhesives for the automotive industry. A few alternatives to this effect have been selected and organized in this chapter and presented below, considering different areas of possible intervention.

- **Substrates:**
  - To improve the level of adhesion on CFRP substrates, a different surface preparation approach would be to perform plasma treatment on the CFRP substrates prior to the SLJ manufacture.
  - Repeat the same sequence of tests performed in this work using high strength steel substrates, a material widely used in the automotive industry.

- **SLJs (geometries and concepts):**
  - Analysis of the influence of different overlap lengths and substrates thicknesses in the SLJs behaviour under impact conditions.
  - Besides the use of single or mixed adhesive SLJs, it would be also important to explore the behaviour of functionally graded joints under impact conditions.
  - Vary the overlap length would enable to better understand the capabilities of mixed adhesive joints, as larger overlaps would provide more area for both adhesives to work in conjunction.
  - Test the use of mixed adhesive joints using other substrates used in the automotive industry such as aluminium, or even studying the performance of joints with dissimilar materials combinations such as steel-CFRP, steel-aluminium or CFRP-aluminium.
  - Attempt to use more adhesives on the overlap length, with the aim of attaining a true graded joint, with smoothly varying properties. The use of this type of joint

with composite substrates might be able to further reduce the onset of delamination.

- As the failure of the joints was mostly by delamination, the use of novel techniques that mitigate this type of failure should also be explored. Usage of fibre metal laminates or geometrical modifications that reduce the peel stresses in the composite are of special interest.
- Study the combination of fibre metal laminates with mixed adhesive joints, two methods which can significantly reduce the negative effect of peel stresses on adhesive joints and minimize delamination.
- Experiment with alternative substrates geometries and mechanical properties to balance the stiffness of the adhesive. By adjusting the substrates, it might be possible to improve significantly the performance of the joints, especially under impact conditions. Other option of optimization of joints geometry could be the introduction of chamfers (internal or external).
- Testing of more complex automotive structures.

- **Experimental tests:**

  - Perform impact tests under higher velocities (using different adhesives, substrates and SLJs).
  - Test the “roof frame header” manufactured with a flexible adhesive to assess the influence of more flexibility of the joint in its resistance.
  - Impact fatigue tests are also a field of study that was not approached in this work and reflects real conditions that automotive structures undergo.

After the completion of this work, it is possible to propose a new and more structured research methodology that should be considered in in further researches using different adhesives (Figure 65).

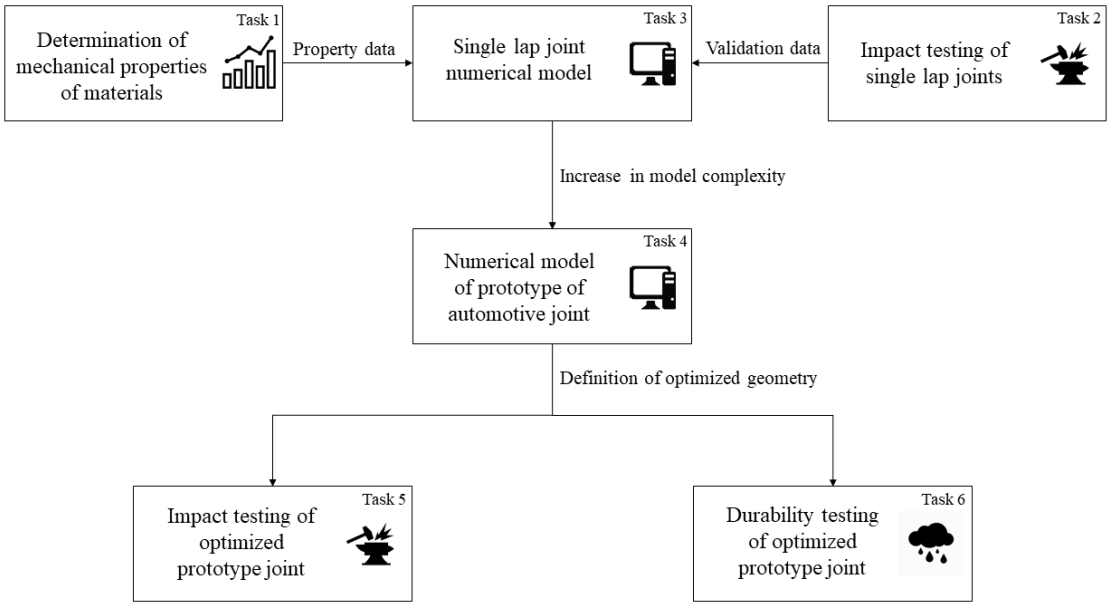

Figure 65 – Schematic representation of the workflow of the tasks proposed for future works.

The proposed sequence of tasks is now designed to focus in the first two tasks in obtaining the mechanical properties of the materials being used (most of it already determined in this work), therefore, to be able to use numerical models (more refined form the knowledge acquired in this work), and finally to perform tests using prototypes to validate the numerical results. It is expected to greatly reduce the time of design of a structure, at the same time being capable of generate more accurate data from numerical simulations.

References

1. da Silva, L.F.M., A. Öchsner, and R.D. Adams, *Handbook of Adhesion Technology*. 2011: Springer Berlin Heidelberg.
2. Petrie, E., *Handbook of Adhesives and Sealants*. 2007: McGraw-Hill Education.
3. Adams, R.D., *Adhesive Bonding: Science, Technology, and Applications*. 2005: Taylor & Francis.
4. Lees, W., *Adhesives in engineering design*. 1984: Springer.
5. Adamvalli, M. and V. Parameswaran, *Dynamic strength of adhesive single lap joints at high temperature.* International Journal of Adhesion and Adhesives, 2008. **28**(6): p. 321-327.
6. da Silva, LFM., A. Öchsner, and R.D. Adams, *Introduction to adhesive bonding technology.* Handbook of adhesion technology, 2018: p. 1-7.
7. Kinloch, A., *Adhesion and adhesives: science and technology*. 2012: Springer Science & Business Media.
8. Adams, R. and J. Harris, *A critical assessment of the block impact test for measuring the impact strength of adhesive bonds.* International journal of adhesion and adhesives, 1996. **16**(2): p. 61-71.
9. Farley, G.L., *Energy absorption of composite materials.* Journal of composite Materials, 1983. **17**(3): p. 267-279.
10. Thornton, P., *Energy absorption in composite structures.* Journal of Composite Materials, 1979. **13**(3): p. 247-262.
11. Körber, H., *Mechanical response of advanced composites under high strain rates*. 2012.
12. da Silva, LFM. and M.J.C. Lopes, *Joint strength optimization by the mixed-adhesive technique.* International Journal of Adhesion and Adhesives, 2009. **29**(5): p. 509-514.
13. da Silva, L.F.M. and R. Adams, *Joint strength predictions for adhesive joints to be used over a wide temperature range.* International Journal of Adhesion and Adhesives, 2007. **27**(5): p. 362-379.
14. Marques, E. and L.F. da Silva, *Joint strength optimization of adhesively bonded patches.* The Journal of Adhesion, 2008. **84**(11): p. 915-934.
15. Pires, I., et al., *Performance of bi-adhesive bonded aluminium lap joints.* International Journal of Adhesion and Adhesives, 2003. **23**(3): p. 215-223.

16. da Silva, LFM. and R. Adams, *Joint strength predictions for adhesive joints to be used over a wide temperature range.* International Journal of Adhesion and Adhesives, 2007. **27**(5): p. 362-379.
17. Marques, E., L. da Silva, and M. Flaviani, *Testing and simulation of mixed adhesive joints for aerospace applications.* Composites Part B: Engineering, 2015. **74**: p. 123-130.
18. Marques, E., LFM. da Silva, and C. Sato, *Testing of Dual Adhesive Ceramic-Metal Joints for Aerospace Applications.* Advances in Modeling and Design of Adhesively Bonded Systems, 2013: p. 171-190.
19. Marques, E., D. Magalhães, and L. da Silva, *Experimental study of silicone-epoxy dual adhesive joints for high temperature aerospace applications.* Materialwissenschaft und Werkstofftechnik, 2011. **42**(5): p. 471-477.
20. Kumar, S. and P. Pandey, *Behaviour of bi-adhesive joints.* Journal of Adhesion Science and Technology, 2010. **24**(7): p. 1251-1281.
21. Temiz, Ş., *Application of bi-adhesive in double-strap joints subjected to bending moment.* Journal of adhesion science and technology, 2006. **20**(14): p. 1547-1560.
22. Sato, C., *Design for impact loads.* Handbook of adhesion technology, 2011: p. 743-763.
23. Dean, G., G. Lord, and B. Duncan. *Comparison of the measured and predicted performance of adhesive joints under impact*. in *NPL Report CMMT (A) 206 Appendix 1 Finite Element Analysis Perforated Single lap Joint NPL Report CMMT (A) 206*. 1999. Citeseer.
24. Field, J.E., et al., *Review of experimental techniques for high rate deformation and shock studies.* International journal of impact engineering, 2004. **30**(7): p. 725-775.
25. Avendaño, R., et al., *Effect of temperature and strain rate on single lap joints with dissimilar lightweight adherends bonded with an acrylic adhesive.* Composite Structures, 2016. **152**: p. 34-44.
26. da Silva, LFM. and R. Adams, *Techniques to reduce the peel stresses in adhesive joints with composites.* International Journal of Adhesion and Adhesives, 2007. **27**(3): p. 227-235.
27. Marques, E., et al., *Adhesive joints for low-and high-temperature use: an overview.* The Journal of Adhesion, 2015. **91**(7): p. 556-585.

28. da Silva, LFM. and C. Sato, *Design of adhesive joints under humid conditions*. Vol. 461. 2013: Springer.
29. Loh, W., et al., *Environmental degradation of the interfacial fracture energy in an adhesively bonded joint.* Engineering fracture mechanics, 2002. **69**(18): p. 2113-2128.
30. Ameli, A., M. Papini, and J. Spelt, *Hygrothermal degradation of two rubber-toughened epoxy adhesives: Application of open-faced fracture tests.* International Journal of Adhesion and Adhesives, 2011. **31**(1): p. 9-19.
31. Viana, G., et al., *A review on the temperature and moisture degradation of adhesive joints.* Proceedings of the Institution of Mechanical Engineers, Part L: Journal of Materials: Design and Applications, 2017. **231**(5): p. 488-501.
32. Wylde, J. and J. Spelt, *Measurement of adhesive joint fracture properties as a function of environmental degradation.* International Journal of Adhesion and Adhesives, 1998. **18**(4): p. 237-246.
33. Costa, M., et al., *Environmental effect on the fatigue degradation of adhesive joints: a review.* The Journal of Adhesion, 2017. **93**(1-2): p. 127-146.
34. Costa, M., et al., *Effect of humidity on the fatigue behaviour of adhesively bonded aluminium joints.* Latin American Journal of Solids and Structures, 2017. **14**(1): p. 174-187.
35. Viana, G., et al., *Behaviour of environmentally degraded epoxy adhesives as a function of temperature.* The Journal of Adhesion, 2017. **93**(1-2): p. 95-112.
36. Zhang, F., et al., *Experimental study of strain rate effects on the strength of adhesively bonded joints after hygrothermal exposure.* International Journal of Adhesion and Adhesives, 2015. **56**: p. 3-12.
37. da Silva, L. and A. Öchsner, *Modeling of adhesively bonded joints*. 2008: Springer.
38. Blackman, B., et al., *The use of a cohesive zone model to study the fracture of fibre composites and adhesively-bonded joints.* International Journal of Fracture, 2003. **119**(1): p. 25-46.
39. He, X., *A review of finite element analysis of adhesively bonded joints.* International Journal of Adhesion and Adhesives, 2011. **31**(4): p. 248-264.
40. Vaziri, A. and H. Nayeb-Hashemi. *Experimental and analytical investigations of the dynamic response of adhesively bonded single lap joints*. in *ASME 2002*

International Mechanical Engineering Congress and Exposition. 2002. American Society of Mechanical Engineers.

41. Cavalli, M. and M. Thouless, *The effect of damage nucleation on the toughness of an adhesive joint.* The Journal of Adhesion, 2001. **76**(1): p. 75-92.
42. Liljedahl, C., et al., *Damage modelling of adhesively bonded joints.* International journal of fracture, 2006. **141**(1-2): p. 147-161.
43. Campilho, R., M. De Moura, and J. Domingues, *Stress and failure analyses of scarf repaired CFRP laminates using a cohesive damage model.* Journal of Adhesion science and technology, 2007. **21**(9): p. 855-870.
44. Marques, E., R. Campilho, and L. da Silva, *Geometrical study of mixed adhesive joints for high-temperature applications.* Journal of adhesion science and Technology, 2016. **30**(7): p. 691-707.
45. Tvergaard, V. and J.W. Hutchinson, *The relation between crack growth resistance and fracture process parameters in elastic-plastic solids.* Journal of the Mechanics and Physics of Solids, 1992. **40**(6): p. 1377-1397.
46. Alfano, G., *On the influence of the shape of the interface law on the application of cohesive-zone models.* Composites Science and Technology, 2006. **66**(6): p. 723-730.
47. Blackman, B., A. Brunner, and J. Williams, *Mode II fracture testing of composites: a new look at an old problem.* Engineering Fracture Mechanics, 2006. **73**(16): p. 2443-2455.
48. Fernlund, G. and J. Spelt, *Mixed-mode fracture characterization of adhesive joints.* Composites science and technology, 1994. **50**(4): p. 441-449.
49. Aymerich, F., F. Dore, and P. Priolo, *Prediction of impact-induced delamination in cross-ply composite laminates using cohesive interface elements.* Composites science and technology, 2008. **68**(12): p. 2383-2390.
50. Carlberger, T. and U. Stigh, *An explicit FE-model of impact fracture in an adhesive joint.* Engineering fracture mechanics, 2007. **74**(14): p. 2247-2262.
51. Avendaño, R., et al., *Impact loading of single lap joints of dissimilar lightweight adherends bonded with a crash-resistant epoxy adhesive.* Journal of Engineering Materials and Technology, 2016. **138**(4): p. 041019.
52. Clarke, M., et al., *Application of the design of experiments procedure to the behaviour of adhesively bonded joints with plastically deformable adherends to*

enable further understanding of strain rate sensitivity. International Journal of Adhesion and Adhesives, 2013. **44**: p. 226-231.

53. Haufe, A., et al. *Modelling of weld and adhesive connections in crashworthiness applications with LS-DYNA*. in *Proceedings of the NAFEMS seminar "simulation of connections and joints in structures". Wiesbaden, Germany*. 2010.
54. May, M., H. Voß, and S. Hiermaier, *Predictive modeling of damage and failure in adhesively bonded metallic joints using cohesive interface elements.* International Journal of Adhesion and Adhesives, 2014. **49**: p. 7-17.
55. Neumayer, J., et al., *Experimental determination of the tensile and shear behaviour of adhesives under impact loading.* The Journal of Adhesion, 2016. **92**(7-9): p. 503-516.
56. Standard, B., *BS 2782*, in *Methods of Testing Plastics, Part*. 1970.
57. *NF T 76-142. Méthode de préparation de plaques d'adhésifs structuraux pour la réalisation d'éprouvettes d'essai de caractérisation.* 1988.
58. Varajão, J.F.D., *Impact of CFRP Adhesive joints for the Automotive Industry*. 2015, Master Thesis, Faculdade de Engenharia da Universidade do Porto.
59. Materials., A.S.f.T.a., *D3433-99: Standard test method for fracture strength in cleavage of adhesives in bonded metal joints.* 1999: Annual Book of ASTM Standards 2000;15(06):226–32.
60. Sato, C. and K. Ikegami, *Strength of adhesively-bonded butt joints of tubes subjected to combined high-rate loads.* The Journal of Adhesion, 1999. **70**(1-2): p. 57-73.
61. Murakami, S., et al., *Strength of cylindrical butt joints bonded with epoxy adhesives under combined static or high-rate loading.* International Journal of Adhesion and Adhesives, 2016. **67**: p. 86-93.
62. da Silva, L.F., et al., *Testing adhesive joints: best practices*. 2012: John Wiley & Sons.
63. ISO, B., *15024: 2001.* Fibre-reinforced plastic composites. Determination of mode I interlaminar fracture toughness, GIC, for unidirectional reinforced materials. BSI, 2002.
64. de Moura, M., R. Campilho, and J. Gonçalves, *Pure mode II fracture characterization of composite bonded joints.* International Journal of Solids and Structures, 2009. **46**(6): p. 1589-1595.

65. Campilho, R.D.S.G., *Repair of composite and wood structures*. 2009, Instituto Superior de Engenharia do Porto.
66. ASTM, D., *1002.* Standard Test Method for Apparent Shear Strength of Single-Lap-Joint Adhesively Bonded Metal Specimens by Tension Loading (Metal-to-Metal), 2005. **15**: p. 45-48.
67. *ISO 4587: Determination of tensile lap-shear strength of rigid-to-rigid bonded assemblies.* 1995.
68. da Silva, M.R.G., *Impact of mixed adhesive joints for the automotive industry.* 2015.
69. 294-3, I., *Plastics-injection moulding of test specimens of thermoplastic materials, part 3: small plates.* 2002: Switzerland.
70. ISO, E., *62 (2008).".* Plastics. Determination of water absorption," EU adoption of International Organization for Standardization, Geneva, Switzerland.
71. da Silva, L.F.M. and C. Sato, *Design of adhesive joints under humid conditions*. Vol. 461. 2013: Springer.
72. da Silva, L.F.M., *Handbook of adhesion technology*. 2011: Springer Science & Business Media.
73. Parker, B., *Some effects of moisture on adhesive-bonded CFRP-CFRP joints.* Composite structures, 1986. **6**(1-3): p. 123-139.
74. Lee, M.C. and N.A. Peppas, *Models of moisture transport and moisture-induced stresses in epoxy composites.* Journal of Composite Materials, 1993. **27**(12): p. 1146-1171.
75. Kumar, S., I. Sridhar, and S. Sivashanker, *Influence of humid environment on the performance of high strength structural carbon fiber composites.* Materials Science and Engineering: A, 2008. **498**(1-2): p. 174-178.
76. Lin, Y. and X. Chen, *Moisture sorption–desorption–resorption characteristics and its effect on the mechanical behavior of the epoxy system.* Polymer, 2005. **46**(25): p. 11994-12003.
77. Crank, J., *The Mathematics of Diffusion: 2d Ed*. 1975: Clarendon Press.
78. Loh, W., et al., *Modelling anomalous moisture uptake, swelling and thermal characteristics of a rubber toughened epoxy adhesive.* International journal of adhesion and adhesives, 2005. **25**(1): p. 1-12.

79. Ameli, A., et al., *Hygrothermal properties of highly toughened epoxy adhesives.* The Journal of Adhesion, 2010. **86**(7): p. 698-725.

80. Zhang, Y., R. Adams, and L. da Silva, *A rapid method of measuring the glass transition temperature using a novel dynamic mechanical analysis method.* The Journal of Adhesion, 2013. **89**(10): p. 785-806.

81. Rittel, D., *On the conversion of plastic work to heat during high strain rate deformation of glassy polymers.* Mechanics of Materials, 1999. **31**(2): p. 131-139.

82. De Moura, M., R. Campilho, and J. Gonçalves, *Crack equivalent concept applied to the fracture characterization of bonded joints under pure mode I loading.* Composites Science and Technology, 2008. **68**(10): p. 2224-2230.

83. De Moura, M., J. Gonçalves, and A. Magalhães, *A straightforward method to obtain the cohesive laws of bonded joints under mode I loading.* International Journal of Adhesion and Adhesives, 2012. **39**: p. 54-59.

84. Da Silva, L.F.M. and A. Öchsner, *Modeling of adhesively bonded joints*. 2008: Springer.

85. Saldanha, D., et al., *Mechanical characterization of a high elongation and high toughness epoxy adhesive.* International Journal of Adhesion and Adhesives, 2013. **47**: p. 91-98.

86. Wang, Y. and J. Williams, *Corrections for mode II fracture toughness specimens of composites materials.* Composites Science and Technology, 1992. **43**(3): p. 251-256.

87. Yoshihara, H. and T. Kawamura, *Mode I fracture toughness estimation of wood by DCB test.* Composites Part A: applied science and manufacturing, 2006. **37**(11): p. 2105-2113.

88. De Moura, M., et al., *Cohesive and continuum mixed-mode damage models applied to the simulation of the mechanical behaviour of bonded joints.* International Journal of Adhesion and Adhesives, 2008. **28**(8): p. 419-426.

89. Dias, G., et al., *Cohesive laws of composite bonded joints under mode I loading.* Composite Structures, 2013. **106**: p. 646-652.

90. Silva, F.G., et al., *Determination of cohesive laws in wood bonded joints under mode I loading using the DCB test.* Holzforschung, 2013. **67**(8): p. 913-922.

91. Banea, M., L.d. Silva, and R. Campilho, *Effect of temperature on tensile strength and mode I fracture toughness of a high temperature epoxy adhesive.* Journal of Adhesion Science and Technology, 2012. **26**(7): p. 939-953.

92. Chaves, F., *Fracture mechanics applied to the design of adhesively bonded joints.* PhD, FEUP, Porto, 2013.
93. Banea, M., L. da Silva, and R. Campilho, *High temperature adhesives for aerospace applications.* Annals of" Dunarea de Jos" University of Galati. Fascicle XII: Welding Equipment and Technology, 2012. **23**: p. 16-20.
94. Silva, F., et al., *Determination of cohesive laws in wood bonded joints under mode II loading using the ENF test.* International Journal of Adhesion and Adhesives, 2014. **51**: p. 54-61.
95. de Moura, M.F., *Numerical simulation of the ENF test for the mode-II fracture characterization of bonded joints.* Journal of adhesion Science and Technology, 2006. **20**(1): p. 37-52.
96. Carlsson, L., J. Gillespie, and R. Pipes, *On the analysis and design of the end notched flexure (ENF) specimen for mode II testing.* Journal of composite materials, 1986. **20**(6): p. 594-604.
97. Xavier, J., et al., *Determining mode II cohesive law of Pinus pinaster by combining the end-notched flexure test with digital image correlation.* Construction and Building Materials, 2014. **71**: p. 109-115.
98. de Moura, M., et al., *Mode II fracture characterization of a hybrid cork/carbon-epoxy laminate.* Composites Part B: Engineering, 2015. **76**: p. 44-51.
99. Campilho, R.D., et al., *Modelling adhesive joints with cohesive zone models: effect of the cohesive law shape of the adhesive layer.* International Journal of Adhesion and Adhesives, 2013. **44**: p. 48-56.
100. Machado, J., et al., *Numerical study of the behaviour of composite mixed adhesive joints under impact strength for the automotive industry.* Composite Structures, 2018. **185**: p. 373-380.
101. Needleman, A., *A continuum model for void nucleation by inclusion debonding.* Journal of applied mechanics, 1987. **54**(3): p. 525-531.
102. Camacho, G.T. and M. Ortiz, *Computational modelling of impact damage in brittle materials.* International Journal of solids and structures, 1996. **33**(20-22): p. 2899-2938.
103. Banea, M.D., L.F. da Silva, and R. Campilho, *Effect of temperature on the shear strength of aluminium single lap bonded joints for high temperature applications.* Journal of Adhesion Science and Technology, 2014. **28**(14-15): p. 1367-1381.

104. da Silva, L.F. and R.D. Campilho, *Advances in numerical modelling of adhesive joints*, in *Advances in numerical modeling of adhesive joints*. 2012, Springer. p. 1-93.

105. Araújo, H.A.M., *Impact and Damping Behaviour of Composite Adhesive Joints.* 2016.

106. Machado, J., et al., *Mode I fracture toughness of CFRP as a function of temperature and strain rate.* Journal of Composite Materials, 2017. **51**(23): p. 3315-3326.

107. Machado, J., et al., *Mode II fracture toughness of CFRP as a function of temperature and strain rate.* Composites Part B: Engineering, 2017. **114**: p. 311-318.

Paper 1

Content of Paper 1

Abstract

1. Introduction

2. Procedures for impact testing of adhesive and adhesive joints

2.1. Procedures for impact testing of adhesives

2.2. Procedures for impact testing of adhesive joints

3. Mechanical behaviour of adhesives under large strain rates

3.1. Effect of the strain rate on tensile and shear properties of adhesives

3.2. Effect of the strain rate on the fracture toughness of adhesives

4. Mechanical behaviour of adhesive joints at large strain rates

4.1. Influence of adhesive and substrate properties

4.2. Effect of adhesive thickness

5. Influence of environmental effects on the impact behaviour of adhesive joints

5.1. Influence o thermal effects on the impact strength of adhesive joints

5.2. Influence of aging on the impact strength of adhesive joints

5.3. Impact fatigue of adhesive joints

6. Modelling the impact behaviour of adhesive joints

6.1. Constitutive modelling of the strain rate dependency of adhesives

6.1.1. Voight/Maxwell models

6.1.2. Cowper-Symonds

6.1.3. Johnson-Cook

6.1.4. Creep curves and isochronous stress-strain curves

6.2. Impact modelling of adhesive joints

6.2.1. Model configurations

6.2.2. Failure load prediction

7. Practical applications

7.1. Automotive

7.2. Ballistics and armour

8. Summary and future trends

References

THE JOURNAL OF ADHESION
2018, VOL. 94, NO. 6, 421–452
https://doi.org/10.1080/00218464.2017.1282349

Taylor & Francis
Taylor & Francis Group

Check for updates

Adhesives and adhesive joints under impact loadings: An overview

J. J. M. Machado[a], E. A. S. Marques[a], and Lucas F. M. da Silva [a,b]

[a]Instituto de Ciência e Inovação em Engenharia Mecânica e Industrial (INEGI), Rua Dr. Roberto Frias, Porto, Portugal; [b]Departamento de Engenharia Mecânica, Faculdade de Engenharia, Universidade do Porto, Rua Dr. Roberto Frias, Porto, Portugal

ABSTRACT

The study of the behaviour of adhesive joints under impact loadings is a very active field of research, driven by significant industrial interest. Many industries, such as the automotive industry, are currently employing adhesive joints extensively, making use of the inherent properties of adhesive joints to improve the mechanical behaviour, reduce weight, and simplify manufacturing. Reduced structural weight is achieved by combining multiple lightweight materials, which is made possible by using adhesive joints. Impact strength is also a major factor, as vehicles must be able to provide adequate safety levels for their occupants during collisions. Another example of industrial application is the defence industry, which uses bonded structures to withstand ballistic impacts, with extremely high impact velocities. Understanding the behaviour of adhesive joints under impact is, therefore, crucial for designing stronger and safer structures. This document aims to review the research that has been previously undertaken in this field. Discussed research topics include high strain rate property determination, adhesive joint testing, effects of coupling environmental conditions with impact loads, and sections on numerical and constitutive modelling procedures. The final sections describe some practical applications of adhesive joints under large strain rates and relate them to the fundamental concepts previously discussed.

ARTICLE HISTORY
Received October 18 2016
Accepted January 11 2017

KEYWORDS
Fatigue; fracture toughness; impact; joint design; strain-rate; stress analysis

1. Introduction

Adhesive bonding is a joining method where an adhesive material is used to create a strong mechanical connection between two components, known as substrates. While many other structural joining methods are available (such as fastening, welding or riveting), adhesive bonding exhibits some particularly interesting advantages over these methods [1–3]. Adhesive joints have been shown to exhibit a very smooth stress distribution along the bonded length which translates into higher fatigue resistance. Bonded structures are also very light, can be relatively cheap to manufacture, and are able to sustain significant damage before the total

CONTACT Lucas F. M. da Silva lucas@fe.up.pt Engenharia (FEUP), Universidade do Porto, Rua Dr. Roberto Frias, 4200-465 Porto, Portugal.

Color versions of one or more of the figures in this article can be found online at www.tandfonline.com/gadh.

© 2018 Taylor & Francis

failure [4]. The ability to effectively join dissimilar materials is perhaps one of the most important advantages as it allows the use of lightweight materials, such as composites that cannot be joined using other conventional methods. Advances in chemical formulations of adhesives coupled with an ever increasing demand for structures with a very high strength to weight ratio has led to a steady increase in the use of adhesive joints. Adhesive joints are now in use in several industries, such as automotive, aerospace, defence, electronics, and naval [5].

Many of these industries manufacture products that are expected to perform adequately under sustained impact loadings. This directly creates the necessity to understand and optimise the behaviour of adhesive joints under high strain rate loads. This is not straightforward, as the mechanical behaviour of materials can vary significantly with the strain rate. Therefore, to fully understand the mechanical behaviour of a joint under impact, the first challenge that arises is the need to fully characterise the behaviour of the joint materials as a function of the strain rate.

The behaviour of adhesives under impact is a very complex subject. One of the reasons for this complexity is the difficulty in experimentally replicating high strain rate conditions and also the high costs associated to testing, as the setups usually require high-performance sensors and data logging systems. Nevertheless, experimental testing is fundamental, as it provides more accurate results which in several cases can even be considered unpredictable and unexpected [3], as the properties can change drastically depending on the strain rate. For example, an adhesive with a non-brittle behaviour under static or quasi-static conditions can exhibit a brittle behaviour when an abrupt loading is applied. This has a direct consequence on the energy absorbing capabilities of a joint [1,3].

To determine the behaviour of an adhesive at large strain rates, impact tests can be performed on bulk adhesives. They can be part of the design process or to check the properties of an adhesive as a quality control [1]. Impact testing is also extensively performed on complete joints, those including the adhesive and the substrates. These joints more closely approximate the behaviour of real structures and the interactions between all the components of the joints. These are usually employed to validate energy absorption, effectivity of surface treatments, type of failure obtained, among many other aspects.

The properties obtained using these characterisation procedures can then be used in analytical or numerical models and applied on the design and analysis of structures undergoing impact conditions. However, in order to achieve reliable and accurate predictions, determination of full material properties is not the only required step. The selection of a suitable model for the material behaviour is fundamental and must be taken into account before any practical implementation is made.

This review offers a discussion of the most important topics related to the use of adhesives under impact conditions. It is divided into various sections,

each discussing one of these topics. After a short discussion on the methods available to test adhesives and adhesive joints at large strain rates, the document presents two sections describing the influence of the strain rate on the mechanical behaviour of adhesives and adhesive joints. Sections on the influence of environmental factors are presented next, including temperature, aging, and impact fatigue. A section on modelling topics is also included in this work. The initial part of this section describes some of the existing constitutive modelling approaches that can be employed to dynamically model the behaviour of adhesives and adhesive joints. The second part is focused on numerical modelling, using finite element analysis (FEA) and its related techniques. Lastly, two practical application examples are given, explaining the particular demands of each application and the techniques and materials used to solve each particular problem.

2. Procedures for impact testing of adhesives and adhesive joints

As discussed in the introductory section of this document, the capability of a material or structure made either from a single, or a combination of materials, to withstand an abrupt loading is of extreme importance in a wide variety of applications. To successfully design joints that are able to safely support dynamic loadings, it is, therefore, fundamental to assess the strain rate dependency of the materials used (both substrates and adhesives) and also to test the actual impact behaviour of a complete joint (substrates and adhesive bonded together) [6]. A variety of impact tests has, therefore, been devised for applying the sudden impact loading and using various parameters to evaluate the joint performance. Several of these procedures have been adopted as standard industry methods while others are employed mainly as a research procedure [7].

Impact testing procedures can be divided into two main groups, distinguishing between the impact tests performed in order to determine the intrinsic properties of the adhesive and those that aim to test the behaviour of a complete adhesive joint.

2.1. *Procedures for impact testing of adhesives*

Knowledge of several properties of a given adhesive is fundamental to enable the design of an adhesive joint under impact conditions. Among the most important properties are the tensile and shear stiffness, the tensile and shear strength, and the fracture toughness (in mode I, mode II, or mixed mode).

Several impact testing methods are described in the literature, usually these consist in quasi-static testing procedures adapted to function in conjunction with drop weight impact testing machines or Split Hopkinson Pressure Bar (SHPB) testing machines, which are able to achieve high strain rates.

Table 1. Mechanical properties and respective experimental procedures used for impact testing of adhesives.

Measured properties	Tests
Tensile stiffness and strength	Tensile test
Shear stiffness and strength	TAST, Torsion, ARCAN
Fracture toughness (Mode I)	DCB, ATDCB, SENB, CT
Fracture toughness (Mode II)	ENF
Fracture toughness (Mixed mode)	Custom specimen designs

The basic strain rate dependent properties of the material (stiffness, yield stresses, and elongation) can be derived from tensile and shear tests performed at high testing rates. Tensile tests are mainly performed on tensile specimens solely comprised of bulk material [8], while shear tests can be performed on a variety of specialised specimens, such as the Thick Adherend Shear Test (TAST) [9], the torsion test [10], or the Notched plate shear method (Arcan) test [8]. Very large strain rates usually require the use of non-contact extensometers to assess the material extension.

The determination of fracture toughness of adhesives under impact is also an important research topic and several different experimental are described in the literature. For mode I testing, the use of the standardised Double Cantilever Beam (DCB) is extremely widespread [11], although other techniques are commonly used, such as the Asymmetric Tapered Double Cantilever Beam (ATDCB) [12], Single Edge Notched Bend (SENB) [13,14], and the Compact Tension (CT) [15] specimen. Mode II fracture toughness determination methods are less varied, with the End-Notched Flexure tests (ENF) being by far the most common. Despite its importance, very few authors present solutions to test mixed mode fracture toughness under impact conditions as these require very specialised specimens and testing setups [16]. All these specific tests allow the determination of several mechanical properties of adhesives for a given strain rate, which can be combined into a numerical model of the adhesive. The material properties and relevant experimental tests are summarised in Table 1.

2.2. *Procedures for impact testing of adhesive joints*

The tests described in the previous section are fundamentally used in materials research and their experimental procedures aim to isolate the properties of the adhesive from other factors. However, in many cases it is also important to assess the impact behaviour of an adhesive joint, where other effects such as the adherent properties, surface preparation, joint geometry among others are also important. These impact tests on adhesive joints are especially useful for use in industrial applications as they allow the assessment of the combined influence of all the parameters that govern joint strength.

Table 2. Impact test classification according to crosshead speed.

Test classification	Testing speed	Suitable test equipment
Low velocity	Up to 5 m/s	Pendulum impact tester
Medium Velocity	Between 5 and 10 m/s	Drop weight tester
High velocity	Between 10 and 100 m/s	SHPB tester

Impact tests of adhesive joints are usually categorised in three ranges, divided in terms of velocity [17], as shown in Table 2.

In the low velocity range, the problems can be treated as a vibrating system, in medium velocity range, the stress and strain propagates as waves in materials, and in high velocity a body collides with another faster than their sound velocity [1].

Several test procedures are available for testing adhesive joints, such as the Impact Wedge-peel test (IWP) [18], Drop-weight test [19], Block Impact test [20], and SHPB test [21], in order to evaluate joint strength with the aim of measuring the energy and force necessary to break the joints. The joint geometries used in this test are varied, but the most common are the Single Lap Joint (SLJ) [22], Double Lap Joint (DLJ) [23], butt joints [24], rod-ring joints, and hat shaped joints [25].

3. Mechanical behaviour of adhesives under large strain rates

Polymeric materials, among which are included most adhesives, are known to be strain rate-dependent. This is caused by the inherent viscoelastic behaviour of the polymeric structures, which makes their mechanical behaviour highly sensitive to the loading rates [25]. To quantify this effect, considerable research work has been devoted to measure the high strain rate properties of adhesives [7]. In this section, the results of experimental studies on the effect of strain rate on the mechanical properties of adhesive materials are described, focusing on tensile, shear and fracture properties of these materials.

3.1. *Effect of the strain rate on tensile and shear properties of adhesives*

Tardif and Marquis in 1963 [26] and Lindholm in 1964 [27] were among the first to explore the strain rate dependency of polymers. These authors performed compression tests of various plastics at strain rates up to order of 1000 s^{-1}, and observed large increases in modulus and an increase in ultimate stress over the static value, together with a significant reduction in ultimate strain. However, restrictive effects of the higher stiffness pressure bars on the specimen under compression have been shown by Adams and Copendale [28] to result in misleading high values of yield and ultimate stress [7]. Nevertheless, all these early experiments indicated that polymers exhibit noticeable increase in mechanical properties with higher strain rates.

Performing shear tests with TAST specimens, Chalkley and Chui [29] and Zgoul [30] found that the yield stress of the adhesive has a very large strain rate dependency, while the shear modulus was largely unchanged, again suggesting a viscoelastic behaviour. The TAST joints also were found to sustain a higher level of shear load in comparison to SLJ when at the same nominal strain rate, as they are subjected to a higher effective strain rate.

Several other different tests have been used to demonstrate the strain rate sensitivity of adhesives. Tension tests [31,32], ARCAN tests [33], tension SHPB [34], torsion SHPB [35], and tensile-compression SHPB [36] tests have all demonstrated the tendency of adhesives to change from a ductile to a brittle behaviour as the strain rate is increased. An increase in the maximum stress is usually coupled with a reduction in elongation. Most of these works report that there is no significant change in elastic or shear modulus.

In several cases, it is necessary to predict mechanical properties over a larger range of strain rates, which can be achieved by extrapolating to strain rates beyond those that can be experimentally tested. The experimental and numerical work of Carlberger *et al.* [37] and Avendaño *et al.* [38] has demonstrated that a logarithmic extrapolation is suitable for this purpose.

3.2. *Effect of the strain rate on the fracture toughness of adhesives*

The improvement of the fracture toughness of adhesives is always an important objective for adhesive manufacturers. Many adhesive users, such as the automotive industry, are constantly demanding tougher adhesives to improve the performance of their products. While there is extensive research in the fracture toughness of adhesives under quasi-statics loads, under impact the published work is considerably more limited. The research on the strain rate dependence of the fracture energy of polymers first started in 1981, with the work of Bascom *et al.* [39]. In this study, Compact Tension (CT) specimens were used to obtain the fracture energies of elastomer-modified epoxy polymers over a range of strain rates from 10^{-2} to 10^{-3} s^{-1}. The authors registered a general decrease in fracture energy within increasing strain rate.

The work of Bitner *et al.* [40] and Hunston *et al.* [41] consisted on a series of tests assessing the relationship between fracture energy and strain rate on rubber toughened epoxy adhesives. Their results indicate that fracture energy decreases substantially as the strain rate increases and that, with regards to fracture energy, decreasing the temperature produces a similar effect to increasing the loading rate. More recently, in 2002, Raghavan *et al.* [42] found similar results for a similar type of adhesive.

In 1994, Lataillade *et al.* [16] developed an experimental device based on the SHPB apparatus, to assess the high strain rate behaviour and fracture energy, G_C, of steel–steel joints bonded with one-part epoxy adhesive, by using the fracture mechanics method. The experimental device allows to

achieve high strain rates subjected to different failure modes (mode I, mode II, and mode I+II), for a range of temperature conditions. For all bondline thicknesses under study, the G_{I+IIC}, G_{IC} and G_{IIC} values were all found to slightly decrease with an increase of strain rate.

Blackman *et al.* [43] in 2000, conducted impact wedge peel testing of a range of structural adhesives (six different types) being used to bond either mild-steel or aluminium–alloy substrates. The results demonstrated that there is a significant reduction of the fracture toughness with an increase in test speed.

Carlberger *et al.* [37] in 2009, performed experiments in a peel mode (1000 mm/s) using DCB specimens and in a shear mode (200 mm/s), using ENF specimens. The authors concluded that in peel mode, the fracture energy increases slightly with the increase of the strain rate and in a shear mode the fracture energy decreases [44], which is in contrast with most of the published work.

Blackman *et al.* [45] in 2009, studied the fracture behaviour of structural adhesives joints (DCB and TDCB) under high strain rates, ranging from quasi-static up to 15 m/s, in mode I. The tests were performed on joints made of an epoxy adhesive and two substrates, a unidirectional carbon-fibre epoxy composite and aluminium. An increase of the test rate over six decades (from 10^{-5} to 10^{1} m/s) decreased the value of the fracture energy, G_{IC}, by approximately about 40% of its quasi-static value, from 3.5 to about 2.2 kJ/m^2. The adhesive fracture energy, G_{IC}, measured at quasi-static loading rates, was revealed to be independent of the substrate material and test geometry. These results were supported by the similar work performed by Karac *et al.* [32] in 2011. Figure 1 shows the results from these works combined in a single graph to illustrate the evolution of G_{IC} with test rate.

The general outlook from these publications is that the fracture energy of structural adhesives generally tends to reduce with the increase of the strain

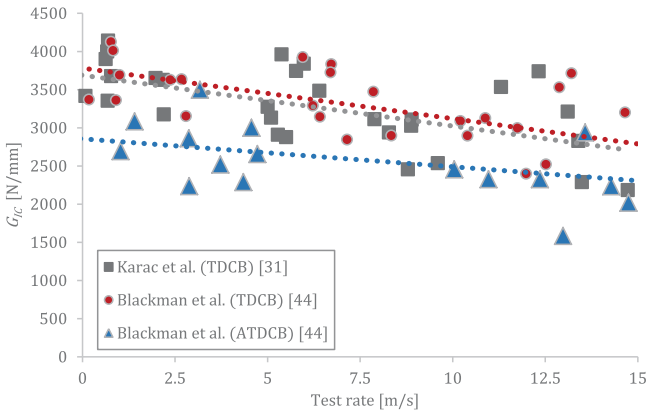

Figure 1. Variation of fracture energy in mode I with the test rate. Adapted from Karac *et al.* [32] and Blackman *et al* [45].

rate. While the basic mechanical properties of adhesives, for example the tensile strength, might increase, the adhesive actually becomes slightly more brittle when subjected to impact loads. This obviously has repercussions in the behaviour of complete adhesive joints, which is described in the following section.

4. Mechanical behaviour of adhesive joints at large strain rates

The behaviour of adhesive joints under impact is a very complex subject which is a target of many studies that aim to understand the governing factors controlling the impact strength of bonded structures. The properties of the substrate, adhesive, joint geometry, and load type are all significant parameters that influence the strength of an adhesive joint under impact

4.1. *Influence of adhesive and substrate properties*

The previous two sections have clearly demonstrated that strain rate has a very significant effect on the mechanical properties of adhesives. However, adhesives are only one component of adhesive joints, and it is the behaviour of the complete assembly that is of interest for a structural designer. A large number of published works have focused on the assessment of the effect of strain rate on the strength of various types of adhesive joints.

The work of Wegman *et al.* [46,47] in 1963 and 1966 is among the first of such studies. By impact testing butt joints, the modification of epoxy adhesives with the introduction of flexibilisers and plasticisers was found to lead to an increase of the absorbed impact energy and impact strength. The difference between the dynamic and static strength was found to depend on the adhesive composition and that generally, rigid adhesives exhibited a smaller percentage change. This behaviour of butt joints was further studied by Wada *et al.* [48] and Hayashida *et al.* [49]. In the following decades, several other authors have confirmed that the strain rate sensitivity of adhesives can lead to increases in joint strength for various types of joints, such as SLJ [50–53], DLJ [54–57], hat joints [58,59], and pin and bush joints [60].

One of the earliest studies on the effect of the substrate properties was conducted by Perry [61] in 1959. By using an instrumented pendulum rig in order to measure the failure load and energy absorption of butt and shear joints, the authors found that the compliance of the metal substrates was substantially larger than that of the adhesive layer. Consequentially, the values of absorbed energy from impact tests on adhesive joints did not necessarily reflect the energy absorbing capabilities of the adhesive itself, but rather of the complete joint. This relationship between adhesive and substrate was further studied by Beevers and Ellis in 1984 [22]. The authors found that in joints with thin and ductile substrates and bonded with a

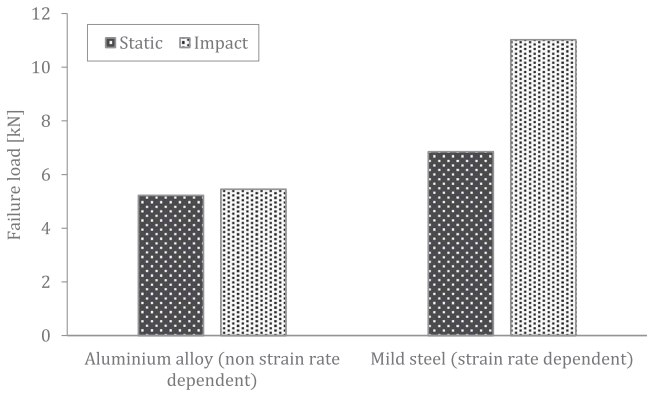

Figure 2. Effect of the strain rate in failure load for two types of substrates. Adapted from Beevers and Ellis [22].

sufficiently strong adhesive, the joint failure has a close relation with the onset of yield in the substrate. Figure 2 demonstrates the results found in this work.

Harris and Adams in 1985 [62] tested more substrates and adhesives types, reinforcing the conclusion that the energy absorption was not directly provided by the adhesive, but is derived instead from the plastic deformation of the substrate. As a ductile and strong adhesive was being used, the plastic deformation of the substrate at high strain rates is what determined the failure load and absorbed energy. High strength substrates produced high failure loads but very low absorbed energy while the opposite occurred for more ductile substrates. Figure 3 and Figure 4 show some of the most important results from this work.

Figure 3 clearly shows that the soft aluminium used in this work is strain rate sensitive. The failure is caused by adherend yielding, which occurs at the same static and impact loads. It also demonstrates that tough, flexible adhesives enable higher failure loads.

Figure 4 shows the effect of the adhesive and substrates in the energy absorption process. It is clearly shown that brittle adhesives break very easily and are unable to plastically deform the metal substrates, leading to very small absorbed energy. In contrast, ductile adhesives are able to hold the joint together during the impact and enable large energy absorption, especially when used in conjunction with, low strength, ductile substrates.

Yokoyama *et al.* [63] in 2003 studied the behaviour of butt joint, with very stiff substrates of two different materials. Their work has shown that if there is no plastic deformation of the substrates, the energy absorption of joint at large strain rates remains constant or can even reduce with an increase in the strain rate. The same phenomenon was described by Clarke *et al.* [64] in the case of SLJ impact testing.

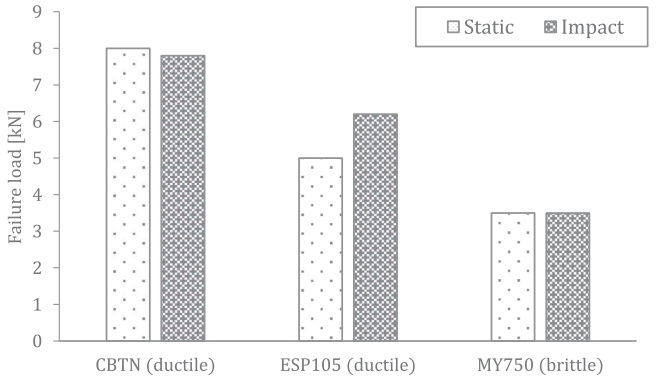

Figure 3. Effect of the strain rate in failure load of joints with soft aluminium substrates and three different adhesives. Adapted from Harris and Adams [62].

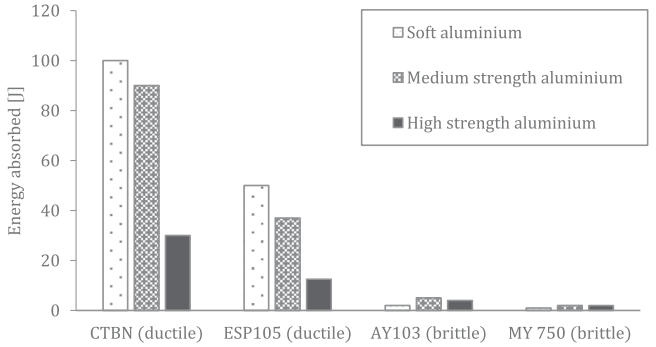

Figure 4. Effect of the strain rate in absorbed energy for three types of substrates and two adhesives. Adapted from Harris and Adams [62].

The impact strength of joints using composite substrates can also be highly dependent on substrate properties. In 2012, Galliot e al. [65] studied joints using carbon fibre composite substrates under impact, with varied fibre orientations. For all cases, the failure was found to be caused by delamination in the substrate and the increase in strength under impact was mostly caused by the strain rate dependency of the composite resin. Several studies were performed demonstrating that the resin matrix of a carbon fibre composite exhibits significant strain rate dependency [66–68].

The impact strength of joints using dissimilar substrates was studied by Sankar *et al.* [69] in 2015, where the dynamic impact of split-cylinder lap joints was studied using a SPHB apparatus and two types of substrates, steel and aluminium. The main conclusion derived from this work was that for dissimilar adherends it is the less stiff adherend that controls the joint strength and energy absorption. This is a phenomenon that has parallels with similar static behaviour, identified by Reis *et al.* [70] in 2011.

Avendaño *et al.* [38] conducted a study concerning the characterisation of the impact strength of a resistant epoxy adhesive as a function of temperature and showed that for joints using steel substrates, the steel strength determines the failure load of SLJs at room temperature. This is due to the high degree of substrate yielding that absorbs most of the impact energy.

It can be concluded that the strength and energy absorption of an adhesive joint under impact conditions is fundamentally governed by substrate ductility when low strength materials are used. The adhesive itself, independently of its properties, is only able to provide a small contribution on the total absorbed energy of a joint. Joints bonded with low ductility adhesives typically exhibit small failure loads and reduced energy absorption as they are unable to maintain the joint cohesion during the impact process. High energy absorption is achieved for tough adhesives used in conjunction with ductile adherends (low strength aluminium or mild steel). High strength adherends bonded with tough adhesives provide high joint strength but are unable to significantly absorb energy.

4.2. *Effect of adhesive thickness*

A very important parameter in adhesive joint design is the thickness of the adhesive layer. Although there are considerable published data regarding the influence of adhesive thickness under static conditions [71,72], for large strain rates there is limited information. In 1998, Bezemer *et al.* [25] used rod-ring type specimens to load a stiff epoxy and a ductile polyurethane adhesive under shear. The optimum bondline thickness for energy absorption was found to be 0.25 mm for the epoxy and 1 mm for the polyurethane. Figure 5 shows the data from this work.

For SLJ specimens bonded with an epoxy adhesive, Goglio and Rossetto [73] found that a thickness of 0.5 mm provided higher strength than 1 mm thickness. These values are generally similar to those identified for static testing where stiff adhesives behave optimally for thicknesses around 0.2 mm [72] and flexible adhesives should be used in 1 mm thick layers [74]. The work of Yokoyama [63,75] and Yokoyama and Shimizu [76] for pin-and-collar specimens bonded with a cyanoacrylate adhesive identified optimum thicknesses ranging between 0.025 mm and 0.035 mm, below the maximum recommended bondline thickness for anaerobic adhesives, which is 0.05 mm [17].

5. Influence of environmental effects on the impact behaviour of adhesive joints

Most adhesively bonded structures are expected to undergo severe environmental conditions during their lifecycles, such as extreme temperatures and adhesive aging caused by water absorption. If such structures are also

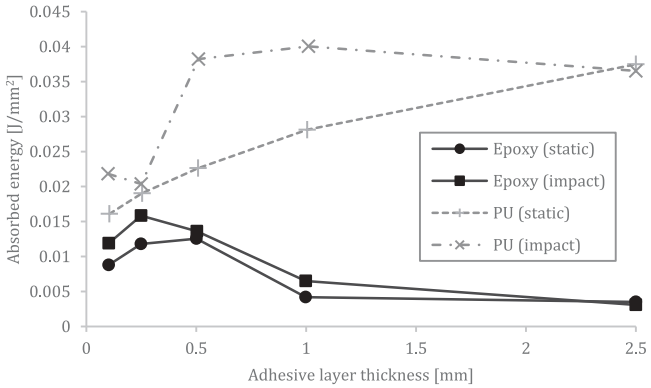

Figure 5. Effect of adhesive layer thickness on energy absorption. Adapted from Bezemer *et al.*[25].

intended to sustain impact loads, it becomes mandatory to comprehend in detail how the combination of dynamic behaviour and durability of the adhesive bonded joints affects the joint behaviour.

5.1. *Influence of thermal effects on the impact strength of adhesive joints*

Temperature variations cause marked changes of the adhesive properties and subsequently lead to significantly different adhesive joint behaviour. Several studies have focused on the effect of temperature on the impact strength of adhesive joints. Their results are discussed in this section.

The work of Bauwens [77] in 1972, built upon the earlier observations of Ree and Eyring [78], was among the first to explore the relationship between the yield stress and loss tangent of a polymeric material with the range of temperature and strain rate at which secondary relaxation occurs. By using measurements from the loss tangent, as a function of temperature and at the frequency corresponding to the strain rate, it was possible to compute compression yield–stress curves, giving the yield stress versus temperature at constant strain rate, which was found to fit the experimental data.

In 1996, Cayssials *et al.* [79] performed tests on the shear yield behaviour of epoxy joints bonded with steel substrates. It was determined that the yield stress of the joint is greatly influenced by the temperature, as well as the energy and the yield strain. The authors have also established a correlation between high impact strength and the presence of the mechanical loss peak in the range of the explored strain rate.

In 2000, Blackman *et al.* [43] conducted a study on the evaluation of the fracture toughness of six different adhesives, using TDCB specimens. Tests were undertaken at temperatures of –40°C and 23°C. It was found that for high testing

speeds (2 m/s) the fracture energy in mode I decreased with a corresponding decrease in temperature. This was evident for all the adhesives tested.

The work of Xu and Dillard [80], published in 2003, studied the behaviour of DCB joints bonded with electrically conductive adhesives subjected to falling wedge-peel tests. An impact velocity of 1.6 m/s was used and DCB specimens were tested at several temperatures, namely, –70°C, room temperature, 60°C and 90°C. The authors found that the impact fracture energy for a given temperature follows a logarithmic relationship with the corresponding loss factor. An increased loss factor was shown to result in improved impact performance. This underlines the fact that thermally induced physical changes in the polymer structure have a significant influence on the joint strength.

In 2003, Srivastava [81] tested SLJ made of a two-component thixotropic adhesive and two different substrates under the effect of temperature and strain rate separately (in quasi-static regime). The main conclusion from this research was that the bond strength decreased by 40–50% at 300°C, revealing an increase with strain rate.

Adamvalli and Parameswaran [82] in 2008 assessed the dynamic strength at different loading rates and temperatures, varying between 25 to 100°C, of SLJ with titanium substrates and an epoxy adhesive. The authors used a SHPB setup in compression in order to load the joint dynamically. The increase of temperature was found to cause the dynamic strength to decrease. At a temperature of 100°C, the dynamic strength is 35% lower when compared to that obtained at 25°C, and it is 50% greater when compared with the static strength at room temperature. The dynamic strength at high temperature was found to be higher than the quasi-static strength at ambient temperature.

In 2009, Carlberger *et al.* [37] assessed the influence of temperature (between –40 °C and 80 °C) and strain rate on the mode I and mode II fracture toughness of a structural epoxy adhesive (Betamate XW1044-3 from DOW Automotive). Although the combined testing of the effects of strain rate and temperature was not performed, the authors used the results to conclude that the viscoelastic nature of the adhesives allows for a good amount of correlation between the effect of temperature and the effect of strain rate in the fracture toughness. It is even postulated that if the correct correlations are established, it might be possible to replace impact tests with temperature testing.

In 2016, Avendaño *et al.* [38] published a work regarding the impact and quasi-static behaviour of SLJ specimens for the automotive industry as a function of temperature (from –30°C to 80°C). The joints were bonded using an acrylic adhesive and a crash resistant epoxy adhesive with CFRP and biopolymer adherends. The authors concluded that the higher the temperature, the higher the ductility of the materials and therefore, the higher its

strain rate dependence. This causes the failure loads at impact to be much higher than those under quasi-static conditions.

All the discussed works have shown that there is strong influence of temperature on the impact strength of adhesive joints. Testing at temperatures below room temperature shows a decrease in joint toughness of the adhesive while testing above room temperature was found to reduce joint strength. These phenomena are directly related to thermally induced physical changes in the polymer structure, such as the glass transition temperature and the loss factor, and are equivalent to those found during quasi-static testing [83]. The existence of a correlation between the thermal effects and strain rate effects was also identified, supported by the viscoelastic nature of adhesives.

5.2. *Influence of aging on the impact strength of adhesive joints*

The main factor causing aging of adhesive joints (loss of mechanical properties over time) is water absorption [84]. If adhesive joints operate in highly humid environments, moisture penetrates the adhesive and significant changes in properties are expected [85]. As is the case for extreme temperatures, this can translate into low impact strength of the joint [86]. Several studies have been performed on the effect of moisture on adhesive properties and strength of adhesive joints under quasi-static loading, even in combination with temperature effects [87–89].

However, there is very limited data regarding the combined effect of aging and impact loadings. The only known work published in this field was by Zhang *et al.* [90] in 2015. The authors conducted a study with the aim to investigate the impact rate effect on the strength of adhesively bonded SLJ specimens after hygrothermal exposure (periods of 10 or 20 days), which consisted on an environmental condition of 80°C and 95% relative humidity. The specimens, bonded with a crash-toughened epoxy adhesive and two different substrates (high strength steel and aluminium alloy), after exposure to hot-wet conditions, were tested at impact rates ranging from 1.6×10^4 to 12 m/s. For all specimens tested and independently of the substrate material, the presence of moisture caused the degradation on the joint strength. The reduction of joint strength increases noticeable with the aging time. The joint strength was also found to increase with the strain rate, even for specimens with the maximum amount of aging time. However, the specimens which used the aluminium substrates were those who exhibited less increase with the strain rate. An ANOVA study was performed to better understand the correlation between these factors and found that the aging effects and the strain rate are independent and their interaction effect is insignificant. This work, therefore, supports the notion that these two effects can be independently modelled.

5.3. *Impact fatigue of adhesive joints*

The performance and reliability of an adhesively bonded structure can be greatly affected by the occurrence of standard fatigue (SF) [91]. A more severe variation of SF is impact fatigue (IF), which can be caused either by a cyclic repetition of low energy impacts or low velocity impacts. These cyclic impact loads, although being insufficient to cause immediate failure, can cause early failure of the joint after a few cycles. Adding to this damaging effect is the fact that, in several cases, the impact fatigue appears concealed in loading records by non-impact loading cycles with higher amplitudes. Although there is a general understanding of the threat of high-energy impact, not a lot of attention has been given to repetitive impact of structures. The existing models of material behaviour are not sufficient, generally employing quasi-static conditions and isothermal temperatures, to predict the reliability of components when exposed to cyclic loading (fatigue).

In 1984, Usui and Sakata [92] were among the first to publish work on the impact fatigue behaviour of adhesive joints. SLJ specimens bonded with an epoxy adhesive were subjected to impact fatigue loadings using a drop weight. Their results have demonstrated that impact-fatigue strength of the joints was dependent on the magnitude of stress and the loading time. Casa-Rodriguez *et al.* [93] in 2007 considered the behaviour of adhesive joints subjected to low-velocity impacts using a pendulum, with the aim to evaluate the IF life and to compare this loading regime with SF (*i.e.* non-impacting, constant amplitude, sinusoidal fatigue). It was demonstrated that the multiple impacting tensile loads are an extremely damaging load regime when compared to standard fatigue. The specimens used were SLJ specimens with aluminium substrates (7075-T6) and rubber toughened adhesive (FM 73M from Cytec Ltd.). The conclusion obtained from the experimental results is that the IF tests of SLJ specimens revealed more damage than the SF.

In 2008, Casa-Rodriguez *et al.* [94,95] investigated and evaluated the behaviour of lap-strap joints (LSJ), with CFRP substrates, under the influence of three fatigue regimes, namely, SF, IF, and a combination of the two types of regimes (CSIF). The specimens were bonded using a rubber modified epoxy adhesive. The occurrence of fatigue fracture at very low load amplitudes was observed for the IF regime.

In 2009, Silberschmidt *et al.* [96] studied the impact fatigue in adhesive joints using two types of substrates, an aluminium alloy and CFRP bonded in LSJ specimens, respectively for fatigue life experiments and fatigue crack growth studies, both in SF and IF regimes. The authors also used two distinct combinations of adhesives regarding the type of test being performed, namely, an epoxy adhesive/primer for aluminium specimens and an epoxy film adhesive for the CFRP. The authors concluded that a decrease of the maximum load parameter for quasi-static (or single impact) loading

conditions, which is more than sufficient for SF, does not assure the integrity of a structure under impact loading condition. In the IF regime, the potential to initiate a crack and to quickly propagate, at levels of loading factors that are significantly lower than quasi-static and dynamic strengths or even the durability limit of joints, is largely increased.

Kemiklioglu *et al.* [97] in 2015 conducted a study using SLJ specimens on the strength comparison under single and repeated impacts of ductile and brittle adhesives using a drop weight impact machine. The authors used as substrate glass fibre epoxy and brittle and ductile adhesives. This study showed that for a given energy, the load sustained by the joint changes with the number of impact loads. For the brittle adhesive, the load on the specimen was found to be higher after repeated impacts, while for the case of the ductile adhesive the load after multiple impacts was lower than the load measured during a single impact.

While limited, the work performed in the field of impact fatigue has generally shown that this is a highly damaging type of loading, where relatively small but repeated loads can cause early failure. It is suggested that the mechanical properties of the adhesive can influence this behaviour, however there is not extensive data to fully support this statement.

6. Modelling the impact behaviour of adhesive joints

To enable the use of adhesives in the design of energy absorbing structures, it is fundamental for designers to have at their disposal methods that allow the prediction of joint strength under impact [98]. For instance, the automotive industry can use these models to validate the crash worthiness of an adhesively bonded structure without the need to carry out expensive mechanical testing. In this section a review is made of the state of the art on modelling the behaviour of adhesive and adhesive joints under large strain rates. It is divided into two sections, the first discusses the work performed in modelling the strain rate dependent mechanical response of adhesives while the second section focuses on the approaches used to model complete bonded joints.

6.1. *Constitutive modelling of the strain rate dependency of adhesives*

The prediction of dynamic strength of adhesive joints is extremely important for various users of this technology. The use of a numerical model suitable for modelling adhesive joints allows the calculation of the stresses and strains, that are present on the adhesive and substrates. As previously shown in Section 0, adhesives can exhibit viscoelastic and viscoplastic behaviour, which can be represented using a constitutive model.

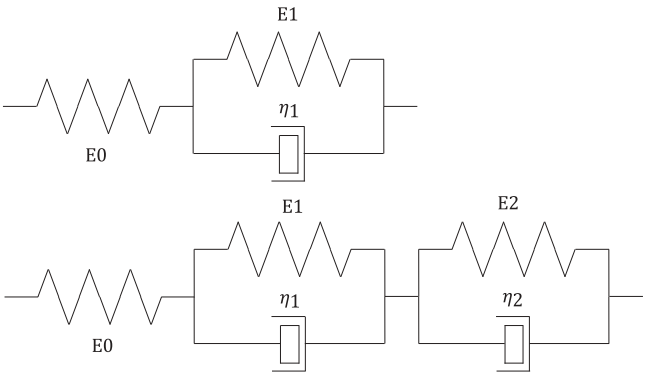

Figure 6. Example of a three element and a five element Voigt viscoelastic model, adapted from Sato and Ikegami [99].

6.1.1. *Voigt/Maxwell models*

The elastic deformation of an adhesive as a function of time can be expressed by Voigt or Maxwell viscoelastic models, which use the sum of stresses on springs and dashpots to model the behaviour of the adhesive. The complexity of these models can be increased by adding additional elements. The parameters used in this model must be determined by experimental observation.

In 2000, Sato and Ikegami [99] conducted a study on the viscoelastic properties of a cured epoxy structural adhesive and attempted to model the dynamic stress of adhesive joints subjected to impact using Voigt models of three and five elements. The authors concluded that the five element Voigt model was able to describe the high rate behaviour of the adhesive and used this model to identify optimum joint geometries. Figure 6 shows a schematic representation of the models used in this work.

Khan *et al.* [100] in 2006 followed a similar approach to model the compressive uniaxial behaviour of a polymer under quasi-static and dynamic operating conditions. Their work used a simple differential form model based on a combination of linear and nonlinear springs. The results were compared with a modified superposition principle. The new model was found to be in good agreement with experimental observations, over a wide range of strain rates and above and below the glass transition temperature regimes. The work of Iwamoto *et al.* [101] in 2010, also employed this type of modelling, with a four element elasto-viscoplastic model being used to model the stress in the joint. The authors were able to successfully express the basic features of the experimental curves of structural adhesives, such as the linear elastic portion, strain softening and strain hardening stages.

6.1.2. *Cowper–Symonds*

A commonly used model for simulating the strain rate dependency of materials is the Cowper–Symonds model [102] material model which can

be characterised as being a simple elasto-plastic and strain rate hardening model which uses the empirical formulation described in a work of Ludwik [103] from 1909, in which materials strengthen when plastic deformations are applied. Goglio *et al.* [36] used this model to fit experimental data of SHPB tests of an epoxy adhesive and obtained reasonably accurate results for high strain rates (above 10^2 s^{-1}). The model was found to be totally unsuitable for smaller rates of deformation.

6.1.3. *Johnson–Cook*

While the Voigt/Maxwell and Cowper–Symonds models are of viscoelastic nature, the Johnson–Cook model [104] is a viscoplastic model which provides a description of the strain rate dependency of equivalent failure strain. Some authors have employed this model to create failure criteria for adhesive materials, such as Morin *et al.* [105]. Goglio *et al.* [36] used this model for SHPB and found that for high strain rates it is not as accurate as the Cowper–Symonds model.*6.1.4. Overstress models*

In these models, the strain rate dependency effect is achieved by allowing the stresses to increase beyond the rate-independent yield surface upon application of a load and then allowing them to relax back to the yield surface over time. In 1989, Kitagawa *et al.* [106] developed a model for describing the rate dependence of a polypropylene based on the Krempl overstress theory for metals [107]. This model was shown to be able to model the viscoelastic properties of polymeric materials, although with some limitations.

In 1995, Chiu *et al.* [108] developed a unified constitutive model for a film adhesive building upon the Kitagawa model and the Ramaswamy [109] unified theory. The model was compared with experimental data and shown to be able to model strain rate dependent behaviour as well as creep and stress relaxation.

In 2001, Crocombe *et al.* [110] have successfully implemented an overstress based model into an ABAQUS finite element code. Based on the previously discussed works of Dean [33] and Crocombe [110], Zgoul and Crocombe [111] employed an overstress based model to predict the strain rate behaviour of SLJ and TAST specimens The overstress model was found to be able to model correctly the response of SLJ specimens, although it failed to predict the behaviour of TAST specimens.

6.1.4. *Creep curves and isochronous stress–strain curves*

A study conducted by Crocombe [112] in 1995 studied the modelling and prediction of the rate-dependent strength of adhesive joints using creep laws and isochronous stress–strain curves with a commercial software package. The author found that creep curves are not suitable for the purpose of modelling ramped strain rates (typical of impact loads) as they require a

considerable amount of time steps to reach an accurate solution. In contrast, a solution based on isochronous stress–strain curves derived from experimental data was shown to be effective for the material and configuration under study.

6.2. *Impact modelling of adhesive joints*

Numerical modelling of the impact behaviour of adhesive joints is currently a very active research topic with direct industrial application. The evaluation of new designs for crashworthy structures may be streamlined using FEA, reducing the large costs inherent in building or testing prototypes. The literature suggests a variety of models of differing complexity to solve this problem, which can include inertial effects and strain rate dependent properties (derived from experimental data or constitutive models). Dynamic models usually are available in commercial or custom designed finite element analysis (FEA) packages [113] and can perform strain rate dependent stress analysis, aiming to identify areas in the adhesive where stress concentrations, which correspond to locations for failure initiation, are present.

6.2.1. *Model configurations*

The process of modelling the impact behaviour of adhesive joints usually demands the use of dynamical models, as for large strain rates the influence of inertial effects becomes significant and introduces added stresses in the joint. Some authors, such as Harris and Adams [62] have employed models without any type of inertial effects but with strain rate dependent properties, which are valid for smaller rates of loading and small masses. Alternatively, if the materials are not shown to be strain rate sensitive and the impact speeds are high, models with quasi-static property descriptions are used in conjunction with inertial modelling to improve accuracy in stress predictions. This is also valid in joints where adherend yield occurs under impact, as in these joints the adhesive does not have a significant contribution on the behaviour of the joint and most metallic adherends do not exhibit strain rate dependency. Sawa *et al.* [114–116] in 2002 used the DYNA3D software package to model the stress distribution propagation in SLJ specimens under diverse impact loadings. This type of dynamic models is formulated according to Equation (1),

$$[M][A] + [K][U] = [F]. \tag{1}$$

where $[M]$ is the mass matrix, $[A]$ is the acceleration vector, $[K]$ is the stiffness matrix, $[U]$ is the displacement vector, and $[F]$ is the external load vector.

Challita and Othman [23] also employed a three-dimensional FEA dynamical model to assess the stresses present in SHPB testing of DLJ specimens with metal substrates. For both substrates and adhesive, an elastic behaviour

was assumed. Similar modelling work was performed by Hazimeh *et al.* [117] in 2015, but using composite substrates in DLJ specimens.

More complex models combine the inertial effects with strain rate dependent properties, either for the adhesive, the adherends or both. In oer to achieve reliable and accurate predictions of impact behaviour of adhesive joints using numerical models, the material properties used in the model should preferably be determined at the appropriate strain rates values [118–120]. The work of Xia *et al.* [121,122] in 2009 aimed to understand in depth the dynamic failure of weld-bonded joints. The models created by the authors used a fully dynamical analysis that treated the adhesive layer as a rigid link between the two strain rate dependent substrates. Yang *et al.* [123] in 2012 evaluated the application of a simplified finite element for modelling of a toughened adhesively bonded joint. The numerical model employed strain rate dependent data for a toughened epoxy adhesive and for the steel substrates by defining curves of the failure parameters versus the effective strain rate. This was complemented by the addition to the model of strain rate dependent data for the pre-failure properties.

As an alternative to the use of experimentally derived strain rate dependent data, the model can directly employ a constitutive model, such as those described in Section 0. In 2000, Zaera *et al.* [124] used a Cowper–Symmonds based model in a finite difference simulation of the impact behaviour of a bonded ceramic/metal armour. The authors were able to use this relatively simple constitutive model to model the experimental data sufficiently well for preliminary design calculations. The work of Sawa *et al.* [125] in 2008, and Liao *et al.* [126,127] further demonstrated that the use of a Cowper–Symonds constitutive model for the adhesive could model the interface stress distributions in various types of joint geometries.

6.2.2. *Failure load predictions*

The failure criteria of adhesive joints have historically been divided into two main categories. These are the strength of materials approach and the fracture mechanics approach. The strength of materials approach is based on the evaluation of the maximum allowable stresses [128,129] or strains [130,131]. The work of Adams *et al.* [2] has demonstrated that the strength of materials approach is not especially suited for adhesive joints, fundamentally due to the presence of stress singularities that prevent the use of any criteria that limits a maximum stress or strain to predict onset of failure and makes this approach extremely mesh dependent. In contrast, the fracture mechanics approach can be applied to points were singularities exist. However, it requires the knowledge of the critical stress intensity factors which cannot always be easily related to the intrinsic material properties [132]. Another fundamental flaw of this approach is the fact that it assumes that for failure

to initiate, a crack should already be present in the adhesive or substrate, which might not always be the case [133].

Dean *et al.* [134] in 1999 conducted a study with the intention to compare the measured and predicted performance of SLJ specimens under impact conditions (strain rates ranging from 2.10^{-5} to 115 s^{-1}), through the use of a drop weight apparatus. Von Mises and Drucker–Prager models implemented in a FEA were used to predict joint failure. The results indicated that the von Mises yield criterion was not suitable for toughened adhesives, but they indicated that the linear Drucker–Prager model seemed applicable. The authors concluded that for toughened adhesives, an elastic–plastic material model is needed and that this model should employ a yield criterion with sensitivity to the hydrostatic component stress.

Zgoul and Crocombe [111] employed a rate dependent von Mises mode and a rate dependent Drucker–Prager to model the numerical behaviour of SLJ and TAST specimens. All models were implemented in a FEA and the results compared with experimental data. The results were not very satisfactory as the von Mises model was found to be inaccurate as it did not account for hydrostatic sensitivity. The Drucker–Prager model was able to accommodate hydrostatic sensitivity but was reported to have convergence problems.

Recently, the strength of materials and fracture mechanics approaches have been combined in cohesive zone models (CZM), with the aim of minimising the flaws of the strength of materials and fracture mechanics approaches [135]. These models can be successfully employed for thin planes of materials, making them especially well-suited for adhesive joints [136]. These models employ traction-separation laws, which model stiffness and degradation of the element. These laws can exhibit several different shapes, the most common being the triangular and the trapezoidal laws. A schematic representation of a triangular traction-separation law for mode I and mode II is shown in Figure 7.

The work of Carlberger and Stigh, published in 2007 [44], demotrated the validity of using this type of approach to predict impact strength. Authorsuch as Haufe *et al.* [137], May *et al.* [138], Clarke *et al.* [64], Avendaño *et al.* [139] and Neumayer *et al*[140] have shown that modern commercial software packages support the accurate prediction of failure loads using complex dynamical cohesive models with strain rate dependent data.

7. Practical applications

7.1. *Automotive*

Currently, one of the major industrial users of adhesive bonding is the automotive industry. Despite an initial reluctance in employing this technology [141], the automotive industry has steadily increased the use of adhesive

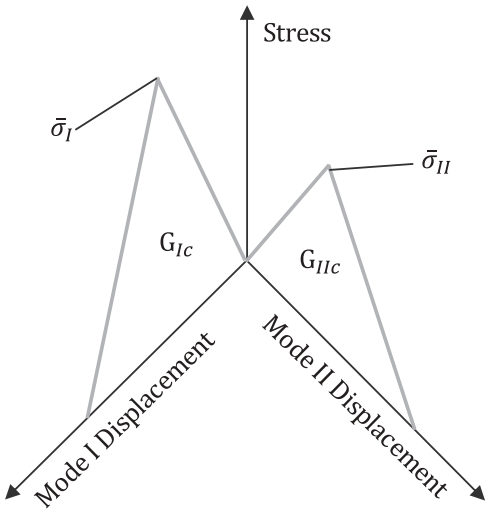

Figure 7. Schematic representation of the traction-separation law for mode I and mode II, where $\bar{\sigma}_I$. and $\bar{\sigma}_{II}$. are the yield stresses in mode I and mode II, respectively, and G_{Ic} and G_{IIc} are the fracture energies in mode I and mode II.

joints in structural automotive components, which has coincided with a steady increase in the use of composite materials [1,5,142]. The combined use of composites and adhesive bonding allows the manufacture of structures with very high mechanical strength and reduced weight, which in turn allows the vehicles to meet stringent emission limits. Adhesive joints are especially suitable for lightweight structures, as the use of rivets and screws inherently weakens the components by causing stress concentrations, which are especially damaging for composite materials. However, the impact strength of adhesive joints must also be assured, as one of the main automotive industry requirements is the safety of the occupants in the event of a collision. Adhesive joints must be able to sustain large impact loads, transmitting the forces to the structure while maintaining joints' integrity.

Significant research has been devoted to the development and testing of adhesives able to withstand this load [143]. These are now known industrially as crash resistant adhesives. Usually they are complex epoxy based formulations, toughened by the addition of rubber particles or a flexible polymer like polyurethane. They differ from standard adhesives by being able to combine high stiffness and strength with high ductility, which provides them with the ability to absorb significant levels of energy. The general behaviour of the flexible and stiff adhesive used in the automotive industry is extremely dissimilar, as shown by the studies of Loureiro *et al.* [50]. In 2013, Cho *et al.* [144] tested a toughened epoxy and found very high fracture toughness values under high strain rates, demonstrating its effectiveness in inhibiting failure under impact. The work of Saldanha *et al.* [51] studied the behaviour

of a modern crash resistant epoxy adhesive under static and impact loads. The adhesive was found to combine the best properties of a polyurethane and an epoxy, with high strength, elongation and toughness.

Drop weight tests using box beam specimens are commonly used to compare the joining techniques used in automotive construction. In 1990, Fay and Suthurst [145] compared the geometry of several bonded box beam structures using a toughened epoxy as an adhesive. As expected, it was found that the box beam geometry has significant effect on the joint behaviour and the weld-bonded solutions were found to provide the most stable type of collapse. At the time, the authors did not recommend the use of adhesives alone. Born [146] shows more results for this type of test and again found that a bonded box beam can sustain considerable impact loads when compared with a spot welded configuration. Box beams with hybrid construction (weld-bonded) were also considered and although they were an improvement on the welded construction, they did not surpass the energy absorbed by the purely bonded specimen, as shown in Figure 8.

These results show that the most of the absorbed energy comes from the plastic deformation of the metal. The main function of the adhesive in crash resistant structures is to ensure that the metal structure does not suffer disassembly during the impact process, leading to maximum energy absorption. The conclusions correlate well with the results found by Harris and Adams [62] for lap joints, where the same fundamental processes were identified.

The use of tough, crash-resistant adhesives ensures the cohesion of the structure and has been show to significantly improve performance on box impact tests. Mirdamadi *et al.* [143], Peroni *et al.* [147] and Avalle *et al.* [148] have all experimentally demonstrated the improvements provided by the tough adhesives in box impact tests. One of the most widely employed mechanical tests for the assessment of joint strength on the automotive industry is the IWP [18], as it provides a quick and simple test to assess the toughness of an adhesive when subjected to the most damaging peel forces [113].

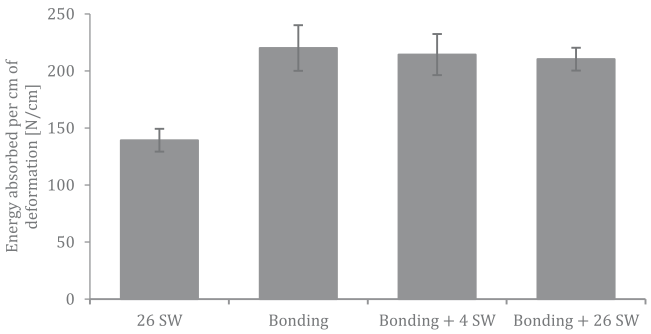

Figure 8. Energy absorption of box beam with spot welded (SW), bonded and weld-bonded configurations. Adapted from Born [146].

The modelling of the mechanical behaviour of adhesively bonded structures under impact is also the subject of considerable effort. Several authors have used numerical modelling to the advancement of numerical modelling procedures of joints and adhesives intended for the automotive industry, such as the work of Clarke *et al.* [64,149], May *et al.* [138] and Avendaño *et al.* [139]. Morin *et al.* [150] have also successfully modelled the dynamical behaviour of automotive impact boxes using a cohesive element with an improved constitutive model to taking into account the viscoplasticity of the adhesive, with different behaviour in tension and compression. These works have demonstrated that the use of cohesive elements can successfully be used to model impact behaviour, failure load and absorbed energy of automotive structures.

Novel techniques based on adhesive bonding are currently being proposed for use in the automotive industry. One of those is the mixed adhesive joint, where two adhesives can be effectively combined with the aim of achieving a synergetic effect, improving joint properties under static and impact loads. The work of Silva *et al.* [151] has approached this technique with promising results. SLJ specimens with mixed adhesive layers were tested under static condition and impact. Although improvements over a joint with single adhesive, the overall strength and energy absorption still did not surpass the performance of a modern crash resistant adhesive. The work of Avendaño *et al.* [38] also demonstrates how the use of adhesives can allow the automotive industry to use environment-friendly materials and structures, while remaining able to withstand impact loads.

According to these research trends and results, it can be concluded that the adhesive joining technology has sufficiently matured and is now being extensively used in automotive structures, not only with the aim of reducing weight, but also as a method to significantly reinforce energy absorption capabilities.

7.2. *Ballistics and armour*

The defence industry manufactures several structures which must resist high energy impacts. These armoured panels usually employ a composite construction, combining different materials in superimposed layers, with the aim of gradually dispersing the impact energy and therefore stop incoming projectiles. This type of construction lends itself to the use of adhesive bonding, as it is an effective method to join armour panels while aiding in energy dissipation. Figure 9 shows a schematic representation of an adhesively bonded ballistic armour structure.

The work of Martínez *et al.* [152] in 1998 was among the first to explore the advantages in the use of an elastic adhesive to bond a ceramic front face to a metallic back plate. Their results suggested that the adhesive thickness can be optimised to minimise energy reflection under strain rates of 1000 s^{-1}

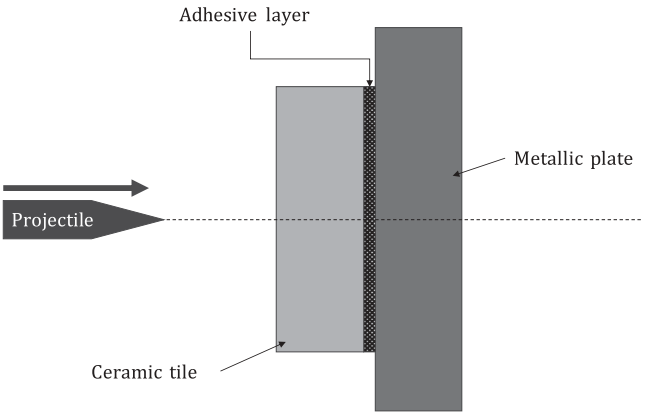

Figure 9. Basic configuration of an adhesively bonded ballistic armour. Adapted from Zaera *et al.* [124].

while still being able to hold the ceramic material in position after the impact load. Zaera *et al.* [124] further explored this technique by testing two different adhesives, a polyurethane and a more rigid rubber-modified epoxy. The comparison between the two adhesives indicates that the stiffer adhesive is in fact able to transmit the incident energy faster to the metallic backing plate, while the flexible adhesive is slower to do so. The flexible adhesive reflects energy back to the ceramic plate and causes early fracture. Lopez-Puente *et al.* [153] built upon these two previous works to determine that the optimum adhesive thickness for these type of ceramic panels is around 0.3 mm. This value was found be high enough to induce low shear stresses on the adhesive layer and ensure sufficient energy absorption while being thin enough to avoid spalling of the ceramic plate. A numerical study on this type of bonded structures was performed by Grujicic *et al.* [154], where a transient nonlinear analysis was employed to investigate the role of the adhesive layer on the effectiveness of these structures. An experimentally derived viscoelastic model, first presented by Amirkhizi *et al.* [155], was employed for modelling the adhesive layer. The model was used to adjust several variables of the viscoelastic model in order to achieve optimum impact performance. These results show that the performance of armour can be successfully improved by using dynamical modelling of the adhesive materials that bond these types of composite structures.

8. Summary and future trends

While the use of adhesive joints in several industries is extensive, there are various aspects of their use that still require substantial research, such as aging, thermal performance and property determination. This literature research paper focused on one of those aspects, the impact behaviour of

adhesive joints. Research on this topic is currently very significant, mainly driven by industrial requirements such as those of the automotive industry.

One of the main topics studied is the strain rate sensitivity of adhesives. The literature shows that adhesives are in fact quite sensitive to the strain rate, not only in tensile and shear properties, but also in their fracture properties. While tensile and shear properties are found to increase with the strain rate, the fracture energy was generally found to reduce with the increase of strain rate as most adhesives become slightly more brittle when subjected to impact loads.

The strain rate sensitivity of adhesive joints was also a focus of this research. Extensive experimental work has been published and has led to the conclusion that the behaviour of a joint under large strain rates is in fact governed not only by the properties of the adhesive but also of the substrates used. To produce joints able to withstand impact loads, it is therefore important to thoroughly understand the properties and strain rate sensitivity of all the materials employed in the joint.

The work published regarding impact strength under environmental effects such as temperature, aging and fatigue has also been discussed. It was generally found that the available literature is limited, with most experimental tests being performed at room temperature and without humidity. While several important conclusions have already been determined, this is still a topic of research with appreciable room for improvement.

A section on the modelling of adhesive joints shows that various authors have proposed several analytical and numerical models able to accurately model the impact behaviour of adhesives and adhesive joints.

Generally speaking, it can be said that consistent improvements in the formulations of adhesives have greatly expanded their ability to withstand plastic deformation without failure. The use of fully bonded and composite automotive structures is bound to increase significantly as the automotive industry pushes for more efficient lightweight vehicles. Crash resistant adhesives and crashworthy joint design will be fundamental to enable the construction of these vehicles. All these advances in material properties, joint design and simulation methods, combined with a detailed knowledge of the potential problems, provide the designer of an adhesive joint with the tools to do it in a safe and efficient manner, with the full understanding of the joint behaviour under impact loads.

Acknowledgments

The authors gratefully acknowledge the funding of Project NORTE-01-0145-FEDER-000022 – SciTech – Science and Technology for Competitive and Sustainable Industries, co-financed by Programa Operacional Regional do Norte (NORTE2020), through Fundo Europeu de Desenvolvimento Regional (FEDER). The authors would also like to thank NAGASE ChemteX for the financial support.

ORCID

Lucas F. M. da Silva http://orcid.org/0000-0003-3272-4591

References

[1] da Silva, L. F. M., Öchsner, A., and Adams, R. D. (Eds.), *Handbook of Adhesion Technology*, (Springer Science & Business Media, 2011).
[2] Adams, R. D., Comyn, J., and Wake, W. C., *Structural Adhesive Joints in Engineering*, (Springer Science & Business Media, 1997).
[3] da Silva, L. F. M., Pirondi, A., and Öchsner, A. (Eds.), *Hybrid Adhesive Joints*, (Springer Science & Business Media, 2011).
[4] Banea, M. D., and da Silva, L. F. M., *Part L: J. Mater. Des. Appl.* **223**, 1–18 (2009).
[5] Banea, M. D., da Silva, L. F. M., Campilho, R. D. S. G., and Sato, C., *J. Adhes.* **90**, 16–40 (2014).
[6] Goglio, L., *Handbook of Adhesion Technology*, (Springer, Heidelberg, Berlin, 2011). 21, 503–532.
[7] Adams, R. D., and Harris, J. A., *Int. J. Adhes. Adhes.* **16**, 61–71 (1996).
[8] da Silva, L. F. M., Dillard, D. A., Blackman, B., and Adams, R. D. (Eds.), *Testing Adhesive Joints: Best Practices*, (Wiley-VCH Verlag & Co., Weinheim, Germany, 2012).
[9] "ISO 11003-2 Determination of shear behaviour of structural adhesives - Part 2: Tensile test method using thick adherends," ed, First issue 2001, last review 2012.
[10] Sato, C., and Ikegami, K., *J. Adhes.* **70**, 57–73 (1999).
[11] "ISO 25217:2009 Adhesives - Determination of the mode 1 adhesive fracture energy of structural adhesive joints using double cantilever beam and tapered double cantilever beam specimens," ed, First issue 2009, last review 2014.
[12] da Silva, L. F. M., Esteves, V. H. C., and Chaves, F. J. P., Materialwissenschaft und Werkstofftechnik, 42, 460–470 (2011).
[13] Kinloch, A. J., and Kodokian, G. A., *J. Adhes.* **24**, 109–126 (1987).
[14] Kinloch, A. J., and Kodokian, G. A., *J. Mater. Sci. Lett.* **6**, 653–655 (1987).
[15] Imanaka, M., Nakamura, Y., Nishimura, A., and Iida, T., *Composites Science and Technology*, **63**, 41–51 (2003).
[16] Lataillade, J. L., Grapotte, D., and Cayssials, F., *Le J. de Physique IV*, **4**, C8-771–C8-776 (1994).
[17] Adams, R. D. (Ed), *Adhesive Bonding: Science, Technology and Applications*, (Woodhead Publishing Limited, Cambridge, England, 2005).
[18] "ISO 11343:2003 Adhesives - Determination of dynamic resistance to cleavage of high-strength adhesive bonds under impact conditions – Wedge impact method," ed, First issue 2003, last review 2013.
[19] Fernie, R., and Warrior, N. A., *Strain* **38**, 69–73 (2002).
[20] "ISO 9653:1998 Adhesives - Test method for shear impact strength of adhesive bonds," ed, First issue 1998, last review 2013.
[21] Gray, G. T., ASM Handbook, Mechanical Testing and Evaluation, **8**, 462–476 (2000).
[22] Beevers, A. and Ellis, M. D., *Int. J. Adhes. Adhes.* **4**, 13–16 (1984).
[23] Challita, G., and Othman, R., *Int. J. Adhes. Adhes.* **30**, 236–244 (2010).
[24] Ikegami, K., Fujii, T., Kawagoe, H., Kyogoku, H., Motoie, K., Nohno, K., et al., *Int. J. Adhes. Adhes.* **16**, 219–226 (1996).
[25] Bezemer, A. A., Guyt, C. B., and Vlot, A., *Int. J. Adhes. Adhes.* **18**, 255–260 (1998).
[26] Tardif, H. P., and Marquis, H., *Can. Aeronaut. Space J.* **9**, 205–213 (1963).

[27] Lindholm, U. S., *J. Mech. Phys. Solids* **12**, 317–335 (1964).
[28] Adams, R. D., and Coppendale, J., *J. Adhes.* **10**, 49–62 (1979).
[29] Chalkley, P. D. and Chiu, W. K., *Int. J. Adhes. Adhes.* **13**, 237–242 (1993).
[30] Zgoul, M., Characterising the rate dependent response of adhesively bonded structures, Doctoral dissertation, University of Surrey, 2002.
[31] Sugaya, T., Obuchi, T., and Sato, C., *J. Solid Mech. Mater. Eng.* **5**, 921–928 (2011).
[32] Karac, A., Blackman, B. R. K., Cooper, V., Kinloch, A. J., Sanchez, S. R., Teo, W. S., et al., *Eng. Fract. Mech.* **78**, 973–989 (2011).
[33] Dean, G. D., Read, B. E., and Duncan, B. C., An evaluation of yield criteria for adhesives for finite element analysis - Report (A)117, (National Physical Laboratory. Great Britain, Centre for Materials Measurement and Technology, 1999).
[34] Chen, W., Lu, F., and Cheng, M., *Polym. Test.* **21**, 113–121 (2002).
[35] Gilat, A., Goldberg, R. K., and Roberts, G. D., *ASCE J. Aerosp. Eng.* **20**, 75–89 (2007).
[36] Goglio, L., Peroni, L., Peroni, M., and Rossetto, M., *Int. J. Adhes. Adhes.* **28**, 329–339 (2008).
[37] Carlberger, T., Biel, A., and Stigh, U., *Int. J. Fract.* **155**, 155–166 (2009).
[38] Avendaño, R., Carbas, R. J. C., Marques, E. A. S., da Silva, L. F. M., and Fernandes, A. A., *Compos. Struct.* **152**, 34–44 (2016).
[39] Bascom, W. D., Ting, R. Y., Moulton, R. J., Riew, C. K., and Siebert, A. R., *J. Mater. Sci.* **16**, 2657–2664 (1981).
[40] Bitner, J. L., Rushford, J. L., Rose, W. S., Hunston, D. L., and Riew, C. K., *J. Adhes.* **13**, 3–28 (1981).
[41] Hunston, D. L., and Bullman, G. W., *Int. J. Adhes. Adhes.* **5**, 69–74 (1985).
[42] Raghavan, D., He, J., Hunston, D., and Hoffman, D., *J. Adhes.* **78**, 723–739 (2002).
[43] Blackman, B. R. K., Kinloch, A. J., Taylor, A. C., and Wang, Y., *J. Mater. Sci.* **35**, 1867–1884 (2000).
[44] Carlberger, T., and Stigh, U., *Eng. Fract. Mech.* **74**, 2247–2262 (2007).
[45] Blackman, B. R. K., Kinloch, A. J., Sanchez, F. S. R., Teo, W. S., and Williams, J. G., *Eng. Fract. Mech.* **76**, 2868–2889 (2009).
[46] Wegman, R. F., and Tanner, W. C., *ASTM Spec. Tech. Publ. Adhes.* **360**, 163–165 (1964).
[47] Wegman, R. F., and O'brien, E. L., *J. Appl. Polym. Sci.* **10**, 291–301 (1966).
[48] Wada, H., Kubo, S., Murase, K., and Kennedy, T., Dynamic tensile strength of PMMA/AL plate butt adhesive joints, in *ICF10, Honolulu (USA)* 2001.
[49] Hayashida, S., Sugaya, T., Kuramoto, S., Sato, C., Mihara, A., and Onuma, T., *Int. J. Adhes. Adhes.* **56**, 61–72 (2015).
[50] Loureiro, A. L., da Silva, L. F. M., Sato, C., and Figueiredo, M. A. V., *J. Adhes.* **86**, 765–787 (2010).
[51] Saldanha, D. F. S., Canto, C., da Silva, L. F. M., Carbas, R. J. C., Chaves, F. J. P., Nomura, K., et al., *Int. J. Adhes. Adhes.* **47**, 91–98 (2013).
[52] Soltannia, B., Ahmadi-Moghadam, B., and Taheri, F., "Influence of tensile impact and strain rate on the response of adhesively bonded single lap joints," presented at the ICCM19, Montreal, 2013.
[53] Kadioglu, F., and Adams, R. D., *Int. J. Adhes. Adhes.* **56**, 73–78 (2015).
[54] Challita, G., Othman, R., Casari, P., and Khalil, K., *Int. J. Adhes. Adhes.* **31**, 146–153 (2011).
[55] Al-Zubaidy, H., Al-Mahaidi, R., and Zhao, X.-L., *Compos. Struct.* **94**, 510–518 (2012).
[56] Al-Zubaidy, H., Zhao, X., and Al-Mahaidi, R., *Procedia Eng.* **14**, 1312–1317 (2011).
[57] Meschut, G., Teutenberg, D., and Henkel, K., "Design of low temperature cured adhesive joints in steel-FRP constructions under crash loads," presented at the METC and 2nd ESTAD, Dusseldorf, 2015.

[58] Yokoyama, T., and Nakai, K., "Determination of impact tensile properties of structural epoxy adhesive butt joints using a hat-shaped specimen," in *EURODYMAT 2006*, Dijon, France, 2006, pp. 789–795.
[59] Yokoyama, T., and Nakai, K., *Int. J. Adhes. Adhes.* **56**, 13–23 (2015).
[60] Amijima, S., and Fujii, T., "The effect of strain rate on mechanical properties of adhesives and adhesive bonded joints," in *International Conference on Fracture Mechanics and Technology, Hong Kong*, 1977, pp. 363–372.
[61] Perry, H. A., *Adhesive Bonding of Reinforced Plastics*, (Woodhead Publishing Limited, Cambridge, England, 1959).
[62] Harris, J. A., and Adams, R. D., *J. Mech. Eng. Sci.* **199**, 121–131 (1985).
[63] Yokoyama, T., *J. Strain Anal. Eng. Des.* **38**, 233–245 (2003).
[64] Clarke, M. I., Broughton, J. G., Hutchinson, A. R., and Buckley, M., *Int. J. Adhes. Adhes.* **44**, 226–231 (2013).
[65] Galliot, C., Rousseau, J., and Verchery, G., *Int. J. Adhes. Adhes.* **35**, 68–75 (2012).
[66] Hiley, M. J., Dong, L., and Harding, J., *Composites Part A* **28**, 171–180 (1997).
[67] Hosur, M. V., Islam, S. M. W., Vaidya, U. K., Kumar, A., Dutta, P. K., and Jeelani, S., *Compos. Struct.* **70**, 295–307 (2005).
[68] Lifshitz, J. M., and Leber, H., *Compos. Sci. Technol.* **58**, 987–996 (1998).
[69] Sankar, H. R., Adamvalli, M., Kulkarni, P. P., and Parameswaran, V., *Int. J. Adhes. Adhes.* **56**, 46–52 (2015).
[70] Reis, P. N. B., Ferreira, J. A. M., and Antunes, F., *Int. J. Adhes. Adhes.* **31**, 193–201 (2011).
[71] Adams, R. D., and Peppiatt, N. A., *J. Strain Anal. Eng. Des.* **9**, 185–196 (1974).
[72] da Silva, L. F. M., Rodrigues, T. N. S. S., Figueiredo, M. A. V., De Moura, M. F. S. F., and Chousal, J. A. G., *J. Adhes.* **82**, 1091–1115 (2006).
[73] Goglio, L. and Rossetto, M., *Int. J. Impact Eng.* **35**, 635–643 (2008).
[74] Banea, M. D., and da Silva, L. F. M., *Materialwissenschaft und Werkstofftechnik*, **41**, 325–335 (2010).
[75] Yokoyama, T., *Key Eng. Mater.* **145-149**, 317–322 (1998).
[76] Yokoyama, T. and Shimizu, H., *JSME Int. J. Ser. A Solid Mech. Mater. Eng.* **41**, 503–509 (1998).
[77] Bauwens, J. C., *J. Mater. Sci.* **7**, 577–584 (1972).
[78] Ree, T., and Eyring, H., *J. Appl. Phys.* **26**, 793–800 (1955).
[79] Cayssials, F., and Lataillade, J. L., *J. Adhes.* **58**, 281–298 (1996).
[80] Xu, S., and Dillard, D. A., *IEEE Trans. Compon. Packag. Technol*, **26**, 554–562 (2003).
[81] Srivastava, V. K., *Int. J. Adhes. Adhes.* **23**, 59–67 (2003).
[82] Adamvalli, M., and Parameswaran, V., *Int. J. Adhes. Adhes.* **28**, 321–327 (2008).
[83] Marques, E. A. S., da Silva, L. F. M., Banea, M. D., and Carbas, R. J. C., *J. Adhes.* **91**, 556–585 (2015).
[84] Gledhill, R. A., and Kinloch, A. J., *J. Adhes.* **6**, 315–330 (1974).
[85] Bowditch, M. R., *Int. J. Adhes. Adhes.* **16**, 73–79 (1996).
[86] Pethrick, R. A., *Proc. Inst. Mech. Eng. Part L*, **229**, 349–379 (2015).
[87] Wylde, J. W., and Spelt, J. K., *Int. J. Adhes. Adhes.* **18**, 237–246 (1998).
[88] Ameli, A., Papini, M., and Spelt, J. K., *Int. J. Adhes. Adhes.* **31**, 9–19 (2011).
[89] Viana, G., Costa, M., Banea, M. D., and da Silva, L. F. M., *Proc. Inst. Mech. Eng. Part L* doi: 10.1177/1464420716671503 (2016)
[90] Zhang, F., Yang, X., Xia, Y., Zhou, Q., Wang, H.-P., and Yu, T.-X., *Int. J. Adhes. Adhes.* **56**, 3–12 (2015).
[91] Costa, M., Viana, G., da Silva, L. F. M., and Campilho, R. D. S. G., *J. Adhes.* **93**, 127–146 (2016).
[92] Usui, Y., and Sakata, O., *Bull. Jpn Soc. Precis. Eng.* **18**, 213–218 (1984).

[93] Casas-Rodriguez, J. P., Ashcroft, I. A., and Silberschmidt, V. V., *J. Sound Vib.* **308**, 467–478 (2007).
[94] Casas-Rodriguez, J. P., Ashcroft, I. A., and Silberschmidt, V. V., *Compos. Sci. Technol.* **68**, 2401–2409 (2008).
[95] Casas-Rodriguez, J. P., Ashcroft, I. A., and Silberschmidt, V. V., *Compos. Sci. Technol.* **68**, 2663–2670 (2008).
[96] Silberschmidt, V. V., Casas-Rodriguez, J. P., and Ashcroft, I. A., "Impact fatigue of adhesive joints," in *Key Engineering Materials*, 2009, pp. 71–78.
[97] Kemiklioglu, U., Sayman, O., Batar, T., Soykok, I. F., Akderya, T., and Akan, E., *Appl. Adhes. Sci.* **3**, 1–9 (2015).
[98] Sato, C., *Handbook of Adhesion Technology*, (Springer, Heidelberg, Berlin, 2011). 29, 743–763.
[99] Sato, C. and Ikegami, K., *Int. J. Adhes. Adhes.* **20**, 17–25 (2000).
[100] Khan, A. S., Lopez-Pamies, O., and Kazmi, R., *Int. J. Plast.* **22**, 581–601 (2006).
[101] Iwamoto, T., Nagai, T., and Sawa, T., *Int. J. Solids Struct.* **47**, 175–185 (2010).
[102] Cowper, G. R., and Symonds, P. S., "Strain-hardening and strain-rate effects in the impact loading of cantilever beams," DTIC Document1957.
[103] Ludwik, P., *Elemente der Technologischen Mechanik*, (Verlag Von Julius Springer, Leipzig, 1909).
[104] Johnson, G. R., and Cook, W. H., *Eng. Fract. Mech.* **21**, 31–48 (1985).
[105] Morin, D., Haugou, G., Bennani, B., and Lauro, F., *Eng. Fract. Mech.* **77**, 3481–3500 (2010).
[106] Kitagawa, M., Mori, T., and Matsutani, T., *J. Polym. Sci. Part B* **27**, 85–95 (1989).
[107] Krempl, E., *J. Eng. Mater. Technol.* **101**, 380–386 (1979).
[108] Chiu, W. and Jones, R., *Int. J. Adhes. Adhes.* **15**, 131–136 (1995).
[109] Ramaswamy, V. G., Stouffer, D. C., and Laflen, J. H., *J. Eng. Mater. Technol.* **112**, 280–286 (1990).
[110] Crocombe, A. D., Yu, X. X., and Richardson, G., *J. Adhes. Sci. Technol.* **15**, 279–302 (2001).
[111] Zgoul, M. and Crocombe, A. D., *Int. J. Adhes. Adhes.* **24**, 355–366 (2004).
[112] Crocombe, A. D., *Int. J. Adhes. Adhes.* **15**, 21–27 (1995).
[113] Sato, C., *Modeling of Adhesively Bonded Joints*, (Springer, Heidelberg, Berlin, 2008). 10, 279–303.
[114] Higuchi, I., Sawa, T., and Suga, H., *J. Adhes. Sci. Technol.* **16**, 1585–1601 (2002).
[115] Sawa, T., Higuchi, I., and Suga, H., *J. Adhes. Sci. Technol.* **17**, 2157–2174 (2003).
[116] Higuchi, I., Sawa, T., and Suga, H., *J. Adhes. Sci. Technol.* **16**, 1327–1342 (2002).
[117] Hazimeh, R., Challita, G., Khalil, K., and Othman, R., *Int. J. Adhes. Adhes.* **56**, 24–31 (2015).
[118] Duncan, B. C., and Pearce, A., Comparison of Impact and High Rate Tests for Determining Properties of Adhesives and Polymers Needed for Design Under Impact Loading: Performance of Adhesives Joints Programme Project PAJ2 - Report (A)134, (National Physical Laboratory. Great Britain, Centre for Materials Measurement and Technology, 1999).
[119] Charalambides, M., and Dean, G., Constitutive models and their data requirements for use in finite element analysis of adhesives under impact loading - Report (A)59, (National Physical Laboratory. Great Britain, Centre for Materials Measurement and Technology, 1997).
[120] Dean, G. D., and Charalambides, M. N., Data requirements for the use of finite element methods to predict the impact performance of plastics - Report (A)58,

(National Physical Laboratory. Great Britain, Centre for Materials Measurement and Technology, 1997).
[121] Xia, Y., Zhou, Q., Wang, P. C., Johnson, N. L., Gayden, X. Q., and Fickes, J. D., *Int. J. Adhes. Adhes.* **29**, 414–426 (2009).
[122] Xia, Y., Zhou, Q., Wang, P. C., Johnson, N. L., Gayden, X. Q., and Fickes, J. D., *Int. J. Adhes. Adhes.* **29**, 427–433 (2009).
[123] Yang, X., Xia, Y., Zhou, Q., Wang, P.-C., and Wang, K., *Int. J. Adhes. Adhes.* **39**, 21–32 (2012).
[124] Zaera, R., Sánchez-Sáez, S., Pérez-Castellanos, J. L., and Navarro, C., *Composites Part A* **31**, 823–833 (2000).
[125] Sawa, T., Nagai, T., Iwamoto, T., and Kuramoto, H., "A Study on Evaluation of Impact Strength of Adhesive Joints Subjected to Impact Shear Loadings," in *ASME* 2008 *International Mechanical Engineering Congress and Exposition*, 2008, pp. 55–61.
[126] Liao, L., Kobayashi, T., Sawa, T., and Goda, Y., *Int. J. Adhes. Adhes.* **31**, 612–619 (2011).
[127] Liao, L., Sawa, T., and Huang, C., *Int. J. Adhes. Adhes.* **44**, 91–98 (2013).
[128] Harris, J. A., and Adams, R. A., *Int. J. Adhes. Adhes.* **4**, 65–78 (1984).
[129] Bigwood, D. A., and Crocombe, A. D., *Int. J. Adhes. Adhes.* **10**, 31–41 (1990).
[130] Crocombe, A. D., and Adams, R. D., *J. Adhes.* **13**, 241–267 (1982).
[131] Lee, S. J., and Lee, D. G., *J. Adhes.* **40**, 1–14 (1992).
[132] Kinloch, A., *Adhesion and Adhesives: Science and Technology*, (Springer Science & Business Media, United Kingdom, 2012).
[133] Sheppard, A., Kelly, D., and Tong, L., *Int. J. Adhes. Adhes.* **18**, 385–400 (1998).
[134] Dean, G., Lord, G., and Duncan, B., Comparison of the measured and predicted performance of adhesive joints under impact - Report (A)206, (National Physical Laboratory. Great Britain, Centre for Materials Measurement and Technology, 1999).
[135] Cavalli, M. N., and Thouless, M. D., *J. Adhes.* **76**, 75–92 (2001).
[136] Campilho, R. D. S. G., De Moura, M. F. S. F., and Domingues, J. J. M. S., *J. Adhes. Sci. Technol.* **21**, 855–870 (2007).
[137] Haufe, A., Pietsch, G., Graf, T., and Feucht, M., "Modelling of weld and adhesive connections in crashworthiness applications with LS-DYNA," in *Proceedings of the NAFEMS seminar "simulation of connections and joints in structures". Wiesbaden, Germany*, 2010.
[138] May, M., Voß, H., and Hiermaier, S., *Int. J. Adhes. Adhes.* **49**, 7–17 (2014).
[139] Avendaño, R., Carbas, R. J. C., Chaves, F. J. P., Costa, M., da Silva, L. F. M., and Fernandes, A. A., *J. Eng. Mater. Technol.* **138**, 041019 (2016)
[140] Neumayer, J., Kuhn, P., Koerber, H., and Hinterhölzl, R., *J. Adhes.* **92**, 503–516 (2016).
[141] Daniels, J., *Int. J. Adhes. Adhes.* **4**, 5–8 (1984).
[142] Moreira, P. M. G. P., da Silva, L. F. M., and Castro, P. M. S. T., *Structural Connections for Lightweight Metallic Structures*, (Springer, New York, USA, 2012).
[143] Mirdamadi, M., and Korchnak, G., "Great automotive designs enabled by advances in adhesive bonding," presented at the AISI Great Design in Steel - Seminar, Livonia, MI, 2006.
[144] Cho, J. U., Kinloch, A., Blackman, B., Sanchez, F. S. R., and Han, M. S., *Int. J. Automot. Technol.* **13**, 1127–1131 (2012).
[145] Fay, P. A., and Suthurst, G. D., *Int. J. Adhes. Adhes.* **10**, 128–138 (1990).
[146] Born, P., *AutoTechnol.* **4**, 44–47 (2004).
[147] Peroni, L., Avalle, M., and Belingardi, G., *Int. J. Impact Eng.* **36**, 498–511 (2009).
[148] Avalle, M., Peroni, L., Peroni, M., and Scattina, A., *J. Adhes.* **86**, 539–560 (2010).

[149] Clarke, M., Broughton, J. G., Hutchinson, A. R., and Buckley, M., *Int. J. Veh. Struct. Syst*. (IJVSS), 3, (2011)
[150] Morin, D., Bourel, B., Bennani, B., Lauro, F., and Lesueur, D., *Int. J. Impact Eng*. **53**, 94–105 (2013).
[151] Silva, M. R. G., Marques, E. A. S., and Silva, L., *Latin Am. J. Solids Struct*. **13**, 835–853 (2016).
[152] Martinez, M. A., Chocron, I. S., Rodriguez, J., Gálvez, V. S., and Sastre, L. A., *Int. J. Adhes. Adhes*. **18**, 375–383 (1998).
[153] López-Puente, J., Zaera, R., and Navarro, C., *Composites Part B* **33**, 559–566 (2002).
[154] Grujicic, M., Pandurangan, B., and D'entremont, B., *Mater. Des*. **41**, 380–393 (2012).
[155] Amirkhizi, A. V., Isaacs, J., Mcgee, J., and Nemat-Nasser, S., *Philos. Mag*. **86**, 5847–5866 (2006).

Paper 2

Content of Paper 2

Abstract

1. Introduction

2. Experimental details

2.1. Crash resistant adhesive

2.2. Specimen fabrication

2.2.1. Glass transition temperature (T_g)

2.2.2. Tensile specimens

2.2.3. DCB specimens

2.2.4. Torsion specimens

2.3. Testing procedures

2.3.1. Glass transition temperature (T_g)

2.3.2. Tensile tests

2.3.3. Fracture toughness in mode I

2.3.4. Torsion tests

3. Determination of the strain rate

4. Experimental results

4.1. Glass transition temperature (T_g)

4.2. Tensile tests results

4.2.1. Stress-strain curves

4.2.2. Tensile strength

4.2.3. Young´s modulus

4.2.4. Strain at failure (%)

4.2.5. Summary of the tensile testing results

4.3. DCB tests results

4.4. Tensile strength as a function of temperature and displacement rate

4.4.1. XNR6852 E-3 adhesive bulk “Dogbone”

4.4.2. XNR6852 E-3 fracture toughness in mode I (G_{IC})

4.5. Young´s modulus as a function of temperature and displacement rate

4.6. Torsion test results

4.7. Analytical considerations

5. Conclusion

References

Check for updates

Original article

Institution of MECHANICAL ENGINEERS

Journal of MATERIALS: DESIGN AND APPLICATIONS

Proc IMechE Part L:
J Materials: Design and Applications
0(0) 1–15
© IMechE 2019
Article reuse guidelines:
sagepub.com/journals-permissions
DOI: 10.1177/1464420719836914
journals.sagepub.com/home/pil

SAGE

Strain rate dependence of a crash resistant adhesive as a function of temperature for the automotive industry

JJM Machado[1], A Hayashi[2], PDP Nunes[3], EAS Marques[1], RJC Carbas[3], C Sato[2] and LFM da Silva[3]

Abstract

The wide and diverse application of adhesives in the automotive industry has increased over the last decades, driven by the need to produce efficient yet strong vehicles, able to meet both fuel economy and safety standards. This method allows to bond a variety of dissimilar materials used for structural parts, as well as to achieve lighter structures, and higher failure loads over other traditional methods such as fastening or welding. It is therefore important to understand the behaviour of adhesives under a wide range of strain rates and temperatures. These data are fundamental to ensure vehicle safety, as adhesives must be able to sustain impact conditions, deforming but at the same time keeping the integrity of the structure and transmitting the loads without damaging the joint. The aim and novelty of this work is the complete mechanical characterization of a high-performance crash resistant adhesive under varied strain rate and temperature conditions, necessary for the validation of structures used in the automotive industry. The mechanical behaviour of these materials is still poorly understood and described in the literature. The results showed a change in the mechanical properties of the adhesive with the variation of strain rate (quasi-static and impact of 3 m/s) and temperature (−30, 24 and 80 °C). With the mechanical properties determined it was possible to define cohesive laws for implementation in finite element simulation, as a function of strain rate and temperature.

Keywords

Crash resistant adhesive, strain rate, impact, mode I, torsion, temperature

Date received: 8 January 2019; accepted: 20 February 2019

Introduction

The application of adhesives has increased over the last decades as it is one of the most effective techniques to join dissimilar materials. It is also the optimal method for joining composites, which cannot be joined using other methods, creating a strong mechanical connection.[1–3] Several industries are using adhesives such as the automotive industry, aerospace, defence, electronics and naval industries.[4] The application of adhesives in the automotive industry has increased over the last years due to strict requirements regarding safety, fuel consumption and emissions, although the automotive designers still face challenges in the design of bonded joints, particularly for complex structural elements.[5] Automotive structures must be able to undergo impact loadings, allowing the structures to deform and absorb the impact energy, and at the same time keeping the occupants safe through the integrity of the structures, it is of great necessity to understand and optimize the behaviour of adhesives and adhesive joints under high strain rate loads under different temperatures.[6] Although there are other available methods (such as fastening, welding or riveting) for joining materials, adhesive bonding offers a very smooth and uniform stress distribution along the bonded overlap, resulting in higher fatigue resistance. This method also presents the advantage of producing very light structures, it can be relatively cheap to manufacture, and also create a structure able to withstand significant damage before total failure.[7]

Adhesives are polymers and therefore present a viscoelastic and viscoplastic behaviour being of extreme importance the knowledge of the variation

[1]Instituto de Ciência e Inovação em Engenharia Mecânica e Engenharia Industrial (INEGI), Porto, Portugal
[2]Institute of Innovative Research (IIR), Tokyo Institute of Technology, Yokohama, Japan
[3]Departamento de Engenharia Mecânica, Faculdade de Engenharia (FEUP), Universidade do Porto, Porto, Portugal

Corresponding author:
Lucas da Silva, FEUP Rua Dr. Roberto Frias, s/n Porto, 4200-465 Portugal.
Email: lucas@fe.up.pt

of its mechanical properties when subjected to strain rates and temperatures since their behaviour is very sensitive to those factors.[8–10] Some authors stated that adhesives characterized as non-brittle under static or quasi-static, conditions being subjected to an abrupt load, can display a brittle behaviour which influences the aptitude of a joint to absorb energy. The demand for structures with high strength to weight ratio has conducted to several developments in the chemical formulation of adhesives as a response.[3] Some of the authors who performed development of epoxy adhesives to make them suitable for impact loadings, being able to offer excellent tensile and shear strength were Ashida et al.[11] and Nakayama et al.[12] (specifically for the automotive industry). Lutz and Schneider[13] in 2006 developed an epoxy adhesive, to be used in the automotive industry, aiming to increase the fracture energy rather than ultimate strength by altering the chemical composition of the adhesive (e.g. adding minerals or thermoplastics). The introduction of particles in the adhesive composition can influence its temperature dependency, requiring new studies of the mechanical behaviour under different temperatures.[14]

The understanding of the behaviour of the mechanical properties of both the adhesives and substrates is essential to design joints which are able to safely withstand dynamic loadings.[15] Some of the most relevant properties are the tensile and shear stiffness, the tensile and shear strength, and the fracture toughness (both in modes I, II, or mixed mode). By performing tensile and shear tests at high strain rates, it is possible to derive the basic strain rate dependent properties of the adhesives, such as the stiffness, yield stress and elongation/strain to failure). Tensile tests are principally performed on tensile specimens constituted of bulk material.[16]

There is a wide diversity of shear tests which can be performed using a variety of specific specimens, namely, the Thick Adherend Shear Test,[17–19] the torsion test,[20] or the notched plate shear method test.[16] Chai[21] used a Napkin Ring test specimen to determine the stress–strain behaviour of a simple structural adhesive in simple shear, as a function of a range of low and high temperature. The ultimate shear strain of the joint was found to be insensitive to the increase of strain rate, decreasing linearly with the increase of temperature.

There are several methods for impact testing available.[22,23] Some of these testing procedures are adapted from quasi-static testing methods and therefore modified to operate in combination with drop weight impact testing machines or Split Hopkinson Pressure Bar (SHPB) testing machines, allowing to achieve high strain rates.[16,24] In the literature, most studies assess the dynamic behaviour of adhesive joints, while only few authors address solely adhesives.[25–27] A study of the strain rate effects on the dynamic mechanical behaviour (using an SHPB) of a bi-component epoxy adhesive for structural bonding was performed by Goglio et al.,[28] focusing on the influence on the tensile and compressive strength, revealing that the strength of the adhesive increases significantly with the increase of the strain rate. The adhesive was found to be brittle under tension and ductile under compression. Goglio et al.[29] performed experimental dynamical testing on two structural epoxy adhesives using an SHPB in tensions and compression, revealing that there was a restrictive effect of the strain rate on the elastic modulus in compression and that no such effect occurs in tension. Using a two-part methacrylate and an epoxy structural adhesives, Yokoyama et al.[30] developed a constitutive model considering high strain rate mechanical compressive properties.

The change of adhesive properties with temperature represents the main challenge for low and high temperature applications. The consideration of thermal effects on an adhesive joint is of extreme importance because it can lead to a strength reduction,[31,32] although that does not occur for all the cases.[33] The stresses caused by the shrinkage effect on an adhesive joints strength is lower than those generated by the substrate thermal divergence.[33] Carlberger et al.[34] studied the effects of low and high values of temperature and strain rate using an engineering epoxy adhesive. The authors used double-cantilever beam (DCB) and end-notched flexure (ENF) specimens to determine the fracture toughness in both mode I and mode II. The results showed that the fracture toughness is not dependent of the temperature variation. It was observed that, with the increase of strain rate, in mode I the fracture toughness marginally increases and in mode II the fracture toughness decreases. Banea and da Silva[35] studied the effect of temperature on the mechanical properties of an epoxy and a polyurethane adhesive using bulk and adhesive joint tests, concluding that failure loads were influenced by this parameter.

The aim of this work is the mechanical characterization of a crash resistant epoxy adhesive under the variation of strain rate (quasi-static and impact at 3 m/s) and temperature (−30, 24 and 80 °C) necessary for the validation of structures used in the automotive industry. With the mechanical properties determined it was possible to define cohesive laws as a function of strain rate and temperature, suitable to implement in finite element simulations, and therefore predict the behaviour of real structures under both quasi-static and impact conditions with the variation of temperature. The analytical and numerical models created can be applied on the design and analysis of real structures undergoing impact conditions.

Experimental details

A description of all the experimental details will be made in terms of the tensile and shear mechanical

characterization tests performed using a crash resistant epoxy adhesive. The main application of the crash resistant epoxy adhesive being studied is the automotive industry. An automotive structure must be designed and evaluated in terms of its mechanical behaviour when being subjected to different loads (ranging from quasi-static to impact) and for cycles of low and high temperatures, at which it might be subjected during its life cycle. Therefore, the aim of this work is the mechanical characterization of a crash resistant adhesive varying the applied load from quasi-static (1 and 100 mm/min) to impact (3 m/s), for three distinct testing temperatures (−30, 24 and 80 °C), corresponding to those necessary for the validation of this type of structures for use in the automotive industry.

Crash resistant adhesive

The adhesive investigated in this work was supplied by Nagase ChemteX® (Osaka, Japan). The crash resistant, tough epoxy adhesive is designated XNR6852 E-3, a one-part component adhesives, specifically developed for the automotive industry. This type of adhesive is well suited for bonding vehicle structures due to the combination of its high strength, ductility and resistance to impact. This material can deform significantly before failure, allowing the bonded structure to deform plastically and absorb the impact energy. The cure cycle of the XNR6852 E-3 adhesive requires a stage of four hours at 150 °C.

Specimen fabrication

The following section describes the experimental procedures involved in the manufacture of all the specimens used to experimentally determine the glass transition temperature (T_g), tensile, shear, and torsion tests.

Glass transition temperature. An important parameter to have in consideration for the type of application of the adhesives is its T_g. The determination of this property is due to the different testing temperatures, once it represents a considerable influence on the strength of an adhesive. When an adhesively bonded joint is tested below this temperature, the adhesive will behave like a low-strain rigid material, while above this temperature it will have a more rubber-like behaviour. For such reason it is important to understand where the glass transition zone is located[36,37] and to ensure that the adhesive is operating bellow T_g. A total of three specimens were machined from XNR6852 E-3 adhesive bulk plates. The geometry and dimensions of the specimens are shown in Figure 1.

Tensile specimens. Following the French NF T 76-142 standard,[38] bulk XNR6852 E-3 adhesive plates with a

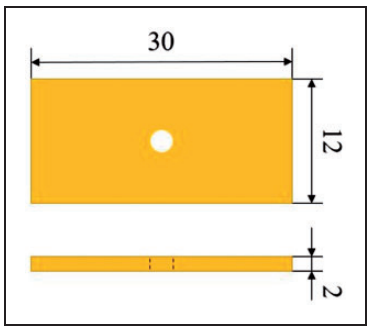

Figure 1. Schematic representation of the geometry of the adhesive XNR6852 E-3 T_g specimens (dimensions in mm).

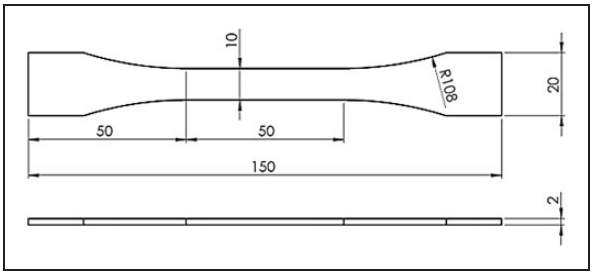

Figure 2. Schematic representation of the geometry of the tensile specimen ("dogbone") according to BS 2782 (dimensions in mm).[39]

thickness of 2 mm were produced between steel plates of mould with a silicone rubber frame in a hot press plates being applied the necessary pressure and temperature in order to follow the curing cycle of the XNR6852 E-3 adhesive. The use of a silicone rubber frame restricts the adhesive from flowing out and it creates a hydrostatic pressure which avoids the formation of voids and provides a good surface finishing of the adhesive plates.

The XNR6852 E-3 adhesive plates were machined into the final dimensions, following the BS 2782 standard[39] (Figure 2). A total of six bulk specimens were manufactured and tested for each strain rate and temperature conditions.

Although the tensile properties of XNR6852 E-3 adhesive can be used to roughly estimate the joint strength, other mechanical properties are fundamental for accurate modelling of the adhesive behaviour. To fully define the strain rate and temperature dependent cohesive laws, it is necessary to include parameters such the fracture toughness in mode I and shear (mode II), the determination of which is therefore described in the following sections.

DCB specimens. The fracture toughness in mode I, G_{IC}, was assessed by using DCB specimens which were manufactured using hard steel (DIN 40 CrMnMo 8-6-4) to avoid the plastic deformation of the substrates. Prior to the application of the adhesive, the joint surfaces were grit blasted and degreased with acetone. The bondline thickness was set at 0.2 mm

with the use of spacers (calibrated metal tape), which were positioned between the adherends at both ends and prior to the application of the adhesive. The schematic representation of the dimensions of the DCB specimens and the applied loads is presented in Figure 3. The value of crack length, a_0, was of 30 mm allowing a stable crack propagation. With the use of a sharp razor blade (0.05 mm thick) positioned in the mid-thickness a sharp pre-crack was introduced and its value measured. A total of six DCB specimens were used for each testing combination.

Torsion specimens. Butt joint specimens with rigid substrates can be used to measure the tensile properties or the shear properties of the adhesive through a torsion test as presented in this work. For tests performed under torsion, the specimen is ideally free of stress concentrations, which enables larger strains to failure than other types of tests where stress concentration is present. Another advantage of this testing method is that the adhesive displacement is higher, which gives a higher accuracy for the strain than other joint testing methods.[1]

The geometry and dimensions of the cylindrical butt-joints used to perform torsion tests are presented in Figure 4.

The first step in the preparation of the surface of the substrates was the use of sandpaper (#600 mesh grit) to remove any particles and achieve a homogenous roughness, being after degreased with acetone. The bottom substrate of the specimen was positioned in a jig,[40] the adhesive was first applied on the top section of that substrate and the upper substrate was then assembled in the mould, positioned by the cylinder support of the jig. The adhesive thickness was controlled by a micrometer installed at the upper part of the jig. The spindle of the micrometer contacted with the inferior part of the jig so that the thickness of the adhesive layer could be controlled.[16]

The substrates are made of steel due to higher stiffness necessary to minimize substrate deformation, and as well as to allow cures at high temperature to prevent residual thermal stresses caused by the difference in thermal expansion between the steel jig and the specimen.

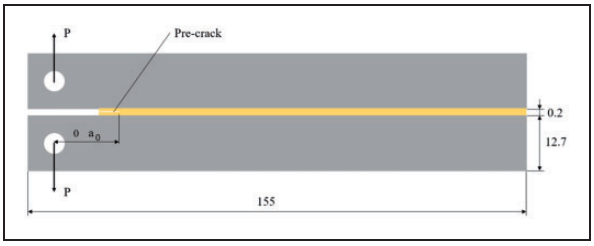

Figure 3. Schematic representation of the geometry of the DCB specimens and loads applied (P is the load and a is the pre-crack length ($a_0 = 30$)) (dimensions in mm).

Testing procedures

Glass transition temperature. The determination of this property was performed using an in-house developed apparatus.[41] The method of the test is a dynamic mechanical type of analysis which involves excitation of the test specimen (a vibrating beam with XNR6852 E-3 adhesive plate bolted in its centre of resonance) during cycles of heating and cooling, and it is based on the phenomenon that there is a peak in the damping value at the T_g of an adhesive.[41] The XNR6852 E-3 adhesive plate is responsible by the introduction of damping in the specimen. The beam is supported by two thin stretched twines, at each side of the vibrating beam. The temperature of the specimen is raised, and the corresponding amplitude of the vibration is then recorded.

From the theory of forced vibration, the damping is proportional to the inverse of the amplitude, allowing to conclude that the value of T_g corresponds to the minimum amplitude of the specimen. The beam should always be kept at the resonance frequency, which varies throughout the test. For such reason, the frequency of the power supply that feeds the driving coil is controlled by a feedback system that considers the frequency read by the pickup coil. Another identical beam (dummy beam) is used just to record the temperature, not being subjected to any vibration.

Because the measurement of T_g using this method is relatively fast (taking only about 10 min), the possibility of inducing a post-cure process of the

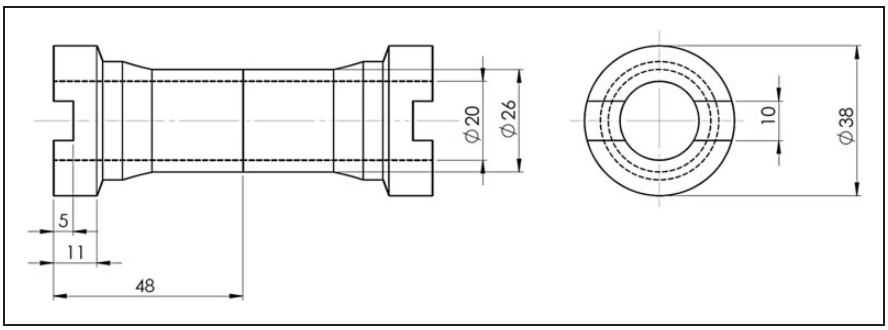

Figure 4. Geometry and dimensions (in mm) of the cylindrical butt-joint torsion specimens (adapted from Sato and Ikegami[20]).

XNR6852 E-3 was avoided. The final value is obtained by averaging the peak values of the heating and cooling curves.

Tensile tests. Two distinct tensile test machines were used to tests the "dogbone" bulk XNR6852 E-3 adhesive specimens. A universal test machine INSTRON® model 3367 (Norwood, Massachusetts, USA) with a load cell of 30 kN was used to perform tests at a cross-head displacement rates of 1 and 100 mm/min. Tests at an initial impact velocity of 3 m/s were performed using a Shimadzu Hydroshot HITS-T10, which allows a maximum impact force of 10 kN and an impact speed of 20 m/s, for a maximum displacement of 300 mm. The specimen was held using a jig, and a striker hits the upper part of this jig with an initial impact velocity of 3 m/s, as represented in Figure 5. The initial and testing impact velocities were recorded, to ensure their consistency with the pre-set value.

The tests were performed under different testing temperatures, namely at −30, 24 and 80 °C. For the low (with nitrogen) and high (internal heating coils) values of temperature, a thermal chamber was used, independently of the tensile equipment used. Prior to the tests, the climatic chambers were kept at the respective temperature for one hour, to ensure homogeneity of the jig and chamber temperatures as well as minimizing any effect of thermal expansion or contraction. Before each test, the specimen remained inside the chamber for a period of 10 min to ensure a homogenous temperature distribution along the specimen (assessed with thermocouples).

For each test performed, load-displacement (P-δ) curves were recorded up to failure. For tests performed at 1 and 100 mm/min, the use of an extensometer would greatly influence the results due to local damage caused to the specimens or slippage during testing. As a solution to avoid these problems, an optical method was used to measure the strain, using two horizontal marks in each specimen as a reference (according to the calibrated length). By using a camera to take pictures every five seconds in the case of 1 mm/min tests and by filming (due to their short duration) for the 100 mm/mm tests, the strain could be recorded. A routine for the software MATLAB® was then used to convert the pictures and the videos into strain data. For the case of tests under impact of 3 m/s, a high-speed camera (Hyper Vision HPV-X2J) was used for recording each test. The frame rate used depended on the testing temperature: −30 °C – 40,000 fps, 24 °C – 50,000 fps, and 80 °C – 10,000 fps.

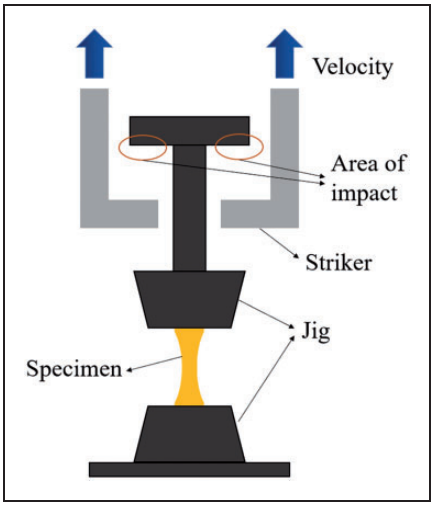

Figure 5. Schematic representation of the setup used to test XNR6852 E-3 adhesive bulk "dogbone" under impact of 3 m/s (tensile equipment Shimadzu Hydroshot HITS-T10).

Fracture toughness in mode I. The DCB specimens were tested according to the ASTM D3433 standard[42] in an INSTRON® model 3367 (Norwood, Massachusetts, USA) universal test machine with a load cell of 30 kN, for cross-head displacements of 1, 10 and 100 mm/min in a tension configuration. The tests were performed under different testing temperatures (−30, 24 and 80 °C) following the previously described experimental process (Section 'Tensile tests').

To avoid a blunt initial crack and ensure a more stable crack propagation, before testing the specimens were lightly loaded in mode I and the new value of a_0 recorded.

For the calculation of the critical fracture energy in mode I, G_{IC}, the compliance-based beam method[43,44] was used. This method has the advantage of not requiring crack length measurement during the test, using instead the crack equivalent concept (equation (1)).

$$G_{IC} = \frac{6P^2}{b^2 h}\left(\frac{2a_{eq}^2}{h^2 E_f} + \frac{1}{5G}\right) \quad (1)$$

where a_{eq} is an equivalent crack length obtained from the experimental compliance and accounting for the fracture process zone at the crack tip, E_f is a corrected flexural modulus to account for all phenomena affecting the P-δ curve, such as stress concentrations at the crack tip and stiffness variability between specimens, and G corresponds to the shear modulus of the adherents.[45]

Torsion tests. The torsion testing machine was originally developed by Shindo et al.[46] and it was based on a machine created by Lindholm,[47] which was modified by Sato et al.[40] The machine is constituted by a hydraulic actuator composed by two oil chambers, one for tensile loading and other for shear loading. The actuator is controlled with a pair of closed-loop feedback systems comprising a load cell, strain amplifiers, displacement sensors, electric circuits, and servo valves. The feedback system was only used for

quasi-static tests as displacement control was possible to achieve when considering the response time. Once the control systems were not able to be used due to the slow response for high values of strain rate, an open-loop control was therefore employed. The increments of the actuator displacement rate were determined by preliminary tests aimed at objectively identifying the stress increment rate. The main advantage of this testing machine is that both oil chambers in the actuator begin simultaneously loading when one of the loads exceeds the static friction. As a result, good synchronisation of the tensile and torsion loading can be established, even for high values of strain rate.

The loads applied to every specimen were measured with a specially made load cell from which tensile and torsional loads could be simultaneously measured. The deformation of XNR6852 E-3 adhesive layer in each specimen was measured with the biaxial extensometer, which uses a pair of eddy current gap sensors placed in the axial and circumferential directions.

The influence of low and high testing temperatures was not assessed in this type of test due to equipment limitations.

Determination of the strain rate

Adhesives are known to be strain rate dependent and such behaviour can be attributed to the inherent viscoelastic properties of polymeric structures.[48] It is therefore important to quantify the level of strain rate dependency, especially on the mechanical properties of adhesives, focusing on the tensile, shear and fracture toughness.

The fundamental concept of strain rate ($\dot{\varepsilon}$) is characterized as being the change in strain (deformation) of a specific material with respect to time. In this work, three distinct values of displacement rate were used in respect to: quasi-static conditions (1 and 100 mm/min) and impact condition (3 m/s). From equation (2) it is possible to determine the values of strain rate for each value of displacement rate.

$$\dot{\varepsilon}(t) = \left(\frac{L(t) - L_0}{L_0}\right) = \frac{v(t)}{L_0} \tag{2}$$

where $v(t)$ corresponds to displacement rate (mm/s), and L_0 to the value of length of the specimen (mm). It is important to state that in the case of the adhesive bulk ''dogbone'' specimens, the length used to determine the value of strain rate was of 120 mm, representing the distance between the bottom and top region of free adhesive where the grips were positioned during the test. For the case of fracture toughness in mode I (G_{IC}), the value of L_0 considered was in respect with the thickness of the adhesive layer, being 0.2 mm. As for the case of the shear tests, the values of strain rate were determined after each test was performed, after the measurement of the deformation of the adhesive layer.

Table 1. Conversion of the displacement rate to strain rate values for the adhesive bulk ''dogbone'' and fracture toughness in mode I (G_{IC}).

Displacement rate	mm/s	Strain rate ($\dot{\varepsilon}$), s^{-1}
Adhesive bulk ''dogbone'' ($L_0 = 120$ mm)		
1 mm/min	0.016	0.00014
100 mm/min	1.66	0.014
3 m/s (180,000 mm/min)	3000	25
Fracture toughness in mode I (G_{IC}) ($L_0 = 0.2$ mm)		
1 mm/min	0.016	0.083
10 mm/min	0.16	0.83
100 mm/min	1.66	8.33
3 m/s (180,000 mm/min)	3000	15,000

Table 2. Measured values of the T_g of XNR6852 E-3 adhesive.

Measurement	Heating (°C)	Cooling (°C)
Specimen 1	134	130
Specimen 2	128	128
Specimen 3	128	136

Average: 132 ± 4.51 °C

Table 1 presents the conversion of the displacement rate to strain rate values for the tensile adhesive bulk ''dogbone'' and fracture toughness in mode I (G_{IC}) experimental tests.

In order to clearly present the experimental results (due to fact that the values of strain rate are very different), all the data presented in this work will be primarily indicated in terms of displacement rate. However, it must be noted that material behaviour is directly related to the strain rate.

Experimental results

In this section, the experimental results obtained for XNR6852 E-3 adhesive are presented. Such results allow to fully characterize the mechanical behaviour of XNR6852 E-3 adhesive as a function of the variation strain rate and temperature, at the same time allowing to perform a comparison of how such parameters can be related.

Glass transition temperature

Table 2 lists the results of three measurements of T_g, for which three specimens were used to perform the test under the same condition. The average value determined was 132 °C; therefore, the maximum testing temperature of 80 °C (and required for the validation of an automotive structure) is within the working range for XNR6852 E-3 adhesive, and no

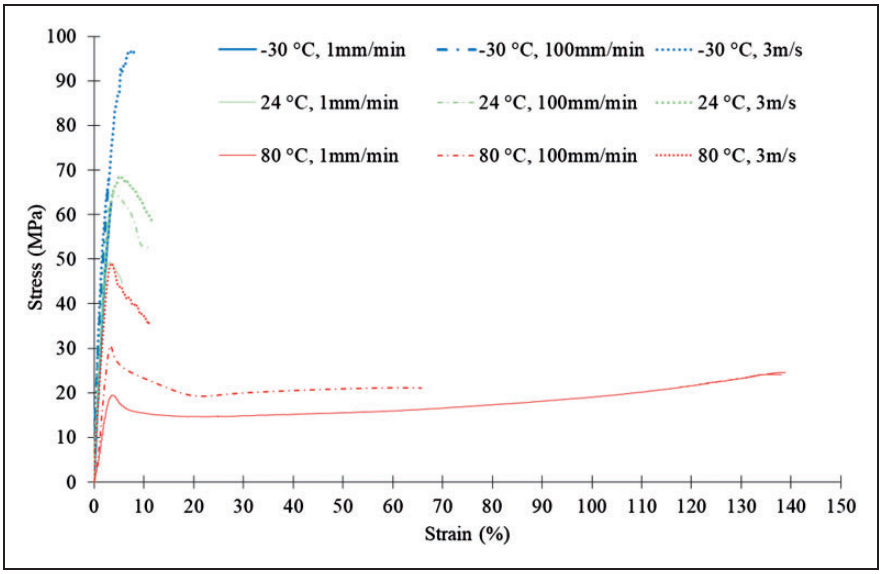

Figure 6. Representative tensile stress–strain curves of XNR6852 E-3 adhesive as a function of displacement rate (1 mm/min, 100 mm/min, and 3 m/s) and varying the testing temperature (−30, 24 and 80 °C).

drastic changes of the mechanical properties are to be expected.

Tensile tests results

The bulk "dogbone" XNR6852 E-3 adhesive specimens were tested at three distinct values of displacement rate (quasi-static: 1 and 100 mm/min, and impact: 3 m/s), varying the testing temperature (−30, 24 and 80 °C). For each specimen, an engineering tensile stress–strain curve was obtained based on load and displacement values, considering each specimen dimensions. From the stress–strain curves it was possible to determine the following mechanical properties, for each testing condition: Young's modulus, tensile strength and strain at failure.

Stress–strain curves. In Figure 6, it is possible to observe representative tensile stress–strain curves of XNR6852 E-3 adhesive tested under quasi-static (1 and 100 mm/min) and impact (3 m/s) conditions, for the three different temperature levels (−30, 24 and 80 °C).

The tensile mechanical properties of XNR6852 E-3 adhesive follow a typical behaviour for polymeric materials. It can be observed that tensile strength decreased with both the increase of temperature and the decrease of the strain rate. The highest values of strength are obtained for the lower testing temperature at high values of strain rate. From the tensile stress–strain curve's behaviour it was also observed that the Young's modulus and strain at failure were strongly affected by changing the strain rates and the testing temperature.

The mechanical behaviour of XNR6852 E-3 adhesive exhibited an initial elastic response followed by yielding, strain softening and, finally, non-linear strain hardening.[49] As stated in other studies,[50] some polymers deformed beyond their yield stress undergo a drop in the stress level described as "strain softening or yield-drop". Strain softening corresponds to the onset of strain localization and plays a critical role in controlling the mechanical properties of polymers.

The increase of the testing temperature revealed a major effect on the tensile stress–strain behaviour, conducting to a thermal softening of XNR6852 E-3 adhesive. The influence of the strain rate thus underlines the importance of understanding the effects of thermo-mechanical coupling during polymer deformations as occurs during impact load together with deformation processing.[51] For tests performed at temperature of 80 °C, especially for displacement rates of 1 and 100 mm/min, there was a considerable softening and plastic type behaviour, allowing to achieve higher values of strain at failure (although with the presence of a shear-band and necking[52]). A slight recovery of the tensile strength was achieved prior to failure of the specimens and after a peak value. Such behaviour resembles the one found for polymers under compression when tested under high temperatures.[53]

Strain at failure (%). Strain at failure results of XNR6852 E-3 adhesive tested, as a function of displacement rate and testing temperature are presented in Figure 7.

The values of strain at failure between −30 and 24 °C were similar and with slight changes for all the displacement rates considered. Only under the presence of high temperatures, most precisely, in the range between 24 and 80 °C significant changes were recorded for tests performed at the two lowest testing rates (1 and 100 mm/min). In the case of impact (3 m/s) load, the value of strain at failure measured

was almost constant through all the testing temperatures, considering average values. At 80 °C, it was observed that lower values of testing rate led to higher strain at failure. Such fact was due to the increased toughness and flexibility of XNR6852 E-3 adhesive.

Tensile strength as a function of temperature and displacement rate

The analysis of the tensile strength of XNR6852 E-3 adhesive under quasi-static (1 and 100 mm/min) and impact (3 m/s = 180,000 mm/min) loads, as a function of the testing temperature, is presented in Figure 8.

The results revealed that, for all the displacement rates tested, with the increase of the testing temperature, a decrease of the tensile strength was observed. Tensile strength variation with the testing temperature was similar for the case of tests performed at the lower testing rates (1 and 100 mm/min). The decrease in strength was higher between 24 and 80 °C for 1 and 100 mm/min – respectively of 49 and 42%, due to increased proximity to the T_g of XNR6852 E-3 adhesive. For the case of tests performed under impact (3 m/s) load, the change in tensile strength as a function of the testing temperature was very consistent throughout the full range of temperature (from −30 to 80 °C), with a value of around 26%, and a linear behaviour.

For the adhesive under study, it also clear that increases in the strain rate will result in an increase in the tensile strength.

It can be also observed that, for all cases of displacement rate, with the increase of the testing temperature there is a decrease of the tensile strength, caused by the increased proximity to the T_g of XNR6852 E-3 adhesive. The results indicate a linear dependence, which can be expressed as an equation (as shown in Figure 8).

A similar analysis was performed on the behaviour of XNR6852 E-3, determining the adhesive tensile strength for each testing temperature, varying the displacement rate (Figure 9).

It can be concluded that with the increase of the displacement rate, an increase of the tensile strength of XNR6852 E-3 adhesive occurs. Simultaneously, as the testing temperature increases towards the T_g, the tensile strength drops, following a logarithmic relationship.

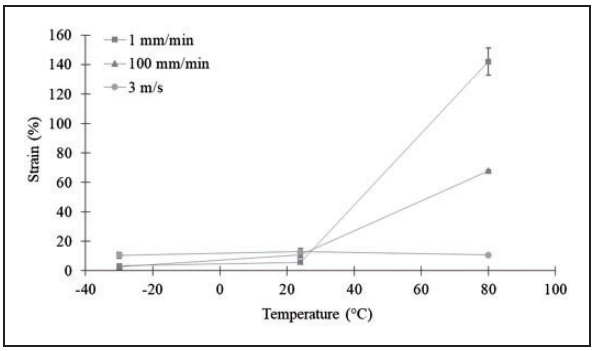

Figure 7. Average values and standard deviation of strain at failure (%) for XNR6852 E-3 adhesive for different values of displacement rate and temperature.

Young's modulus as a function of temperature and displacement rate

An analysis of the Young's modulus and the strain at failure of XNR6852 E-3 adhesive was performed, correlating the results with both the displacement rate and the testing temperature.

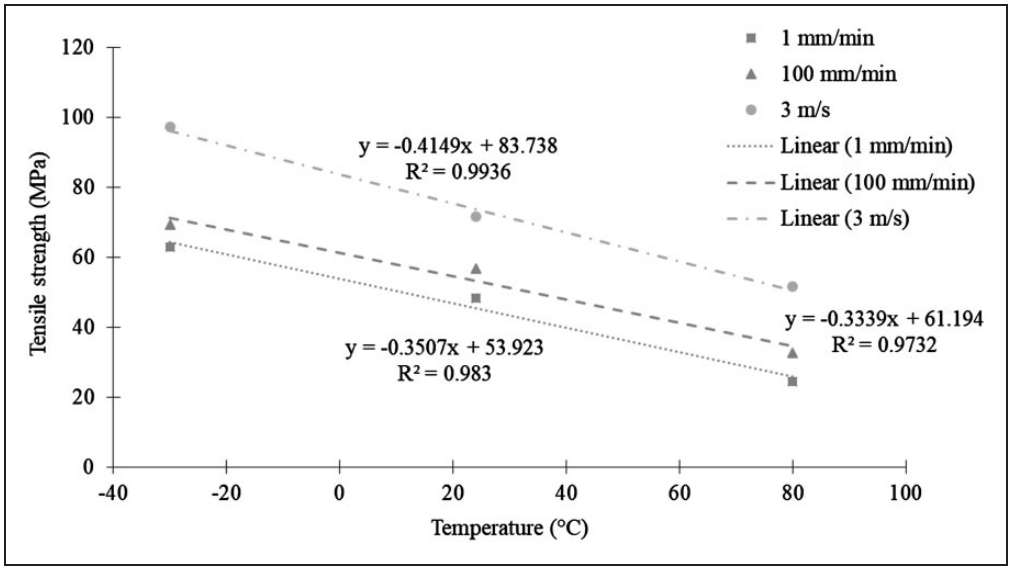

Figure 8. Comparison of the tensile strength of XNR6852 E-3 adhesive between the different displacement rates as a function of the testing temperature.

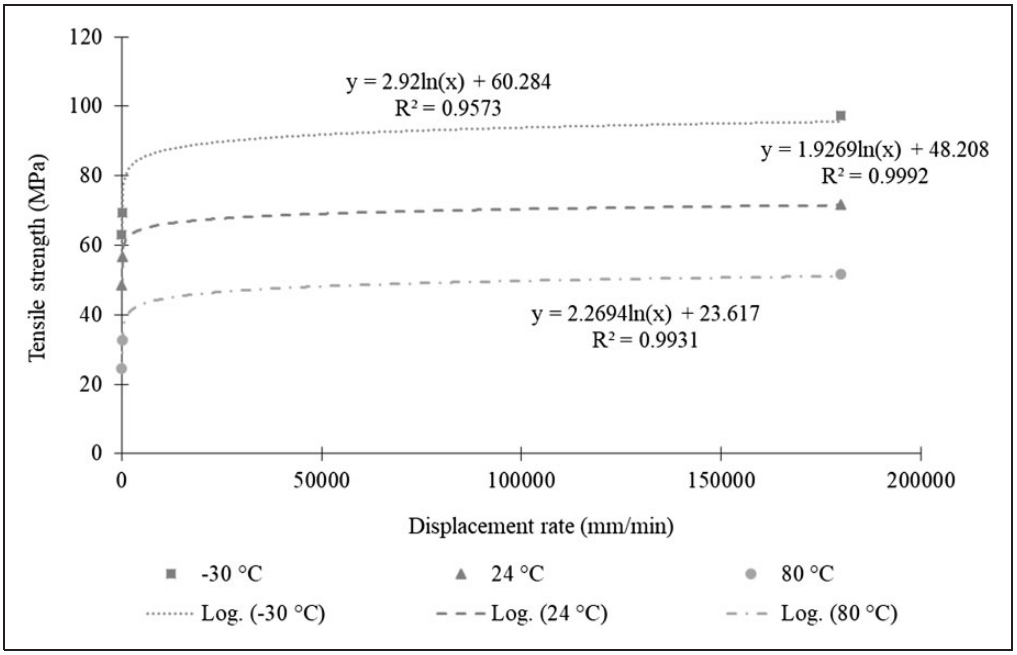

Figure 9. Comparison of the tensile strength of XNR6852 E-3 adhesive between the different displacement rates as a function of the testing temperature.

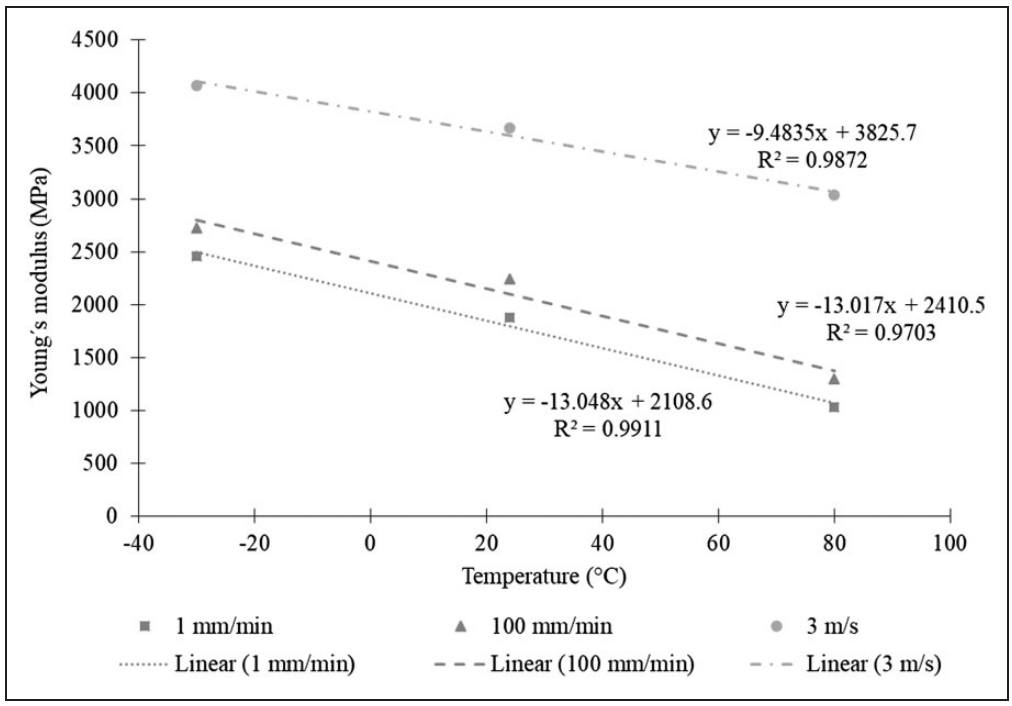

Figure 10. Comparison of the Young's modulus of XNR6852 E-3 adhesive between the different testing temperatures as a function of the displacement rates.

Figure 10 represents the Young's modulus results varying the testing temperature and as a function of displacement rate.

Considering the average values, there is a noticeable decrease of the Young's modulus with the increase of temperature, independently of the displacement rate, with a more pronounced decrease between 24 and 80 °C. As previously stated for the case of tensile strength, for tests performed at the lower testing speeds (1 and 100 mm/min), the variation follows in Young's modulus from low to high temperatures follow the same trend. The decrease of

Young's modulus under these conditions was found to be higher between 24 and 80 °C, being of approximately 43%. Under impact (3 m/s) load, the drop of Young's modulus between 24 and 80 °C (around 20%) is twice the value obtained between −30 and 24 °C.

As stated for the tensile strength results, for the adhesive under study there was a measurable increase of the stiffness as the strain rate increased.

With the increase of the testing displacement rate, an increase of the Young's modulus was observed, independently of the testing temperature considered, being possible to determine a linear behaviour. This behaviour can be related to plasticization of XNR6852 E-3 adhesive as its temperature increases towards the T_g value.

The Young's modulus results varying the displacement rate and as a function of the testing temperature is shown in Figure 11.

With the increase of the testing temperature, a decrease of the Young's modulus was observed, independently of the displacement rate, which followed a logarithmical behaviour. Such behaviour can be attributed to the increased ductility and flexibility of XNR6852 E-3 adhesive as its temperature increases towards the T_g value.

XNR6852 E-3 fracture toughness in mode I (G_{IC})

Experimental results regarding the fracture toughness in mode I (G_{IC}) of XNR6852 E-3 adhesive were obtained for tests performed at 1, 10 and 100 mm/min values of displacement rate. Direct measurement was not performed for 3 m/s and an extrapolation process was used to determine the properties at this rate. The logarithmic law used for the extrapolation process is given by equation (3).

$$\text{Property to determine} = A\ln(\dot{\varepsilon}) + B \tag{3}$$

where A and B are constants obtained from experimental data, and $\dot{\varepsilon}$ is the strain rate in s^{-1}. This logarithmic extrapolation process has been first proposed by the work of Zgoul and Crocombe[54] and further validated by the work of Avendaño et al.[55]

As for the values of fracture toughness in mode II (G_{IIC})[56] of XNR6852 E-3 adhesive, these could not be experimentally determined due to the extremely high fracture toughness that this adhesive presents in mode II, which caused plastic deformation of the metallic substrates in all studied End-notched flexure (ENF) specimens. Saldanha et al.[57] and Avendaño et al.[58] have studied previous versions of Nagase XNR6852 E-3 adhesive and in their works the experimentally determined G_{IIC} value was 6 to 10 times higher than the G_{IC} value. Considering this previous data, and due to the high ductility of the adhesive, the value for G_{IIC} was assumed to be 8 times higher than for the case of G_{IC}.

From Figure 12, it is possible to observe a linear relation of G_{IC} with the increasing temperature, valid for all displacement rates. Higher displacement rates led to higher values of G_{IC}. This can be attributed to the viscoelastic and viscoplastic effects inherent to this type of crash resistant adhesive.[48] The value of G_{IC} increases with the increase of both temperature and strain rate. As the temperature approaches T_g the adhesive becomes more tough and ductile.

The influence of the testing temperature on the values of G_{IC} of XNR6852 E-3 adhesive as a function of the displacement rate is shown in Figure 13.

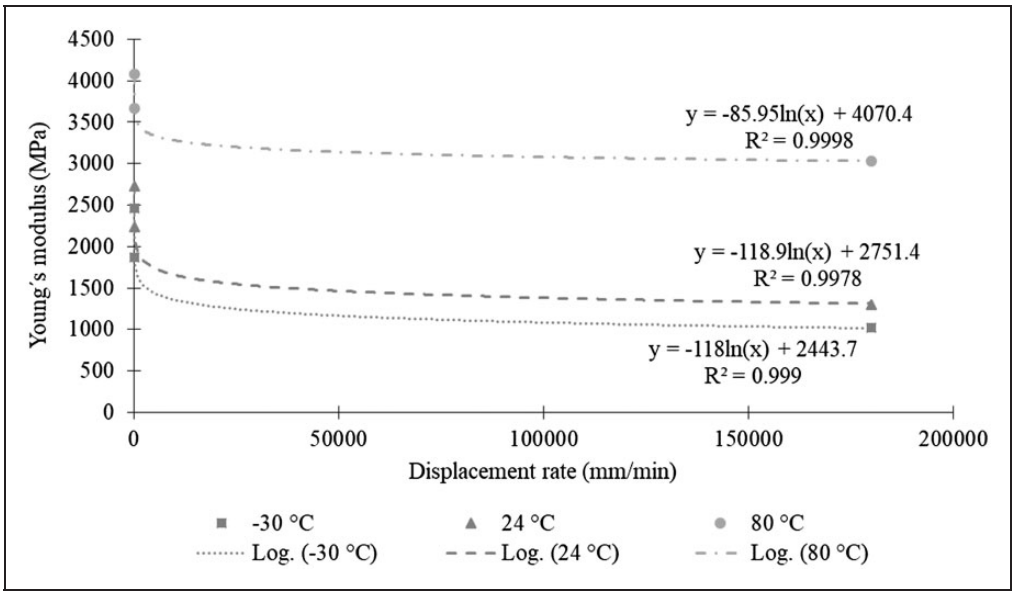

Figure 11. Comparison of the Young's modulus of XNR6852 E-3 adhesive between the different displacement rates as a function of the testing temperature.

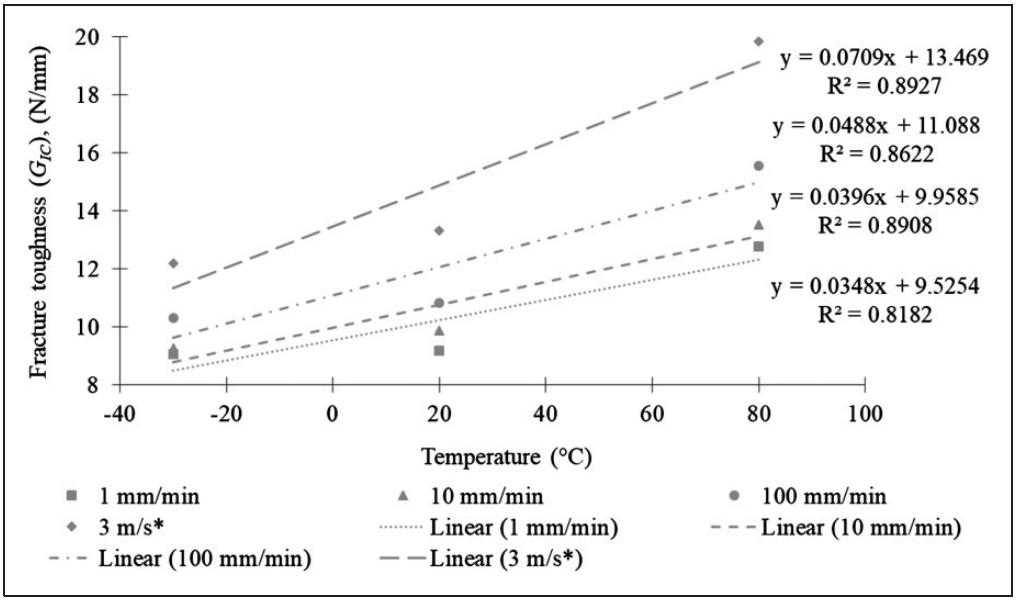

Figure 12. Comparison of the G_{IC} of XNR6852 E-3 adhesive between the different displacement rates as a function of the testing temperature.

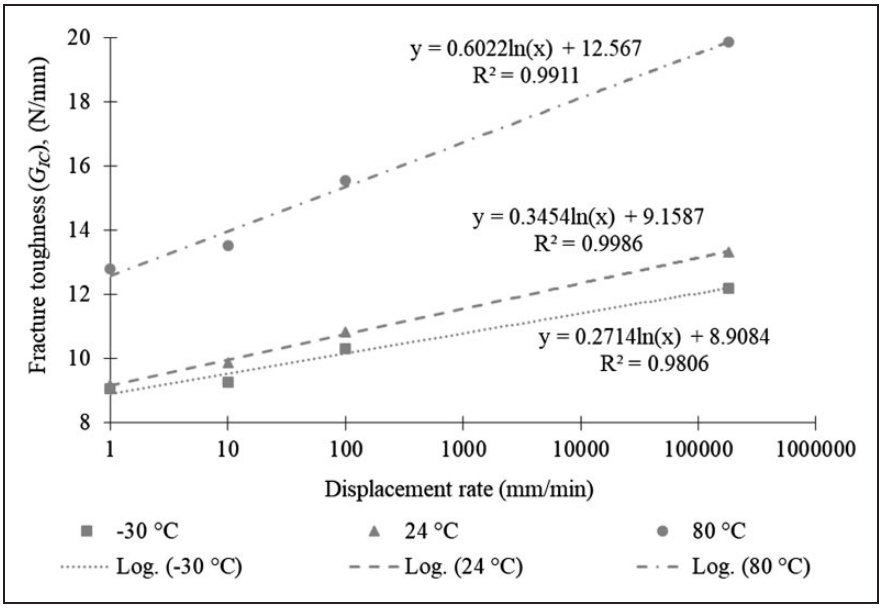

Figure 13. Comparison of the G_{IC} of XNR6852 E-3 adhesive between the different displacement rates as a function of the testing temperature.

Contrary to the results obtained in terms of tensile strength, with the increase of the testing temperature an increase of the G_{IC} was observed. This is valid for all displacement rates tested.

Torsion test results

The experimental results of shear stress of XNR6852 E-3 adhesive were obtained by performing torsion tests. Due to the absence of an environmental chamber, only tests at 24 °C were performed. Considering the capabilities of the torsion machine, three distinct strain rate ranges were selected for testing, namely, low (0.0014 s^{-1}), intermediate (0.002 s^{-1}) and high (11.4 s^{-1}) (Figure 14).

In order to facilitate the analysis of the results, the value of strain rate was plotted as $\log_{10}$. It can be concluded that with the increase of the value of strain rate there was an increase of the shear strength, which follows an almost logarithmic trend.

Analytical considerations

Analysing the experimental results, it is possible to infer analytical relations between the studied tensile mechanical properties, which can serve as support

for the design of adhesive joints loaded under thermal and impact conditions. From the experimentally obtained data it is possible to assess that the tensile strength varies linearly with the testing temperature and logarithmically as a function of the displacement rate.

From the work of Chai,[21] the following relationship can be deduced

$$\sigma = A_1\left[1 + A_2\left(\frac{T}{T_g}\right)\log\left(\frac{\gamma}{\gamma_0}\right)\right] \quad (4)$$

where σ is the tensile strength (in MPa), T the temperature (in °C), and γ the displacement rate (in mm/min). The remaining variables, i.e.: A_1, A_2, and γ_0, are the material constants, which were determined by solving the equations system obtained by introducing each value previously determined by testing under the different values of displacement rate and temperature, matching such results with those obtained experimentally, by using the software Matlab®.

Figure 15 shows comparisons between the experimentally determined tensile strength average values and the predicted trend obtained by equation (4) as a function of the testing temperature, respectively, for displacement rates of 1, 100 and 180,000 mm/min.

The determined equations were able to fit with good agreement the experimentally obtained results. The coefficients obtained are reported in Table 3.

A more fundamental understanding of the dependences of the strength on temperature and strain rate are offered by Airing's theory of molecular activation, where the coefficients A_1 and A_2 are interpreted in terms of activation energy and activation volume.[21]

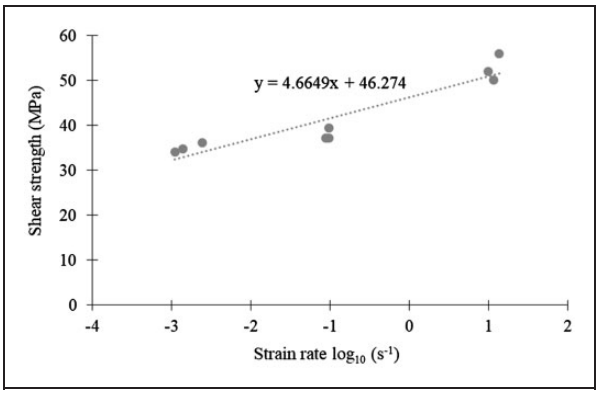

Figure 14. Values of shear strength of XNR6852 E-3 adhesive tested under three distinct stages at 24 °C.

Table 3. Coefficients obtained using equation (3) to predict the values of tensile strength of XNR6852 E-3 adhesive as a function of testing temperature and displacement rate.

	Displacement rate (mm/min)		
Coefficient	1	100	180,000
A_1	53.8	61.1	83.7
A_2	0.19	0.19	0.22
γ_0	3.24×10^{-5}	1.48×10^{-4}	1.36×10^{-3}

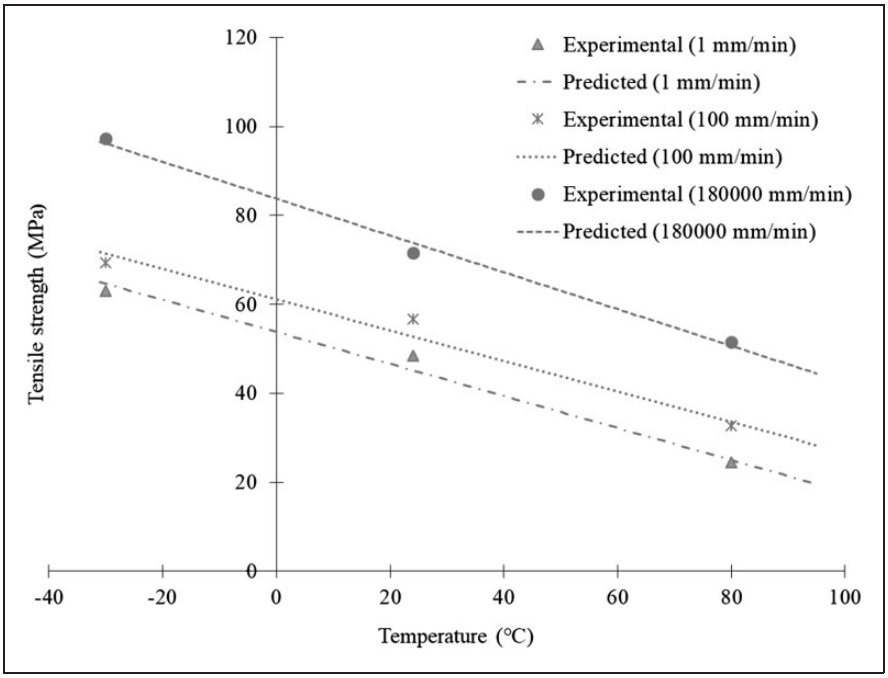

Figure 15. Comparison between the tensile strength experimentally determined (average values) and the predicted trend of XNR6852 E-3 adhesive between the different testing temperatures at a displacement rate of 1, 100 and 180,000 mm/min.

Conclusions

The aim of this work is the mechanical characterization of a crash resistant epoxy adhesive under the variation of strain rate (quasi-static and impact at 3 m/s) and temperature (−30, 24 and 80 °C) necessary for the validation of structures used in the automotive industry. With the mechanical properties determined it was possible to define cohesive laws as a function of strain rate and temperature, suitable to implement in finite element simulations and therefore predict the behaviour of real structures under both quasi-static and impact conditions with the variation of temperature. The analytical and numerical models created can be applied on the design and analysis of real structures subjected to impact loads.

The main conclusions which can be drawn from this work are:

- The experimental results indicate that the tensile stress–strain response of XNR6852 E-3 adhesive at high strain rates exhibited the non-linear characteristics including the obvious yielding and strain softening. The tension behaviour is strongly dependent on the strain rate and temperature.
- Experimental testing demonstrated that, for all the displacement rates tested, with the increase of the testing temperature, a decrease of the tensile strength was observed, and that with the increase of the strain rate values there was an increase of the values of the tensile strength.
- A decrease of the Young's modulus values was found to occur with the increase of temperature, independently of the displacement rate. This decrease was more pronounced between 24 and 80 °C.
- The value of G_{IC} increases with the increase of both temperature and strain rate, since the temperature approaches T_g the adhesive becomes more ductile and tough. This is due to the increased viscoelastic and viscoplastic effects that become as the material operates closer to T_g.
- With the increase of the value of strain rate there was an increase of the shear strength.

Declaration of conflicting interests

The author(s) declared no potential conflicts of interest with respect to the research, authorship, and/or publication of this article.

Funding

The author(s) disclosed receipt of the following financial support for the research, authorship, and/or publication of this article: Funding provided by PhD grant SFRH/BD/139341/2018 "Impact strength optimization with cohesive zone elements of multi-material bonded structures used in the automotive industry", Project No. 028473 POCI-01-0145-FEDER-028473 "Design methodology for impact resistant bonded multi-material automotive structures (ImpactBondDesign)", Project NORTE-01-0145-FEDER-000022 – "SciTech – Science and Technology for Competitive and Sustainable Industries", co-financed by Programa Operacional Regional do Norte (NORTE2020), through Fundo Europeu de Desenvolvimento Regional (FEDER). The authors would also like to thank NAGASE ChemteX® for the financial support provided.

ORCID iD

JJM Machado http://orcid.org/0000-0002-1094-0114

References

1. Adams RD, Comyn J and Wake WC. *Structural adhesive joints in engineering*. Berlin: Springer Science & Business Media, 1997.
2. da Silva LFM, Pirondi A and Öchsner A. *Hybrid adhesive joints*. Berlin: Springer Science & Business Media, 2011.
3. da Silva LFM, Öchsner A and Adams RD. *Handbook of adhesion technology*. Berlin: Springer Science & Business Media, 2018.
4. Banea MD, da Silva LFM, Campilho RDSG, et al. Smart adhesive joints: an overview of recent developments. *J Adhes* 2014; 90: 16–40.
5. Grant L, Adams R and da Silva LFM. Effect of the temperature on the strength of adhesively bonded single lap and T joints for the automotive industry. *Int J Adhes Adhes* 2009; 29: 535–542.
6. Amijima S and Fujii T. The effect of strain rate on mechanical properties of adhesives and adhesive bonded joints. *International Conference on Fracture Mechanics and Technology, Hong Kong*1977, p. 363–372.
7. Banea MD and da Silva LFM. Adhesively bonded joints in composite materials: an overview. *Proc IMechE, Part L: J Materials: Design and Applications* 2009; 223: 1–18.
8. Wegman RF and Tanner WC. Strength of epoxy adhesives when stressed to failure in milliseconds. *ASTM Special Techn Publ – Adhes* 1964; 360: 163–165.
9. Hartshorn S. *Structured adhesives: chemistry and technology*. New York: Plenum Press, 1986.
10. Wake W. Theories of adhesion and uses of adhesives: a review. *Polymer* 1978; 19: 291–308.
11. Ashida T, Ohnishi M, Nagase T, et al. Epoxy resin adhesive composition. Google Patents, 1994. US5290857A. USA.
12. Nakayama A, Nagase T, Ashida T, et al. Epoxy resin structural adhesive composition. Google Patents, 1997.
13. Lutz A and Schneider D. Toughened epoxy adhesive composition. Google Patents, 2013.
14. Banea MD, da Silva LFM, Carbas RJ, et al. Mechanical and thermal characterization of a structural polyurethane adhesive modified with thermally expandable particles. *Int J Adhes Adhes* 2014; 54: 191–199.
15. Machado JJ, Marques EA, da Silva LF. Adhesives and adhesive joints under impact loadings: an overview. *The Journal of Adhesion* 2018; 94(6): 421–452.
16. LFM da Silva, DA Dillard, B Blackman, et al. (eds) *Testing adhesive joints: best practices*. New York: John Wiley & Sons, 2012.

17. 11003-2 I. ISO 11003-2. *Determination of shear behaviour of structural adhesives – Part 2: tensile test method using thick adherends*, First issue 2001, last review 2012.
18. Banea MD, da Silva LFM and Campilho RD. Moulds design for adhesive bulk and joint specimens manufacturing. *Assembly Autom* 2012; 32: 284–292.
19. da Silva LFM and Adams R. Measurement of the mechanical properties of structural adhesives in tension and shear over a wide range of temperatures. *J Adhes Sci Technol* 2005; 19: 109–141.
20. Sato C and Ikegami K. Strength of adhesively-bonded butt joints of tubes subjected to combined high-rate loads. *J Adhes* 1999; 70: 57–73.
21. Chai H. The effects of bond thickness, rate and temperature on the deformation and fracture of structural adhesives under shear loading. *Int J Fracture* 2004; 130: 497–515.
22. Falk AH. Impact testing of adhesives. *ASTM Bulletin* 1946; 42–44.
23. Ilkka G and Scott R. Impact testing of adhesive bonds. In: *Proceedings of the symposium on adhesion and cohesion*. Warren, Mich: General Motors Research Laboratories, 1961, pp.65–73.
24. Kolsky H. An investigation of the mechanical properties of materials at very high rates of loading. *Proc Phys Soc Sect B* 1949; 62: 676.
25. Harris JA and Adams RD. An assessment of the impact performance of bonded joints for use in high energy absorbing structures. *Proc IMechE, Part C: J Mechanical Engineering Science* 1985; 199: 121–131.
26. Yokoyama T. Experimental determination of impact tensile properties of adhesive butt joints with the split Hopkinson bar. *J Strain Anal Eng Des* 2003; 38: 233–245.
27. Martinez MA, Chocron IS, Rodriguez J, et al. Confined compression of elastic adhesives at high rates of strain. *Int J Adhes Adhes* 1998; 18: 375–383.
28. Goglio L, Peroni L, Peroni M, et al. High strain-rate compression and tension behaviour of an epoxy bi-component adhesive. *Int J Adhes Adhes* 2008; 28: 329–339.
29. Goglio L, Peroni M and Rossetto M. Effect of the strain rate on the mechanical behaviour of epoxy adhesives. In: Garibaldi L, Surace C, Holford K and Ostachowicz WM (eds) *Key engineering materials*. Switzerland: Trans Tech Publ, 2007, pp.671–676.
30. Yokoyama T, Nakai K and Mohd Yatim NH. High strain-rate compressive properties and constitutive modeling of bulk structural adhesives. *J Adhes* 2012; 88: 471–486.
31. Apalak MK, Apalak ZG, Gunes R, et al. Steady-state thermal and geometrical non-linear stress analysis of an adhesively bonded tee joint with double support. *Int J Adhes Adhes* 2003; 23: 115–130.
32. Al-Samhan A and Darwish S. Factors influencing thermo-mechanical stresses developed in bonded tools. *Int J Adhes Adhes* 2005; 25: 379–388.
33. da Silva LFM, Adams R and Gibbs M. Manufacture of adhesive joints and bulk specimens with high-temperature adhesives. *Int J Adhes Adhes* 2004; 24: 69–83.
34. Carlberger T, Biel A and Stigh U. Influence of temperature and strain rate on cohesive properties of a structural epoxy adhesive. *Int J Fracture* 2009; 155: 155–166.
35. Banea M and da Silva LFM. The effect of temperature on the mechanical properties of adhesives for the automotive industry. *Proc IMechE, Part L: J Materials: Design and Applications* 2010; 224: 51–62.
36. Marques E, da Silva LFM, Banea M, et al. Adhesive joints for low- and high-temperature use: an overview. *J Adhes* 2015; 91: 556–585.
37. Marques E, Banea M, da Silva LFM, et al. Effect of low temperature on tensile strength and mode I fracture energy of a room temperature vulcanizing silicone adhesive. *J Test Eval* 2015; 44: 1284–1293.
38. AFNOR. NF T 76-142. Méthode de préparation de plaques d'adhésifs structuraux pour la réalisation d'éprouvettes d'essai de caractérisation, 1988.
39. British Standard. BS 2782-0:2011. *Methods of testing plastics*, Part 2011.
40. Murakami S, Sekiguchi Y, Sato C, et al. Strength of cylindrical butt joints bonded with epoxy adhesives under combined static or high-rate loading. *Int J Adhes Adhes* 2016; 67: 86–93.
41. Zhang Y, Adams R and da Silva LFM. A rapid method of measuring the glass transition temperature using a novel dynamic mechanical analysis method. *J Adhes* 2013; 89: 785–806.
42. ASTM. D3433-99. Standard test method for fracture strength in cleavage of adhesives in bonded metal joints. *Annual book of ASTM standards* 2000; 15: 226–232.
43. de Moura M, Campilho R and Gonçalves J. Crack equivalent concept applied to the fracture characterization of bonded joints under pure mode I loading. *Compos Sci Technol* 2008; 68: 2224–2230.
44. de Moura M, Gonçalves J, Chousal J, et al. Cohesive and continuum mixed-mode damage models applied to the simulation of the mechanical behaviour of bonded joints. *Int J Adhes Adhes* 2008; 28: 419–426.
45. Banea M, Silva LFM and Campilho R. Effect of temperature on tensile strength and mode I fracture toughness of a high temperature epoxy adhesive. *J Adhes Sci Technol* 2012; 26: 939–953.
46. Shindo MS, Yamashita A and Hagiwara T. Trial manufacture of dynamic combined load testing machine and a few experiments on mild steel. In: *Proc Jpn S Mech Eng Kansai Branch 234th Meet, 754-10 (1975)* 1975; 45–47.
47. Lindholm U and Yeakley L. A dynamic biaxial testing machine. *Exp Mech* 1967; 7: 1–7.
48. Bezemer A, Guyt C and Vlot A. New impact specimen for adhesives: optimization of high-speed-loaded adhesive joints. *Int J Adhes Adhes* 1998; 18: 255–260.
49. Mulliken A and Boyce M. Mechanics of the rate-dependent elastic–plastic deformation of glassy polymers from low to high strain rates. *Int J Solids Struct* 2006; 43: 1331–1356.
50. Jancar J, Hoy RS, Jancarova E, et al. Effect of temperature, strain rate and particle size on the yield stresses and post-yield strain softening of PMMA and its composites. *Polymer* 2015; 63: 196–207.
51. Arruda EM, Boyce MC and Jayachandran R. Effects of strain rate, temperature and thermomechanical coupling on the finite strain deformation of glassy polymers. *Mech Mater* 1995; 19: 193–212.
52. Abdel-Wahab AA, Ataya S and Silberschmidt VV. Temperature-dependent mechanical behaviour of PMMA: experimental analysis and modelling. *Polym Test* 2017; 58: 86–95.

53. Cao K, Wang Y and Wang Y. Experimental investigation and modeling of the tension behavior of polycarbonate with temperature effects from low to high strain rates. *Int J Solids Struct* 2014; 51: 2539–2548.
54. Zgoul M and Crocombe AD. Numerical modelling of lap joints bonded with a rate-dependent adhesive. *Int J Adhes Adhes* 2004; 24: 355–366.
55. Avendaño R, Carbas R, Marques E, et al. Effect of temperature and strain rate on single lap joints with dissimilar lightweight adherends bonded with an acrylic adhesive. *Compos Struct* 2016; 152: 34–44.
56. Azevedo J, Campilho R, da Silva F, et al. Cohesive law estimation of adhesive joints in mode II condition. *Theor Appl Fract Mech* 2015; 80: 143–154.
57. Saldanha DFS, Canto C, da Silva LFM, et al. Mechanical characterization of a high elongation and high toughness epoxy adhesive. *Int J Adhes Adhes* 2013; 47: 91–98.
58. Avendaño R, Carbas R, Chaves F, et al. Impact loading of single lap joints of dissimilar lightweight adherends bonded with a crash-resistant epoxy adhesive. *J Eng Mater Technol* 2016; 138: 041019.

Paper 3

Content of Paper 3

Abstract

1. Introduction

2. Experimental details

2.1. Material and properties

2.2. Fabrication and testing

2.3. Data reduction schemes

3. Results

3.1. Experimental data

3.2. Numerical analysis

4. Conclusions

References

Check for updates

Article

JOURNAL OF COMPOSITE MATERIALS

Journal of Composite Materials
2017, Vol. 51(23) 3315–3326
© The Author(s) 2016
Reprints and permissions:
sagepub.co.uk/journalsPermissions.nav
DOI: 10.1177/0021998316682309
journals.sagepub.com/home/jcm
SAGE

Mode I fracture toughness of CFRP as a function of temperature and strain rate

JJM Machado[1], EAS Marques[1], RDSG Campilho[2] and Lucas FM da Silva[3]

Abstract

Composite structures currently used in the automotive industry must meet strict requirements for safety reasons. They need to maintain strength under varied temperatures and strain rates, including impact. It is therefore critical to fully understand the impact behaviour of composites. This work presents experimental results regarding the influence of a range of temperature and strain rates on the fracture energy in mode I, G_{IC}, of carbon fibre reinforced plastic plates. To determine G_{IC} as a function of temperature and strain rate, double cantilever beam specimens were tested at 20, 80 and -30°C, with strain rates of 0.2 and 11 s^{-1}. A complementary numerical study was performed with the aim of predicting strength using the measured values. This work has demonstrated a significant influence of the strain rate and temperature on G_{IC} of the composite materials, with higher strain rates and lower temperatures causing a decrease in the G_{IC} values.

Keywords

Carbon fibre reinforced plastic, impact, strain rates, temperature, fracture energy in mode I, double cantilever beam

Introduction

The wide use of fibre reinforced composite materials, namely carbon fibre reinforced plastic (CFRP), in the automotive industry can offer several advantages, such as lower structural weight, high strength and excellent stiffness to weight ratios.[1] While initially the use of carbon fibre in the automotive industry was restricted to non-structural components, nowadays these materials are starting to be used in crash absorbing structures. In order to achieve the technical requirements for safety, the structures designed in the automotive industry have to be able to undergo a variety of load conditions, deforming and absorbing energy but at the same time being capable to maintain their integrity. When in use, these structures can be subjected to wide ranges of temperature and strain rates (including impact loads), and therefore a complete knowledge of the behaviour of CFRP when operating under those circumstances is necessary.[2,3]

The use of composite materials is driven by the need to reduce the weight of vehicles, decreasing the quantity of material used and the fuel consumption as well. Composite materials are made of combinations of two or more different materials and combine their constituent's mechanical properties, providing in general high values of stiffness and strength as well as low density. When bonded, composite materials exhibit a completely different behaviour from metals and in the literature only a few studies can be found focusing on the behaviour of composites under impact loads. Regarding the composite materials, it is possible to consider that the automotive industry main interest is on the delamination resistance of CFRP laminates and/or the fracture behaviour of joints.

The mechanical properties of composite materials are sensitive to the variation of strain rate.[4] The concept of strain rate is characterized as being the change in strain (deformation) of a specific material with respect to time. In comparison to metals, the damage and failure

[1]Instituto de Ciência e Inovação em Engenharia Mecânica e Engenharia Industrial (INEGI), Portugal
[2]Instituto Superior de Engenharia do Porto (ISEP), Portugal
[3]Departamento de Engenharia Mecânica, Faculdade de Engenharia (FEUP), Universidade do Porto, Portugal

Corresponding author:
Lucas FM da Silva, Departamento de Engenharia Mecânica, Faculdade de Engenharia (FEUP), Universidade do Porto, Rua Dr. Roberto Frias, 4200-465 Porto, Portugal.
Email: lucas@fe.up.pt

mechanisms of composite materials are not entirely understood, particularly for the case of high strain rates of loading. The strain rate effect on composite tensile properties was investigated by several authors. In 1983, Harding and Welsh[3] studied the high strain rate longitudinal tensile behaviour of unidirectional carbon-epoxy laminates using a modified tensile split Hopkinson pressure bar (SHPB) apparatus, and found no significant strain rate effects. Other authors who obtained experimentally identical results were Taniguchi et al.[5] in 2007, and another conclusion from this research was the fact that the tensile properties in the transverse direction and the shear properties increased with the strain rate. In 2004, Ochola et al.[6] performed compressive tests (using a SHPB apparatus) on rod CFRP specimens and concluded about the strain rate sensitivity of the strain to failure. Another conclusion was the fact that as the strain rates increases the material experiences full disintegration, due to the higher energy value, which is the prevailing failure mode at low strain rates.

In 2000, Hou and Ruiz[7] tested woven CFRP using a SHPB apparatus at different strain rates in tension, compression and in-plane shear. The authors concluded that the properties that are dominated by the matrix are compression strength, Poisson's ratio, in-plane shear modulus, shear modulus and shear strength, being these properties strain rate dependent. The properties dominated by the fibres are tensile modulus and strength, which are virtually rate independent.

With the aim to summarize and understand the trends regarding the strain rate behaviour, Körber[8] in 2012 made a comparison of the available literature results of polymer composites. In the case of transverse modulus and strength, the strain rate influences the results because these properties are dominated by the resin.

The effects of extreme temperature variations on the impact damage of CFRP (orthotropic laminated plates) were experimentally determined by Kwang-Hee et al.[9] in 2001, using an air gun. The authors found that with the increase of temperature, the areas with delamination within the damaged areas were reduced. Also, the authors observed a linear relation between the impact energy and the areas where the delamination occurred, for the cases of extreme temperatures (low and high). Additionally, the ultimate tensile strength decreased with temperature in both laminates. With the decrease of temperature, the stiffness of the quasi-isotropic laminate increases.

López-Puente et al.[10] studied in 2002 the effect of low temperature on the intermediate and high velocity impact response of CFRP (tape and woven). The woven laminates were more capable of dealing with impact than the quasi-isotropic laminates. Impact behaviour of the tape laminate is negatively affected by the low temperature. Above the ballistic limit, a damage saturation was observed, and the temperature has no influence on the damage extension.

Damage in CFRP at low temperature, caused by low impact velocity, was studied by Gómez-del Río et al.[11] in 2005. Results revealed that decreasing the laminate temperature prior to impact introduces an effect on damage identical to that of increasing the impact energy, leading to a larger matrix cracking and deeper indentation on the impacted side. The same authors[12] also performed dynamic tests using a SHPB apparatus on CFRP with unidirectional and quasi-isotropic configurations. The influence of temperature and strain rate on the tensile strength is of little expression, in the case unidirectional laminates loaded in the fibre direction. Conversely, in the transverse direction, the strength increases. For the quasi-isotropic laminates, the influence of temperature doesn't present a significant effect on the in-plane properties, although a slight increase in tensile strength was registered regarding strain rate.

The vast majority of tests performed with the aim to characterize the material fracture energy in mode I, G_{IC}, are performed though the use of double cantilever beam (DCB) specimens.[2,13–17] The two main standards for this test are the ASTM D3433-99 and ISO 25217.[16]

Cohesive zone models (CZM) have been increasingly implemented in the last decades to simulate crack initiation as well propagation in delamination, being other applications cohesive and interfacial failure problems.[18] Several shapes of cohesive laws have been developed, namely, the triangular law.[19–24] The damage initiation is simulated by the CZMs, which occurs at a given node when the local strength of the material is attained. After an initial elastic phase, softening initiates, leading to damage growth when the stresses in that specific node reach zero. The evolution of damage is defined by an energetic criterion. The use of this methodology enables the complete numerical characterization of the structures behaviour until failure.[13]

In order to correctly perform numerical simulations, using CZM, it is necessary to accurately define the traction separation laws. While some information is available for static loads and at room temperature, there is the requirement to create traction separation laws able to model the behaviour of the CFRP under large strain rates and within large thermal amplitudes.

To enable the design of high performance and lightweight composite structures, to withstand large impact loads under varied conditions, these CZM models must be defined using data that covers many temperatures and strain rate. Therefore, the aim of this work was to assess experimentally and numerically the influence of a range of temperatures (20, 80 and -30°C) and strain rate conditions (0.2 and $11\,s^{-1}$) on the fracture

energy in mode I, G_{IC}, of CFRP, using DCB specimens. Three data reduction schemes were used to determine the value of fracture energy: compliance-based beam method (CBBM), corrected beam theory (CBT) and compliance calibration method (CCM). The models created using these properties were validated against experimental data to ensure their usefulness in the design of advanced composite structures.

Experimental details

Material and properties

The CFRP specimens used in this work were made of plies of carbon/epoxy pre-preg (SEAL® Texipreg HS 160 RM).

The properties of this material were previously determined in the work of Campilho[13] in 2009, and are presented in Table 1.

An important property to characterize the CFRP resin is the glass transition temperature, T_g. This property can be related to the strength of a polymer at a given temperature, therefore it is important to understand where the glass transition zone is located.[25,26] An in-house developed apparatus (based on the device proposed by Zhang et al.[27]) was used, based on the phenomenon that there is a corresponding peak in the damping value at the T_g of a polymer. For measuring the T_g using this apparatus, the specimen (an aluminium beam with a portion of adhesive bonded to it) is subjected to a constant vibrational movement at the beam's resonance frequency. The temperature at which the specimen displacement is lower can be identified by varying the temperature in a chamber containing the specimen and registering the amplitude of its movement. At this temperature maximum damping occurs, which can be understood as the temperature corresponding to the glass transition phase. A dummy static specimen is also used to register the temperature. The measurement of the resin T_g showed a value of 105°C.

Fabrication and testing

The specimens tested in this work consisted on unidirectional laminates of CFRP cut from bulk laminates, which were produced by hand lay-up and cured in a hot plate press. The bulk laminates with dimensions of $300 \times 300\,mm^2$ were fabricated from stacking of unidirectional 0° lay-up (with the aim to obtain better properties in the loading direction) in a total of 20 plies of carbon/epoxy pre-preg (SEAL® Texipreg HS 160 RM) with 0.15 mm of ply thickness. The cure cycle applied was of 130°C during 1 h.

Table 1. Properties of CFRP elastic orthotropic.[13]

Elastic modulus (MPa)	Poisson's ratio	Shear modulus (MPa)
$E_1 = 1.09E5$	$\nu_{12} = 0.342$	$G_{12} = 4315$
$E_2 = 8819$	$\nu_{13} = 0.342$	$G_{13} = 4315$
$E_3 = 8819$	$\nu_{23} = 0.380$	$G_{23} = 3200$

After to the removal from the press, the laminates were cut into smaller specimens using a diamond disc cutting machine. Edge finishing was carried out manually with 120 grit sandpaper in order to remove the loose fibres and smoothen the sharp edges.

The geometry of the CFRP DCB specimens was based on the ISO 15024 standard[28] from 2001, which is used to determine, in mode I, the interlaminar fracture toughness, G_{IC}, for unidirectional reinforced fibre-reinforced plastic composites.

Following the indications from ISO 15024 standard,[28] the dimensions (Figure 1) of each DCB specimen are the following: length of 125 mm, width of 25 mm and thickness of 3 mm. A pre-crack of $a_0 = 45$ mm was introduced, using a thin sheet of Teflon® with a thickness of 0.075 mm, to induce stable crack-propagation.

ISO 15024 standard[28] also indicates that the crack-opening mode due to a load applied perpendicularly to the plane of delamination using the DCB specimen can be achieved with the use of hinges or load blocks. In this work, load blocks were selected.

For each stage of strain rate and temperature, five specimens were tested, according to ISO 15024 standard.[28]

With the aim of correctly measuring the crack propagation, one side of the specimen was painted using a white paint spray. The value of the initial crack, a_0, was measured after a pre-crack inducing procedure, where the specimens were gradually loaded until the crack starts to propagate. To prepare the specimens for testing, the Teflon® sheet was removed from the specimens and a measurement scale was glued on the side starting from that point.

By changing the cross-head speed of the universal testing machine, the specimen can be subjected to different strain rates. The values of strain rate studied in this work and their respective cross-head displacement speeds are presented in Table 2.

The DCB tests were performed in an INSTRON® model 3367 universal test machine (Norwood, Massachusetts, USA) with a load capacity of 30 kN. For the tests performed with high temperature, a heating chamber was used, and for the low temperature range, nitrogen was injected inside the chamber. For the high and low temperatures, each specimen remained inside the chamber for a period of 10 min to ensure a homogenous temperature distribution along the specimen (measured with a thermocouple) before testing.

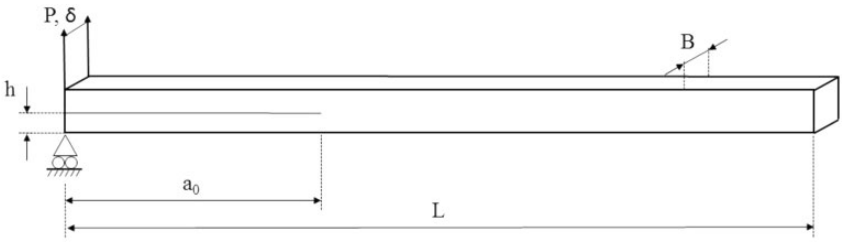

Figure 1. Dimensions of DCB CFRP specimens following ISO 15024 standard (L = 125 mm, B = 25 mm, h = 3 mm, a_0 = 45 mm).

Table 2. Conversion of values of cross-head displacement speed to strain rate.

	Cross-head displacement speed		
Conversion	2 mm/min	100 mm/min	120,000 mm/min[a]
Strain rates	0.2 s^{-1}	11 s^{-1}	13,333 s^{-1}

[a]Impact velocity of 2 m/s (values extrapolated for this range).

Table 3. Range of tests performed: Temperature and strain rates.

	Temperatures		
Tests to perform	−30°C	20°C	80°C
Strain rates	0.2 s^{-1} 11 s^{-1}	0.2 s^{-1} 11 s^{-1}	0.2 s^{-1} 11 s^{-1}

In the literature, different impact tests have been used to quantify the maximum load and energy absorbed using composite adherends, although the determination of the influence of temperature over different strain rates has never been previously considered. Therefore, the main goal of this work is to measure the fracture energy in mode I, G_{IC}, of DCB specimens at different strain rates and at different temperatures (Table 3).

During the testing procedure, the onset of stable delamination growth was monitored and the delamination initiation and propagation readings were recorded. For the case of 0.2 s^{-1} strain rate, pictures were taken every 5 s, and for 11 s^{-1} strain rate a video was logged. This was only performed for the 20°C tests, as the climatic chamber did not allow the direct measurement of delamination growth for other temperatures. This data was used to perform a comparison between different data reduction schemes.

Data reduction schemes

There are several methods described in the literature that allow the determination of the fracture toughness from the experimental results of DCB test specimens. The CCM and CBT methods depend on the measurement of the crack length during the test procedure, affecting the accuracy of the results since the crack propagation might be unstable.[29,30] In contrast, the more recently developed CBBM method does not require the measurement of the crack length. According to the literature, the two methods which provide the most accurate measurements of G_{IC} are the CBBM and the CBT.[13,14]

The CCM is a technique based on Irwin's approach, which is defined as the energy release rate. Equation (1) is derived from the Irwin–Kies theory, where G_{IC} represents the energy available for an increment of the crack extension.[31,32]

$$G_1 = \frac{P^2\, dC}{2B\, da} \tag{1}$$

In equation (1), P is the applied load, B represents the width of the specimen, C is the compliance (based on the flexibility of the material) and a is the crack length.

The values are fitted into a cubic polynomial approximation being the compliance, C, a function of a crack length, a.

The CBT also derives from the Irwin–Kies theory (equation (1)). The corrected crack has a deviation from the one assumed in the CCM, as the deformation around the crack tip is taken into account. The fracture toughness can then be determined by equation (2)[32,33]:

$$G_1 = \frac{3P\delta}{2B(a + |\Delta|)} \tag{2}$$

where δ is the loading line displacement and Δ is a correction factor for the crack tip rotation and deflection of the substrates, first proposed in 1992 by Wang and Williams.[33]

With the CBBM developed by de Moura et al.[14] in 2008, contrarily to the other methods, the crack length measurement is not necessary. By using the crack equivalent concept, this method depends only on the specimen's compliance during the test.[14,34] At the end

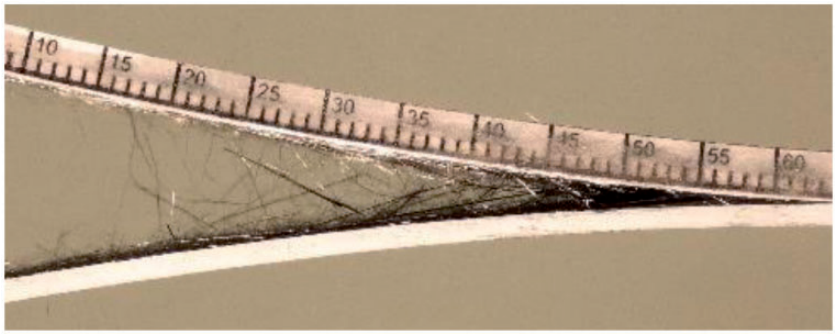

Figure 2. Presence of the effect of fibre bridging in a DCB specimen.

of the crack, a fracture process zone (FPZ) develops.[35] This region is characterized by the development of multiple micro-cracks and plasticization zones, which absorb some of the energy. For ductile adhesives, the energy dissipated in the FPZ is higher, and therefore should be considered in the calculations. This method is based on the beam theory of Timoshenko.[14,36,37]

By applying the CBBM, it is possible to determine G_{IC} using equation (3)[14,32,38,39]:

$$G_1 = \frac{6P^2}{B^2 h}\left(\frac{2a_{eq}^2}{h^2 F_f} + \frac{1}{5G}\right) \quad (3)$$

where a_{eq} is an equivalent crack length obtained from the experimental compliance and accounting for the FPZ, where a progressive softening occurs at the crack tip.[31] E_f is a corrected flexural modulus to account for all phenomena affecting the load-displacement (P-δ) curve, such as the stress concentration at the crack tip and stiffness variability between specimens. G is the shear modulus of the adherends and h represents the height of each specimen arm.[40]

Results

Experimental data

The methods used to quantify the value of the fracture energy under mode I loading, G_{IC}, using the DCB specimens were CCM, CBT and CBBM. As it is difficult to reliably measure the crack propagation during tests involving high and low temperature, the CCM and CBT methods have only been considered for specimens tested at 20°C, and for the remaining cases, the method CBBM was applied exclusively.

The fracture surface of all specimens tested were found to be very similar with very homogeneous appearance and a few broken fibres, typical of interlaminar failure in composite materials.

In 2000, a study conducted by Bui et al.[41] focused on the imperfect interlaminar interfaces in laminated composites. The authors stated the necessity to consider the presence of two values of strain energy release rates in the case of interlaminar fracture characterization, namely a value referring to characterization of the delamination onset ($G_{IC(\text{ini})}$), and a value related to delamination in a steady-state of growth ($G_{IC(\text{s/s-prop})}$). It was considered that ($G_{IC(\text{ini})}$) is identical to the energy release rate obtained during delamination growth. The authors specified that for a more realistic approach to the analysis of delamination, both values should be considered in the characterization of the resistance curve (R-curve) effects.

Some authors[42,43] estimated quantitatively the effect of cutting the fibre bridging during tests. The effect of fibre bridging is to increase the fracture toughness during crack propagation.

The effect of the phenomenon of fibre bridging (Figure 2) on the measured fracture energy, G_{IC}, was considered as it is not possible to perform the cutting of fibre during the execution of tests requiring the use of an environmental chamber.

Two different values of G_{IC} were considered for each R-curve. The first value, $G_{IC(\text{ini})}$, corresponds to the maximum value of force, when the crack starts to propagate. A second value, $G_{IC(\text{stab})}$, corresponds to the zone of stabilized crack propagation.

During the analysis of the test results, a distinction between values of fracture energy in the initiation of delamination (values taken from the maximum value of force), $G_{IC(\text{ini})}$, and for the crack stabilization, $G_{IC(\text{stab})}$ were considered.

The results of fracture energy corresponding to the crack initiation ($G_{IC(\text{ini})}$), using the maximum value of force from the P-δ curves, are presented in Figure 3.

It is possible to observe that with the increase of the strain rate from 0.2 to 11 s^{-1}, there was a decrease of the measured value of fracture energy, a situation which occurred for the three different ranges of temperature studied. The higher values of fracture energy, G_{IC}, occur for the highest value of temperature being tested since it is closer to the T_g of the resin used in the CFRP. The lower values of fracture energy, G_{IC}, occur

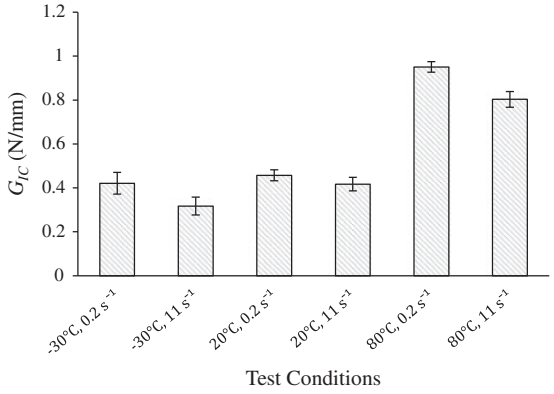

Figure 3. Values of fracture energy at the beginning of crack propagation ($G_{IC(ini)}$).

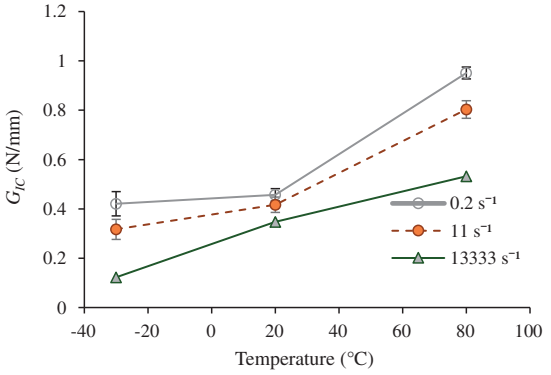

Figure 5. Prediction of fracture energy at the beginning of crack propagation ($G_{IC(ini)}$) for impact (13,333 s^{-1}) at the three ranges of temperature being studied.

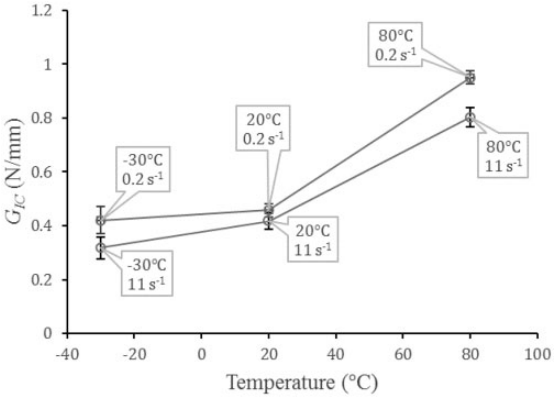

Figure 4. Fracture energy at the beginning of crack propagation ($G_{IC(ini)}$) as a function of temperature considering a strain rate of 0.2 s^{-1} and a strain rate of 11 s^{-1}.

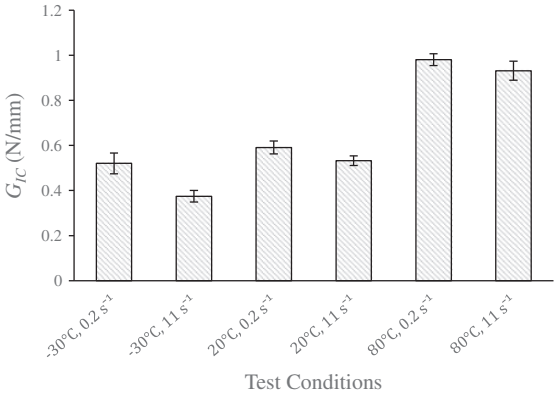

Figure 6. Fracture energy with stabilized crack propagation ($G_{IC(stab)}$).

for the lowest temperature as the resin presents a brittle behaviour and, at this temperature, the CFRP is more prone to premature failure caused by defects.

From Figure 4, it is possible to verify that, for both values of strain rate, there is a significant increase in the fracture energy ($G_{IC(ini)}$) as the temperature rises from 20 to 80°C. Between −30 and 20°C, the change of the fracture energy value is less noticeable. This effect can be basically explained by the behaviour of the resin of the CFRP matrix, which is brittle at lower temperatures but increases its ductility at temperatures nearing the T_g.

With the use of a logarithmic trend function (equation (4)),[44,45] it was possible to extrapolate the value of the fracture energy at the beginning of crack propagation ($G_{IC(ini)}$) for the three different temperatures being studied (Figure 5), when subjected to low speed impact conditions (a 2 m/s impact was considered, corresponding to 13,333 s^{-1}).

$$G_{IC(ini)} = A \times \ln(\dot{\varepsilon}) + B \quad (4)$$

A and B coefficients were determined from the logarithmic trend function, and $\dot{\varepsilon}$ corresponds to the strain rate.

The extrapolation results show a behaviour generally similar to that identified for lower strain rates, with a constant increase of the fracture energy as the temperature rises. Also, the higher the strain rate conditions, the lower will be the values of fracture energy, a behaviour observed for all ranges of temperature studied.

The results of fracture energy corresponding to stable crack propagation ($G_{IC(stab)}$) are presented in Figure 6.

The values considered were taken from the stabilization value, measured in the stabilized central section of the *R*-curve of each specimen tested.

As for the case of initiation fracture energy ($G_{IC(inic)}$), it is possible to observe that with the increase of the strain rate from 0.2 to 11 s^{-1}, there was a decrease of the value of the measured fracture energy, which occurred for the three temperatures studied in this work.

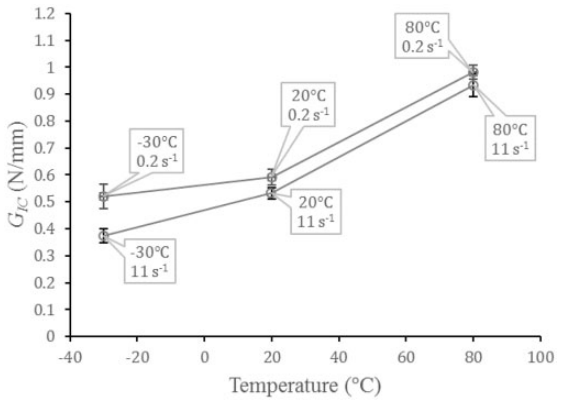

Figure 7. Fracture energy with stabilized crack propagation ($G_{IC(stab)}$) as a function of temperature considering: (a) strain rate of 0.2 s^{-1} and (b) strain rate of 11 s^{-1}.

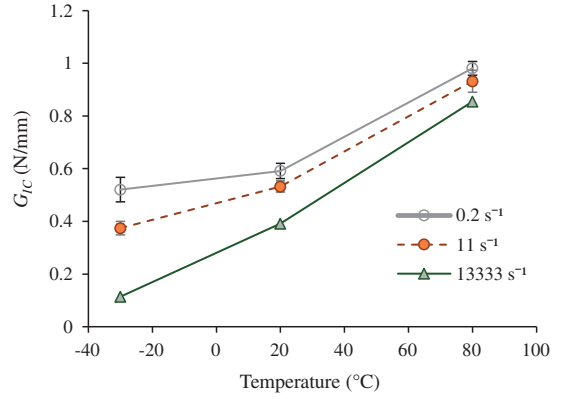

Figure 8. Prediction of fracture energy with stabilized crack propagation ($G_{IC(stab)}$) for impact (13,333 s^{-1}) at the three ranges of temperature being studied.

For the different strain rates and ranges of temperature studied, it is possible to observe the same behaviour in the fracture energy in both stages of crack propagation (Figure 7). In the case of stabilized crack propagation ($G_{IC(stab)}$), all values of fracture energy are higher than those for crack initiation ($G_{IC(inic)}$).

With the use of a logarithmic trend function (equation (4)), it was possible to extrapolate the value of the fracture energy with stabilized crack propagation ($G_{IC(stab)}$) for the three different temperatures being studied (Figure 8) of DCB specimens subjected to impact conditions (2 m/s or 120,000 mm/min).

The predicted trend indicates that the higher the temperature, the lower is the variation of fracture energy, which could be explained by the brittle properties of the resin impregnating the CFRP. It is also important to mention that, for all ranges of temperature, with the increase of strain rate there is an associated decrease of the fracture energy.

For 20°C and a strain rate of 0.2 s^{-1}, it is possible to observe an example of *R*-curves obtained by applying the CBBM, CCM and CBT methods (Figure 9). The results from these three methods are generally similar, without very significant differences.

An example of *R*-curves obtained by applying the CBBM, CCM and CBT methods is presented in Figure 10 for 20°C and a strain rate of 11 s^{-1}. As stated in the analysis of the tests performed with the strain rate of 0.2 s^{-1}, the values of fracture energy obtained in the three methods are relatively similar. The higher value of the fracture energy with stabilized crack propagation ($G_{IC(stab)}$) is obtained when using the CBBM method.

The values of the fracture energy, with stabilized crack propagation ($G_{IC(stab)}$), for the CBBM, CCM and CBT methods are presented in Table 4.

The values of fracture energy ($G_{IC(stab)}$) obtained by the CCM method were lower in comparison with the values obtained by the other two methods. Such fact is directly related with the adjustment of the polynomic function C = f(a).

Numerical analysis

A finite element analysis was performed using the software ABAQUS® with the objective of reproducing the experimental results. The model employed cohesive elements with a triangular (bilinear) traction-separation law, based on the mechanical and cohesive properties of the CFRP. Although the DCB geometry theoretically leads to a pure-mode loading, a mixed mode formulation was considered, using the quadratic stress criterion for damage initiation and the linear energetic criterion for damage propagation. A non-linear geometric analysis was performed. Regarding the loading and restraining conditions, a node at the edge of the lower arm was restrained in the plane, and a node at the edge of the upper arm was restrained horizontally and pulled vertically. The two-dimensional (2D) mesh applied in the models was constructed with plain-strain four-node quadrilateral solid finite elements (CPE4 from ABAQUS®), and four-node cohesive elements (COH2D4 from ABAQUS®). For each specimen arm, six elements were used through-thickness.[46,47] The mesh was refined to reduced element sizes in regions with large stress gradient. The mesh size of the cohesive elements was $0.2 \times 0.2\,mm^2$. The stiffness of the CFRP was considered to be the value of E_2 presented in Table 1.

The material properties used to characterize the elastic behaviour of the CFRP were previously presented in Table 1. The properties used to model the interlaminar fracture of the specimens are given in Table 5. It should be mentioned that the shear fracture energies in this

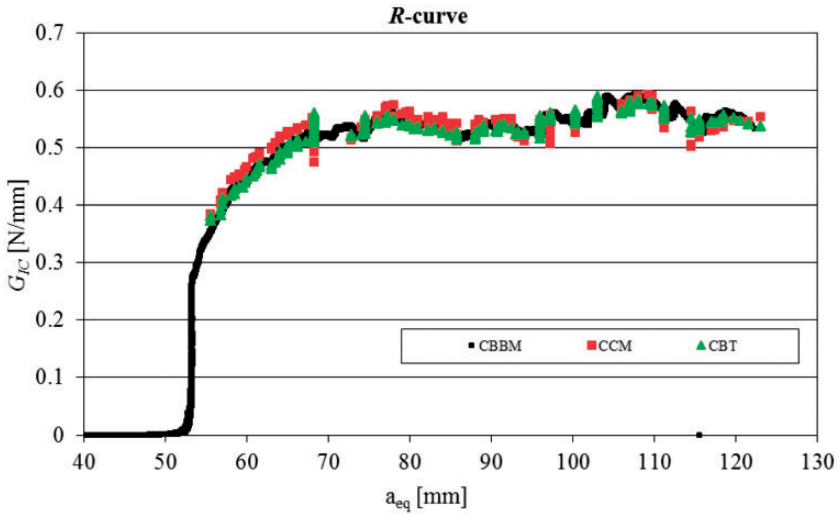

Figure 9. Comparison of fracture energy with stabilized crack propagation ($G_{IC(stab)}$) at 20°C and strain rate of 0.2 s^{-1} using the methods: CBBM, CCM and CBT.

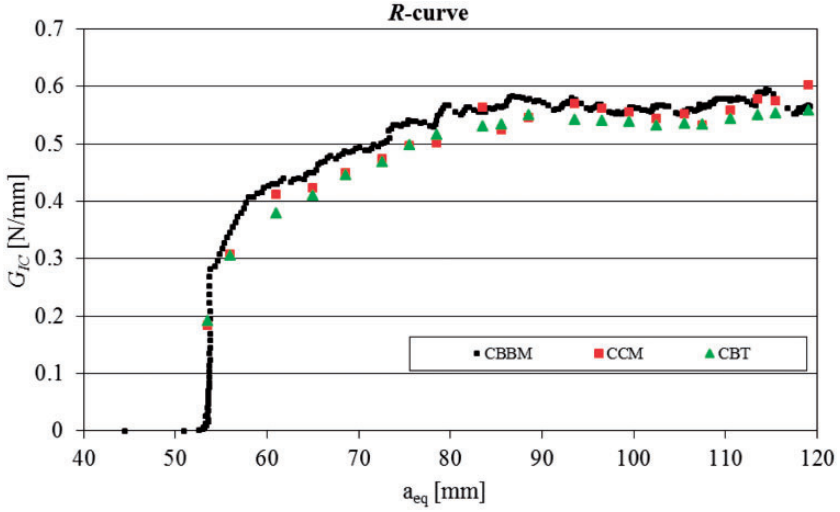

Figure 10. Comparison of fracture energy with stabilized crack propagation ($G_{IC(stab)}$) at 20°C and strain rate of 1 s^{-1} using the methods: CBBM, CCM and CBT.

Table 4. Comparison of fracture energy with stabilized crack propagation ($G_{IC(stab)}$) and standard deviation at 20°C and strain rate of 1 s^{-1} using the methods: CBBM, CCM and CBT.

Methods applied	20°C and 0.2 s^{-1}	20°C and 1 s^{-1}
CBBM		
$G_{IC(stab)}$ (N/mm)	0.59	0.53
Standard deviation (N/mm)	0.028	0.021
CBT		
$G_{IC(stab)}$ (N/mm)	0.59	0.58
Standard deviation (N/mm)	0.024	0.036
CCM		
$G_{IC(stab)}$ (N/mm)	0.58	0.47
Standard deviation (N/mm)	0.034	0.070

Table 5. CFRP cohesive properties used in the software ABAQUS®.[48]

CFRP cohesive properties	Value	Units
Nominal stress (normal)	25.0	MPa
Nominal stress (first direction)	13.5	MPa
Nominal stress (second direction)	13.5	MPa
Normal mode fracture energy	0.33	N/mm
Shear mode fracture energy (first direction)	0.79	N/mm
Shear mode fracture energy (second direction)	0.79	N/mm

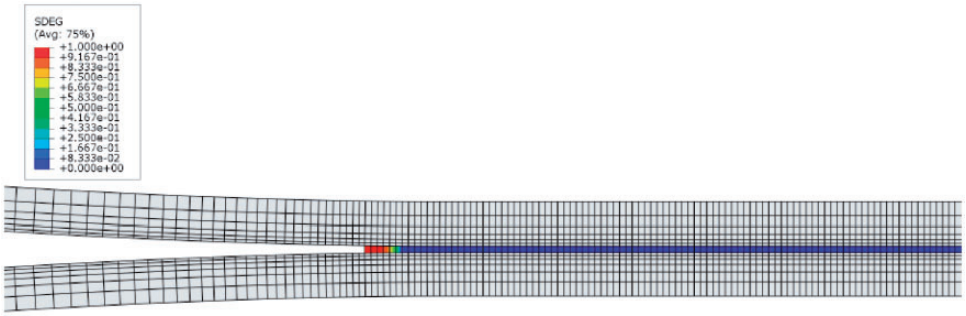

Figure 11. Example of the damage in the cohesive elements (SDEG) for the simulation performed at 20°C with a strain rate of $0.2\,s^{-1}$ for a CFRP DCB specimen.

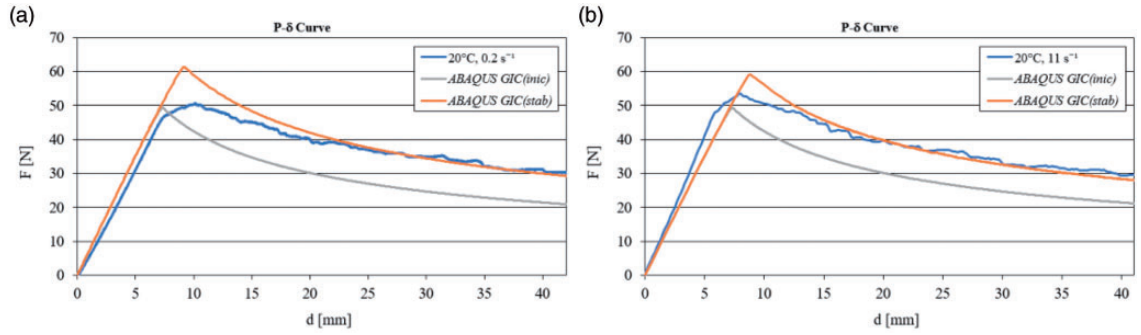

Figure 12. Comparison between the *P-δ* curves from the experimental test and simulations taking into account the value of $G_{IC(inic)}$ and $G_{IC(stab)}$ at 20°C: (a) Strain rate of $0.2\,s^{-1}$ and (b) strain rate of $11\,s^{-1}$.

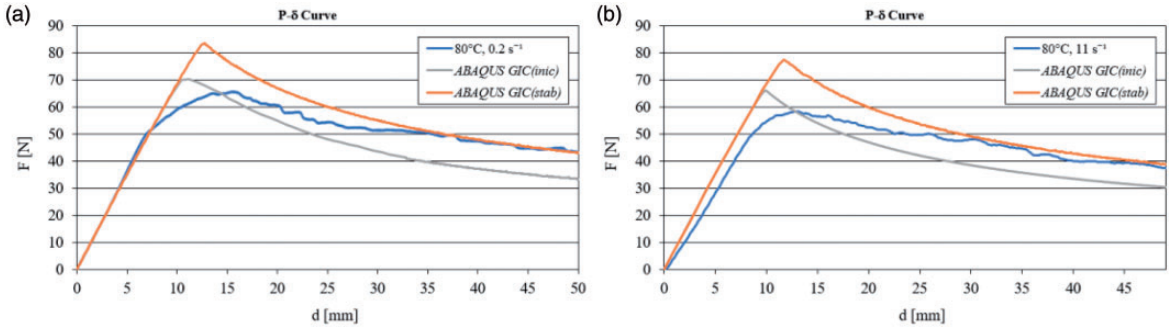

Figure 13. Comparison between the *P-δ* curves from the experimental test and simulations taking into account the value of $G_{IC(inic)}$ and $G_{IC(stab)}$ at 80°C: (a) Strain rate of $0.2\,s^{-1}$ and (b) strain rate of $11\,s^{-1}$.

table are merely indicative because for each numerical specimen the respective properties obtained in the experiments by the CBBM method were used.

An example of the model used and the result from the simulation is shown in Figure 11 for a strain rate of $0.2\,s^{-1}$ at 20°C.

Two different models were created, one using the values of fracture energy (G_{IC}) obtained for the initiation stage and another using the stabilization of crack propagation. As the practical results have a variation in the value of the fracture energy due to fibre bridging, it was expected to obtain an experimental *P-δ* curve between the two curves from the simulations.

Figures 12 to 14 present a comparison between the *P-δ* curves from the experimental test (a single representative curve was selected for each stage being analysed) and the simulations taking into account the value of $G_{IC(inic)}$ and $G_{IC(stab)}$. From each experimental *P-δ* curve, it was possible to obtain the value of $G_{IC(inic)}$ as

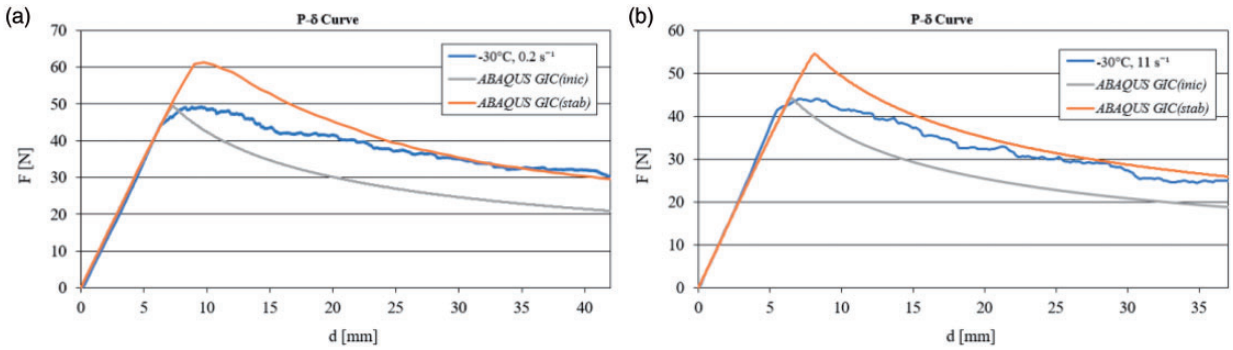

Figure 14. Comparison between the *P*-δ curves from the experimental test and simulations taking into account the value of $G_{IC(inic)}$ and $G_{IC(stab)}$ at -30°C: (a) Strain rate of $0.2\,s^{-1}$ and (b) strain rate of $11\,s^{-1}$.

the maximum value of fracture energy, and the value of ($G_{IC(stab)}$) from the average fracture energy.

The results show that the numerical results satisfactorily predict the value of fracture energy in mode I, G_{IC}, and that, in all cases, the *P*-δ curves obtained experimentally are between the curves obtained using the simulation considering both $G_{IC(inic)}$ and $G_{IC(stab)}$.

Conclusions

This work described the strain rate and temperature dependence of the fracture energy in mode I of CFRP specimens. The resultant data were used to create cohesive zone models, which were validated using existing experimental data. The main conclusions drawn from this work are presented below:

- For both values of strain rate, in the case of high temperature (80°C), the value of fracture energy ($G_{IC(inic)}$) has a larger increase in comparison to that observed at -30 and 20°C. The higher the temperature, the higher the value of fracture energy ($G_{IC(inic)}$). Such fact can be explained by the behaviour induced by the brittle resin of the CFRP matrix.
- For different strain rates and ranges of temperature, similar behaviour was identified in the fracture energy in both stages of crack propagation. As expected and in the case of stabilized crack propagation, all values of fracture energy ($G_{IC(stab)}$) were found to be higher than at the beginning of crack propagation ($G_{IC(inic)}$).
- At 20°C and a strain rate of $11\,s^{-1}$, *R*-curves were calculated applying the CBBM, CCM and CBT methods. The values of fracture energy obtained using the three methods were found to be relatively similar. The higher value of the fracture energy with the crack stabilized ($G_{IC(stab)}$) was obtained for the CBBM method.
- The CCM method presents the lowest values of fracture energy ($G_{IC(stab)}$) in comparison with the other two methods. Such fact can be directly related with the process of adjustment of the polynomic function C = f(a).
- The measured properties were used to validate finite element models, using cohesive elements. The models were found to be in good agreement with the experimental data.

Declaration of Conflicting Interests

The author(s) declared no potential conflicts of interest with respect to the research, authorship, and/or publication of this article.

Funding

The author(s) disclosed receipt of the following financial support for the research, authorship, and/or publication of this article: The authors gratefully acknowledge the funding of Project NORTE-01-0145-FEDER-000022 - SciTech - Science and Technology for Competitive and Sustainable Industries, co-financed by Programa Operacional Regional do Norte (NORTE2020), through Fundo Europeu de Desenvolvimento Regional (FEDER). The authors would also like to thank NAGASE ChemteX® for the financial support provided.

References

1. Campilho R, de Moura M, Ramantani D, et al. Tensile behaviour of three-dimensional carbon-epoxy adhesively bonded single-and double-strap repairs. *Int J Adhes Adhes* 2009; 29: 678–686.
2. da Silva L. *Handbook of adhesion technology*. Berlin, Germany: Springer Science & Business Media, 2011.
3. Harding J and Welsh L. A tensile testing technique for fibre-reinforced composites at impact rates of strain. *J Mater Sci* 1983; 18: 1810–1826.
4. Chaves F, da Silva L, de Moura M, et al. Fracture mechanics tests in adhesively bonded joints: a literature review. *J Adhes* 2014; 90: 955–992.
5. Taniguchi N, Nishiwaki T and Kawada H. Tensile strength of unidirectional CFRP laminate under high strain rate. *Adv Compos Mater* 2007; 16: 167–180.

6. Ochola R, Marcus K, Nurick G, et al. Mechanical behaviour of glass and carbon fibre reinforced composites at varying strain rates. *Compos Struct* 2004; 63: 455–467.
7. Hou J and Ruiz C. Measurement of the properties of woven CFRP T300/914 at different strain rates. *Compos Sci Technol* 2000; 60: 2829–2834.
8. Körber H. *Mechanical response of advanced composites under high strain rates*. Phd Thesis, University of Porto, Porto, Portugal, 2012.
9. Im K, Cha C, Kim S, et al. Effects of temperature on impact damages in CFRP composite laminates. *Compos B: Eng* 2001; 32: 669–682.
10. López-Puente J, Zaera R and Navarro C. The effect of low temperatures on the intermediate and high velocity impact response of CFRPs. *Compos B: Eng* 2002; 33: 559–566.
11. Gómez-del Rio T, Zaera R, Barbero E, et al. Damage in CFRPs due to low velocity impact at low temperature. *Compos B: Eng* 2005; 36: 41–50.
12. Gomez-del Rio T, Barbero E, Zaera R, et al. Dynamic tensile behaviour at low temperature of CFRP using a split Hopkinson pressure bar. *Compos Sci Technol* 2005; 65: 61–71.
13. Campilho R. *Repair of composite and wood structures*. Instituto Superior de Engenharia do Porto. Phd Thesis, Porto, Portugal, 2009.
14. de Moura M, Campilho R and Gonçalves J. Crack equivalent concept applied to the fracture characterization of bonded joints under pure mode I loading. *Compos Sci Technol* 2008; 68: 2224–2230.
15. Banea MD and da Silva L. Mechanical characterization of flexible adhesives. *J Adhes* 2009; 85: 261–285.
16. Canto C. *Strength and fracture energy of adhesives for the automotive industry*. MSc Thesis, Porto, Portugal, 2013.
17. Brunner A, Blackman B and Davies P. A status report on delamination resistance testing of polymer–matrix composites. *Eng Fract Mech* 2008; 75: 2779–2794.
18. Alfano G. On the influence of the shape of the interface law on the application of cohesive-zone models. *Compos Sci Technol* 2006; 66: 723–730.
19. Hillerborg A, Modéer M and Petersson P. Analysis of crack formation and crack growth in concrete by means of fracture mechanics and finite elements. *Cement Concr Res* 1976; 6: 773–781.
20. Mi Y, Crisfield M, Davies G, et al. Progressive delamination using interface elements. *J Compos Mater* 1998; 32: 1246–1272.
21. Mi Y, Crisfield M, Hellweg H, et al. Finite element method and progressive failure modelling of composite structures. *Comput Plast: Fundam Appl* 1997; 1: 239–254.
22. Alfano G and Crisfield M. Finite element interface models for the delamination analysis of laminated composites: mechanical and computational issues. *Int J Numer Methods Eng* 2001; 50: 1701–1736.
23. Campilho R. *Modelação numérica de reparações por sobreposição simples e dupla em materiais compósitos*. MSc Thesis, Porto, Portugal, 2007.
24. de Moura M, Fernandez M, de Morais A, et al. Numerical analysis of the edge crack torsion test for mode III interlaminar fracture of composite laminates. *Eng Fract Mech* 2009; 76: 469–478.
25. Marques EA, Banea MD, da Silva LF, et al. Effect of low temperature on tensile strength and mode I fracture energy of a room temperature vulcanizing silicone adhesive. *J Test Eval* 2015; 44: 1284–1293.
26. Marques E, da Silva L, Banea M, et al. Adhesive joints for low-and high-temperature use: an overview. *J Adhes* 2015; 91: 556–585.
27. Zhang Y, Adams R and da Silva L. A rapid method of measuring the glass transition temperature using a novel dynamic mechanical analysis method. *J Adhes* 2013; 89: 785–806.
28. ISO B. 15024: 2001. Fibre-reinforced plastic composites: Determination of mode I interlaminar fracture toughness, GIC, for unidirectional reinforced materials. BSI, 2002.
29. Bader M, Hamerton I, Hay J, et al. Double cantilever beam testing of repaired carbon fibre composites. *Compos A: Appl Sci Manuf* 2000; 31: 603–608.
30. Ducept F, Davies P and Gamby D. Mixed mode failure criteria for a glass/epoxy composite and an adhesively bonded composite/composite joint. *Int J Adhes Adhes* 2000; 20: 233–244.
31. da Silva L and Öchsner A. *Modeling of adhesively bonded joints*. Berlin, Germany: Springer, 2008.
32. Saldanha D, Canto C, da Silva L, et al. Mechanical characterization of a high elongation and high toughness epoxy adhesive. *Int J Adhes Adhes* 2013; 47: 91–98.
33. Wang Y and Williams J. Corrections for mode II fracture toughness specimens of composites materials. *Compos Sci Technol* 1992; 43: 251–256.
34. de Moura M, Campilho R and Gonçalves J. Pure mode II fracture characterization of composite bonded joints. *Int J Solids Struct* 2009; 46: 1589–1595.
35. Fernandes R, Chousal J, De Moura M, et al. Determination of cohesive laws of composite bonded joints under mode II loading. *Compos B: Eng* 2013; 52: 269–274.
36. Dias G, de Moura M, Chousal J, et al. Cohesive laws of composite bonded joints under mode I loading. *Compos Struct* 2013; 106: 646–652.
37. de Moura M, Gonçalves J and Magalhães A. A straightforward method to obtain the cohesive laws of bonded joints under mode I loading. *Int J Adhes Adhes* 2012; 39: 54–59.
38. de Moura M, Gonçalves J, Chousal J, et al. Cohesive and continuum mixed-mode damage models applied to the simulation of the mechanical behaviour of bonded joints. *Int J Adhes Adhes* 2008; 28: 419–426.
39. Silva F, Xavier J, Pereira F, et al. Determination of cohesive laws in wood bonded joints under mode I loading using the DCB test. *Holzforschung* 2013; 67: 913–922.
40. Banea M, da Silva L and Campilho R. Effect of temperature on tensile strength and mode I fracture toughness of a high temperature epoxy adhesive. *J Adhes Sci Technol* 2012; 26: 939–953.
41. Bui V, Marechal E and Nguyen-Dang H. Imperfect interlaminar interfaces in laminated composites: interlaminar

stresses and strain-energy release rates. *Compos Sci Technol* 2000; 60: 131–143.
42. de Moura M, Campilho R, Amaro A, et al. Interlaminar and intralaminar fracture characterization of composites under mode I loading. *Compos Struct* 2010; 92: 144–149.
43. Iwamoto M, Ni Q, Fujiwara T, et al. Intralaminar fracture mechanism in unidirectional CFRP composites: Part I: Intralaminar toughness and AE characteristics. *Eng Fract Mech* 1999; 64: 721–745.
44. Zgoul M and Crocombe A. Numerical modelling of lap joints bonded with a rate-dependent adhesive. *Int J Adhes Adhes* 2004; 24: 355–366.
45. Avendaño R, Carbas R, Marques E, et al. Effect of temperature and strain rate on single lap joints with dissimilar lightweight adherends bonded with an acrylic adhesive. *Compos Struct* 2016; 152: 34–44.
46. Daghyani HR, Ye L and Mai Y-W. Mixed-mode fracture of adhesively bonded CF/epoxy composite joints. *J Compos Mater* 1996; 30: 1248–1265.
47. Campilho RDSG, De Moura M, Barreto A, et al. Fracture behaviour of damaged wood beams repaired with an adhesively-bonded composite patch. *Compos A: Appl Sci Manuf* 2009; 40: 852–859.
48. Neto J, Campilho R and Da Silva L. Parametric study of adhesive joints with composites. *Int J Adhes Adhes* 2012; 37: 96–101.

Paper 4

Content of Paper 4

Abstract

1. Introduction

2. Experimental details

2.1. Material and properties

2.2. Fabrication and testing

2.3. Data reduction schemes

3. Results

3.1. Experimental data

3.2. Numerical analysis

4. Conclusions

References

Composites Part B 114 (2017) 311–318

Contents lists available at ScienceDirect

Composites Part B

journal homepage: www.elsevier.com/locate/compositesb

Mode II fracture toughness of CFRP as a function of temperature and strain rate

J.J.M. Machado [a], E.A.S. Marques [a], R.D.S.G. Campilho [b], Lucas F.M. da Silva [c, *]

[a] Instituto de Ciência e Inovação Em Engenharia Mecânica e Engenharia Industrial (INEGI), Rua Dr. Roberto Frias, 4200-465 Porto, Portugal
[b] I Instituto Superior de Engenharia Do Porto (ISEP), Instituto Politécnico Do Porto, Rua São Tomé, 4200-485 Porto, Portugal
[c] Departamento de Engenharia Mecânica, Faculdade de Engenharia (FEUP), Universidade Do Porto, Rua Dr. Roberto Frias, 4200-465 Porto, Portugal

ARTICLE INFO

Article history:
Received 5 December 2016
Received in revised form
25 January 2017
Accepted 9 February 2017
Available online 14 February 2017

Keywords:
CFRP
Impact
Strain rates
Temperature
Fracture energy in mode II
End notched flexure

ABSTRACT

Knowledge of the fracture properties of composite materials is fundamental to predict the impact behaviour of the lightweight structures currently used in the automotive industry. Although there is substantial research on mode I fracture behaviour of composites, limited information exists on mode II behaviour. This work aims to fulfil this gap, presenting experimental data regarding the influence of temperature and strain rate on the fracture energy in mode II, G_{IIC}, of composite plates. Significant influence of the strain rate and temperature on G_{IIC} of the composite materials was found. Higher strain rates led to a decrease of G_{IIC} up to 17%. An increase of temperature corresponded to an increase of G_{IIC} up to 15% and a decrease of temperature originated a decrease of G_{IIC} up to 7%.

© 2017 Elsevier Ltd. All rights reserved.

1. Introduction

Fibre reinforced composite materials, such as carbon fibre reinforced composite (CFRP), are extensively employed in the automotive industry as they can offer several advantages over traditional materials, such as lower structural weight, high strength and excellent stiffness to weight ratios [1]. While initially the use of carbon fibre in the automotive industry was restricted to non-structural components, nowadays these materials are starting to be used in adhesively bonded crash absorbing structures. To pass the most recent safety requirements, the bonded composite structures designed in the automotive industry must be able to undergo a variety of load conditions, deforming and absorbing energy but at the same time being capable to maintain their integrity. When in use, these structures can be subjected to wide ranges of temperature and strain rates (including impact loads), and therefore a complete knowledge of the behaviour of CFRP when operating under those circumstances is necessary [2–6].

The mechanical properties of composite materials are sensitive to the variation of strain rate [7]. The concept of strain rate is characterized as being the change in strain (deformation) of a specific material with respect to time. In comparison to metals, the damage and failure mechanisms of composite materials are not entirely understood, particularly for the case of large rates of loading [8]. The strain rate effect on the tensile properties of composites was investigated by several authors. In 1983, Harding and Welsh [3] studied the high strain rate (from 10^{-4} s^{-1} to 1000 s^{-1}) longitudinal tensile behaviour of unidirectional carbon-epoxy laminates using a modified tensile split Hopkinson pressure bar (SHPB) apparatus, and found no significant strain rate effects. Other authors that obtained experimentally identical results were Taniguchi et al. [9] in 2007. Their work, performed from quasi-static conditions to 100 s^{-1}, also identified of an increase of the tensile properties in the transverse direction and the shear properties with the strain rate. In 2004, Ochola et al. [10] performed compressive tests (using a SHPB apparatus) on rod CFRP specimens, with strain rates ranging from 10^{-3} to 450 s^{-1} and concluded that strain at failure is strain rate sensitive. Another conclusion was the fact that as the strain rates increases the material experiences full disintegration, due to the higher energy value, which is the prevailing failure mode at low strain rates.

In 2000, Hou and Ruiz [11] tested woven CFRP using a SHPB apparatus at different strain rates in tension, compression and in-

* Corresponding author.
E-mail address: lucas@fe.up.pt (L.F.M. da Silva).

http://dx.doi.org/10.1016/j.compositesb.2017.02.013
1359-8368/© 2017 Elsevier Ltd. All rights reserved.

plane shear. The authors concluded that the properties that are dominated by the matrix are: compression strength, Poisson's ratio, in-plane shear modulus, shear modulus and shear strength, with all these properties being strain rate dependent. The properties dominated by the fibres are the tensile modulus and strength, which are virtually rate independent.

With the aim to summarize and understand the trends regarding the strain rate behaviour, Körber [12] in 2012 made a comparison of the available literature results of polymer composites. From a range of strain rates from 10^{-4} to 10^{3} s^{-1} the effect of the strain rate on longitudinal tensile modulus and strength is not significant. In the case of transverse modulus and strength, strain rates above 10^{2} s^{-1} influence the results. This is mainly due to the strain rate sensitivity of the resin, which absorbs most of the loads in the transverse direction.

The effects of extreme temperature variations on the impact damage of CFRP (orthotropic laminated plates) were experimentally determined by Kwang-Hee et al. [13] in 2001, using an air gun. The authors found that with an increase of temperature, the areas with delamination within the damaged areas were reduced. Also, the authors observed a linear relation between the impact energy and the areas where the delamination occurred, for the cases of extreme temperatures (low and high). Additionally, the tensile strength decreased with temperature in both laminates. With a decrease of temperature, the stiffness of the quasi-isotropic laminate increases.

López-Puente et al. [14] studied in 2002 the effect of low temperature on the intermediate and high velocity impact response of CFRP (tape and woven). The woven laminates were more capable of dealing with impact than the quasi-isotropic laminates. Impact behaviour of the tape laminate was negatively affected by the low temperature. Above the ballistic limit, a damage saturation was observed, and the temperature had no influence on the damage extension.

Damage in CFRP at low temperature, caused by low impact velocity, was studied by Gómez-del Río et al. [15] in 2005. Results revealed that decreasing the laminate temperature prior to impact has an effect on damage identical to that of increasing the impact energy, leading to a larger matrix cracking and deeper indentation on the impacted side. The same authors [16] also performed dynamic tests using a SHPB apparatus on CFRP with unidirectional and quasi-isotropic configurations. The influence of temperature and strain rate on the tensile strength is of little expression, in the case of unidirectional laminates loaded in the fibre direction which is line with the results previously shown by Körber [12]. Conversely, in the transverse direction, the strength increases. For the quasi-isotropic laminates, the influence of temperature revealed no significant effect on the in-plane properties, although a slight increase in tensile strength was registered regarding strain rate.

Although there are several tests to determine G_{IIC}, the shear fracture characterization of CFRP is still a relatively unexplored field due to some inherent aspects of those tests. Tests that can be performed are: end notched flexure (ENF) test, end loaded split (ELS) and four-point end notched flexure (4ENF) [17]. The ENF test was first proposed by Russel and Street [18]. In their study the crack propagated abruptly, and G_{IIC} initiation was then determined. The ELS testing method has the advantage of having a larger range of crack length that propagates stably [19,20]. A problem of the ELS test is the necessity of having a clamp which causes a variability and increases the complexity of data reduction [21]. A complex setup is required for the 4ENF test and, due to friction effects, data might be influenced by errors [22]. The most suitable test for mode II fracture characterization of bonded joints is the ENF, although problems of unstable crack growth and crack monitoring during propagation have not yet been fully addressed. In tests to characterize G_{IIC} the crack tends to close due to direction of the applied load, obstructing the accurate visualization of its tip [23].

Hiroaki et al. [24] evaluated the G_{IIC} of CFRP using substrates with two values of thickness, concluding that the fracture toughness increased linearly with the increase of substrates thickness.

Tadaharu et al. [25] assessed G_{IIC} of unidirectional CFRP laminates, and concluded that for carbon/epoxy laminates the dynamic interlaminar fracture toughness depends on the deflection rate. Similarly, Briggs and Ramulu [26], evaluated the G_{IIC} of ENF specimens with CFRP adherends and also found a clear rate dependence.

Chou *el al.* [27] studied the correlation of damage resistance under low velocity impact and mode II delamination resistance of CFRP laminates. The authors studied five different materials and divided them into two types, a compatible type, demonstrating high impact resistance under low velocities with high mode II delamination resistance, and a second type designated by non-compatible, presenting a poor resistance at low velocities, although presenting a higher resistance to delamination in mode II. The main difference between these two types was that in the case of the compatible types the resistance to delamination in mode II is superior in both sub-critical crack growth region and propagation.

Stevnovic et al. [28] investigated the influence of pre-crack conditions on the behaviour of unidirectional composite materials in mode II. Two different sets of specimens were used: one set with a blunt starter crack and another with a fatigue induced pre-crack. Authors observed that there was no influence of the pre-crack condition on the fracture toughness of the composite.

Machado et al. [29] have recently explored the effect of temperature and strain rate on the mode I fracture toughness of CFRP DCB specimens. The results have demonstrated that mode I fracture energy increases with temperature, while higher strain rates will result in a decrease in stiffness.

Cohesive zone models (CZM) have been increasingly implemented in the last decades to simulate crack initiation and progression, as well as delamination in composite materials. Other applications include cohesive and interfacial failure problems [30]. Several shapes of cohesive laws have been developed, namely, the triangular law [31–36]. Damage initiation is simulated by CZM's, which occurs at a given node when the local strength of the material is attained. After an initial elastic phase, softening initiates, leading to damage growth when the stresses in that specific node reach zero. The evolution of damage is defined by an energetic criterion. The use of this methodology enables the complete numerical characterization of the structures behaviour until failure [37].

In order to correctly perform numerical simulations, using CZM, it is necessary to accurately define the traction separation laws. While some information is available for static loads and at room temperature, there is the requirement to create traction-separation laws able to model the behaviour of the CFRP under large strain rates and within large thermal amplitudes.

To enable the design of high performance and lightweight composite structures, to withstand large impact loads under varied conditions, these CZM models must be defined using data that covers many temperatures and strain rates. Therefore, the aim of this work was to experimentally and numerically assess the influence of a range of temperatures (20, 80 and −30 °C) and strain rate conditions (0.2 and 11 s^{-1}) on G_{IIC} of CFRP, using ENF specimens. There is limited information regarding the influence of strain rate on the fracture toughness of composite materials and these strain rates were selected to complement the work previously performed by the authors on mode I fracture toughness using a similar experimental procedure [29]. Three data reduction schemes were used to determine the value of G_{IIC}: compliance-based beam method (CBBM), corrected beam theory (CBT) and compliance

Table 1
Elastic orthotropic properties of CFRP (1–fibres direction, 2–transverse direction, 3–out-of-plane direction [37].

Elastic Modulus (GPa)	Poisson's Ratio	Shear Modulus (GPa)
$E_1 = 109$	$\nu_{12} = 0.342$	$G_{12} = 4.315$
$E_2 = 8.819$	$\nu_{13} = 0.342$	$G_{13} = 4.315$
$E_3 = 8.819$	$\nu_{23} = 0.380$	$G_{23} = 3.200$

calibration method (CCM). The models created using these properties were validated against experimental data to ensure their accuracy and suitability for the design of advanced composite structures.

2. Experimental details

2.1. Material and properties

The CFRP specimens were comprised of twenty plies of carbon/epoxy pre-preg (SEAL® Texipreg HS 160 RM), oriented in a single direction. The elastic mechanical properties of this material were previously determined in the work of Campilho [37] in 2009, and are presented in Table 1.

As this study concerns the temperature dependence of the fracture energy, it is also important to be aware of the glass transition temperature, T_g, of the composite resin. This property has considerable influence on the strength of a polymer at a given temperature. Below T_g the composite resin is stiff while above it is flexible. It is therefore important to understand where the glass transition zone is located [38,39] and ensure that the material operates below T_g. An in-house developed apparatus [40] was used, based on the phenomenon that there is a peak in the damping value at the T_g of a polymer. Using this apparatus, the resin T_g showed a value of 105 ± 2 °C.

2.2. Fabrication and testing

The specimens tested in this work are unidirectional laminates of CFRP cut from bulk laminates. The bulk laminates were fabricated by stacking unidirectional 0° lay-up (with the aim of obtaining better properties in the loading direction) in a total of twenty plies of carbon/epoxy pre-preg material (SEAL® Texipreg HS 160 RM), each ply 0.15 mm thick. The cure cycle consisted of applying a temperature cycle of 130 °C during 1 h.

After removal from the press (the average pressure was of 0.30 MPa), the laminates were cut into smaller specimens using a diamond blade saw equipped cutting machine. Edge finishing procedures were carried out manually with a 120-grit sandpaper to remove the loose fibres and smoothen the sharp edges.

The dimensions (Fig. 1) of each ENF specimen are the following: length ($2L$) of 200 mm, width (B) of 25 mm and thickness ($2 \times h$) of 3 mm. The total length of the specimen was slightly superior to the 200 mm indicated, in order to allow the correct support of the specimen (not in its edges and keeping it centred) during testing. A pre-crack of $a_0 = 70$ mm (considered to be equal to 70% of half-length of the specimen) was introduced during the manual stacking procedure in order to provide crack growth stability [41], using a thin sheet of Teflon® with a thickness of 0.075 mm.

Table 2
Conversion of values of cross-head displacement speed to strain rate.

Conversion	Cross-head displacement speed	
	2 mm/min	100 mm/min
Strain Rates	0.2 s^{-1}	11 s^{-1}

For each stage of strain rate and temperature, five specimens were tested.

With the aim of correctly measure and monitor the crack propagation, one side of the specimen was painted with a white paint spray and a measurement scale was glued to the upper edge of each specimen. The initial crack, a_0, was introduced by gradually loading the specimens until a small amount of crack propagation could be detected. To prepare the specimens for testing, the Teflon® sheet was removed from the specimens.

By changing the cross-head speed of the universal testing machine, the specimen can be subjected to different strain rates. The values of strain rate studied in this work and their respective cross-head displacement speeds are presented in Table 2.

The ENF tests were performed in an INSTRON® model 3367 universal test machine (Norwood, Massachusetts, USA) with a load capacity of 30 kN. For the tests performed at high temperature, a heated climatic chamber was employed, and for the low temperature range nitrogen was injected inside the chamber. Before testing, each specimen remained inside the chamber for a period of 10 min to ensure a homogenous temperature distribution along the specimen (measured with a thermocouple).

In the literature, different impact tests have been used to quantify the maximum load and energy absorbed using composite adherends, although the determination of the influence of temperature and different strain rates on the fracture energy has never been previously considered. Therefore, the main goal of this work is to measure G_{IIC} of ENF specimens at different strain rates and at different temperatures (Table 3).

Table 3
Range of tests performed: temperature and strain rates.

Tests to Perform	Temperatures		
	−30 °C	20 °C	80 °C
Strain Rates	0.2 s^{-1} 11 s^{-1}	0.2 s^{-1} 11 s^{-1}	0.2 s^{-1} 11 s^{-1}

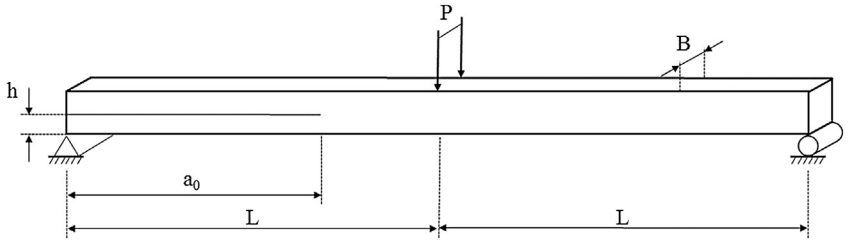

Fig. 1. Dimensions of ENF CFRP specimens (L = 100 mm, B = 25 mm, h = 1.5 mm, a_0 = 70 mm).

During the testing procedure, the onset of stable delamination growth was monitored and the delamination initiation and propagation readings were recorded. For each specimen, the load-displacement (P-δ) curve was obtained. For mode II fracture characterization tests, it is very difficult to monitor the crack propagation, as the crack often grows without a visible opening [21]. For tests performed at 20 °C, and for the case of 0.2 s^{-1} strain rate, pictures were taken every 5 s. For 20 °C and 11 s^{-1} strain rate, a video was logged instead to provide more data points. For −30 °C and 80 °C, the use of the climatic chamber precluded the direct measurement of crack growth.

2.3. Data reduction schemes

Several methods are described in the literature that allow the determination of the fracture toughness from the experimental results of ENF test specimens. The CCM and CBT methods depend on the measurement of the crack length during the test procedure, affecting the accuracy of the results since the crack propagation might be unstable [42,43]. In contrast, the more recently developed CBBM method does not require such measurement. According to the literature, the two methods which provide the most accurate measurements of G_{IIC} are the CBBM and the CBT [37,44].

The CCM is a technique based on the Irwin's approach which is defined as the energy release rate. Equation (1) is derived from the Irwin-Kies theory [45], where G_{IIC} represents the energy available for an increment of the crack extension [46,47].

$$G_{IIC} = \frac{P^2}{2B}\frac{dC}{da} \tag{1}$$

In Equation (1), P is the applied load (which is applied monotonically), B represents the width of the specimen, $C = \frac{\delta}{P}$ is the compliance (based on the flexibility of the material) and a is the crack length. The use of cubic polynomials ($C = C_1 a^3 + C_0$) to fit the $C = f(a)$ curves leads to Equation (2) [23].

$$G_{IIC} = \frac{3P^2 C_1 a^2}{2B} \tag{2}$$

The values are fitted into a cubic polynomial approximation, with C as a function of a.

The CBT also derives from the Irwin-Kies theory (Equation (1)). The corrected crack has a deviation from the one assumed in the CCM, as the deformation around the crack tip is taken into account. G_{IIC} can then be determined by Equation (3) [47,48]:

$$G_{IIC} = \frac{9(a + 0.42\Delta_I)^2 P^2}{16B^2 h^3 E_1} \tag{3}$$

where E_1 is the axial modulus, h corresponds to half height of the specimen and Δ_I is the crack length correction to account for shear deformation and it is given by Equation (4), first proposed in 1992 by Wang and Williams [48].

$$\Delta_I = h\sqrt{\frac{E_1}{11G_{13}}\left[3 - 2\left(\frac{\Gamma}{1+\Gamma}\right)^2\right]} \tag{4}$$

Γ is determined by Equation (5):

$$\Gamma = 1.18\frac{\sqrt{E_1 E_3}}{G_{13}} \tag{5}$$

being E_3 the transverse moduli and G_{13} the shear moduli.

With the CBBM developed by de Moura et al. [44] in 2008, contrarily to the other methods, measurement of a crack length is not necessary. By using the crack equivalent concept, this method depends only on the specimen's compliance during the test [23,44]. At the end of the crack, a fracture process zone (FPZ) develops [49]. This region is characterized by the development of multiple micro-cracks and plasticization zones, which absorb some of the energy. For ductile matrices, the energy dissipated in the FPZ is higher, and therefore it should be considered in the calculations. This method is based on the beam theory of Timoshenko [44,50,51].

By applying the CBBM, it is possible to determine G_{IIC} using Equation (6) [44,47,52,53]:

$$G_{IIC} = \frac{9P^2 a_{eq}^2}{16B^2 E_f h^3} \tag{6}$$

where a_{eq} is an equivalent crack length obtained from the experimental compliance and accounting for the FPZ, where a progressive softening occurs at the crack tip [46]. E_f is a corrected flexural modulus to account for all phenomena affecting the P-δ curve, such as the stress concentrations at the crack tip and stiffness variability between specimens. G is the shear modulus of the adherends, h represents the height of and B is the width of each specimen arm [54].

3. Results

3.1. Experimental data

The methods used to quantify G_{IIC} using the ENF specimens were the CCM, CBT and CBBM. As previously stated, it is difficult to reliably measure the crack propagation during tests involving high and low temperature, so methods that rely on crack measurement, such as the CCM and CBT methods, have only been considered for the specimens tested at 20 °C, while for the remaining cases only the CBBM method was applied.

The results of G_{IIC} using the maximum value of P from the P-δ curves were obtained by the CBBM method and are presented in Fig. 2.

It is possible to observe that with the increase of the strain rate from 0.2 to 11 s^{-1}, there was a decrease of the measured G_{IIC}, which occurred for the three different ranges of temperature studied. Higher values of G_{IIC} occur for the highest value of temperature being tested since it is closer to the T_g of the resin used in the CFRP. Lower values of G_{IIC} occur for the lowest temperature as the resin

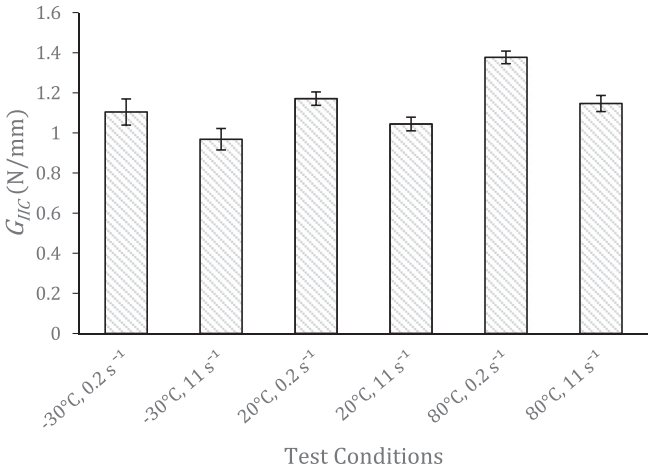

Fig. 2. Values of G_{IIC} for all the conditions tested.

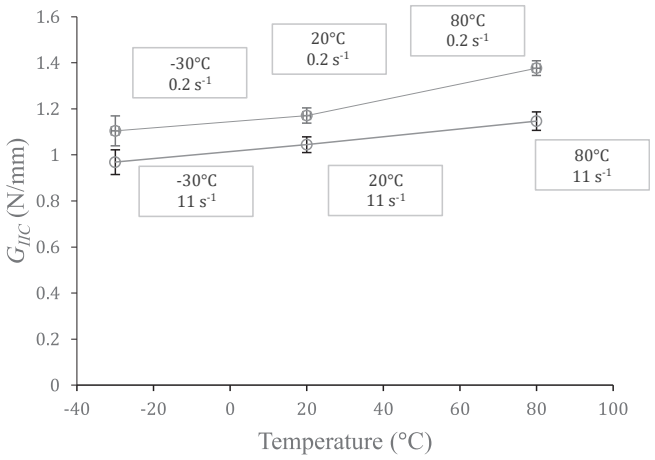

Fig. 3. G_{IIC} as a function of temperature considering strain rates of 0.2 and 11 s^{-1}.

presents a brittle behaviour and at this temperature the CFRP is more prone to premature failure caused by defects.

From Fig. 3 it is possible to verify that, for both values of strain rate, there is a significant increase of G_{IIC} as the temperature rises from 20 to 80 °C. Between −30 and 20 °C, the change of the fracture energy value is less noticeable. This effect can be explained by the behaviour of the resin of the CFRP matrix, which is brittle at lower temperatures but increases its ductility at temperatures nearing the T_g.

The experimental results allowed the extrapolation as well as the calculation of each property under impact speed conditions. With the use of a logarithmic trend function (Equation (7)), it was possible to extrapolate the value of G_{IIC} for the three different temperatures being studied (Fig. 4), when subjected to low speed impact conditions (a 2 m/s impact was considered, corresponding to 13333 s^{-1}).

$$G_{IIC} = A \times ln(\dot{\varepsilon}) + B \tag{7}$$

A and B coefficients were determined from the logarithmic trend function, and $\dot{\varepsilon}$ corresponds to the strain rate. This logarithmic extrapolation process has been first proposed by the work of Zgoul and Crocombe [55] and further validated by the work of Avendaño et al. [56].

The extrapolation results show that the variation of G_{IIC} is less pronounced for high strain rates, with an almost constant value as the temperature rises. This effect is due to the fact that the difference between the fracture energy of the 0.2 s^{-1} and 11 s^{-1} conditions increases with an increase in temperature. Using this data, the logarithmic law used predicts lower values of G_{IIC}, between 0.7 and 0.8 N/mm.

For 20 °C and a strain rate of 0.2 s^{-1}, it is possible to observe an example of R-curves obtained by applying the CBBM, CCM and CBT methods (Fig. 5). The results from these three methods are generally similar, without very significant differences. A steady-state propagation value of G_{IIC} is also observed.

The R-curves for 20 °C and a strain rate of 11 s^{-1} were not obtained since the measurement of the crack propagation was not possible and the length of test was extremely short, making the crack length, a, impossible to retrieve even from the video data.

The values of G_{IIC} for the CBBM, CCM and CBT methods are presented in Table 4.

The values of G_{IIC} obtained by the CCM were lower in comparison with the values obtained by the other two methods. Such fact is directly related with the adjustment of the polynomic function $C = f(a)$.

3.2. Numerical analysis

The FEM analysis was performed using the software ABAQUS® with the main goal of creating a validated and representative cohesive law for each strain rate and temperature under study. This law, implemented in a CZM should be able to reproduce the experimental results obtained at different temperatures and strain rates tested experimentally. The model employed cohesive elements with a triangular (bilinear) traction-separation law, based on the mechanical and cohesive properties of the CFRP. Although the ENF geometry theoretically leads to a pure-mode loading, a mixed mode formulation was considered, using the quadratic stress criterion for damage initiation and the linear energetic criterion for damage propagation. A non-linear geometric analysis was performed. Regarding the boundary conditions, they consisted of fixing the supporting cylinders in the xy plane and restraining the loading cylinder in the horizontal direction. The model was also restrained in a discrete point located in the lower adherend in the

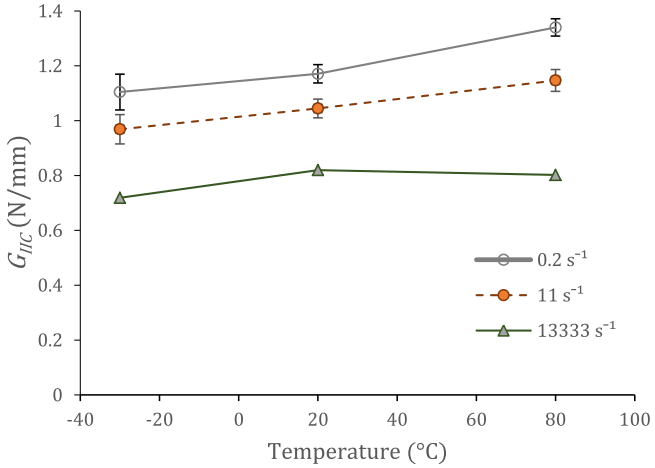

Fig. 4. Prediction of G_{IIC} for impact (13333 s^{-1}) at the three ranges of temperature being studied.

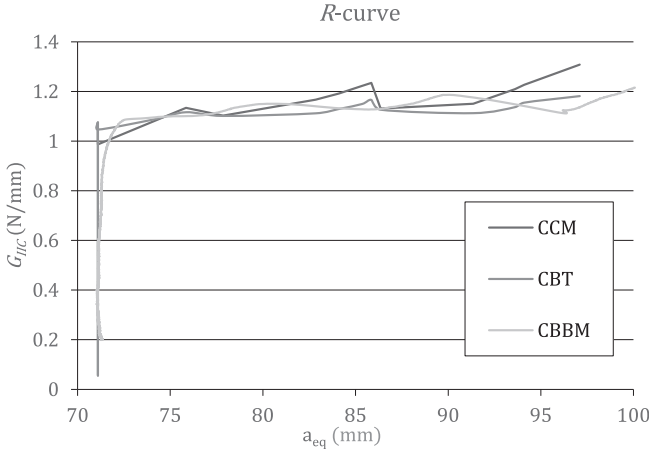

Fig. 5. R-curve at 20 °C and strain rate of 0.2 s^{-1} using the: CBBM, CCM and CBT methods.

Table 4
Comparison of G_{IIC} and standard deviation at 20 °C using the: CBBM, CCM and CBT methods.

	Methods applied		
	CBBM	CBT	CCM
Fracture energy (G_{IIC}) (N/mm)	**1.17**	**1.14**	**1.13**
Standard Deviation (N/mm)	0.026	0.020	0.029

Table 5
CFRP cohesive properties used in the software ABAQUS® [60].

CFRP cohesive properties	Value	Units
Nominal stress (normal)	25.0	MPa
Nominal stress (first direction)	13.5	MPa
Nominal stress (second direction)	13.5	MPa

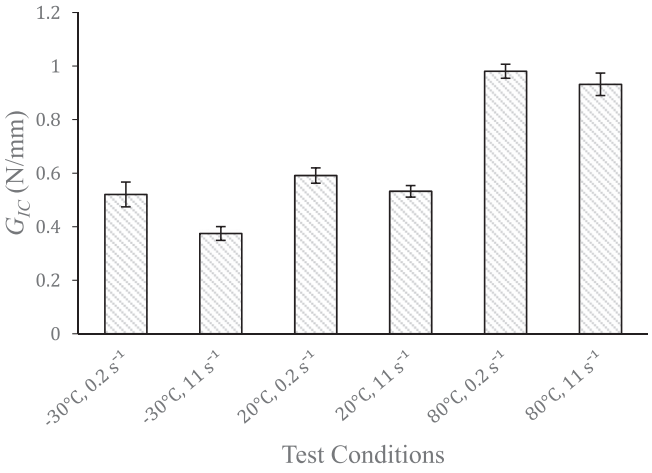

Fig. 6. –Mode I fracture energy (G_{IC}) for unidirectional CFRP DCB specimens, determined by Machado et al. [29].

horizontal direction, to avoid rigid body movement. Between all the cylinders and the respective contacting surfaces, contact conditions were imposed, and also between the adherends at the initially non-bonded section with the aim to prevent interpenetration [57]. The two-dimensional (2D) mesh applied in the models was constructed with plain-strain four-node quadrilateral solid finite elements (CPE4 from ABAQUS®), and four-node cohesive elements (COH2D4 from ABAQUS®). For each specimen arm, six elements were used through-thickness [58,59]. The mesh was refined to reduce the element sizes in regions with large stress gradients, such as the regions near the cylinders. The mesh size of the cohesive elements was 0.2 × 0.2 mm. The experimental tests were reproduced individually with the value of a_0 of each tested specimen.

The elastic material properties used to characterize the elastic behaviour of the CFRP were previously presented in Table 1. The peak stresses employed in the definition of the cohesive zone model are given in Table 5.

Mode I properties were extracted from the previously published work by Machado et al. [29], shown in Fig. 6.

The model used the mode II fracture energy (G_{IIC}) measured in the current work, already shown in Fig. 2.

An example of the model used and the result from the simulation is shown in Fig. 7 for a strain rate of 0.2 s^{-1} at 20 °C.

Figs. 8–10 present a comparison between the *P-δ* curves from the experimental tests (a single representative curve was selected for each stage being analysed) and the simulations. From each experimental *P-δ* curve it was possible to obtain the value of G_{IIC} as the value of fracture energy.

The results show that the numerical results satisfactorily predict the value of G_{IIC}.

4. Conclusions

This work experimentally studied the strain rate and temperature dependence of G_{IIC} of CFRP specimens. The resultant data was also used to estimate shear CZM laws of the composite, which were validated against the existing experimental data. The main conclusions drawn from this work are as follows:

- For both strain rates under study, in the case of high temperature (80 °C), the value of G_{IIC} has a larger increase in comparison to that observed at −30 and 20 °C. The higher the temperature, the higher the value of G_{IIC}. Such fact can be explained by the behaviour induced by the brittle resin of the CFRP matrix.
- For different strain rates and ranges of temperature, a similar behaviour was identified in the fracture behaviour in both stages of crack propagation.
- At 20 °C and a strain rate of 11 s^{-1}, *R*-curves were calculated applying the CBBM, CCM and CBT methods. The values of G_{IIC} obtained using the three methods were found to be relatively similar. The higher value of G_{IIC} was obtained for the CBBM method.
- The CCM method presents the lowest values of G_{IIC} in comparison with the other two methods. Such fact can be directly related with the process of adjustment of the polynomic function $C = f(a)$.

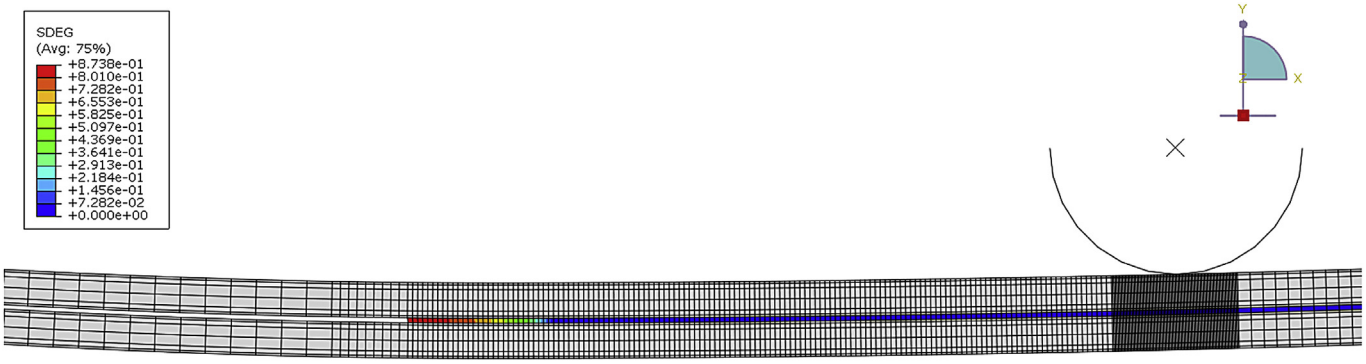

Fig. 7. Example of the damage in the cohesive elements (SDEG) for a simulation performed at 20 °C with a strain rate of 0.2 s^{-1}.

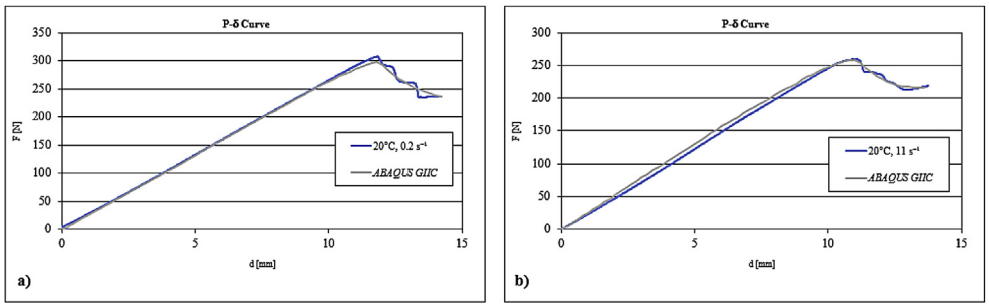

Fig. 8. Comparison between the *P*-δ curves from the experimental test and simulations taking into account the value of G_{IIC} at 20 °C: a) strain rate of 0.2 s^{-1} and b) strain rate of 11 s^{-1}.

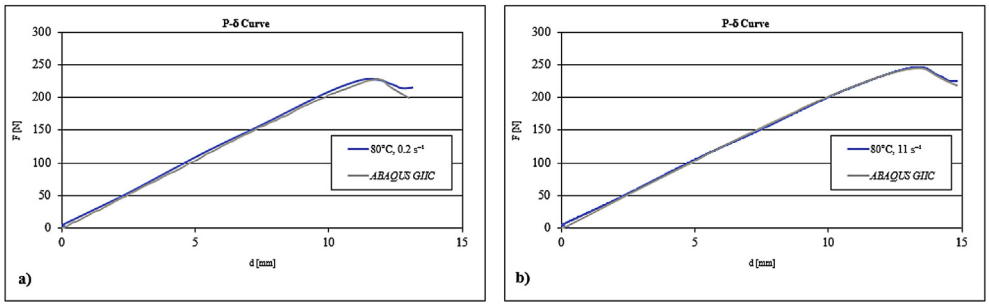

Fig. 9. Comparison between the *P*-δ curves from the experimental test and simulations taking into account the value of G_{IIC} at 80 °C: a) strain rate of 0.2 s^{-1} and b) strain rate of 11 s^{-1}.

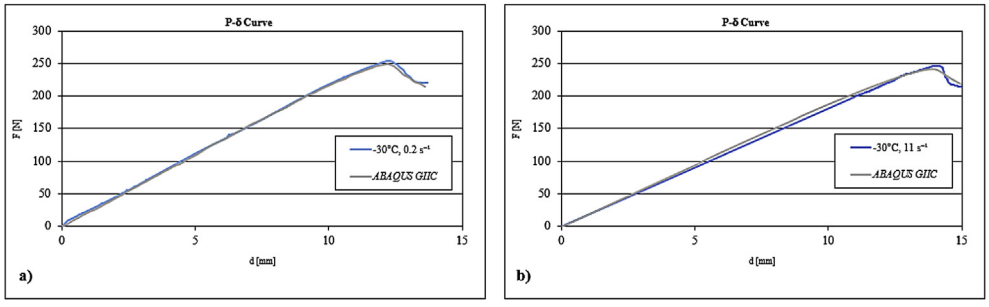

Fig. 10. Comparison between the *P*-δ curves from the experimental test and simulations considering the value of G_{IIC} at −30 °C: a) strain rate of 0.2 s^{-1} and b) strain rate of 11 s^{-1}.

- The measured properties were used to validate estimated CZM laws, using cohesive elements. The models were found to be in good agreement with the experimental data.

Acknowledgments

The authors gratefully acknowledge the funding of Project NORTE-01-0145-FEDER-000022 - SciTech - Science and Technology for Competitive and Sustainable Industries, co-financed by Programa Operacional Regional do Norte (NORTE2020), through Fundo Europeu de Desenvolvimento Regional. The authors would also like to thank NAGASE ChemteX® for the financial support provided.

References

[1] Campilho R, de Moura M, Ramantani D, Morais J, Domingues J. Tensile behaviour of three-dimensional carbon-epoxy adhesively bonded single-and double-strap repairs. Int J adhesion adhesives 2009;29(6):678–86.
[2] da Silva L. Handbook of adhesion technology. Springer Science & Business Media; 2011.
[3] Harding J, Welsh L. A tensile testing technique for fibre-reinforced composites at impact rates of strain. J Mater Sci 1983;18(6):1810–26.
[4] Banea M, da Silva L, Campilho R. High temperature adhesives for aerospace applications. Ann of" Dunarea de Jos" Univ Galati Fascicle XII Weld Equip Technol 2012;23:16–20.
[5] Ou Y, Zhu D, Zhang H, Yao Y, Mobasher B, Huang L. Mechanical properties and failure characteristics of CFRP under intermediate strain rates and varying temperatures. Compos Part B Eng 2016;95:123–36.
[6] Amaro A, Reis P, Neto M. Experimental study of temperature effects on composite laminates subjected to multi-impacts. Compos Part B Eng 2016;98:23–9.
[7] Chaves F, da Silva L, de Moura M, Dillard D, Esteves V. Fracture mechanics tests in adhesively bonded joints: a literature review. J Adhesion 2014;90(12):955–92.
[8] Machado J, Marques E, da Silva LF. Adhesives and adhesive joints under impact loadings: An Overview. Received 18 Oct 2016, Accepted 11 Jan 2017, Accepted author version posted online: 20 Jan 2017.
[9] Taniguchi N, Nishiwaki T, Kawada H. Tensile strength of unidirectional CFRP laminate under high strain rate. Adv Compos Mater 2007;16(2):167–80.
[10] Ochola R, Marcus K, Nurick G, Franz T. Mechanical behaviour of glass and carbon fibre reinforced composites at varying strain rates. Compos Struct 2004;63(3):455–67.
[11] Hou J, Ruiz C. Measurement of the properties of woven CFRP T300/914 at different strain rates. Compos Sci Technol 2000;60(15):2829–34.
[12] Körber H. Mechanical response of advanced composites under high strain rates. Faculty of Engineering of the University of Porto; 2012.
[13] Im K, Cha C, Kim S, Yang I. Effects of temperature on impact damages in CFRP composite laminates. Compos Part B Eng 2001;32(8):669–82.

[14] López-Puente J, Zaera R, Navarro C. The effect of low temperatures on the intermediate and high velocity impact response of CFRPs. Compos Part B Eng 2002;33(8):559–66.
[15] Gómez-del Rio T, Zaera R, Barbero E, Navarro C. Damage in CFRPs due to low velocity impact at low temperature. Compos Part B Eng 2005;36(1):41–50.
[16] Gomez-del Rio T, Barbero E, Zaera R, Navarro C. Dynamic tensile behaviour at low temperature of CFRP using a split Hopkinson pressure bar. Compos Sci Technol 2005;65(1):61–71.
[17] Blackman B, Brunner A, Williams J. Mode II fracture testing of composites: a new look at an old problem. Eng Fract Mech 2006;73(16):2443–55.
[18] Russell A, Street K. Factors affecting the interlaminar fracture energy of graphite/epoxy laminates. Prog Sci Eng Compos 1982:279–86.
[19] Ilcewicz L, Keary P, Trostle J. Interlaminar fracture toughness testing of composite mode I and mode II DCB specimens. Polym Eng Sci 1988;28(9):592–604.
[20] Prel YJ, Davies P, Benzeggagh ML, de Charentenay FX. Mode I and mode II delamination of thermosetting and thermoplastic composites. Compos Mater Fatigue Fract Second Volume ASTM Int 1989. http://dx.doi.org/10.1520/STP10419S.
[21] Blackman B, Kinloch A, Paraschi M. The determination of the mode II adhesive fracture resistance, G IIC, of structural adhesive joints: an effective crack length approach. Eng Fract Mech 2005;72(6):877–97.
[22] Schuecker C, Davidson BD. Effect of friction on the perceived mode II delamination toughness from three-and four-point bend end-notched flexure tests. Compos Struct Theory Pract ASTM Int 2001. http://dx.doi.org/10.1520/STP14518S.
[23] de Moura M, Campilho R, Gonçalves J. Pure mode II fracture characterization of composite bonded joints. Int J Solids Struct 2009;46(6):1589–95.
[24] Miyagawa H, Sato C, Ikegami K. Experimental determination of fracture toughness of CFRP in mode II by Raman spectroscopy. Appl Compos Mater 2001;8(1):25–41.
[25] Adachi T, Arai M, Sakabe N, Matsumoto H. Evaluation of dynamic fracture toughness of unidirectional CFRP laminates. JSME Int J Ser A Solid Mech Material Eng 2000;43(2):179–85.
[26] Briggs TM. Influence of mode II behavior and processing on CFRP composite materials. SAMPE 2010 Conference and Exhibition" New Materials and Processes for a New Economy" 2010.
[27] Chou I, Inutake T, Namba K. Correlation of damage resistance under low velocity impact and mode II delamination resistance in CFRP laminates. Adv Compos Mater 1999;8(2):167–76.
[28] Stevanovic D, Jar PY, Kalyanasundaram S, Lowe A. On crack-initiation conditions for mode I and mode II delamination testing of composite materials. Compos Sci Technol 2000;60(9):1879–87.
[29] Machado J, Marques E, Campilho R, da Silva LF. Mode I fracture toughness of CFRP as a function of temperature and strain rate. J Compos Mater 2016. http://dx.doi.org/10.1177/0021998316682309. First Published December 5, 2016.
[30] Alfano G. On the influence of the shape of the interface law on the application of cohesive-zone models. Compos Sci Technol 2006;66(6):723–30.
[31] Hillerborg A, Modéer M, Petersson P. Analysis of crack formation and crack growth in concrete by means of fracture mechanics and finite elements. Cem Concr Res 1976;6(6):773–81.
[32] Mi Y, Crisfield M, Davies G, Hellweg H. Progressive delamination using interface elements. J Compos Mater 1998;32(14):1246–72.
[33] Mi Y, Crisfield M, Hellweg H, Davies G. Finite element method and progressive failure modelling of composite structures. Comput plasticity Fundam Appl Part 1997;1:239–54.
[34] Alfano G, Crisfield M. Finite element interface models for the delamination analysis of laminated composites: mechanical and computational issues. Int J Numer methods Eng 2001;50(7):1701–36.
[35] Campilho R. Modelação numérica de reparações por sobreposição simples e dupla em materiais compósitos [MSc Thesis]. 2007.
[36] de Moura M, Fernandez M, de Morais A, Campilho R. Numerical analysis of the edge crack torsion test for mode III interlaminar fracture of composite laminates. Eng Fract Mech 2009;76(4):469–78.
[37] Campilho R. Repair of composite and wood structures. Instituto Superior de Engenharia do Porto; 2009.
[38] da Silva L, Sato C, Marques E, Banea M, Carbas R. Effect of low temperature on tensile strength and mode I fracture energy of a room temperature vulcanizing silicone adhesive. J Test Eval 2015;44(3).
[39] Marques E, da Silva L, Banea M, Carbas R. Adhesive joints for low-and high-temperature use: an overview. J Adhesion 2015;91(7):556–85.
[40] Zhang Y, Adams R, da Silva L. A rapid method of measuring the glass transition temperature using a novel dynamic mechanical analysis method. J Adhesion 2013;89(10):785–806.
[41] Carlsson L, Gillespie J, Pipes R. On the analysis and design of the end notched flexure (ENF) specimen for mode II testing. J Compos Mater 1986;20(6):594–604.
[42] Bader M, Hamerton I, Hay J, Kemp M, Winchester S. Double cantilever beam testing of repaired carbon fibre composites. Compos Part A Appl Sci Manuf 2000;31(6):603–8.
[43] Ducept F, Davies P, Gamby D. Mixed mode failure criteria for a glass/epoxy composite and an adhesively bonded composite/composite joint. Int J Adhesion Adhesives 2000;20(3):233–44.
[44] de Moura M, Campilho R, Gonçalves J. Crack equivalent concept applied to the fracture characterization of bonded joints under pure mode I loading. Compos Sci Technol 2008;68(10):2224–30.
[45] Kanninen MF, Popelar CL. Advanced fracture mechanics. 1985.
[46] da Silva L, Öchsner A. Modeling of adhesively bonded joints. Springer; 2008.
[47] Saldanha D, Canto C, da Silva L, Carbas R, Chaves F, Nomura K, et al. Mechanical characterization of a high elongation and high toughness epoxy adhesive. Int J Adhesion Adhesives 2013;47:91–8.
[48] Wang Y, Williams J. Corrections for mode II fracture toughness specimens of composites materials. Compos Sci Technol 1992;43(3):251–6.
[49] Fernandes R, Chousal J, De Moura M, Xavier J. Determination of cohesive laws of composite bonded joints under mode II loading. Compos Part B Eng 2013;52:269–74.
[50] Dias G, de Moura M, Chousal J, Xavier J. Cohesive laws of composite bonded joints under mode I loading. Compos Struct 2013;106:646–52.
[51] de Moura M, Gonçalves J, Magalhães A. A straightforward method to obtain the cohesive laws of bonded joints under mode I loading. Int J Adhesion Adhesives 2012;39:54–9.
[52] de Moura M, Gonçalves J, Chousal J, Campilho R. Cohesive and continuum mixed-mode damage models applied to the simulation of the mechanical behaviour of bonded joints. Int J Adhesion Adhesives 2008;28(8):419–26.
[53] Silva F, Xavier J, Pereira F, Morais J, Dourado N, de Moura M. Determination of cohesive laws in wood bonded joints under mode I loading using the DCB test. Holzforschung 2013;67(8):913–22.
[54] Banea M, da Silva L, Campilho R. Effect of temperature on tensile strength and mode I fracture toughness of a high temperature epoxy adhesive. J Adhesion Sci Technol 2012;26(7):939–53.
[55] Zgoul M, Crocombe A. Numerical modelling of lap joints bonded with a rate-dependent adhesive. Int J adhesion adhesives 2004;24(4):355–66.
[56] Avendaño R, Carbas R, Marques E, da Silva L, Fernandes A. Effect of temperature and strain rate on single lap joints with dissimilar lightweight adherends bonded with an acrylic adhesive. Compos Struct 2016;152:34–44.
[57] Azevedo J, Campilho R, da Silva F, Faneco T, Lopes R. Cohesive law estimation of adhesive joints in mode II condition. Theor Appl Fract Mech 2015;80:143–54.
[58] Daghyani HR, Ye L, Mai YW. Mixed-mode fracture of adhesively bonded CF/epoxy composite joints. J Compos Mater 1996;30(11):1248–65.
[59] Campilho RDSG, De Moura M, Barreto A, Morais J, Domingues J. Fracture behaviour of damaged wood beams repaired with an adhesively-bonded composite patch. Compos Part A Appl Sci Manuf 2009;40(6):852–9.
[60] Neto J, Campilho R, Da Silva L. Parametric study of adhesive joints with composites. Int J Adhesion Adhesives 2012;37:96–101.

Paper 5

Content of Paper 5

Abstract

1. Introduction

2. Experimental details

2.1. Material and properties

2.2. Fabrication and testing

2.3. Data reduction scheme

3. Results and discussion

4. Conclusions

References

Theoretical and Applied Fracture Mechanics 103 (2019) 102257

Contents lists available at ScienceDirect

Theoretical and Applied Fracture Mechanics

journal homepage: www.elsevier.com/locate/tafmec

Dynamic behaviour in mode I fracture toughness of CFRP as a function of temperature

J.J.M. Machado[a], A. Hayashi[b], Y. Sekigushi[b], R.D.S.G. Campilho[c], E.A.S. Marques[a], C. Sato[b], Lucas F.M. da Silva[d,*]

[a] Instituto de Ciência e Inovação em Engenharia Mecânica e Engenharia Industrial (INEGI), Rua Dr. Roberto Frias, 4200-465 Porto, Portugal
[b] Institute of Innovative Research (IIR), Tokyo Institute of Technology, 4259 Nagatsuta-cho, Midori-Ku Ward, Yokohama, Kanagawa Prefecture 226-8503, Japan
[c] Departamento de Engenharia Mecânica, Instituto Superior de Engenharia do Porto (ISEP), Instituto Politécnico do Porto, Rua Dr. António Bernardino de Almeida, 431, 4200-072 Porto, Portugal
[d] Departamento de Engenharia Mecânica, Faculdade de Engenharia (FEUP), Universidade do Porto, Rua Dr. Roberto Frias, 4200-465 Porto, Portugal

ARTICLE INFO

Keywords:
CFRP
Impact
Fracture toughness in mode I
Temperature
Finite element analysis

ABSTRACT

The aim of this work is to assess the influence of high strain rates and testing temperature on the fracture energy in mode I, G_{IC}, of carbon fibre reinforced plastic (CFRP) plates. Double cantilever beam (DCB) specimens were tested to determine G_{IC} as a function of temperature (24 and 80 °C) under an impact load of 4.7 m/s (using a falling-wedge impact test machine), with the results being compared with the values previously determined by the authors under quasi-static loads. This work has demonstrated a significant influence of the testing temperature on the G_{IC} of composite materials, as this value greatly increased for higher temperatures. On the other hand, a less significant influence of the strain rate on G_{IC} was found, which slightly decreased by increasing the strain rate.

1. Introduction

The use of composites in the automotive industry has greatly increased in the last decades. Composites offer a distinct number of advantages over other commonly used structural materials (e.g. steel and aluminium). These include the possibility to achieve tailored structures, higher specific strength and stiffness, superior corrosion resistance, as well an improvement of the fatigue properties [1].

One of the major concerns in terms of design and maintenance of composite structures is their behaviour when subjected to dynamic and impact loads. Due to their use in vehicle construction, composite structures are likely to be subjected during these loads during collisions, for example. To enable the formulation of advanced numerical models describing the strain rate dependent behaviour of this material, it therefore becomes fundamental to understand how the mechanical properties of composites change with the loading rate. It is also important to consider how temperature affects the mechanical properties, due to the wide range of environmental conditions that road vehicles are subjected to during regular usage.

It is known that the composites have a limited ability to plastically deform under impact, which leads to the onset of large areas of fracture damage with ensuing reductions in both specific strength and stiffness [2]. One possible type of failure induced by an impact load is the interlaminar fracture (failure by delamination). This type of failure is critical in composite structures, and is often associated with a transverse load scenario, governed by the fracture toughness in mode I (G_{IC}). Moreover, G_{IC} is usually lower than G_{IIC}, which further emphasizes the severity of mode I loadings. However, this type of failure can also occur in mode II or mixed-mode (I + II) [3]. In fact, in many cases, including impact, mode II and mixed-mode are prevalent over mode I. For such cases, delamination still occurs, but ruled by these modes of failure and the corresponding fracture [4].

Delamination growth in composite materials can be described in three distinct stages, namely: initiation, slow growth and ply separation [5], with the majority of the published works being performed to mechanically characterize these materials under quasi-static loadings. It is therefore highly complex to accurately measure the G_{IC} of composites as a function of strain rate, as some specific requirements must be addressed, such as: the necessity to ensure symmetrical opening of the specimens, implementing a viable method to accurately measure the crack propagation, and the elimination of oscillation in the load signal acquisition [6].

The failure mode in composite materials can change due to the variation of loading rate, which has considerable influence on the

* Corresponding author.
E-mail address: lucas@fe.up.pt (L.F.M. da Silva).

https://doi.org/10.1016/j.tafmec.2019.102257
Received 9 January 2019; Received in revised form 24 May 2019; Accepted 24 May 2019
Available online 27 May 2019
0167-8442/ © 2019 Elsevier Ltd. All rights reserved.

measured fracture toughness. A reduction of the fracture toughness was found to occur when increasing the load rate, associated to a transition from ductile to brittle failure mode [7]. The effect of loading rate on mode I fracture toughness was studied by several authors with different conclusions, as some [8–12] observed that the fracture toughness in mode I increased with the increase of strain rate; and others [13,14] concluded that it remained independent.

A review of the most representative experimental results of G_{IC} of composites was performed by Jacob et al. [15], stating that there is no agreement on how strain rate influences the fracture toughness. Several experimental observations can justify this lack of consistency in the G_{IC} variation with the strain rate, namely (1) the strain rate sensitivity of the polymer matrix, which may affect the composite behaviour and (2) the transition from ductile to brittle type of failure by increasing the strain rate, which results in a decrease of fracture toughness. On the other hand, it is known that high strain rates introduce additional problems on the correct measurement of G_{IC}. Aiming to minimize any effects that might influence the measurement of G_{IC}, Blackman et al. [13] used an equation which did not require data from measured loads, avoiding the influence of the dynamic effects. It was found that, as the strain rate increases the crack becomes unstable.

The tensile and shear properties can follow similar trends. Daniel et al. [16] has demonstrated that the moduli and strengths of unidirectional carbon epoxy varied linearly varied with the logarithm of strain rate. The effect of strain rate on the compressive and shear behaviour of carbon/epoxy composite materials was investigated by Hsiao et al. [17], determining that higher strength and strain values were obtained with increasing strain rate, while the modulus increased slightly over the quasi-static value.

The impact damage of CFRP was experimentally determined by Im et al. [18] when subjected to extreme temperature variations, considering two different laminates: CFRP composites with either epoxy or PEEK resin. It was found that, when increasing the temperature, the areas with delamination within the damaged areas were reduced. A linear trend, correlating the impact energy with the delamination areas for all tested temperatures, was found, characterized by a nearly proportional increase of the delamination area with G_{IC}. Finally, G_{IC} typically increased with the temperature in both laminates.

Numerous tests [1,19,20] can be performed to determine the G_{IC} of composite materials, although no standard tests have yet been defined for cases of tests performed under high strain rates. May [6] performed a review of the experimental tests and data acquisition used to measure G_{IC} of composite materials under high strain rates, identifying the double cantilever beam (DCB) as the specimen most commonly used to determine the loading rate effect on both initiation and propagation of delamination [21]. To ensure the symmetric opening of DCB specimens under impact, which can be a major issue in these tests, two distinct test procedures are available. One of the possible solutions is to perform a conventional DCB test, as described by Hug [22], which considered the direct correlation between the vertical movement of the cross-head displacement and the horizontal opening of the specimen (not suitable for high strain rates and requiring a complex setup). Alternatively, the wedge loaded setup can be considered (suitable for high strain rates and simpler to implement but requiring the determination of the friction coefficient between the wedge and the composite fracture surface) [14,23,24].

This work has been carried out with the objective of assessing the influence of the testing temperature and high strain rate on the fracture energy in mode I, G_{IC}, of carbon fibre reinforced plastic (CFRP) plates, providing novel data that can be used as a basis to construct constitutive models for representing the mechanical behaviour of composite materials. Double cantilever beam (DCB) specimens were tested to determine G_{IC} as a function of temperature (24 and 80 °C) and impact load of 2.5 m/s (using a falling-wedge impact test machine), with a comparison being performed against quasi-static values previously determined by the authors [25].

Table 1
Properties of CFRP elastic orthotropic [27].

Elastic Modulus (MPa)	Poisson's Ratio	Shear Modulus (MPa)
E_1 = 1.09E5	ν_{12} = 0.342	G_{12} = 4315
E_2 = 8819	ν_{13} = 0.342	G_{13} = 4315
E_3 = 8819	ν_{23} = 0.380	G_{23} = 3200

The results obtained with this work demonstrate that both the testing temperature and the strain rate have influence on the G_{IC} of the composite material being tested, although the effect of temperature is significantly greater.

2. Experimental details

2.1. Material and properties

The composite DCB specimens tested in this work are composed of a carbon/epoxy pre-preg material (SEAL® Texipreg HS 160 RM). The use of DCB specimens in this work is due to the fact that this specimen configuration is commonly used to determine G_{IC} [26], and also because it allows a direct comparison to be made with results obtained at quasi-static conditions, previously determined by the authors [25].

The mechanical properties of this specific material, which were previously determined in the work of Campilho [27] in 2009 at room temperature, are presented in Table 1.

As the experimental testing was performed at two distinct temperatures, it is fundamental to determine the glass transition temperature, T_g, of the CFRP resin. This property is strongly related to the strength of a polymer at a given temperature, therefore being a crucial parameter to understand if the material is operating above or below the glass transition zone [28,29].

An in-house developed apparatus was used to measure the T_g (based on the device proposed by Zhang et al. [30]), searching for a peak in the damping of the adhesive that is known to occur at the T_g of a polymer. The procedure to measure the T_g using this apparatus consists in the use of a specimen (an aluminium beam with a portion of adhesive bonded to it) that is subjected to a constant vibrational movement at the beam's resonance frequency. The temperature at which the specimen displacement is lower can be identified by a variation of the temperature in a chamber containing the specimen and registering the amplitude of its movement. Damping occurs at this maximum temperature, which can be understood as the temperature corresponding to the glass transition phase. A dummy static specimen is also used to register the temperature. Only the resin of the pre-preg was used to produce the T_g specimen (obtained from the excess of resin which flowed out of the mould during the curing process), as when testing a section of the CFRP, due to the damping properties of the fibres, it is not possible to directly measure this property. The measurement of the brittle resin T_g showed a value of 105 °C [25].

2.2. Fabrication and testing

The manufacturing process of the DCB specimens under study, composed entirely of CFRP, consisted on the manual stacking of pre-preg unidirectional (0°) plies, creating a laminate that was cured in a hot plate press of 130 °C for 1 h. Each ply of CFRP has a thickness of 0.15 mm, with a total of twenty plies being used to manufacture each plate. The unidirectional setup was selected to ensure that better properties are obtained in the loading direction.

A small Teflon® sheet with a thickness of 0.075 mm was partially laminated into each CFRP plate during the manufacture process (positioned between ply ten and eleven, of the total of twenty), to create a pre-crack of a_0 = 45 mm, with the objective of achieving stable crack-propagation during the DCB test. Due to the significant thickness of this

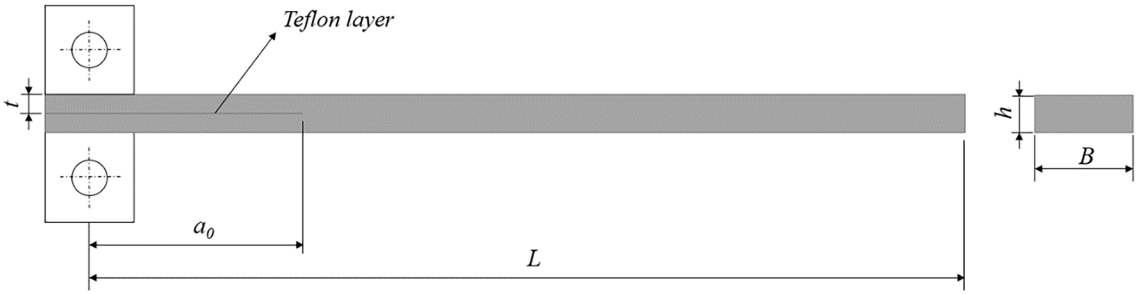

Fig. 1. Dimensions of DCB CFRP specimens following ISO 15024 standard (L = 125 mm, B = 25 mm, h = 3 mm, a_0 = 45 mm, and t = 1.5 mm which is half of the specimen thickness).

sheet (which is much thicker than an actual natural crack), an initial pre-crack must be manually created and propagated before actual testing, avoiding errors in measurement of the initial G_{IC} which can occur due to blunt effects at the crack tip [31]. Nonetheless, the length of the manual pre-crack should be short enough not to induce fibre bridging that would affect the initial G_{IC} measurement.

The CFRP plates were then cut according to the DCB geometry using a diamond disc cutting machine. Edge finishing was carried out manually with 120 grit sandpaper in order to remove the loose fibres and smoothen the sharp edges. The geometry of the CFRP DCB specimens was based on the ISO 15024 standard [26] from 2001 (Fig. 1), which is used to determine, in mode I, the interlaminar fracture toughness, G_{IC}, for unidirectional reinforced fibre-reinforced plastic composites. It is indicated in the ISO 15024 standard [26] that the crack-opening mode due to a load applied perpendicularly to the plane of delamination using the DCB specimen can be achieved with the use of hinges or loading blocks. Steel loading blocks were used for this purpose in this work, being bonded to the specimens with the Nagase ChemteX® XNR3324FT adhesive (cured at room temperature for 24 h, to avoid damaging the DCB CFRP specimens).

With the aim of correctly measuring the crack propagation, one side of each specimen was painted using a white spray paint, and a measurement scale was drawn using black lines spaced by 10 mm. The initial crack length, a_0, was measured after a pre-crack inducing procedure, where the specimens were gradually loaded until the crack starts to propagate. To prepare the specimens for testing, the Teflon® sheet was removed, and the new value of a_0 registered.

A total of four specimens were tested under impact (4.7 m/s) conditions at 24 and 80 °C, according to the ISO 15024 standard [26]. The room temperature was set at 24 °C and, for the tests performed at 80 °C, heating strips were held against the top and bottom of specimens. After the pre-set temperature was attained, it was kept constant for 10 min, to ensure homogeneous temperature distribution along the DCB CFRP specimens. At this point, the heating strips were released to perform the test. To ensure that there wasn't any change in the specimens' temperature, at the same time a heat gun was pointed towards the specimens with the temperature being registered and monitored using thermocouples. Trial specimens with the DCB exact geometry were used to assess of the specimen's temperature at several points. Thermocouples were positioned on the bottom surface and heat was applied on the top of the specimen, which ensured that the 10 min exposure was sufficient to uniformize the temperature in the specimen.

The impact tests were performed using a falling-wedge machine, with an initial velocity of 4.7 m/s. The schematic representation of the setup used for this technique is shown in Fig. 2. The test method was based on the work of Xu and Dillard [32]. The setup comprises of two polycarbonate wedges (with an incident angle of 30°) assembled in parallel to form the impactor of a drop weight machine, that when released acts as a striker that splits the DCB CFRP specimens. Polycarbonate is used for the wedge's construction due to its transparency (as this allows for clear a view of the specimen) and due to its relatively high strength (which provides resistance to damage under impact situations). For this type of testing setup, the acting load is not directly measured to calculate G_{IC} of CFRP, as no load cells or load transducers are installed. During the tests, the impactor (which is comprised of the two polycarbonate wedges and weights) was released, impacting the pins positioned in the centre of the load blocks (bonded to one end of the DCB CFRP specimens), splitting the specimens (which were secured vertically at the base of the drop tower).

The initial impact velocity was determined considering the maximum height and the weight attached to the wedge striker. A mass of 13.4 kg was introduced to perform the test, and the striker was released from a height of 1130 mm, providing an impact energy of 148 J. The pins were lubricated, reducing to a minimum any friction that might influence the results of G_{IC}, which is a prominent problem of this type of setup [6]. Tracking markers were added in the pins, allowing to assess the displacement of each section of the substrates during the test. The fracture process during the test was recorded using a high-speed camera (CRYSTA, PI-1PS, Photron CO., Ltd., Tokyo, Japan) at a rate of 5000 fps. A focused LED light was used to improved visualization of the crack growth and it was positioned in a way as not to compromise recording of the tests.

The general concept of strain rate ($\dot{\varepsilon}$) is characterized as being the change in strain (deformation) of a specific material with respect to time. Three distinct values of displacement rate have been considered (to perform a comparison) and include quasi-static conditions (2 and 100 mm/min) from a previous work [25] performed by the authors and impact condition (4.7 m/s). As the material is being loaded in pure mode I, for practical purposes the nominal strain rate in this analysis is considered to be the tensile strain rate corresponding to the straining of a layer of material in the thickness direction. From Eq. (1) it is possible to determine the values of the nominal tensile strain rate of the displacement rate tested.

$$\dot{\varepsilon}(t) = \frac{v(opening)}{L_0} \tag{1}$$

where $v(opening)$ corresponds to lateral displacement rate (mm/s), and L_0 to the value of length of the specimen (mm). In the case of G_{IC} of DCB CFRP specimens, the value of L_0 considered was in respect with the thickness of the a CFRP ply, being of 0.15 mm.

It is possible to determine $v(opening)$ by using Eq. (2).

$$v(opening) = 2 \times v(pin) = \frac{\Delta h}{\frac{1}{v(impactor)}} = \frac{tg\alpha}{1/2500} \tag{2}$$

Being $v(pin)$ the velocity of the pins moving during the impact, $v(impactor)$ the velocity of the impactor, Δh the corresponding displacement of the specimens opening during the test, and α is the angle of the striker wedges.

Table 2 presents the conversion of the previously measured quasi-static [25] and impact values in terms of strain rate.

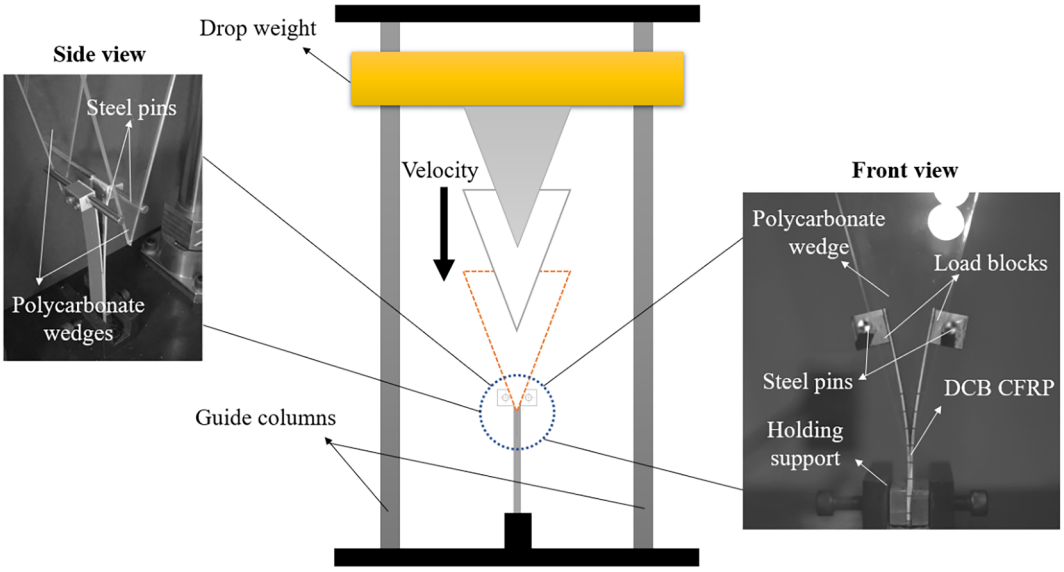

Fig. 2. Schematic representation of the falling wedge impact test machine (left), and a photo of the test being performed (right) – wedge angle is 30°.

Table 2
Conversion of values of lateral displacement rate to strain rate, quasi-static [25] and impact values.

Conversion	Lateral displacement rate		
	2 mm/min*	100 mm/min*	80370 mm/min**
Strain Rates	0.16 s^{-1}	8.33 s^{-1}	1880000 s^{-1}

* Quasi-static results determined in a previous work.
** Initial impact velocity of 2.5 m/s.

2.3. Data reduction scheme

The determination of G_{IC}, can performed following using a fracture mechanics approach, and it is based on the Linear Elastic Fracture Mechanics (LEFM), which relies on Irwin's approach and is defined as the energy release rate. Eq. (2) is derived from the Irwin-Kies theory, where G_{IC} represents the energy available for an increment of the crack extension [33,34].

$$G_I = \frac{P^2}{2B}\frac{dC}{da} \tag{3}$$

Being P the applied load, B the specimen width, C the compliance ($C = \delta/P$, where δ is the opening displacement – and it is based on the flexibility of the material) and a is the crack length. The compliance can be expressed using a Euler beam theory:

$$C = \frac{\delta}{P} = \frac{2a^3}{3EI} \tag{4}$$

Using the simple beam theory (SBT), dC/da is given by:

$$\frac{dC}{da} = \frac{2a^2}{EI} \tag{5}$$

where E and $I = \frac{bh^3}{12}$ (being h the height of the substrate) are the Young's modulus and second moment of area of the substrates, respectively.

The values are fitted into a cubic polynomial approximation being the compliance, C, a function of a crack length, a.

Therefore, the measurement of the values of load, opening displacement and crack length are required to determine the value of G_{IC}, and some correction must be applied to truthfully measure this parameter due to deviation from the SBT. In order to achieve that, the Corrected Beam Theory (CBT) method derives from the Irwin-Kies theory (Eq. (2)). The corrected crack has a deviation from the one assumed in the Compliance Calibration Method (CCM), as the deformation around the crack tip is considered. The fracture toughness can then be determined by Eq. (6) [34,35]:

$$G_I = \frac{3P\delta}{2B(a + |\Delta|)} \tag{6}$$

Being δ the loading line displacement and Δ a correction factor for the crack tip rotation and deflection of the substrates, proposed in 1992 by Wang and Williams [35].

In order to reduce crack length measurement, which is a difficult and time-consuming task, the Compliance Based Beam Method (CBBM) was considered instead. With this method which, developed by de Moura et al. [36] in 2008, direct crack length measurement is not necessary. By using the crack equivalent concept, this method only requires the specimen's compliance during the test [36,37]. At the end of the crack, a fracture process zone (FPZ) develops [38]. This region is characterized by the development of multiple micro-cracks and plasticization zones, which absorb some of the energy. This method is based on the beam theory of Timoshenko [36,39].

By applying the CBBM, it is possible to determine G_{IC} using Equation (6) [36,40,41]:

$$G_I = \frac{6P^2}{B^2h}\left(\frac{2a_{eq}^2}{h^2E_f} + \frac{1}{5G}\right) \tag{7}$$

where a_{eq} is an equivalent crack length obtained from the experimental compliance and accounting for the FPZ, where a progressive softening occurs at the crack tip [33]. E_f is a corrected flexural modulus to account for all phenomena affecting the load-displacement (P-δ) curve, such as the stress concentration at the crack tip and stiffness variability between specimens. G is the shear modulus of the adherends, and h represents the height of each specimen arm [42].

Since this work relates to high strain rate fracture tests, the load under impact conditions cannot be directly measured. Consequently, a load reduction scheme is required to accurately calculate G_{IC}. As the relationship between the load, displacement and crack length is achieved using the beam theory, the load independent method (LIM) [13,43] can be applied to calculate G_{IC}. Although for LIM the crack length correction is still essential for the accurate calculation of G_{IC}, such correction requires the measurement of the applied load. As the correction contains the large influence of high strain rate effects, G_{IC} values previously determined for tests performed under quasi-static conditions [25] are used to calculate the fracture energy overall. When

LIM is determined using the crack length correction (|Δ|), it is denoted as LIM_{Δ}. When using the CBBM crack length correlation (Δ_{CBBM}), LIM is addressed as LIM_{CBBM}. Therefore, G_{IC} is given by Equation (8) for cases when LIM_{Δ}.

$$G_I = \frac{9\delta^2 EIF}{4B(a + |\Delta|)^4} \tag{8}$$

In the cases when LIM_{CBBM}, the value of G_{IC} is given by Eq. (9).

$$G_I = \frac{9\delta^2 EIF}{4b(a + \Delta_{CBBM})^4} \tag{9}$$

The dynamic effect of the DCB CFRP specimens (related to its inertia) on G_{IC} is not considered in this case, since the kinetic energy contribution of the substrate [13] is small in comparison to the G_{IC} measured in the testing conditions.

Impact loading greatly differs from quasi-static conditions, and the approach to data analysis is completely distinct. Blackman et al. [13] demonstrated that the load signal in tests performed at high loading rates was significantly influenced by dynamic effects, which could lead to unreliable load values being registered. Another important conclusion is that if a displacement-based approach (Eq. (8)) (obtained with the aid of high-speed camera) is used for the calculation of G_{IC} under high-speed loading conditions, errors can be reduced. It is also important to state that this type of wedge loading induces a degree of longitudinal compression in the DCB CFRP specimens, due to both the geometry of the wedge and the friction between the wedges and the pins, however this effect was neglected in the formulation. It was considered that this effect has a minor influence on the strain field around the crack-tip, because of the high longitudinal stiffness of CFRP, and due to fact that this is a longitudinal component to the stress.

As load blocks (Fig. 3) were used to transfer the load, it is also necessary to consider a displacement correction factor.

Being l_1 the distance (in the vertical direction) from the centre of the loading block until half of the thickness of the upper section of the DCB CFRP, and l_2 the distance from the centre of the loading block (in the horizontal direction) to the end of the block.

The displacement correction factor is determined by the relation of: F (Eq. (10)) and N (Eq. (11)). F is the crack length correction factor accounting for beam root rotation and shear effects, and N is the large beam displacements and load block stiffening effects.

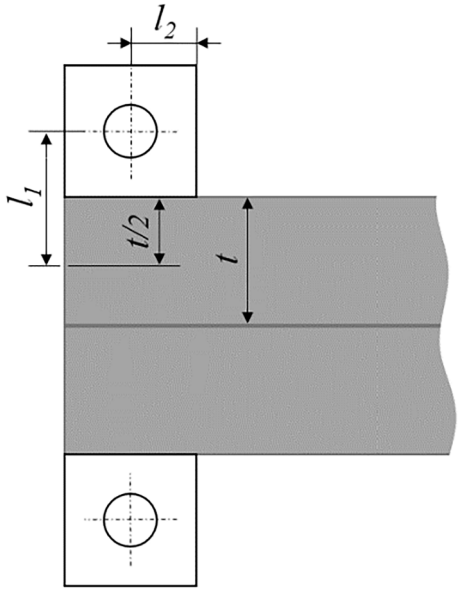

Fig. 3. Schematic representation of the DCB specimen with load blocks (t is the thickness of the upper substrate, l_1 and l_2 are respectively the vertical and horizontal dimensions of the centre of the load blocks).

$$F = 1 - 0.3\left(\frac{\delta}{a}\right)^2 - 1.5\left(\frac{l_1\delta}{a^2}\right) \tag{10}$$

$$N = 1 - \left(\frac{l_2}{a}\right)^3 - \frac{9}{8}\frac{\delta l_1}{a^2}\left\{1 - \left(\frac{l_2}{a}\right)^2\right\} - \frac{9}{35}\left(\frac{\delta}{a}\right)^2 \tag{11}$$

The correlation between N and F used was set to be $\left(\frac{N}{F}\right)^2$.

3. Results and discussion

During experimental testing, specific care was taken to avoid unsymmetrical opening of the DCB CFRP specimens, a challenge in this type of tests. Prior to performing the tests, each specimen was positioned and clamped, to ensure that the falling wedge (Fig. 2) was able to strike each pin uniformly. To assess if the experimental setup achieved symmetrical opening of the specimen, an analysis of the opening path was digitally performed by tracking Points A and B (Fig. 4), using the Photron FASTCAM Analysis 1.3.2.0 software. The results show that the displacement of each section of the substrate is similar, which creates a balanced test condition.

As previously referred, the fracture process during the test was recorded using a high-speed camera, and the opening displacement and the crack length was extracted from the digital images of the test, considering that the resolution of the images was of 0.2 mm per pixel. Figs. 5 and 6 represent the relationship between the crack length and time, respectively for the specimens tested at 24 and 80 °C.

All the curves presented started with a plateau corresponding to a region without crack propagation. The crack length versus time curves for the three specimens' tests were similar for each testing temperature.

Another conclusion is that, for both testing temperatures, all crack length versus time curves evidence a stable crack growth, which occurs when an a continuously growing crack propagates through the specimen being tested in a constant manner.

An analysis of the "average" crack velocity was performed considering the impact tests (initial velocity of 2.5 m/s) at 24 °C (Fig. 7) and 80 °C (Fig. 8). The crack length versus time curves shown correspond to the average and most representative measurements for each testing temperature.

A drop of the average crack velocity through the test could be identified for both cases, below the initial impact velocity set to 4.7 m/s. For the impact tests performed at 24 °C, there was a drop of about 6% of the average crack velocity from the initial testing velocity. The most significant reduction was found for the impact tests performed at 80 °C, which has likely been caused by the high temperature being close to T_g of the brittle CFRP resin. In this case, the resin becomes more ductile which greatly reduces the average crack velocity to 44% due to an increase in the resistance to crack propagation [44,45]. This type of behaviour is expected from this type of testing setup, and was also observed by Im et al. [18].

Using a logarithmic trend function, represented in Eq. (4) [46,47], and considering the previously determined quasi-static (2 and 100 mm/min) [25] values, it was possible to extrapolate G_{IC} for different testing temperatures under an initial impact velocity of 2.5 m/s impact (corresponding to 282,514 s^{-1}) (Eq. (12)).

$$G_{IC} = A \times ln(\dot{\varepsilon}) + B \tag{12}$$

The A and B coefficients were determined from the logarithmic trend function, and $\dot{\varepsilon}$ corresponds to the strain rate.

The experimental results of G_{IC} obtained for the impact tests, considering an initial impact velocity of 4.7 m/s and for testing temperature of 24 and 80 °C are presented in Fig. 9. A comparison with the values of G_{IC} previously determined under quasi-static (2 and 100 mm/min) [25] conditions is also presented, as well as the extrapolated values for the impact condition. The values of G_{IC} were measured using the CFRP DCBs, considering variable opening velocity.

It can be observed that, for the case of impact (initial velocity of

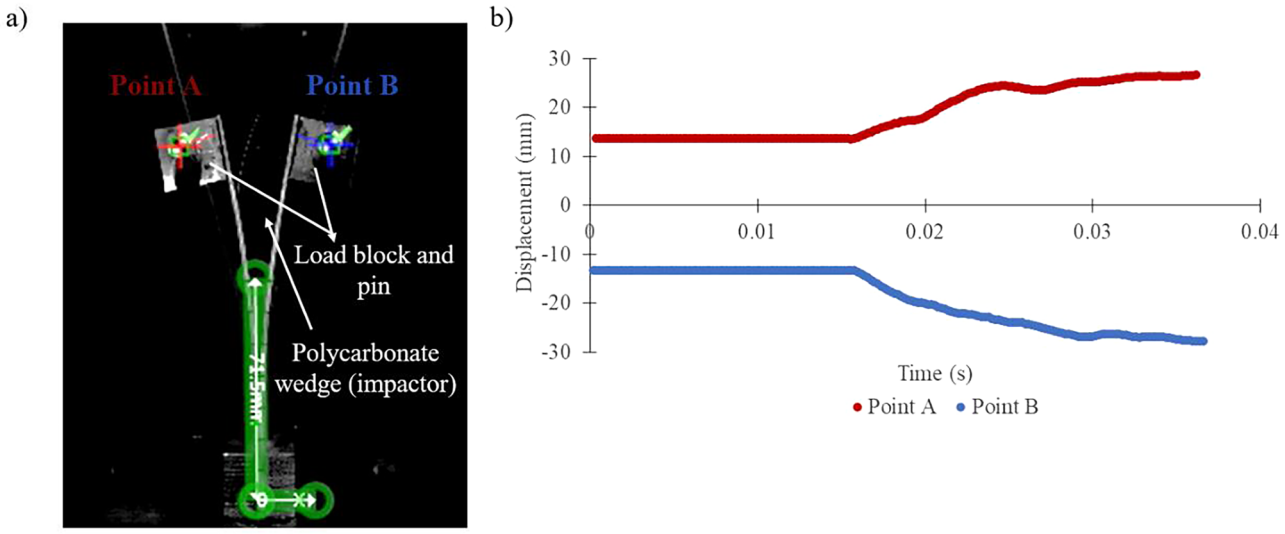

Fig. 4. Example of a measurement of DCB CFRP test under impact (initial impact velocity of 2.5 m/s: a) Setting the reference points A and B in the software (Photron FASTCAM Analysis Version 1.3.2.0) to measure the displacement between the load blocks; and b) example of the measurements of displacement between the two reference points as a function of time.

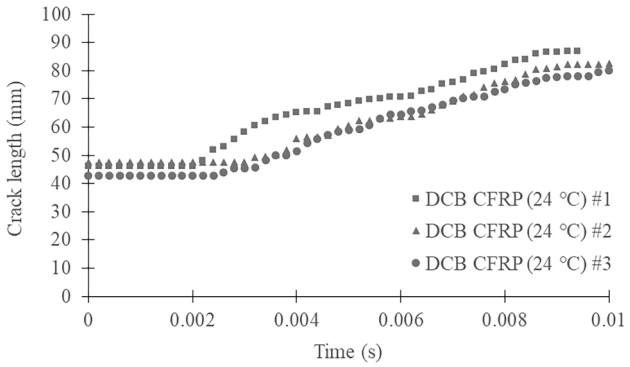

Fig. 5. Relationship between the crack length and time of the three DCB CFRP specimens tested at an initial impact velocity of 2.5 m/s at 24 °C.

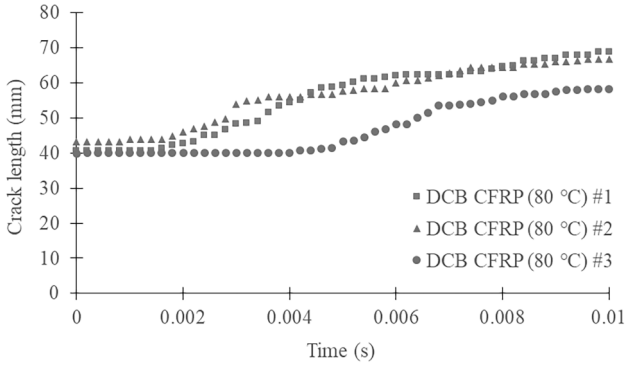

Fig. 6. Relationship between the crack length and time of the three DCB CFRP specimens tested at an initial impact velocity of 2.5 m/s at 80 °C.

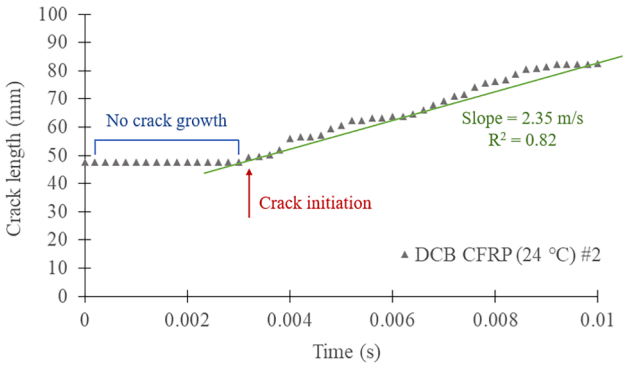

Fig. 7. Determination of the "average" crack velocity (stable crack growth) from the plot of crack length versus time for the case of impact test with an initial velocity of 2.5 m/s at 24 °C (considering the DCB CFRP specimen number 2).

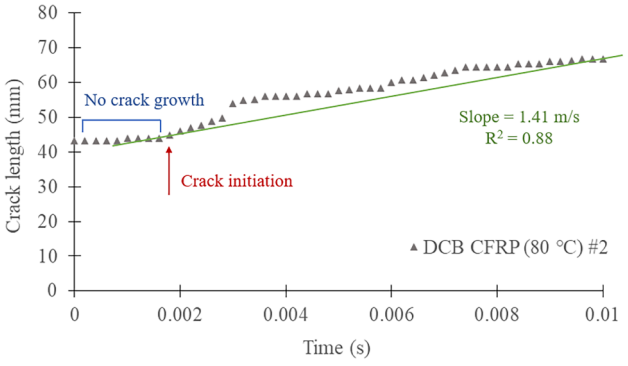

Fig. 8. Determination of the "average" crack velocity (stable crack growth) from the plot of crack length versus time for the case of impact test with an initial velocity of 2.5 m/s at 80 °C (considering the DCB CFRP specimen number 2).

2.5 m/s) tests, an increase of the testing temperature leads to an increase of about 50% of the G_{IC}. Such fact can be explained by the change in the mechanical properties of the brittle resin of the CFRP, which becomes more ductile with the increase of temperature [43]. Considering the average values of G_{IC}, with the increase of the testing displacement rate, the values of G_{IC} decreased independently of the testing temperature. This allows to conclude that the strain rate influences the value of G_{IC}, although with limited significance if the standard deviation for the tests performed at 80 °C (near T_g of the CFRP brittle resin) is considered. For high temperature tests, this behaviour can also be related to the drop of the average crack velocity induced by the increased compliance of the CFRP resin near the T_g [48]. The extrapolation method was found to be in agreement with the experimentally obtained values of G_{IC} under the impact condition and for both testing

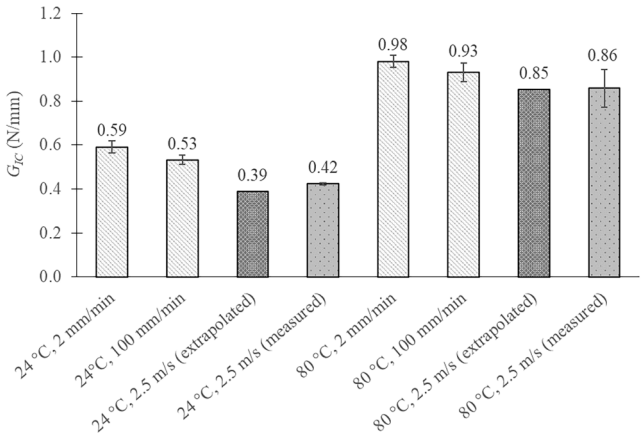

Fig. 9. Comparison between the G_{IC} (average and standard deviation) results for impact (2.5 m/s) and previously determined quasi-static (2 and 100 mm/min) [25] results, for tests performed at 24 and 80 °C.

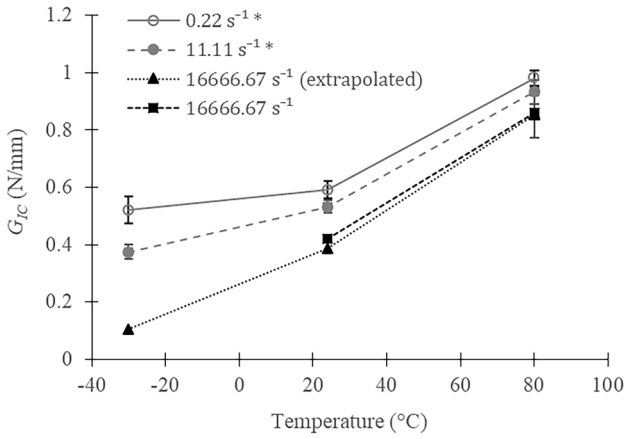

Fig. 10. Comparison between the G_{IC} results for impact (2.5 m/s) and previously determined quasi-static* (2 and 100 mm/min) [25] results for tests performed at −30, 24 and 80 °C, also introducing the values extrapolated.

temperatures.

Fig. 10 summarizes the evolution of G_{IC} values, as a function of strain rate and temperature. It considers the previously determined quasi-static (2 and 100 mm/min) [25] results, the extrapolated values for the three testing temperatures for the case of impact (4.7 m/s) condition, as well as the values measured under the impact condition.

The prediction trend (created using an extrapolation from quasi-static experimental results) indicates that the higher the temperature, the lower is the rate of change of the G_{IC}, which appears to be governed by the naturally brittle behaviour of the resin of the CFRP. This is supported by the fact that, at low testing temperatures, the mechanical properties of CFRP are significantly influenced by the strain rate. The extrapolated values of G_{IC} for the impact condition were relatively close to the experimentally obtained average values, although, in the case of the lowest testing temperature (−30 °C) no experimental results were determined. For this case, the expected G_{IC} value calculated by extrapolation was of 0.1 N/mm.

4. Conclusions

This work consisted on an experimental study of the effect of strain rate and testing temperature on the G_{IC} of a unidirectional CFRP material. For this purpose, DCB specimens were tested at two different temperatures (24 and 80 °C) and under an impact load of 4.7 m/s (using a falling-wedge impact test machine). A comparison was performed with experimental values determined at quasi-static rates in a previous work by the authors [25]. The main conclusions drawn from this work are presented below:

- Using a falling-wedge impact test machine it was possible to assess the dynamic effect on G_{IC} using CFRP DCB specimens tested at 24 and 80 °C. Three distinct strain rates were considered, two at quasi-static (0.22 and 11.11 s^{-1}) conditions which were previously determined by the authors [25], and under impact (282514 s^{-1}).
- The values of G_{IC} were measured using CFRP DCB specimens and considering a variable opening velocity. Symmetrical opening of the CFRP DCB specimens was achieved, minimizing the effect of one the common problems in this type of testing setup.
- For the case of impact tests, with the increase of the testing temperature, an increase of about 50% of G_{IC} was registered, explained by the change in the mechanical properties of the brittle resin impregnating the CFRP. As the temperature becomes closer to T_g, the resin becomes noticeably more ductile. The average values of G_{IC} indicate that, with the increase of the testing displacement rate, the fracture toughness decreases independently of the testing temperature. It can be concluded that, at all temperature levels, the strain rate has some influence on the value of G_{IC}. However, this effect is much less significant for tests performed at 80 °C (near T_g of the CFRP brittle resin) as the changes in G_{IC} fall within the standard deviation.
- The test velocity was not constant, due to the type of testing setup, with a gradual decrease of the velocity occurring through the test. Again, due to the increased ductility of the resin near the T_g, this reduction of velocity was much more noticeable at 80 °C.

Acknowledgments

The authors gratefully acknowledge the funding provided by PhD grant SFRH/BD/139341/2018 “Impact strength optimization with cohesive zone elements of multi-material bonded structures used in the automotive industry”, Project N° 028473 POCI-01-0145-FEDER-028473 “Design methodology for impact resistant bonded multi-material automotive structures (ImpactBondDesign)”, Project NORTE-01-0145-FEDER-000022 – “SciTech – Science and Technology for Competitive and Sustainable Industries”, co-financed by Programa Operacional Regional do Norte (NORTE2020), through Fundo Europeu de Desenvolvimento Regional (FEDER). The authors would also like to thank NAGASE ChemteX® for the financial support provided.

References

[1] W. Cantwell, J. Morton, The impact resistance of composite materials—a review, Composites 22 (5) (1991) 347–362.
[2] A. Rotem, Residual flexural strength of FRP composite specimens subjected to transverse impact loading, Sampe J. 3 (1988) 19–25.
[3] S. Benmedakhene, M. Kenane, M. Benzeggagh, Initiation and growth of delamination in glass/epoxy composites subjected to static and dynamic loading by acoustic emission monitoring, Compos. Sci. Technol. 59 (2) (1999) 201–208.
[4] M.S. Islam, L. Tong, Effects of hygrothermal and ambient humidity conditioning on shear strength of metal–GFRP single lap joints co-cured in and out of water, Int. J. Adhes. Adhes. 68 (2016) 305–316.
[5] S. Mall, G. Law, M. Katouzian, Loading rate effect on interlaminar fracture toughness of a thermoplastic composite, J. Compos. Mater. 21 (6) (1987) 569–579.
[6] M. May, Measuring the rate-dependent mode I fracture toughness of composites – a review, Compos. A Appl. Sci. Manuf. 81 (2016) 1–12.
[7] F. Chaves, et al., Fracture mechanics tests in adhesively bonded joints: a literature review, J. Adhes. 90 (12) (2014) 955–992.
[8] A. Aliyu, I. Daniel, Effects of strain rate on delamination fracture toughness of graphite/epoxy, Delamination and Debonding of Materials, ASTM International, 1985.
[9] I.M. Daniel, I. Shareef, A.A. Aliyu, Rate effects on delamination fracture toughness of a toughened graphite/epoxy, Toughened Composites, ASTM International, 1987.
[10] I.M. Daniel, G. Yaniv, J.W. Auser, Rate effects on delamination fracture toughness of graphite/epoxy composites, in: I.H. Marshall (Ed.), Composite Structures 4, Springer Netherlands, Dordrecht, 1987, pp. 258–272.
[11] G. Yaniv, I.M. Daniel, Height-tapered double cantilever beam specimen for study of rate effects on fracture toughness of composites, Composite Materials: Testing and Design (Eighth Conference), ASTM International, 1988.

[12] H. You, Y.-J. Yum, Loading rate effect on mode I interlaminar fracture of carbon/epoxy composite, J. Reinf. Plast. Compos. 16 (6) (1997) 537–549.
[13] B. Blackman, et al., The failure of fibre composites and adhesively bonded fibre composites under high rates of test, J. Mater. Sci. 30 (23) (1995) 5885–5900.
[14] T. Kusaka, et al., Rate dependence of mode I fracture behaviour in carbon-fibre/epoxy composite laminates, Compos. Sci. Technol. 58 (3–4) (1998) 591–602.
[15] G.C. Jacob, et al., The effect of loading rate on the fracture toughness of fiber reinforced polymer composites, J. Appl. Polym. Sci. 96 (3) (2005) 899–904.
[16] I. Daniel, B. Werner, J. Fenner, Strain-rate-dependent failure criteria for composites, Compos. Sci. Technol. 71 (3) (2011) 357–364.
[17] H. Hsiao, I. Daniel, Strain rate behavior of composite materials, Compos. B Eng. 29 (5) (1998) 521–533.
[18] K. Im, et al., Effects of temperature on impact damages in CFRP composite laminates, Compos. B Eng. 32 (8) (2001) 669–682.
[19] W. Cantwell, M. Blyton, Influence of loading rate on the interlaminar fracture properties of high performance composites – a review, Appl. Mech. Rev. 52 (6) (1999) 199–212.
[20] M. Sohn, X. Hu, Impact and high strain rate delamination characteristics of carbon fibre epoxy composites, Theor. Appl. Fract. Mech. 25 (1) (1996) 17–29.
[21] T.K. O'Brien, Interlaminar fracture toughness: the long and winding road to standardization, Compos. B Eng. 29 (1) (1998) 57–62.
[22] G. Hug, et al., Effect of the loading rate on mode I interlaminar fracture toughness of laminated composites, Eng. Fract. Mech. 73 (16) (2006) 2456–2462.
[23] J. Kalthoff, et al. On the Determination of the Crack Arrest Toughness, in: ICF4, Waterloo (Canada), 1977, 1977.
[24] N. Sridhar, et al., Delamination dynamics in through-thickness reinforced laminates with application to DCB specimen, Int. J. Fract. 118 (2) (2002) 119–144.
[25] J. Machado, et al., Mode I fracture toughness of CFRP as a function of temperature and strain rate, J. Compos. Mater. 51 (23) (2017) 3315–3326.
[26] ISO, B., 15024: 2001. Fibre-reinforced plastic composites. Determination of mode I interlaminar fracture toughness, GIC, for unidirectional reinforced materials. BSI, 2002.
[27] R. Campilho, Repair of Composite and Wood Structures, Instituto Superior de Engenharia do Porto, 2009.
[28] L. da Silva, et al., Effect of low temperature on tensile strength and Mode I fracture energy of a room temperature vulcanizing silicone adhesive, J. Test. Eval. 44 (3) (2015).
[29] E. Marques, et al., Adhesive joints for low-and high-temperature use: an overview, J. Adhes. 91 (7) (2015) 556–585.
[30] Y. Zhang, R. Adams, L. da Silva, A rapid method of measuring the glass transition temperature using a novel dynamic mechanical analysis method, J. Adhes. 89 (10) (2013) 785–806.
[31] R. Fernandes, R. Campilho, Testing different cohesive law shapes to predict damage growth in bonded joints loaded in pure tension, J. Adhes. 93 (1–2) (2017) 57–76.
[32] S. Xu, D.A. Dillard, Determining the impact resistance of electrically conductive adhesives using a falling wedge test, IEEE Trans. Compon. Packag. Technol. 26 (3) (2003) 554–562.
[33] L. da Silva, A. Öchsner, Modeling of Adhesively Bonded Joints, Springer, 2008.
[34] D. Saldanha, et al., Mechanical characterization of a high elongation and high toughness epoxy adhesive, Int. J. Adhes. Adhes. 47 (2013) 91–98.
[35] Y. Wang, J. Williams, Corrections for mode II fracture toughness specimens of composites materials, Compos. Sci. Technol. 43 (3) (1992) 251–256.
[36] M. De Moura, R. Campilho, J. Gonçalves, Crack equivalent concept applied to the fracture characterization of bonded joints under pure mode I loading, Compos. Sci. Technol. 68 (10) (2008) 2224–2230.
[37] M. de Moura, R. Campilho, J. Gonçalves, Pure mode II fracture characterization of composite bonded joints, Int. J. Solids Struct. 46 (6) (2009) 1589–1595.
[38] R. Fernandes, et al., Determination of cohesive laws of composite bonded joints under mode II loading, Compos. B Eng. 52 (2013) 269–274.
[39] G. Dias, et al., Cohesive laws of composite bonded joints under mode I loading, Compos. Struct. 106 (2013) 646–652.
[40] M. De Moura, et al., Cohesive and continuum mixed-mode damage models applied to the simulation of the mechanical behaviour of bonded joints, Int. J. Adhes. Adhes. 28 (8) (2008) 419–426.
[41] F. Silva, et al., Determination of cohesive laws in wood bonded joints under mode I loading using the DCB test, Holzforschung 67 (8) (2013) 913–922.
[42] M. Banea, L.d. Silva, R. Campilho, Effect of temperature on tensile strength and mode I fracture toughness of a high temperature epoxy adhesive, J. Adhes. Sci. Technol. 26 (7) (2012) 939–953.
[43] Y. Yamagata, et al., Experimental investigation of mode I fracture energy of adhesively bonded joints under impact loading conditions, Appl. Adhes. Sci. 5 (1) (2017) 7.
[44] R. Suvarna, et al., Effect of temperature on low velocity impact damage and post-impact flexural strength of CFRP assessed using ultrasonic C-scan and micro-focus computed tomography, Compos. B Eng. 66 (2014) 58–64.
[45] L. Sorrentino, et al., Effect of temperature on static and low velocity impact properties of thermoplastic composites, Compos. Part B: Eng. 113 (2017) 100–110.
[46] M. Zgoul, A. Crocombe, Numerical modelling of lap joints bonded with a rate-dependent adhesive, Int. J. Adhes. Adhes. 24 (4) (2004) 355–366.
[47] R. Avendaño, et al., Effect of temperature and strain rate on single lap joints with dissimilar lightweight adherends bonded with an acrylic adhesive, Compos. Struct. 152 (2016) 34–44.
[48] B. Blackman, et al., The fracture behaviour of structural adhesives under high rates of testing, Eng. Fract. Mech. 76 (18) (2009) 2868–2889.

Paper 6

Content of Paper 6

Abstract

1. Introduction

2. Experimental details

2.1. Material and properties

2.1.1. CFRP

2.1.2. Adhesive

2.2. Specimen configurations

2.3. Specimen fabrication

2.4. Quasi-static and impact testing procedure

2.5. Dynamic testing procedure

3. Numerical details

3.1. Quasi-static modelling

3.2. Impact modelling

4. Results

4.1. Experimental results

4.1.1. Quasi-static testing

4.1.2. Impact testing

4.1.3. Dynamic testing

4.2. Numerical analysis results

4.2.1. Quasi-static models

4.2.2. Impact models

4.2.3. Dynamic testing

5. Conclusions

References

Composite Structures 171 (2017) 549–561

Contents lists available at ScienceDirect

Composite Structures

journal homepage: www.elsevier.com/locate/compstruct

Dynamic behaviour of composite adhesive joints for the automotive industry

H.A.M. Araújo [a], J.J.M. Machado [b], E.A.S. Marques [b], L.F.M. da Silva [a,*]

[a] Departamento de Engenharia Mecânica, Faculdade de Engenharia (FEUP), Universidade do Porto, Rua Dr. Roberto Frias, 4200-465 Porto, Portugal
[b] Instituto de Ciência e Inovação em Engenharia Mecânica e Engenharia Industrial (INEGI), Rua Dr. Roberto Frias, 4200-465 Porto, Portugal

ARTICLE INFO

Article history:
Received 7 February 2017
Revised 20 March 2017
Accepted 21 March 2017
Available online 22 March 2017

Keywords:
Composite
Static
Impact
Single lap joints
Numerical simulation

ABSTRACT

The automotive industry has significantly increased the use of adhesive joints in vehicle construction, which can be explained in part by the widespread adoption of composite materials and structures. The combined use of composites and bonding allows the manufacture of structures with high mechanical strength and reduced weight. However, to ensure vehicle safety, these adhesive joints must be able to sustain large impact loads, transmitting the load to the structure without damaging the joint. This work aims to study the impact behaviour of composite adhesive joints bonded with a ductile epoxy adhesive, comparing different overlap lengths. For this purpose, a characterization of the behaviour of single lap joints was performed under quasi-static and impact conditions. Dynamic tests were also performed using vibration analysis to assess the damping capabilities of the studied joints. Numerical models were developed with cohesive elements in ABAQUS® software, including both quasi-static and dynamic models. It was demonstrated that joints manufactured with this type of adhesives and substrates can exhibit excellent impact strength and damping capabilities. It was also shown that the behaviour of these joints can be successfully modelled using static and dynamic finite element analysis.

© 2017 Elsevier Ltd. All rights reserved.

1. Introduction

The wide use of fibre reinforced composite materials, such as carbon-fibre reinforced polymer (CFRP), in the automotive industry has led to lighter structures, with excellent strength and stiffness to weight ratios [1,2]. In order to satisfy mandatory safety requirements, structures used in this industry must be able to sustain dynamic load conditions, deforming and absorbing energy while at the same time maintaining their integrity. It is therefore important to ensure that carbon fibre structures can also bear impact loadings without premature failure.

The design of a composite adhesive joint for these conditions must be carefully considered, as geometrical parameters have a significant effect on the mechanical behaviour of bonded composite joints. Li et al. [3] analysed the influence of the overlap length, adherend thickness, width and scarf angle on single lap joints (SLJs), double lap joints (DLJs) and scarf joints, all using composite substrates and under static conditions. As the overlap increased, the ultimate failure also increased, as did the equivalent stiffness of the joint. In contrast, the overlap lap shear strength reduces with larger overlap lengths. Analysing the surfaces of the tested joints, the fracture modes changed from cohesive in the adhesive to cohesive in the adherend with an increase in the overlap length.

Neto et al. [4] further studied the effect of overlap length, performing a static strength comparison between a polyurethane adhesive and a two-component epoxy adhesive using CFRP adherends. In the case of the epoxy adhesive, the failure load increased until it reached a plateau from the overlap length of 30 mm. From this point further, the failure load was dictated by the composite. For the ductile adhesive, a linear behaviour of the failure load was noticed, since the failure mode was cohesive in the adhesive.

The effect of high strain rates in CFRP was studied by different authors. Harding and Welsh [5] showed that tensile properties of unidirectional carbon-epoxy were not influenced by strain rate. Taniguchi et al. [6] reached the same conclusion and also determined that the tensile properties in the transverse direction and the shear properties increased with an increase of the strain rate. Körber [7] showed that while strain rate had no significant effect on the longitudinal tensile modulus and strength, the same did not occur for the transverse tensile modulus and strength. A variation of the transverse tensile modulus and strength with the strain rate was observed. In this case, it is the resin that controls the failure, instead of the carbon fibres, which mostly influence

* Corresponding author.
E-mail address: lucas@fe.up.pt (L.F.M. da Silva).

http://dx.doi.org/10.1016/j.compstruct.2017.03.071
0263-8223/© 2017 Elsevier Ltd. All rights reserved.

the longitudinal properties. In 2000, Hou and Ruiz [8] tested woven CFRP using a split Hopkinson pressure bar (SHPB) apparatus under different strain rates and in tension, compression and in-plane shear. The authors concluded that the properties which are dominated by the matrix are: compression strength, Poisson's ratio, in-plane shear modulus, shear modulus and shear strength, being those properties strain rate dependent; the properties dominated by the fibres are: tensile modulus and strength which are virtually rate independent.

After understanding the mechanical behaviour of the CFRP substrate under impact loads, it is then fundamental to evaluate the adhesive behaviour under these same loads. Harris and Adams [9] compared the variation of joint strength in static and high rates of loading and the energy absorption by the structures under impact loads. In this research, different epoxy adhesives were used in the experiments. The first important conclusion was that the joint strength did not vary significantly when comparing static to dynamic loading of these adhesives. Concerning energy absorption by the structures, it was shown that in the case of bonded joints, energy absorption comes from the deformation of adherend material, and not from the adhesive itself. Bonded structures can withstand impact loads if the joints have sufficient strength to undergo plastic deformation in the adherend layers. In another study performed by Saldanha et al. [10] where low yield strength steel adherends and a high elongation and high ductility adhesive were used, drop weight impact tests were performed. It was possible to observe that in the impact tests the failure load increased and the elongation decreased. The adherends deformed less and absorbed less energy. Despite this, for both cases the failure occurred in the adherends. The behaviour of flexible adhesives under impact loads was studied by Kadioglu and Adams [11]. The authors determined that when the strain rate increased, the maximum tensile shear stress also increased and the tensile strain to failure decreased. This can be explained by considering that under high strain rates, the natural molecular rearrangement of the adhesive does not take place, because of the short period of load applications.

Cohesive zone models (CZM) are a very powerful tool for studying the behaviour of adhesive joints under static or impact loads. These numerical models are extensively used and give accurate predictions of failure loads. Authors such as Needleman [12], Tvergaard et al. [13] and Camacho et al. [14] were among the first to demonstrate the validity of this technique. A CZM combines the elastic stress calculations with classical fracture mechanics, being able to fully model the fracture process and location. A CZM model uses cohesive elements, which contain both strength and energy parameters to simulate the nucleation and advance of a fracture crack [15,16]. A traction separation law is used to establish a relation between the stresses and displacements. Fig. 1 shows a triangular traction separation law, typically available in many finite element software packages such as ABAQUS®. In Fig. 1, σ_n and τ_s are the cohesive strengths in tension and shear, respectively, E and G correspond to the stiffness in tension and shear, and G_{IC} and G_{IIC} are the critical fracture energies in mode I and mode II.

The work of Carlberger et al., published in 2007 [17] was the first that demonstrated the validity of using this type of approach to predict impact strength of adhesive joints. Authors such as Haufe et al. [18], May et al. [19], Clarke et al. [20], Avendaño et al. [21], Neumayer et al. [22] and Morin et al. [23] employed similar approaches and have shown that modern commercial software packages enable accurate prediction of failure loads, using complex dynamic cohesive models with strain rate dependent data.

The damping of adhesive joints is also an important property for the automotive industry, as manufacturers demand stiff structures that are still able to absorb vibrations. Damping of an adhesive joint can be expressed by different parameters such as specific damping capacity, damping ratio, logarithmic decrement and loss factor. Limited research has been undertaken on the damping behaviour of SLJs by studying the effect of variables such as the overlap ratio, temperature and bondline thickness. One of the earliest works on this subject, performed by Saito et al. [24] found that damping of SLJs is highly dependent on vibrational mode and overlap length. Adams et al. [25] studied four different adhesives with five different overlap lengths, employing a high strength low-damping steel for adherends This research determined that the optimum overlap ratio (overlap length divided by total specimen length) is around 0.25 for SLJs and that the damping provided by adhesives in vibrating structures is relatively limited and cannot be expected to significantly enhance the damping of the complete structure.

The main aim of this work was to experimentally assess the impact behaviour of composite adhesive joints bonded with a ductile epoxy adhesive. The behaviour of SLJs with different overlap lengths was studied under quasi-static and impact conditions. The damping capabilities of these joints was also examined. Lastly, CZMs were used to develop numerical simulations, which were validated using the experimental quasi-static and dynamic results, ensuring their usefulness in the design of crash resistant composite structures.

2. Experimental details

2.1. Material and properties

2.1.1. CFRP

The SLJ specimens used in this work used CFRP substrates bonded with a high ductility, crash resistant adhesive (Nagase ChemteX® XNR6852E-3). The CFRP substrates were composed of stacked plies of a carbon/epoxy pre-preg (SEAL® Texipreg HS 160 RM). A unidirectional configuration was used, selected to ensure maximum strength in the loading direction of SLJs.

The properties of this material were previously determined in the work of Campilho et al. [26] in 2008, and are presented in Table 1.

As shown in the introduction, the tensile properties of unidirectional CFRP are known to not vary significantly with the strain rate along the fibre direction [6,7,27]. Due to this fact, the strain rate dependent characterization of the Young's modulus and the tensile strength was not performed in these experimental procedures. However, there is limited information regarding strain rate dependence of fracture energy, which prompted the use of fracture toughness testing to obtain this data. Additionally, some authors have demonstrated sudden drop-offs in fracture toughness due to adiabatic heating. In some cases, there is also pointed the absence of the effect of fracture toughness [28]. While the tensile strength in the off-axis direction and the shear strength are also known to be sensitive to the rate of loading [29], these effects were not considered on this study due to the loads being applied mainly in the fibre direction.

For mode I fracture testing double cantilever beam (DCB) specimens were used. The geometry of the CFRP DCB specimens was based on ISO 15024 [30] standard, from 2001, which is used to determine, in mode I, the interlaminar fracture toughness, G_{IC}, for unidirectional reinforced fibre-reinforced plastic composites.

Mode II fracture testing was performed using end notch flexure (ENF) specimens. The same manufacture procedure described for the DCB specimens was followed for ENF specimens. This test consists of a 3-point bending load, where the specimen is supported at both ends and loaded in the opposite side at mid-span, promoting a shear mode loading in the adhesive layer [31]. Since there is no standard defined for these experiments [32], the geometry of the

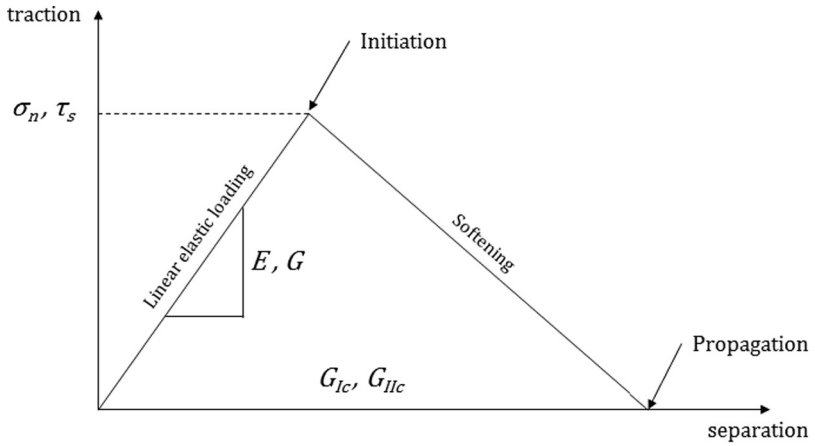

Fig. 1. Triangular cohesive law with mode I and mode II properties.

Table 1
Elastic orthotropic properties of CFRP (1 – fibres direction, 2 – transverse direction, 3 – out of plane direction) [26].

Elastic modulus (MPa)	Poisson's ratios	Shear modulus (MPa)
E_1 = 1.09E5	ν_{12} = 0.342	G_{12} = 4315
E_2 = 8819	ν_{13} = 0.342	G_{13} = 4315
E_3 = 8819	ν_{23} = 0.380	G_{23} = 3200

specimens was defined instead by studying the behaviour of numerical models, a technique based on the work developed by de Moura et al. [33]. The main purpose of this step was to assess if stable crack propagation could be achieved with a given geometry. The experimental results allowed the extrapolation as well as the calculation of each property under impact speed conditions. The logarithmic law used in this process is given by Eq. (1).

$$\text{Property to determine} = A\ \ln(\dot{\varepsilon}) + B \quad (1)$$

where A and B are constants obtained from experimental data, and $\dot{\varepsilon}$ is the strain rate in s^{-1}. This logarithmic extrapolation process has been first proposed by the work of Zgoul and Crocombe [34] and further validated by the work of Avendaño et al. [35].

Table 2 lists the experimentally measured mechanical properties for the CFRP material as well as the extrapolated properties for impact velocity.

The strain rates are relatively low for complete impact characterization but very limited work exists relating the fracture toughness of composites with the strain rate. Therefore, this is still an early first step in work, and it is intended to explore higher strain rates in further works.

2.1.2. Adhesive

The adhesive used in this work is a crash resistant adhesive that combines the toughness of a polyurethane with the high strength of an epoxy [36]. This type of adhesive is particularly relevant for the automotive industry due to the combination of its high strength, ductility and resistance to impact. This material can deform significantly without breaking, allowing the bonded structure to deform plastically and absorb the impact energy. This epoxy adhesive was experimentally characterized under two different displacement rates: 1 and 100 mm/min. Tensile and shear tests were performed as well as fracture energy tests in mode I and II [37,38].

In order to characterize the tensile properties of the adhesive, bulk tests were performed and the specimen geometry used was in accordance with EN ISO 527-2 [39–41].

Thick adherend shear tests (TAST) were employed to characterize the shear properties of the ductile adhesive. The TAST specimens are composed of two steel substrates (DIN C45 E), joined by the adhesive layer. The stiffness of the steel substrate combined with the short overlap length introduces an almost pure shear stress in the adhesive layer [42,43]. The geometry used is in accordance to ISO 11003-2 [44].

DCB tests [45] were performed in order to obtain the critical strain energy release rate in mode I of XNR6852E-3 adhesive. High strength steel (DIN 40 CrMnMo 8-6-4) specimens were used to avoid plastic deformations of the substrates. The geometry used was per D 3433-99 ASTM standard [46] .

Mode II characterization [47] of the XNR6852E-3 could not be experimentally performed due to the extremely high fracture toughness that this adhesive presents in mode II, which caused plastic deformation of the metallic substrates in all studied ENF specimens. Saldanha et al. [10] and Avendaño et al. [21] have studied previous versions of Nagase XNR6852 adhesive and in their works G_{IIC} determined experimentally was 6–10 times higher than G_{IC}. Considering this previous data, and due to the high ductility of the adhesive, the value for G_{IIC} was therefore assumed to be 8 times higher than the fracture toughness in mode I.

Table 3 lists the experimentally measured mechanical properties (average values) for the XNR6852E-3 adhesive as well as the extrapolated properties for impact velocity.

Table 2
Mechanical properties of CFRP under quasi-static and impact conditions.

Properties	1 mm/min	100 mm/min	Impact*
Young's modulus, E [MPa]	108000	108000	108000
Shear modulus, G [MPa]	4315	4315	4315
Tensile strength, σ_n [MPa]	40	40	40
Shear strength, t_s [MPa]	35	35	35
Fracture energy (mode I), G_{IC}[N/mm]	0.59	0.53	0.39
Fracture energy (mode II), G_{IIC}[N/mm]	1.17	1.04	0.82

* Impact velocity of 2 m/s.

Table 3
Mechanical properties of Nagase ChemteX® XNR6852E-3 epoxy adhesive under quasi-static and impact conditions (average values).

Properties	1 mm/min	100 mm/min	Impact
Young's modulus, E [MPa]	1728	1728	1728
Shear modulus, G [MPa]	665	645	603
Tensile strength, σ_n [MPa]	51.5	60.5	77.7
Shear strength, t_s [MPa]	44.9	44	42.9
Fracture energy (mode I), G_{IC}[N/mm]	6.4	7.1	8
Fracture energy (mode II), G_{IIC}[N/mm]	51	58.2	64.1

2.2. Specimen configurations

The specimens used for impact testing were SLJs with 2.1 mm thick CFRP substrates. The geometry chosen can be considered as representative of automotive industry applications, with thin substrates and single overlap bonding.

The different overlap lengths used for SLJs tested at quasi-static conditions were 12.5, 25 and 50 mm, and for impact conditions 12.5 and 25 mm. The 50 mm overlap was not tested under impact due to limitations in the maximum capacity of the drop weight machine. The free length was kept constant, to allow direct comparison between the results of the various overlap lengths. The thickness of the adhesive layer used was 0.2 mm. Three specimens were tested for each quasi-static test and seven for each impact test.

The dimensions of the SLJ specimens are shown in Fig. 2.

2.3. Specimen fabrication

The substrates used for the SLJs consisted on unidirectional laminates of CFRP cut from bulk laminates, which were produced by hand lay-up and cured in a hot plate press. The bulk laminates with dimensions of 300 mm by 300 mm were fabricated by stacking unidirectional 0° plies. The unidirectional lay-up was chosen with the aim of obtaining better properties in the loading direction. A total of twenty plies of carbon/epoxy pre-preg (SEAL® Texipreg HS 160 RM) were stacked, each with 0.15 mm of ply thickness. The stacked lay-up was placed in a hot plate press and subjected to a cure cycle of 130 °C during 1 h.

After removal from the press, the laminates were cut into smaller specimens using a diamond disc cutting machine. Edge finishing was carried out manually with 120 grit sandpaper to remove the loose fibres and smoothen the sharp edges.

The joints were assembled using a mould to ensure both the correct alignment of the joint and the intended overlap length. To complete the joint manufacture process, the mould was placed under pressure and temperature in a hot plate press. The curing cycle of the epoxy adhesive was 150 °C during 3 h.

2.4. Quasi-static and impact testing procedure

The static tests of specimens with 12.5 mm and 25 mm of overlap length were performed in an INSTRON® model 3367 universal testing machine (Norwood, Massachusetts, USA) with a capacity of 30 kN. The static tests of 50 mm overlap length were performed in a Material Test System® 810 universal testing machine with a capacity of 100 kN. The use of different testing machines was necessary as the failure loads of the specimens with the larger overlap length were higher than the maximum capacity of the first machine. All tests were performed with a constant cross-head rate of 1 mm/min, corresponding to a strain rate of 0.08 s^{-1}.

The impact tests were performed in a Rosand® Instrumented Falling weight impact tester, type 5 H.V. (Stourbridge, West Midlands, U.K.). This device consists of a mass that is dropped from a certain height, until it impacts the specimen. The specimen is mounted vertically with the use of a specially designed grip. The impactor collides with the lower section of the grip, accelerating the test assembly such that the specimen is loaded in tension-shear. During the setup of the testing machine, the mass was set to the maximum value of 26 kg. For testing specimens with 12.5 mm of overlap length, the height was adjusted to attain a test speed of 2 m/s, providing an impact energy of 50 J. For specimens with 25 mm of overlap length, the speed test was increased to 3 m/s, to provide a higher impact energy of 117 J. The increase on the displacement speed was due to the need to achieve larger values of energy to break the bond of the SLJs with higher overlap length. As the maximum mass capacity of the drop weight machine was already being used (limited to 26 kg), the only method available to increase the energy was to increase the test speed.

The value of strain rate applied in the case of SLJs with overlap length of 12.5 mm was of 10,000 s^{-1} (which corresponds to a displacement speed of 2 m/s), and for the case of overlap length of 25 mm, the value of strain rate was of 15,000 s^{-1} (corresponding to a displacement speed of 3 m/s).

2.5. Dynamic testing procedure

A modal test, simulating the cantilever beam case, was performed to study the damping capabilities of the CFRP/high ductility adhesive combination. One of the ends was clamped, while the other remained free. Three overlap lengths were studied (12.5, 25 and 50 mm). The clamped portion of the specimen was 15 mm long. Flexural (bending) vibration was the studied load, as this is one of the most common forms of vibration in automotive applications. While this research focus on the analysis of CFRP substrates, the damping capabilities of steel specimens with geometries representative of automotive structures were also assessed, allowing for a direct comparison between CFRP and steel substrates.

The dynamic excitation was applied into the free end of the specimens, using an impact hammer from Dytran® 5800 SL. An accelerometer was used to measure the response of the specimen. This device was placed at the free end of the specimens. Fig. 3 shows a schematic representation of the test setup.

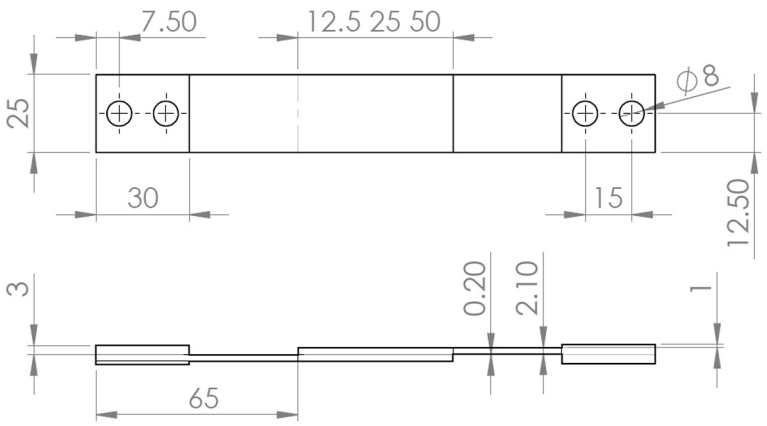

Fig. 2. Dimensions in mm of the CFRP SLJs used for quasi-static and impact tests.

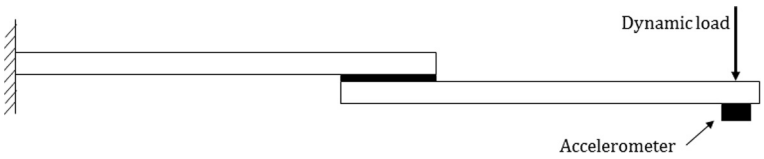

Fig. 3. Scheme of the vibration testing setup.

The natural frequencies and damping characteristics were obtained from the frequency response function (FRF). Every FRF was obtained by an average of three hammer impact tests. The magnitude of each frequency response function of acceleration was obtained by the data acquired from the accelerometer and the impact hammer. The natural frequencies were directly obtained from the frequency response function of each specimen, while the damping ratio was obtained using the half power bandwidth method [48]. Data was acquired for the first and second modes of vibration.

3. Numerical details

3.1. Quasi-static modelling

A finite element analysis (FEA) was performed using the commercial software ABAQUS®. The experimental results were used to validate the numerical model. For all joints, the adhesive layer was modelled as a triangular (bilinear) traction-separation law using cohesive elements with the same height as the adhesive thickness. The adherends were modelled with elastic elements as well as cohesive elements, which were modelled as a traction separation law. The two-dimensional (2D) mesh applied to the models was constructed with plain-strain four-node quadrilateral solid finite elements (CPE4 from ABAQUS®), and four-node cohesive elements (COH2D4 from ABAQUS®). The mesh was refined to reduce element size in regions with large stress gradients. The triangular CZM was chosen due to its reduced complexity and application in previous studies. The properties used were those previously shown in Tables 2 and 3.

All the experiments were modelled as two-dimensional studies due to the simplicity of the SLJ geometry. A single layer of cohesive elements was introduced on each adherend, with a thickness of 0.015 mm, located near the adhesive layer between two layers of CFRP continuum elements. This layer is implemented to simulate delamination of the CFRP layers, a technique which has been used previously in the literature with success for static and impact models [49,50]. Another cohesive layer was introduced in the adhesive layer, with the same thickness of the adhesive (0.2 mm). This layer simulates failure in the adhesive. This element size was defined according to previous experience using this type of cohesive element, however, it is important to stress that cohesive zone models are note especially sensitive to element size [35].

In the FE model, one of the ends was clamped, restrained in the two directions, while a longitudinal displacement was applied in the other end of the model, restrained in the transverse direction as well. These boundary conditions, shown in Fig. 4, allow the simulation of the effect of the grips used in the experimental tests.

3.2. Impact modelling

A two-dimensional explicit model was developed to predict and simulate the behaviour of CFRP SLJs under impact conditions. Two-dimensional models have been shown to be able to model the impact performance of CFRP materials [51]. The explicit model allows the simulation of high speed tests, including drop weight tests and crash analysis. To simulate the drop weight, a mass was added to the non-clamped edge and a velocity field was introduced to represent the impact velocity. The value of the mass was changed to match the 50 J and 117 J of energy used in the experi-

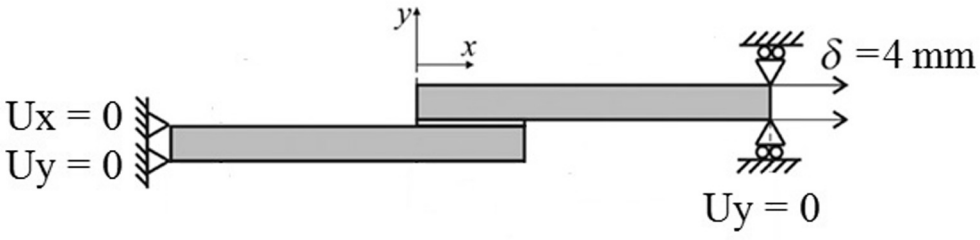

Fig. 4. Schematic representation of the boundary conditions used for static modelling.

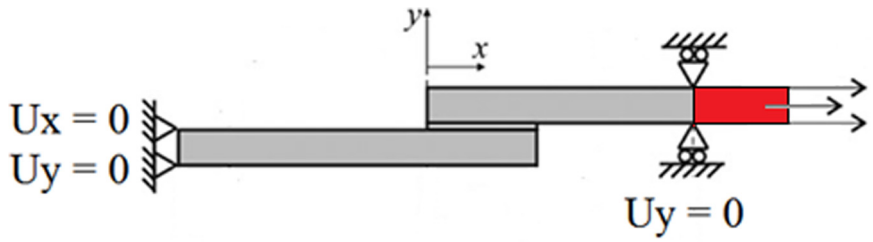

Fig. 5. Schematic representation of the boundary conditions used for dynamic modelling.

mental testing procedures. Fig. 5 illustrates the boundary conditions used for the impact models.

4. Results

4.1. Experimental results

4.1.1. Quasi-static testing

The results for the failure load and displacement of the CFRP SLJs tested at quasi-static conditions are presented for each overlap length in Table 4, as well as the values of standard deviation.

Table 4
Failure load and displacement at failure of CFRP SLJs under quasi-static condition.

Overlap length (mm)	Failure load (kN)	Displacement (mm)
12.5	10.2 ± 0.4	0.78 ± 0.03
25	21.3 ± 1.4	1.13 ± 2.23
50	38.9 ± 2.0	1.58 ± 0.68

Representative force-displacement (P-δ) curves of the CFRP SLJs tested under quasi-static conditions are shown in Fig. 6. The results revealed that with an increase of the overlap length there is an increase in the failure load and displacement.

For all the specimens tested under quasi-static conditions, delamination was found in all CFRP substrates. Representative images of the fracture surface for each overlap length are presented in Fig. 7.

4.1.2. Impact testing

The results of failure load and absorbed energy of the CFRP SLJs tested under impact are presented for each overlap length in

Table 5
Failure load and absorbed energy of CFRP SLJs under impact conditions.

Overlap length (mm)	Failure load (kN)	Absorbed energy (J)
12.5	17.5 ± 4.5	18.9 ± 5.9
25	32.5 ± 3.0	76.6 ± 27.6

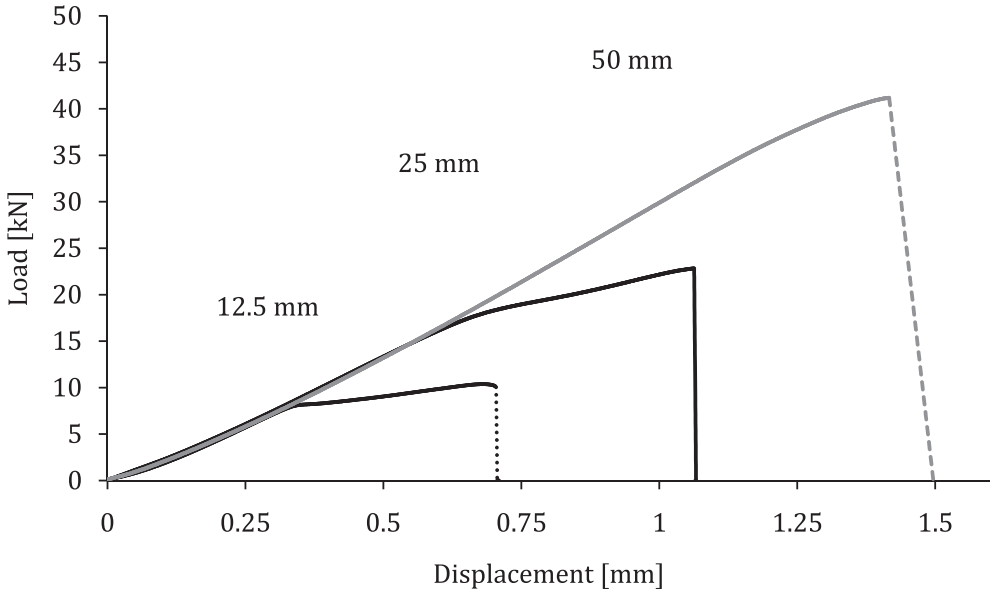

Fig. 6. Representative P-δ curves of SLJs for the three overlap lengths studied under quasi-static conditions.

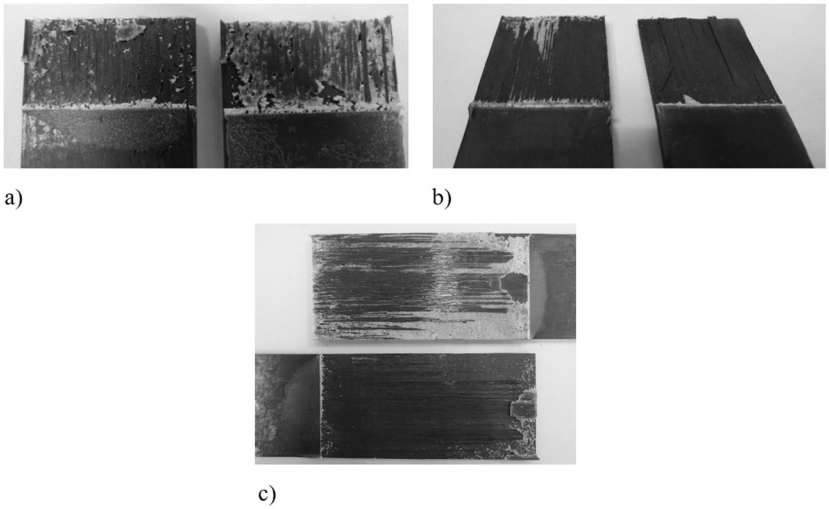

Fig. 7. Representative failure surfaces of CFRP SLJs specimens for three overlap lengths tested under quasi-static conditions: a) 12.5 mm, b) 25 mm, and c) 50 mm.

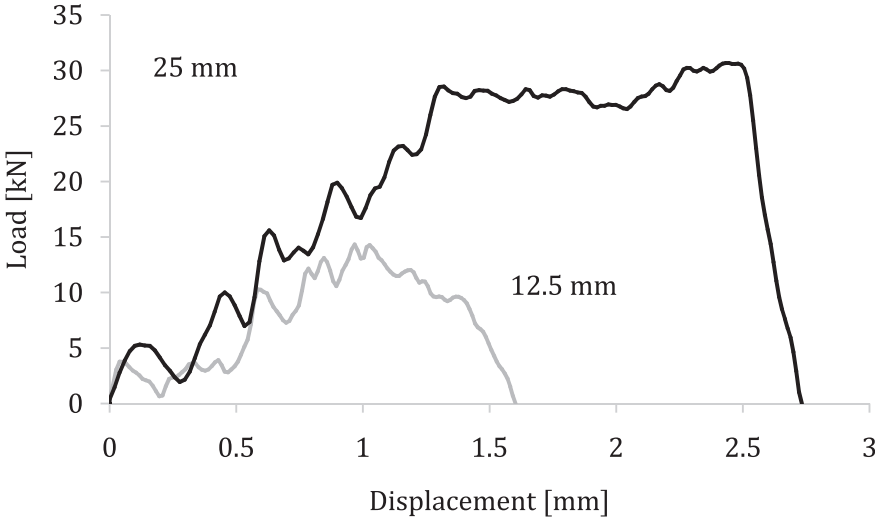

Fig. 8. Representative P-δ curves of CFRP SLJs tested under impact conditions for two overlap lengths (12.5 mm and 25 mm).

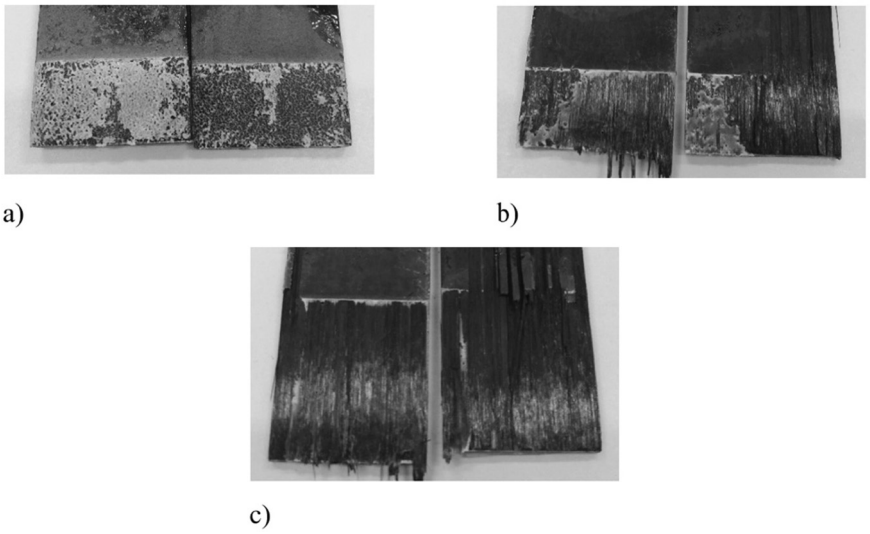

Fig. 9. Failure modes of impact tests of CFRP SLJs: a) cohesive failure of 12.5 mm, b) delamination failure of 12.5 mm, and c) delamination failure of 25 mm.

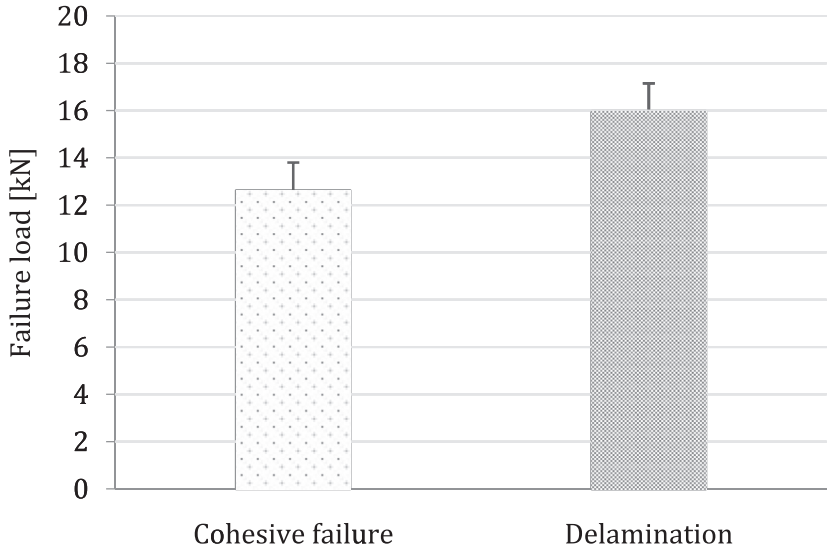

Fig. 10. Failure loads for different failure modes of 12.5 mm overlap length specimens, tested under impact conditions.

Table 5, as well the values of standard deviation. It is possible to notice a clear increase in the average failure load and absorbed energy with the increasing overlap length.

Representative P-δ curves of impact tests are presented in Fig. 8.

When analysing the failure mode, it was found that the specimens with 12.5 mm overlap length exhibited cohesive failure of the adhesive in some cases, while others presented delamination of the CFRP substrate. In the case of 25 mm overlap length, severe delamination occurred in all the specimens. Fig. 9 shows the fracture surfaces found for these tests.

Fig. 10 illustrates how delamination and cohesive failure of the adhesive influences the failure load of the specimens with a 12.5 mm overlap.

The results show that the higher value of the failure load occurred in case of delamination in the composite, which happens when the adhesive is strong enough to induce peel loads that lead to delamination of the CFRP. This was not the case in all specimens tested and can be explained by the dispersion in results typical for impact testing.

In Fig. 11 it is possible to observe a comparison between the results of SLJs tested under quasi-static and impact conditions, as a function of the overlap length. There is a clear increase in the failure load as the overlap increases. It is also evident that there is no linearity for both load cases. This phenomenon is discussed in more detail in the numerical modelling section.

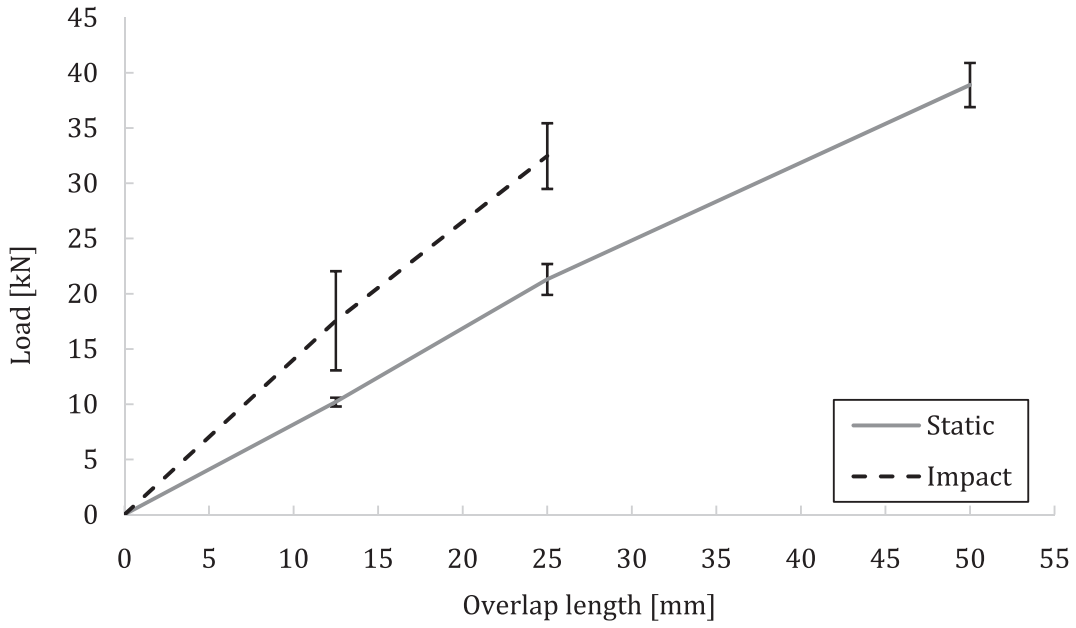

Fig. 11. Comparison of the quasi-static and impact results of SLJs.

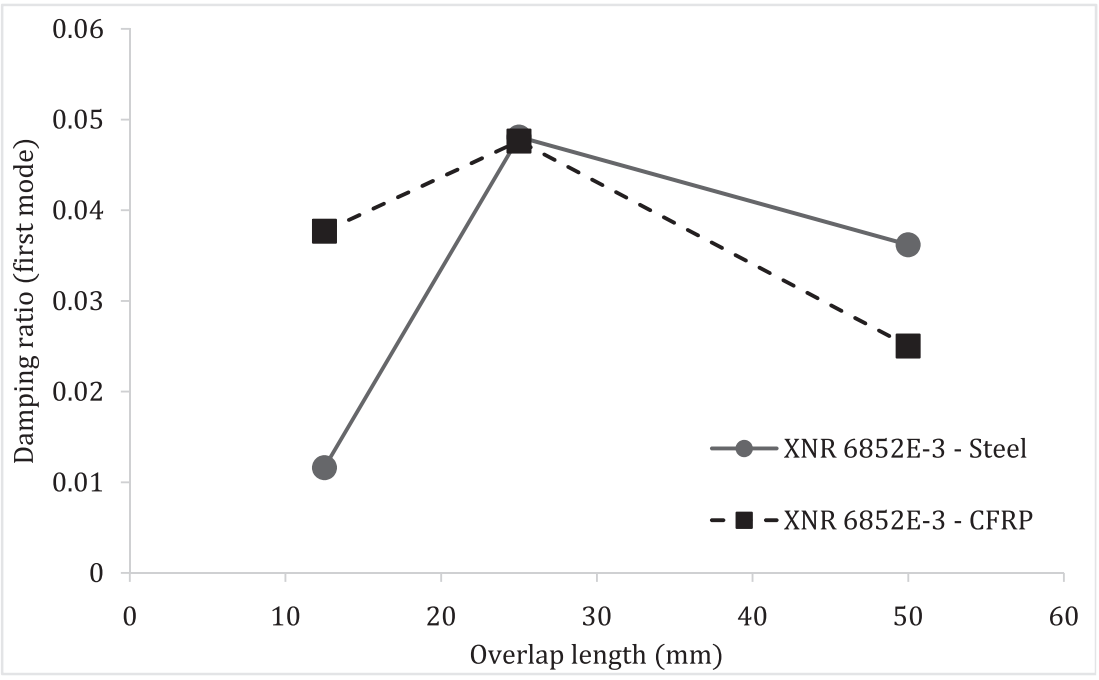

Fig. 12. Damping ratio as a function of the overlap length for CFRP and steel SLJ specimens for the first mode of vibration.

4.1.3. Dynamic testing

Fig. 12 shows the damping ratios calculated for the first mode of vibration, for both substrate materials. The damping ratio for the tested specimens is shown plotted as function of the overlap length.

The figure shows that for the first mode of vibration peak damping is achieved for an overlap of 25 mm for both cases (steel and CFRP specimens), which corresponds to an overlap ratio of 0.17. For shorter overlap lengths, the use of CFRP substrates leads to better damping performance while for higher overlap lengths the use of steel provides slightly better results.

Fig. 13 shows the damping ratios calculated for the second mode of vibration, for both substrate materials.

For the second mode of vibration the specimens with CFRP substrates exhibited higher damping ratios for all the overlap lengths under study. This is expected, as the substrate has significantly higher displacements in this mode of vibration. The maximum damping value is again obtained for an overlap length of 25 mm. This length appears to achieve the best ratio of bonded area to the free length of the substrate. This effect is more pronounced for the CFRP specimens.

Although there is a complex relationship between overlap lengths and damping, these results show that adhesive joints with CFRP specimens can exhibit noticeable improvements in the damping capabilities, surpassing those presented by a typical bonded steel joint.

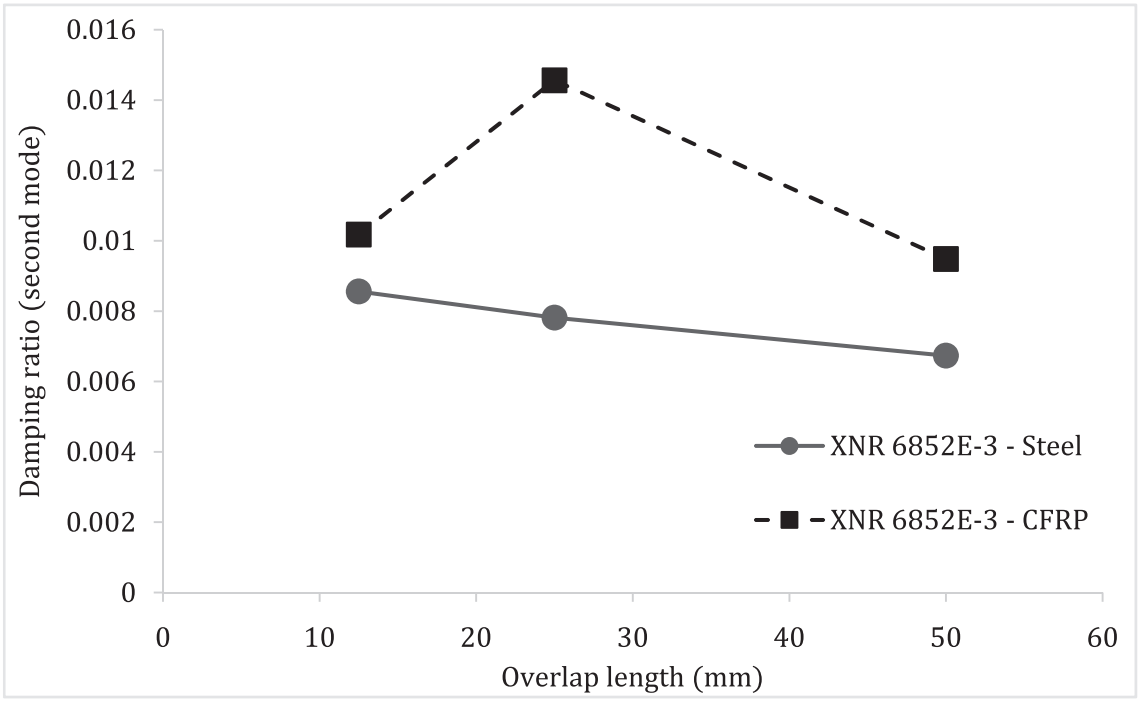

Fig. 13. Damping ratio as a function of the overlap length for CFRP and steel SLJ specimens for the second mode of vibration.

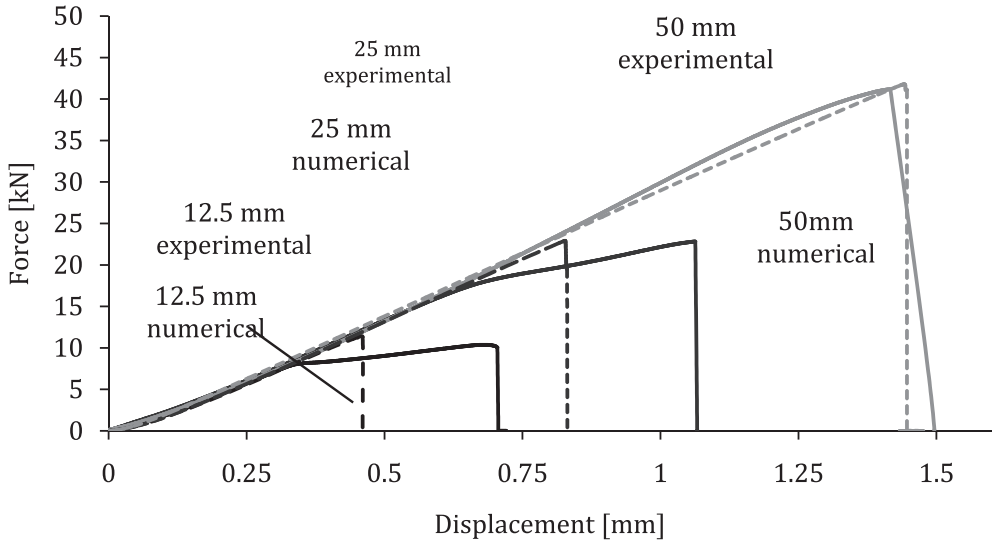

Fig. 14. Experimental vs Numerical results of SLJs tested at quasi-static conditions.

4.2. Numerical analysis results

4.2.1. Quasi-static models

The comparison between experimental and numerical results of SLJs tested at quasi-static conditions and for all the overlap lengths used is presented in Fig. 14.

The numerical curves match the experimental data quite well in failure load and stiffness. However, for the two shortest overlap lengths, there is difficulty in modelling yielding of the joint, which results in inaccurate displacements at failure. This can be explained by the increased influence of the adhesive plasticity for shorter overlaps, which is not correctly captured by the triangular cohesive zone mode. For longer overlaps, higher stress concentrations reduce the influence of the adhesive's plasticity on the joint's overall behaviour. For specimens with 50 mm of overlap, the fracture of the CFRP matrix, a brittle material, is the dominant effect. In this case, the use of a triangular cohesive law is optimal.

Fig. 15 analyses in more detail the failure loads obtained experimentally and numerically. Good agreement was found for all the SLJs tested at quasi-static condition and for the full range of overlap lengths.

The FEA results revealed that the same failure mode (delamination) occurred for all the static simulations for the different overlap lengths, which is in accordance with the experimentally obtained results.

Although not following a perfectly linear trend, a constant increase of the failure load with the increase of overlap length was identified, always with delamination in the CFRP adherend (Fig. 15). Such fact was unexpected, as when the strength of the joint is controlled only by failure of the substrate, its failure load should reach a plateau as described by Neto el al. [4]. Instead of the plateau, there is only a slight decrease of the failure load. This can be explained by the fact that as the overlap increases there is less global yielding of the adhesive and local strains increase, leading to early delamination failure of the CFRP substrate [52,53]. Although the failure is mainly by delamination, the adhesive was simultaneously working in the plastic region. To corroborate this assumption, additional data was extracted from the numerical models, with the objective of identifying the existence of adhesive yielding before any delamination. A step immediately before delamination was selected and the AC YIELD parameter (yielding of the material) requested. As shown in Fig. 16, plotting this

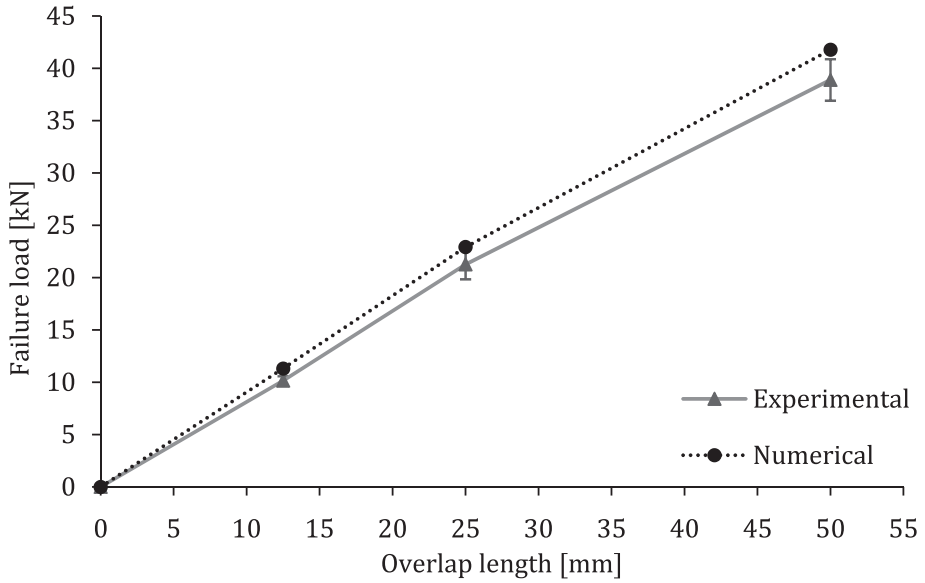

Fig. 15. Experimental vs numerical prediction of the failure load of SLJs tested at quasi-static conditions and for all overlap lengths studied.

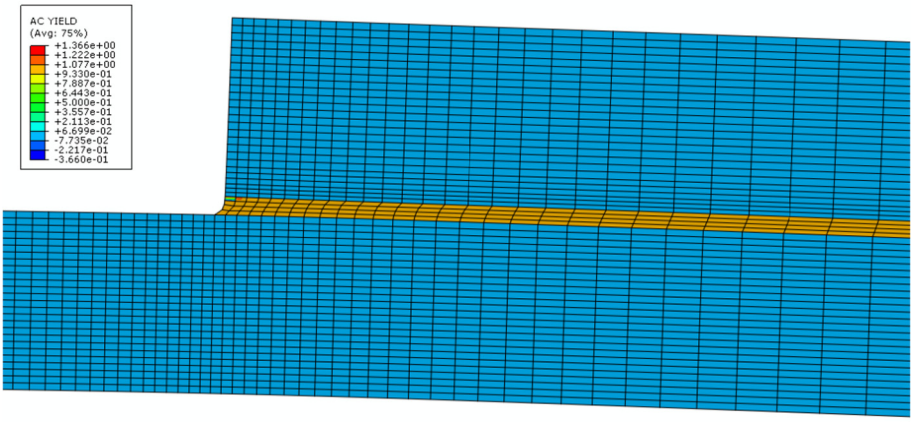

Fig. 16. AC YIELD parameter of a SLJs at quasi-static condition.

parameter reveals that there is already a large amount of plasticization in the adhesive at that point.

It was also possible to obtain the peel stress distribution along the overlap length in the CFRP adherend (Fig. 17). The values were found to be slightly below the interlaminar strength of the CFRP, supporting the idea that there is plastic deformation of the adhesive immediately before the CFRP failure.

4.2.2. Impact models

Regarding the numerical results of the SLJs under impact, representative *P-δ* curves under impact are presented, comparing experimental and numerical results of SLJs with 12.5 mm of overlap length (Fig. 18). The failure load obtained from the numerical simulation is quite close to the experimental failure load.

In Fig. 19 it is possible to observe representative *P-δ* curves comparing experimental and numerical results of SLJs with 25 mm of overlap length under impact.

The failure loads obtained with the FEA are in accordance with the experimentally obtained values. There is however a noticeable difference in the shape of the two curves, as the experimental curve presents a plateau while the numerical drops after reaching the peak load. As described for the quasi-static analysis, this difference can be attributed to the use of a triangular cohesive laws in the model, which is not able to model the plastic plateau. The failure mode in the FEA was delamination in the composite substrates, which also occurred in the experimental results.

4.2.3. Dynamic testing

Using the ABAQUS® software, a complementary FEA analysis of the shape of the two first modes of vibration was performed. A three-dimensional (3D) mesh was constructed with 8 node, linear and reduced integration finite elements. The model was clamped on one end to simulate the test configuration. A frequency analysis calculation step was performed using a Lanczos eigensolver algorithm. The first two modal shapes for specimens with 25 mm of overlap are shown in Figs. 20 and 21.

The influence of the type of substrate on the damping capacity was assessed by taking into account steel and CFRP in the simulations. The dimensions and adhesive properties was considered constant in the simulations using the two different substrates.

According to the numerical data, the higher stiffness of the overlap area leads to limited displacement on the adhesive layer

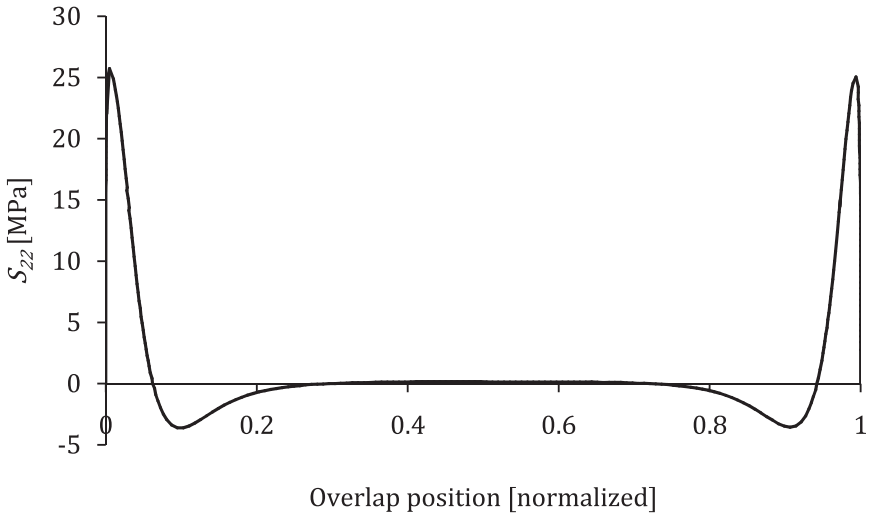

Fig. 17. Numerical peel stress distribution along the overlap length in the CFRP layer.

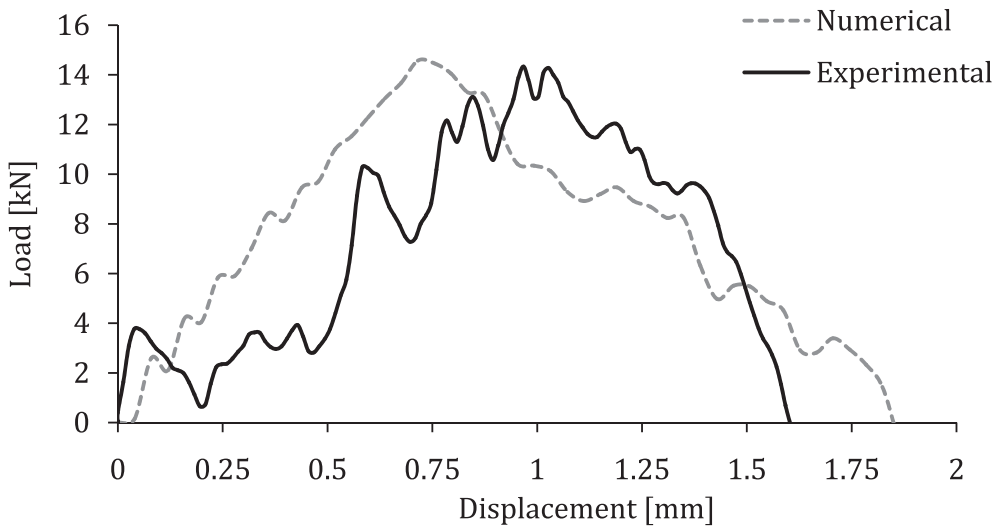

Fig. 18. Experimental and numerical impact results for SLJs with 12.5 mm of overlap.

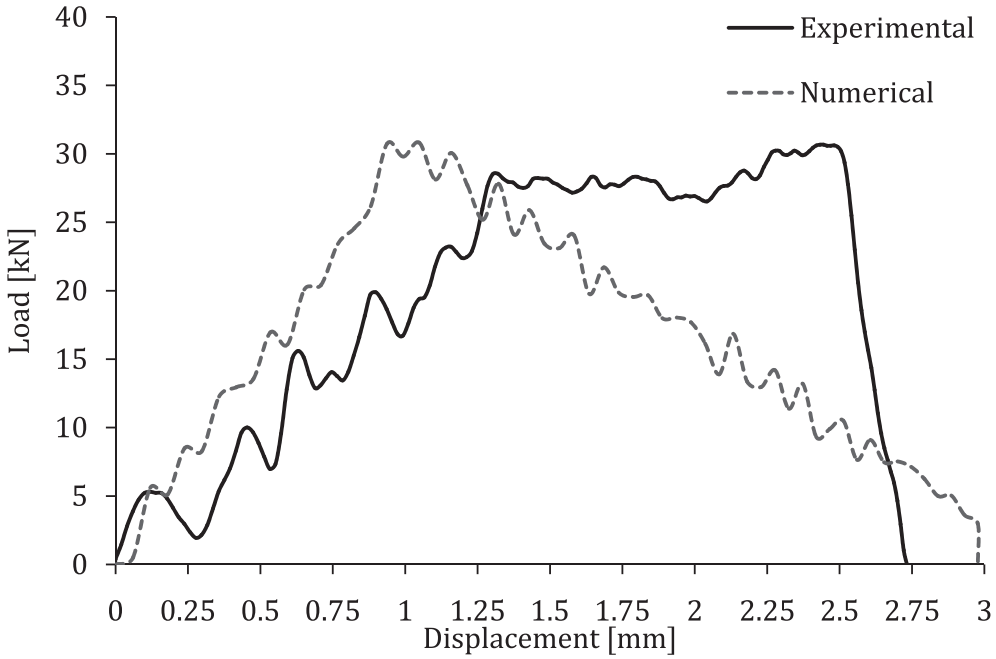

Fig. 19. Experimental and numerical impact results of SLJs with 25 mm overlap length.

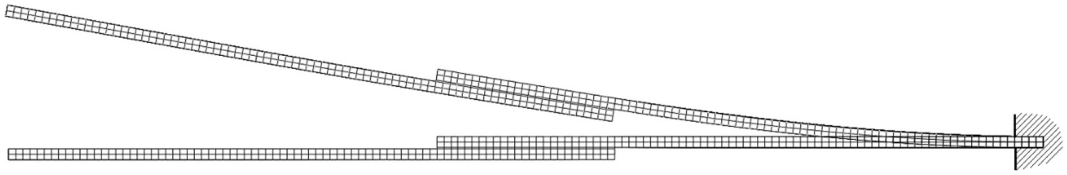

Fig. 20. Finite element representation of the first mode of vibration for SLJ specimens.

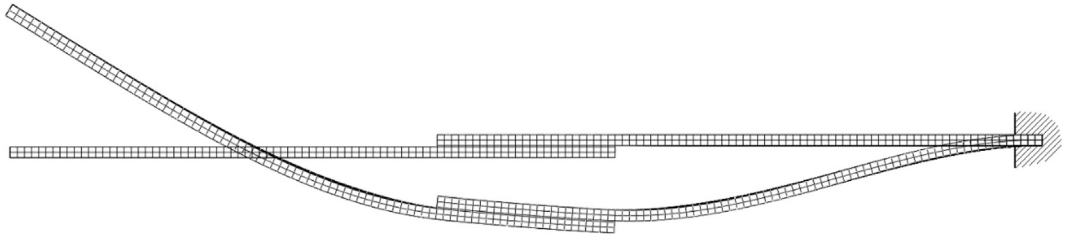

Fig. 21. Finite element representation of the second mode of vibration for SLJ specimens.

for both modes, with most of the movement being transmitted to the free length of the substrates. The maximum deformation of the substrate was found for the second mode of vibration.

5. Conclusions

This work consisted in a complete study of the dynamic behaviour of composite adhesive joints, bonded with a crash resistant adhesive. Impact and vibration tests were performed on composite adhesive joints to determine their strength and damping capabilities. Numerical models were also developed and validated using the experimental data. This research can be used in the design of crashworthy composite structures for the automotive industry. The main conclusions drawn from this work are the following:

- A crash resistant adhesive (Nagase ChemteX® XNR6852E-3) was fully characterized at room temperature and under two strain rates, with the determination of tensile and shear strengths, tensile and shear moduli and mode I and mode II fracture energies. This data was used to extrapolate the mechanical behaviour of the adhesive under impact strain rates;
- During SLJ testing it was found that, for the Nagase ChemteX® XNR6852E-3 adhesive, an increase in the overlap length led to an increase in the failure load, under both testing conditions, quasi-static and impact;
- Independently of the overlap length, the same failure mode (delamination of the CFRP substrates) occurred in the quasi-static tests. On the other hand, under impact conditions, and for the overlap length of 12.5 mm, both failure modes occurred: cohesive in the adhesive and delamination of the CFRP;
- The linear increase of the failure load combined with consistent failure by delamination of the static tests was explained by the fact that the adhesive was fully plasticized immediately before failure of the composite. This was demonstrated using numerical models;

- Failure loads under impact are significantly higher for both overlap lengths tested. This is expected and mainly due to the strain rate sensitivity exhibited by adhesive and the resin of the composite;
- Finite element models were used to simulate the static and impact behaviour of the SLJ specimens. The simulations used cohesive zone modelling, with properties derived from the characterization procedures performed during this work. The failure loads predicted by the models were found to be in agreement with the experimental results.
- A dynamic study was performed to assess the damping capabilities of bonded joints with CFRP and steel specimens. When compared with steel substrates, CFRP substrates were found to provide higher damping levels, especially for shorter overlap lengths. The overlap length of 25 mm was found to provide the highest damping values.

Acknowledgments

The authors gratefully acknowledge the funding of Project NORTE-01-0145-FEDER-000022 – SciTech – Science and Technology for Competitive and Sustainable Industries, co-financed by Programa Operacional Regional do Norte (NORTE2020), through Fundo Europeu de Desenvolvimento Regional (FEDER). The authors would also like to thank NAGASE ChemteX® for the financial support. The help provided by Professor José Dias Rodrigues for the damping tests is gratefully acknowledged.

References

[1] Campilho R, de Moura M, Ramantani D, Morais J, Domingues J. Tensile behaviour of three-dimensional carbon-epoxy adhesively bonded single-and double-strap repairs. Int J Adhes Adhes 2009;29(6):678–86.
[2] da Silva LFM, Dillard DA, Blackman B, Adams RD. Testing adhesive joints: best practices. John Wiley & Sons, 2012.
[3] Li J, Yan Y, Zhang T, Liang Z. Experimental study of adhesively bonded CFRP joints subjected to tensile loads. Int J Adhes Adhes 2015;57:95–104.
[4] Neto JABP, Campilho RDSG, da Silva LFM. Parametric study of adhesive joints with composites. Int J Adhes Adhes 2012;37:96–101.
[5] Harding J, Welsh LM. A tensile testing technique for fibre-reinforced composites at impact rates of strain. J Mater Sci 1983;18(6):1810–26.
[6] Taniguchi N, Nishiwaki T, Kawada H. Tensile strength of unidirectional CFRP laminate under high strain rate. Adv Compos Mater 2007;16(2):167–80.
[7] Körber H. Mechanical response of advanced composites under high strain rates. Faculty of Engineering of the University of Porto; 2012.
[8] Hou J, Ruiz C. Measurement of the properties of woven CFRP T300/914 at different strain rates. Compos Sci Technol 2000;60(15):2829–34.
[9] Harris J, Adams R. An assessment of the impact performance of bonded joints for use in high energy absorbing structures. Proc Inst Mech Eng Part C J Mech Eng Sci 1985;199(2):121–31.
[10] Saldanha D, Canto C, da Silva LFM, Carbas R, Chaves F, Nomura K, et al. Mechanical characterization of a high elongation and high toughness epoxy adhesive. Int J Adhes Adhes 2013;47:91–8.
[11] Kadioglu F, Adams RD. Flexible adhesives for automotive application under impact loading. Int J Adhes Adhes 2015;56:73–8.
[12] Needleman A. A continuum model for void nucleation by inclusion debonding. J Appl Mech 1987;54(3):525–31.
[13] Tvergaard V, Hutchinson JW. The relation between crack growth resistance and fracture process parameters in elastic-plastic solids. J Mech Phys Solids 1992;40(6):1377–97.
[14] Camacho GT, Ortiz M. Computational modelling of impact damage in brittle materials. Int J Solids Struct 1996;33(20):2899–938.
[15] da Silva LFM, Campilho RD. Advances in numerical modelling of adhesive joints. Springer; 2012.
[16] Banea MD, da Silva LFM, Campilho R. Effect of temperature on the shear strength of aluminium single lap bonded joints for high temperature applications. J Adhes Sci Technol 2014;28(14–15):1367–81.
[17] Carlberger T, Stigh U. An explicit FE-model of impact fracture in an adhesive joint. Eng Fract Mech 2007;74(14):2247–62.
[18] Haufe A, Pietsch G, Graf T, Feucht M. Modelling of weld and adhesive connections in crashworthiness applications with LS-DYNA. Proceedings of the NAFEMS seminar "simulation of connections and joints in structures" Wiesbaden, Germany; 2010.
[19] May M, Voß H, Hiermaier S. Predictive modeling of damage and failure in adhesively bonded metallic joints using cohesive interface elements. Int J Adhes Adhes 2014;49:7–17.
[20] Clarke M, Broughton JG, Hutchinson AR, Buckley M. An investigation into the use of an embedded process zone model for predicting the structural behaviour of adhesive bonded joints. Int J Vehicle Struct Syst (IJVSS) 2011;3(3).
[21] Avendaño R, Carbas R, Chaves F, Costa M, da Silva LFM, Fernandes A. Impact loading of single lap joints of dissimilar lightweight adherends bonded with a crash-resistant epoxy adhesive. J Eng Mater Technol 2016;138(4):041019.
[22] Neumayer J, Koerber H, Hinterhölzl R. An explicit cohesive element combining cohesive failure of the adhesive and delamination failure in composite bonded joints. Compos Struct 2016;146:75–83.
[23] Morin D, Bourel B, Bennani B, Lauro F, Lesueur D. A new cohesive element for structural bonding modelling under dynamic loading. Int J Impact Eng 2013;53:94–105.
[24] Saito H, Tani H. Vibrations of bonded beams with a single lap adhesive joint. J Sound Vib 1984;92(2):299–309.
[25] Adams RD, Cooper DG, Pearson S. Vibration damping of adhesively bonded joints. In: Oeschner A, da Silva LFM, editors. Handbook of Adhesion Technology. Springer; 2011. p. 765–86.
[26] Campilho RD, De Moura M, Domingues J. Using a cohesive damage model to predict the tensile behaviour of CFRP single-strap repairs. Int J Solids Struct 2008;45(5):1497–512.
[27] Harding J, Welsh L. A tensile testing technique for fibre-reinforced composites at impact rates of strain. J Mater Sci 1983;18(6):1810–26.
[28] Jacob GC, Starbuck JM, Fellers JF, Simunovic S, Boeman RG. The effect of loading rate on the fracture toughness of fiber reinforced polymer composites. J Appl Polym Sci 2005;96(3):899–904.
[29] Daniel I, Werner B, Fenner J. Strain-rate-dependent failure criteria for composites. Compos Sci Technol 2011;71(3):357–64.
[30] ISO, BSEN 15024: 2001 Fibre-reinforced plastic composites. Determination of mode I interlaminar fracture toughness, GIC, for unidirectional reinforced materials. BSI. ISO, BSEN, 2002.
[31] da Silva LFM, Öchsner A, Adams RD. Handbook of adhesion technology. Heidelberg: Springer-Verlag; 2011.
[32] Chaves FJ, da Silva LFM, De Moura M, Dillard D, Esteves V. Fracture mechanics tests in adhesively bonded joints: a literature review. J Adhes 2014;90(12):955–92.
[33] de Moura M, Campilho R, Gonçalves J. Pure mode II fracture characterization of composite bonded joints. Int J Solids Struct 2009;46(6):1589–95.
[34] Zgoul M, Crocombe A. Numerical modelling of lap joints bonded with a rate-dependent adhesive. Int J Adhes Adhes 2004;24(4):355–66.
[35] Avendaño R, Carbas R, Marques E, da Silva LFM, Fernandes A. Effect of temperature and strain rate on single lap joints with dissimilar lightweight adherends bonded with an acrylic adhesive. Compos Struct 2016;152:34–44.
[36] Loureiro A, da Silva LFM, Sato C, Figueiredo M. Comparison of the mechanical behaviour between stiff and flexible adhesive joints for the automotive industry. J Adhes 2010;86(7):765–87.
[37] Amijima S, Fujii T. The effect of strain rate on mechanical properties of adhesives and adhesive bonded joints. International Conference on Fracture Mechanics and Technology, Hong Kong; 1977. p. 363–72.
[38] Bodnar M, Wegman R. Tensile and impact strengths of ten commercial epoxy adhesive formulations. Mater Des Eng 1960;51:136–8.
[39] ISO, EN 527-2 Plastics–Determination of tensile properties. ISO, EN 1996.
[40] Banea M, da Silva LFM, Campilho R. High temperature adhesives for aerospace applications. Annals of "Dunarea de Jos" University of Galati Fascicle XII: Welding Equipment and Technology, vol. 23, 2012. p. 16–20.
[41] Banea MD, da Silva LFM. Mechanical characterization of flexible adhesives. J Adhes 2009;85(4–5):261–85.
[42] Gilat A, Goldberg RK, Roberts GD. Strain rate sensitivity of epoxy resin in tensile and shear loading. J Aerospace Eng 2007.
[43] Takiguchi M, Izumi S, Yoshida F. Rate-dependent shear deformation of ductile acrylic adhesive and its constitutive modelling. Proc Inst Mech Eng Part C J Mech Eng Sci 2004;218(6):623–9.
[44] ISO 11003-2 Determination of shear behaviour of structural adhesives – Part 2: Tensile test method using thick adherends. First issue 2001, last review 2012.
[45] Lopes RM. Comparação dos ensaios DCB e TDCB para determinação da tenacidade em tração de adesivos estruturais. 2014.
[46] ASTM D3433-99. Standard Test Method for Fracture Strength in Cleavage of Adhesives in Bonded Metal Joints. 2012.
[47] Azevedo J, Campilho R, da Silva F, Faneco T, Lopes R. Cohesive law estimation of adhesive joints in mode II condition. Theor Appl Fract Mech 2015;80:143–54.
[48] Wang I. An analysis of higher order effects in the half power method for calculating damping. J Appl Mech 2011;78(1):014501.
[49] Park H, Kim H. Damage resistance of single lap adhesive composite joints by transverse ice impact. Int J Impact Eng 2010;37(2):177–84.
[50] Waimer M, Siemann M, Feser T. Simulation of CFRP components subjected to dynamic crash loads. Int J Impact Eng 2016.
[51] Davies G, Zhang X. Impact damage prediction in carbon composite structures. Int J Impact Eng 1995;16(1):149–70.
[52] Fernandes TA, Campilho RD, Banea MD, da Silva LFM. Adhesive selection for single lap bonded joints: Experimentation and advanced techniques for strength prediction. J Adhes 2015;91(10–11):841–62.
[53] Banea MD, da Silva LFM, Carbas R, Campilho RD. Effect of material on the mechanical behaviour of adhesive joints for the automotive industry. J Adhes Sci Technol 2016:1–14.

Paper 7

Content of Paper 7

Abstract

1. Introduction

2. Experimental details

2.1. Mechanical properties of CFRP substrates and epoxy adhesive

2.1.1. CFRP substrates

2.1.2. Adhesive

2.2. Specimens manufacturing

2.3. Specimens configurations

2.4. Testing procedure

2.4.1. Quasi-static conditions

2.4.2. Impact conditions

3. Experimental results

3.1. Quasi-static tests

3.1.1. Fracture surface of quasi-static tests

3.1.2. Failure load

3.1.3. Energy absorbed

3.2. Impact tests

3.2.1. Fracture surface of impact tests

3.2.2. Failure load

3.2.3. Energy absorbed

4. Comparison between quasi-static and impact results

4.1. Comparison of failure load between quasi-static and impact results

4.2. Comparison of energy absorbed between quasi-static and impact results

5. Conclusions

References

Check for updates

Article

JOURNAL OF COMPOSITE MATERIALS

Journal of Composite Materials
2018, Vol. 52(26) 3621–3635
© The Author(s) 2018
Article reuse guidelines:
sagepub.com/journals-permissions
DOI: 10.1177/0021998318766641
journals.sagepub.com/home/jcm
SAGE

Mechanical behaviour of adhesively bonded composite single lap joints under quasi-static and impact conditions with variation of temperature and overlap

JJM Machado[1], EAS Marques[1] and LFM da Silva[2]

Abstract

The use of adhesively bonded joints in structural components for the automotive industry has significantly increased over the last years, supported by the widespread integration of composite materials. This synergy allows vehicle manufacturers to offer a significant weight reduction of the vehicle allowing for fuel and emissions reduction and, at the same time, providing high mechanical strength. However, to ensure vehicle safety, the crashworthiness of these adhesive joints must be assessed, to evaluate if the structures can sustain large impact loads, transmitting the load and absorbing the energy, without damaging the joint. The novelty of this work is the study of the strain rate dependent behaviour of unidirectional composite adhesive joints bonded with a ductile epoxy crash resistant adhesive, subjected to low and high testing temperatures and using different overlap lengths. It was demonstrated that joints manufactured with this type of adhesive and composite substrates can exhibit excellent quasi-static and impact performance for the full range of temperatures tested. Increasing the overlap length, and independently of the testing temperature, it was observed an increase of energy absorbed for both quasi-static and impact loads, this is of considerable importance for the automotive industry, demonstrating that composite joints exhibit higher performance under impact.

Keywords

Composite material, quasi-static, impact, single lap joints, temperature

Introduction

The introduction of carbon fibre composite materials in the automotive industry has increased over the last decades as a response to strict requirements in terms of fuel efficiency and emissions and demanding safety standards, which require light and strong structures. Consolidated parts as well design freedom, reduction of tolling cost and reduction of materials in addition to manufacturing costs represent other benefits.[1–4] The application of composite materials over more conventional steel and aluminium materials has several advantages such as higher specific strength and stiffness, higher resistance to corrosion and better fatigue properties.[5]

The use of adhesive joints in these structures provides several advantages, as adhesively bonded joints exhibit more uniform stress fields at the bonding region than conventional techniques such as the use of fasteners and rivets. The adhesive layer also prevents corrosion and compensates different thermal expansion of the substrates.[6,7] These advantages conducted to an extensive use of adhesives to join composite materials[8] as they solve the problem of stress concentration induced by the application of bolts[9–11] and lead to an increase of the joint failure load and weight reduction.

The occurrence of an impact load on a composite structure has the potential to seriously compromise its integrity due to the high loads and large incident energy. It is therefore of great importance to gather

[1]Instituto de Ciência e Inovação em Engenharia Mecânica e Engenharia Industrial (INEGI), Portugal
[2]Departamento de Engenharia Mecânica, Faculdade de Engenharia (FEUP), Universidade do Porto, Portugal

Corresponding author:
JJM Machado, Faculty of Engineering of the University of Porto, R. Dr. Roberto Frias s/n, Porto 4200-465, Portugal.
Email: jmachado@inegi.up.pt

data regarding the performance of composites under impact. This type of loading can cause several different types of failure, with the interlaminar fracture being one of the most severe and predominant in composite structures.[12–17] Another important type of failure is delamination,[18] which can be the result of flaws during the manufacturing process or even from the composite structure being subjected to impact load during the service life, which can reduce the overall stiffness.[19] Under impact conditions the process of delamination is complex and composed by multiple translaminar cracking, fibre and matrix failure.[20] The occurrence of delamination on composite structures may not be perceptible on the surface causing unexpected failure due to substantial reduction of stiffness and strength of the material, potentially causing the structure integrity to be compromised. Several authors[21–26] focused on the characterisation of the composite resistance to delamination, as well as on the understanding of the delamination process under impact loads.[27]

Unidirectional composite materials, such as carbon fibre reinforced plastic (CFRP), are not used as structural components due to their anisotropic properties since each laminate undergoes stresses in line and transverse to the fibres. The behaviour of composites is very anisotropic with respect to both stiffness and strength. In the fibre direction, unidirectional composites can be very strong and stiff whereas the transverse and shear properties are significantly inferior. This type of configuration offers higher fracture strength and stiffness along the fibre direction.[28] The matrix of the CFRP, being a polymer, presents a viscoelastic behaviour dependent of the time and temperature conditions, controlling the resistance of the CFRP. The appearance of cracks along the fibres also may occur even before they are broken. For this reason, the assessment of the mechanical properties of unidirectional CFRP with the variation of strain rate and temperature is necessary. An important fact is that CFRP under impact conditions is too brittle meaning that its mechanical properties can be therefore significantly reduced.[29]

Miyano et al.,[30] using unidirectional CFRP specimens, experimentally studied the time and temperature dependence of tensile, compressive and flexural strengths considering the longitudinal and transverse directions, concluding that these properties behaved as the matrix epoxy resin. Another conclusion was that the longitudinal compressive and flexural fracture strengths were dominated by the deformation properties of the matrix, therefore, the transverse tensile, compressive and flexural fracture strength were greatly affected by the fracture strength of the matrix.

Hsiao and Daniel,[31] using a drop weight machine, assessed how compressive and shear behaviour of unidirectional of a carbon/epoxy composite material was affected with the increase of strain rate. The authors observed a higher strength and strain values with the increase of strain rate, although the modulus increase was only slightly higher than the quasi-static value. The increase in strength and ultimate strain observed may be related to the shear behaviour of the composite and the change in failure modes. The stiffening was found to be lower in the longitudinal case and higher in the transverse and shear cases. Gilat et al.[32] using a split Hopkinson pressure bar (SHPB) apparatus experimentally studied the strain rate dependency of a carbon/epoxy composite material using different layups and concluded that for all the different combinations with the increase of strain rate the stiffness of the material also increased. Following the same experimental methodology, Daniel et al.[33] found a constant ratio of transverse to in-plane shear modulus, independent of the strain rate. The transverse tensile and compressive strength and the in-plane shear strength were found to vary linearly with the logarithm of strain rate, maintaining proportionality throughout the entire strain rate range under study. More recently, Al-Zubaidy et al.[34] performed tests at medium strain rates using CFRP and carbon/epoxy composite materials (two distinct adhesives). In the case of CFRP, the increase of strain rate conducted to an increase of tensile strength, tensile stiffness, strain to failure and energy absorption. For the cases of carbon/epoxy composites the same behaviour was observed.

Taniguchi et al.[35] using an SHPB determined the tensile strength of unidirectional CFRP specimens under impact loads, concluding that the tensile modulus and strength in the longitudinal direction are independent of the strain rate, while, in the transverse direction the tensile and shear properties increase with the strain rate. Another conclusion was that the strain rate dependence of the shear strength is significantly higher to the one obtained for the transverse direction.

The viscoelastic properties of CFRP under temperature dependence were studied by Melo and Radford[36] through a dynamic mechanical analysis (DMA) revealing a decrease in the storage moduli and an increase in the damping loss factors with the increase of temperature. The effect of low temperature (LT) and high temperature (HT) on impact damage of CFRP (with different lay-up configurations) was studied by Im et al.[37] demonstrating that delamination areas of impact decreased with at higher temperatures, which indicated that temperature has a great influence in the impact failure of CFRP.

Adhesively bonded composite joints can undergo peel loading, causing the composite to fail in transverse tension prior the failure of the adhesive. In general, failure strength of adhesively bonded joints in metal substrates is proportional to adhesion strength of

adhesive. But it is expected that composite adhesively bonded joints have a different behaviour due to weakness of delamination failure.[39] Separation of the composite substrates can occur locally due to peel stresses, destroying the shear transfer capacity between the inner and outer substrates.[38] It is therefore important to study the failure mode of such joints and try to find reliable ways to predict the strength of joints with composite substrates. Studies on adhesively bonded composite joints have been performed by Budhe et al.[39] with a comprehensive review on the bond strength prediction as well type of failure, and da Silva et al.[40,41] with analytical models of adhesively bonded single lap joints (SLJs). In the work of Soltannia and Taheri[42] and Soltannia et al.,[43] composite SLJs were tested under impact conditions using a modified instrumented pendulum, observing an increase of the overall stiffness and strength while increasing the loading rate.

Neto et al.[44] tested SLJs using unidirectional CFRP substrates and two distinct adhesives (a stiff and a ductile) under quasi-static conditions and different overlap lengths, observing an increase of the failure load for higher overlap lengths when using the ductile adhesive (obtaining cohesive failure in the adhesive). However, for the case of the brittle adhesive, increasing the overlap length led to a plateau in the failure load, as the failure transitioned from cohesive in the adhesive to interlaminar failure of the composite. Li et al.[45] experimentally tested SLJs made of CFRP using an epoxy adhesive and varying the substrate thickness, the results revealed that the ultimate failure load and lap shear strength are not dependent of the thickness of the CFRP substrate.

The knowledge of the capability of a composite structure to absorb energy through-controlled failure mechanisms (crashworthiness) is critical to improve safety of a vehicle under impact conditions. The energy absorption depends on parameters such as: type of fibre and matrix, fibre architecture, specimen geometry, fibre volume and processing conditions and testing speed. The rate at which the structure is loaded has an important effect on both the material's behaviour and the structure response of the target.[46] The energy absorbed response of composite materials has been assessed by several authors with distinct outcomes. While some authors[47–51] have found a decrease of the energy absorption of composite structures with the increase of strain rate; other authors such as Thornton[52] and Farley[53] found a significant increase of the energy absorption of composites with the increase of strain rate. These works suggest that that the configuration and the materials comprising the composite have significant influence on the energy absorption process.

Given the complexity of designing adhesively bonded composite joints for impact loads, this work aims generate experimental data able to shed light on the factors affecting the mechanical behaviour of these joints, considering materials, temperatures and strain rates typical for the automotive industry. For this purpose, composite single lap joints bonded with a ductile epoxy crash resistant adhesive were subjected to quasi-static and impact loads. The experimental results are shown for LT (−30°C), room temperature (RT) (24°C) and HT (80°C), which are the temperatures typically required to validate structures used in the automotive industry; as well as for different overlap lengths (12.5 and 25 mm, also representative of the geometries used in the automotive industry). It was demonstrated that joints manufactured with this type of adhesives and substrates can exhibit excellent impact strength capabilities within the range of temperatures tested.

Experimental details

This section presents the mechanical properties of an epoxy crash resistant adhesive and CFRP substrates used in SLJs experimentally tested under different temperatures, namely, LT (−30°C), RT (24°C) and HT (80°C). The detailed manufacturing process and joint configuration is also described.

Mechanical properties of CFRP substrate and epoxy adhesive

CFRP substrates. CFRP was selected as substrate for the SLJs tested in this work. The CFRP substrates were comprised of stacked plies of a carbon/epoxy pre-preg (SEAL® Texipreg HS 160 RM). A unidirectional configuration of 0° was used, to ensure maximum strength in the loading direction of SLJs.

Table 1 presents the elastic orthotropic mechanical properties of this material at RT and quasi-static conditions, which were previously determined by Campilho et al.[54]

Low and high testing temperatures were used in this study, which necessitates knowledge of the glass transition temperature, T_g, of the composite resin as its value can greatly influence the mechanical behaviour

Table 1. Elastic orthotropic properties of carbon fibre reinforced plastic.[54]

Elastic modulus (MPa)	Poisson's ratios	Shear modulus (MPa)
$E_1 = 1.09E5$	$\nu_{12} = 0.342$	$G_{12} = 4315$
$E_2 = 8819$	$\nu_{13} = 0.342$	$G_{13} = 4315$
$E_3 = 8819$	$\nu_{23} = 0.380$	$G_{23} = 3200$

1: fibres direction; 2: transverse direction; 3: out of plane direction.

Table 2. Mechanical properties of CFRP under quasi-static and impact conditions.

	1 mm/min			Impact[a]		
Properties	−30°C	24°C	80°C	−30°C	24°C	80°C
Young's modulus, E (MPa)	108,000	108,000	108,000	108,000	108,000	108,000
Shear modulus, G (MPa)	4315	4315	4315	4315	4315	4315
Tensile strength, σ_n (MPa)	40	40	40	40	40	40
Shear strength, t_s (MPa)	35	35	35	35	35	35
Fracture energy (mode I), G_{IC} (N/mm)	0.52	0.59	0.98	0.11	0.39	0.86
Fracture energy (mode II), G_{IIC} (N/mm)	1.10	1.17	1.37	0.71	0.82	0.80

[a]Values extrapolated for an impact velocity of 3 m/s.

of the joint.[55,56] T_g has a considerable influence on the strength of a polymer at a given temperature, namely, below T_g the composite resin presents a stiff characteristic while above behaves in a flexible manner.[15,57,58] The determination of T_g was performed in previous works developed by the authors[57] and the composite resin presented a value of 105 ± 2°C, above the higher testing temperature.

As mentioned in the introduction, the tensile properties of the unidirectional CFRP were determined not to vary significantly with the strain rate along the fibre direction.[35,59,60] For that reason, the strain rate dependent characterisation of the Young's modulus and the tensile strength was not performed with the variation of strain rate and temperature. However, there is limited information regarding strain rate dependence of the fracture energy, which prompted the use of fracture toughness testing to obtain this data.

Table 2 lists the mechanical properties, from quasi-static (1 mm/min) to impact (considering an impact velocity of 3 m/s) conditions for the same testing temperatures. The CFRP properties at RT were determined in previous works performed by the authors.[15,57]

Adhesive. The adhesive used in this work is a crash resistant epoxy based adhesive that combines the toughness of a polyurethane with the high strength of an epoxy.[61] The adhesive is designated XNR6852 E-3 manufactured by Nagase ChemteX®. This type of adhesive is particularly relevant for the automotive industry due to the combination of its high strength, ductility and resistance to impact. This material can deform significantly without breaking, allowing the bonded structure to deform plastically and absorb the impact energy. This epoxy adhesive was experimentally characterised under quasi-static load (1 mm/min) for different temperatures (−30, 24 and 80°C).

Table 3. Mechanical properties of Nagase ChemteX® XNR6852E-3 epoxy adhesive under quasi-static conditions (average values).

	1 mm/min		
Properties	−30°C	24°C	80°C
Young's modulus, E (MPa)	2460	1874	1026
Tensile strength, σ_n (MPa)	6.95	48.44	24.43
Fracture energy (mode I), G_{IC} (N/mm)	9.18	8.84	12.78

Table 3 lists the experimentally measured mechanical properties (average values) for the adhesive under quasi-static conditions and at three temperatures.

Saldanha et al.[62] and Avendaño et al.[63] have studied previous versions of adhesive XNR6852 E-3 and in their works the G_{IIC} determined experimentally was 6–10 times higher than G_{IC}. Considering this previous data, and due to the high ductility of the adhesive, the value for G_{IIC} was therefore assumed to be 8 times higher than the fracture toughness in mode I.

The determination of T_g was performed and the measured value was of 132 ± 4°C, which is higher than the applied testing HT and therefore not representing a problem for the tests.

Specimens manufacturing

The manufacturing process of the SLJs can be divided in two distinct steps, the first being the manufacture of the CFRP substrates and the second the adhesive joint itself.

The CFRP substrates used in the SLJs consisted on unidirectional (with 0° plies orientation) laminates obtained from laminates bulk plate, which were produced by hand lay-up and cured in a hot plate press. The laminate bulk plates with dimensions of 300 by

300 mm were manufactured by stacking the unidirectional 0° plies. To obtain a final thickness of 2.1 mm, a total of fourteen plies of carbon/epoxy pre-preg (SEAL® Texipreg HS 160 RM) were stacked, each 0.15 mm thick. The stacked lay-up was cured in a hot plate press subjected a curing cycle of 130°C for 1 h under a pressure of 400 bar. After the curing cycle was completed, the laminate bulk plates were cut into smaller specimens using a diamond disc cutting machine. The final step was to use a 120-grit sandpaper to achieve edge finishing and to remove the loose fibres allowing to smoothen the sharp edges.

To assemble the SLJs, a steel mould was used to ensure both the correct alignment of the joint and the intended overlap length (12.5 mm or 25 mm). To complete the joint manufacture process, the mould was placed under pressure and temperature in a hot plate press and subjected to a curing cycle of 150°C for 3 h.

Specimen configurations

The geometry used in both quasi-static and impact tests was chosen as its configuration is representative of the joints used in an automotive structure, with the thickness, overlap length of substrates and adhesive layer thickness being defined to be as close as possible to those used in the final application.

The CFRP substrates of the SLJs used have a thickness of 2.1 mm. The different overlap lengths used were 12.5 and 25 mm for all ranges of temperature tested. The free length of each SLJ was kept constant (at 65 mm), to allow a direct comparison between the results of the two overlap lengths. The main goal was to assess the influence of overlap length on the joint behaviour, being aware that the bending moments are different. Using the two different overlaps allows to better understand the trade-off between additional bonding area and the increase in peel stress. The bending rotation factor is not changed once in a real application it cannot be controlled. The thickness of the adhesive layer used was 0.2 mm. A total of six specimens were tested for each quasi-static and impact testing condition and different testing temperature. The dimensions of the SLJ specimens used are shown in Figure 1. The specimens were manufactured with two different overlap lengths (12.5 and 25 mm), and are based on the ASTM D1002-99[64] and ISO 4587:1995[65] standards.

Testing procedure

Quasi-static conditions. The quasi-static tests of SLJs were performed in a universal testing machine, of the type INSTRON® 3367 (Norwood, Massachusetts, USA) with a load cell capacity of 30 kN. All tests were performed at a constant cross-head rate of 1 mm/min, which corresponds to an average strain rate of 0.08 s^{-1} in the adhesive layer.

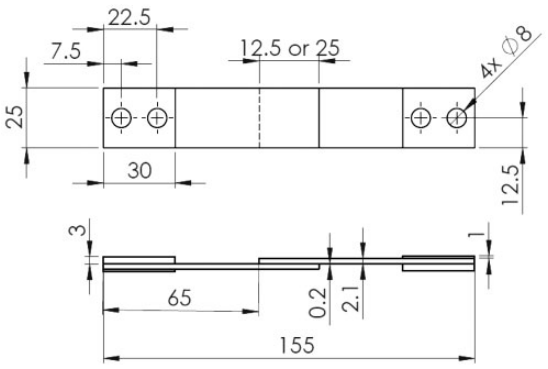

Figure 1. Dimensions in mm of the CFRP SLJs used for quasi-static and impact tests (adapted from literature[64,65]).
CFRP: carbon fibre reinforced plastic; SLJs: single lap joints.

For both overlap lengths, in tests performed under LT and HT, a heated climatic chamber was integrated in the testing machine. In the case of LT, the same chamber was used, with pressurised liquid nitrogen being injected in a controlled manner to achieve the LT. With the use of a thermocouple positioned in contact with each SLJ the temperature was measured, to ensure a homogeneous temperature distribution. Each test was only performed after a period of 10 min at the intended temperature. While the tests were being performed the SLJs remained enclosed in the chamber under a constant temperature.

A total of six specimens were tested for each overlap and temperature condition, and force–displacement (P–δ) curves were obtained for all SLJs tested.

Impact conditions. The impact tests were performed in a Rosand® Instrumented Falling weight impact tester, type 5 H.V. (Stourbridge, West Midlands, U.K.) coupled with a load cell of 60 kN. This equipment consists of a mass being dropped from a certain height, until it impacts the specimen. The specimen is mounted and kept vertically with the use of a specially designed grip (Figure 2). The impactor strikes the lower section of the grip, accelerating the test assembly such that the specimen is loaded in tension-shear. A total impactor weight of 26 kg was used in the setup of the testing machine. The test speed was of 3 m/s, which provides a total impact energy of 117 J using the maximum mass capacity of the drop weight machine (limited to 26 kg). Considering the load rate and the adhesive layer geometry, the average strain rate in the adhesive layer was calculated to be 15,000 s^{-1}. It is important to refer that for this calculation only the deformation of adhesive was considered.

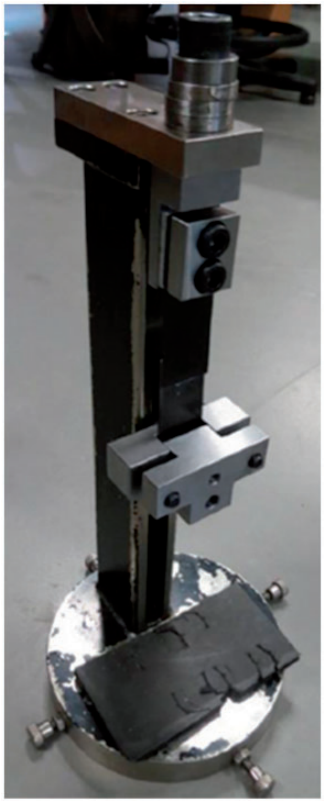

Figure 2. Setup used to hold the specimen in position for the impact test.

For tests performed at LT, gaseous nitrogen was applied to cool the SLJs. In the case of HT, an induction coil to heat-up the SLJs was used. In both stages of temperature, a thermocouple was attached in the beginning of the area of overlap length to measure and control the temperature of the specimen. Each test occurred when the adhesive layer temperature was found to be stabilised at the desired value (controlled using type K-thermocouples).

A total of six specimens were tested for each overlap and temperature condition, and a P–δ curve was obtained for each SLJ tested.

Experimental results

In this section, the experimental results of all SLJs tested are presented and analysed in terms of fracture surface, failure load and energy absorbed (which is the fraction of the incident energy that was dissipated by the failure process of the SLJs) during the quasi-static and impact conditions. Three distinct testing temperatures were used, namely, −30°C (LT), 24°C (RT) and 80°C (HT).

Quasi-static tests

Tests at quasi-static conditions were performed at a cross-head displacement of 1 mm/min. The different overlap lengths of the CFRP SLJs tested were of 12.5 and 25 mm.

Fracture surface of quasi-static tests. For all the specimens tested under quasi-static conditions, the type of failure was delamination in all CFRP substrates, independently of the overlap length and testing temperature, even though the severity of delamination presented some changes regarding the testing conditions. Representative images of the fracture surface regarding each overlap length and testing temperature are presented in Table 4.

In tests at quasi-static conditions, for an overlap length of 12.5 mm and at RT and HT, the failure surface includes both delamination of CFRP and cohesive failure in the adhesive. The same type of failure was observed at impact conditions for an overlap of 25 mm at HT. The less severe delamination at impact for the 12.5 mm overlap can, in part be attributed to the less severe peel stresses that occur for this shorter overlap length. For both cases, it was possible to conclude that under those testing conditions the strength of the adhesive was lower, and therefore causing the adhesive to fail simultaneously with the CFRP. Such differences in the failure mode are due to the viscoelastic and viscoplastic behaviour of the brittle CFRP resin and the epoxy crash-resistant adhesive under the different testing temperatures. As the testing temperature approaches T_g, the adhesive and substrate mechanical properties vary significantly.

Failure load. Figure 3 shows the average values and standard deviation of failure load of the CFRP SLJs tested at quasi-static conditions, varying the testing temperature and for two overlap lengths (12.5 and 25 mm).

In tests performed at LT, the failure load was similar for both overlap lengths (both results fall within standard deviation) which, when associated with the severe delamination as failure mode, is an indicator of the higher strength of the adhesive over the more brittle resin of the CFRP substrate. The LT causes the resin of the CFRP substrate to become more brittle and more prone to delamination while the adhesive is significantly tougher. For specimens with 25 mm overlap length at LT, no improvement in joint strength was found. This is due to the high level of peel stresses present which induce CFRP delamination. The resin of the CFRP substrate is again limiting the SLJs failure load and causes the joint strength to perform similarly despite the overlap length.

Considering RT, the failure load was higher for SLJs with overlap length of 25 mm. At this testing temperature, delamination of CFRP substrates was observed, with cohesive failure in the adhesive for SLJs with

Table 4. Representative failure surfaces of CFRP SLJs specimens tested under quasi-static conditions (1 mm/min), at different testing temperatures (LT, RT and HT), and for different overlap lengths: (a) 12.5 mm and (b) 25 mm.

Testing temperature	Overlap of 12.5 mm	Overlap of 25 mm
−30 °C (LT)		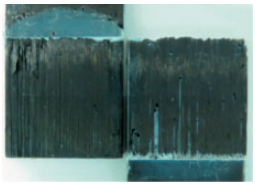
	Delamination of CFRP	Delamination of CFRP
24 °C (RT)	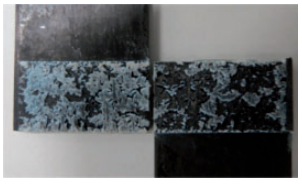	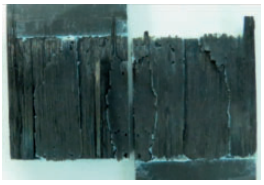
	Delamination of CFRP[a]	Delamination of CFRP
80 °C (HT)	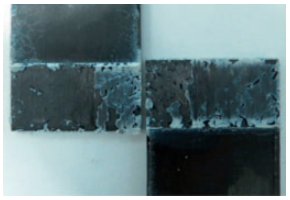	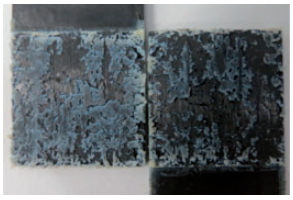
	Delamination of CFRP[a]	Delamination of CFRP[a]

CFRP: carbon fibre reinforced plastic; SLJs: single lap joints; LT: low temperature; RT: room temperature; HT: high temperature.
[a]Partially cohesive in the adhesive.

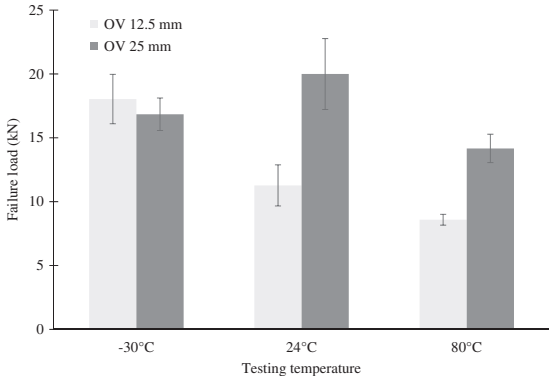

Figure 3. Average values and standard deviation of failure load of SLJs tested at quasi-static conditions (1 mm/min) with the variation of overlap length (12.5 and 25 mm) and testing temperature.
SLJs: single lap joints.

overlap length of 12.5 mm, and severe delamination of CFRP substrate for SLJs with the overlap length of 25 mm. For SLJs with the larger the overlap length, the failure load was found to increase slightly over the values reached at LT, probably induced by the improved toughness of the resin at RT. In the case of SLJs with the lower overlap length, the mixed failure mechanism has led to a slightly lower joint strength.

The lowest values of failure mode were obtained for tests at HT when analysing both overlap lengths, with the highest value being obtained for SLJs with 25 mm of overlap length. At this temperature, the mechanical properties of the brittle resin of the CFRP substrate and adhesive are weakened, due its viscoelastic and viscoplastic behaviour. The specimens with 25 mm of overlap length, due to higher peel loads generated fail only by delamination, which occurs at lower loads than those encountered at LT and RT as the resin matrix is closer to its T_g. In the case of SLJs with overlap length of 12.5 mm the delamination process was less severe, and the combination of delamination with cohesive failure in the adhesive suggests that the adhesive has become weakened at HT and is causing the joint to fail at relatively low loads.

Energy absorbed. The average and standard deviation values of energy absorbed by the SLJs tested at quasi-

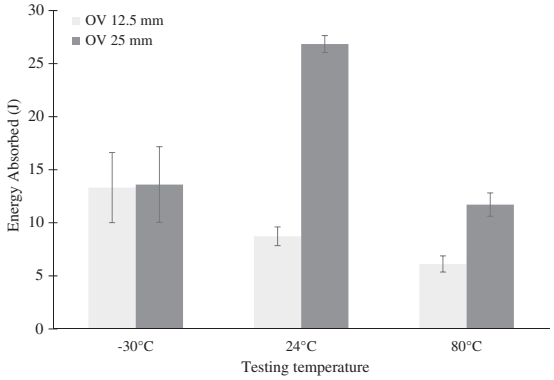

Figure 4. Average values and standard deviation of energy absorbed of SLJs tested at quasi-static conditions (1 mm/min) with the variation of overlap length (12.5 and 25 mm) and testing temperature.
SLJs: single lap joints.

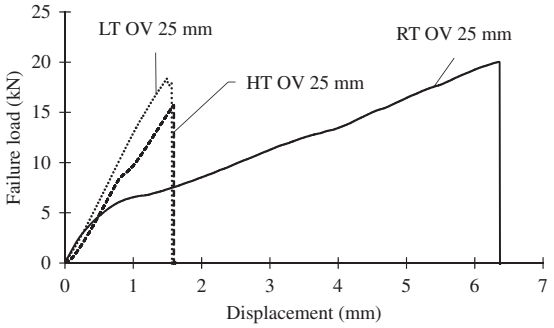

Figure 5. Examples of P–δ curves of SLJs tested at quasi-static conditions with overlap length of 25 mm and for the various testing temperatures.
SLJs: single lap joints.

static conditions are presented in Figure 4, with the variation of overlap length and testing temperature.

As mentioned previously, regarding failure load at LT, the energy absorbed by the SLJs was independent of the overlap length. The fracture surface indicated severe delamination for both overlap lengths, which indicates that the failure of the SLJs was determined and limited by the stiff resin of the CFRP substrate.

The results for tests performed at RT revealed higher energy absorbed by the SLJs for the cases of 25 mm overlap length. This is in accordance with the value of failure load obtained, which also increases significantly when using higher overlap length. The failure surface revealed severe delamination in the case of SLJs with overlap length of 25 mm, and delamination with cohesive failure in the adhesive for 12.5 mm overlap, therefore evidencing that for SLJs with overlap 12.5 mm the adhesive is approaching failure earlier in comparison with SLJs with the higher overlap length.

At HT, the same behaviour of the failure load occurred, and the lowest values of energy absorbed by the SLJs was registered for both overlap lengths, though, the highest value of energy absorbed was obtained in the cases of overlap length of 25 mm. For this testing temperature delamination was observed with cohesive failure of the adhesive for SLJs with an overlap length of 25 mm, indicating that the adhesive (due to its viscoelastic and viscoplastic properties) softened fails at lower loads.

The analysis of the load–displacement (P–δ) curves allows to better visualise this type of phenomena. For example, observing Figure 5, it is evident that although the failure loads are not very distinct, the area underneath the curve for the RT test is substantially higher.

Impact tests

Tests at impact conditions were performed at an impact velocity of 3 m/s. The overlap lengths of the CFRP SLJs tested were of 12.5 and 25 mm, and the testing temperatures were of −30°C (LT), 24°C (RT) and 80°C (HT).

Fracture surface of impact tests. The type of failure observed in all the tests performed at impact conditions was delamination in all CFRP substrates, independently of the overlap length and testing temperature, but the severity of delamination presented some changes depending on the testing conditions. Representative images of the fracture surface regarding each overlap length and testing temperature are presented in Table 5.

Although all specimens under study suffered failure by CFRP delamination, some of the fracture surfaces exhibited the presence of cohesive failure in the adhesive. This occurred for the SLJs tested at LT and HT, independently of the overlap length. Such behaviour can be explained due to the viscoelastic and viscoplastic behaviour of the brittle resin of the CFRP substrate, as well the adhesive, which are dependent on both the strain-rate and temperature. The crash-resistant epoxy adhesive becomes stiffer at LT and more flexible at HT. A similar behaviour can be found for the brittle resin of the CFRP substrate. The failure surfaces of SLJs tested at LT and HT, for both 12.5 and 25 mm of overlap length, revealed that besides delamination of the CFRP substrate, there is a presence of adhesive in both substrates, indicating that the adhesive is being loaded to failure, due to a decrease of its mechanical properties with the variation of temperature.

Failure load. The average values and standard deviation of failure load of the CFRP SLJs tested at impact conditions, with the variation of the testing temperature

Table 5. Representative failure surfaces of CFRP SLJs specimens tested under impact conditions (3 m/s), at different testing temperatures (LT, RT and HT) and for different overlap lengths: (a) 12.5 mm and (b) 25 mm.

Testing temperature	Overlap of 12.5 mm	Overlap of 25 mm
−30 °C (LT)	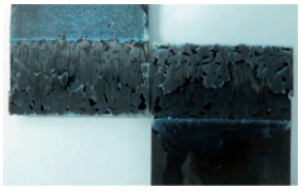	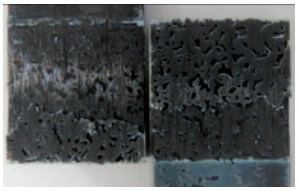
	Delamination of CFRP[a]	Delamination of CFRP[a]
24 °C (RT)	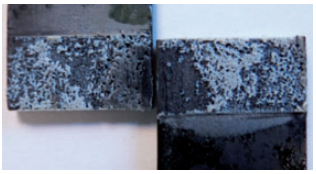	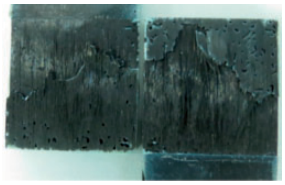
	Delamination of CFRP[a]	Delamination of CFRP
80 °C (HT)	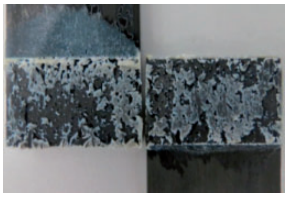	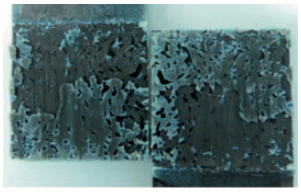
	Delamination of CFRP[a]	Delamination of CFRP[a]

CFRP: carbon fibre reinforced plastic; SLJs: single lap joints; LT: low temperature; RT: room temperature; HT: high temperature.
[a]Partially cohesive in the adhesive.

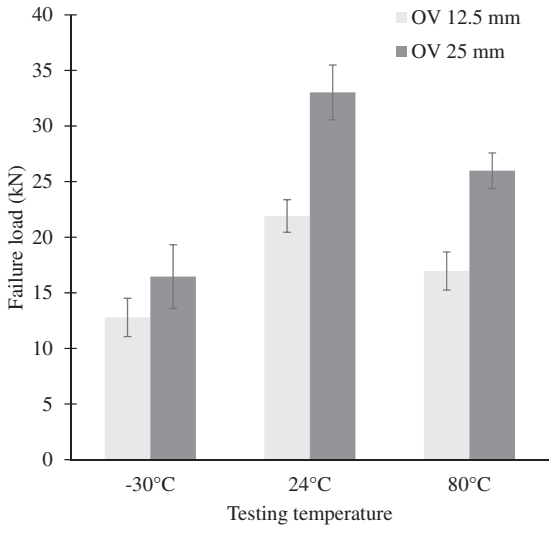

Figure 6. Average values and standard deviation of failure load of SLJs tested at impact (m m/s) with the variation of overlap length (12.5 and 25 mm) and testing temperature.
SLJs: single lap joints.

overlap length (12.5 and 25 mm) is presented in Figure 6.

The lowest values of failure load were obtained for tests performed at LT, and for both SLJs overlap length. From the fracture surfaces, it is possible to observe that at LT, the adhesive becomes very stiff and the SLJs failure occurred by delamination, a process which is controlled by the brittle resin of the CFRP substrates.

At RT, the highest values of failure load were registered (in comparison with the other testing temperatures) for both overlap lengths. The fracture surface was severe delamination for both SLJs overlap length. Between the different SLJs overlap length, the highest value of failure load was registered for the higher overlap length. At this temperature, the adhesive becomes more flexible, and can redistribute the stresses more evenly through the overlap length. This delays the onset of delamination and leads to high failure loads.

At HT, intermediate values of failure load were reached. The fracture surface revealed delamination

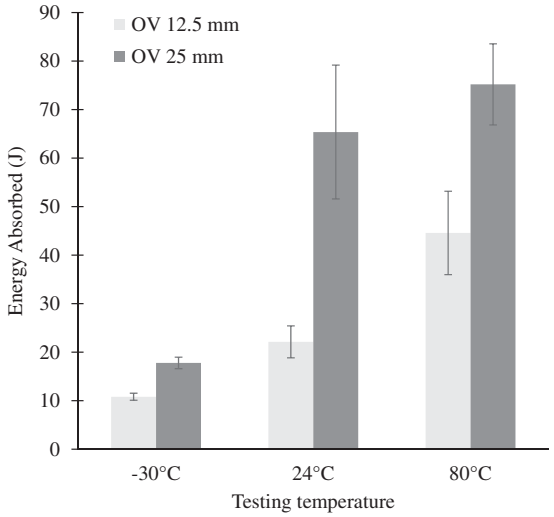

Figure 7. Average values and standard deviation of energy absorbed of SLJs tested at impact conditions (3 m/s) with the variation of overlap length (12.5 and 25 mm) and testing temperature.
SLJs: single lap joints.

with cohesive failure in the adhesive, but less prominently than in the case of LT. Although the adhesive becomes more flexible and reduces the peel loads, the proximity to the T_g also leads to lower tensile and shear strength, even considering strain rate dependency. It is the occurrence of localised cohesive failure that leads to the lower failure loads.

Energy absorbed. Figure 7 shows the average and standard deviation values of energy absorbed by the SLJs tested at impact conditions, with the variation of overlap length and testing temperature.

The energy absorbed by the SLJs at LT, for both overlap lengths, is expressively lower than for other test temperatures. From the fracture surfaces (delamination with cohesive failure in the adhesive), it is possible to conclude that due to the viscoelastic and viscoplastic behaviour of both crash-resistant epoxy adhesive and brittle resin of the CFRP substrates (both become stiffer under LT), both materials become so stiff that the SLJs had lower failure load and therefore absorbed less energy during the impact. The opposite phenomena occurred at HT, where the increased adhesive and substrate flexibility allowed the joint to absorb more energy during impact, delaying the onset of delamination and offering a failure load higher than tests in LT but inferior to tests performed at RT.

At RT, the fracture surfaces revealed severe delamination for SLJs made with both overlap lengths. The values of failure load are in between the ones obtained for tests at LT and HT, once the adhesive strength controls the type of failure.

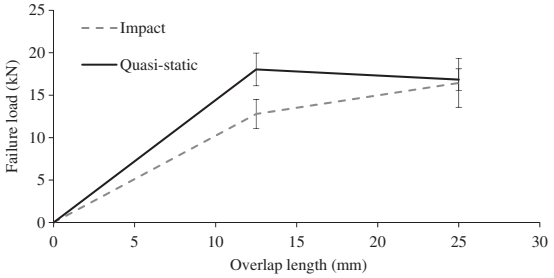

Figure 8. Comparison of the average values and standard deviation of failure load between SLJs tested at quasi-static (1 mm/min) and impact (3 m/s) conditions with the variation of overlap length (12.5 and 25 mm) and testing temperature of −30 °C (LT).
SLJs: single lap joints; LT: low temperature.

In all the tested temperatures, a higher value of energy absorbed by the SLJs made with the higher overlap length (25 mm) was observed, but such difference was more expressive in the case of tests performed at RT. Another conclusion is that for both overlap lengths, the higher the temperature, the higher the capacity of an SLJ to absorb energy during an impact condition.

Comparison between quasi-static and impact results

In this section, a comparison of the results obtained, in terms of failure load and energy absorbed are made between tests performed at quasi-static (1 mm/min) and impact conditions (3 m/s) considering the variation of SLJs overlap length and testing conditions, i.e. −30°C (LT), 24°C (RT) and 80°C (HT).

Comparison of failure load between quasi-static and impact results

The comparison of failure load between quasi-static and impact conditions at LT is shown in Figure 8.

The fracture surface of SLJs tested at LT revealed delamination of CFRP substrate for both overlap lengths. For SLJs with the overlap length of 12.5 mm, the highest value of failure load was measured at quasi-static conditions. Once the adhesive becomes stiffer at LT, it loses capacity to elastically and plastically deform, increasing the peel loads and therefore causing failure by CFRP delamination. Considering SLJs with overlap length of 25 mm, the value of failure load is identical in both quasi-static and impact conditions, once the high stiffness of the adhesive commands the failure mode over the brittle resin of the CFRP substrates. It is possible to conclude that at LT the overlap length has no significant effect in terms of failure load, especially under quasi-static conditions. At this

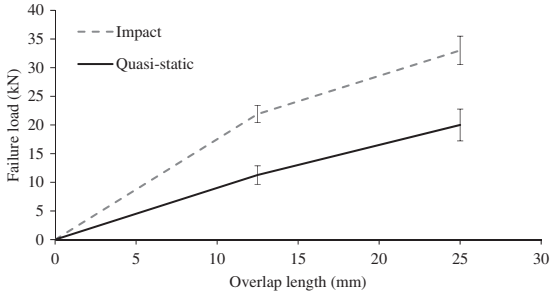

Figure 9. Comparison of the average values and standard deviation of failure load between SLJs tested at quasi-static (1 mm/min) and impact (3 m/s) conditions with the variation of overlap length (12.5 and 25 mm) and testing temperature of 24 °C (RT).
SLJs: single lap joints; RT: room temperature.

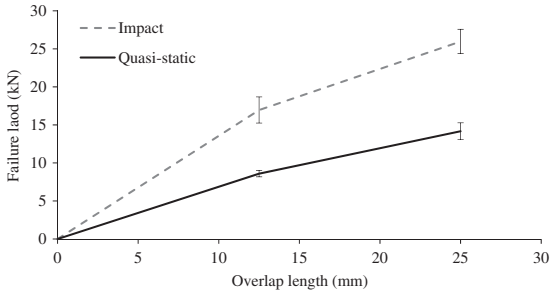

Figure 10. Comparison of the average values and standard deviation of failure load between SLJs tested at quasi-static (1 mm/min) and impact (3 m/s) conditions with the variation of overlap length (12.5 and 25 mm) and testing temperature of 80 °C (HT).
SLJs: single lap joints; HT: high temperature.

temperature, the CFRP resin exhibits a highly brittle behaviour, which increases the susceptibility to delamination failure and leads to the creation of a plateau in the failure loads. This is consistent with the results found by Neto et al.[44] for composite joints bonded with a brittle adhesive being tested at RT.

Under impact, the fracture surfaces demonstrate a combination of delamination and localised cohesive failure of the adhesive. In this case, higher sensitivity to the overlap length is found, due to the more significant contribution of the adhesive on the failure process.

The comparison of failure load between quasi-static and impact conditions at RT and HT is shown in Figures 9 and 10.

It is possible to observe that the trend of the failure load increase at quasi-static and impact conditions, and for both overlap lengths, is the same at RT and HT. For all the cases being analysed, the fracture surface mainly evidenced delamination of the CFRP substrate, with partially cohesive failure in the adhesive identified only for the two following situations: SLJs with overlap length of 12.5 mm at RT, and SLJs with overlap length of 25 mm at HT.

By increasing the SLJs overlap length, an increase of the failure load was found for both testing temperatures and for the quasi-static and impact conditions. The failure loads of the SLJs tested under impact conditions were also found to be higher than the ones measured at quasi-static conditions.

The highest values of failure load at both quasi-static and impact conditions, and for different overlap lengths, were measured for tests at RT. As the epoxy crash-resistant adhesive and brittle resin of the CFRP substrates are viscoelastic and viscoplastic, in the presence of HT, they experience a softening behaviour and their mechanical properties decrease. This viscoelastic softening also explains the improved behaviour at higher strain rates, as the materials will have a rubber like behaviour and exhibit higher failure loads.[66]

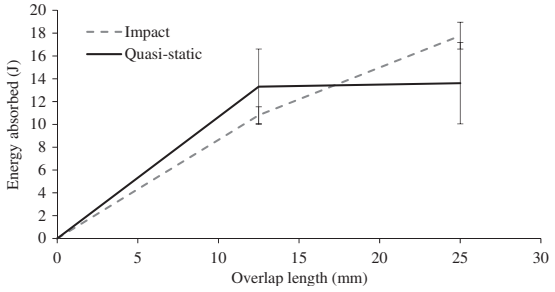

Figure 11. Comparison of the average values and standard deviation of energy absorbed between SLJs tested at quasi-static (1 mm/min) and impact (3 m/s) conditions with the variation of overlap length (12.5 and 25 mm) and testing temperature of −30 °C (LT).
SLJs: single lap joints; LT: low temperature.

Comparison of energy absorbed between quasi-static and impact results

Figure 11 shows the comparison of failure load between quasi-static and impact conditions at LT.

It is possible to observe that for SLJs with an overlap length of 12.5 mm, the value of energy absorbed is slightly superior to the cases of SLJs with the overlap length of 25 mm. The higher peel stresses induced by the higher overlap length cause the resin of the CFRP substrate to fail. At quasi-static conditions, the increase of overlap length did not introduce significant changes in the measured value of energy absorbed, due to the type of failure being controlled by the still brittle resin of the CFRP substrate.

The comparison of energy absorbed between quasi-static and impact conditions at RT and HT is shown in Figures 12 and 13.

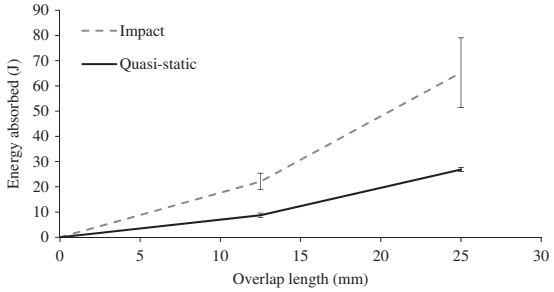

Figure 12. Comparison of the average values and standard deviation of energy absorbed between SLJs tested at quasi-static (1 mm/min) and impact (3 m/s) conditions with the variation of overlap length (12.5 and 25 mm) and testing temperature of 24 °C (RT).
SLJs: single lap joints; RT: room temperature.

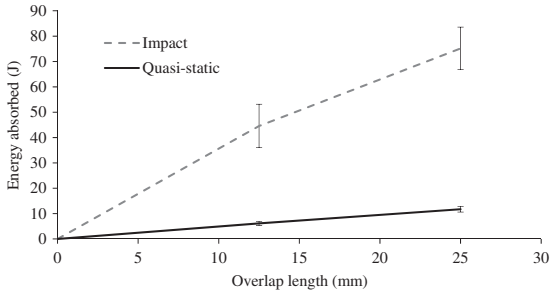

Figure 13. Comparison of the average values and standard deviation of energy absorbed between SLJs tested at quasi-static (1 mm/min) and impact (3 m/s) conditions with the variation of overlap length (12.5 and 25 mm) and testing temperature of 80 °C (HT).
SLJs: single lap joints; HT: high temperature.

As previously stated for the case of HT, it is possible to conclude that the overlap length has an important influence with the increase of temperature, being better under impact than at quasi-static conditions.

The trend in energy absorption at quasi-static and impact conditions, and for both overlap lengths, is the same at RT and HT. With the increase of the overlap length there is a noticeable increase of the energy absorbed in both quasi-static and impact conditions, and for both testing temperatures. The values of energy absorbed at impact conditions are also considerably higher than the values obtained at quasi-static conditions, which follows the results obtained for the failure load. The values of energy absorbed by the SLJs tested at HT are the highest values obtained from the range of tested temperatures.

The increase in energy absorption level under impact conditions can result from a combination of factors. As stated in the introduction, the literature describes cases where composite structures are able to sustain higher loads and absorb more energy under impact.[52,53] Several authors[67,68] have presented works demonstrating that during the failure process of composite materials, the frictional sliding of the fibre within the matrix might be responsible for a large fraction of energy absorption. This type of frictional sliding has been shown to be a complex phenomenon[69] involving both the Van der Walls forces and the mobility of macromolecules at the interface, which results in larger energy absorption for higher impact strain rates.[70]

However, increased energy absorption under impact conditions cannot be solely attributed to the process of delamination and fibre pull-out. The energy absorption and toughness of bulk polymeric materials (which include both the adhesive and the matrix of the composite under study) has been described to increase with the strain rate.[71] Such effect may be due to secondary connections between the polymeric chains, which are affected by both the temperature and the strain rate and result in higher energy absorption.[72] The secondary connections have been previously identified as responsible for a significant level of rate sensitivity of material properties, which occurs close to strain rate and temperature conditions related to the β-transition viscoelastic behaviour.[73]

Overall, the results of this experimental procedure strongly suggest that the impact performance of composite adhesive single lap joints is similar (at LT) or superior (at RT and HT) to that exhibited by the same joint under quasi-static conditions. This indicates that the dimensioning of such joints for the automotive industry can be made considering only the quasi-static properties and tests. The design process can be greatly simplified, as the tools for this type of dimensioning are already well established.

Conclusions

This work consisted in a complete study of the quasi-static and impact behaviour of composite adhesive joints (CFRP substrates), bonded with an epoxy crash-resistant adhesive, varying the testing temperature accordingly to the automotive industry requirements and using two distinct SLJs overlap lengths (12.5 and 25 mm). The main conclusions drawn from this work are the following:

- The use of the epoxy crash-resistant adhesive (Nagase ChemteX® XNR6852 E-3) presented excellent capability to join CFRP substrates under both quasi-static and impact conditions for a range of LT to HT, being therefore suitable for the application in the automotive industry.
- For the range of testing conditions analysed, the type of fracture surface obtained was delamination of CFRP substrates, although for some cases there

was also the presence of partially cohesive failure in the adhesive.

- For both quasi-static and impact conditions, the failure load was found to be highly dependent on temperature. At higher temperatures, the adhesive becomes less stiff and the delamination process is not as severe, with direct influence on the joint performance.
- The highest values of energy absorbed by the CFRP SLJs were measured for SLJs tested for tests at LT (for SLJs overlap length of 12.5 mm) and at LT (for SLJs length of 25 mm) at RT. At impact condition, the highest values of energy absorbed by the SLJs (independently of the overlap length) were obtained at HT. This increase of toughness with the strain rate is determined by several factors such as the effect of strain rate on the secondary transitions of polymeric networks and the frictional energy dissipation caused by fibre-matrix slippage.
- The energy absorption and failure load of adhesively bonded composite single lap joints was found to remain constant (at LT) or improve (at RT and HT) under impact conditions. This indicates that the design process of composite bonded structures for impact energy absorption can be validated under quasi-static loads using simpler and better understood design tools.

Declaration of Conflicting Interests

The author(s) declared no potential conflicts of interest with respect to the research, authorship and/or publication of this article.

Funding

The author(s) disclosed receipt of the following financial support for the research, authorship and/or publication of this article: The authors gratefully acknowledge the funding of Project NORTE-01-0145-FEDER-000022 – SciTech – Science and Technology for Competitive and Sustainable Industries, co-financed by Programa Operacional Regional do Norte (NORTE2020), through Fundo Europeu de Desenvolvimento Regional (FEDER). The authors would also like to thank NAGASE ChemteX® for the financial support.

References

1. Stewart R. Rebounding automotive industry welcome news for FRP. *Reinf Plast* 2011; 55: 38–44.
2. Jacob GC, Starbuck JM, Fellers JF, et al. The effect of loading rate on the fracture toughness of fiber reinforced polymer composites. *J Appl Polym Sci* 2005; 96: 899–904.
3. Mayyas A, Qattawi A, Omar M, et al. Design for sustainability in automotive industry: a comprehensive review. *Renew Sustain Energy Rev* 2012; 16: 1845–1862.
4. Beardmore P and Johnson C. The potential for composites in structural automotive applications. *Compos Sci Technol* 1986; 26: 251–281.
5. Cantwell W and Morton J. The impact resistance of composite materials – a review. *Composites* 1991; 22: 347–362.
6. da Silva LFM. *Handbook of adhesion technology*. Berlin, Germany: Springer Science & Business Media, 2011.
7. da Silva LFM, Pirondi A and Öchsner A. *Hybrid adhesive joints*. Berlin, Germany: Springer Science & Business Media, 2011.
8. Adams RD, Comyn J and Wake WC. *Structural adhesive joints in engineering*. Berlin, Germany: Springer Science & Business Media, 1997.
9. Collings T. The strength of bolted joints in multi-directional CFRP laminates. *Composites* 1977; 8: 43–55.
10. Kolesnikov B, Herbeck L and Fink A. CFRP/titanium hybrid material for improving composite bolted joints. *Compos Struct* 2008; 83: 368–380.
11. Smith P, Pascoe K, Polak C, et al. The behaviour of single-lap bolted joints in CFRP laminates. *Compos Struct* 1986; 6: 41–55.
12. Machado J, Marques E, Campilho R, et al. Mode II fracture toughness of CFRP as a function of temperature and strain rate. *Compos Part B Eng* 2017; 114: 311–318.
13. Chou I, Inutake T and Namba K. Correlation of damage resistance under low velocity impact and mode II delamination resistance in CFRP laminates. *Adv Compos Mater* 1999; 8: 167–176.
14. Iwamoto M, Ni Q, Fujiwara T, et al. Intralaminar fracture mechanism in unidirectional CFRP composites: part I: intralaminar toughness and AE characteristics. *Eng Fract Mech* 1999; 64: 721–745.
15. Machado J, Marques E, Campilho R, et al. Mode I fracture toughness of CFRP as a function of temperature and strain rate. *J Compos Mater* 2016; 0021998316682309.
16. Mehrabadi FA and Khoshravan M. Mode III interlaminar fracture and damage characterization in woven fabric-reinforced glass/epoxy composite laminates. *J Compos Mater* 2013; 47: 1583–1592.
17. Szekrényes A. The influence of crack length and delamination width on the mode-III energy release rate of laminated composites. *J Compos Mater* 2011; 45: 279–294.
18. Johnson A and Holzapfel M. Influence of delamination on impact damage in composite structures. *Compos Sci Technol* 2006; 66: 807–815.
19. Benmedakhene S, Kenane M and Benzeggagh M. Initiation and growth of delamination in glass/epoxy composites subjected to static and dynamic loading by acoustic emission monitoring. *Compos Sci Technol* 1999; 59: 201–208.
20. Sohn M and Hu X. Impact and high strain rate delamination characteristics of carbon fibre epoxy composites. *Theor Appl Fract Mech* 1996; 25: 17–29.
21. Welsh L and Harding J. Effect of strain rate on the tensile failure of woven reinforced polyester resin composites. *Le Journal de Physique Colloques* 1985; 46: C5-405-C5–414.
22. Daniel I, Yaniv G and Auser J. Rate effects on delamination fracture toughness of graphite/epoxy composites. *Compos Struct 4* 1987; 258–272.

23. Brunner A, Blackman B and Davies P. A status report on delamination resistance testing of polymer-matrix composites. *Eng Fract Mech* 2008; 75: 2779–2794.
24. Tamuzs V, Tarasovs S and Vilks U. Delamination properties of translaminar-reinforced composites. *Compos Sci Technol* 2003; 63: 1423–1431.
25. Williams JG and Rhodes MD. Effect of resin on impact damage tolerance of graphite/epoxy laminates. In: *Composite materials: testing and design (6th conference)*, West Conshohocken, PA, EUA. ASTM International, 1982.
26. Mines R, Worrall C and Gibson A. The static and impact behaviour of polymer composite sandwich beams. *Composites* 1994; 25: 95–110.
27. Machado J, Marques E and da Silva LFM. Adhesives and adhesive joints under impact loadings: an overview. *J Adhes* 2017; DOI: 10.1080/00218464.2017.1282349).
28. Adachi T, Arai M, Sakabe N, et al. Evaluation of dynamic fracture toughness of unidirectional CFRP laminates. *JSME Int J Ser A Solid Mech Mater Eng* 2000; 43: 179–185.
29. Tanaka K, Kurokawa T, Fujinaga S, et al. Damage and residual bending strength of graphite/epoxy composite laminates subjected to normal impact. *Jpn Soc Aeronaut Space Sci J* 1989; 37: 285–292.
30. Miyano Y, Kanemitsu M, Kunio T, et al. Role of matrix resin on fracture strengths of unidirectional CFRP. *J Compos Mater* 1986; 20: 520–538.
31. Hsiao H and Daniel I. Strain rate behavior of composite materials. *Compos Part B Eng* 1998; 29: 521–533.
32. Gilat A, Goldberg RK and Roberts GD. Experimental study of strain-rate-dependent behavior of carbon/epoxy composite. *Compos Sci Technol* 2002; 62: 1469–1476.
33. Daniel I, Werner B and Fenner J. Strain-rate-dependent failure criteria for composites. *Compos Sci Technol* 2011; 71: 357–364.
34. Al-Zubaidy H, Zhao X-L and Al-Mahaidi R. Mechanical characterisation of the dynamic tensile properties of CFRP sheet and adhesive at medium strain rates. *Compos Struct* 2013; 96: 153–164.
35. Taniguchi N, Nishiwaki T and Kawada H. Tensile strength of unidirectional CFRP laminate under high strain rate. *Adv Compos Mater* 2007; 16: 167–180.
36. Melo JDD and Radford DW. Time and temperature dependence of the viscoelastic properties of CFRP by dynamic mechanical analysis. *Compos Struct* 2005; 70: 240–253.
37. Im K, Cha C, Kim S, et al. Effects of temperature on impact damages in CFRP composite laminates. *Compos Part B Eng* 2001; 32: 669–682.
38. da Silva LFM and Adams R. Techniques to reduce the peel stresses in adhesive joints with composites. *Int J Adhes Adhes* 2007; 27: 227–235.
39. Budhe S, Banea M, de Barros S, et al. An updated review of adhesively bonded joints in composite materials. *Int J Adhes Adhes* 2017; 72: 30–42.
40. da Silva LFM, das Neves PJ, Adams R, et al. Analytical models of adhesively bonded joints – part I: literature survey. *Int J Adhes Adhes* 2009; 29: 319–330.
41. da Silva LFM, das Neves PJ, Adams R, et al. Analytical models of adhesively bonded joints – part II: comparative study. *Int J Adhes Adhes* 2009; 29: 331–341.
42. Soltannia B and Taheri F. Static, quasi-static and high loading rate effects on graphene nano-reinforced adhesively bonded single-lap joints. *J Compos Mater* 2013; 3: 181–190.
43. Soltannia B, Ahmadi-Moghadam B and Taheri F. Influence of tensile impact and strain rate on the response of adhesively bonded single lap joints. In: *ICC19 international conference on composite materials*, 2013.
44. Neto J, Campilho R and da Silva LFM. Parametric study of adhesive joints with composites. *Int J Adhes Adhes* 2012; 37: 96–101.
45. Li J, Yan Y, Zhang T, et al. Experimental study of adhesively bonded CFRP joints subjected to tensile loads. *Int J Adhes Adhes* 2015; 57: 95–104.
46. Jacob GC, Fellers JF, Simunovic S, et al. Energy absorption in polymer composites for automotive crashworthiness. *J Compos Mater* 2002; 36: 813–850.
47. Ramakrishna S. Energy absorption characteristics of knitted fabric reinforced epoxy composite tubes. *J Reinf Plast Compos* 1995; 14: 1121–1141.
48. Mamalis AG, Yuan YB and Viegelahn G. Collapse of thin–wall composite sections subjected to high speed axial loading. *Int J Veh Des* 1992; 13: 564–579.
49. Schmueser D and Wickliffe L. Impact energy absorption of continuous fiber composite tubes. *J Eng Mater Technol* 1987; 109: 72–77.
50. Farley GL. Energy absorption of composite materials. *J Compos Mater* 1983; 17: 267–279.
51. Thornton P. Energy absorption in composite structures. *J Compos Mater* 1979; 13: 247–262.
52. Thornton P. The crush behavior of pultruded tubes at high strain rates. *J Compos Mater* 1990; 24: 594–615.
53. Farley GL. The effects of crushing speed on the energy-absorption capability of composite tubes. *J Compos Mater* 1991; 25: 1314–1329.
54. Campilho RD, de Moura M and Domingues J. Using a cohesive damage model to predict the tensile behaviour of CFRP single-strap repairs. *Int J Solids Struct* 2008; 45: 1497–1512.
55. da Silva LFM, Sato C, Marques E, et al. Effect of low temperature on tensile strength and mode I fracture energy of a room temperature vulcanizing silicone adhesive. *J Test Eval* 2015; 44.
56. Marques E, da Silva LFM, Banea M, et al. Adhesive joints for low-and high-temperature use: an overview. *J Adhes* 2015; 91: 556–585.
57. Machado J, Gamarra P-R, Marques E, et al. Improvement in impact strength of composite joints for the automotive industry. *Compos Part B Eng* 2018; 138: 243–255.
58. Araújo H, Machado J, Marques E, et al. Dynamic behaviour of composite adhesive joints for the automotive industry. *Compos Struct* 2017; 171: 549–561.
59. Harding J and Welsh L. A tensile testing technique for fibre-reinforced composites at impact rates of strain. *J Mater Sci* 1983; 18: 1810–1826.

60. Körber H. *Mechanical response of advanced composites under high strain rates*. PhD Thesis, Faculty of Engineering of the University of Porto, 2012.
61. Loureiro A, da Silva LFM, Sato C, et al. Comparison of the mechanical behaviour between stiff and flexible adhesive joints for the automotive industry. *J Adhes* 2010; 86: 765–787.
62. Saldanha D, Canto C, da Silva LFM, et al. Mechanical characterization of a high elongation and high toughness epoxy adhesive. *Int J Adhes Adhes* 2013; 47: 91–98.
63. Avendano R, Carbas RJC, Chaves FJP, et al. Impact loading of single lap joints of dissimilar lightweight adherends bonded with a crash-resistant epoxy adhesive. *J Eng Mater Technol ASME* 2016; 138.
64. ASTM D1002:2005. Standard test method for apparent shear strength of single-lap-joint adhesively bonded metal specimens by tension loading (metal-to-metal); 15: 45–48.
65. ISO 4587:1995. Determination of tensile lap-shear strength of rigid-to-rigid bonded assemblies.
66. Fatt MH and Ouyang X. The behavior of elastomers at high strain rates. In: *WIT transactions on the built environment*, 2006; 87.
67. Lauke B, Schultrich B and Barthel R. Contribution to the micromechanical interpretation of fracture work of short-fibre-reinforced thermoplastics. *Compos Sci Technol* 1985; 23: 21–35.
68. Gupta V, Mittal R and Goel M. Energy absorbing mechanisms in short-glass-fibre-reinforced polypropylene. *Compos Sci Technol* 1990; 37: 353–369.
69. Lavielle L and Lamouri S. Polymer-polymer friction: adhesion dependence. *Lubr Sci* 1995; 12: 125–131.
70. Tanoglu M, McKnight SH, Palmese GR, et al. The effects of glass-fiber sizings on the strength and energy absorption of the fiber/matrix interphase under high loading rates. *Compos Sci Technol* 2001; 61: 205–220.
71. Perkins WG. Polymer toughness and impact resistance. *Polym Eng Sci* 1999; 39: 2445–2460.
72. Turley S and Keskkula H. A survey of multiple transitions by dynamic mechanical methods. *J Polyp Sci Polymer Symposia* 1966; 14(1): 69–87.
73. Mulliken A and Boyce M. Mechanics of the rate-dependent elastic–plastic deformation of glassy polymers from low to high strain rates. *Int J Solids Struct* 2006; 43: 1331–1356.

Paper 8

Content of Paper 8

Abstract

1. Introduction
2. Experimental details
2.1. Material and properties
2.1.1. Adhesive
2.1.2. CFRP
2.1.3. Aluminium alloys
2.2. Fabrication and testing
2.2.1. Preparation of CFRP plates
2.2.2. SLJ manufacture, geometry and joint configurations
2.2.3. Quasi-static testing procedures
2.2.4. Dynamic testing procedure
3. Experimental results
3.1. Quasi-static tests
3.1.1. Fracture surface
3.1.1.1. Joints with similar substrates
3.1.1.2. Joints with dissimilar substrates
3.1.2. Failure load
3.1.2.1.Joints with similar substrates
3.1.2.2. Joints with dissimilar substrates
3.1.3. Energy absorbed
3.1.3.1.Joints with similar substrates
3.1.3.2. Joints with dissimilar substrates
3.2. Impact tests
3.2.1. Fracture surface
3.2.1.1. Joints with similar substrates
3.2.1.2. Joints with dissimilar substrates
3.2.2. Failure load
3.2.2.1. Joints with similar substrates
3.2.2.2. Joints with dissimilar substrates
3.2.3. Energy absorbed
3.2.3.1. Joints with similar substrates
3.2.3.2. Joints with dissimilar substrates
3.3. Analysis of the combined effect of temperature and strain-rate
3.3.1. Failure load
3.3.1.1. Joints with similar substrates
3.3.1.2. Joints with dissimilar substrates
3.3.2. Energy absorbed
3.3.2.1. Joints with similar substrates
3.3.2.2. Joints with dissimilar substrates
4. Conclusions

References

Composites Part B 158 (2019) 102–116

Contents lists available at ScienceDirect

Composites Part B

journal homepage: www.elsevier.com/locate/compositesb

Adhesive joints using aluminium and CFRP substrates tested at low and high temperatures under quasi-static and impact conditions for the automotive industry

J.J.M. Machado[a], P.D.P. Nunes[b], E.A.S. Marques[a], Lucas F.M. da Silva[b,*]

[a] Instituto de Ciência e Inovação em Engenharia Mecânica e Engenharia Industrial (INEGI), Rua Dr. Roberto Frias, 4200-465, Porto, Portugal
[b] Departamento de Engenharia Mecânica, Faculdade de Engenharia (FEUP), Universidade do Porto, Rua Dr. Roberto Frias, 4200-465, Porto, Portugal

ARTICLE INFO

Keywords:
CFRP
Aluminium
Adhesives
Single lap joints
Temperature
Impact

ABSTRACT

The use of adhesives to bond metallic and composite structural components has increased substantially over the last decades. The aim of this work is to understand and predict the behaviour of dissimilar adhesive joints, using composite and aluminium substrates, under quasi-static and impact loads. Several testing temperatures (−30 to 80 °C) were considered, following the requirements for the automotive industry. It was possible to conclude that dissimilar adhesive joints, if used in conjunction with modern crash resistant adhesives, can effectively be used for the construction of automotive structures, without significant sacrifices in joint performance, with good energy absorption capabilities under impact.

1. Introduction

The increasingly strict requirements for fuel consumption and emissions reduction imposed on the automotive industry have created an opportunity to expand the use of lightweight composite materials, employing them as replacements for several metallic automotive components such as roofs, doors, and outer body panels. However, the use of composites in conjunction with more traditional methods of joining such as fasteners and rivets can damage both the reinforcement and the matrix, introduce stress concentration points and consequentially causing the reduction of structure integrity. Another important prerequisite is that automotive structures must be able to withstand an impact loading, deforming and absorbing the energy but at the same time maintaining the integrity of the structure. As a response to these challenges, the application of adhesives to bond structures has increased in the last decades providing benefits such as allowing to bond composite and dissimilar materials, increased design flexibility, time savings due to less preparation work required, reduction of stress concentrations over the overlap area and higher joint strength [1,2].

The intensification of the use of adhesives in the automotive industry for joining structural parts is in part dependent on the knowledge of their behaviour under different loading conditions as a function of temperature. Different factors such as the type of adhesive, substrates properties and surface preparation, joint geometry, as well as loading and temperature conditions introduce significant changes in a joint strength, being of extreme importance the understanding of the behaviour of the different combinations of adhesives and substrates [3].

Several studies can be found focusing on the effect of substrates stiffness on the joint strength under quasi-static conditions using similar and dissimilar substrates. The analysis of the stress distribution in joints made using dissimilar substrates and different thicknesses was performed by Cheng et al. [4] demonstrating that the maximum shear and normal stresses in the adhesive layer is greatly affected by the ratio of the elastic moduli. Sawa et al. [5] subjected to tensile loads SLJs made with dissimilar substrates and assessed the effect of the elastic modulus of each substrate on the stress at the interface between the epoxy adhesive and each substrate, observing that a reduction of the elastic modulus of one of the substrates, will lead to reduction of the edge stress near the interface with the low elastic modulus substrate increases. Reis et al. [6] tested SLJs with dissimilar substrates (carbon/epoxy laminate, high elastic limit steel and an aluminium alloy) at quasi-static conditions to relate substrate stiffness to the tensile shear strength, concluding that the higher the substrate stiffness the higher the value of shear strength obtained being the joint limited by the lowest stiffness of the substrates combination. Similar results were found by Afendi et al. [7] testing adhesively bonded scarf joints of dissimilar substrates, namely stainless steel and an aluminium alloy. Gültekin et al. have found the in composite-aluminium dissimilar joints the stacking sequence and thickness of the composite in adhesively bonded substantially influences the load-carrying capacity of the joint

* Corresponding author.
E-mail addresses: jmachado@inegi.up.pt (J.J.M. Machado), lucas@fe.up.pt (L.F.M. da Silva).

https://doi.org/10.1016/j.compositesb.2018.09.067
Received 29 May 2018; Received in revised form 23 July 2018; Accepted 21 September 2018
Available online 22 September 2018
1359-8368/ © 2018 Elsevier Ltd. All rights reserved.

[8].

The response of SLJs under impact conditions is also of extreme importance and has been previously studied by several authors [9–13] considering a variety of joints, substrates (generally joints composed of metal and similar materials and adhesives. Raykhere et al. [14] performed an experimental study focusing on the evaluation of the shear strength of butt joints made with three adhesives in combination with aluminium and glass fibre reinforced plastics (GFRP) substrates under quasi-static and dynamic loadings, concluding that the dynamic strength was not dependent to the type of substrate combination when the joint failure occurred in the adhesive. Sankar et al. [15] used butt joints made of similar and dissimilar materials (steel and aluminium) to assess the dynamic strength as a function of the substrate. The results revealed that the type of substrate influences the joint strength, and that for the case of dissimilar substrates the strength was lower in comparison with both joints using similar materials.

He and Ge [16] studied the effect on the dynamic strength (with a split Hopkinson pressure bar (SHPB) equipment) of similar and dissimilar SLJs, using titanium, aluminium and composite substrates. The dynamic strength of the SLJs was largely influenced by the stiffness of each substrate, being the highest strength achieved by joints made with stiffer substrates.

The influence of temperature on the strength of adhesive and adhesive joints is an important factor to assess as it can greatly influence the design phase [17,18], as for the automotive industry the structures must be validated ranging from low to high temperatures. In the case of tests performed at low temperatures, the adhesive strength might be compromised due to the formation of micro-cracks. Sharon et al. [19] studied the effects of loading rate and temperature on the viscoelastic related properties of four structural adhesives, concluding that the yield stress and modulus decreased with temperature while the loading rate presented a pronounced effect on the yield stress which increased with increasing loading rate and had a negligible influence on the modulus. A similar study was performed by Banea et al. [20] aiming to determine the tensile properties of a high temperature epoxy with a T_g of 155 °C. It was observed that the ultimate tensile stress decreased linearly with temperature while increased logarithmically with the loading rate. The Young's modulus presented a similar behaviour to the ultimate tensile stress, as function of loading rate while the decrease as function of temperature as nonlinear, being also stated that the effect of temperature on the properties was more significant than that of the strain rate.

A numerical evaluation and comparison of the behaviour of SLJs made with two epoxy adhesives and dissimilar substrates (aluminium and titanium) at low temperature was performed by Anes et al. [21]. The authors concluded that for dissimilar joints stresses arise able to surpass the adhesive lap shear strength, making the selection of adhesives and dissimilar substrates an important issue. Recently, Qin et al. have also found that high and low temperatures can have direct influence on the strength failure mode of dissimilar composite-aluminium joints [22].

The aim of this work is to describe, understand and model the behaviour of dissimilar adhesive joints, using composite and aluminium substrates, under quasi-static and impact loads. A variety of testing temperatures (ranging from −30 to 80 °C) was considered, considering the environmental requirements for the automotive industry. It was possible to conclude that dissimilar adhesive joints, if used in conjunction with modern crash resistant adhesives, can effectively be used for the construction of automotive structures, without significant sacrifices in joint performance, with good energy absorption capabilities under impact.

2. Experimental details

This section presents the mechanical properties of an epoxy crash resistant adhesive, as well of the three substrates (two aluminium alloys: 5754-H22 and 6060-T6, and CFRP) used in SLJs experimentally tested under different temperatures, specifically, low temperature (−30 °C – LT), room temperature (24 °C – RT) and high temperature (80 °C – HT). The SLJs were manufactured in similar and dissimilar substrates combinations, representative of those used on the automotive industry. The detailed manufacturing process and joint configuration is also described in detail.

2.1. Material and properties

2.1.1. Adhesive

The adhesive used in this work is a crash resistant epoxy-based adhesive that combines the toughness of a polyurethane with the high strength of an epoxy. The adhesive is designated XNR6852 E−3 manufactured by Nagase ChemteX®. This type of adhesive is particularly relevant for the automotive industry due to the combination of its high strength, ductility and impact resistance. This material can withstand significant plastic deformation before failure, allowing the bonded structure to absorb the impact energy. This epoxy adhesive was experimentally characterized under quasi-static load (1 and 100 mm/min) for different temperatures (LT, RT and HT).

The quasi-static tests (1 and 100 mm/min) were performed in a universal testing machine, of the type INSTRON® 3367 (Norwood, Massachusetts, USA) equipped with a 30 kN load cell.

To allow tests to be performed at LT and HT, a heated climatic chamber was integrated in the testing machine. Electric resistors were used to achieve the HT, while in the case of LT, liquid nitrogen was injected in a controlled manner. A thermocouple was positioned in contact with each specimen to control the temperature. To ensure homogeneous temperature distribution each test was only performed after a period of 10 min at the target temperature and the specimens remained enclosed in the chamber under a constant temperature during load application.

To characterize the tensile properties of the adhesive, bulk specimens were manufactured and tested. The specimen geometry used was in accordance with EN ISO 527-2 [23–25].

For the determination of shear properties, thick adherend shear tests (TAST) were employed. These tests were performed at RT only. The TAST specimens are composed of two steel substrates (DIN C45 E), joined by the adhesive layer. The stiffness of the steel substrate combined with the short overlap length introduces an almost pure shear stress in the adhesive layer [26,27]. The geometry used is in accordance to ISO 11003-2 [28].

DCB tests [29] were performed in order to obtain the critical strain energy release rate in mode I of XNR6852E-3 adhesive. High strength steel (DIN 40 CrMnMo 8-6-4) specimens were used to avoid plastic deformations of the substrates. The geometry used was per D 3433-99 ASTM standard [30].

Mode II characterization [31] of the XNR6852E-3 adhesive could not be experimentally performed due to the extremely high fracture toughness that this adhesive presents in mode II, which causes early plastic deformation of the metallic substrates before crack propagation occurs. Saldanha et al. [32] and Avendaño et al. [33] have studied previous versions of Nagase XNR6852 E−3 adhesive and in their works G_{IIC} determined experimentally was 6–10 times higher than G_{IC}. Considering this previous data, and due to the high ductility of the adhesive, the value for G_{IIC} was therefore assumed to be 8 times higher than the fracture toughness in mode I.

As many of these tests do not lend themselves to characterization under impact conditions (initial impact velocity of 3 m/s) and extrapolation process was employed for estimating the properties at higher strain rates. A logarithmic law used in this process as given by Equation (1).

$$\textit{Property to determine} = A \ln(\dot{\varepsilon}) + B \quad (1)$$

Where A and B are constants obtained from experimental data, and $\dot{\varepsilon}$ is the strain rate in s^{-1}. This logarithmic extrapolation process has been

Table 1
Mechanical properties of Nagase ChemteX® XNR6852E-3 epoxy adhesive under quasi-static and impact conditions (average values), as a function of temperature (low temperature (−30 °C – LT), room temperature (24 °C – RT) and high temperature (80 °C – HT)).

Mechanical Properties	1 mm/min			100 mm/min			180000 mm/min[a]		
	LT	RT	HT	LT	RT	HT	LT	RT	HT
Young's modulus, E [MPa]	2460	1874	1026	2727	2243	1268	1320	3813	2392
Shear modulus, G [MPa]	–	665	–	–	645	–	–	603	–
Tensile strength, σ_n [MPa]	63	48	24	69	57	33	95	95	72
Shear strength, t_s [MPa]	–	45	–	–	44	–	–	43	–
Fracture energy (mode I), G_{IC} [N/mm]	9	9	13	9	10	14	12	13	20
Fracture energy (mode II), G_{IIC} [N/mm]	72	72	104	72	80	112	96	104	160

[a] Extrapolated properties considering an initial impact velocity of 3 m/s.

first proposed by the work of Zgoul and Crocombe [34] and later further validated by the work of Avendaño et al. [35].

Table 1 lists the experimentally measured mechanical properties (average values) for the XNR6852 E−3 adhesive as well as the extrapolated properties for the impact velocity (initial impact velocity of 3 m/s).

As low and high testing temperatures were employed in this study, the glass transition temperature, T_g, of the adhesive was experimentally determined, as its value can greatly influence the mechanical behaviour of the joint [36,37]. Below T_g the adhesive presents a stiff characteristic while above behaves in a flexible manner [38,39]. The determination of T_g was performed and the measured value was of 132 ± 4 °C, which is higher than the applied testing HT and ensures the mechanical performance of the adhesive is not drastically changed.

2.1.2. CFRP

The CFRP specimens used in this work were manufactured with plies of carbon/epoxy pre-preg (SEAL® Texipreg HS 160 RM) which were oriented in a single direction. The elastic properties of this material were previously determined in the work of Campilho [40] in 2009. Table 2 presents the Young's modulus (E), the shear modulus (G), and the Poisson's ratio (ν), in the three-axis direction (x,y,z), being E_1 the normal direction, E_2 the transverse direction and E_3 the out plane direction.

The mechanical properties of CFRP have been previously experimentally determined for 1 mm/min and 100 mm/min by the authors [38,41]. The properties for high impact speed (3 m/s) have been determined using the same extrapolation process described for the adhesives [37]. Table 3 lists the cohesive properties of CFRP for three testing speeds. As additional strain rate data for this material is not experimentally available, the Young's modulus, shear modulus and tensile strength were not considered to be strain rate dependent in this model. The mechanical properties for the case of an impact velocity of 3 m/s were again logarithmically extrapolated using the previously described Equation (1).

Table 2
Properties of CFRP elastic orthotropic [40].

Elastic Modulus (MPa)	Poisson's Ratio	Shear Modulus (MPa)
E_1 = 109000	ν_{12} = 0.342	G_{12} = 4315
E_2 = 8819	ν_{13} = 0.342	G_{13} = 4315
E_3 = 8819	ν_{23} = 0.380	G_{23} = 3200

Table 3
Cohesive properties of CFRP under quasi-static and impact conditions.

Properties	1 mm/min	100 mm/min	180000 mm/min[a]
Young's modulus, E [MPa]	109000	109000	109000
Shear modulus, G [MPa]	4315	4315	4315
Tensile strength, σ_n [MPa]	40	40	40
Shear strength, t_s [MPa]	35	35	35
Fracture energy (mode I), G_{IC} [N/mm]	0.59	0.53	0.39
Fracture energy (mode II), G_{IIC} [N/mm]	1.17	1.04	0.82

[a] Extrapolated properties considering an initial impact velocity of 3 m/s.

The determination of Tg was performed in previous works developed by the authors [37] and the composite resin presented a value of 105 ± 2 °C, above the higher testing temperature.

2.1.3. Aluminium alloys

Two aluminium alloys commonly applied in the automotive industry were used in this work, namely, the 5754-H22 and 6060-T6.

The thickness of each aluminium alloy is different, as are representative of the average value of the different thicknesses used in the automotive industry, being of 1.5 mm for the 5754-H22 alloy and of 2.0 mm for the 6060-T6 alloy; both alloys are designated in the results as Al 1.5 and Al 2.0, respectively to easy perform a comparison. Both aluminium alloys were provided with an anodization surface treatment, required to improve the adhesion process. Table 4 presents the mechanical elastic properties of the aluminium alloys used.

Using a hardness testing machine (Otto Wolpert-Werke Dia tester 2RC), measurements were performed on both aluminium alloys, provided in their natural state and after being subjected to the same temperature used to cure the adhesive, to verify if such temperature would cause any significant changes in the materials hardness. It was possible to conclude that the curing temperature of the adhesive did not cause any change regarding the hardness of both substrates. The aluminium 5754-H22 registered a hardness of 72 HV and the aluminium 6060-T6 of 76 HV.

2.2. Fabrication and testing

2.2.1. Preparation of CFRP plates

The specimens tested in this work consisted of unidirectional laminates of CFRP cut from bulk laminates, which were produced by hand lay-up and cured in a hot plate press. The bulk laminates, with dimensions of 300 mm by 300 mm, were fabricated by stacking unidirectional 0° lay-up plies (with the aim of obtaining better properties in the loading direction). Each plate had a total of 14 plies of carbon/epoxy pre-preg (SEAL® Texipreg HS 160 RM) with 0.15 mm of ply thickness. The cure cycle applied was 130 °C for 1 h.

Subsequently to the removal from the press, the laminates were cut into smaller specimens using a diamond disc cutting machine. Edge finishing was carried out manually with 120-grit sandpaper to remove the loose fibres and smoothen the sharp edges. Being the CFRP

Table 4
Elastic properties of the used aluminium alloys: Al 5754-H22 and Al 6060-T6.

Aluminium designation	Mechanical Properties	
	Elastic Modulus (*GPa*)	Poisson's ratio
Al 5754-H22 (Thickness of 1.5 mm) – **Al 1.5**	69	0.33
Al 6060T6 (Thickness of .0 mm) – **Al 2.0**	69	0.33

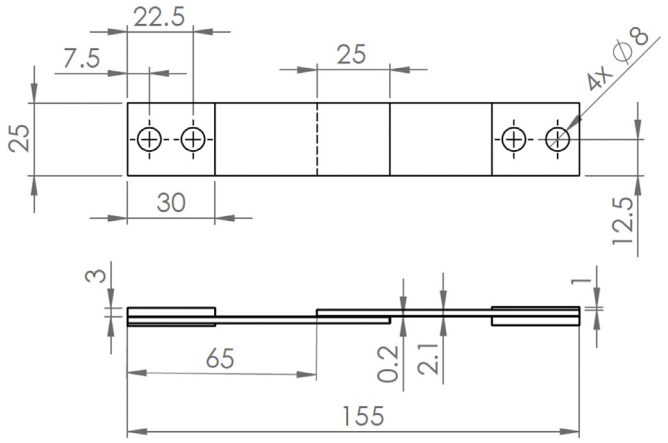

Fig. 1. Geometry of SLJ specimens (dimensions in mm).

substrates made of 14 plies, a total thickness of 2.1 mm was achieved, and the adhesive thickness used in the SLJ was of 0.2 mm.

2.2.2. SLJ manufacture, geometry and joint configurations

Before bonding the CFRP substrates, 120-grit sandpaper was used to remove the top layer to improve the adhesion through the surface rugosity, the process consisted in abrading in both directions of the overlap area at 45° to ensure a homogeneous surface. Both aluminium alloys used were already provided with surface treatment of anodization, the process of cleaning involved a sequence of placing the substrates in an oven at 190 °C for 30 min finalized with the use of alcohol isopropanol to remove any particles or contaminants of the surface.

The SLJs were tested with one overlap length of 25 mm. The geometry chosen is representative of automotive industry applications, with thin substrates and single overlap bonding (Fig. 1). The overlap of 25 mm was already studied by several authors where a comparison was made with several values of overlap length being tested [42–44].

Considering the three distinct substrates (CFRP, aluminium alloys: 5754 H22 and 6060 T6), it is possible to perform several combinations of SLJs made of similar and dissimilar substrates. The SLJ combinations used in this work are presented in Table 5.

A total of four specimens were tested for each overlap and temperature condition, and force-displacement (P-δ) curves were obtained for all the SLJs tested, respectively for quasi-static and impact conditions.

2.2.3. Quasi-static testing procedure

The quasi-static tests were performed using an INSTRON® 3367 (Norwood, Massachusetts, USA) universal testing machine, with a load cell with a capacity of 30 kN. All quasi-static tests were performed at room temperature and with a constant cross head displacement rate of 1 mm/min, corresponding to an average shear strain rate of 0.08 s^{-1}. Six specimens were tested for each condition, and for each joint a P-δ curve was obtained.

Three distinct testing temperatures were used, namely, low temperature (− 30 °C – LT), room temperature (24 °C – RT) and high temperature (80 °C – HT).

Table 5
Different SLJ combinations of similar and dissimilar substrates.

Combinations with similar substrates	Al 5754-H22 + Al 5754-H22 Al 6060-T6 + Al 6060-T6 CFRP + CFRP
Combinations with dissimilar substrates	Al 5754-H22 + Al 6060-T6 Al 5754-H22 + CFRP Al 6060-T6 + CFRP

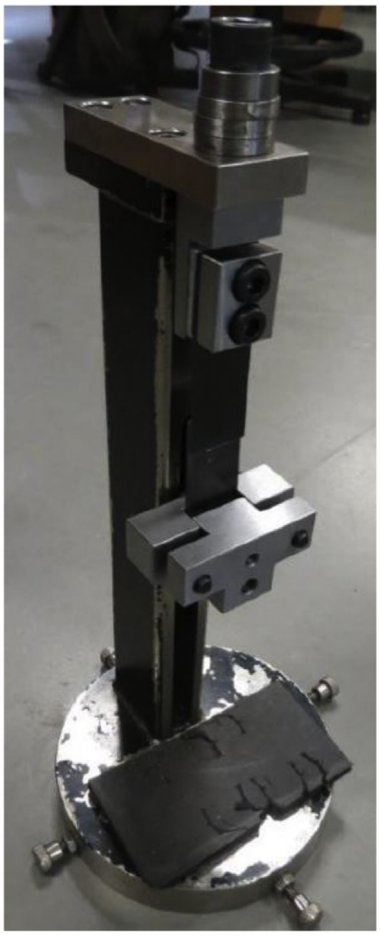

Fig. 2. Setup used to hold the specimen in position for the impact test.

In tests performed under LT and HT, a heated climatic chamber was integrated in the testing machine. In the case of LT, the same chamber was used, with nitrogen being injected in a controlled manner to achieve the lower temperature. With the use of a thermocouple positioned in contact with each SLJ the temperature was measured, ensuring a homogeneous temperature distribution. Each test was only performed after a period of 10 min at the intended temperature. While the tests were being performed the SLJs remained enclosed in the chamber under a constant temperature.

2.2.4. Dynamic testing procedure

For the impact tests, metallic tabs were added to the ends of the composite SLJ specimens. This was performed to align the load, evenly distribute the gripping force and prevent hole failure by reinforcing the clamped area.

A Rosand® Instrumented Falling weight impact tester, type 5 H.V. (Stourbridge, West Midlands, U.K), with a load cell with a capacity of 60 kN, was used for the impact tests. This equipment allows to achieve 300 J (using 29 kg of weight) and a maximum impact speed of 4.5 m/s. The procedure consists in dropping a weighted mass, which falls until it impacts a clamp bolted to the lower substrate of the SLJ specimen. In Fig. 2, it is possible to observe the setup used to hold the specimen in position. The impact velocity can then be defined by selecting a drop height. Likewise, the energy applied in the impact is controlled by adjusting the weight of the impact mass.

The average strain rate in the adhesive layer, was of 15000 s^{-1} (corresponding to a displacement speed of 3 m/s). A mass of 26 kg was used for the impactor, corresponding to an impact energy of 117 J, sufficient to break all specimen configurations. For each adhesive

configuration, six specimens were tested.

Impact testing was performed at the same three temperatures used for quasi-static testing. For tests performed at LT, gaseous nitrogen was applied directly in every SLJ. In the case of HT, a heat gun to heat-up the SLJs was used. In both stages of temperature, a thermocouple was attached in the beginning of the area of overlap length to measure and control the temperature of the specimen. Each test occurred when the adhesive layer temperature was found to be stabilized at the desired value.

3. Experimental results

In this section, the experimental results of all SLJs tested (similar and dissimilar substrates configurations) are presented and analysed in terms of fracture surface, failure load and energy absorbed (which is the fraction of the incident energy that was dissipated by the failure process of the SLJs) during the quasi-static and impact conditions. As previously referred, for all the testing results, the aluminium substrates will be designated differently to facilitate the identification of its specific thickness value, being the Al 5754-H22 also identified as Al 1.5 and the Al 6060-T6 presented as Al 2.0, which corresponds to the thickness values of each substrate.

3.1. Quasi-static tests

The results are presented in respect to similar and dissimilar combination of substrates of the SLJs as a function of the testing temperature (LT, RT and HT).

From representative load-displacement (P-δ) curves of SLJs tested at RT and using similar substrates combinations (Fig. 3), it is possible to observe that joints made with aluminium substrates exhibit a significantly large deformation within the plastic domain, opposite to the behaviour found for when using CFRP substrates which, even though presenting higher failure load, are quite prone to the occurrence of delamination.

In the case of the P-δ curve related to the joints made with the Al 5754-H22 (Al 1.5), instability during plastic deformation occurs, being caused by the Portevin-Le Chatellier effect [45–47] which is a typical and well described behaviour of the aluminium alloys from the 5xxx series.

Noticeable from the P-δ curve of CFRP joints is a light decrease in stiffness near the failure point, which can be attributed to the gradual breakage of fibres during the test (and can be heard during the test in the moments preceding the failure by delamination).

3.1.1. Fracture surface

3.1.1.1. Joints with similar substrates. The type of failure surface is a critical parameter to study and better understand the mechanical behaviour of adhesive joints. Table 6 shows the typical quasi-static failure surface of all joints made with similar substrates configurations and tested at different temperatures (LT, RT and HT).

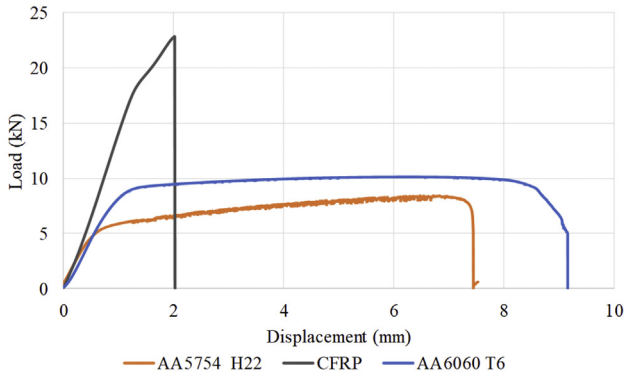

Fig. 3. Representative P-δ curves of SLJs using similar substrates tested at quasi-static conditions and RT.

The images in Table 6 show that the type of failure of the joints which employ aluminium substrates is either by cohesive failure in the adhesive, or cohesive failure in the substrate. Even when cohesive failure in the adhesive occurs prior to failure (more common for the 5754 H22 alloy), large deformation in the aluminium substrates is noticeable, thus the aluminium also controls the failure process. In the case of SLJs made with Al 6060-T6 (Al 2.0) substrates and tested at RT, the failure mode can be characterized as unstable, as half of the joints failed by the adhesive and the other half by the substrate, although the failure load values remained constant for both situations. It is possible to conclude that the SLJs using aluminium substrates fail due to onset of plastic deformation of the material, therefore, introducing high peel stresses at the end of the overlap length, specifically for the cases when the failure occurs in the adhesive. For SLJs using CFRP substrates, and as evidenced in Table 6, delamination of the substrate occurs at LT and at RT, while at high temperature the adhesive becomes more ductile and less strong, failing before the composite.

3.1.1.2. Joints with dissimilar substrates. The different types of failure surface for SLJs made with dissimilar substrates and tested at quasi-static conditions varying the testing temperature (LT, RT and HT) are presented in Table 7.

As shown in Table 7, the SLJs combining Al 5754-H22 + Al 6060-T6 (Al 1.5 + Al 2.0) substrates, the type of joint failure is mainly cohesive in the adhesive but accompanied of a noticeable degree of plastic deformation of the aluminium alloys. It is this plastic deformation that ultimately leads to adhesive failure, as it results in the introduction of high peel stresses in the adhesive layer. Combining Al 5754-H22 + CFRP (Al 1.5 + CFRP) substrates, the figure shows a combination of failure by delamination and cohesive failure in the adhesive, which occurs at HT and RT. At LT, there is a more unstable behaviour, where two distinct types of failure may occur alternatively, either by delamination of CFRP or by complete failure of the aluminium substrate. The last row of Table 7 shows the type of failure surface obtained for joints combining Al 6060-T6 + CFRP (Al 2.0 + CFRP) substrates. Complete failure of the aluminium is found, as these substrates are generally weaker than both the CFRP and the adhesive layer.

A key factor for understanding the difference of failure mode between the two different aluminium substrates (Al 5754-H22 (Al 1.5) and Al 6060-T6 (Al 2.0)), when combined with the CFRP substrate, is the difference in thickness of each substrate. As previously mentioned, the Al 6060-T6 (Al 2.0) substrate is 2 mm thick, in contrast to 1.5 mm for the Al 5754-H22 (Al 1.5) substrate, which is closer to the 2.1 mm thickness of the CFRP substrates. The lower value of thickness means that lower peel stress distribution along the overlap length will be present, causing the type of failure of the joint to change from delamination of CFRP, in the case of the combination of Al 5754-H22 + CFRP (Al 1.5 + CFRP) substrates, to being cohesive in the aluminium substrate, for the substrates combination of Al 6060-T6 + CFRP (Al 2.0 + CFRP), as shown in Table 7.

3.1.2. Failure load

3.1.2.1. Joints with similar substrates. The results in term of failure load of SLJs made using similar substrates and tested at quasi-static conditions as a function of temperature (LT, RT and HT), are presented in Fig. 4.

It is possible to observe that SLJs made with aluminium substrates are not sensitive to the different testing temperatures due to the intrinsic mechanical properties of metals. However, considering joints made with CFRP substrates, it is observed a significant decrease of failure load as the testing temperature increases from RT to HT. Such behaviour can be explained by the higher influence of the testing temperature on the mechanical properties of the epoxy resin of the

Table 6
Failure surfaces of SLJs using similar substrates (CFRP and aluminium alloys) tested at quasi-static conditions as a function of temperature.

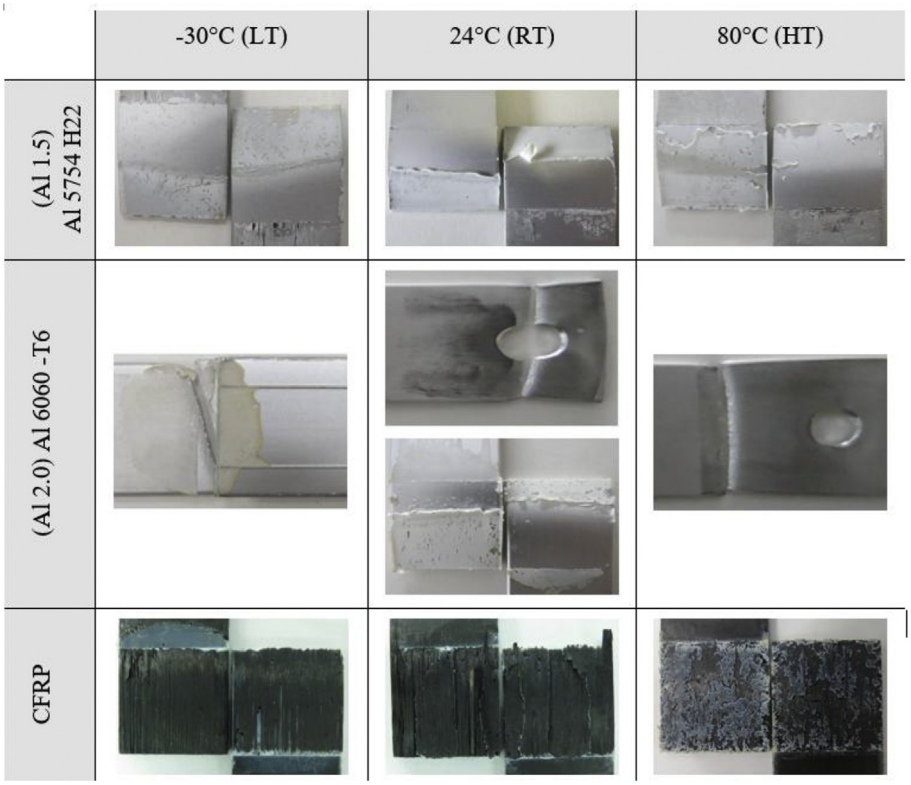

CFRP substrate, even though the change in the mechanical properties of the adhesive with the temperature is a major factor to consider.

The adhesive is ductile enough through the range of testing temperatures to avoid high stress concentration and therefore to cause early failure, ergo the decrease of tensile strength is more noticeable. It can be also stated that the SLJs made with CFRP substrates present higher failure load in comparison with joints made using aluminium substrates (Al 5754-H22 (Al 1.5) and Al 6060-T6 (Al 2.0)), allowing to conclude

Table 7
Failure surfaces of SLJs using dissimilar substrates (CFRP and aluminium alloys) tested at quasi-static conditions as a function of temperature.

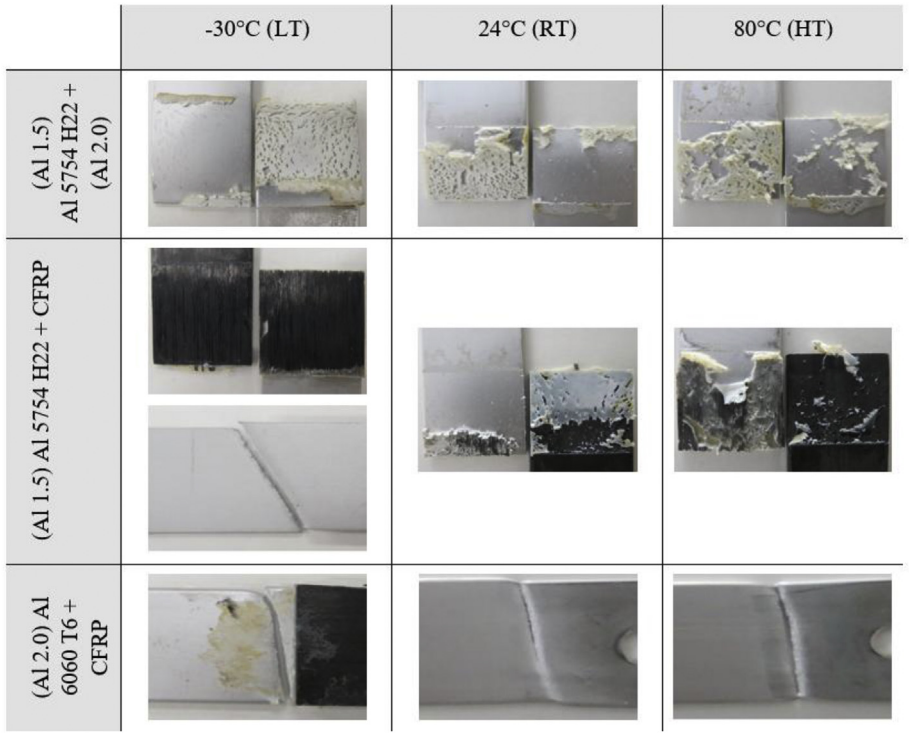

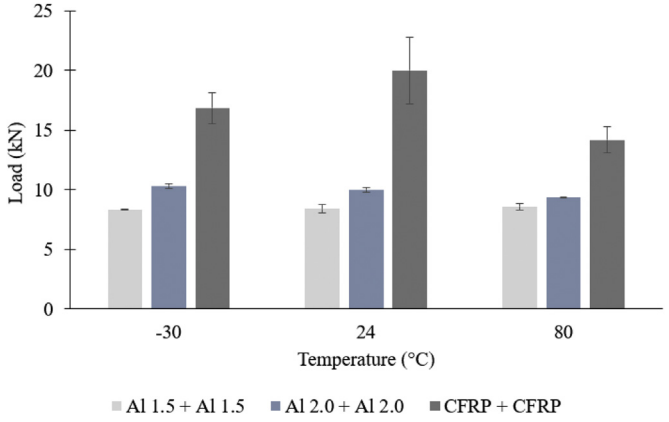

Fig. 4. Failure load of SLJs using similar substrates (CFRP and aluminium alloys) tested at quasi-static conditions as a function of testing temperature.

that the failure is in fact heavily dependent on the mechanical properties of the substrates being used.

3.1.2.2. Joints with dissimilar substrates. The results in term of failure load of SLJs made with dissimilar substrates are presented in Fig. 5.

The maximum failure load obtained for each SLJ made with dissimilar substrates is controlled by the weakest substrate of the combination. In the case of SLJs made with following substrate combinations: Al 5754-H22 + Al 6060-T6 (Al 1.5 + Al 2.0) and Al 5754-H22 + CFRP (Al 2.0 + CFRP), the failure of the joint is commanded by the weaker Al 5754-H22 (Al 1.5) substrates. As for SLJs combining Al 6060-T6 + CFRP (Al 2.0 + CFRP), the joint failure is limited by the Al 6060-T6 (Al 2.0) substrate. From the results obtained no temperature dependence was observed since the only substrate sensitive to testing temperatures is the CFRP.

3.1.3. Energy absorbed

3.1.3.1. Joints with similar substrates. Another important characteristic to assess the mechanical behaviour of SLJs is the energy absorbed, which is the fraction of the incident energy that is dissipated by the failure process of the SLJs. Fig. 6 shows the results of similar substrates combinations of SLJs tested at quasi-static conditions as a function of different temperatures (LT, RT and HT).

The energy absorbed by SLJs made with aluminium alloys (Al 5754-H22 (Al 1.5) and Al 6060-T6 (Al 2.0)) is significantly higher than the values obtained for joints using CFRP substrates, despite the higher values in terms of failure load exhibited by the joints made with CFRP substrates. SLJs made using aluminium alloys (Al 5754-H22 (Al 1.5) and Al 6060-T6 (Al 2.0)) undergo significantly higher plastic deformation prior to failure in comparison with joints using CFRP

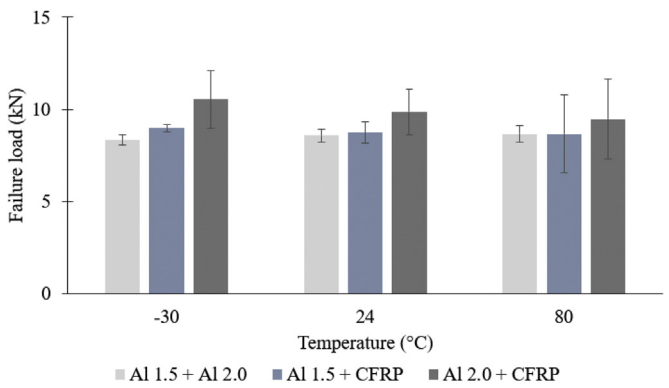

Fig. 5. Failure load of SLJs using dissimilar substrates (CFRP and aluminium alloys) tested at quasi-static conditions as a function of temperature.

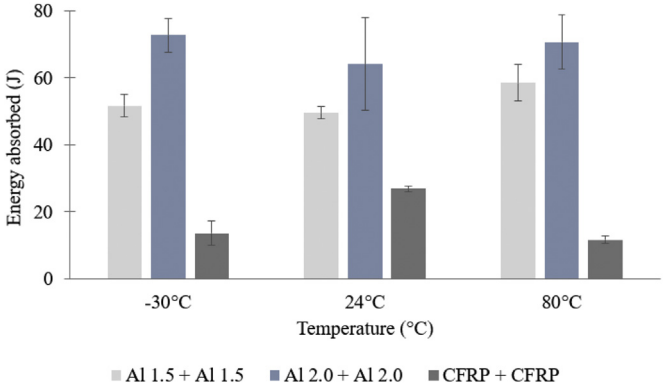

Fig. 6. Energy absorbed by SLJs using similar substrates (CFRP and aluminium alloys) tested at quasi-static conditions as a function of temperature.

substrates.

Comparing both aluminium substrates, it can be concluded that the energy absorbed by the Al 6060-T6 (Al 2.0) alloy is higher than the one found for the Al 5754-H22 (Al 1.5) alloy, allowing for this material to withstand higher deformation before failure. Considering the standard deviation of the test results there is no temperature dependence regarding the absorbed energy of SLJs made using aluminium substrates (Al 5754-H22 (Al 1.5) and Al 6060-T6 (Al 2.0)).

For the case of SLJs made with CFRP substrates, due to the epoxy resin of the composite sensitivity to testing temperature, more energy was absorbed by the SLJs at RT. Comparing with SLJs made with aluminium substrates, such disparity of energy absorbed was not found for the different testing temperatures, allowing to conclude that for SLJs made with CFRP, the epoxy resin was too brittle at LT, and became unable to absorb energy, therefore losing its mechanical properties as it approached T_g.

3.1.3.2. Joints with dissimilar substrates. The values of energy absorbed during quasi-static tests varying the temperature, for SLJs made using dissimilar combination of substrates, are presented in Fig. 7.

It is possible to observe that the values of energy absorbed for SLJs with dissimilar substrates combination are in between of those obtained in the case of joints with similar substrates (Fig. 6). This can be explained by the fact that in a joint with a dissimilar combination of substrates, the deformation of an aluminium substrate (Al 5754-H22 (Al 1.5) or Al 6060-T6 (Al 2.0)) when combined with the stiffer and less flexible CFRP will occur, as for joints with similar substrates of aluminium the deformation is symmetric until the peel stress disrupts the adhesive.

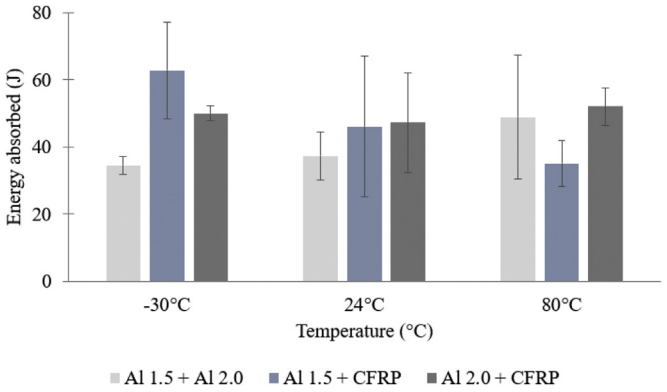

Fig. 7. Energy absorbed by SLJs using dissimilar substrates (CFRP and aluminium alloys) tested at quasi-static conditions as a function of temperature.

Table 8
Failure surfaces of SLJs using similar substrates (CFRP and aluminium alloys) tested at impact conditions as a function of temperature.

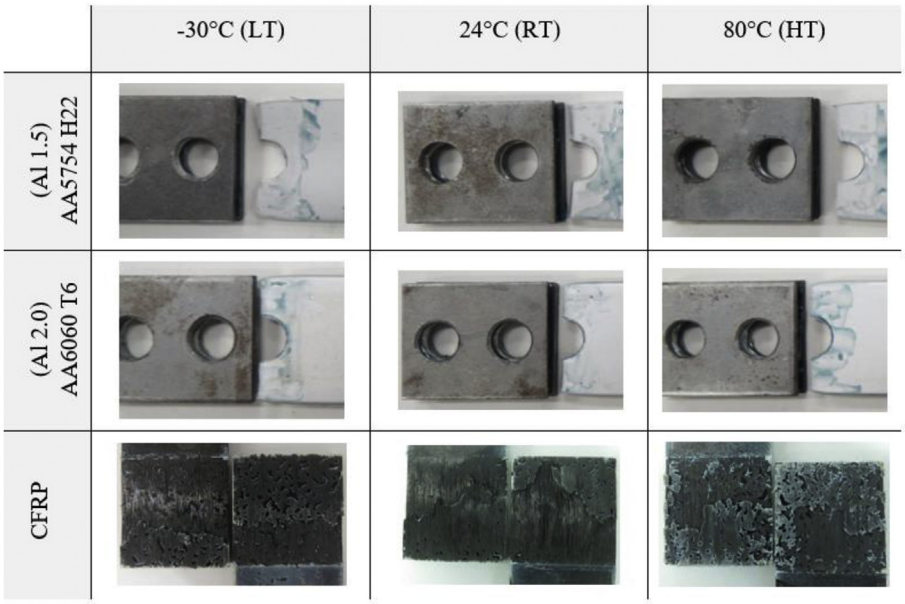

3.2. Impact tests

The impact results were performed at an initial impact velocity of 3 m/s using a drop weight impact testing machine, in which a mass of 26 kg was used for the impactor, achieving an impact energy of 117 J, adequate to break all SLJs configurations. The results are presented in respect to similar and dissimilar combination of substrates of the SLJs as a function of the testing temperature (LT, RT and HT).

3.2.1. Fracture surface

3.2.1.1. Joints with similar substrates. The type of failure surface is a critical parameter to study and better understand the mechanical behaviour of adhesive joints. The typical impact failure surface of all joint made with similar substrates configurations and tested at different temperatures (LT, RT and HT) are shown in Table 8.

Regarding the SLJs made with similar aluminium substrates (Al 5754-H22 (Al 1.5) or Al 6060-T6 (Al 2.0)), the failure took place on the clamped area for both substrates and for all testing temperatures (LT, RT and HT). Such behaviour can be explained by the higher mechanical properties with the increase of the strain rate, and the stress concentrations due to the presence of holes in the clamping area which were created to hold the specimens in place while testing, being the second phenomena the most probable to cause the premature failure of the joints.

Considering SLJs made with CFRP substrates, failure of the joint by delamination was present for all the testing temperatures (LT, RT and HT), although, some changes were found as a function of temperature. For tests performed at LT and HT, cohesive failure in the adhesive was found since it became stiffer at LT and more flexible at HT, having the same behaviour occurred for the resin of the CFRP. The presence of such mixed failure mode allows to conclude that the adhesive was being loaded until failure, due to the decrease of its, as well the resin of the CFRP, mechanical properties.

3.2.1.2. Joints with dissimilar substrates. Table 9 shows the typical impact failure surface of all joint made with dissimilar substrates configurations and tested at different temperatures (LT, RT and HT).

As previously stated for the case of SLJs made with similar substrates combinations, the introduction of aluminium substrates (Al 5754-H22 (Al 1.5) or Al 6060-T6 (Al 2.0)) causes the joints to fail in the clamped area due to the presence of holes. The only exception is the case of SLJs combining Al 6060-T6 (Al 2.0) + CFRP substrates, having the joints failed by severe delamination of CFRP at LT, due to the viscoelastic and viscoplastic behaviour of both the adhesive and resin of the CFRP, which translate in both materials becoming more brittle at LT. Since joint failure by delamination of CFRP substrates, it is possible to state that at LT the effect on the resin of the CFRP is significantly higher than of the adhesive. It is also important to remark that due to the general occurrence of failure on the metal substrate under impact conditions it becomes difficult to truly assess the influence of the factors under study on the adhesive. This work therefore serves to validate a given adhesive layer configuration and ensure that it is not the weak link. Nonetheless it is still possible to assess the joint performance as a complete unit, which is performed in the following sections with regards to failure load and energy absorption.

3.2.2. Failure load

3.2.2.1. Joints with similar substrates. The results in term of failure load of SLJs made using similar substrates and tested under impact conditions as a function of temperature (LT, RT and HT) are presented in Fig. 8.

For test performed at HT, the adhesive becomes more flexible, therefore reducing the peel loads in SLJs made with CFRP substrates; the HT tests proximity to the T_g conducts to lower values of tensile and shear strength, even when considering strain rate dependency. It is the occurrence of a mixed failure mode, with simultaneous delamination and cohesive failure that leads to the lower failure loads obtained.

Both the adhesive and the resin of the CFRP become more brittle when tested at LT. The failure load results obtained testing SLJs made with Al 6060-T6 (Al 2.0) substrates revealed to be higher than the values obtained for joint made with CFRP substrates, allowing to conclude that under LT the resin of the CFRP is significantly more affected, therefore controlling the failure of the joint.

In the case of SLJs made with Al 6060-T6 (Al 2.0) substrates, despite a noticeable decrease of the average value of maximum failure load from LT to RT, no tendency can be considered since these values fall under the respective standard deviations. The same behaviour can be observed in SLJs using Al 5754-H22 (Al 1.5) substrates.

3.2.2.2. Joints with dissimilar substrates. The failure load results of SLJs

Table 9
Failure surfaces of SLJs using dissimilar substrates (CFRP and aluminium alloys) tested at impact conditions as a function of temperature.

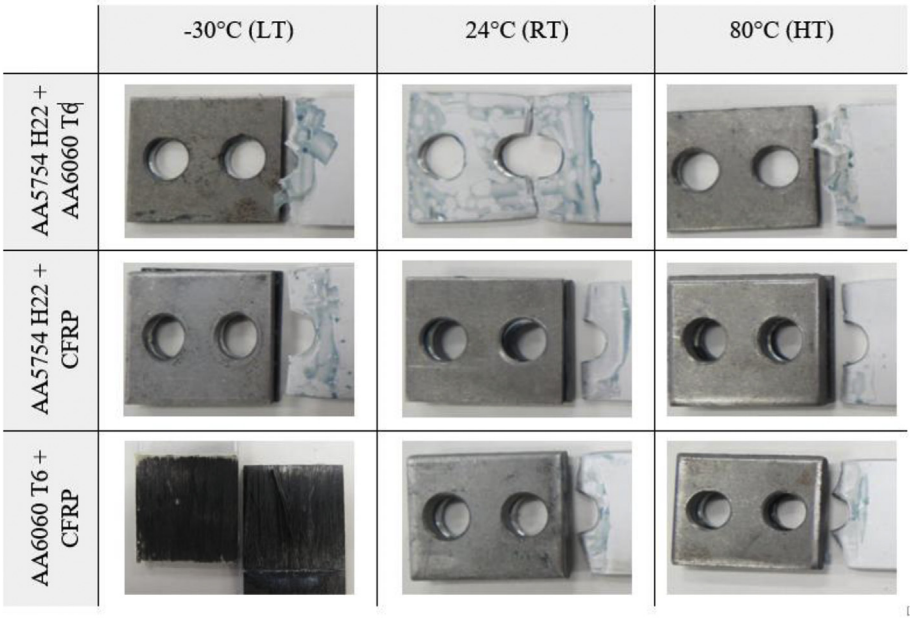

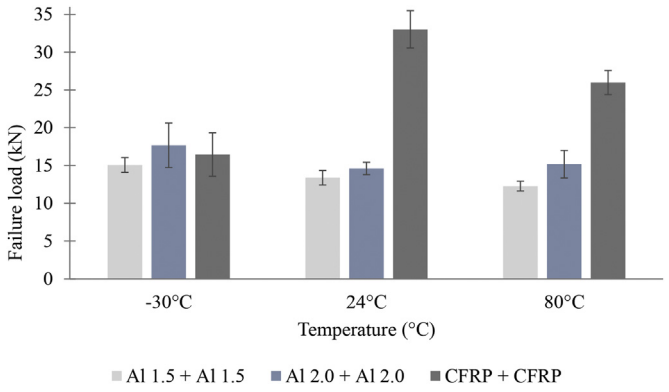

Fig. 8. Failure load of SLJs using similar substrates (CFRP and aluminium alloys) tested at impact conditions as a function of temperature.

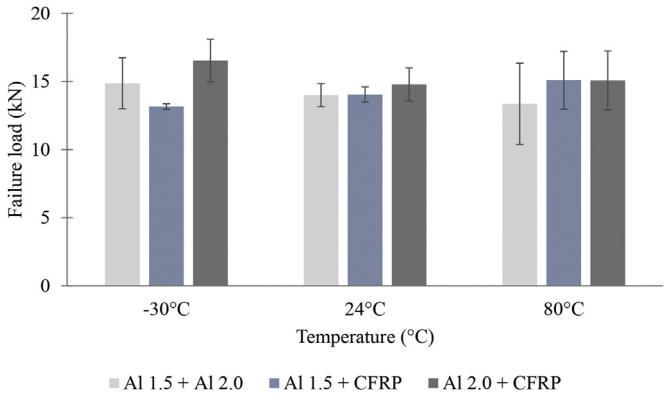

Fig. 9. Failure load of SLJs using dissimilar substrates (CFRP and aluminium alloys) tested at impact conditions as a function of temperature.

made with dissimilar substrates under impact conditions for all testing temperatures (LT, RT and HT) are presented in Fig. 9.

No clear tendency was found in terms of failure load of joints made with dissimilar substrates (CFRP and aluminium alloys: Al 5754-H22 (Al 1.5) or Al 6060-T6 (Al 2.0)) as a function of testing temperature (LT, RT and HT). It is possible to observe that the maximum failure load was defined by the weakest substrate, in the case of joints combining Al 5754-H22 (Al 1.5) + Al 606-T6 (Al 2.0) and Al 5754-H22 (Al 1.5) + CRP, that the weakest substrate was the Al 5754-H22 (Al 1.5); and that for joints made with Al 6060-T6 (Al 2.0) + CFRP, the weakest substrate was the Al 6060-T6 (Al 2.0) substrate.

3.2.3. Energy absorbed

3.2.3.1. Joints with similar substrates. Another important characteristic to assess the mechanical behaviour of SLJs is the energy absorbed, which is the fraction of the incident energy that is dissipated by the failure process of the SLJs. Fig. 10 shows the results of similar substrates combinations of SLJs tested under impact conditions as a function of different temperatures (LT, RT and HT).

Considering SLJs made with similar aluminium substrates (Al 5754-H22 (Al 1.5) and Al 6060-T6 (Al 2.0)), no clear tendency of the energy absorbed was found as a function of temperature and under impact conditions. However, for the case of joints made with similar substrates of CFRP there was an increase of the energy absorbed under impact conditions with the increase of the testing temperature, as observed from the representative *P-δ* curves (Fig. 11) obtained under impact as a function of testing temperature (LT, RT and HT).

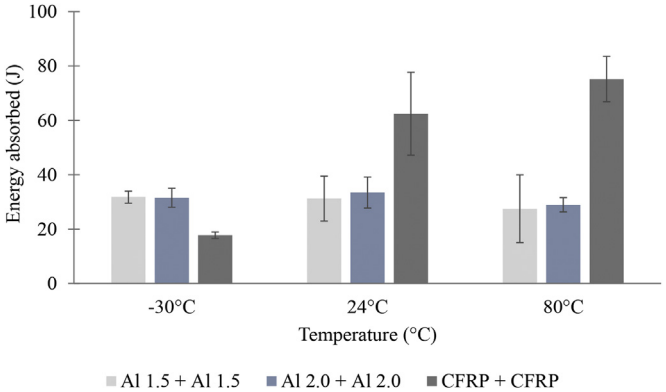

Fig. 10. Energy absorbed by SLJs using similar substrates (CFRP and aluminium alloys) tested at impact conditions as a function of temperature.

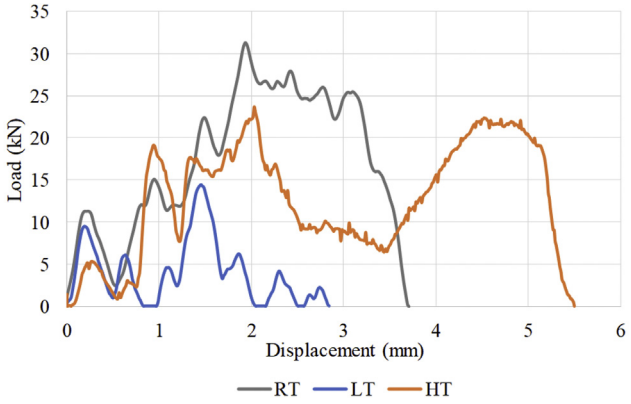

Fig. 11. Representative P-δ curves of SLJs using CFRP similar substrates tested at impact conditions as a function of temperature.

As found in the literature, some authors found that composites structures can sustain higher loads and absorb more energy under impact conditions [48,49].

Also, in some works [50,51] it was stated that through the failure process of composite materials, the frictional sliding of the composite fibres within the matrix might be responsible for a large fraction of the energy absorption (Fig. 12). This type of frictional sliding has been shown to be a complex phenomenon [52] involving both the Van der Waals forces and the mobility of macromolecules at the interface, which results in larger energy absorption for higher impact strain rates [53]. However, increased energy absorption under impact conditions cannot be totally due to the process of delamination and fibre pull-out. The energy absorption and toughness of bulk polymeric materials (which include both the adhesive and the matrix of the composite under study) has been described to increase with the strain rate [54]. Such effect may be due to secondary connections between the polymeric chains, which are affected by both the temperature and the strain rate and result in higher energy absorption [55]. The secondary connections have been previously identified as responsible for a significant level of rate sensitivity of material properties, which occurs close to strain rate and temperature conditions related to the β-transition viscoelastic behaviour [56].

3.2.3.2. Joints with dissimilar substrates. The energy absorbed results obtained from SLJs made with dissimilar substrates combinations tested under impact conditions as a function of different temperatures (LT, RT and HT) are shown in Fig. 13.

Independently of the type of dissimilar substrates configuration, the higher values of energy absorbed were obtained for tests performed at

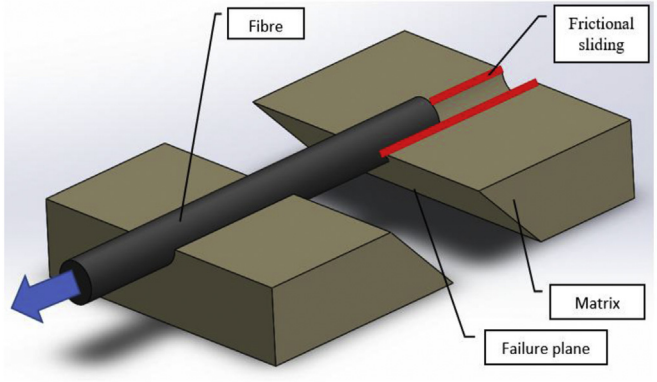

Fig. 12. Schematic representation of the frictional sliding phenomenon of a fibre in a matrix in composite materials.

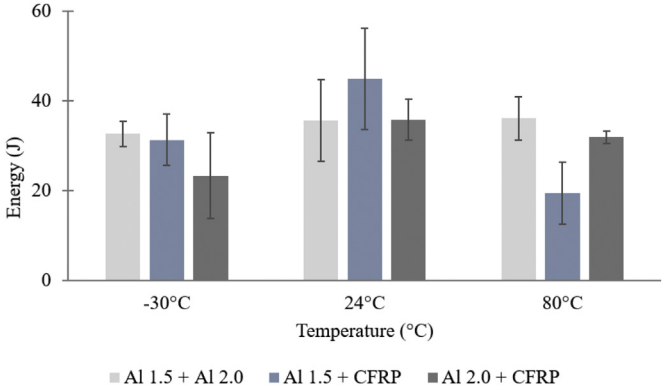

Fig. 13. Energy absorbed by SLJs using dissimilar substrates (CFRP and aluminium alloys) tested at impact conditions as a function of temperature.

RT. This phenomenon can be explained by the fact that the adhesive, due to its viscoelastic and viscoplastic behaviour as a function of temperature, becomes stiffer at LT and more flexible at HT, as the testing temperature approaches the T_g.

3.3. Analysis of the combined effect of temperature and strain-rate

This section aims to describe the evolution of the combined effect of temperature and strain rate on the mechanical behaviour of SLJs made using similar and dissimilar substrates combinations, by using three dimensional plots of the failure load and absorbed energy.

3.3.1. Failure load

3.3.1.1. Joints with similar substrates. The failure load of SLJs made using similar substrates combinations (Al 5754-H22 (Al 1.5), Al 6060-T6 (Al 2.0) and CFRP), as a function of temperature and strain rate, is shown from Figs. 14 to 16.

Independently of the type of substrate used, higher values of failure load were found with the increase of strain rate. Regarding SLJs made using aluminium substrates (Al 5754-H22 (Al 1.5) or Al 6060-T6 (Al 2.0)), it can be concluded that the influence of the testing temperature (LT, RT and HT) mainly affects the adhesive properties, with the failure load slightly diminishing with the increase of temperature. In the case of SLJs made with CFRP substrates, a peak in the value of the failure load was found at RT, which revealed to be independent of the strain rate. The higher values of failure load were found for SLJs made with CFRP substrates, such behaviour (in comparison with the aluminium substrates (Al 5754-H22 (Al 1.5) or Al 6060-T6 (Al 2.0)) can be explained by the higher stiffness of this material, allowing the adhesive to

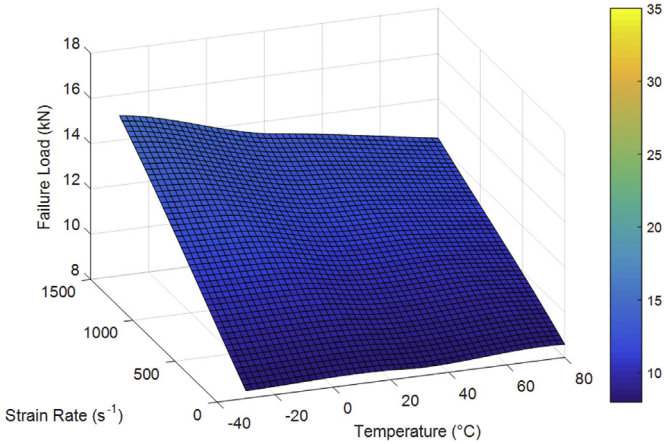

Fig. 14. Failure load of SLJs with Al 5754-H22 (Al 1.5) similar substrates as function of temperature (LT, RT and HT) and strain rate.

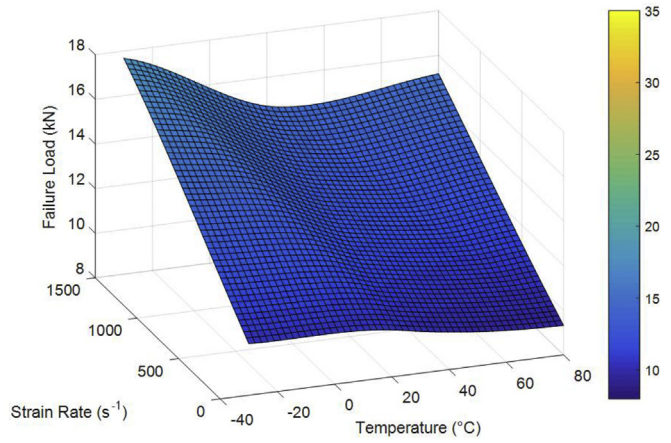

Fig. 15. Failure load of SLJs with Al 6060-T6 (Al 2.0) similar substrates as function of temperature (LT, RT and HT) and strain rate.

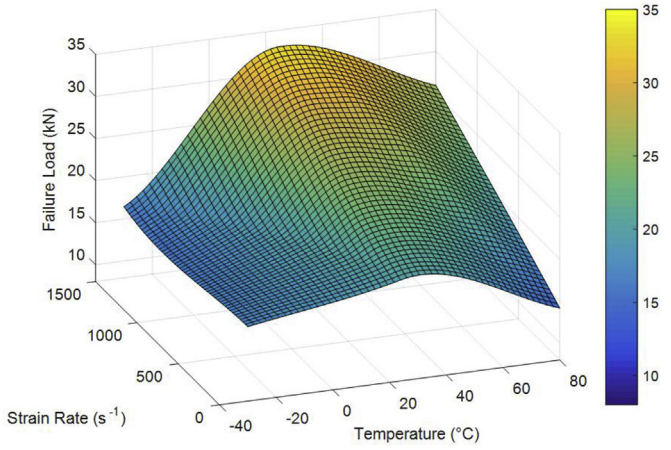

Fig. 16. Failure load of SLJs with CFRP similar substrates as function of temperature (LT, RT and HT) and strain rate.

undergo higher shear loads instead of peeling.

The main conclusion is that the improvement of the SLJs, in terms of failure load, was achieved with the increase of the strain rate, for all the substrates tested (CFRP, Al 5754-H22 (Al 1.5) or Al 6060-T6 (Al 2.0)). However, the influence of testing temperature (LT, RT and HT) has a significant effect in SLJs made with CFRP substrates, and for joints with aluminium substrates (Al 5754-H22 (Al 1.5) or Al 6060-T6 (Al 2.0)) such effect is almost negligible.

3.3.1.2. Joints with dissimilar substrates. The failure load of SLJs made using dissimilar substrates combinations (Al 5754-H22 (Al 1.5), Al 6060-T6 (Al 2.0) and CFRP), as a function of temperature and strain rate, is shown from Figs. 17–19.

Joints with the dissimilar substrates combination of Al 5754-H22 (Al 1.5) + CFRP presented a slight increase of failure load when increasing the testing temperature and the strain rate, although this variation falls under the standard deviation, meaning that the influence of testing temperature does not play a major role. The same behaviour was found for the two other dissimilar substrates combinations, Al 600-T6 (Al 2.0) + CFRP and Al 5754-H22 (Al 1.5) + Al 6060-T6 (Al 2.0).

It can be therefore concluded that for joints made with dissimilar substrates configurations, the failure load will be imposed by the weakest substrate being used, as expected. With the increase of strain rate there was observed an improvement of the SLJs performance, that was regarding of the type of substrate combination. Every joint configuration using dissimilar substrates has at least an aluminium

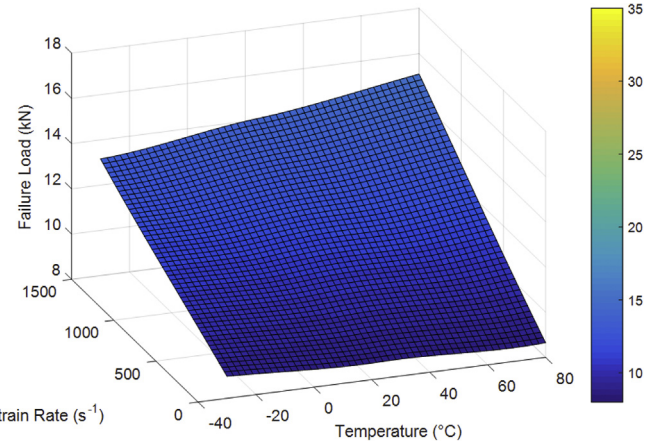

Fig. 17. Failure load of SLJs with Al 5754-H22 (Al 1.5) + CFRP dissimilar substrates as function of temperature (LT, RT and HT) and strain rate.

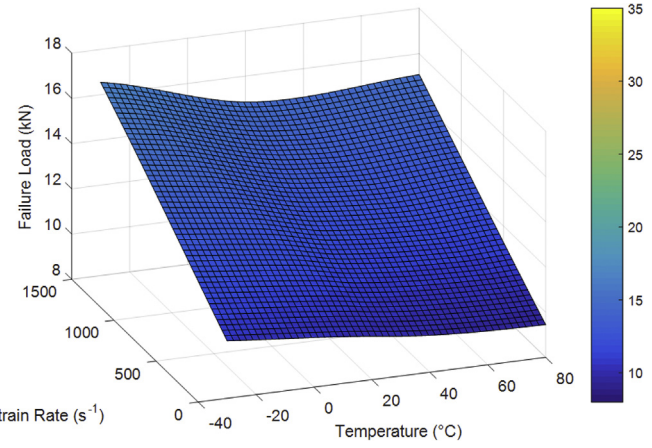

Fig. 18. Failure load of SLJs with Al 6060-T6 (Al 2.0) + CFRP dissimilar substrates as function of temperature (LT, RT and HT) and strain rate.

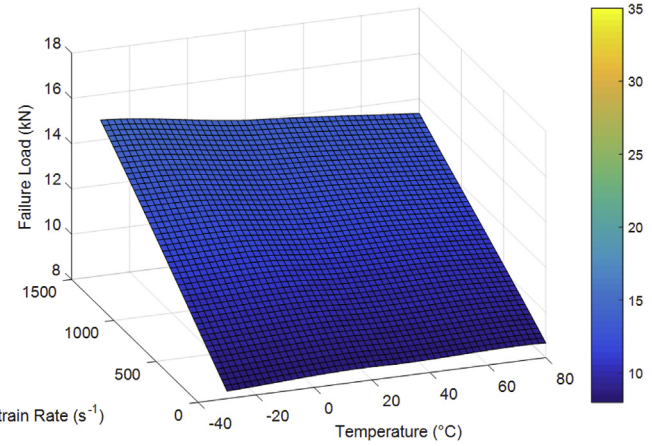

Fig. 19. Failure load of SLJs with Al 5754-H22 (Al 1.5) + Al 6060-T6 (Al 2.0) dissimilar substrates as function of temperature (LT, RT and HT) and strain rate.

substrate (Al 5754-H22 (Al 1.5) or Al 6060-T6 (Al 2.0)), therefore, the behaviour in terms of failure load is the same as for SLJs made using only aluminium, as the failure was controlled manly by the onset of its plastic deformation.

3.3.2. Energy absorbed

3.3.2.1. Joints with similar substrates. The values of energy absorbed as

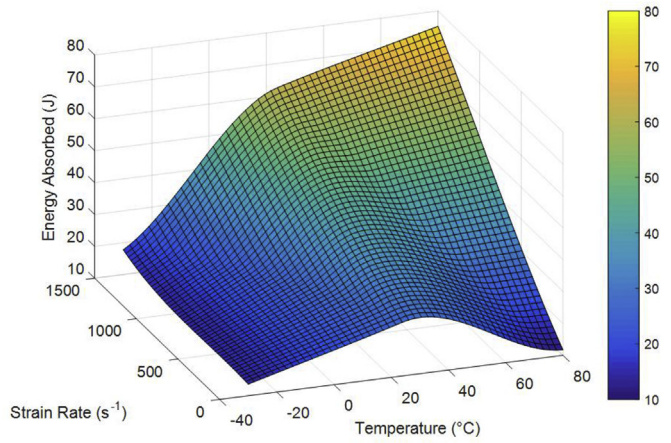

Fig. 20. Energy absorbed by SLJs with CFRP similar substrates as function of temperature and strain rate.

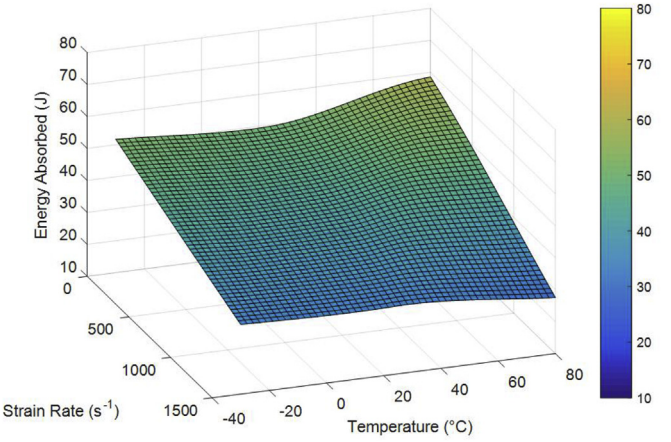

Fig. 21. Energy absorbed by SLJs with Al 5754-H22 (Al 1.5) similar substrates as function of temperature (LT, RT and HT) and strain rate.

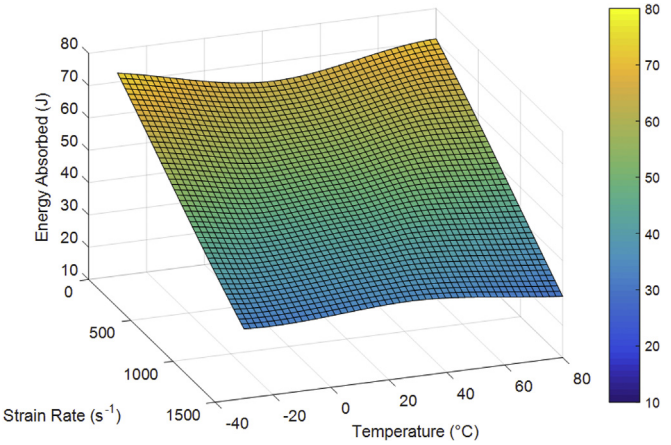

Fig. 22. Energy absorbed by SLJs with Al 6060-T6 (Al 2.0) similar substrates as function of temperature (LT, RT and HT) and strain rate.

a function of strain rate and testing temperatures (LT, RT and HT), for SLJs made using similar combination of substrates (CFRP, AL 5754-H22 (Al 1.5) and Al 6060-T6 (Al 2.0)), are presented from Figs. 20–22. It can be noted that, for the results of SLJs made with CFRP substrates (Fig. 20), the axis orientation is different than the ones with aluminium substrates (Fig. 21 (Al 5754-H22 (Al 1.5)) and Fig. 22 (Al 6060-T6 (Al 2.0)) to improve the visualization of the graphic surface.

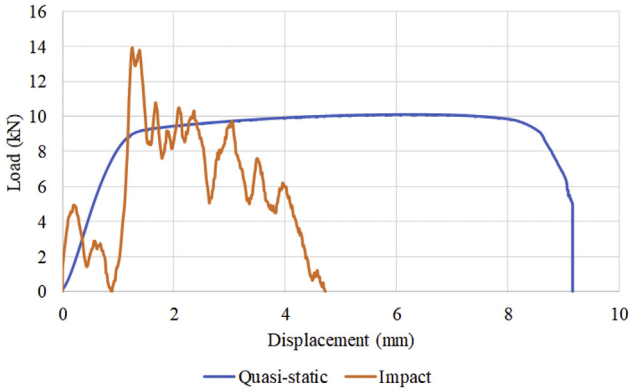

Fig. 23. P-δ curves of SLJs with Al 6060-T6 (Al 2.0) similar substrates tested at RT as function of strain rate.

Notwithstanding the fact that the failure load increases with the strain rate, SLJs with aluminium alloys substrates (Al 5754-H22 (Al 1.5) or Al 6060-T6 (Al 2.0)) also present higher energy absorption capabilities at quasi-static conditions, something especially evident in Fig. 23. This occurrence can be explained by the fact that, when impact conditions are presented, the shock wave is transmitted through the overlap, where the adhesive, due to its viscoelastic behaviour at high strain rates, does not allow large deformations, and propagates along the length of the substrate until encounters a weak spot, that is the hole in the clamped zone, where the stress concentration is high. Early failure occurs in this weakened section with limited energy absorption. The propagation of the stress wave along the joint during an impact test is shown in Fig. 24, created using finite element analysis with Abaqus CAE©. Whereas, in a quasi-static situation, all the SLJs were under a uniformly increasing stress state, until, at some point, the onset of plastic deformation occurs in the region of the overlap. Under quasi-static loads, the adhesive is more ductile due to the relaxation of the polymeric chains, thus permitting larger deformations in both substrates and absorbing more energy. Fig. 25 shows schematically the evolution of stress distribution during a quasi-static test.

Figs. 24 and 25 also clearly demonstrate that the performance of adhesively bonded joints under impact is not only a function of the intrinsic material properties under large strain rates but also of the stress fields present.

Regarding the SLJs with similar CFRP substrates, there is a noticeable increase in the energy absorption level under impact conditions, which can result from a combination of factors. While both the adhesive and the CFRP matrix become tougher and more flexible with temperature, the phenomenon of frictional sliding of the fibre within the matrix during the delamination process might be responsible for a significant part of the energy absorption.

3.3.2.2. Joints with dissimilar substrates. The values of energy absorbed as a function of strain rate and testing temperatures (LT, RT and HT), for SLJs made using dissimilar combination of substrates (Al 5754-H22 (Al 1.5), Al 6060-T6 (Al 2.0) and CFRP), are presented from Figs. 26–28.

Regarding the SLJs with dissimilar substrates, for the combination of aluminium Al 6060-T6 (Al 2.0) + CFRP, the behaviour encountered is consistent with the one presented by SLJs with similar substrates of Al 6060-T6. In these cases, lower energy is absorbed for quasi-static conditions, since only the aluminium Al 6060-T6 (Al 2.0) substrate tends to significantly deform. The lower peak of energy absorbed for impact conditions at LT is due to the failure mode which was by delamination of CFRP substrate. Joints with dissimilar substrates of aluminium (Al 5754-H22 (Al 1.5) and Al 6060-T6 (Al 2.0)) offer strong LT dependence with regards to absorbed energy. The dissimilar joints with CFRP substrates were slightly more sensitive to temperature, although

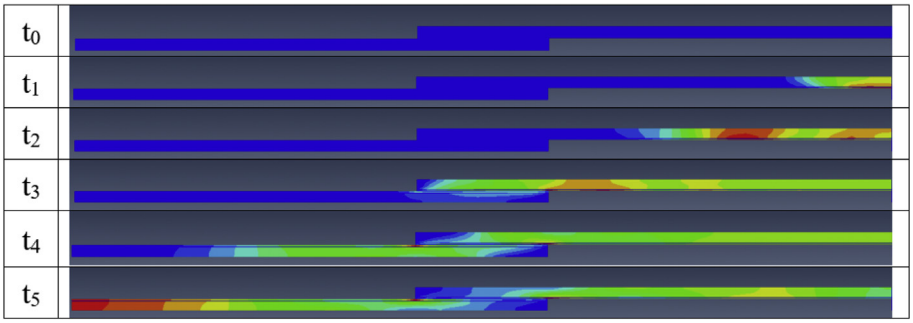

Fig. 24. Stress propagation through the SLJ in impact conditions.

the effect was much less pronounced than that of SLJs made with similar substrates of CFRP.

4. Conclusions

An in-depth analysis of the quasi-static and impact behaviour of dissimilar adhesive joints subjected to a wide range of temperatures was performed in this work. The main conclusions drawn are therefore presented:

- The CFFR-CFRP joint configuration exhibited the highest failure load for all conditions except for the impact test at −30 °C, where the performance of all joints under study was similar. The aluminium joints with similar substrates exhibited low temperature sensitivity and failure loads significantly lower than those exhibited by the CFRP-CFRP joints.
- The performance of the dissimilar joints, in terms of maximum load, was found to be limited by the aluminium deformation in all conditions tested.
- In quasi-static conditions the aluminium-aluminium similar joints absorbed the most energy for all temperatures tested due to large level of plastic deformation present. In impact conditions, the CFRP-CFRP joints were those that absorbed more energy due to frictional sliding during delamination. At low temperatures this effect is less pronounced, and the aluminium alloys absorb more energy;
- A significant difference in absorbed energy from quasi-static to impact was found when testing the joints with aluminium substrates. This is since failure mostly occurred in the clamped section during impact testing. The locus of failure does not allow to directly assess the influence of the factors under study on the adhesive, but still enables the comparative study of joint performance, if failure outside the adhesive layer is considered as the optimal type of failure.
- The effect of temperature on joint performance is only pronounced for the CFRP-CFRP SLJs, due to the large temperature dependence of these materials as they approach T_g. As expected, in joints bonded with a crash resistant adhesive and containing aluminium substrates the effect of temperature is very limited, as the substrate is temperature insensitive and the adhesive, although losing strength, becomes tougher.

As a final remark, it is possible to conclude that dissimilar adhesive joints, if used in conjunction with modern crash resistant adhesives, can effectively be used for the construction of automotive structures, without significant sacrifices in joint performance, including energy

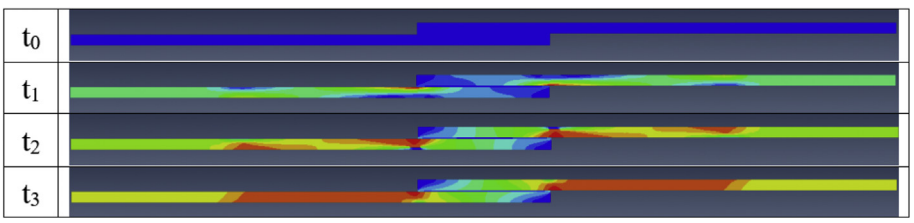

Fig. 25. Stress propagation through the SLJ in quasi-static conditions.

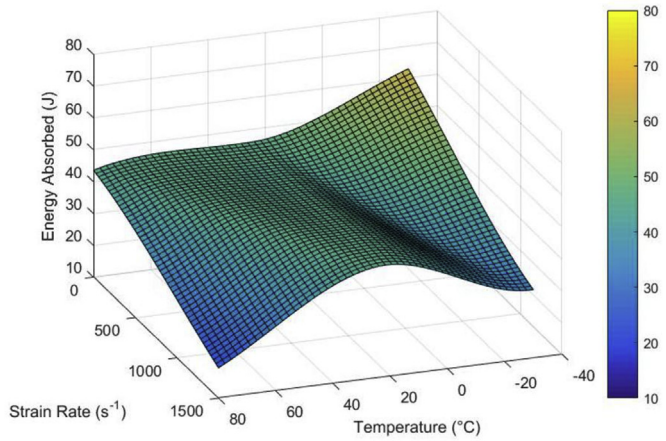

Fig. 26. Energy absorbed by SLJs with Al 5754-H22 (Al 1.5) + CFRP dissimilar substrates as function of temperature (LT, RT and HT) and strain rate.

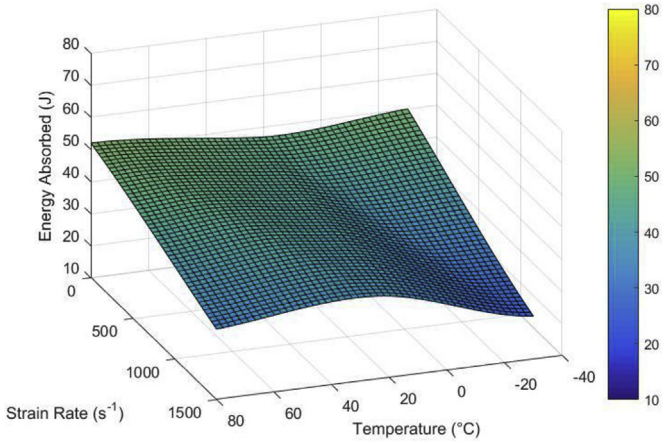

Fig. 27. Energy absorbed by SLJs with Al 6060-T6 (Al 2.0) + CFRP dissimilar substrates as function of temperature (LT, RT and HT) and strain rate.

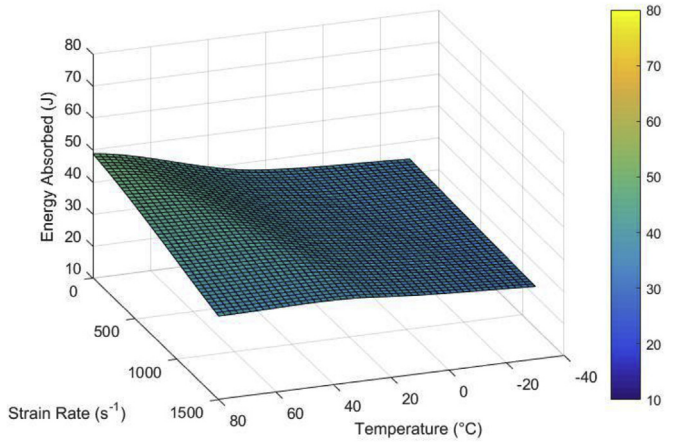

Fig. 28. Energy absorbed by SLJs with Al 5754-H22 (AL 1.5) + Al 6060-T6 (Al 2.0) dissimilar substrates as function of temperature (LT, RT and HT) and strain rate.

absorption under impact.

Acknowledgments

The authors gratefully acknowledge the funding of Project NORTE-01-0145-FEDER-000022 - SciTech - Science and Technology for Competitive and Sustainable Industries, co-financed by Programa Operacional Regional do Norte (NORTE2020), through Fundo Europeu de Desenvolvimento Regional. The authors would also like to thank NAGASE ChemteX® for the financial support provided, as well to Aston Martin Lagonda® for supplying the aluminium substrates.

References

[1] da Silva LFM, das Neves PJ, Adams R, Spelt J. Analytical models of adhesively bonded joints—Part I: literature survey. Int J Adhesion Adhes 2009;29(3):319–30.
[2] da Silva LFM, Öchsner A, Adams RD. Handbook of adhesion technology. second ed. Springer Science & Business Media; 2018.
[3] Machado J, Marques E, da Silva L. Adhesives and adhesive joints under impact loadings: an Overview. J Adhes 2017. https://doi.org/10.1080/00218464.2017.1282349.
[4] Cheng S, Chen D, Shi Y. Analysis of adhesive-bonded joints with nonidentical adherends. J Eng Mech 1991;117(3):605–23.
[5] Sawa T, Liu J, Nakano K, Tanaka J. A two-dimensional stress analysis of single-lap adhesive joints of dissimilar adherends subjected to tensile loads. J Adhes Sci Technol 2000;14(1):43–66.
[6] Reis PNB, Ferreira JAM, Antunes F. Effect of adherend's rigidity on the shear strength of single lap adhesive joints. Int J Adhesion Adhes 2011;31(4):193–201.
[7] Afendi M, Teramoto T, Bakri HB. Strength prediction of epoxy adhesively bonded scarf joints of dissimilar adherends. Int J Adhesion Adhes 2011;31(6):402–11.
[8] Gültekin K, Akpinar S, Özel A, Öner GA. Effects of unbalance on the adhesively bonded composites-aluminium joints. J Adhes 2017;93(9):674–87.
[9] Harris JA, Adams RD. An assessment of the impact performance of bonded joints for use in high energy absorbing structures. Proc IME C J Mech Eng Sci 1985;199(2):121–31.
[10] Beevers A, Ellis MD. Impact behaviour of bonded mild steel lap joints. Int J Adhesion Adhes 1984;4(1):13–6.
[11] Yokoyama T, Shimizu H. Evaluation of impact shear strength of adhesive joints with the split Hopkinson bar. JSME Int J A Solid Mech Materl Eng 1998;41(4):503–9.
[12] Sato C, Ikegami K. Dynamic deformation of lap joints and scarf joints under impact loads. Int J Adhesion Adhes 2000;20(1):17–25.
[13] Goglio L, Rossetto M. Impact rupture of structural adhesive joints under different stress combinations. Int J Impact Eng 2008;35(7):635–43.
[14] Raykhere SL, Kumar P, Singh R, Parameswaran V. Dynamic shear strength of adhesive joints made of metallic and composite adherents. Mater Des 2010;31(4):2102–9.
[15] Sankar HR, Adamvalli M, Kulkarni PP, Parameswaran V. Dynamic strength of single lap joints with similar and dissimilar adherends. Int J Adhesion Adhes 2015;56:46–52.
[16] He B, Ge D. Dynamic strength of adhesively bonded composite joints with similar and dissimilar assembled adherends. J Reinforc Plast Compos 2017;36(23):1683–92.
[17] Marques EAS, da Silva LFM, Banea MD, Carbas RJC. Adhesive joints for low-and high-temperature use: an Overview. J Adhes 2015;91(7):556–85.
[18] Viana G, Costa M, Banea MD, da Silva LFM. A review on the temperature and moisture degradation of adhesive joints. Proc IME J Mater Des Appl 2016. https://doi.org/10.1177/1464420716671503.
[19] Sharon G, Dodiuk H, Kenig S. Effects of loading rate and temperature on the mechanical properties of structural adhesives containing a Carrier. J Adhes 1989;31(1):21–31.
[20] Banea M, De Sousa F, Da Silva L, Campilho R, de Pereira AB. Effects of temperature and loading rate on the mechanical properties of a high temperature epoxy adhesive. J Adhes Sci Technol 2011;25(18):2461–74.
[21] Anes V, Pedro R, Henriques E, Freitas M, Reis L. Bonded joints of dissimilar adherends at very low temperatures-An adhesive selection approach. Theor Appl Fract Mech 2016;85:99–112.
[22] Qin G, Na J, Tan W, Mu W, Ji J. Failure prediction of adhesively bonded CFRP-Aluminum alloy joints using cohesive zone model with consideration of temperature effect. J Adhes 2018:1–24.
[23] ISO. EN 527-2 Plastics–Determination of tensile properties. EN: ISO; 1996.
[24] Banea MD, da Silva LFM, Campilho RDSG. High temperature adhesives for aerospace applications vol. 23. Annals of "Dunarea de Jos" University of Galati Fascicle XII: Welding Equipment and Technology; 2012. p. 16–20.
[25] Banea MD, da Silva LFM. Mechanical characterization of flexible adhesives. J Adhes 2009;85(4–5):261–85.
[26] Gilat A, Goldberg RK, Roberts GD. Strain rate sensitivity of epoxy resin in tensile and shear loading. ASCE J Aerospace Eng 2007;20:75–89.
[27] Takiguchi M, Izumi S, Yoshida F. Rate-dependent shear deformation of ductile acrylic adhesive and its constitutive modelling. Proc IME C J Mech Eng Sci 2004;218(6):623–9.
[28] ISO 11003-2 Determination of shear behaviour of structural adhesives - Part 2: tensile test method using thick adherends. First issue 2001, last review 2012.
[29] Lopes RM. Comparação dos ensaios DCB e TDCB para determinação da tenacidade em tração de adesivos estruturais. 2014.
[30] ASTM D3433-99. Standard test method for fracture strength in cleavage of adhesives in bonded metal joints vol. 2012. 2012.
[31] Azevedo J, Campilho R, da Silva F, Faneco T, Lopes R. Cohesive law estimation of adhesive joints in mode II condition. Theor Appl Fract Mech 2015;80:143–54.
[32] Saldanha DFS, Canto C, da Silva LFM, Carbas RJC, Chaves FJP, Nomura K, et al. Mechanical characterization of a high elongation and high toughness epoxy adhesive. Int J Adhesion Adhes 2013;47:91–8.
[33] Avendano R, Carbas RJC, Chaves FJP, Costa M, da Silva LFM, Fernandes AA. Impact loading of single lap joints of dissimilar lightweight adherends bonded with a crash-resistant epoxy adhesive. J Eng Mater-T Asme 2016;138(4).
[34] Zgoul M, Crocombe AD. Numerical modelling of lap joints bonded with a rate-dependent adhesive. Int J Adhesion Adhes 2004;24(4):355–66.
[35] Avendano R, Carbas RJC, Marques EAS, da Silva LFM, Fernandes AA. Effect of temperature and strain rate on single lap joints with dissimilar lightweight adherends bonded with an acrylic adhesive. Compos Struct 2016;152:34–44.
[36] Marques EAS, Banea MD, da Silva LFM, Carbas RJC, Sato C. Effect of low temperature on tensile strength and mode I fracture energy of a room temperature vulcanizing silicone adhesive. J Test Eval 2015;44(3):1284–93.
[37] Araújo HAM, Machado JJM, Marques EAS, da Silva LFM. Dynamic behaviour of composite adhesive joints for the automotive industry. Compos Struct 2017;171:549–61.
[38] Machado J, Marques E, Campilho R, da Silva L. Mode I fracture toughness of CFRP as a function of temperature and strain rate. J Compos Mater 2016;51(23):3315–26.
[39] Harding J, Welsh LM. A tensile testing technique for fibre-reinforced composites at impact rates of strain. J Mater Sci 1983;18(6):1810–26.
[40] Campilho RDSG. Repair of composite and wood structures. Instituto Superior de Engenharia do Porto; 2009.
[41] Machado JJM, Marques EAS, Campilho RDSG, da Silva LFM. Mode II fracture toughness of CFRP as a function of temperature and strain rate. Compos B Eng 2017;114:311–8.
[42] Fitton MD, Broughton JG. Variable modulus adhesives: an approach to optimised joint performance. Int J Adhesion Adhes 2005;25(4):329–36.
[43] da Silva L, Adams R. Joint strength predictions for adhesive joints to be used over a wide temperature range. Int J Adhesion Adhes 2007;27(5):362–79.
[44] da Silva LFM, Adams RD. Adhesive joints at high and low temperatures using similar and dissimilar adherends and dual adhesives. Int J Adhesion Adhes 2007;27(3):216–26.
[45] Abbadi M, Hähner P, Zeghloul A. On the characteristics of Portevin–Le Chatelier bands in aluminum alloy 5182 under stress-controlled and strain-controlled tensile testing. Mater Sci Eng 2002;337(1):194–201.
[46] Clausen AH, Børvik T, Hopperstad OS, Benallal A. Flow and fracture characteristics of aluminium alloy AA5083–H116 as function of strain rate, temperature and triaxiality. Mater Sci Eng 2004;364(1):260–72.
[47] Naka T, Yoshida F. Deep drawability of type 5083 aluminium–magnesium alloy sheet under various conditions of temperature and forming speed. J Mater Process Technol 1999;89:19–23.
[48] Thornton P. The crush behavior of pultruded tubes at high strain rates. J Compos Mater 1990;24(6):594–615.
[49] Farley GL. The effects of crushing speed on the energy-absorption capability of composite tubes. J Compos Mater 1991;25(10):1314–29.
[50] Lauke B, Schultrich B, Barthel R. Contribution to the micromechanical interpretation of fracture work of short-fibre-reinforced thermoplastics. Compos Sci Technol 1985;23(1):21–35.
[51] Gupta VB, Mittal RK, Goel M. Energy absorbing mechanisms in short-glass-fibre-reinforced polypropylene. Compos Sci Technol 1990;37(4):353–69.
[52] Lavielle L, Lamouri S. Polymer-polymer friction: adhesion dependence. Lubric Sci 1995;12(2):125–31.

[53] Tanoglu M, McKnight SH, Palmese GR, Gillespie Jr. J. The effects of glass-fiber sizings on the strength and energy absorption of the fiber/matrix interphase under high loading rates. Compos Sci Technol 2001;61(2):205–20.
[54] Perkins WG. Polymer toughness and impact resistance. Polym Eng Sci 1999;39(12):2445–60.
[55] Turley SG, Keskkula H. A survey of multiple transitions by dynamic mechanical methods. Journal of Polymer Science: polymer Symposia. Wiley Online Library; 1966. p. 69–87.
[56] Mulliken A, Boyce M. Mechanics of the rate-dependent elastic–plastic deformation of glassy polymers from low to high strain rates. Int J Solid Struct 2006;43(5):1331–56.

Paper 9

Content of Paper 9

Abstract

1. Introduction

2. Experimental details

2.1. Material and properties

2.1.1. Adhesives

2.1.2. CFRP

2.2. Fabrication and testing

2.2.1. Preparation of CFRP plates

2.2.2. SLJ geometry and manufacture

2.2.3. Quasi-static testing procedure

2.2.4. Dynamic testing procedure

3. Results

3.1. Experimental data

3.1.1. Quasi-static tests

3.1.2. Fracture surface of quasi-static tests

3.1.2.1. SLJs using a single adhesive

3.1.2.2. SLJs using mixed adhesives

3.1.3. Impact tests

3.1.4. Fracture surface of quasi-static tests

3.1.4.1. SLJs using a single adhesive

3.1.4.2. SLJs using mixed adhesives

3.2. Comparison between quasi-static and impact tests

3.3. Comparison between CFRP and steel substrates

4. Conclusions

References

Composites Part B 138 (2018) 243–255

Contents lists available at ScienceDirect

Composites Part B

journal homepage: www.elsevier.com/locate/compositesb

Improvement in impact strength of composite joints for the automotive industry

J.J.M. Machado[a], P.M.-R. Gamarra[b], E.A.S. Marques[a], Lucas F.M. da Silva[b,*]

[a] Instituto de Ciência e Inovação em Engenharia Mecânica e Engenharia Industrial (INEGI), Rua Dr. Roberto Frias, 4200-465 Porto, Portugal
[b] Departamento de Engenharia Mecânica, Faculdade de Engenharia (FEUP), Universidade do Porto, Rua Dr. Roberto Frias, 4200-465 Porto, Portugal

ARTICLE INFO

Keywords:
CFRP
Mixed adhesive joints
Single lap joints
Quasi-static
Impact

ABSTRACT

The use of composite structures in the automotive industry aims to produce vehicles able to meet both fuel economy and safety standards. This work focused on the improvement of static and impact strength of composite adhesive joints, avoiding early delamination of the composite. The techniques applied are mixed adhesive combinations (use of two adhesives in one overlap) and the use of crash resistant adhesives. Experimental results demonstrated that a crash resistant adhesive provides the best mechanical performance under quasi-static and impact loads. A mixed adhesive configuration provided good results and improvements over single adhesives.

1. Introduction

High tech transportation industries are constantly under pressure to produce better performing structures [1], with lower weights and higher strength, being at the same time capable of withstanding impact without compromising the integrity of the structure. This has led to an increase in the use of adhesive joints and composite materials, creating the necessity of evaluating the effect of impact loads in the affected components [2]. However, most materials used in these structures exhibit some form of strain rate sensitivity, which coupled with the presence of inertial effects makes the impact behaviour of an adhesive joint very different from its static behaviour. To fully understand how large strain rates affect composite joints, it is therefore important to study in detail the strain rate dependency of adhesives, substrates and of the complete joint [3–5].

The effect of strain rate in carbon fibre reinforced polymers (CFRP) has been widely studied by different authors, due to their importance in the mechanical response of composite structures [6–8]. Harding and West [9] and Taniguchi et al. [10] demonstrated that while the tensile properties of unidirectional CFRP were not influenced by the strain rate, in the transverse direction the composite properties do have strong dependence of strain rate, as in this case the main contributor for strength is the matrix and not the fibres. Similarly, Körber et al. [11] showed that strain rate does not have a significant effect on the longitudinal tensile modulus and strength but influences the transverse tensile modulus and strength. In 2000, Hou and Ruiz [12] concluded that the properties which are dominated by the matrix are: compression strength, Poisson's ratio, in-plane shear modulus, shear modulus and shear strength, being those properties strain rate dependent; the properties dominated by the fibres are: tensile modulus and strength which are virtually rate independent.

Harris and Adams [13] compared the strength and energy absorption of single lap joints (SLJs) in static and high rates of loading. It was shown that most of the energy absorption comes from the deformation of the adherend material, and not from the adhesive. To ensure large energy absorption, the adhesive joints must suffer plastic deformation in the substrates. Similar results were obtained by Saldanha et al. [14], where mild steel joints with a high ductility adhesive were tested under static and drop weight impact tests. The impact strength of joints using composite substrates can also depend on the fibre orientations. In 2012, Galliot et al. [15] studied joints using carbon fibre composite substrates under impact, with varied fibre orientations. For all cases, the failure was found to be caused by delamination in the substrate and the increase in strength under impact was mostly caused by the strain rate dependency of the composite resin. The work of Kadioglu and Adams [16] tested SLJs with flexible adhesives. Their work has determined that, for these materials, when the strain rate increases, the maximum tensile stress also increases and tensile strain to failure decreases.

The selection of the adhesive is crucial to provide impact strength. Some adhesives are optimized to exhibit excellent properties under large strain rates. These adhesives are usually known as crash suitable structural adhesives, combining strength and ductility, with excellent fracture toughness. They can withstand very significant deformation before failure occurs, which is important for energy absorption under impact [17]. A crash resistant suitable structural adhesive has higher initial peel resistance, higher average peel force, and withstands the

* Corresponding author.
E-mail address: lucas@fe.up.pt (L.F.M. da Silva).

https://doi.org/10.1016/j.compositesb.2017.11.038
Received 1 August 2017; Received in revised form 2 November 2017; Accepted 27 November 2017
Available online 28 November 2017
1359-8368/ © 2017 Elsevier Ltd. All rights reserved.

force for a longer period [18,19]. These adhesives also have higher absorption energy, as evidenced by the larger area beneath the load-displacement curves (P-δ) typical of these materials [17]. Several studies such as Loureiro et al. [20], Cho et al. [21] and Saldanha et al. [14] analysed adhesives with diverse mechanical properties, searching an optimal adhesive for the use in the automotive industry and crash suitable adhesives were shown to provide best results. Another possibility for improving the impact strength of adhesive joints is the combination of two adhesives in the same joint, a concept known as the mixed adhesive joint.

Mixed adhesive joints were first introduced by Raphael [22], which proposed the use of a more flexible adhesive at the ends of the overlap and a stiffer stronger adhesive in the central section, ultimately achieving a more uniform stress distribution. Fitton and Broughton [23] demonstrated that the right combination of adhesives with different modulus can reduce stress concentration, as well as change the mode of failure. However, a good selection of adhesives is not only based on the mechanical properties but will also require compatible working characteristics [24]. Hart-Smith [25] recognized that the use of mixed adhesive joints could yield significant improvements in mechanical strength for joints subjected to large temperature range. da Silva and Adams [26] further expanded this concept and predicted improvements in the mechanical behaviour of a joint under a large temperature range. Neves et al. [27] proposed an analytical solution to assess the shear deformation in the substrates as well the nonlinear geometric effect which is characteristic of SLJs, developing a model of mixed adhesive joints and performing a comparison with a finite element analysis. The same authors [28] later performed a parametric study of several joint parameters focusing on the stress distribution of mixed adhesive joints.

da Silva and Lopes [29] experimentally studied mixed adhesive SLJs under static conditions using three different ductile adhesives. Better results were found using mixed adhesive joints compared to a brittle adhesive in single adhesive application. The work of Silva et al. [30] consisted in testing mixed adhesive SLJs with aluminium substrates under static and impact conditions. While the configuration using a stiff epoxy and room temperature vulcanising silicone performed poorly, the configuration with the stiff epoxy and an acrylic adhesive outperformed both adhesives used individually. In addition to the use of mixed adhesives, several other possibilities have been proposed by the researchers to achieve similar effects such as modifying the geometry in the overlap through tapering or fillets [26,31].

It is also important to determine the behaviour of an adhesive joint under impact taking into consideration the influence of the different adhesive and substrates in the joint. Among the first authors to assess the influence of substrate behaviour in butt and shear joints using an instrumented pendulum rig was Perry [32] in 1959. The compliance of the metal substrates was found to be considerably higher than that of the adhesive layer. For such reason, the values obtained in terms of absorbed energy from the impact tests did not revealed the capability of the adhesive of absorbing energy, but it was relative to the adding effect of adhesive and substrates. In 1984, Beevers and Ellis [33] concluded that for joints bonded with a sufficiently strong adhesive and using thin and ductile substrates, the onset of the yield in the substrates had a close relation to the joint failure, namely, similar failure load in quasi-static and impact when using an aluminium alloy (not strain rate dependent) and higher values of failure load under impact for the case of mild steel substrates (strain rate dependent). The failure of composite substrates can also significantly influence the strength of adhesive joints The work of Araújo et al. [34] has demonstrated that modern crash resistant adhesives can cause delamination of composite substrates under impact.

In this work, single and mixed adhesive SLJs with composite substrates were manufactured and experimentally tested under quasi-static and impact loads with the objective of assessing the feasibility of using the mixed adhesive joint concept for increasing the impact strength of adhesive joints. The results revealed that the use of a crash resistant adhesive offers the best mechanical performance in both quasi-static and impact load, although, with this adhesive delamination of CFRP occurs. With the use of mixed adhesives, it was possible to find one combination where the performance of the joint represented an improvement over the use of single adhesives. Finally, a comparison was made between the behaviour of CFRP mixed adhesive joints and the previously tested behaviour of joints using the same concept but using steel substrates.

2. Experimental details

2.1. Material and properties

2.1.1. Adhesives

For this work, five different adhesives were used, two stiff and three flexible adhesives. These adhesives were selected with the aim of testing adhesives with very different mechanical properties. This section lists the adhesives used (ordered from the stiffest to the least stiff) and their main mechanical properties:

1. **Araldite AV 138** (Salt Lake City, UT, USA) – stiff adhesive: An epoxy adhesive with very stiff and brittle mechanical behaviour. When used alone in adhesive joints, it normally leads to low strength due to the large stress concentration it creates. It is therefore a good candidate for obtaining improvements when combined with a second, less stiff adhesive. The properties of this adhesive were determined by da Silva et al. [35].
2. **Nagase-Chemtex XNR6852 E-3** (Osaka, Japan) – stiff adhesive: A one-part system epoxy adhesive, formulated for use in automotive structures. It was selected due to its high strength and ductility, which provide excellent impact behaviour to this adhesive. It is commonly known as a crash resistant adhesive and was selected for this work to represent an actual adhesive employed by the automotive industry. The mechanical properties of this adhesive were determined by Araújo [34].
3. **SikaFast 5211 NT** (Baar, Switzerland): A two-component structural acrylic adhesive with a very fast curing time and good ductility. This adhesive was selected for use in mixed adhesive joints due to its ductile behaviour. Unlike the first two adhesives, this adhesive has not been fully characterized and some of its mechanical properties were obtained from the literature [36].
4. **3M DP 8005** (Maplewood, Minnesota, USA): A two-component structural acrylic adhesive specially formulated to bond polymers such as polyvinyl chloride (PVC), polyvinyl ether (PVE) or polypropylene (PP). This adhesive has good resistance to water, humidity and chemical substances. It has already been tested in mixed adhesive joints, demonstrating good results [30]. The properties were determined by da Silva et al. [37] and Pinto et al. [38].
5. **Momentive RTV 106** (Albany, NY, USA): A silicone rubber acetoxy type adhesive. It is a very ductile adhesive, with excellent thermal properties. It has low mechanical strength but very high ductility, enabling good impact performance [39]. This adhesive was selected for this work as it has already been tested in mixed adhesive joint research with promising results. The properties of this adhesive were determined by Banea et al. [40].

Due to strain rate dependency, knowledge of the material properties at higher testing speeds are necessary to perform accurate numerical simulations. However, the adhesives were not fully characterized for high strain rate (3 m/s). To obtain these values, most of the adhesives were first tested at 1 mm/min and 100 mm/min. An extrapolation process based in a logarithmic trend function was then used to estimate the properties at higher strain rates [41,42], shown in Equation (1).

$$\textit{Property to determine} = A \ln(\dot{\varepsilon}) + B \quad (1)$$

where A and B are constrains obtained from experimental data, and $\dot{\varepsilon}$ is

Table 1
Mechanical properties of the stiff and flexible adhesives (properties not available are marked as n/a).

Adhesive	Test speed (mm/min)	Young's modulus [MPa]	Shear modulus [MPa]	Tensile strength [MPa]	Shear strength [MPa]	Mode I fracture energy [N/mm]	Mode II fracture energy [N/mm]
AV 138	1	4890	1560	41	30.2	0.35	4.9
	100			49.1	36.2		
	180000			72.1	45.9		
XNR6852 E-3	1	1728	665	51.5	44.9	6.4	51
	100		645	60.5	44	7.1	58.2
	180000		603	77.7	42.9	8	64.1
SikaFast 5211 NT	1	260	n/a	5.06	n/a	n/a	n/a
	100	n/a					
	180000	n/a					
DP 8005	1	590	159	6.3	8.4	1.1	6
	100			13	17.4		
	180000			32	32		
RTV 106	1	1.6	0.86	2.3	1.97	2.73	5
	100						
	180000						

the strain rate in s^{-1}.

Likewise, $\dot{\varepsilon}$ (strain rate) was determined with Equation (2):

$$\dot{\varepsilon} = \frac{v}{L_o} \tag{2}$$

Being v the velocity of the test and L_o the initial calibrated longitudinal deformation length of the specimen section where the strain is measured.

Table 1 summarizes all the adhesive mechanical properties for three different testing speeds, ranging from quasi-static (1 mm/min) to impact (180000 mm/min or 3 m/s).

The properties available in the literature for each adhesive vary, with some having their strain rate dependency fully characterized (XNR6852 E-3) while others only have some properties represented as strain rate dependent (DP 8005 and AV 138).

RTV106 adhesive is a special case, due to the difficulty in testing this material at high strain rates. This adhesive was therefore not considered as strain rate dependent in this work. There is also limited information regarding SikaFast 5211 NT. Some properties are not available in the literature and all correspond to quasi-static loadings.

2.1.2. CFRP

The CFRP specimens used in this work were manufactured with plies of carbon/epoxy pre-preg (SEAL® Texipreg HS 160 RM) which were orientated in a single direction. The elastic properties of this material were previously determined in the work of Campilho [43] in 2009. Table 2 presents the Young's modulus (E), the shear modulus (G), and the Poisson's ratio (v), in the three axis direction (x,y,z), being E_1 the normal direction, E_2 the transverse direction and E_3 the out plane direction. As stated in the introduction, the tensile and shear properties of CFRP are known not to vary significantly with the strain rate.

The mechanical properties of CFRP have been previously experimentally determined for 1 mm/min and 100 mm/min by the authors [6,44]. The properties for high impact speed (3 m/s) have been determined using the same extrapolation process described for the adhesives [34]. Table 3 lists the cohesive properties of CFRP for three testing speeds, and Young's modulus, shear modulus and tensile strength were not found to be strain rate dependent.

Table 2
Properties of CFRP elastic orthotropic [43].

Elastic Modulus (MPa)	Poisson's Ratio	Shear Modulus (MPa)
E_1 = 109000	ν_{12} = 0.342	G_{12} = 4315
E_2 = 8819	ν_{13} = 0.342	G_{13} = 4315
E_3 = 8819	ν_{23} = 0.380	G_{23} = 3200

Table 3
Cohesive properties of CFRP under quasi-static and impact conditions.

Properties	1 mm/min	100 mm/min	180000 mm/min
Young's modulus, E [MPa]	109000	109000	109000
Shear modulus, G [MPa]	4315	4315	4315
Tensile strength, σ_n [MPa]	40	40	40
Shear strength, t_s [MPa]	35	35	35
Fracture energy (mode I), G_{IC} [N/mm]	0.59	0.53	0.39
Fracture energy (mode II), G_{IIC} [N/mm]	1.17	1.04	0.82

2.2. Fabrication and testing

2.2.1. Preparation of CFRP plates

The specimens tested in this work consisted of unidirectional laminates of CFRP cut from bulk laminates, which were produced by hand lay-up and cured in a hot plate press. The bulk laminates, with dimensions of 300 mm by 300 mm, were fabricated by stacking unidirectional 0° lay-up plies (with the aim of obtaining better properties in the loading direction). Each plate had a total of 14 plies of carbon/epoxy pre-preg (SEAL® Texipreg HS 160 RM) with 0.15 mm of ply thickness. The cure cycle applied was 130 °C for 1 h.

Subsequently to the removal from the press, the laminates were cut into smaller specimens using a diamond disc cutting machine. Edge finishing was carried out manually with 120-grit sandpaper to remove the loose fibres and smoothen the sharp edges. Being the CFRP substrates made of 14 plies, a total thickness of 2.1 mm was achieved, and the adhesive thickness used in the SLJ was of 0.2 mm.

2.2.2. SLJ geometry and manufacture

The SLJs were tested with one overlap length of 25 mm for all the different combinations of single and mixed adhesives. The geometry chosen is representative of automotive industry applications, with thin substrates and single overlap bonding (Fig. 1). The overlap of 25 mm was already studied by several authors where a comparison was made with several values of overlap length being tested [23,45,46].

Five different adhesives were used in ten different configurations. In total, eleven different combinations could have been developed. However, the DP 8005 + XNR6852 E-3 combination was discarded due to previously identified adhesive compatibility problems [47]. The adhesive combinations tested in this work are listed below:

- **AV 138** (full overlap) – stiff adhesive;
- **XNR6852 E-3** (full overlap) – stiff adhesive;
- **SikaFast 5211 NT** (full overlap) – flexible adhesive;

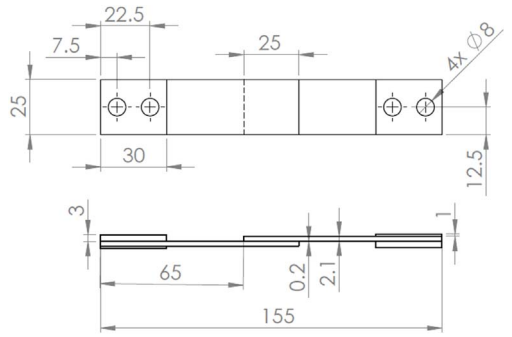

Fig. 1. Geometry of SLJ specimens (dimensions in mm).

- **DP 8005** (full overlap) – flexible adhesive;
- **RTV 106** (full overlap) – flexible adhesive;
- **AV 138** (centre) – stiff adhesive + **SikaFast 5211 NT** (edges) – flexible adhesive;
- **AV 138** (centre) – stiff adhesive + **DP 8005** (edges) – flexible adhesive;
- **AV 138** (centre) – stiff adhesive + **RTV 106** (edges) – flexible adhesive;
- **XNR6852 E-3** (centre) – stiff adhesive + **SikaFast 5211 NT** (edges) – flexible adhesive;
- **XNR6852 E-3** (centre) – stiff adhesive + **RTV 106** (edges) – flexible adhesive.

The mixed adhesive joints used a stiff adhesive in the central section and a flexible adhesive at the overlap ends. The schematic representation of the adhesive ratio used is presented in Fig. 2. This ratio was selected because it has been previously [47] used with good results in joints with metallic substrates. The separation between the two adhesive types is achieved in practice using a 0.2 mm nylon wires which were glued to one of the substrates of each SLJ. This method is minimally intrusive and does not causes voids or large separation between the adhesives in the overlap.

For the manufacture of single adhesive specimens, ASTM D 1002 standard [48] was followed. The curing cycles for all the adhesives used are presented in detail in Table 4.

For the mixed adhesive joints, the curing cycle was governed by the stiff adhesive. Mixed adhesive joints containing XNR6852 E-3 were cured for 3 h at 150 °C, while those containing AV 138 were subjected to 120 °C for 1 h. Due to these cure cycles, differences in mechanical properties are expected between the flexible adhesives cured at room temperature and those cured at high temperatures when used in a mixed adhesive joint. However, these curing cycles were selected according to manufacturing concerns, and therefore the joints must be compared in these different states to consider these practical concerns.

2.2.3. Quasi-static testing procedure

The quasi-static tests were performed using an INSTRON® 3367 (Norwood, Massachusetts, USA) universal testing machine, with a load cell with a capacity of 30 kN. All quasi-static tests were performed at room temperature and with a constant cross head displacement rate of 1 mm/min, corresponding to a shear strain rate of 0.08 s^{-1}. Six specimens were tested for each condition, and for each joint a *P-δ* curve

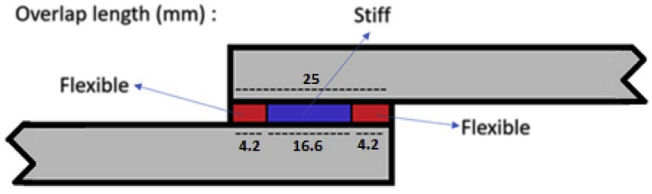

Fig. 2. Schematic representation of the mixed-adhesive configuration.

Table 4
Cure time of the adhesives employed.

Adhesive:	Curing cycle:
AV 138	1 h (120 °C)
XNR6852 E-3	3 h (150 °C)
SikaFast 5211 NT	2 days (Room temperature)
DP 8005	8–24 h (Room temperature)
RTV106	1 week (Room temperature)

was obtained.

2.2.4. Dynamic testing procedure

For the impact tests, metallic tabs were added to the ends of the composite SLJ specimens. This was performed to align the load, improve the gripping force and preventing hole failure by reinforcing the clamped area.

A Rosand® Instrumented Falling weight impact tester, type 5 H.V. (Stourbridge, West Midlands, U.K), with a load cell with a capacity of 60 kN, was used for the impact tests. This equipment allows to achieve 300 J (using 29 kg of weight) and a maximum impact speed of 4.5 m/s. The procedure consists in dropping a weighted mass, which falls until it impacts a clamp bolted to the lower substrate of the SLJ specimen. In Fig. 3 it is possible to observe the setup used to hold the specimen in position. The speed of the drop, can be defined by selecting a drop height. Likewise, the energy applied in the impact is controlled by adjusting the weight of the impact mass.

The specimens were tested with a speed of 3 m/s. A mass of 26 kg was used for the impactor, corresponding to an impact energy of 117 J, sufficient to break all specimen configurations. For each adhesive configuration, six specimens were tested.

3. Results

3.1. Experimental data

The experimental results presented in this section were obtained by testing six specimens for each adhesive configuration under study. Ten different configurations of adhesive combinations were tested, under

Fig. 3. Setup used to hold the specimen in position for the impact test.

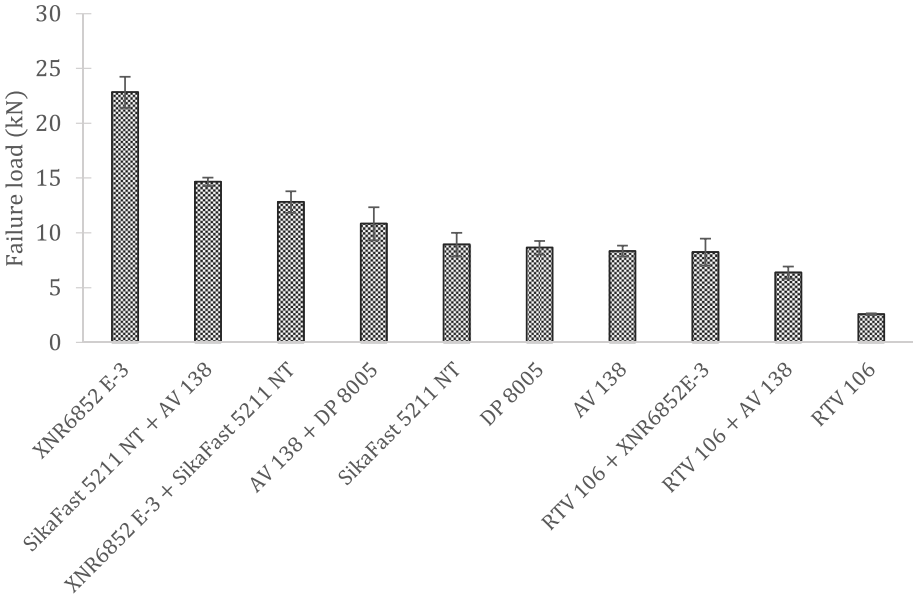

Fig. 4. Comparison of failure load between the single and mixed adhesive SLJs combinations under quasi-static conditions.

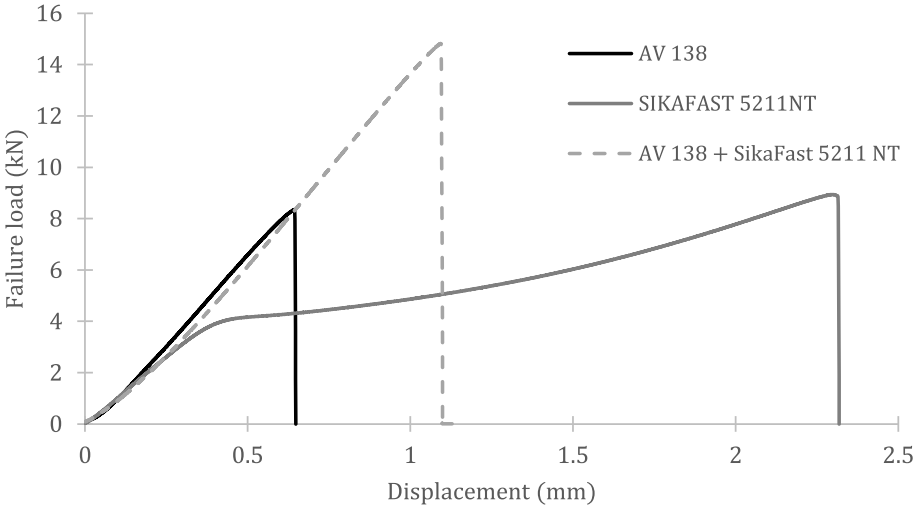

Fig. 5. Comparison between representative P-δ curves of AV 138 and SikaFast 5211 NT single and mixed-adhesive SLJs.

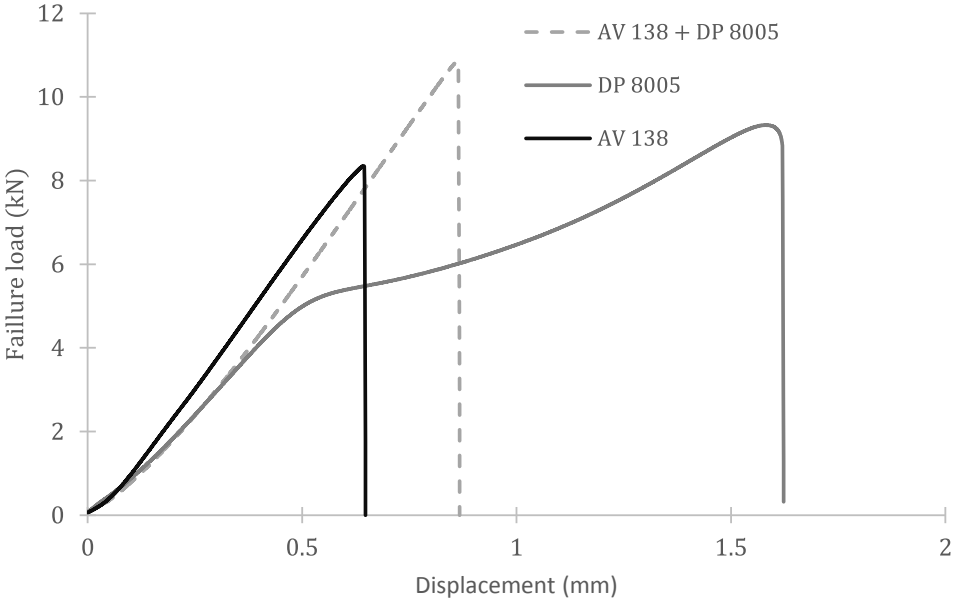

Fig. 6. Comparison between representative P-δ curves of DP 8005 + AV 138 both single and mixed-adhesive SLJs.

Table 5
Summary of the maximum failure load and displacement for all SLJs tested under quasi-static conditions.

Adhesive combination	Failure load (kN)	Standard deviation (kN)	Displacement at maximum load (mm)	Standard deviation (mm)
AV 138	8.34	0.50	0.61	0.04
XNR6852 E-3	22.82	1.42	2.53	0.80
SikaFast 5211 NT	8.93	1.08	2.14	0.20
DP 8005	8.64	0.63	1.58	0.14
RTV 106	2.57	0.08	1.46	0.42
AV 138 + SikaFast 5211 NT	14.65	0.38	1.06	0.04
AV 138 + DP 8005	10.83	1.51	0.94	0.22
AV 138 + RTV 106	6.37	0.56	0.82	0.32
XNR6852 E-3 + SikaFast 5211 NT	12.81	0.97	3.72	2.34
XNR6852 E-3 + RTV 106	8.23	1.23	1.71	0.19

quasi-static loads (1 mm/min) and impact loads (3 m/s). All specimens tested had an overlap length of 25 mm.

3.1.1. Quasi-static tests

The failure loads (a comparison between tests performed using single adhesives and mixed adhesive SLJs was performed) and representative load displacement curves are shown, with a brief description of the failure type exhibited by each specimen.

Fig. 4 shows a comparison of the static failure loads of single and mixed adhesive SLJs with the indication of the standard deviations for all the results.

Analysing this data, it becomes evident that the configuration with XNR6852 E-3 as single adhesive is considerably stronger than any other configuration under study, with full delamination of the CFRP substrate. It is also clear that the two mixed adhesive combinations with XNR6852 E-3 resulted in failure loads below that of the single XNR6852 E-3. The mixed adhesive configuration notably worsened the strength of the joint (36% of the failure load of XNR6852 E-3 when combined with RTV 106 and 47% of the failure load of XNR6852 E-3 when combined with SikaFast 5211 NT).

From the results obtained in the quasi-static experimental tests, two combinations of adhesive have exhibited improvement over the SLJs. The combination of AV 138 with SikaFast 5211 NT acrylic adhesive is one of those combinations. Fig. 5 shows the relevant P-δ curves. It is clear that a synergetic effect is successfully obtained using this adhesive combination, with improved ductility over AV 138 and a much higher failure load than that achieved by each adhesive individually.

The other combination which has led to improvements is the mixed-joint with AV 138 and DP 8005. Fig. 6 shows the P-δ curves obtained with this mixed joint as well as the single adhesive curves.

A summary of all the experimental results under quasi-static conditions is presented in Table 5, in terms of maximum failure load and

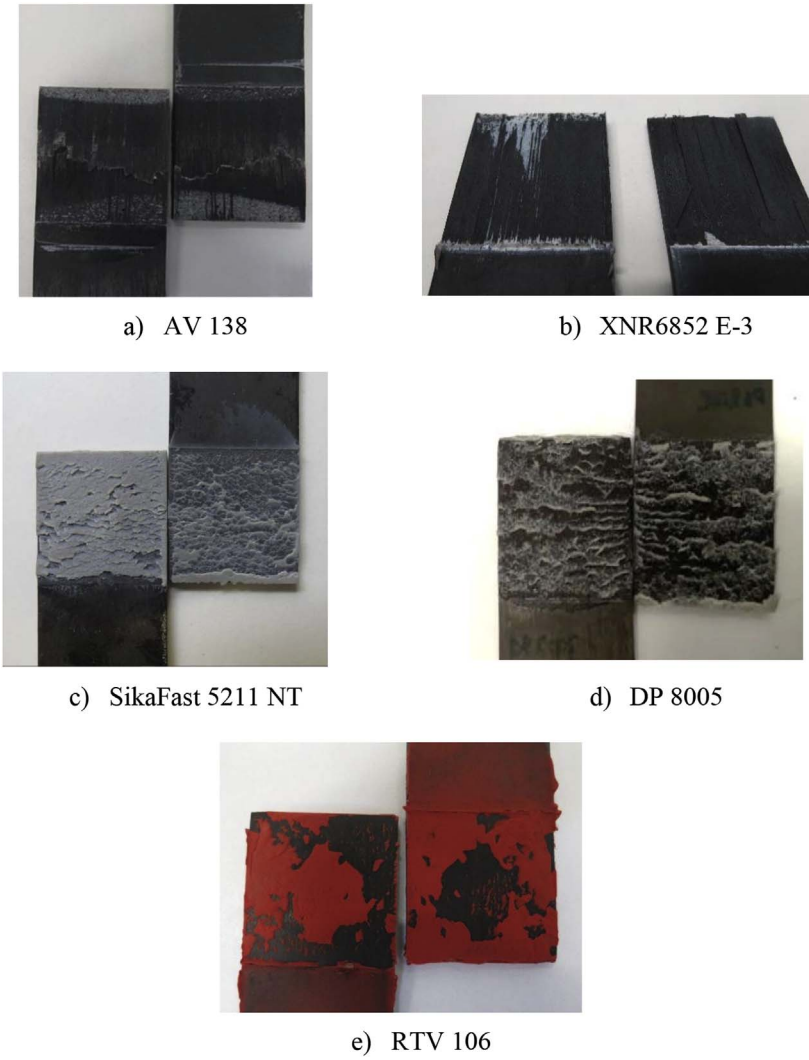

Fig. 7. Typical fracture surfaces of SLJs using a single adhesive configuration tested under quasi-static condition.

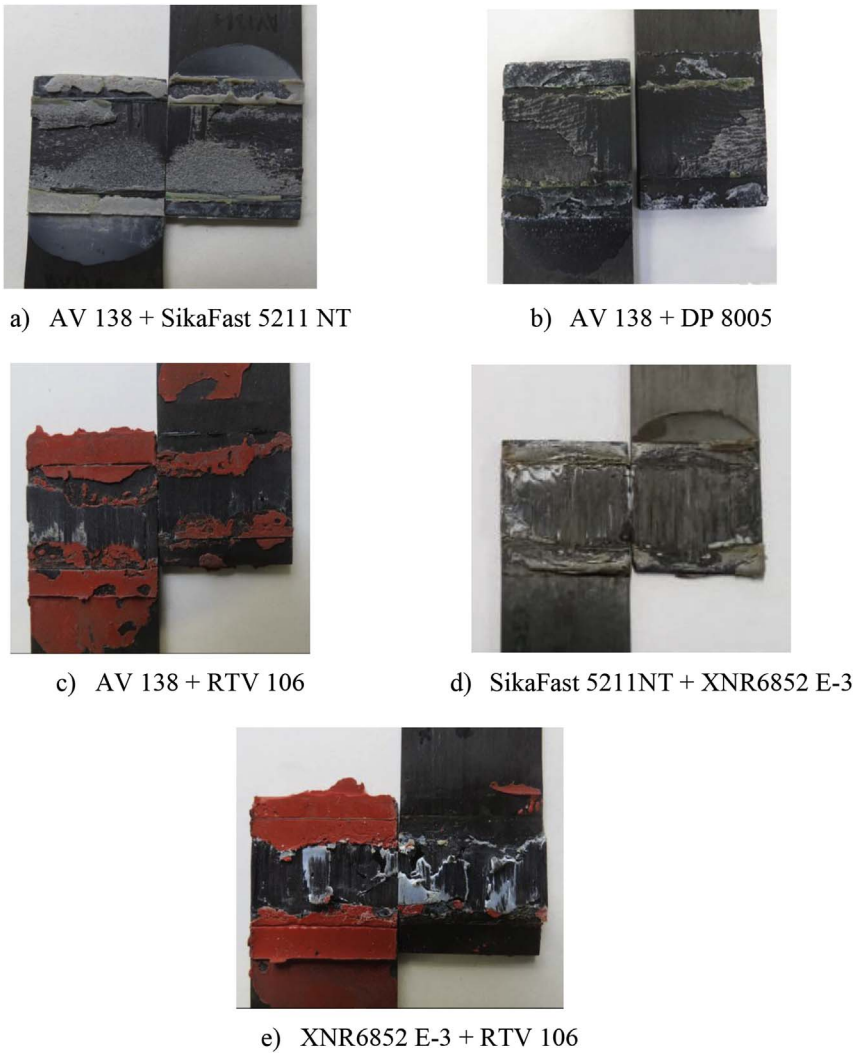

Fig. 8. Typical fracture surfaces of SLJs using mixed adhesive configuration tested under quasi-static condition.

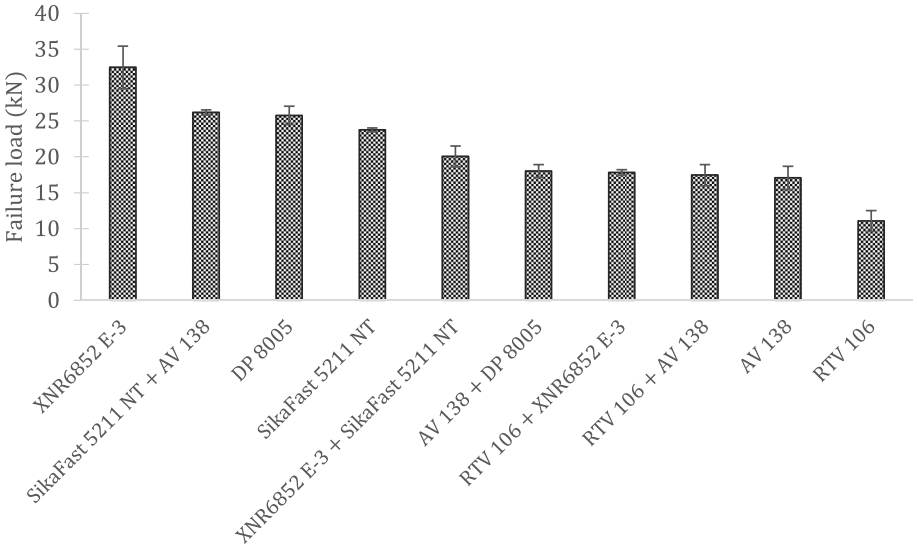

Fig. 9. Comparison of failure load between the single and mixed adhesive SLJs combinations under dynamic conditions.

corresponding displacement.

3.1.2. Fracture surface of quasi-static tests

The failure mode exhibited by each specimen and respective description are presented in this section for all the specimens tested under quasi-static conditions. The different types of failure surface are divided in SLJs using a single adhesive and mixed adhesives.

3.1.2.1. SLJs using a single adhesive. The failure surface of SLJs using the AV 138 adhesive exhibited a clear delamination for all the tested

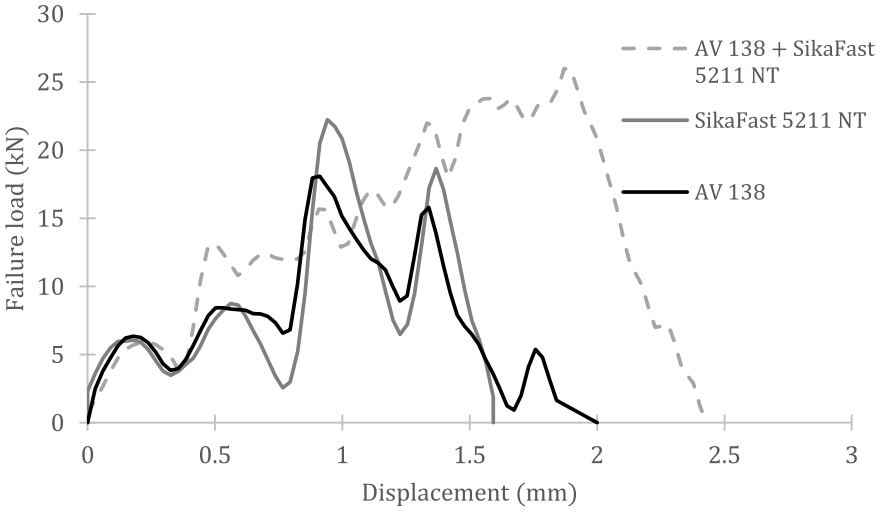

Fig. 10. Comparison between representative P-δ curves of SikaFast 5211 NT + AV 138 both single and mixed-adhesive SLJs.

Table 6
Summary of the maximum failure load and displacement for all SLJs tested under impact conditions.

Adhesive combination	Failure load (kN)	Standard deviation (kN)	Displacement at maximum load (mm)	Standard deviation (mm)
AV 138	17.05	1.63	1.14	0.42
XNR6852 E-3	32.47	2.97	2.91	1.22
SikaFast 5211 NT	23.75	0.27	1.85	0.24
DP 8005	25.77	1.7	2.32	0.39
RTV 106	11.06	1.46	1.35	0.77
AV 138 + SikaFast 5211 NT	26.19	0.36	1.75	0.21
AV 138 + DP 8005	18.01	0.89	1.01	0.20
AV 138 + RTV 106	17.45	1.48	1.01	0.22
XNR6852 E-3 + SikaFast 5211 NT	20.05	1.46	1.01	0.14
XNR6852 E-3 + RTV 106	17.82	0.39	1.25	0.34

specimens, demonstrating that high peel loads are generated for relatively low tensile loads. Fig. 7a is representative of this behaviour.

In the specimens with XNR6852 E-3 adhesive, the mode of failure found was delamination, as represented in Fig. 7b. A very large failure load was reached by the joints containing this adhesive, confirming the excellent mechanical properties.

Cohesive failure in the adhesive region (Fig. 7c) was obtained using the SikaFast 5211 NT adhesive, which demonstrates the low level of peel stress generated by this flexible adhesive.

Another adhesive which presented cohesive failure was the DP 8005 (Fig. 7d).

Furthermore, RTV 106 demonstrated mostly adhesive failures on the interface between composite and adhesive. This resulted in joints with very low failure load. An example of this failure is shown in Fig. 7e. Unlike the other adhesives under study, RTV 106 is a sealant designed for applications with temperature, not especially well suited for structural applications. The tendency for adhesive failure was previously identified in another research work [47].

3.1.2.2. SLJs using mixed adhesives. In the combination of SikaFast 5211 NT and AV 138, a relatively high failure load was identified for this configuration, which can be partially explained by the aspect of the fracture surface (Fig. 8a). The area bonded with SikaFast 5211 NT exhibited cohesive failure in the adhesive, while the central portion exhibited limited delamination with a large portion having suffered cohesive failure of the adhesive. This enabled the joint to perform better under static conditions.

This mixed adhesive configuration shows a small improvement in failure load over the single adhesives (AV 138 and DP 8005). There is also a small improvement in displacement, however it is still far from the performance of DP 8005 used alone. The use of AV 138 induces severe delamination of CFRP substrate, which is reduced when a flexible adhesive is introduced (Fig. 8b).

The failure mode obtained using the combination of AV 138 and RTV 106 was adhesive failure, which was also identified with RTV 106 as the single adhesive. In the central section of the joint, containing stiff adhesive, delamination was found in all the specimens tested. This was consistent with the failure type obtained when using AV 138 alone. Also noteworthy is the contamination/intrusion of RTV 106 of the central area reserved for AV 138 (Fig. 8c).

Attending to the failure mode of the combination of XNR6852 E-3 and SikaFast 5211 NT, a cohesive failure occurred for the SikaFast 5211 while the failure in XNR6852 E-3 was severe delamination (Fig. 8d).

For the combination of XNR6852 E-3 and RTV 106, the failure mode was identical to the previous combination analysed, being adhesive failure in the flexible adhesive (RTV 106) and delamination in the stronger adhesive (XNR6852 E-3) (Fig. 8e), likewise, the contamination of the central area by the flexible adhesive was also found.

3.1.3. Impact tests

The failure loads of the single and mixed adhesive SLJs configurations are shown in Fig. 9 with the indication of the standard deviations for all the results.

The data shows that joints with XNR6852 E-3 exhibit the highest failure load under impact, followed by the combination between AV 138 + SikaFast 5211 NT, which is also close to the performance of DP 8005 as well.

Despite the good performance of XNR6852 E-3 alone, all the combinations of this adhesive plus another adhesive, resulted in modest performance, even when mixed with extremely ductile adhesives. The delamination that this adhesive induces in the CFRP was impossible to reduce with any combination, despite the use of flexible adhesives to mitigate the effects of the peel stress at the ends of the joints.

The impact results for RTV 106 showed that while this adhesive has extremely low mechanical properties, under impact conditions the results were found to be surprisingly good. However, poor adhesion between the RTV 106 and the CFRP was found in most specimens. It becomes evident that if this adhesion problem can be solved, RTV106 might provide excellent impact performance in CFRP structures.

SikaFast 5211 NT and DP8005 used alone have led to cohesive failure in the adhesive, demonstrating to be valid alternatives for bonding composites, exhibiting relatively high failure loads. The mixed-

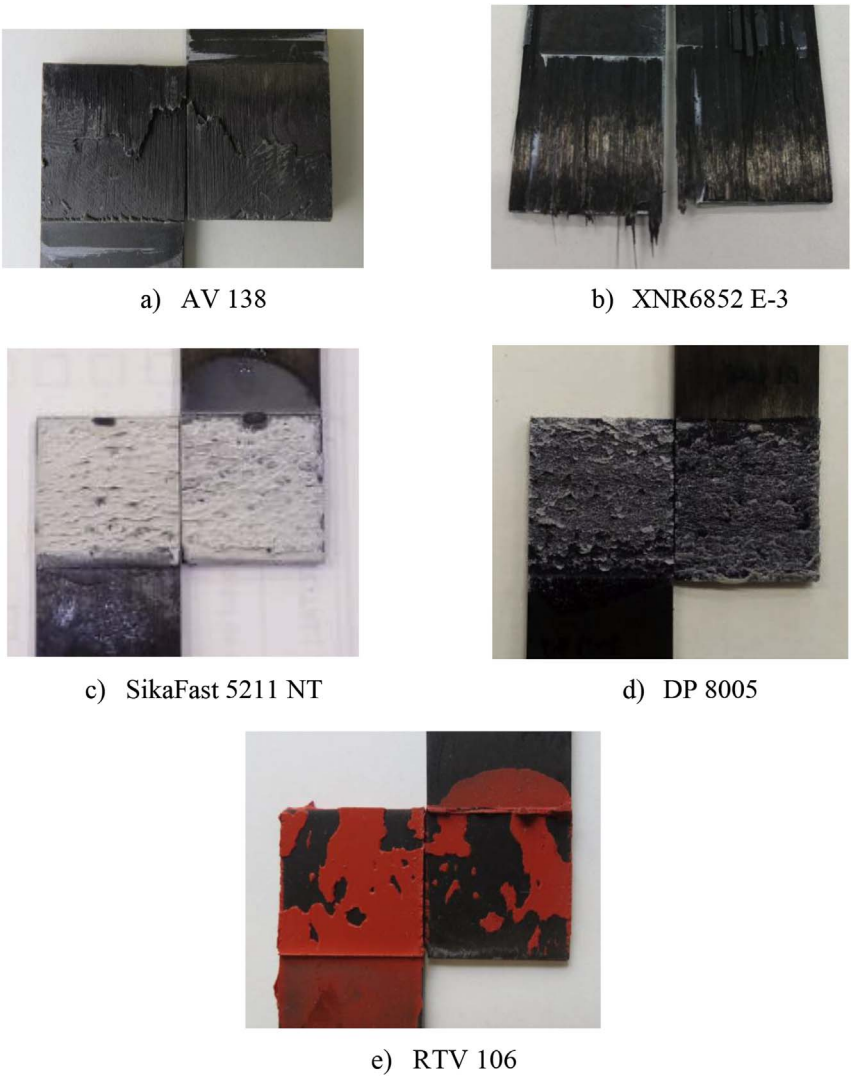

Fig. 11. Typical fracture surfaces of SLJs using a single adhesive configuration tested under impact condition.

adhesive configurations using these adhesives always had the same type of cohesive failure, demonstrating that these adhesives can carry all the load, without compromising the adherend.

Under impact, only one mixed adhesive combination has achieved better performance than the use of single adhesives. The SikaFast 5211 NT + AV 138 configuration (Fig. 10) reached a high failure load, resulting in a clear improvement over the SikaFast 5211 NT or AV 138 used alone.

Although the bonded area containing AV 138 suffered delamination, the presence of the flexible SikaFast 5211 NT at the ends of the overlap has delayed its onset significantly. This configuration demonstrated the possibility of using a mixed adhesive joint to improve the impact strength in composites.

A summary of all the experimental results under impact conditions is presented in Table 6 in terms of maximum failure load and correspondent displacement.

3.1.4. Fracture surface of impact tests

The failure mode exhibited by each specimen and respective description are presented in this section for all the specimens tested under impact conditions. The different types of failure surface are divided in SLJs using a single adhesive and mixed adhesives.

3.1.4.1. SLJs using a single adhesive. With the use of the AV 138 adhesive a clear delamination was found in all the tested specimens, again due to the large peel stresses induced by this stiff adhesive (Fig. 11a).

Using the XNR6852 E-3 adhesive, it is possible to conclude that this adhesive can carry high values of loads under impact. Observing the failure mode (Fig. 11b), this adhesive again exhibits a large amount of delamination of the CFRP substrates.

SikaFast 5211 NT adhesive exhibited good performance under impact. Regarding the failure mode, a clear cohesive failure in the adhesive (Fig. 11c) was found for all specimens. This indicates the good level of adhesion between the adhesive and CFRP, as well as the low peel stresses generated.

A clear cohesive failure in DP 8005 adhesive was found in all the specimens tested, as seen in Fig. 11d. As commented for the static results, the behaviour of this adhesive is similar to that of SikaFast 5211 NT.

However, bad adhesion between RTV 106 and the CFRP was found in the fracture surfaces (Fig. 11e). It becomes evident that if this adhesion problem can be solved, RTV106 might provide excellent impact performance in CFRP structures.

3.1.4.2. SLJs using mixed adhesives. In the combination of SikaFast 5211 NT and AV 138, the failure type (Fig. 12a) was the same as the one founded in the configuration using DP 8005 and AV138, i.e. cohesive failure in the adhesive for the flexible adhesive and a light delamination in the stiff adhesive area.

Fig. 12. Typical fracture surfaces of SLJs using mixed adhesive configuration tested under impact condition.

The failure type of the combination of DP 8005 and AV 138 was cohesive failure in the adhesive for the area governed by the DP 8005 and light delamination in AV 138's area (Fig. 12b).

In terms of type of failure of the combination of AV 138 and RTV 106, RTV 106 suffered again adhesive failure and AV 138 led to delamination in the adherend. Analysing in more detail (Fig. 12c), it is possible to observe a contamination of the RTV 106 into the central adhesive area. This manufacture problem is due to the low viscosity of RTV 106; when the joint is closed, the adhesive moves and can debond the fishing wire. This invasion causes problems with the results accuracy, because the central area is not fully occupied by the stiff adhesive, providing apparently less strength in the joint. Similar problems were identified and commented in the quasi-static test results.

Regarding the failure mode for the combination of XNR6852 E-3 and SikaFast 5211 NT, cohesive failure occurred in the SikaFast 5211 NT adhesive combined with large delamination in the XNR6852 E-3. This can be observed in Fig. 12d.

For the combination of XNR6852 E-3 and RTV 106, the same type of failure identified for the combination of AV 138 + RTV 106 was found (Fig. 12e), with RTV 106 contamination and a more pronounced delamination in the central section.

3.2. Comparison between static and impact tests

Using the experimental data, a comparison can be made between the average maximum loads in static and impact tests with the indication of the standard deviations for all the results (Fig. 13). This comparison is made to assess which SLJ configuration represents an improvement under impact conditions and if there are mixed adhesives joints that can provide an improvement over the use of a single adhesive.

Strain rate dependence can be identified for all adhesives and adhesive combinations. This is very evident for RTV 106 and SikaFast 5211 NT, demonstrating that the flexibility of the adhesives leads to increased impact performance. Even stiff adhesives, such as AV 138, show marked improvements.

To break a SLJ specimen of RTV 106 under impact conditions, the force required is four times the static force, despite the common occurrence of adhesive failure. However, the adhesion problems with RTV 106 reduce its effectiveness when integrated in a mixed-adhesive combination. For example, when RTV 106 is combined with AV 138, a remarkable improvement is attained, but better results could probably be achieved with improved adhesion.

In terms of energy absorbed under impact, once the case of mixed adhesive combination using AV 138 + SikaFast 5211 NT revealed to offer better failure load, in Fig. 14 it is possible to observe a comparison between SLJs made of single adhesive and the mixed adhesive combination mentioned. The results show that the energy absorbed by the mixed adhesive SLJs is slightly higher to SLJs using the flexible adhesive SikaFast 5211 NT and more than double of the values obtained

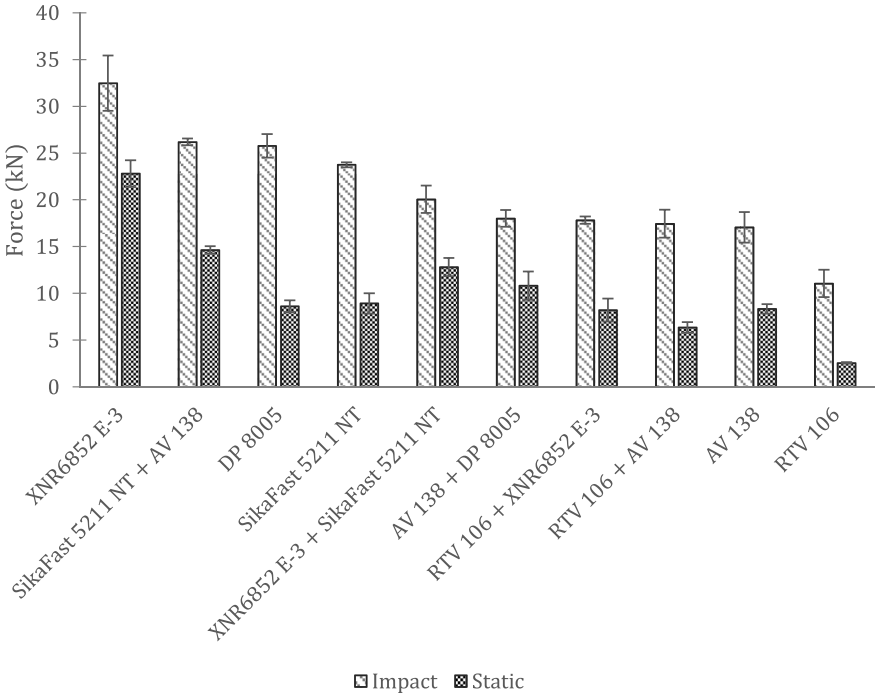

Fig. 13. Comparison between static and impact failure loads.

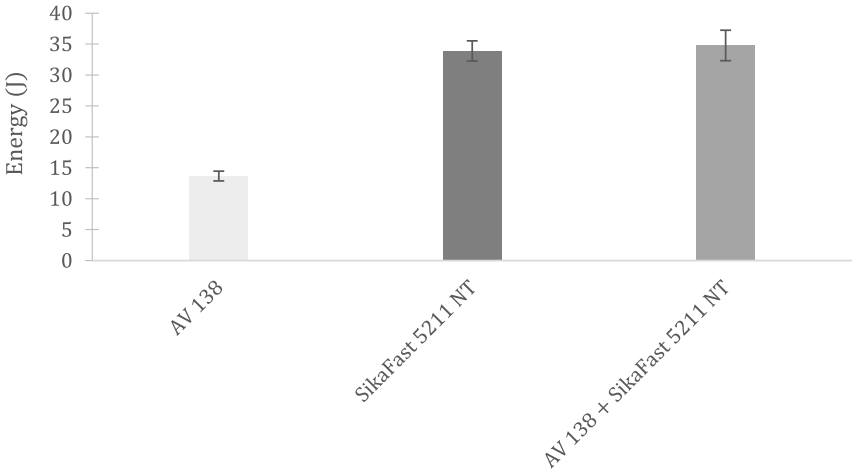

Fig. 14. Comparison between energy absorbed during impact tests using single and mixed adhesive configuration of AV 138 + SikaFast 5211 NT.

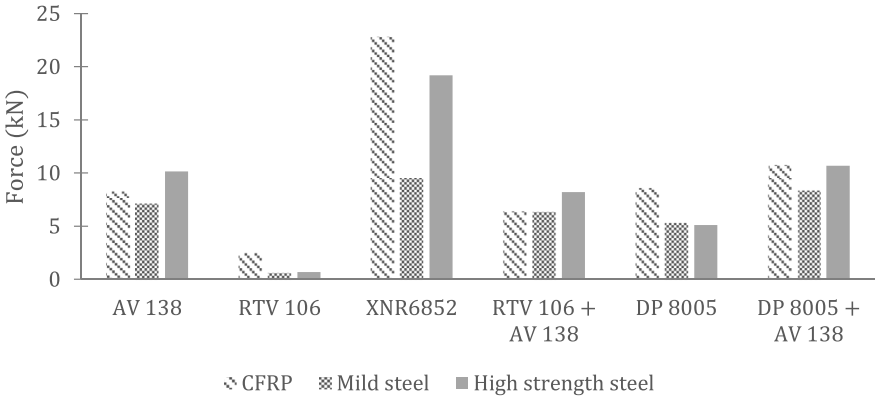

Fig. 15. Comparison in terms of failure load of SLJs between different substrates using the same adhesive combination in quasi-static conditions.

using the stiff adhesive AV 138.

3.3. Comparison between CFRP and steel substrates

A comparison between different substrates (CFRP and metal) was made using data from this work combined with data available from a previous work by the same authors [30]. The dimensions of the two types metal substrates (mild and high strength steel) are very close to the CFRP substrates used in this work. The only difference is the thickness which is 0.1 mm higher in the CFRP specimen's. The thickness

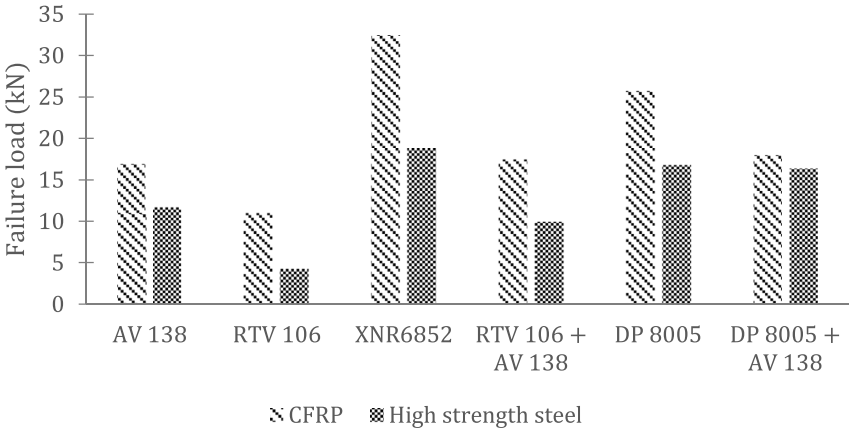

Fig. 16. Comparison in terms of failure load of SLJs between different substrates using the same adhesive combination under impact conditions.

of both materials accurately represents the typical dimensions used in the manufacture of automotive structures. It is also important to notice that the adhesives used in both works are the same, although XNR6852 E-2 used in the specimens with steel substrates is a previous version of the adhesive XNR6852 E-3 used in the CFRP specimens, being the mechanical properties of the latest version slightly lower. All these similarities enable direct comparison between results. In Fig. 15 it is possible to observe the influence of using the different substrates in terms of failure load when testing the SLJs under quasi-static conditions.

The results demonstrated that under quasi-static conditions, the use of CFRP and high strength steel substrates allows to obtain the highest failure loads for all the combinations. Joints with mild steel exhibit low failure loads and the difference is more pronounced when the XNR6852 adhesive (considered in both versions) is used. This is mainly due to the occurrence of plastic deformation in the mild steel substrates, which does not occur for the CFRP and the high strength steel. The results also clearly demonstrate that tough, flexible adhesives enable higher failure loads. The same behaviour was revealed by Harris and Adams [49] for the use of three aluminium (soft, mild and hard) substrates and using four types of adhesives (two brittle and two ductile).

The comparison between impact tests results for the different substrates is shown in Fig. 16. It is important to notice that in the previous work considered for this analysis [30], mild steel was not tested under impact loads, so it is only possible to establish a comparison between CFRP and high strength steel substrates.

The results demonstrated that CFPR substrates are the best performing configuration for all cases tested, with extremely high values of force obtained. High values are obtained with the crash resistant adhesive XNR6852 with CFRP substrates, which despite suffering complete delamination achieves almost double failure load of the joints with high strength steel substrates. This increase in strength can be attributed to the lower stiffness of the CFRP in the fibre direction, which reduces the stresses in the adhesive layer when compared with the high strength steel substrates.

4. Conclusions

The main goal of this work was the improvement of the static and impact strength of composite adhesive joints, aiming to avoid early delamination of the composite substrates. The techniques selected for this purpose were the mixed adhesive joints and the use of a crash resistant adhesive, which were experimentally tested. The main conclusions drawn from this work are presented below:

- A new technique for the manufacture of mixed adhesive joints using composite specimens has been successfully developed. Further improvements are still needed for some adhesives, which were not adequately contained by the nylon wire.
- The effectiveness of the mixed-adhesive in composites has been demonstrated in static and impact tests, with the combination between AV 138 + SikaFast 5211 NT, exhibiting significant improvements in both cases.
- Failure loads under impact conditions were found to be considerably higher than static loads, due to the strain rate dependence of the adhesives.
- The XNR6852 E-3 adhesive exhibited very high strength under quasi-static and impact conditions, significantly higher than those attained by another single adhesive or mixed adhesive combination. This adhesive was therefore shown to be a valid crash resistant adhesive for use in composite structures. Moreover, the flexible adhesives combined with XNR6852 E-3 were not found to be useful.
- Flexible adhesives such as the SikaFast 5211 NT and DP 8005 were also found to be able to join CFRP substrates without inducing delamination, albeit with failure loads below those presented by XNR6852 E-3.
- When compared with the results from a previous work [30] where metal substrates were used (namely, mild and high strength steel), CFRP specimens were generally found to provide higher failure loads under impact than high strength steel substrates.

Acknowledgments

The authors gratefully acknowledge the funding of Project NORTE-01-0145-FEDER-000022 - SciTech - Science and Technology for Competitive and Sustainable Industries, co-financed by Programa Operacional Regional do Norte (NORTE2020), through Fundo Europeu de Desenvolvimento Regional (FEDER). The authors would also like to thank NAGASE ChemteX® for the financial support provided.

References

[1] Galvez P, Quesada A, Martinez MA, Abenojar J, Boada MJL, Diaz V. Study of the behaviour of adhesive joints of steel with CFRP for its application in bus structures. Compos Part B Eng 2017;129:41–6.
[2] Wu Y, Liu Q, Fu J, Li Q, Hui D. Dynamic crash responses of bio-inspired aluminum honeycomb sandwich structures with CFRP panels. Compos Part B Eng 2017:122–33.
[3] Machado J, Marques E, da Silva LFM. Adhesives and adhesive joints under impact loadings: an Overview. J Adhesion 2017. http://dx.doi.org/10.1080/00218464.2017.1282349.
[4] Banea M, da Silva LFM, Campilho R. Effect of temperature on tensile strength and mode I fracture toughness of a high temperature epoxy adhesive. J Adhesion Sci Technol 2012;26(7):939–53.
[5] Agarwal A, Foster SJ, Hamed E. Testing of new adhesive and CFRP laminate for steel-CFRP joints under sustained loading and temperature cycles. Compos Part B Eng 2016;99:235–47.
[6] Machado J, Marques E, Campilho R, da Silva LFM. Mode I fracture toughness of CFRP as a function of temperature and strain rate. J Compos Mater 2016. 0021998316682309.
[7] Daniel I, LaBedz R, Liber T. New method for testing composites at very high strain rates. Exp Mech 1981;21(2):71–7.

[8] Al-Hassani S, Kaddour A. Strain rate effects on GRP, KRP and CFRP composite laminates. Key Eng Mater Trans Tech Publ 1998;141-143:427–52.
[9] Harding J, Welsh L. A tensile testing technique for fibre-reinforced composites at impact rates of strain. J Mater Sci 1983;18(6):1810–26.
[10] Taniguchi N, Nishiwaki T, Kawada H. Tensile strength of unidirectional CFRP laminate under high strain rate. Adv Compos Mater 2007;16(2):167–80.
[11] Korber H. Mechanical response of advanced composites under high strain rates PhD Thesis Faculty of Engineering of the University of Porto; 2010
[12] Hou J, Ruiz C. Measurement of the properties of woven CFRP T300/914 at different strain rates. Compos Sci Technol 2000;60(15):2829–34.
[13] Adams R, Harris J. A critical assessment of the block impact test for measuring the impact strength of adhesive bonds. Int J adhesion adhesives 1996;16(2):61–71.
[14] Saldanha D, Canto C, da Silva LFM, Carbas R, Chaves F, Nomura K, et al. Mechanical characterization of a high elongation and high toughness epoxy adhesive. Int J Adhesion Adhesives 2013;47:91–8.
[15] Galliot C, Rousseau J, Verchery G. Drop weight tensile impact testing of adhesively bonded carbon/epoxy laminate joints. Int J Adhesion Adhesives 2012;35:68–75.
[16] Kadioglu F, Adams RD. Flexible adhesives for automotive application under impact loading. Int J Adhesion Adhesives 2015;56:73–8.
[17] Delfosse D, Poursartip A. Energy-based approach to impact damage in CFRP laminates. Compos Part A Appl Sci Manuf 1997;28(7):647–55.
[18] Neumayer J, Kuhn P, Koerber H, Hinterholzl R. Experimental determination of the tensile and shear behaviour of adhesives under impact loading. J Adhes 2016;92(7–9):503–16.
[19] May M, Hesebeck O, Marzi S, Böhme W, Lienhard J, Kilchert S, et al. Rate dependent behavior of crash-optimized adhesives–Experimental characterization, model development, and simulation. Eng Fract Mech 2015;133:112–37.
[20] Loureiro A, da Silva LFM, Sato C, Figueiredo M. Comparison of the mechanical behaviour between stiff and flexible adhesive joints for the automotive industry. J Adhesion 2010;86(7):765–87.
[21] Cho J, Kinloch A, Blackman B, Sanchez FR, Han M. High-strain-rate fracture of adhesively bonded composite joints in DCB and TDCB specimens. Int J Automot Technol 2012;13(7):1127–31.
[22] Raphael C. Variable-adhesive bonded joints. Appl Polym Symp 1966:99–108.
[23] Fitton M, Broughton J. Variable modulus adhesives: an approach to optimised joint performance. Int J Adhesion Adhesives 2005;25(4):329–36.
[24] Breto R, Chiminelli A, Duvivier E, Lizaranzu M, Jiménez M. Functionally graded bond-lines for metal/composite joints. European conference on composite materials, Sville, Spain. 2014.
[25] Hart-Smith LJ. Adhesive-bonded single-lap joints. Hampton, VA: Langley Research Center; 1973.
[26] da Silva LFM, Adams R. Techniques to reduce the peel stresses in adhesive joints with composites. Int J Adhesion Adhesives 2007;27(3):227–35.
[27] das Neves PJ, da Silva LFM, Adams R. Analysis of mixed adhesive bonded joints part I: theoretical formulation. J Adhesion Sci Technol 2009;23(1):1–34.
[28] das Neves PJ, da Silva LFM, Adams R. Analysis of mixed adhesive bonded joints part II: parametric study. J Adhesion Sci Technol 2009;23(1):35–61.
[29] da Silva LFM, Lopes MJC. Joint strength optimization by the mixed-adhesive technique. Int J Adhesion Adhesives 2009;29(5):509–14.
[30] Silva M, Marques E, da Silva LFM. Behaviour under impact of mixed adhesive joints for the automotive industry. Lat Am J Solids Struct 2016;13(5):835–53.
[31] Adams R, Atkins R, Harris J, Kinloch A. Stress analysis and failure properties of carbon-fibre-reinforced-plastic/steel double-lap joints. J Adhesion 1986;20(1):29–53.
[32] Perry HA. Adhesive bonding of reinforced plastics. McGraw-Hill; 1959.
[33] Beevers A, Ellis M. Impact behaviour of bonded mild steel lap joints. Int J Adhesion Adhesives 1984;4(1):13–6.
[34] Araújo H, Machado J, Marques E, da Silva LFM. Dynamic behaviour of composite adhesive joints for the automotive industry. Compos Struct 2017. http://dx.doi.org/10.1016/j.compstruct.2017.03.071.
[35] da Silva LFM, De Magalhaes F, Chaves F, De Moura M. Mode II fracture toughness of a brittle and a ductile adhesive as a function of the adhesive thickness. J Adhesion 2010;86(9):891–905.
[36] Netusil M, Eliasova M. Trends and requirements for adhesives with load bearing role. Proc Challenging Glass 2014;4:369–74.
[37] da Silva LFM, da Silva R, Chousal J, Pinto A. Alternative methods to measure the adhesive shear displacement in the thick adherend shear test. J Adhesion Sci Technol 2008;22(1):15–29.
[38] Pinto AMG, Magalhães A, Campilho RDSG, De Moura M, Baptista A. Single-lap joints of similar and dissimilar adherends bonded with an acrylic adhesive. J Adhesion 2009;85(6):351–76.
[39] de Sousa Marques EA. High temperature mixed-adhesive joints for aerospace applications PhD Thesis Faculty of Engineering of the University of Porto; 2016
[40] Banea MD, da Silva L. Mechanical characterization of flexible adhesives. J Adhesion 2009;85(4–5):261–85.
[41] Zgoul M, Crocombe A. Numerical modelling of lap joints bonded with a rate-dependent adhesive. Int J adhesion adhesives 2004;24(4):355–66.
[42] Avendaño R, Carbas R, Marques E, da Silva L, Fernandes A. Effect of temperature and strain rate on single lap joints with dissimilar lightweight adherends bonded with an acrylic adhesive. Compos Struct 2016;152:34–44.
[43] Campilho R. Repair of composite and wood structures PhD Thesis Faculty of Engineering of the University of Porto; 2009
[44] Machado J, Marques E, Campilho R, da Silva LFM. Mode II fracture toughness of CFRP as a function of temperature and strain rate. Compos Part B Eng 2017;114:311–8.
[45] da Silva LFM, Adams R. Joint strength predictions for adhesive joints to be used over a wide temperature range. Int J Adhesion Adhesives 2007;27(5):362–79.
[46] da Silva LFM, Adams R. Adhesive joints at high and low temperatures using similar and dissimilar adherends and dual adhesives. Int J Adhesion Adhesives 2007;27(3):216–26.
[47] da Silva MRG. Impact of mixed adhesive joints for the automotive industry Master Thesis Faculty of Engineering of the University of Porto; 2015
[48] ASTM D 1002. Standard test method for apparent shear strength of single-lap-joint adhesively bonded metal specimens by tension loading (Metal-to-Metal) vol. 15. 2005. p. 45–8.
[49] Harris J, Adams R. An assessment of the impact performance of bonded joints for use in high energy absorbing structures. Proc Institution Mech Eng Part C J Mech Eng Sci 1985;199(2):121–31.

Paper 10

Content of Paper 10

Abstract

1. Introduction

2. Experimental details

2.1. Material and properties

2.1.1. Adhesives

2.1.2. CFRP

2.2. Fabrication and testing

2.2.1. Preparation of CFRP plates

2.2.2. SLJ geometry and manufacture

2.2.3. Quasi-static testing procedure

2.2.4. Dynamic testing procedure

3. Results

3.1. Quasi-static tests

3.1.1. Fracture surface

3.1.2. Failure load

3.1.3. Energy absorbed

3.2. Impact tests

3.2.1. Fracture surface

3.2.2. Failure load

3.2.3. Energy absorbed

3.3. Comparison between quasi-static and impact tests

4. Conclusions

References

Composite Structures 194 (2018) 68–79

Contents lists available at ScienceDirect

Composite Structures

journal homepage: www.elsevier.com/locate/compstruct

Influence of low and high temperature on mixed adhesive joints under quasi-static and impact conditions

J.J.M. Machado[a], E.A.S. Marques[a], Lucas F.M. da Silva[b,*]

[a] Instituto de Ciência e Inovação em Engenharia Mecânica e Engenharia Industrial (INEGI), Rua Dr. Roberto Frias, 4200-465 Porto, Portugal
[b] Departamento de Engenharia Mecânica, Faculdade de Engenharia (FEUP), Universidade do Porto, Rua Dr. Roberto Frias, 4200-465 Porto, Portugal

ARTICLE INFO

Keywords:
Mixed adhesive joints
Composites
Temperature
Single lap joints
Quasi-static
Impact

ABSTRACT

The increasing use of composite structures in the automotive industry is due to strict regulations regarding fuel efficiency and safety standards. The main advantage of the use of adhesives is the possibility of joining dissimilar materials, particularly composites. The technique studied was the mixed adhesive joints, as two or more adhesives can be used in a single lap joint combining the properties of those adhesives to attain mechanical performance superior to that obtained using those adhesives individually. The main goal was to assess if a previously validated combination of mixed adhesives in a composite joint, tested under quasi-static and impact conditions, offers the same advantage over the use of a single adhesive when subjected to low (−30 °C) and high (80 °C) temperatures. The influence of temperature on the behaviour of the composite joints was assessed in quasi-static and impact conditions allowing to infer the effect on each adhesive. Another important aspect of the use of this type of technique is to avoid the early delamination of the composite substrates. This method was found to improve the performance under quasi-static and impact conditions although its behaviour under the wide range of temperature tested was found to vary significantly.

1. Introduction

The constant requirements to produce lighter and stronger structures in the automotive industry, to decrease the fuel consumption and emissions, has led to the introduction of a larger amount of lightweight materials, including composites [1–3]. With the application of composite materials, traditional joining methods, such for example fasteners, require both the fibres and the matrix to be cut and hence introduce stress concentrations that negatively impact the strength of the material. The use of adhesive joint avoids these problems, as this joining method is able to easily join dissimilar materials without damaging the substrates. However, most composite materials are sensitive to transverse loads which can cause delamination and early failure of the substrates. If an adhesive joint is not designed taking this effect into account, it can introduce large peel stresses in the extremities of the bonded area that lead to failure by delamination. Such failure mode can be avoided by employing less strong but flexible adhesives that spread the stresses evenly through the bonded area and reducing the presence of features which cause stress concentrations. Although the use of flexible adhesives is able to avoid delamination, joint strength can be relatively low. A possible solution to minimize delamination without sacrificing joint strength is the use of mixed adhesive joints, which employ a stiff adhesive aiming at the reduction of stress concentrations of brittle adhesives.

Composite materials such as carbon fibre reinforced polymers (CFRP) are composed of carbon fibres in a polymer matrix [4–7]. The mechanical properties, such as the fracture toughness of this type of material, are affected by changes in the loading rate as it is controlled by the polymer matrix which is strain rate dependent [8,9]. For such reason, the failure mode in composite materials can change in respect to the variation of loading rate, causing a significant influence on the fracture toughness properties. A reduction of the fracture toughness with the increase of loading rates was found to occur when increasing the loading rates in a transition from ductile to a brittle failure mode [10]. The effect of loading rate on mode I fracture toughness was studied by several authors with different conclusions. Some authors [11–15] found that the fracture toughness in mode I increased with the increase of strain rate; and other authors [16,17] concluded that it remained independent. A general agreement is that the fracture toughness in mode II decreases with the increase of strain rate [18–21]. Daniel et al. [22] characterized a unidirectional carbon/epoxy material in quasi-static and impact conditions at different biaxial states of stress with the combination of compression and shear. It was concluded that the moduli and strengths linearly varied with the logarithm of strain

* Corresponding author.
E-mail address: lucas@fe.up.pt (L.F.M. da Silva).

https://doi.org/10.1016/j.compstruct.2018.03.093
Received 30 January 2018; Received in revised form 19 March 2018; Accepted 26 March 2018
Available online 31 March 2018
0263-8223/ © 2018 Elsevier Ltd. All rights reserved.

rate.

The effect of strain rate on the compressive and shear behaviour of carbon/epoxy composite materials was investigated by Hsiao et al. [23]. The composite configuration using fibres with an overlap of 0° revealed higher strength and strain values with increasing strain rate, while the modulus increased slightly over the quasi-static value. The dynamic stress-strain curves were found to stiffen with the strain rate, with the stiffening being lowest in the longitudinal case and highest in the transverse and shear directions.

To ensure high impact strength, the selection of the adhesive is of extreme importance. There are adhesives developed to exhibit excellent properties under a wide range of strain rates namely crash structural adhesives which combine strength and ductility at the same time with excellent fracture toughness. They are characterized by being able to withstand a very significant deformation prior to failure, which is vital for energy absorption under impact [24]. When compared to a typical structural adhesive, a crash resistant adhesive has generally higher peel resistance and withstands loads for a longer period [25,26]. Such adhesives have higher absorption energy, as demonstrated by the larger area beneath the load-displacement curves (P-δ) typical of these materials [24].

An important aspect to consider when designing an adhesive joint is the influence of temperature on its strength, especially in the case of the automotive industry where bonded structures must operate within a wide range of temperatures [2,27]. The main factors which determine the joint strength over low and high temperatures are the adhesive shrinkage [28], the coefficients of thermal expansion (CTE) [29–32], as well the temperature dependency of mechanical properties [31,33,34]. Adhesives suitable for high temperature perform poorly at low temperatures, exhibiting brittle behaviour. Conversely, adhesives better suited for low temperatures lose their strength or suffer degradation at high temperatures [30].

Some authors experimentally tested structural adhesives (mainly epoxies) at low and high temperatures, concluding that at low temperatures the joint strength decreases due to high thermal residual stresses, and at high temperatures the joint strength also decreases due to low adhesive strength [31,34–36]. Adams et al. [34] experimentally tested SLJs with CFRP/aluminium substrates, using three different epoxy adhesives at room and low temperature. Unidirectional CFRP has a smaller coefficient of linear expansion than that of aluminium, leading to a stress state affected by the thermal effects. Banea et al. [37] assessed the effect of temperature on the mechanical properties of an epoxy and a polyurethane adhesives, using bulk specimens and adhesive joints and concluding that the failure loads vary with temperature and, for polyurethane adhesives, SLJs can determine the adhesive shear strength. Owens et al. [38] tested composite/aluminium SLJs bonded with a stiff and a flexible adhesives at room and low temperatures, concluding that SLJs stiffness is more affected by the behaviour of the substrates than the modulus of the thin adhesive layer for low temperature tests.

The reduction of the localized stresses at the end of the overlaps in SLJs has been a significant focus of investigation. Previous works have experimented with simple geometrical modifications, such as tapering of substrates or applying fillets to the joint ends [39–41]. However, industrially, these modifications are still quite complex and costly and, thus, its practical use is limited [42]. Raphael [43] was the first author to introduce the concept of mixed adhesive joints as an alternative solution for the reduction of stresses. This type of joints proposed the use of a stiff adhesive in the centre and a more flexible adhesive at the ends of the overlap, aiming to achieve a more uniform stress distribution. Authors such Fitton and Broughton [44] verified a reduction of stress concentration and change of type of failure by using the right combination of adhesives with different modulus. Nevertheless, the most suitable selection and combination of adhesives is not only based on the mechanical properties but will also require compatible working characteristics [45]. Another important factor is the ratio between the use of both adhesives which has been determined to be of 0.5 by Öz et al. [46]. Hart-Smith [47] was one of the first authors to recognize that the use of mixed adhesive joints could yield substantial improvements in mechanical strength for joints subjected to large temperature range. This effect can be achieved by using an adhesive better suited for high temperature (HTA) in the middle of the joint, combined with a low-temperature adhesive (LTA) at the ends of the overlap. At low-temperatures, the LTA supports the load, while the HTA is unstressed. The mixed adhesive joint concept was experimentally proven by da Silva and Adams [39] which found improvements in the mechanical behaviour of a joint under a large temperature range. An analytical solution for modelling mixed adhesive joints was proposed by Neves et al. [48], including the nonlinear geometric effect characteristic of SLJs. This initial study was followed by a parametric study [49], considering several parameters of mixed adhesive joints. da Silva and Lopes [50] tested mixed adhesive SLJs under quasi-static conditions, using three different ductile adhesives and found that the mixed adhesive joints offered better results over the use of single adhesives.

Silva et al. [51] tested mixed adhesive SLJs using aluminium substrates under quasi-static and impact conditions. The configuration using a stiff epoxy and room temperature vulcanising silicone was found to perform poorly, while the configuration with the stiff epoxy and an acrylic adhesive outperformed both adhesives used individually.

The influence between different testing temperatures and strain rate on an adhesive joint strength is also a very important matter to evaluate for the automotive industry and in literature most studies focus separately the effect of both factors. Banea et al. [52] experimentally tested an high temperature epoxy adhesive under different strain rates and high temperature values concluding that the ultimate tensile stress decreased linearly with the increase of temperature and at the same time increased logarithmically with the loading rate. Carlberger et al. [53] proposed a method to assess the temperature and strain rate dependence of cohesive laws for a structural epoxy, determining that the fracture energy of this material is virtually independent of temperature and strain rate.

The technique studied in this work was the use of mixed adhesive joints. The main goal was to assess if a previously validated combination of mixed adhesives in composite SLJ, tested under quasi-static and impact conditions, offers the same advantage over the use of a single adhesive when subjected to low (−30 °C) and high (80 °C) temperatures required for the validation of automotive structures. This is an innovative work as no previous research has been performed on the impact behaviour of composite mixed adhesive joints in combination with temperature. It was demonstrated that this type of technique can avoid early delamination of the composite substrates for some of the tested temperatures, achieving improvements over the use of a single adhesive, while for other cases no improvements can be found due to low mechanical performance of the adhesives.

2. Experimental details

2.1. Material and properties

2.1.1. Adhesives

The concept of mixed adhesive joints studied in this work requires the use of a stiff adhesive in the centre and a flexible at the edges of the overlap length. The two distinct adhesives used were the adhesive Araldite AV 138 (Huntsman, Salt Lake City, UT, USA) as the stiff adhesive and SikaFast 5211 NT (Sika, Baar, Switzerland) as the flexible adhesive. In a previous work developed by the authors [54], using ten different combinations of mixed adhesive joints, using two stiff and three flexible adhesives, it was possible to conclude that the combination of these two adhesives represented an improvement over the use of adhesive joints using a single adhesive.

Adhesive Araldite AV 138 can be characterized as being an epoxy adhesive with very stiff and brittle mechanical behaviour. Adhesive

joints made using this adhesive reveal low strength values due to the large stress concentration created. The properties of this adhesive were determined in da Silva et al. [55]. The glass transition temperature (T_g) of the stiff adhesive (AV 138) is of 85 °C, accordingly to datasheet provided by the supplier.

Adhesive SikaFast 5211 NT is a structural two-component acrylic adhesive which offers good ductility and a very fast curing time. Regarding its mechanical properties, it has not been fully characterized although some mechanical properties can be found in [56]. The T_g value of this adhesive is of 60 °C, from the datasheet provided by the supplier.

Due to strain rate dependency, knowledge of the material properties at higher testing speeds are necessary to perform accurate numerical simulations. However, the adhesives were not fully characterized for high strain rate (3 m/s). To obtain these values, most of the adhesives were first tested at 1 mm/min and 100 mm/min. An extrapolation process based in a logarithmic trend function was then used to estimate the properties at higher strain rates [57,58], shown in Equation (1).

$$Property\ to\ determine = A\ \ln(\dot{\varepsilon}) + B \quad (1)$$

where A and B are constrains obtained from experimental data, and $\dot{\varepsilon}$ is the strain rate in s^{-1}.

Likewise, $\dot{\varepsilon}$ (strain rate) was determined with Eq. (2):

$$\dot{\varepsilon} = \frac{v}{L_o} \quad (2)$$

Being $v$the velocity of the test and L_o the initial calibrated longitudinal deformation length of the specimen section where the strain is measured.

The mechanical properties of both stiff (AV 138) and flexible (SikaFast 5211 NT) adhesives can be found in Table 1.

2.1.2. CFRP

The composite material (CFRP) used in this work was the carbon/epoxy pre-preg (SEAL® Texipreg HS 160 RM). The T_g value of the CFRP was previously determined by the authors [4,59] being of 105 °C. The specimens were fabricated by stacking plies oriented in a single direction. The elastic properties of this material were previously determined in the work of Campilho [60]. Table 2 presents the Young's modulus (E), the shear modulus (G), and the Poisson's ratio (ν), in the three axis direction (x, y, z), being E_1 the normal direction, E_2 the transverse direction and E_3 the out plane direction.

The tensile and shear strength properties of CFRP were determined under quasi-static conditions by Campilho et al. [61]. The values of fracture toughness in mode I and mode II were previously determined by the authors [4,59] as a function of strain rate and temperature. In both mode I and mode II it was observed that with the increase of temperature there was an increase of the fracture toughness. Increasing the strain rate also revealed a decrease of fracture toughness in both modes. All the values of fracture toughness measured for mode II were higher than the values measured in mode I. The mechanical properties of CFRP can be found in Table 3.

Table 2
Properties of CFRP elastic orthotropic [60].

Elastic Modulus (MPa)	Poisson's Ratio	Shear Modulus (MPa)
E_1 = 109,000	ν_{12} = 0.342	G_{12} = 4315
E_2 = 8819	ν_{13} = 0.342	G_{13} = 4315
E_3 = 8819	ν_{23} = 0.380	G_{23} = 3200

Table 3
Mechanical properties of the CFRP at room temperature (properties not available are marked as n/a).

Material	Test speed (mm/min)	Tensile strength [MPa]	Shear strength [MPa]	Mode I fracture energy [N/mm]	Mode II fracture energy [N/mm]
CFRP	1	25	13.5	0.59	1.17
	100	n/a	n/a	0.53	1.04
	180,000*	n/a	n/a	0.39	0.82

* Mechanical properties extrapolated considering an initial impact velocity of 3 m/s.

2.2. Fabrication and testing

2.2.1. Preparation of CFRP plates

The dimensions of the bulk laminates were of 300 x 300 mm, having each ply a thickness of 0.15 mm a stack of a total of 14 plies was performed by hand lay-up to achieve a final thickness of 2.1 mm. All the plies were stacked following a unidirectional 0° lay-up plies (with the aim of obtaining better properties in the loading direction). The curing cycle applied was 130 °C for 1 h by using a hot plate press.

Afterward, the laminates were cut into the dimensions required for each substrate using a diamond disc cutting machine. The final step was the use of a 120-grit sandpaper to remove the loos fibres and smoothen the sharp edges of each side of the substrates.

2.2.2. SLJ geometry and manufacture

The overlap length used in the SLJs was of 25 mm and was kept constant for the different combinations of single and mixed adhesive joints. Such value of overlap length was chosen accordingly to previous studies performed by several authors [44,62,63] which performed a comparison and assessed the best value to use in experimental tests aiming the optimal geometry representative of a real applications.

The geometry chosen is representative of automotive industry applications, with thin substrates and bondline, joined in single overlap bonding (Fig. 1).

The different SLJ configurations, using single and mixed adhesives, tested in this work are listed below:

- **AV 138** (full overlap) – stiff adhesive;
- **SikaFast 5211 NT** (full overlap) – flexible adhesive;
- **AV 138** (centre) – stiff adhesive + **SikaFast 5211 NT** (edges) – flexible adhesive.

Table 1
Mechanical properties of the stiff (AV 138) and flexible (SikaFast 5211 NT) adhesives at room temperature (properties not available are marked as n/a).

Adhesive	Test speed (mm/min)	Young's modulus [MPa]	Shear modulus [MPa]	Tensile strength [MPa]	Shear strength [MPa]	Mode I fracture energy [N/mm]	Mode II fracture energy [N/mm]
AV 138	1	4890	1560	41	30.2	0.35	4.9
	100			49.1	36.2		
	180,000*			72.1	45.9		
SikaFast 5211 NT	1	260	n/a	5.06	n/a	n/a	n/a
	100	n/a					
	180,000*	n/a					

* Mechanical properties extrapolated considering an initial impact velocity of 3 m/s.

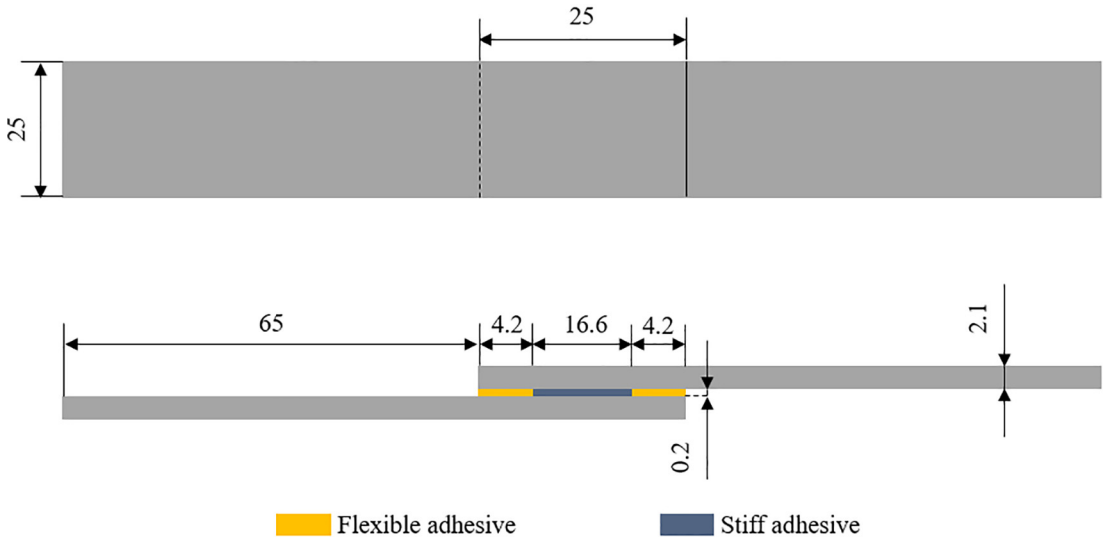

Fig. 1. Schematic representation of the geometry and dimensions of the mixed-adhesive SLJ specimens (dimensions in mm).

The mixed adhesive joints used the stiff adhesive (AV 138) in the centre of the overlap length and the flexible adhesive (SikaFast 5211 NT) at the overlap ends. A schematic representation of the adhesive ratio in terms of lengths used is presented in Fig. 1. This specific ratio was selected since it has been previously [64] used with good results in joints with steel substrates. The use of nylon wires bonded to one of the substrates and with a thickness of 0.2 mm allowed physical separation between the two adhesives types. This method causes a minimal intrusion in the SLJs adhesive layer, defines the thickness of the adhesive layer and does not cause voids or large separation between the adhesives in the overlap.

The manufacture of single adhesive specimens followed the standard ASTM D 1002 [65]. The curing cycle of AV 138 can be performed at room temperature, although in this case temperature was applied as performed in a previous work performed by the authors [54]. The strength of this adhesive is higher when curing with temperature [66]. The curing cycle applied for the stiff adhesive (AV 138) is of one hour at 120 °C, and for the flexible adhesive (SikaFast 5211 NT) of two days at room temperature. In the case of the mixed adhesive SLJs (AV 138 + SikaFast 5211 NT), only the stiff adhesive (AV 138) required high curing temperature. The flexible adhesive (SikaFast 5211 NT), although it can be cured a room temperature, can be more rapidly cured with high temperature. According to these conditions, the cure cycle applied was the same as for the joints made using the stiff adhesive (AV 138).

2.2.3. Quasi-static testing procedure

Using a universal testing machine, model Instron 3367 (Norwood, Massachusetts, USA), quasi-static tests were performed at a constant cross-head displacement rate of 1 mm/min, which corresponds to a shear strain rate of 0.08 s^{-1}. A load cell with a capacity of 30 kN was used.

Tests were performed at −30, 24 and 80 °C. For tests performed at low and high temperature, a heated climatic chamber was integrated to the testing machine. To achieve the high temperature, the heated climatic chamber was used and for the low temperature, nitrogen was injected inside the chamber in a controlled way. Prior to testing, each SLJ was subjected to the specific testing temperature for a period of 10 min to ensure a homogeneous temperature distribution (measured with a thermocouple). While the tests were being performed the specimens remained enclosed in the chamber with the designated temperature being kept constant. Six SLJs were tested for each condition of joint configuration and temperature, and for each joint a P-δ curve was obtained.

2.2.4. Dynamic testing procedure

The impact tests were performed in a Rosand® Instrumented Falling weight impact tester, type 5H.V. (Stourbridge, West Midlands, U.K), with a load cell with a capacity of 60 kN. The maximum energy of the falling weight impact tester is 300 J (when using 29 kg of weight) allowing a maximum impact speed of 4.5 m/s.

The impact procedure consists in dropping a weighted impactor, which falls vertically until it collides with the SLJ specimen holder. The upper substrate of the specimen is firmly clamped to a test fixture. The impact load is directly applied to the lower substrate, which is laterally guided but free to move in the vertical direction. In the test procedure followed, the impact velocity is defined by the pre-selected drop height. The energy applied in the impact is therefore a function of impact mass and the impact velocity. Low temperature tests were performed by applying gaseous nitrogen directly to the SLJs and high temperature tests were performed using an induction coil to heat-up the SLJs. For both low and high temperature, a thermocouple attached in the beginning of the area of overlap was used to measure the temperature. The testing occurred when the desired temperature was reached in the adhesive layer. The specimens were tested at a speed of 3 m/s and a mass of 26 kg was used for the impactor, corresponding to an impact energy of 117 J, determined to be sufficient to break all specimen configurations. For each adhesive configuration under study, six specimens were tested.

3. Results

A total of six specimens were tested for each adhesive configuration and temperature. A total of three different configurations of adhesive were tested (two using single adhesive and one using mixed adhesives), under quasi-static loads (1 mm/min) and impact loads (3 m/s).

3.1. Quasi-static tests

3.1.1. Fracture surface

The fracture surface exhibited by each specimen and respective description are presented in Table 4, for all the specimens tested under quasi-static conditions and as a function of temperature.

It is possible to observe that for the case of the stiff adhesive (AV 138), the fracture surface revealed the occurrence of delamination of CFRP at both LT and RT; as for the case of HT the type of failure was cohesive in the adhesive, with adhesive being present in both substrates. Discoloration of the adhesive layer also indicates that at HT the adhesive suffered significant plastic deformation. The main failure

Table 4
Example of fracture surface for all SLJs tested under quasi-static conditions as a function of temperature.

Adhesive combination	− 30 °C (LT)	24 °C (RT)	80 °C (HT)
AV 138		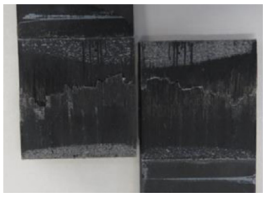	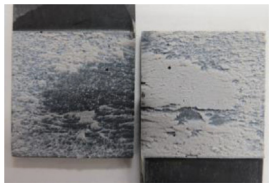
SikaFast 5211 NT	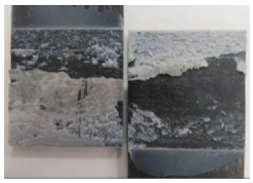	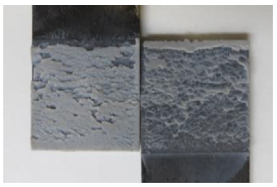	
AV 138 + SikaFast 5211 NT	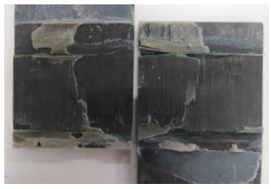	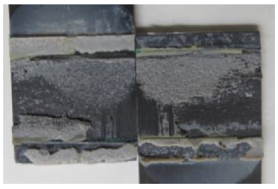	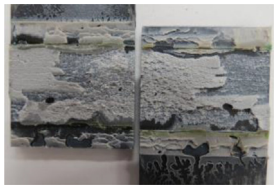

mechanism in this case was controlled by shear and not peel (and subsequent delamination) as was the case for the other range of temperatures tested.

For the flexible adhesive (SikaFast 5211 NT), delamination of CFRP did not occur for any of the tested temperatures. The type of failure surface was found to be cohesive in the adhesive for all the testing temperatures, although, it is noticeable that with the increase of temperature there is also an increase in the shear plastic deformation in the adhesive layer.

In the case of the mixed adhesive configuration (AV 138 + SikaFast 5211 NT), the type of failure surface was found to be delamination of CFRP for LT and RT (more severe in the case of LT), and for tests at HT the type of failure was shown to be cohesive in the adhesives and delamination of CFRP was avoided.

3.1.2. Failure load

In Fig. 2 it is possible to observe the average values of failure load as well standard deviation of the CFRP SLJs tested at quasi-static conditions under varied temperatures.

The plot shows that optimal performance is attained with the mixed adhesive joint (AV 138 + SikaFast 5211 NT) for RT. At this temperature, the mixed adhesive joint is able to perform better than the stiff adhesive (AV 138) or flexible (SikaFast 5211 NT) adhesives used alone, redistributing the peel stresses and avoiding delamination failure. By avoiding this type of failure, it is possible for the adhesive layer to attain its maximum load carrying capabilities. The influence of the adhesive layer configuration on the peel stress distribution of the SLJ is shown schematically in Fig. 3.

At LT, the behaviour of the stiff adhesive (AV 138) and the mixed adhesive layer is excessively stiff, causing early failure of the composite substrate by delamination, an undesirable type of failure. However, the

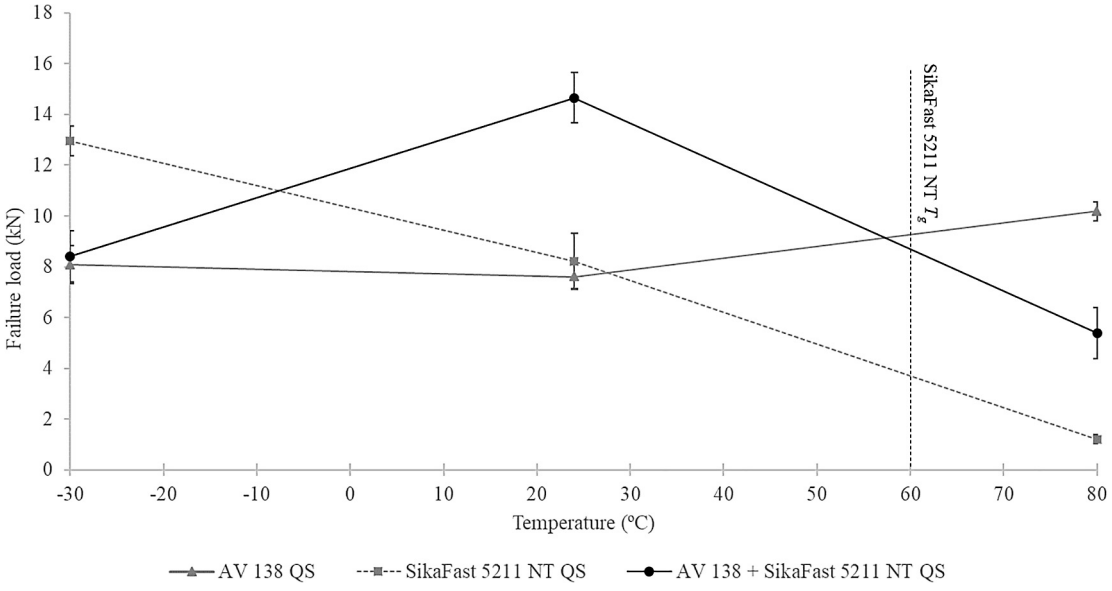

Fig. 2. Values of average failure load and standard deviation of all the combinations of SLJs tested at quasi-static conditions as a function of temperature.

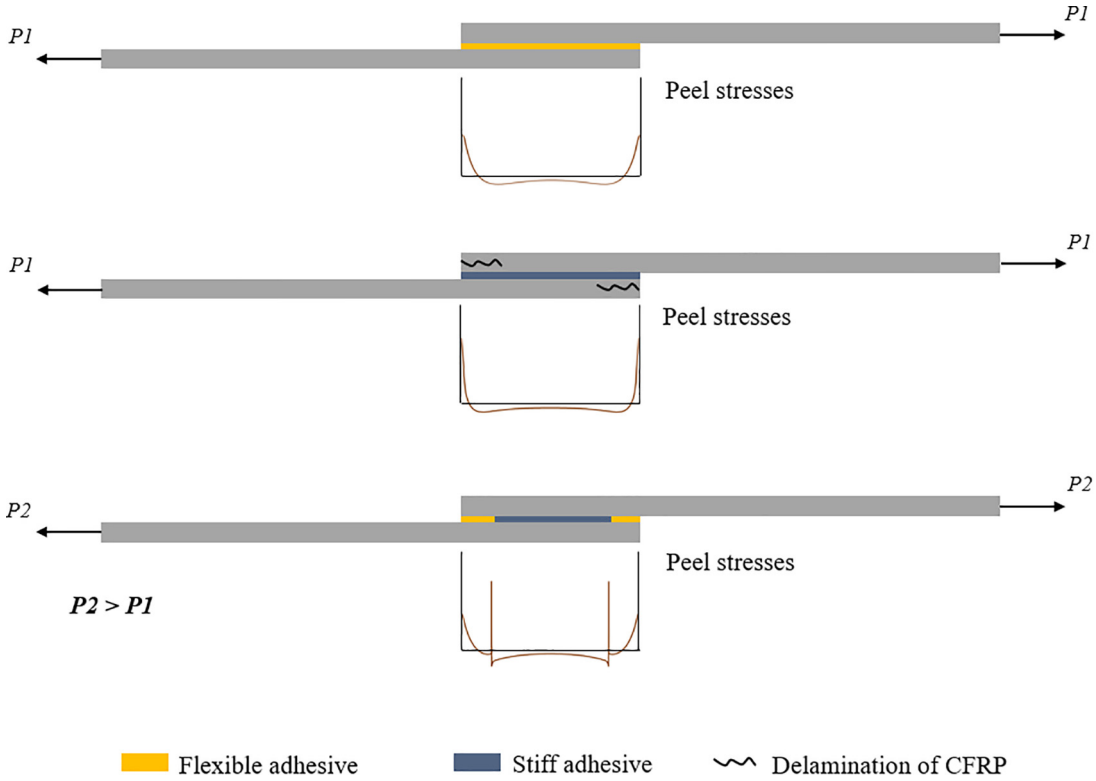

Fig. 3. Schematic representation of the peel stresses acting on SLJs with different adhesive layer configurations.

flexible adhesive (SikaFast 5211 NT) retains some of its ductility and avoids delamination failure of the composite, providing a considerably higher failure load. This behaviour is in accordance with that described by Neto et al. [67], which experimentally identified early delamination for stiff adhesives while a more flexible adhesive was found to carry significantly more load.

At RT, the stiff adhesive (AV 138) is still stiff enough to cause delamination of the CFRP substrate but at HT, it is now being tested substantially closer to its glass transition temperature and becomes more ductile, providing a failure load roughly equivalent to that of the flexible adhesive (SikaFast 5211 NT) at LT. At HT, the flexible adhesive (SikaFast 5211 NT) is found to behave very poorly, as the HT test is performed significantly above its glass transition temperature. This fact is also behind the poor performance of the mixed adhesive joint, which loses the load carrying contribution of the flexible adhesive (SikaFast 5211 NT).

3.1.3. Energy absorbed

Fig. 4 shows the average values of absorbed energy as well as standard deviation of the CFRP SLJs tested at quasi-static conditions varying the temperature.

The higher values of absorbed energy were obtained at LT and RT for SLJs using the flexible adhesive (SikaFast 5211 NT), again due to the flexibility still retained by this adhesive at LT and RT. The high energy absorption capabilities of flexible adhesives under impact have already been observed by the authors during a previous work [51]. At HT, the loss in strength above the glass transition temperature is so significant that the absorbed energy for the flexible adhesive (SikaFast 5211 NT) is almost negligible. The performance of the mixed adhesive joint (AV 138 + SikaFast 5211 NT) is also affected by this behaviour, dropping significantly at HT. For HT, the combination which revealed the highest value of absorbed energy was the stiff adhesive (AV 138), which becomes more ductile as it approaches its glass transition temperature.

Using the data from these tests it is evident that, under quasi-static loadings, the proposed mixed adhesive joint configuration is best suited for operating in temperatures around RT. At HT or LT, the performance of this joint is compromised by the limitations of the adhesives used.

3.2. Impact tests

3.2.1. Fracture surface

The fracture surface exhibited by each specimen and respective description are presented in Table 5, for all the specimens tested under impact conditions and as a function of temperature.

Independently of the testing temperature, it is possible to observe failure by delamination of CFRP when using the stiff adhesive (AV 138), being more severe at LT and RT.

The flexible adhesive (SikaFast 5211 NT) presented cohesive failure in the adhesive for all the testing temperatures, although, at RT and HT the adhesive layer seems to undergo higher shear loadings which is an indication that in this type of SLJs the adhesive layer is undergoing full plasticization.

Failure by delamination of CFRP occurred for the case of the mixed adhesive configuration (AV 138 + SikaFast 5211 NT) at LT. Cohesive failure in the adhesives was present in both RT and HT testing temperatures; once delamination of CFRP was avoided (especially in the case of tests at HT), it is possible to verify that under those circumstances both adhesives undergo full plasticization and experienced large shear loads.

3.2.2. Failure load

Fig. 5 presents the average values of failure load as well as the standard deviation of the CFRP SLJs tested in impact conditions varying the temperature.

As found during the quasi-static tests, the figure shows that optimal performance is provided by the mixed adhesive joint (AV 138 + SikaFast 5211 NT) for RT. At this temperature, the mixed adhesive configuration is again able to avoid delamination and distributes the load by both adhesives, enabling it to sustain higher loads.

For impact tests performed at LT, the failure loads of the three

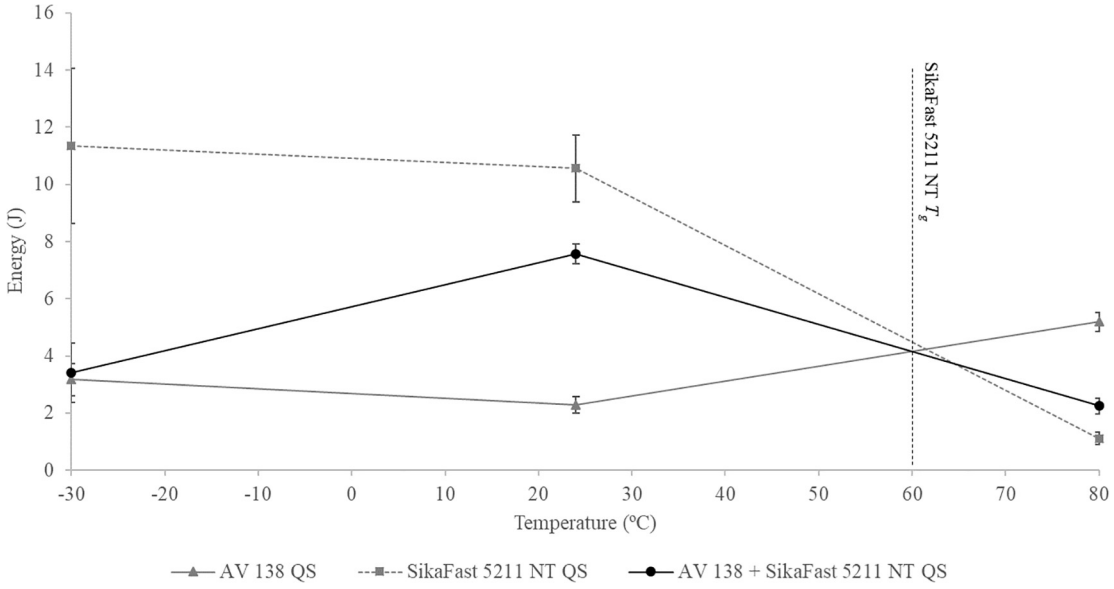

Fig. 4. Values of absorbed energy and standard deviation of all the combinations of SLJs tested at quasi-static conditions as a function of temperature.

specimen configurations under study are relatively similar. The SLJs bonded with the stiff adhesive (AV 138) and the mixed adhesive joints (AV 138 + SikaFast 5211 NT) both fail by delamination of the composite substrate, which results in nearly identical failure loads. Although the SLJ bonded with the flexible adhesive (SikaFast 5211 NT) also provides a similar failure load, its fracture surface indicates a different failure mode, where the adhesive has failed cohesively.

The mixed adhesive (AV 138 + SikaFast 5211 NT) configuration was found to offer an improvement of failure load under impact for RT and HT ranges. In the case of RT, the failure load was 10% higher than that achieved with SLJs made with the flexible (SikaFast 5211 NT) adhesive and 54% higher than that achieved with stiff adhesive (AV 138). The type of failure load of the mixed adhesive SLJs revealed to be cohesive in the adhesive, which is another advantage that this configuration offers over the use of the stiff adhesive (AV 138).

At HT, above the glass transition temperature of the flexible adhesive (SikaFast 5211 NT), there is a marked decrease in failure load for SLJs using only this adhesive and those that use it in a mixed adhesive (AV 138 + SikaFast 5211 NT) configuration. These two configurations exhibit cohesive failure of the adhesive layer, which, due to mechanical property degradation at high temperature, occurs at lower failure loads.

At this temperature, the mixed adhesive joint still presents an improvement (approximately 21%) over the use of single stiff (AV 138) or flexible (SikaFast 5211 NT) adhesive. The failure load was almost identical for SLJs made with stiff (AV 138) and the flexible (SikaFast 5211 NT) adhesive.

In the case of SLJs made using the stiff adhesive (AV 138), it is possible to observe that the value of failure load is essentially identical, and controlled by the CFRP delamination, which was found to not depend greatly on the temperature.

Table 5
Example of fracture surface for all SLJs tested under impact conditions as a function of temperature.

Adhesive combination	−30 °C (LT)	24 °C (RT)	80 °C (HT)
AV 138	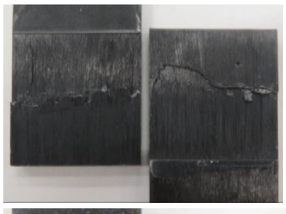	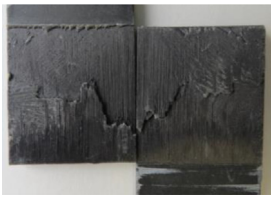	
SikaFast 5211 NT			
AV 138 + SikaFast 5211 NT	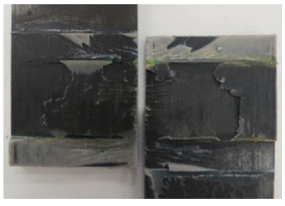	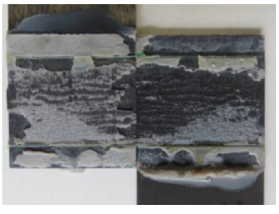	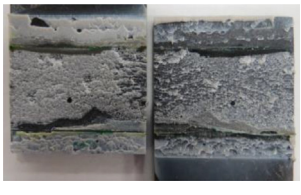

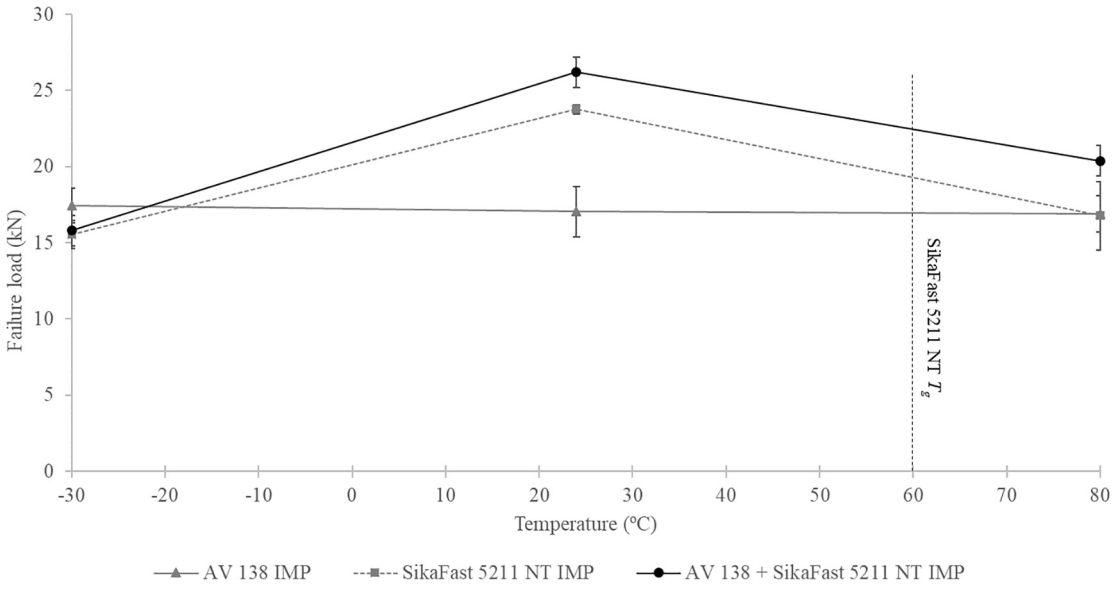

Fig. 5. Values of average failure load and standard deviation of all the combinations of SLJs tested at impact conditions as a function of temperature.

3.2.3. Energy absorbed

In Fig. 6 it is possible to observe the average values of absorbed energy as well as the standard deviation of the CFRP SLJs tested under impact conditions and three different temperatures.

The energy absorbed by the CFRP SLJs tested at LT is very similar and independent of the adhesive configuration used, which is in conformity with the results obtained regarding the failure load. This is to be expected as the main contributor for this energy absorption is the failure of the resin during delamination the CFRP.

At RT, an increase of approximately 150% of absorbed energy was achieved by SLJs made with flexible adhesive (SikaFast 5211 NT) and the mixed adhesive (AV 138 + SikaFast 5211 NT) configuration over the use of the stiff adhesive (AV 138). The lower value of absorbed energy by SLJs made with the stiff adhesive (AV 138) can be explained by the failure of the SLJs by delamination of CFRP.

At HT, the highest value of energy absorbed was by SLJs made with mixed adhesives (AV 138 + SikaFast 5211 NT), and the lowest value was registered when using the stiff adhesive (AV 138) once failure by delamination of CFRP was present.

As determined for quasi-static loadings, under impact loadings, the proposed mixed adhesive joint configuration is again best suited for operating in temperatures around RT. However, due to viscoelastic and viscoplastic effects, the strain rate dependent performance of the flexible adhesive (SikaFast 5211 NT) above its glass transition temperature enables this joint to provide significant impact strength and energy absorption, extending the working range of this joint.

3.3. Comparison between quasi-static and impact tests

A comparison between the quasi-static and impact failure loads for the SLJs manufactured with stiff adhesive (AV 138) and the flexible adhesive (SikaFast 5211 NT) is shown in Fig. 7.

For both adhesives, it is possible to conclude that the failure loads are higher under impact loads for all ranges of temperature tested. However, the joints bonded with flexible adhesive (SikaFast 5211 NT) exhibited an increase in strain rate dependency as the temperature increases and the glass transition temperature is surpassed. This can be attributed to viscoelastic and viscoplastic effects that occur in adhesives

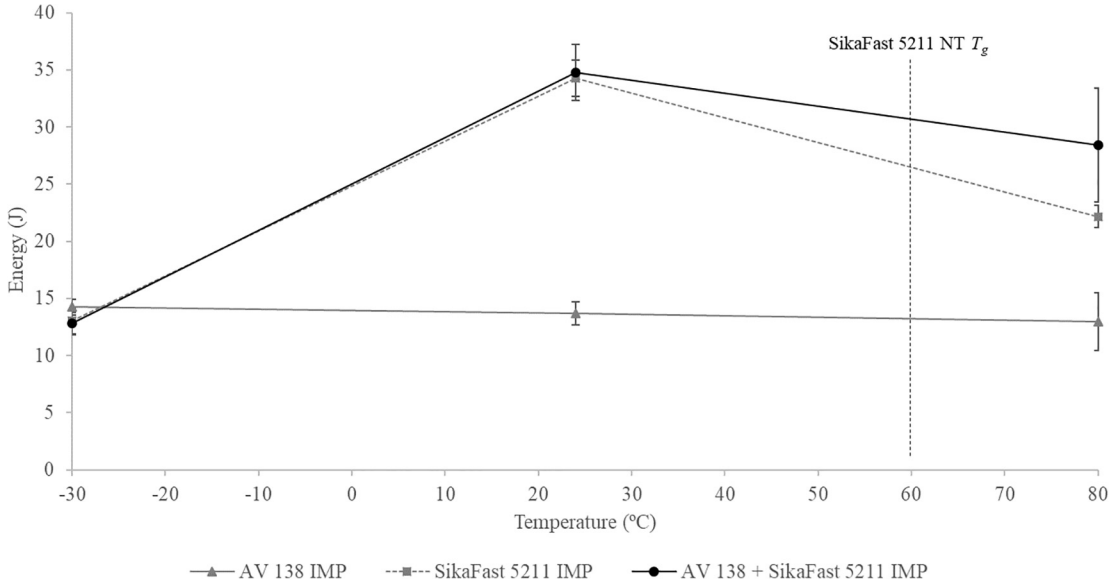

Fig. 6. Values of absorbed energy and standard deviation of all the combinations of SLJs tested at impact conditions as a function of temperature.

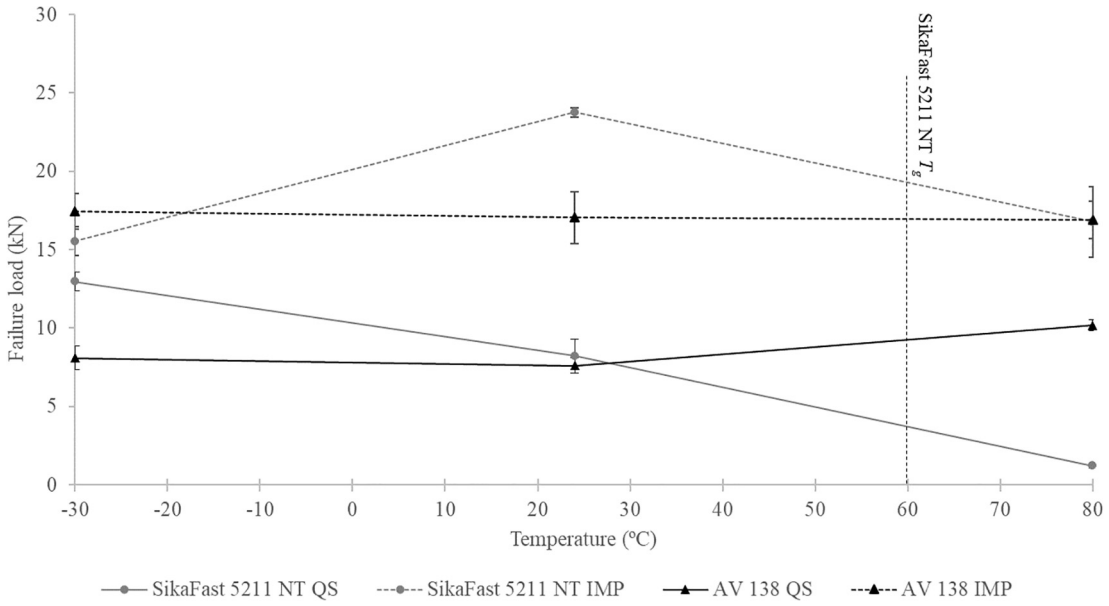

Fig. 7. Comparison of average failure load for single adhesive SLJ combinations tested at quasi-static conditions as a function of temperature.

working close or above their glass transition temperature.

For joints bonded with the stiff adhesive (AV 138), there was no noticeable variation of the strain rate dependency (e.g., the variation between quasi-static and impact failure loads remains roughly constant independently of testing temperature). For this configuration, the failure is mostly dependent on the fracture of the composite, which is further from glass transition temperature and less affected by the previously described viscoelastic and viscoplastic effects.

A comparison between the energy absorbed during quasi-static and impact tests for the SLJs manufactured with stiff adhesive (AV 138) and the flexible adhesive (SikaFast 5211 NT) is shown in Fig. 8.

Energy absorption as a function of temperature shows a behaviour similar to that found for the failure load, with increased strain rate dependence at higher temperatures for the flexible adhesive (SikaFast 5211 NT) and a nearly constant increase of the absorbed energy for the SLJs bonded with the stiff adhesive (AV 138).

A comparison between the quasi-static and impact failure loads for the mixed adhesive SLJs (AV 138 + SikaFast 5211 NT) is shown in Fig. 9.

The behaviour of the mixed adhesive joints follows that of the joints using a single adhesive, which were also found to be strain rate dependent. Additionally, as found for the SLJs bonded only with SikaFast 5211 NT adhesive, with increasing temperature the difference in failure load between quasi-static and impact tests increases.

A comparison between the energy absorbed during quasi-static and impact tests for the mixed adhesive SLJs (AV 138 + SikaFast 5211 NT) is shown in Fig. 10.

The energy absorbed under impact by the mixed adhesive joint (AV 138 + SikaFast 5211 NT) is again shown to be substantially higher than that absorbed under quasi-static conditions.

4. Conclusions

The main goal of this work was to understand the temperature dependent behaviour of CFRP mixed adhesive joints, under quasi-static and impact loads. The mixed adhesive joints studied in this work used a

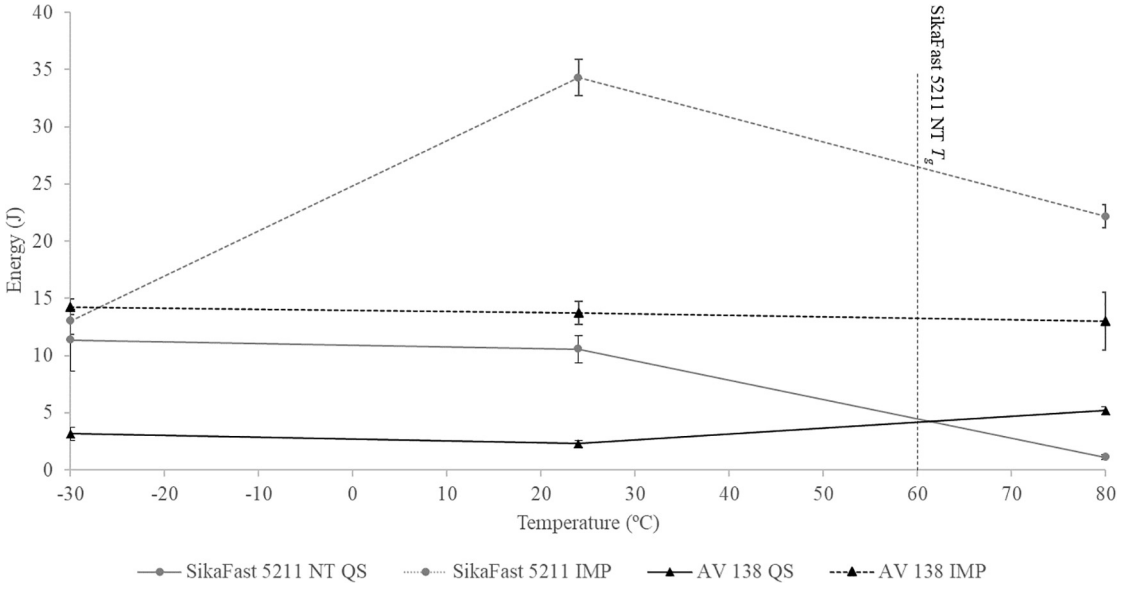

Fig. 8. Comparison of absorbed energy for single adhesive SLJ combinations tested at quasi-static conditions as a function of temperature.

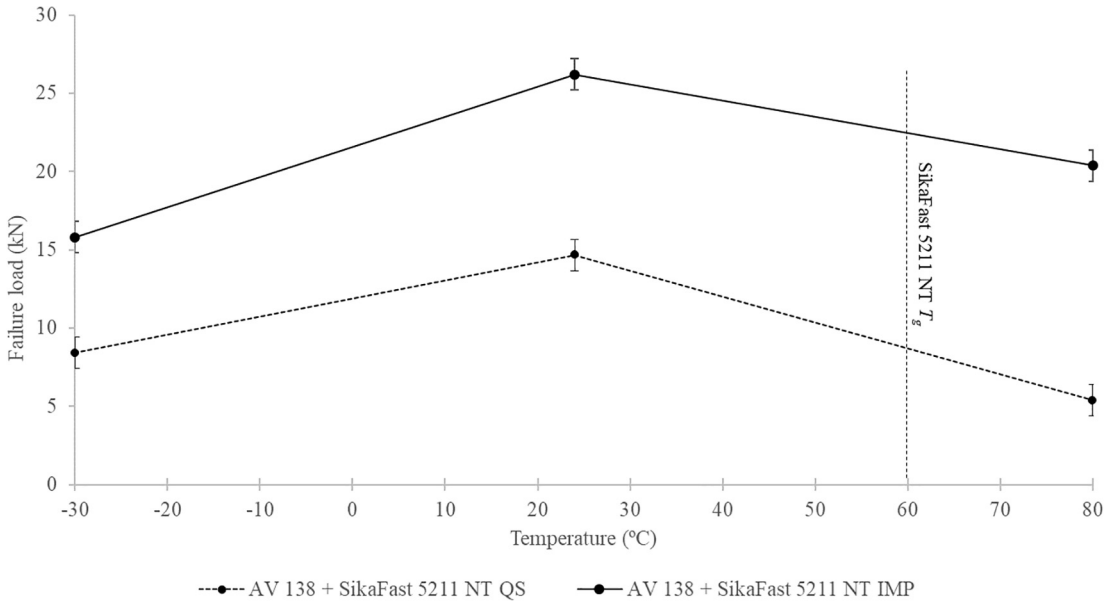

Fig. 9. Comparison of failure load for mixed adhesive SLJs tested under impact conditions as a function of temperature.

stiff (AV 138) and a flexible (SikaFast 5211 NT) adhesive. The performance of the mixed adhesive joint was compared with that of the individual adhesives by experimentally testing SLJs. The main conclusions drawn from this work are presented below.

Quasi-static conditions:

- A considerable improvement of the failure load at RT was obtained by using the mixed adhesive configuration (AV 138 + SikaFast 5211 NT), which exhibited cohesive failure of the adhesive. At LT CFRP delamination occurred and reduced the failure load to match that of the stiff adhesive (AV 138) At high temperature this type of combination performed poorly, as the flexible adhesive (SikaFast 5211 NT) is operating well above glass transition temperature.
- The flexible adhesive (SikaFast 5211 NT) exhibited the highest energy absorption for LT and RT, with the mixed adhesive joint performing well only at RT. At HT all joints were found to have limited energy absorption capabilities.
- Under quasi-static conditions the proposed mixed adhesive joint configuration was found to be best suited for operating in temperatures around RT. At HT or LT, the performance of this joint is severely compromised by the limitations of the adhesives used.

Impact conditions:

- Failure by delamination of the CFRP occurred for the case of the mixed adhesive configuration (AV 138 + SikaFast 5211 NT) at LT. Cohesive failure in the adhesives was present in both RT and HT testing temperatures; once delamination of CFRP was avoided (especially in the case of tests at HT), it is possible to verify that under those circumstances both adhesives undergo full plasticization under shear.
- The mixed adhesive (AV 138 + SikaFast 5211 NT) configuration was found to offer an improvement of failure load under impact for RT and HT ranges. The improved performance at HT over quasi-static tests can be attributed to the viscoelasticity and viscoelasticity that occurs in the flexible adhesive (SikaFast 5211 NT) operating

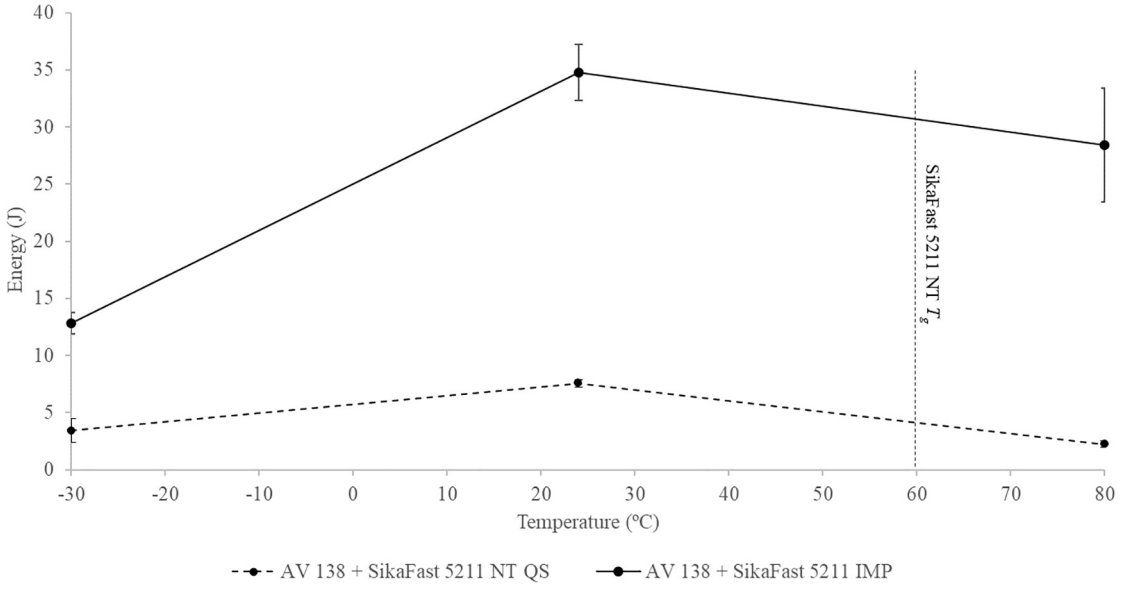

Fig. 10. Comparison of absorbed energy for mixed adhesive SLJs tested under impact conditions as a function of temperature.

above its glass transition temperature.

- The highest value of energy absorbed was obtained with the mixed adhesive SLJs. The lowest value of energy was registered when using the stiff adhesive (AV 138) due to delamination failure of the CFRP.

Comparison between quasi-static and impact conditions:

- All SLJs tested were found to exhibit strain rate dependency. SLJs which used the flexible adhesive (SikaFast 5211 NT) were found to have increased strain rate dependency with higher temperatures.
- Under impact conditions the proposed mixed adhesive joint configuration has a widened range of operation, with improved performance at RT and HT. At LT, the higher stiffness of adhesives causes early delamination failure.

As a conclusion, with the experimental data gathered it becomes evident that the proposed composite mixed adhesive joint configuration is not suitable for operation under impact in this wide range of temperatures. The complex balance between low stiffness at low temperatures (to avoid delamination of CFRP) and high strength at high temperatures (to avoid low mechanical performance) requires further iterations in adhesive selection.

Acknowledgments

The authors gratefully acknowledge the funding of Project NORTE-01-0145-FEDER-000022 – SciTech – Science and Technology for Competitive and Sustainable Industries, co-financed by Programa Operacional Regional do Norte (NORTE2020), through Fundo Europeu de Desenvolvimento Regional (FEDER). The authors would also like to thank NAGASE ChemteX® for the financial support provided.

The authors declare that they have no conflict of interest.

References

[1] da Silva LM. Handbook of adhesion technology. Springer Science & Business Media; 2011.
[2] Burchardt B. Automotive Industry. Handbook of Adhesion Technology. Springer; 2011. p. 1185–212.
[3] Ishikawa T, Amaoka K, Masubuchi Y, Yamamoto T, Yamanaka A, Arai M, et al. Overview of automotive structural composites technology developments in Japan. Compos Sci Technol 2017.
[4] Machado J, Marques E, Campilho R, da Silva LFM. Mode I fracture toughness of CFRP as a function of temperature and strain rate. J Compos Mater 2016;0021998316682309.
[5] Daniel I, LaBedz R, Liber T. New method for testing composites at very high strain rates. Exp Mech 1981;21(2):71–7.
[6] Al-Hassani S, Kaddour A. Strain rate effects on GRP, KRP and CFRP composite laminates. Key engineering materials. Trans Tech Publ; 1998. p. 427–52.
[7] Takeda T, Narita F. Fracture behavior and crack sensing capability of bonded carbon fiber composite joints with carbon nanotube-based polymer adhesive layer under Mode I loading. Compos Sci Technol 2017;146:26–33.
[8] Harding J, Welsh L. A tensile testing technique for fibre-reinforced composites at impact rates of strain. J Mater Sci 1983;18(6):1810–26.
[9] Taniguchi N, Nishiwaki T, Kawada H. Tensile strength of unidirectional CFRP laminate under high strain rate. Adv Compos Mater 2007;16(2):167–80.
[10] Jacob GC, Starbuck JM, Fellers JF, Simunovic S, Boeman RG. The effect of loading rate on the fracture toughness of fiber reinforced polymer composites. J Appl Polym Sci 2005;96(3):899–904.
[11] Aliyu A, Daniel I. Effects of strain rate on delamination fracture toughness of graphite/epoxy. Delamination and debonding of materials. ASTM International; 1985.
[12] Daniel IM, Shareef I, Aliyu AA. Rate effects on delamination fracture toughness of a toughened graphite/epoxy. Toughened composites. ASTM International; 1987.
[13] Daniel I, Yaniv G, Auser J. Rate effects on delamination fracture toughness of graphite/epoxy composites. Composite Structures 4. Springer; 1987. p. 258-72.
[14] Yaniv G, Daniel IM. Height-tapered double cantilever beam specimen for study of rate effects on fracture toughness of composites. Composite materials: testing and design (Eighth Conference). ASTM International; 1988.
[15] You H, Yum Y-J. Loading rate effect on mode I interlaminar fracture of carbon/epoxy composite. J Reinf Plast Compos 1997;16(6):537–49.
[16] Blackman B, Dear J, Kinloch A, Macgillivray H, Wang Y, Williams J, et al. The failure of fibre composites and adhesively bonded fibre composites under high rates of test. J Mater Sci 1995;30(23):5885–900.
[17] Kusaka T, Hojo M, Mai Y-W, Kurokawa T, Nojima T, Ochiai S. Rate dependence of mode I fracture behaviour in carbon-fibre/epoxy composite laminates. Compos Sci Technol 1998;58(3–4):591–602.
[18] Kageyama K, Kimpara I. Delamination failures in polymer composites. Mater Sci Eng, A 1991;143(1–2):167–74.
[19] Maikuma H, Gillespie Jr JW, Wilkins DJ. Mode II interlaminar fracture of the center notch flexural specimen under impact loading. J Compos Mater 1990;24(2):124–49.
[20] Todo M, Nakamura T, Takahashi K. Mode II interlaminar fracture behavior of fiber reinforced polyamide composites under static and dynamic loading conditions. J Reinf Plast Compos 1999;18(15):1415–27.
[21] Chapman T, Smiley A, Pipes R. Rate and temperature effects on Mode II interlaminar fracture toughness in composite materials. Proc ICCM VI/ECCM 1987;2:3.295-3.305.
[22] Daniel I, Werner B, Fenner J. Strain-rate-dependent failure criteria for composites. Compos Sci Technol 2011;71(3):357–64.
[23] Hsiao H, Daniel I. Strain rate behavior of composite materials. Compos B Eng 1998;29(5):521–33.
[24] Delfosse D, Poursartip A. Energy-based approach to impact damage in CFRP laminates. Compos A Appl Sci Manuf 1997;28(7):647–55.
[25] Neumayer J, Kuhn P, Koerber H, Hinterholzl R. Experimental determination of the tensile and shear behaviour of adhesives under impact loading. J Adhes 2016;92(7–9):503–16.
[26] May M, Hesebeck O, Marzi S, Böhme W, Lienhard J, Kilchert S, et al. Rate dependent behavior of crash-optimized adhesives–Experimental characterization, model development, and simulation. Eng Fract Mech 2015;133:112–37.
[27] Sanchez FSR. Fracture Behaviour of Automotive Adhesive Joints: Imperial College London; 2008.
[28] Lu D, Wong C. Effects of shrinkage on conductivity of isotropic conductive adhesives. Int J Adhes Adhes 2000;20(3):189–93.
[29] da Silva LFM, Adams R. Stress-free temperature in a mixed-adhesive joint. J Adhes Sci Technol 2006;20(15):1705–26.
[30] da Silva LFM, Adams R. Measurement of the mechanical properties of structural adhesives in tension and shear over a wide range of temperatures. J Adhes Sci Technol 2005;19(2):109–41.
[31] Adams R, Mallick V. The effect of temperature on the strength of adhesively-bonded composite-aluminium joints. J Adhes 1993;43(1–2):17–33.
[32] Deb A, Malvade I, Biswas P, Schroeder J. An experimental and analytical study of the mechanical behaviour of adhesively bonded joints for variable extension rates and temperatures. Int J Adhes Adhes 2008;28(1):1–15.
[33] Marques E, da Silva LFM, Banea M, Carbas R. Adhesive joints for low-and high-temperature use: an Overview. J Adhes 2015;91(7):556–85.
[34] Adams R, Coppendale J, Mallick V, Al-Hamdan H. The effect of temperature on the strength of adhesive joints. Int J Adhes Adhes 1992;12(3):185–90.
[35] Kang S-G, Kim M-G, Kim C-G. Evaluation of cryogenic performance of adhesives using composite–aluminum double-lap joints. Compos Struct 2007;78(3):440–6.
[36] Banea MD, da Silva LFM, Carbas RJ, Campilho R. Mechanical and thermal characterization of a structural polyurethane adhesive modified with thermally expandable particles. Int J Adhes Adhes 2014;54:191–9.
[37] Banea M, da Silva LFM. The effect of temperature on the mechanical properties of adhesives for the automotive industry. Proc Inst Mech Eng Part L 2010;224(2):51–62.
[38] Owens JF, Lee-Sullivan P. Stiffness behaviour due to fracture in adhesively bonded composite-to-aluminum joints II. Experimental. Int J Adhes Adhes 2000;20(1):47–58.
[39] da Silva LFM, Adams R. Techniques to reduce the peel stresses in adhesive joints with composites. Int J Adhes Adhes 2007;27(3):227–35.
[40] Adams R, Atkins R, Harris J, Kinloch A. Stress analysis and failure properties of carbon-fibre-reinforced-plastic/steel double-lap joints. J Adhes 1986;20(1):29–53.
[41] Tang J, Sridhar I, Srikanth N. Static and fatigue failure analysis of adhesively bonded thick composite single lap joints. Compos Sci Technol 2013;86:18–25.
[42] Fessel G, Broughton J, Fellows N, Durodola J, Hutchinson A. Evaluation of different lap-shear joint geometries for automotive applications. Int J Adhes Adhes 2007;27(7):574–83.
[43] Raphael C. Variable-adhesive bonded joints. Appl Polym Symp 1966:99–108.
[44] Fitton M, Broughton J. Variable modulus adhesives: an approach to optimised joint performance. Int J Adhes Adhes 2005;25(4):329–36.
[45] Breto R, Chiminelli A, Duvivier E, Lizaranzu M, Jiménez M. Functionally graded bond-lines for metal/composite joints; 2014.
[46] Öz Ö, Özer H. An experimental investigation on the failure loads of the mono and bi-adhesive joints. J Adhes Sci Technol 2017;31(19–20):2251–70.
[47] Hart-Smith LJ. Adhesive-bonded single-lap joints. Hampton, VA: Langley Research Center; 1973.
[48] das Neves PJ, da Silva LFM, Adams R. Analysis of mixed adhesive bonded joints part I: theoretical formulation. J Adhes Sci Technol 2009;23(1):1–34.
[49] das Neves PJ, da Silva LFM, Adams R. Analysis of mixed adhesive bonded joints part II: parametric study. J Adhes Sci Technol 2009;23(1):35–61.
[50] da Silva LFM, Lopes MJC. Joint strength optimization by the mixed-adhesive technique. Int J Adhes Adhes 2009;29(5):509–14.
[51] Silva M, Marques E, da Silva LFM. Behaviour under Impact of Mixed Adhesive Joints for the Automotive Industry. Latin Am J Solids Struct 2016;13(5):835–53.
[52] Banea M, De Sousa F, da Silva LFM, Campilho R, de Pereira AB. Effects of temperature and loading rate on the mechanical properties of a high temperature epoxy adhesive. J Adhes Sci Technol 2011;25(18):2461–74.
[53] Carlberger T, Biel A, Stigh U. Influence of temperature and strain rate on cohesive properties of a structural epoxy adhesive. Int J Fract 2009;155(2):155–66.
[54] Machado J, Gamarra P, Marques E, da Silva LFM. Improvement in impact strength of composite joints for the automotive industry. Compos Part B: Eng 2017. Accepted

for publication.
[55] da Silva LFM, De Magalhaes F, Chaves F, De Moura M. Mode II fracture toughness of a brittle and a ductile adhesive as a function of the adhesive thickness. J Adhes 2010;86(9):891–905.
[56] Netusil M, Eliasova M. Trends and requirements for adhesives with load bearing role. Proc Challenging Glass 2014;4:369–74.
[57] Zgoul M, Crocombe A. Numerical modelling of lap joints bonded with a rate-dependent adhesive. Int J Adhes Adhes 2004;24(4):355–66.
[58] Avendaño R, Carbas R, Marques E, da Silva LFM, Fernandes A. Effect of temperature and strain rate on single lap joints with dissimilar lightweight adherends bonded with an acrylic adhesive. Compos Struct 2016;152:34–44.
[59] Machado J, Marques E, Campilho R, da Silva LFM. Mode II fracture toughness of CFRP as a function of temperature and strain rate. Compos B Eng 2017;114:311–8.
[60] Campilho R. Repair of composite and wood structures [Ph.D. Thesis]. Faculdade de Engenharia da Universidade do Porto; 2009.
[61] Campilho RDSG, de Moura MFSF, Domingues JJMS. Stress and failure analyses of scarf repaired CFRP laminates using a cohesive damage model. J Adhes Sci Technol 2007;21(9):855–70.
[62] da Silva LFM, Adams R. Joint strength predictions for adhesive joints to be used over a wide temperature range. Int J Adhes Adhes 2007;27(5):362–79.
[63] da Silva LFM, Adams R. Adhesive joints at high and low temperatures using similar and dissimilar adherends and dual adhesives. Int J Adhes Adhes 2007;27(3):216–26.
[64] da Silva MRG. Impact of mixed adhesive joints for the automotive industry; 2015.
[65] ASTM D. 1002. Standard Test Method for Apparent Shear Strength of Single-Lap-Joint Adhesively Bonded Metal Specimens by Tension Loading (Metal-to-Metal) 2005;15:45–8.
[66] Carbas R, Marques E, da Silva LFM, Lopes A. Effect of cure temperature on the glass transition temperature and mechanical properties of epoxy adhesives. J Adhes 2014;90(1):104–19.
[67] Neto J, Campilho R, da Silva LFM. Parametric study of adhesive joints with composites. Int J Adhes Adhes 2012;37:96–101.

Paper 11

Content of Paper 11

Abstract

1. Introduction

2. Experimental details

2.1. CFRP mechanical properties

2.2. Joint geometry

2.3. Dynamic testing details

2.4. Data reduction scheme

3. Numerical simulation details

3.1. Cohesive zone modelling

3.2. Dynamic model

3.2.1. Geometry and boundary conditions

3.2.2. Material properties

3.2.3. Mesh

3.2.4. Result output

4. Results and discussion

4.1. DCB opening displacement

4.2. Crack propagation and fracture toughness

4.3. Variation of strain rate

5. Conclusions

References

Check for updates

Original article

Institution of MECHANICAL ENGINEERS

Journal of MATERIALS: DESIGN AND APPLICATIONS

Proc IMechE Part L:
J Materials: Design and Applications
0(0) 1–9
© IMechE 2019
Article reuse guidelines:
sagepub.com/journals-permissions
DOI: 10.1177/1464420719871390
journals.sagepub.com/home/pil

SAGE

Numerical study of mode I fracture toughness of carbon-fibre-reinforced plastic under an impact load

JJM Machado[1], PDP Nunes[1], EAS Marques[1], RDSG Campilho[1,2] and Lucas FM da Silva[3]

Abstract

The main objective of this work is, by using cohesive zone modelling, to compute the fracture toughness behaviour in mode I of unidirectional carbon-fibre-reinforced plastic subjected to an impact load at 4.7 m/s. To perform this task, double-cantilever beam specimens were simulated, with its opening displacement and crack propagation being assessed, as well as the evolution of strain rate through the test. Therefore, by plotting the crack propagation, it was possible to calculate the fracture toughness in mode I (G_{IC}). A comparison of the numerical results with experimental tests previously performed by using a drop weight falling-wedge impact test equipment was made, allowing to infer that the numerical approach, based on a triangular cohesive zone modelling, is capable to predict the behaviour of such specimens under impact, accurately obtain G_{IC}, and to determine the value of strain rate achieved through the test.

Keywords

Carbon-fibre-reinforced plastic, impact, fracture toughness in mode I, finite element analysis

Date received: 21 June 2019; accepted: 1 August 2019

Introduction

The application of composite materials within the automotive industry has increased in the last years, since these type of materials offers several advantages over other commonly used structural materials, such as steel and aluminium. Among those advantages, some can be pointed out, such as the opportunity to easily design custom-made structures, higher strength-to-weight ratios over the other materials, higher corrosion resistance and an improvement of the fatigue properties.[1] However, understanding the behaviour of composites under an impact load is crucial in the design phase since, when applied in vehicles, composites might undergo high strain rates due to collisions (and due to their stiffness, which does not allow them to deform plastically).[2]

A common type of failure of composites under impact load is the interlaminar fracture, in which the material fails by delamination. This is often related to a transverse load situation, governed by G_{IC}. The mechanical properties of composites are known to vary as a function of the loading rate.[3–6] Some studies,[7,8] considering composites with 0° ply orientation, observed a considerable effect of the strain rate on both tensile and compressive loads (also, the stiffness is higher with increasing strain rates for both cases). Jacob et al.[4] made a review on the experimental G_{IC} results of composites, not finding any agreement on how the strain rate affects such parameter. Blackman et al.[9] avoided the influence of the dynamical effects to measure G_{IC} by using an equation which did not require data from measured loads.

No standard exists to determine G_{IC} of composites under high strain rates, but several can be found[1,10,11] for quasi-static conditions. According to May,[12] the most suitable test to determine the G_{IC} of composite materials under high strain rates is the double-cantilever beam (DCB) test.[13] A common problem

[1]Instituto de Ciência e Inovação em Engenharia Mecânica e Engenharia Industrial (INEGI), Rua Dr. Roberto Frias, Porto, Portugal
[2]Departamento de Engenharia Mecânica, Instituto Superior de Engenharia do Porto (ISEP), Instituto Politécnico do Porto, Rua Dr. António Bernardino de Almeida, Porto, Portugal
[3]Departamento de Engenharia Mecânica, Faculdade de Engenharia (FEUP), Universidade do Porto, Rua Dr. Roberto Frias, Porto, Portugal

Corresponding author:
Lucas FM da Silva, Departamento de Engenharia Mecânica, Faculdade de Engenharia (FEUP), Universidade do Porto, Rua Dr. Roberto Frias, Porto 4200-465, Portugal.
Email: lucas@fe.up.pt

when testing DCB specimens made of composites is the absence of symmetry[14] while opening under impact, therefore, the wedge loaded setup is an option to avoid such problem.[15–17] Numerical analyses of composite plates under an impact load were performed by several authors[18–20] with good agreement with the experimental results. The use of cohesive elements to simulate the behaviour of composite materials has been studied,[21–24] allowing to conclude that such integration is able to correctly assess the G_{IC} behaviour. Numerical studies regarding the measurement of G_{IC} of composite materials are not currently available in the literature for the case of impact conditions, which then constitutes a field to explore.

The main goal of this work is, by using cohesive zone modelling (CZM), to compute G_{IC} of unidirectional CFRP specimens subjected to an impact load at a speed of 4.7 m/s. DCB specimens were simulated, with its opening displacement and crack propagation being assessed, as well the evolution of strain rate through the test. Therefore, by plotting the crack propagation as a function of testing time, it was possible to calculate G_{IC}. A comparison of the numerical results with previously performed experimental tests[25] by using a drop weight falling-wedge impact test equipment was made, allowing to infer that the numerical approach, based on a triangular CZM, is capable to predict the behaviour of such specimens under impact, to accurately obtain G_{IC}, and to determine the value of strain rate achieved through the test.

Experimental details

CFRP mechanical properties

The composite material used in this work to manufacture the DCB specimens consisted of a carbon/epoxy CFRP in the form of prepreg, designated as SEAL® Texipreg HS 160 RM. This material was used with a configuration of 0° lay-up plies, to ensure that optimal properties are obtained in the loading direction.

The CFRP elastic properties (namely, Young's modulus (E), shear modulus (G) and Poisson's ratio (ν)) with this specific configuration in the three directions were previously determined by Campilho et al.[21] and are presented in Table 1.

One of the few known work regarding the impact characterization of CFRP in which the G_{IC} was experimentally determined, was performed by the authors.[25] As only experimental data are available for the case of quasi-static conditions,[22,26] the mechanical properties of CFRP under impact were not considered to be strain rate dependent in the numerical models, and were based on the quasi-static values (Table 2).

Table 1. Properties of CFRP elastic orthotropic of an unidirectional ply of CFRP aligned in direction 1, 2 is the transverse direction and 3 is the out-of-plane direction.[21]

Elastic modulus (MPa)	Poisson's ratio	Shear modulus (MPa)
$E_1 = 1.09E5$	$\nu_{12} = 0.342$	$G_{12} = 4315$
$E_2 = 8819$	$\nu_{13} = 0.342$	$G_{13} = 4315$
$E_3 = 8819$	$\nu_{23} = 0.380$	$G_{23} = 3200$

Table 2. CFRP mechanical properties under impact (4.7 m/s) conditions in the fibre direction.

Properties	4.7 m/s
Young's modulus, E	109,000 MPa
Shear modulus, G	4315 MPa
Tensile strength, σ_n	40 MPa
Shear strength, t_s	35 MPa
Fracture energy (mode I), G_{IC}	0.42 N/mm
Fracture energy (mode II), G_{IIC}	0.82 N/mm

Joint geometry

The DCB joint geometry was used to estimate the G_{IC} of CFRP under impact loadings, which is one of the most commonly used specimens for such purpose.[27]

The DCB specimen geometry followed the ISO 15024 standard[27] (Figure 1), used to determine G_{IC} of unidirectional fibre-reinforced plastic composites. The standard states that the applied load should be perpendicular to the delamination plane of the DCB specimens, which was achieved by using loading blocks, in the case of the previously performed experimental tests.[25]

Dynamic testing details

The numerical simulation will be based on the experimental tests previously performed[25] to accurately replicate the dynamical testing process.

A drop weight falling-wedge equipment was used to perform the impact tests (Figure 2), and the initial impact velocity of 4.7 m/s was achieved by releasing the impactor at a height 1130 mm, providing a maximum impact energy of 148 J. The impactor (that includes two polycarbonate wedges and a set of weights) was released from the set height, impacting the pins positioned in the centre of the load blocks, opening the specimens and promoting crack growth.

Strain rate ($\dot{\varepsilon}$) is the change in strain (deformation) of a specific material with respect to time. The strain value under impact can be determined from equation (1)

$$\dot{\varepsilon}(t) = \frac{v(opening)}{L_0} \quad (1)$$

where $v(opening)$ is the lateral displacement rate (mm/s), and L_0 the length of the specimen (mm).

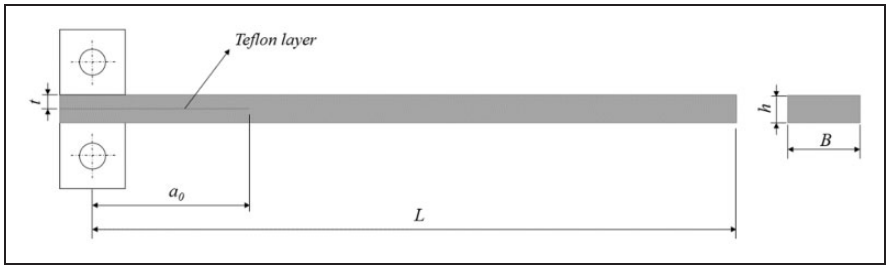

Figure 1. Geometry and dimensions of DCB CFRP specimens following ISO 15024 standard ($L = 125$ mm, $B = 25$ mm, $h = 3$ mm, $a_0 = 45$ mm and $t = 1.5$ mm, which is half of h).

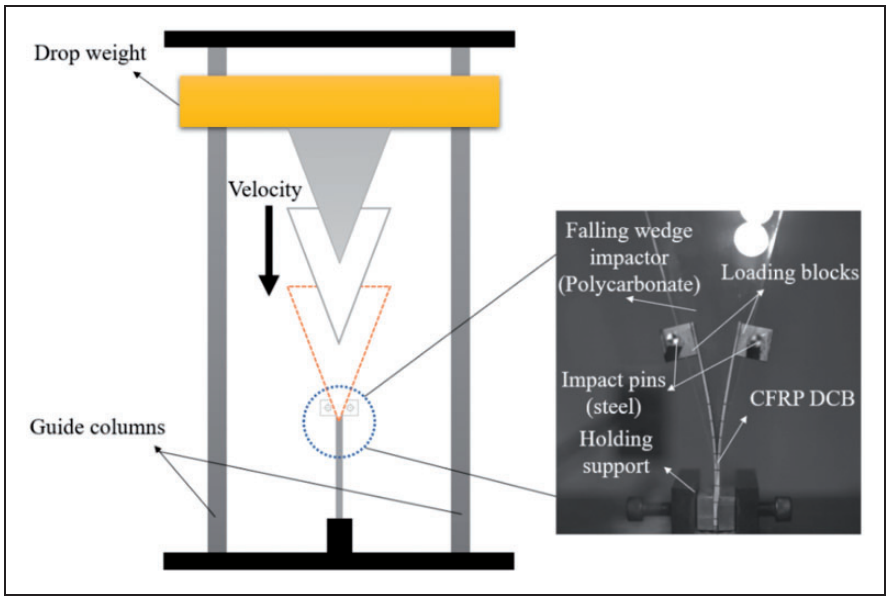

Figure 2. Schematic representation of the impact falling-wedge equipment (left), as well a photo of the test being performed (right) – wedge angle of 30°.

In this specific case, for the DCB specimen made of CFRP, the value of L_0 considered was in respect with the thickness of the a CFRP ply, equal to 0.15 mm.

Equation (2) is used to determine $v(opening)$

$$v(opening) = 2 \times v(pin) = \frac{\Delta h}{\frac{1}{v(impactor)}} = \frac{tg\alpha}{1/2500} \quad (2)$$

From equation (2), the required variables are defined as: the velocity of the pins movement during the impact is specified by $v(pin)$, the velocity of the impactor during the test by $v(impactor)$, Δh corresponds to the displacement of the specimens opening during the test and α is the angle of the striker wedges.

Data reduction scheme

The load under impact conditions cannot be directly measured in this type of tests, therefore it was necessary to use a load reduction scheme to determine G_{IC}.

The load independent method (LIM)[9,28] can be used to calculate G_{IC} (based on the beam theory). For the LIM, it is necessary to accurately measure the crack length to determine G_{IC}. Since the crack length correction ($|\Delta|$) comprises the large influence of high strain rate effects, G_{IC} values determined under quasi-static conditions[22] can be used to calculate the fracture energy overall. When the LIM is determined using $|\Delta|$, it is represented as LIM_{Δ}. By using the compliance based beam method (CBBM) crack length correlation (Δ_{CBBM}), LIM must be addressed as LIM_{CBBM}, and G_{IC} is given by equation (3) when LIM_{Δ}

$$G_I = \frac{9\delta^2 EIF}{4B(a + |\Delta|)^4} \quad (3)$$

For LIM_{CBBM}, the value of G_{IC} is determined by the following equation

$$G_I = \frac{9\delta^2 EIF}{4B(a + \Delta_{CBBM})^4} \quad (4)$$

Load blocks (Figure 3) were used to transfer the impact load.

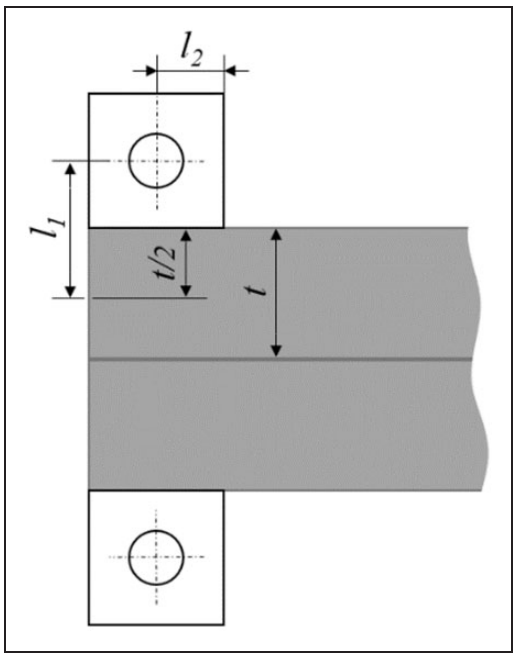

Figure 3. Schematic representation of the DCB specimen with load blocks (t is the thickness of the upper substrate, l_1 and l_2 are respectively the vertical and horizontal dimensions of the centre of the load blocks).

In Figure 3, l_1 is the distance (in the vertical direction) from the centre of the loading block up to half of the upper section thickness of the DCB specimen, and l_2 is half the block length.

The displacement correction factor is determined by the ratio between F (equation (5)) and N (equation (6)). F is the crack length correction factor accounting for beam root rotation and shear effects, N is the large beam displacements and load block stiffening effects, δ is the opening displacement and a is the crack length.

$$F = 1 - 0.3\left(\frac{\delta}{a}\right)^2 - 1.5\left(\frac{l_1\delta}{a^2}\right) \tag{5}$$

$$N = 1 - \left(\frac{l_2}{a}\right)^3 - \frac{9}{8}\frac{\delta l_1}{a^2}\left\{1 - \left(\frac{l_2}{a}\right)^2\right\} - \frac{9}{35}\left(\frac{\delta}{a}\right)^2 \tag{6}$$

The correlation between the variables N and F used was set to be $\left(\frac{F}{N}\right)$, which should then be multiplied by equation (4).

Numerical simulation details

Cohesive zone modelling

A CZM numerical study was performed to assess several parameters during an impact test (drop weight falling-wedge) of a DCB specimen made of CFRP under mode I fracture toughness, such as δ and $\dot{\varepsilon}$ through the tests. For such purpose, the finite element software Abaqus® (Dassault Systèmes, Suresnes, France) was used.

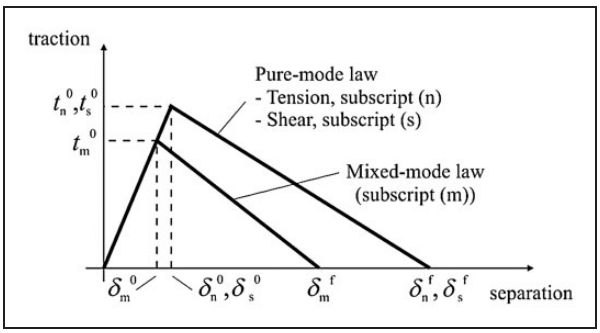

Figure 4. Triangular traction-separation law with linear softening: pure and mixed-mode models available in Abaqus®.[29]

The numerical model performed consisted of cohesive elements based on a triangular (bilinear) traction-separation law, placed in a 0.15 mm thick layer to simulate decohesion in a CFRP ply, which was defined according to the CFRP mechanical cohesive properties (considering inexistent any defects on the material).

The schematic representation of the applied triangular traction-separation law can be observed in Figure 4. It can be defined that t_n^0 and t_s^0 are, respectively, the cohesive strengths in tension and shear, δ_n^0 and δ_s^0 are the respective displacements and δ_n^f and δ_s^f correspond to the tensile and shear displacements at failure.

With respect to the mechanical properties of the CFRP, the parameters of the triangular law can be altered to satisfactorily fit the simulated properties. The initial elastic portion is defined by a constitutive matrix (K) and it is kept constantly linear, containing the stiffness parameters and relating current stresses (t) and strains (ε) in three loading modes across the interface (equation (7))

$$t = \begin{Bmatrix} t_n \\ t_{s1} \\ t_{s2} \end{Bmatrix} = \begin{bmatrix} K_{nn} & K_{ns1} & K_{ns2} \\ K_{ns1} & K_{s1s1} & K_{s1s2} \\ K_{ns2} & K_{s1s2} & K_{s2s2} \end{bmatrix} \cdot \begin{Bmatrix} \varepsilon_n \\ \varepsilon_{s1} \\ \varepsilon_{s2} \end{Bmatrix} = K\varepsilon \tag{7}$$

After the mixed-mode cohesive strength is reached (defined by t_m^0 in Figure 2), the material stiffness is degraded. A linear power law then predicts failure by the required fracture energies in the pure modes, as shown in equation (8)

$$\frac{G_I}{G_I^c} + \frac{G_{II}}{G_{II}^c} = 1 \tag{8}$$

Based on equation (8), it is possible to describe G_I and G_{II} as the parameters denoting the strain energy release rates of each loading mode, and G_{II}^c and G_{II}^c being the respective critical values. Several other shapes can simulate the softening portion of the curve, according to the type of material properties, such as the polynomial,[22] exponential,[25] trapezoidal[23]

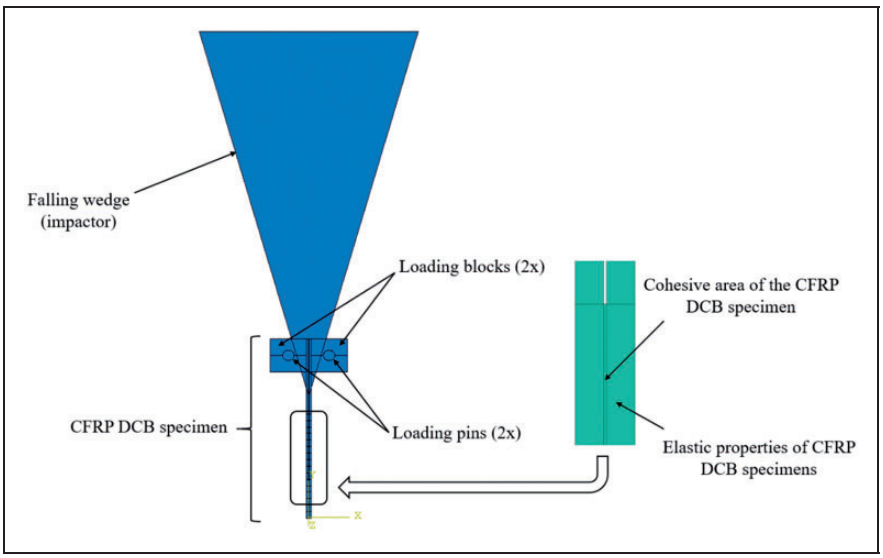

Figure 5. Geometry of the numerical model (assembly).
CFRP: carbon-fibre-reinforced plastic; DCB: double-cantilever beam.

or triangular.[28] When using stiff and brittle resins, triangular laws are known to be the most appropriate type, as for the case of ductile resins the trapezoidal cohesive laws are the most consistent.[30]

Dynamic model

A two-dimensional model was created in Abaqus®/Explicit to replicate the impact conditions of the experimental drop weight falling-wedge impact test previously performed using a DCB specimen made of CFRP.[25]

Geometry and boundary conditions. The geometry of the numerical model comprised three different parts, following the experimental setup, which included the CFRP DCB specimen, the falling wedge and the impact pins (two units), as shown in Figure 5.

The three distinct parts were created separately and were assembled afterwards using interactions, namely surface-to-surface contacts (explicit), where the mechanical constraint formulation used was the penalty contact method. The contact interaction property was defined as a frictionless tangential behaviour as the LIM data reduction scheme does not require force values, but instead only needs the crack length values. The same contact interaction was used between the falling-wedge impactor and the impacting pins, as well as between the pins and the CFRP DCB specimen.

The bottom section of the CFRP DCB was set as clamped, and a velocity field of 4.7 m/s was applied to the falling wedge (impactor), as shown in Figure 6. The impactor falling wedge density was set in order to guarantee a mass of 13.4 kg, to replicate the experimental tests.

Material properties. The falling wedge impactor was modelled using elastic elements. A high stiffness value was attributed to this part, in order to approximate its behaviour to a rigid body. As mentioned before, the density of this part was defined to ensure the 13.4 kg of mass.

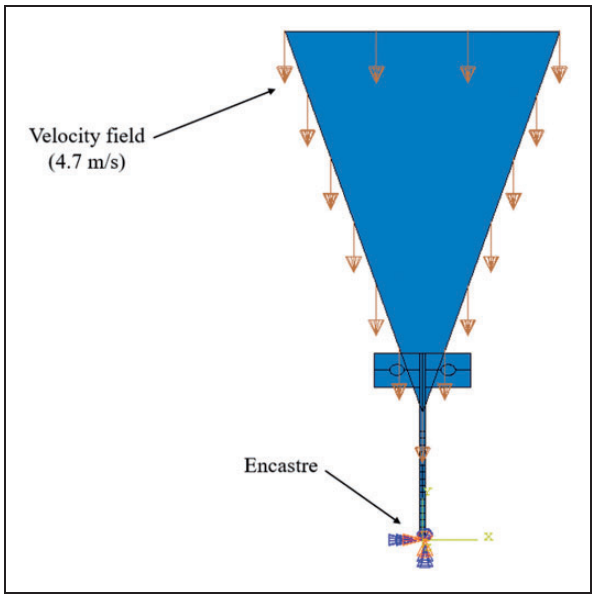

Figure 6. Boundary conditions of the numerical model.

For the impactor pins, mechanical properties of steel were considered, namely, $E = 210$ GPa, $\nu = 0.30$ and density of 7800 kg/m^3.

The triangular cohesive laws in both modes I and II, considered for the CFRP under impact modelling, are shown in Figure 7, corresponding to a thickness of 0.15 mm (the same thickness of a single ply of CFRP) in the centre of the CFRP DCB specimens. The presented values were previously determined by the authors. Elastic orthotropic properties were applied in the remaining specimen area, as specified in Table 1.

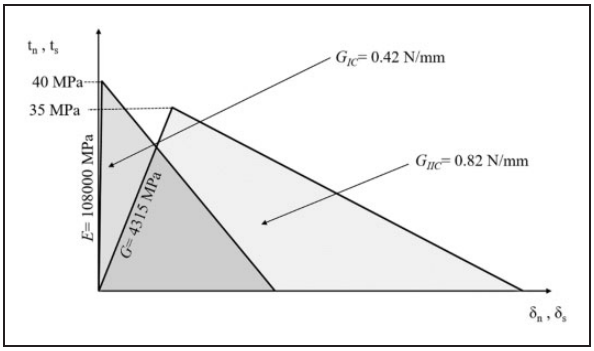

Figure 7. Triangular law for CFRP at impact conditions.

Mesh. The mesh geometry was constructed with square elements (1×1 mm^2), to allow for a refined analysis along the cohesive area of the CFRP DCB specimens. A less refined mesh was applied to the falling wedge impactor, since it was not necessary to retrieve data from this part.

A mapped mesh was applied to all areas, with the exception of the impactor pins and the area of the loading blocks, where a free meshing technique was used due to the parts curvature. The model mesh (with the exception of the cohesive area of the CFRP DCB specimen) was created with four-node bilinear plane strain quadrilateral elements, including reduced integration and hourglass control (CPE4R) (Figure 8). Two-dimensional four-node cohesive elements (COH2D4) were used to model the central area of the CFRP DCB specimen, where delamination is expected to occur.

A total of 2100 elements were created for the CFRP DCB part, 1515 elements for the falling wedge impact and 83 elements for the impactor pins.

Results output. To visualize the cohesive zone degradation, the scalar stiffness degradation (SDEG) variable was used, which provides the direct visualization of the degradation state of the cohesive element, and it ranges between 0 (undamaged) to one (fully damaged). The crack propagation can also be visually monitored using this approach (Figure 9).

Results and discussion

A comparison between the numerical and the previously experimentally determined results will be performed in terms of DCB CFRP specimens opening displacement, crack length and G_{IC}. The experimental curve presented was selected as one of the most representative obtained from a previous work performed by the authors.[25]

DCB opening displacement

Considering the centre of each loading pin of the DCB CFRP specimen being tested in the drop weight falling-wedge equipment (Figure 2), an

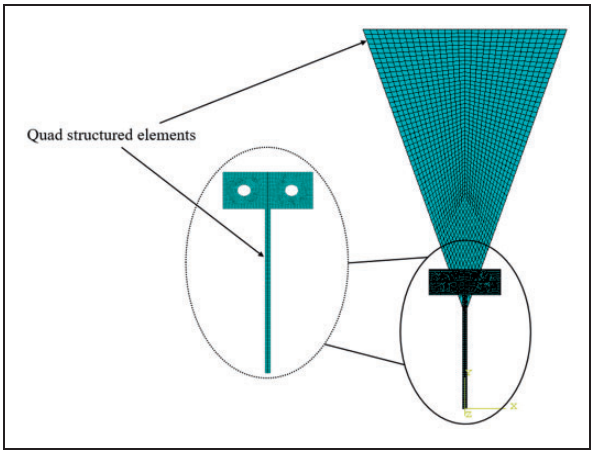

Figure 8. Example and details of the applied mesh (indication of the type of element).

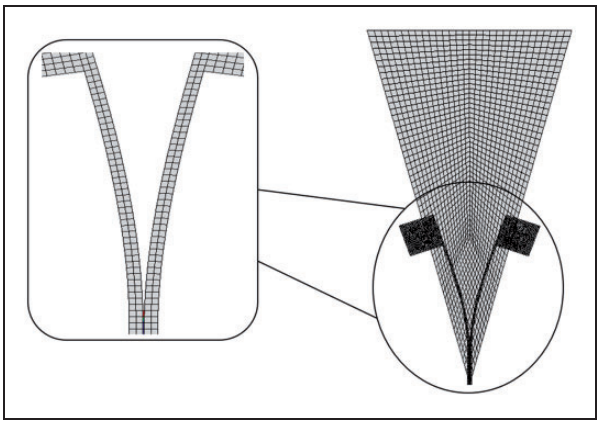

Figure 9. Example of the numerical results of the CFRP DCB under impact.

analysis of the displacement of each point during the impact test (initial impact velocity of 4.7 m/s) was performed numerically to assess its agreement with the experimental results,[25] as shown in Figure 10.

A good agreement between the numerical and experimental results was found, although the simulated final displacement is about 50% higher than the experimental one. The numerical simulation was able to replicate a plateau corresponding to a region without crack propagation, which matched the time necessary for the wedge to fall in the time period prior to it striking the specimen.

Although some deviation of the numerical values of displacement from experimental results occurred between the interval of 0.025 to 0.035 s, such difference might be explained by the fact that in the experimental tests previously performed by the authors,[25] the specimens were clamped at the base of the drop tower. The numerical model was created considering such constrain, but the joining effect of energy and velocity decrease during the experimental impact test cannot be so accurately replicated numerically to

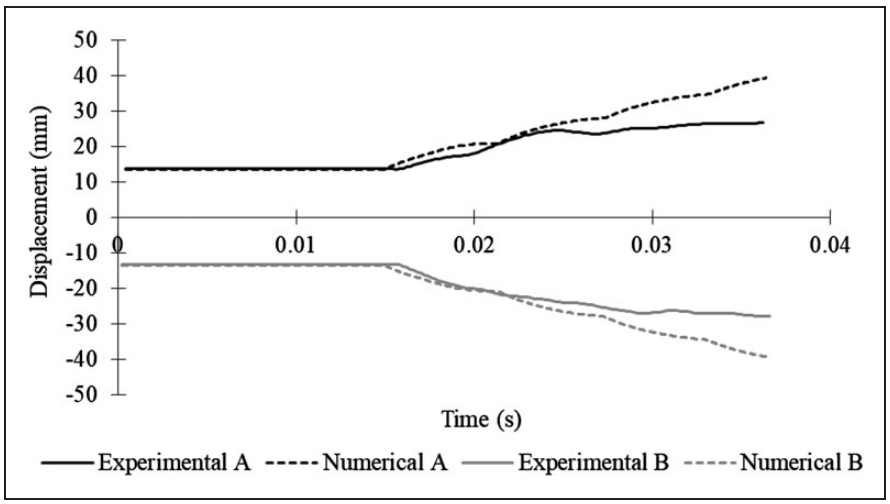

Figure 10. Comparison between the experimental[25] and numerical simulation of the measurement of displacement between the centre of the pins being loaded under impact through the testing time.

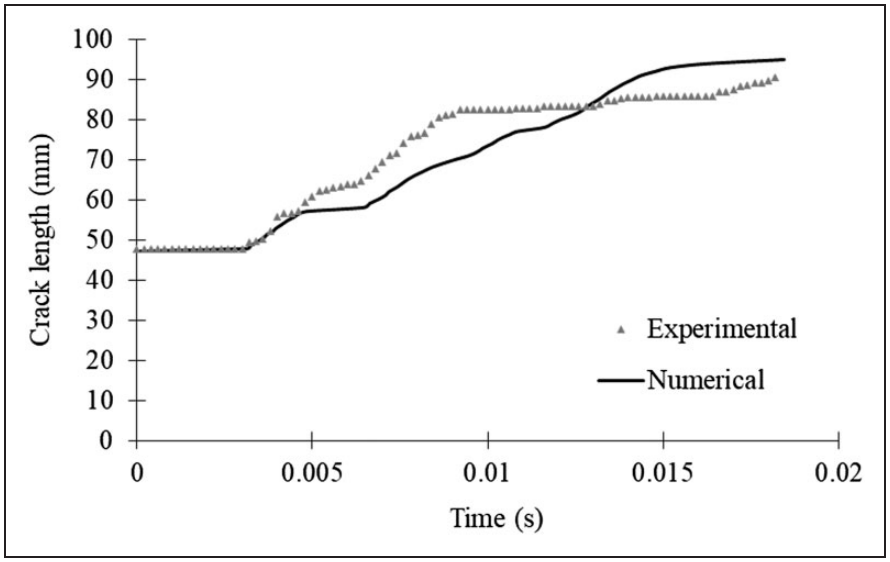

Figure 11. Comparison between the experimental[25] and numerical simulation of the measurement of the crack length of the DCB CFRP specimen under impact through the testing time.

determine such difference, since the velocity was assumed constant in the model.

Crack propagation and fracture toughness

The numerical simulation was used to predict the crack length during the impact test (Figure 11), with the final value of crack length consistent between the numerical and experimental[25] results.

Both the numerical and experimental curves presented the same region without crack propagation. The numerical curve presented a trend similar to the experimental curve, with the crack growing in a stable and continuous form. Between the time interval from 0.005 to 0.010 s, the crack length values of the numerical results deviated below the experimental data, but from 0.010 to 0.018 s better agreement occurred.

The experimentally determined average value of G_{IC}[25] was of 0.42 N/mm, and introducing the numerical data obtained in equation (4), it was possible to determine that the numerical calculated value of G_{IC} was of 0.44 N/mm, a quite similar value which evidences the validity of this approach. The value of G_{IC} was not constant during both experimental testing and numerical simulation, and the presented value refers to a plateau of R-curve.

Variation of strain rate

An analysis of the strain rate evolution through the impact test was performed numerically (Figure 12), being executed at the crack tip.

It was stated in the section "Dynamic testing details" that by using equation (1) and considering

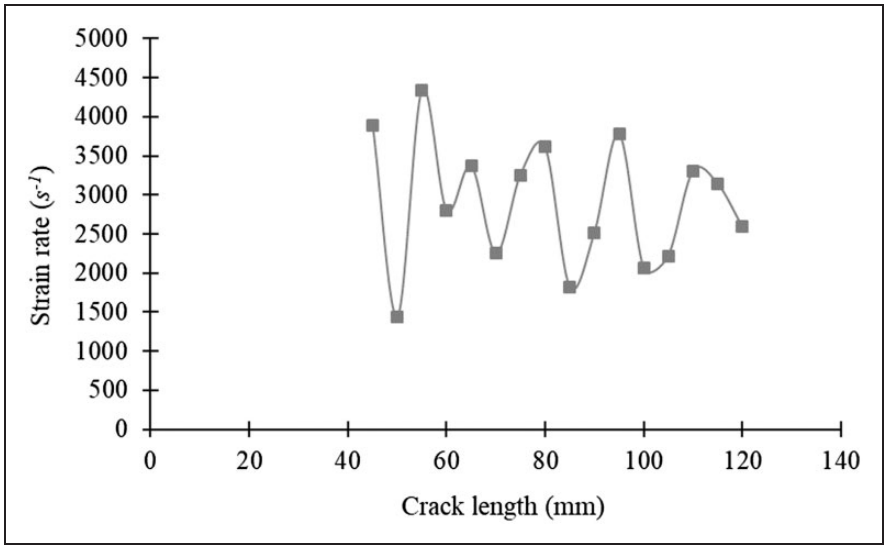

Figure 12. Numerical estimation of the strain rate evolution through the impact test of DCB CFRP specimen under impact (4.7 m/s).

the thickness of one CFRP ply (0.15 mm) it would be possible to calculate the value of strain rate during an impact, also corresponding to the region of the crack tip propagation,[12] which can potentially be the crack propagation speed that can directly be measured. A crack propagation speed cannot be translated into a local transverse strain rate.[12] The numerical analysis was also performed considering the strain rate corresponding to one ply of CFRP at the centre of the specimen.

It can be concluded that the value of $\dot{\varepsilon}$ varies during the impact test presenting strain rate fluctuations that progressively diminish, although the mean value remains approximately constant. As a result, it was stated that $\dot{\varepsilon}$ does not remain constant in a cohesive element after damage has initiated.[12]

Conclusions

In this work, a numerical model was developed using cohesive zone elements (based on a triangular traction-separation law) to simulate the impact behaviour (4.7 m/s) on a DCB specimen made of unidirectional (0° lay-up) CFRP, allowing to deduce the value of G_{IC}. Aiming to verify the accuracy of this model, a comparison with a previous work performed by the authors[25] was performed. The numerical impact setup was based on the experimental drop weight falling-wedge impact test. The main conclusions which can by drawn from this work are:

- Since the values of G_{IC} obtained from the DCB made of CFRP were experimentally obtained[25] considering the variable opening velocity of the specimen, a numerical evaluation of the opening process of the DCB during the impact test was performed, exhibiting a trend consistent with the experimental data, although it was found to be +50% higher at the end of the impact test (which might be due to the decrease of velocity in the experimental tests);
- The numerical evaluation of the crack length propagation (necessary to calculate G_{IC} by using LIM) through the impact test was similar to the one obtained,[25] with the value of G_{IC} calculated by using the numerical data similar to the one experimentally measured;
- An analysis of $\dot{\varepsilon}$ evolution though the impact was numerically performed, allowing to conclude that its value changes along the test and it is lower at the end of the test;
- The numerical model based on the drop weight falling-wedge impact test was able to replicate and provide data necessary to assess the dynamic effect on G_{IC} by using DCB CFRP specimens, considering an impact load of 4.7 m/s.

As a future scope of this work, other displacement rates and testing temperatures should be considered, aiming the full characterization of the material.

Declaration of conflicting interests

The author(s) declared no potential conflicts of interest with respect to the research, authorship, and/or publication of this article.

Funding

The author(s) disclosed receipt of the following financial support for the research, authorship, and/or publication of this article: This study was funded by PhD grant SFRH/BD/139341/2018 "Impact strength optimization with cohesive zone elements of multi-material bonded structures used in the automotive industry", Project No. 028473 POCI-01-0145-FEDER-028473 "Design methodology for impact resistant bonded multi-material automotive structures (ImpactBondDesign)",

Project NORTE-01-0145-FEDER-000022 – ''SciTech – Science and Technology for Competitive and Sustainable Industries'', co-financed by Programa Operacional Regional do Norte (NORTE2020), through Fundo Europeu de Desenvolvimento Regional (FEDER). The authors would also like to thank NAGASE ChemteX® for the financial support provided.

ORCID iD

JJM Machado https://orcid.org/0000-0002-1094-0114
RDSG Campilho https://orcid.org/0000-0003-4167-4434

References

1. Cantwell W and Morton J. The impact resistance of composite materials—a review. *Composites* 1991; 22: 347–362.
2. Rotem A. Residual flexural strength of FRP composite specimens subjected to transverse impact loading. *Sampe J* 1988; 3: 19–25.
3. Daniel I, Werner B and Fenner J. Strain-rate-dependent failure criteria for composites. *Compos Sci Technol* 2011; 71: 357–364.
4. Jacob GC, et al. The effect of loading rate on the fracture toughness of fiber reinforced polymer composites. *J Appl Polym Sci* 2005; 96: 899–904.
5. Bouette B, Cazeneuve C and Oytana C. Effect of strain rate on interlaminar shear properties of carbon/epoxy composites. *Compos Sci Technol* 1992; 45: 313–321.
6. Al-Zubaidy H, Zhao X-L and Al-Mahaidi R. Mechanical characterisation of the dynamic tensile properties of CFRP sheet and adhesive at medium strain rates. *Compos Struct* 2013; 96: 153–164.
7. Hsiao H and Daniel I. Strain rate behavior of composite materials. *Compos Part B: Eng* 1998; 29: 521–533.
8. Gilat A, Goldberg RK and Roberts GD. Experimental study of strain-rate-dependent behavior of carbon/epoxy composite. *Compos Sci Technol* 2002; 62: 1469–1476.
9. Blackman B, et al. The failure of fibre composites and adhesively bonded fibre composites under high rates of test. *J Mater Sci* 1995; 30: 5885–5900.
10. Cantwell W and Blyton M. Influence of loading rate on the interlaminar fracture properties of high performance composites-A review. *Appl Mech Rev* 1999; 52: 199–212.
11. Sohn M and Hu X. Impact and high strain rate delamination characteristics of carbon fibre epoxy composites. *Theoret Appl Fract Mech* 1996; 25: 17–29.
12. May M. Measuring the rate-dependent mode I fracture toughness of composites–A review. *Compos Part A: Appl Sci Manuf* 2016; 81: 1–12.
13. O'Brien TK. Interlaminar fracture toughness: the long and winding road to standardization. *Compos Part B: Eng* 1998; 29: 57–62.
14. Hug G, et al. Effect of the loading rate on mode I interlaminar fracture toughness of laminated composites. *Eng Fract Mech* 2006; 73: 2456–2462.
15. Kalthoff J, et al. On the determination of the crack arrest toughness. In: *ICF4*, Waterloo, Canada, 1977.
16. Kusaka T, et al. Rate dependence of mode I fracture behaviour in carbon-fibre/epoxy composite laminates. *Compos Sci Technol* 1998; 58: 591–602.
17. Sridhar N, et al. Delamination dynamics in through-thickness reinforced laminates with application to DCB specimen. *Int J Fract* 2002; 118: 119–144.
18. Heimbs S, et al. Low velocity impact on CFRP plates with compressive preload: test and modelling. *Int J Impact Eng* 2009; 36: 1182–1193.
19. Heimbs S, Heller S and Middendorf P. Simulation of low velocity impact on composite plates with compressive preload. In: *7th German LS-DYNA forum*, Bamberg, Germany, September 2008.
20. Juntikka R and Olsson R. Experimental and modelling study of hail impact on composite plates. In: *Proceedings of the 17th international conference of composite materials*, Edinburgh, 27–31 July 2009.
21. Campilho RD, De Moura M and Domingues J. Modelling single and double-lap repairs on composite materials. *Compos Sci Technol* 2005; 65: 1948–1958.
22. Machado J, et al. Mode I fracture toughness of CFRP as a function of temperature and strain rate. *J Compos Mater* 2016; 51: 3315–3326.
23. Campilho RD, et al. Modelling adhesive joints with cohesive zone models: effect of the cohesive law shape of the adhesive layer. *Int J Adhes Adhes* 2013; 44: 48–56.
24. Amaro A, et al. The influence of the boundary conditions on low-velocity impact composite damage. *Strain* 2011; 47: e220–e226.
25. Machado J, et al. Dynamic behaviour in mode I fracture toughness of CFRP as a function of temperature. *Theoret Appl Fract Mech* 2019.
26. Machado JJM, et al. Mode II fracture toughness of CFRP as a function of temperature and strain rate. *Compos Part B: Eng* 2017; 114: 311–318.
27. ISO B, 15024: 2001. Fibre-reinforced plastic composites. Determination of mode I interlaminar fracture toughness, G_{IC}, for unidirectional reinforced materials. BSI, 2002.
28. Yamagata Y, et al. Experimental investigation of mode I fracture energy of adhesively bonded joints under impact loading conditions. *Appl Adhes Sci* 2017; 5: 7.
29. Machado J, et al. Numerical study of the behaviour of composite mixed adhesive joints under impact strength for the automotive industry. *Compos Struct* 2018; 185: 373–380.
30. Fernandes R and Campilho R. Numerical evaluation of dissimilar cohesive models to predict the behavior of Double-Cantilever Beam specimens. *Procedia Struct Integr* 2016; 1: 42–49.

Paper 12

Content of Paper 12

Abstract

1. Introduction

2. Numerical simulation procedure

2.1. Mechanical properties

2.2. Quasi-static simulations

2.2.1. Comparison study between 2D and 3D models (quasi-static)

2.3. Impact simulations

2.3.1. Comparison study between 2D and 3D models (impact)

2.3.2. Mesh refinement study

2.3.3. Study on the influence of strain rate dependency and inertial effects

3. Numerical results

3.1. Quasi-static tensile test results

3.2. Impact test results

4. Conclusions

References

International Journal of Adhesion and Adhesives 84 (2018) 92–100

Contents lists available at ScienceDirect

International Journal of Adhesion and Adhesives

journal homepage: www.elsevier.com/locate/ijadhadh

Numerical study of impact behaviour of mixed adhesive single lap joints for the automotive industry

J.J.M. Machado[a], E.A.S. Marques[a], M.R.G. Silva[b], Lucas F.M. da Silva[b,*]

[a] Instituto de Ciência e Inovação em Engenharia Mecânica e Engenharia Industrial (INEGI), Rua Dr. Roberto Frias, 4200-465 Porto, Portugal
[b] Departamento de Engenharia Mecânica, Faculdade de Engenharia, Universidade do Porto, Rua Dr. Roberto Frias, 4200-465 Porto, Portugal

ARTICLE INFO

Keywords:
Mixed adhesive joints
Impact
Simulation
Cohesive zone elements

ABSTRACT

The automotive industry is now extensively using multi-material structures to reduce vehicle weight. Joining these dissimilar materials effectively in a single structure demands the use of adhesive bonding, but the presence of stress concentrations leads to low mechanical performance. Mixed adhesive joints have been proposed as a solution for this issue, using two adhesives in the same joint, combining stiffness and flexibility on the same overlap, improving performance. This work focuses on the numerical modelling of the mechanical behaviour of these joints, using previously published experimental data for validation. The proposed models use cohesive laws with strain rate dependent data to simulate quasi-static and impact loads on several configurations of mixed adhesive joints, using four different adhesives. The models were able to predict the behaviour of most configurations under study, especially for the stiffer adhesives. The model was found to be less effective for modelling high ductility adhesives under impact.

1. Introduction

The use of adhesive bonding is currently being expanded in many industries requiring lightweight structures, such as the aeronautical, automotive and aerospace industries [1]. In the automotive industry, one of the main applications of adhesive bonding is the joining of complex composite and lightweight structures such as carbon fibre panels, to produce lighter, safer and more efficient vehicles. Due to the high importance of vehicle safety, these bonded structures must be capable to withstand high impact loads, such as those found during a collision.

The selection process of adhesives for the automotive industry is an especially complex topic due to extremely large variety of adhesives available. The selection process should not necessary focus on the strength of the adhesive, as this does not necessarily create stronger joints [2,3]. Many high-performance adhesives, with high tensile and shear, exhibit high quasi-static strength, but their low toughness leads to poor impact performance. During the selection process of adhesives for impact is therefore critical to select those with good ductility, shear strength and peel resistance under impact [4,5], enhancing energy absorption and damage tolerance. These extremely tough hybrid adhesives are colloquially known as crash resistant adhesives, and are able to provide excellent strength at all strain rates and good energy absorption [6].

Flexibility and ductility are therefore the most desirable properties for adhesives intended for bonding impact resistant structures such as those found in the automotive industry. A comparison of the quasi-static and impact behaviour of stiff and flexible adhesive joints for the automotive industry was performed by Loureiro et al. [7] and demonstrated that although less stiff, joints bonded with polyurethane are stronger than epoxy bonded joints when subjected to high deformations or high strain energy. However, if the designer intends to achieve maximum possible stiffness and strength, the use of strong and rigid adhesives cannot be discarded. To use these adhesives without their inherent disadvantages, some authors have proposed the creation of mixed adhesive joints, which combine two highly distinct adhesives in a single joint, leading to increased mechanical performance. Typically, these joints combine a stiff adhesive with a flexible adhesive. The rigid adhesive provides overall stiffness and strength while the flexible adhesive can provide toughness and impact resistance.

Raphael [8] first proposed the use of mixed adhesive joints in 1966, as a method to reduce the stress concentration at the ends of overlaps of single lap joints (SLJ). By applying a ductile adhesive in these areas, premature joint failure could be avoided. The stiff adhesive, located in the centre of the overlap and less subjected to deformations, provided strength without being subjected to peak stress concentrations. The concept was expanded by Fitton and Broughton [9] and da Silva and Adams [5] which have achieved strength improvements with the use of

* Corresponding author.
E-mail address: lucas@fe.up.pt (L.F.M. da Silva).

https://doi.org/10.1016/j.ijadhadh.2018.02.036
Accepted 21 February 2018
Available online 23 February 2018
0143-7496/ © 2018 Elsevier Ltd. All rights reserved.

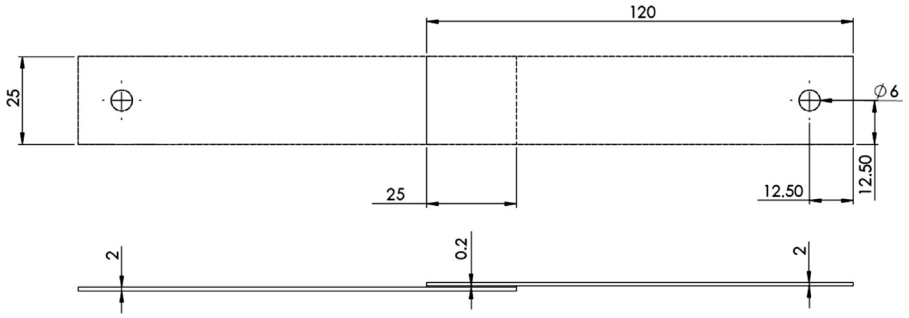

Fig. 1. Dimensions of the SLJs used (in mm).

composite adherends and an epoxy mixed adhesive on a SLJ.

In a related research work, da Silva and Lopes [10] studied the combination of a stiff adhesive and a ductile acrylic adhesive, determining that the average shear strength of the mixed adhesive joint was higher than that achieved by joints where the same adhesives were used alone. Although most of the experimental work on mixed adhesive joints studied the quasi-static behaviour of these joints, the work of Silva et al. [11] was the first to experimentally demonstrate the usefulness of this concept for impact loadings, where stiff and flexible adhesives were used in SLJs with steel substrates.

Finite element analysis (FEA) is a powerful technique which can be applied for the design and analysis of structures, i.e. containing plastics or adhesive bonds, undergoing impact conditions. Nevertheless, in order to achieve reliable and accurate predictions, a suitable model for the material behaviour and material properties at appropriate values of strain rates should be used [1,2,6]. Adams and Harris in 1985 [12] were among the first to demonstrate that a prediction of the joint strength under impact and quasi-static loads can be successfully performed using the correct failure criteria to the FEA.

Several other authors have further explored the use of FEA to model impact loadings in adhesive and adhesive joints, usually employing constitutive models to represent the strain rate sensitive behaviour of the adhesives and substrates. Sawa et al. [13,14] in 2002, performed research on the influence of stress-wave propagations and stress distributions in SLJs using a model with dynamical effects, identifying the locations of the maximum principal stress. In 2008 Sawa et al. [15] added a Cowper-Symonds model to allow the description of the plastic flow characteristic of the thermosetting epoxy adhesive.

Yang et al. [16] in 2012 evaluated the application of a simplified finite element for modelling of the toughened adhesively bonded joint, creating an elastoplasticity model in which the strain rate effort of both the pre-failure material properties and the failure criterion can be characterized.

In 2013, Wada et al. [17] assessed the dynamic strength taking into account the fracture toughness and the average fracture stress of the adhesive., achieving an effective technique for determining the singular stress field parameter at the fracture initiation time was developed.

An alternative method to establish constitutive models is the use of cohesive zone models (CZM), which were created with the objective of aim of combining the strength of materials and fracture mechanics approaches [18]. These models are especially well-suited for adhesive joints, as they work best for simulating failure thin planes of materials [19]. Traction-separation laws, introduced for each material, are used to model stiffness and degradation of the element. These laws can exhibit several different shapes, the most common being the triangular and the trapezoidal laws.

Although the use of CZM is extensive in adhesive modelling, the work of Carlberger and Stigh, published in 2007 [20], was the first to demonstrate the validity of using this type of approach to predict impact strength. Other authors, such as Haufe et al. [21], May et al. [22], Clarke et al. [23], Avendaño et al. [24] and Neumayer et al. [25] have used this approach and achieved accurate prediction of failure loads using complex dynamical cohesive models with strain rate dependent data.

The work presented in this article concerns the dynamical numerical modelling of the mechanical behaviour of mixed adhesive SLJs with metallic substrates, using previously published experimental data as a validation tool. It describes a novel procedure for modelling joints containing two different adhesives in the same joint using strain rate dependent cohesive zone models. Quasi-static and impact numerical simulations were employed for several configurations of mixed adhesive joints with four adhesives in different combinations.

2. Numerical simulation procedure

The mechanical behaviour of varied mixed adhesive joint configurations has already been studied experimentally by the authors. In this work [11], the authors have tested six joint configurations under quasi-static and impact loads. The work presented in this document aims to numerically model this available experimental data using implicit and explicit finite element models and using strain rate dependent data. In this section, the development process of the models is described in detail, including parametric studies to determine optimal model configurations.

The numerical models created in this work are divided in quasi-static and dynamic (referring to impact models). The type of specimen used in the simulations were SLJs, using high strength steel adherends. The use of high strength steel aims to avoid the plasticization of the adherends, and consequently, premature failure of the adhesive. The dimensions of the SLJs are according to the ASTM D 1002 [26] and ISO 4587 [27] standards and are illustrated in Fig. 1.

Four different adhesives were selected for use in the mixed adhesive joints, two stiff adhesives (AV 138 from Araldite and XNR6852 E-2 from Nagase ChemteX®) and two flexible adhesives (RTV 106 from Momentive and DP 8005 from 3M).

The distinction between flexible and stiff adhesive is important, as mixed adhesive joints require the use of a high modulus adhesive combined with a low modulus for stress reduction at the ends of the overlap. The ductile adhesive at the ends of the overlap length provides flexibility to the joint while the brittle adhesive in the middle provides increases its strength (Fig. 2). The physical separation of the two adhesives is achieved by the introduction of two nylon wires, with 0.2 mm of diameter.

Four mixed adhesive joint combinations were used (always keeping the stiff adhesive in the middle and the flexible adhesive at the end of the overlap), being the following:

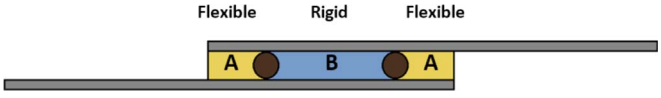

Fig. 2. Schematic representation of the mixed adhesive SLJ (the two dark circles correspond to the nylon wires).

Table 1
Stiffness data for numerical models at quasi-static testing speeds.

Adhesive	Tensile modulus [MPa]	Shear modulus [MPa]	Ref.
DP 8005	590	159	[28,29]
AV 138	4890	1560	[30]
XNR6852 E-2	1742	645.2	[31]
RTV 106	1.6	0.86	[32]

- RTV 106 (edges) with AV 138 (middle);
- DP 8005 (edges) with AV 138 (middle);
- RTV 106 (edges) with XNR6852 E-2 (middle);
- DP 8005 (edges) with XNR6852 E-2 (middle).

In addition, single adhesive joints were also studied, acting as a benchmark for comparison with the mixed adhesive joints.

2.1. Mechanical properties

The mechanical data for the four adhesives used for the quasi-static and impact simulations is presented in Tables 1 and 2.

Tensile properties for XNR6852 E-2, DP 8005 and AV 138 were obtained from bulk tests at 1 and 100 mm/min of crosshead speed as described by Silva et al. [11]. The impact tensile strength (t_n) and shear strength (t_s), which correspond to the yield strengths of the mode I and mode II cohesive zone laws were extrapolated by a logarithmic trend function (Eq. (1)) that determines their values at 105,000 mm/min using the values from 1 mm/min and 100 mm/min tests.

$$\sigma = A \cdot ln(\dot{\varepsilon}/\dot{\varepsilon}_0) + B \tag{1}$$

A and B coefficients were determined from the logarithmic trend function. The strain can be calculated using Eq. (2):

$$\dot{\varepsilon} = \frac{v}{L_0} \tag{2}$$

where v is the velocity of the test and L_0 is the initial calibrated longitudinal deformation length of the specimen section where the strain is measured.

This extrapolation process has previously been used with success by some authors [34,35]. Fig. 3 shows graphically the extrapolation process for the tensile yield strength, where x is the strain rate and y corresponds to the tensile strength. The shear yield strength (t_s) was estimated using the same relationship of proportionality as described for the tensile strength between the 1 mm/min and 100 mm/min tests.

For the RTV 106 adhesive, this extrapolation process was not performed. This was due to adhesion problems encountered both in quasi-static and impact experimental tests. As the failure was always of the adhesive type it was decided not to introduce higher mechanical properties for the dynamic models. For all materials studied, and to simplify the simulation, the elastic moduli and the mode I and mode II fracture energy were considered as not being strain rate dependent. While it is known that fracture toughness exhibits some degree of strain rate dependence, previous works [34,36] have shown that changes are not drastic, and this was the reason behind the decision to not consider strain rate dependency.

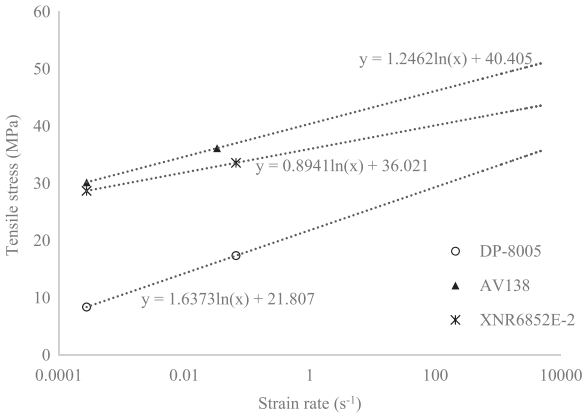

Fig. 3. Tensile stress extrapolation curves.

To introduce damage evolution on the cohesive zone model, a quadratic stress criterion was used. Fig. 4 shows the pure-mode (traction or shear) and mixed-mode traction separation laws, where t_n^0 and t_s^0 are the cohesive strengths in tension and shear, respectively, and δ_n^0 and δ_s^0 are the respective displacements, and δ_n^f and δ_s^f are the tensile and shear displacements at failure, respectively.

The quadratic stress criterion is given by Eq. (3).

$$\left\{\frac{\langle t_n \rangle}{t_n^0}\right\}^2 + \left\{\frac{t_{s1}}{t_{s1}^0}\right\}^2 + \left\{\frac{t_{s2}}{t_{s2}^0}\right\}^2 = 1 \tag{3}$$

where $\langle\ \rangle$ are the Macaulay brackets, emphasizing that a purely compressive stress state does not initiate damage. After the mixed-mode cohesive strength is attained (t_m^0 in Fig. 4) by the fulfilment of Eq. (4), the material stiffness is degraded. Complete separation is predicted by a linear power law form of the required energies for failure in the pure modes

$$\frac{G_n}{G_n^c} + \frac{G_{s1}}{G_{s1}^c} + \frac{G_{s2}}{G_{s2}^c} = 1 \tag{4}$$

G_n and G_s are the current strain energy release rates in each loading mode, while G_n^c and G_s^c are the respective critical values.

2.2. Quasi-static simulations

A FEA was performed using the ABAQUS® (Dassault Systèmes,

Table 2
Material data for numerical models at strain-rate speeds [33].

Adhesive	Speed (mm/min)	L_0 (mm)	Strain-rate (s^{-1})	Tensile strength [MPa]	Shear strength [MPa]	Mode I fracture energy [N/mm]	Mode II fracture energy [N/mm]
DP 8005	1	60	2.78 E−4	6.3	8.4	1.1	6
	100	25	6.67 E−2	13	17.4		
	105,000 (extrapolated)	0.2	8750	27.5	36.7		
AV 138	1	60	2.78 E−4	41	30.2	0.35	4.9
	100	50	3.33 E−2	49.1	36.2		
	105,000 (extrapolated)	0.2	8750	70.2	51.7		
XNR6852 E-2	1	28	5.95 E−4	42.9	28.7	1.68	18
	100	25	6.67 E−2	46	33.6		
	105,000 (extrapolated)	0.2	8750	53.7	45.8		
RTV 106	1	60	2.78 E−4	2.3	1.97	2.73	5
	100	25					
	105,000 (extrapolated)	0.2					

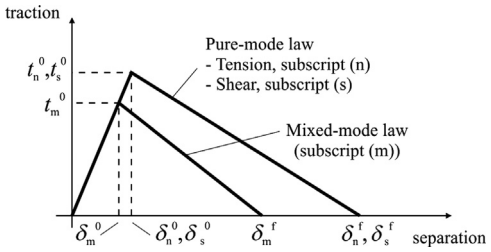

Fig. 4. Traction-separation law with linear softening: pure and mixed-mode models.

Suresnes, France) package to obtain the load-displacement curves (*P-δ*) and a prediction of the failure load. All models created use CZMs, which can represent the fracture process and location, advancing beyond the classical continuum mechanics modelling. Several authors have proposed their use for impact simulations of adhesive joints [37–39]. A CZM is constructed by including in the model a series of discontinuities modelled by cohesive elements, which use both strength and energy parameters to simulate the occurrence and advance of a fracture crack [40,41]. This technique is especially useful for adhesives, as they present a discrete zone, the adhesive layer, where failure can be expected and therefore can be easily modelled. The adhesive properties applied in the model were the same as the properties shown in Table 1 and were converted to a cohesive triangular law.

The numerical model for the quasi-static simulation consisted in an implicit model, computed in a general/quasi-static analysis, with cohesive elements applied to the bondline. To assist in model development, an initial study was performed, comparing the performance of two-dimensional (2D) and a three-dimensional (3D) model.

2.2.1. Comparison study between 2D and 3D models (quasi-static)

To perform the comparison between 2D and 3D models, the combination of AV138 and DP 8005 adhesive was considered. The 2D quasi-static models for this configuration were constructed with plane-strain four-node quadrilateral solid finite elements (CPE4 from ABAQUS®), and four-node cohesive elements (COH2D4 from ABAQUS®). A uniform mesh was used, employing elements with 1 mm long edges. Fig. 5 shows the mesh used for the 2D model.

The geometry and boundary conditions of the specimens of the numerical model were defined to be representative of the experimental specimens and are shown in Fig. 6.

The 3D quasi-static models were constructed with 3D stress, 8 node linear brick solid finite elements (C3D8R from ABAQUS®), and eight node cohesive elements (COH3D8 from ABAQUS®). To match the mesh used for the 2D model as closely as possible, 1 mm long *hex* shaped elements were used. Fig. 7 shows the mesh used for the 3D model.

The geometry and boundary conditions of the specimens of the 3D numerical model are shown in Fig. 8.

The *P-δ* curves obtained with the 2D and 3D quasi-static models are shown in Fig. 9.

The results show good similarity between the two models, with a slightly higher predicted failure load for the 2D model (only around 1.6% higher). For the quasi-static analysis, the 3D models are shown not to provide significant advantages.

2.3. Impact simulations

To simulate the impact conditions, the impact model followed the same approach described in quasi-static simulations, consisting of a deformable part with cohesive modelling of the adhesive layer. Mesh

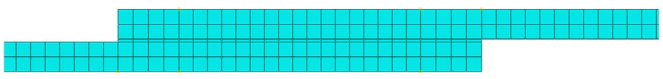

Fig. 5. Mesh geometry for the 2D quasi-static validation model.

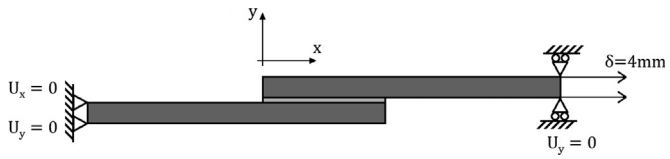

Fig. 6. Boundary conditions applied for the 2D quasi-static validation model.

element types were changed to explicit elements with the same controls as for the quasi-static simulation. The explicit type of formulation enables the model to consider the inertial effects, which can be an important factor on joint strength. Also, the material properties were altered to match the strain rate dependent material properties.

The experimental tests were performed using a drop weight impact testing machine [4]. To replicate the impact's kinetic energy, a 26-kg mass block (the same mass used in the experimental tests) was introduced in the last 25 mm length of the free adherend, as shown in Fig. 10. The volume of the block is 1250 mm^3 and to simulate an impact with 38.3 J of energy and an initial velocity of 1.75 m/s, the density was set to 2.08E + 7 kg/m^3. A predefined velocity field was applied to this mass, replacing the 4 mm of horizontal displacement boundary condition used in the quasi-static simulation.

For the impact analysis, the quasi-static step was replaced with a dynamical explicit calculation with a period of 0.005 seconds and considering non-linear geometry effects. Element stiffness degradation as well as the reaction forces and displacements of the boundary condition nodes were requested to extract the *P-δ* curves and determine the status of the cohesive elements.

2.3.1. Comparison study between 2D and 3D models (impact)

As performed for the quasi-static model, an auxiliary study was carried to understand if there was a need to use a more computational intensive 3D model. The adhesive configuration was again the mixed joint with AV 138 and DP 8005 The elements and mesh used were the same as described for the quasi-static analysis (already shown in Figs. 5 and 7). Only the mechanical properties (which were made to be strain rate dependence in accordance with Table 2) and the boundary conditions were changed. For the 2D model the boundary conditions used are shown in Fig. 10.

Fig. 11 shows schematically the boundary conditions for the 3D impact model.

The *P-δ* curves obtained with the 2D and 3D impact models are shown in Fig. 12.

As was the case for the quasi-static analysis, the results show good agreement between the two models, in this case with a difference below 1%. Again, the 3D models are shown not to provide significant advantages.

In accordance to the data obtained with quasi-static and impact models, it was decided to employ only 2D models for this work.

2.3.2. Mesh refinement study

The ensure accurate performance of the numerical models, a study on mesh performance was performed for the 2D impact model (again considering the mixed adhesive joint with AV 138 and DP 8005). Table 3 shows the four different mesh configurations considered for this study, listing the element size and the number of elements.

Three meshes with uniform element size were compared with a mesh which uses variable element size. The element size in this mesh ranges from 0.2 mm of size (near the adhesive layer edges and the interfaces between the two adhesives) to 4 mm near the boundary conditions. This mesh was adjusted to achieve a low number of elements while ensuring high mesh density near the critical areas. The numerical *P-δ* curves obtained with these four meshes are shown in Fig. 13.

The result clears show reduced mesh dependency of the results with mesh configuration, even with very coarse meshes. This demonstrates that cohesive element modelling is suitable for modelling of large and

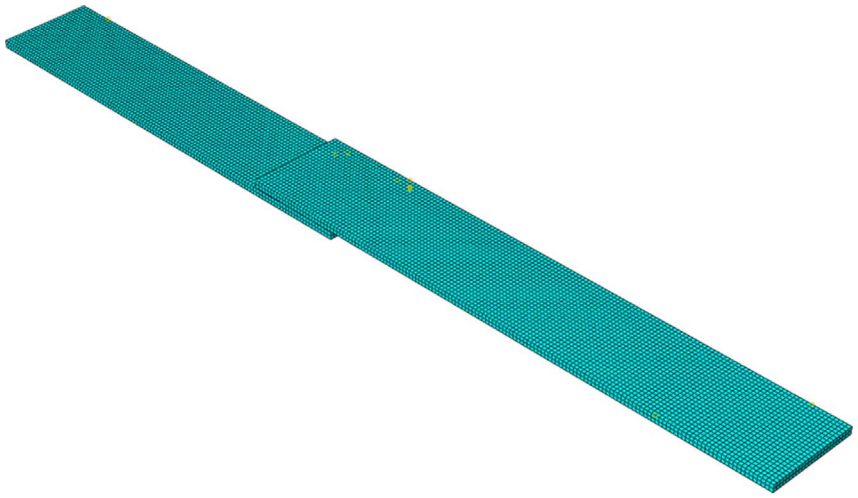

Fig. 7. Mesh geometry for the 3D quasi-static validation model.

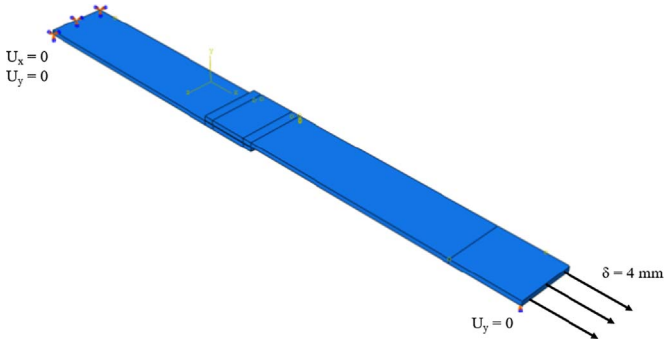

Fig. 8. Boundary conditions applied for the 3D quasi-static model.

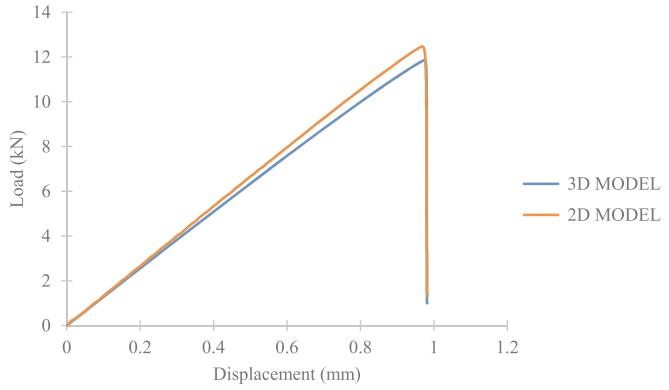

Fig. 9. Numerical P-δ curves for mixed joints with AV 138 + DP 8005 adhesive, obtained by comparing the 2D and 3D quasi-static models.

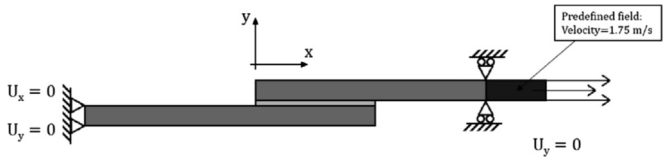

Fig. 10. Boundary conditions applied for the 2D impact validation model.

complex structures, as the need for refinement is minimal. The work carried out in the remainder of this work uses the variable mesh previously described.

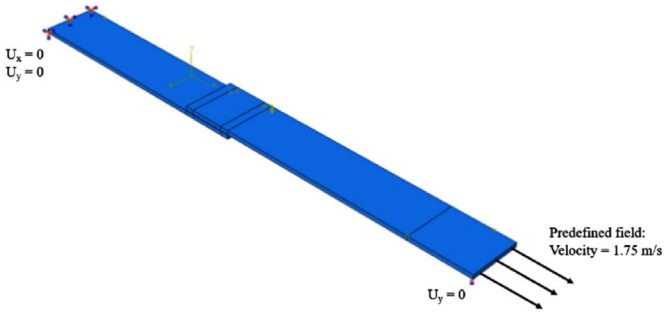

Fig. 11. Boundary conditions applied for the 3D impact model.

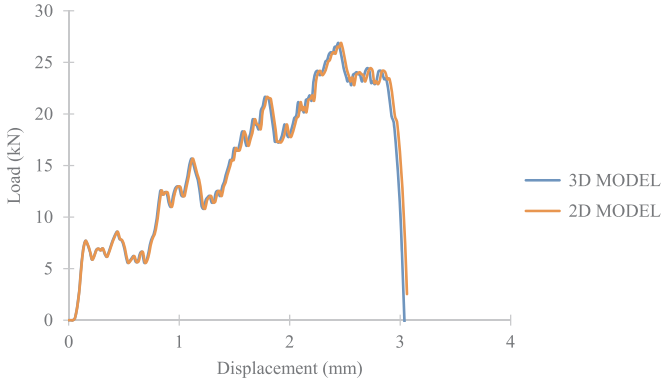

Fig. 12. Numerical P-δ curves for mixed joints with AV138 + DP 8005 adhesive, obtained by comparing the 2D and 3D impact models.

2.3.3. *Study on the influence of strain rate dependency and inertial effects*

To conclude the initial parametric study on the impact models, a study was performed to assess the influence of the strain rate dependent properties and the inertial effects on the model behaviour. For this purpose, data was obtained considering the impact numerical model (for the mixed adhesive joint with AV 138 and DP 8005) with and without strain rate dependent properties for the adhesives. The results for this study are shown in Fig. 14. To aid in the interpretation of the results the data obtained with the quasi-static model is also included.

These results demonstrate that the use of strain rate dependent data is critical for the failure load, with the model failing significant earlier without the improved strain rate dependent properties. It is also noticeable that the initial portion of the two dynamical curves is quite similar, owing to similar elastic responses. When comparing the behaviour of the quasi-static model with the dynamical model without strain

Table 3
Mesh configurations tested.

Element size	Number of elements	Mesh shape
2 × 2 mm	147	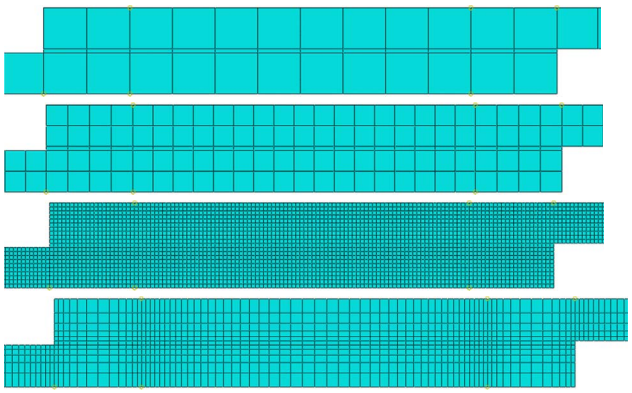
1 × 1 mm	565	
0.2 × 0.2 mm	14,872	
Variable	1536	

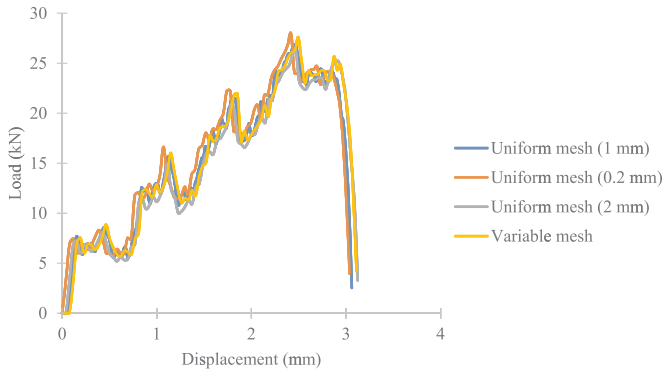

Fig. 13. Numerical P-δ curves under impact for mixed joints with AV 138 + DP 8005 adhesives, using four different mesh configurations.

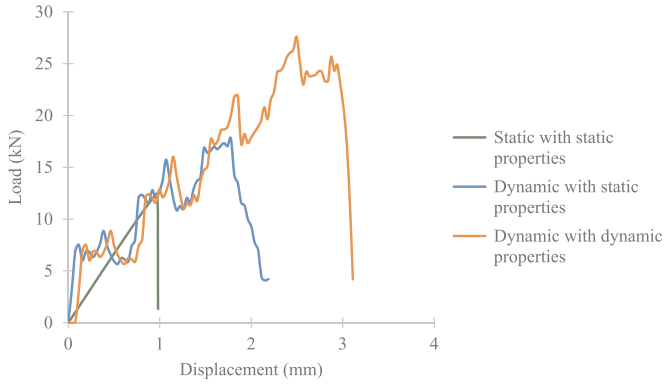

Fig. 14. Numerical P-δ curves for the quasi-static analysis, an impact analysis without strain rate dependent data and finally an impact analysis with strain rate dependent adhesive data, using AV 138 + DP 8005.

rate dependent data (two models which use the same material properties) it is evident that the dynamical effects are significant, causing by themselves an increase of almost 10kN. This change in behaviour can be attributed to the time dependent stress state that occurs under dynamic loading to model this type of joint under impact conditions, it is therefore important to consider the both the strain rate dependency of the adhesives and the inertial effects.

3. Numerical results

In this section, data derived from the numerical analysis is compared with experimental data available from a previously published study [11]. The quasi-static and numerical models described in Section 2 were used to obtain the *P-δ* curves for the six adhesive joint configurations under consideration. The results shown are divided into quasi-static and impact testing conditions.

3.1. Quasi-static tensile test results

Fig. 15 shows a comparison of the numerical results with the experimental data for the failure loads. For many of the cases the numerical model exhibited slightly higher strength values when compared to the experimental data.

The predicted load for XNR6852 E-2 is, however, below the experimental data. This is an indication that the experimentally determined properties are slightly conservative. Due to its extremely large strength and ductility, the characterization of this adhesive poses significant challenges and it reflects in these conservative property values.

Although no large discrepancy occurs, it is important to refer that the data for RTV 106 is of limited use. Due to the existence of adhesive failure for the joints containing RTV 106 adhesive, a cohesive zone model will always overestimate the failure load.

To enable a better understanding of the model capabilities and limitations, a few examples of experimental and numerical *P-δ* curves are compared and discussed in the following paragraphs.

Starting with an analysis of the results for AV 138 (Fig. 16), the

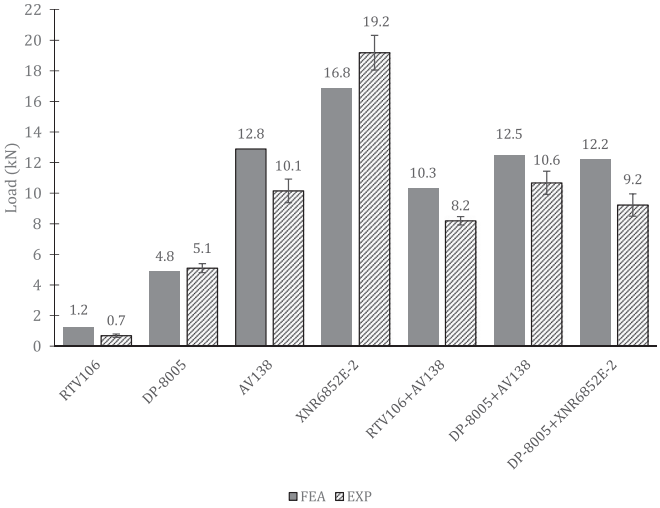

Fig. 15. Failure load results comparison between numerical and experimental.

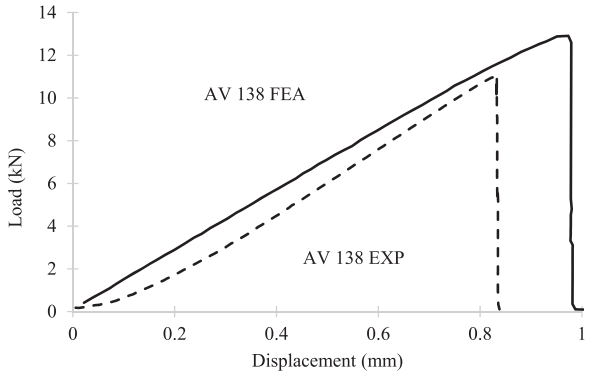

Fig. 16. Numerical and experimental P-δ curves for AV 138.

numerical model generally matched the stiffness of the experimental data, with the predicted failure load being slightly higher. The stiffness in the initial portion of the curve (caused by the non-linearity of the SLJ test) is however not captured by the numerical model, is a factor of the boundary conditions inherently stiffer than those imposed on the experimental specimen. The most significant difference between numerical and experimental curves was the displacement at failure, which is expected to be lower experimentally due to the presence of defects. The triangular cohesive law was found to be suitable for this brittle adhesive. The difference between the predicted and experimental failure load, although significant, can be attributed also to the naturally higher performance of the perfectly modelled SLJ specimen.

Moving on to an analysis of the model of the joints bonded with DP 8005 (Fig. 17), it is evident that in this case, despite a good prediction of the failure load, the ductile behaviour of the adhesive could not be accurately modelled.

A possible solution for improving the model is the use of a trapezoidal law, which should improve the shape of curve. The trapezoidal law is known to be better suited for more ductile adhesives, being the case of DP 8005. A similar behaviour has previously been described in the work of Jousset and Rachik [42], although the authors noted that more complex geometries are not as affected by the shape of the cohesive law. To assess this effect, a basic trapezoidal law was implemented in the numerical model, constructed using the same material properties used for the trapezoidal law but using a central plateau. The results obtained with a numerical trapezoidal CZM, for the quasi-static test of DP 8005, are shown in Fig. 18, where the performance of the trapezoidal law is compared with that of the triangular law and the experimental data.

It is visible that the use of this law predicts the same failure load as obtained for the triangular CZM, the behaviour of the plastic portion of the DP 8005 *P-δ* curve is still not accurately modelled. The demonstrates that in this case, the use of this type of law does bring sufficient advantages for modelling the behaviour of this highly ductile adhesive.

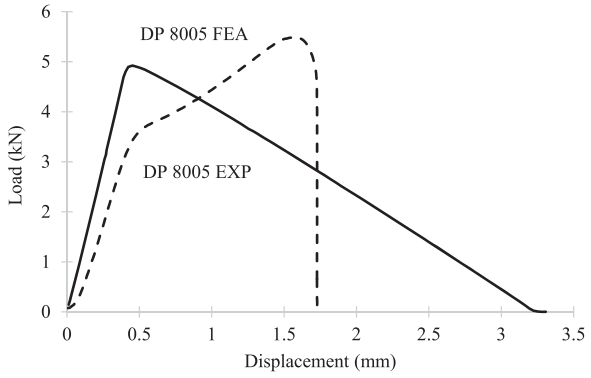

Fig. 17. Numerical and experimental P-δ curves for DP 8005.

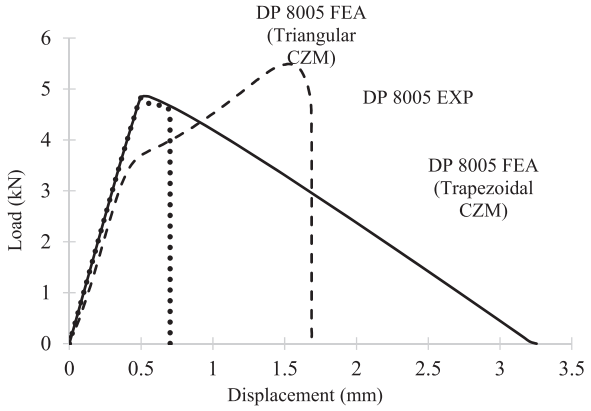

Fig. 18. Comparison between triangular and trapezoidal numerical P-δ curves for DP 8005.

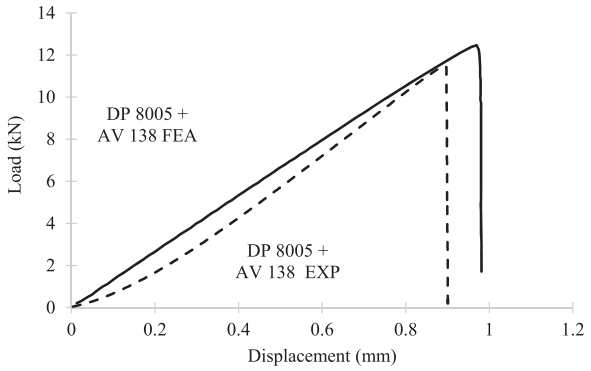

Fig. 19. Numerical and experimental P-δ curves for DP 8005 + AV 138.

Lastly, the performance of a mixed adhesive model is examined in Fig. 19. The model of the mixed adhesive joint containing DP 8005 and AV 138 exhibited results closely matching the experimental curve. Both the stiffness and the failure load are similar. Although DP 8005 was shown to be complex to model using this type of cohesive law, its influence in this model is limited, as most of the bonded area corresponds to the stiffer AV 138 adhesive.

3.2. Impact test results

Fig. 20 shows a comparison of the numerical with the experimental results for the maximum impact load of each SLJ configuration analysed.

The numerical model again exhibited higher strength results compared to the experimental data. The deviation can also be justified by

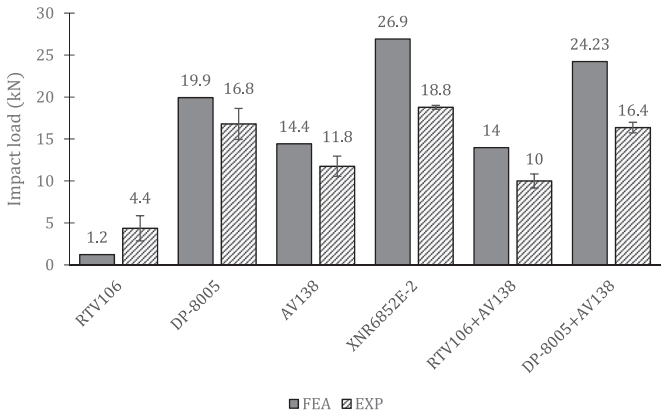

Fig. 20. Comparison between numerical and experimental impact failure load results.

the mechanical properties applied to the model and by manufacture problems of the experimental specimens, which can include defects that cause strength degradation of the joints. In addition, the fracture energy properties were considered as not strain rate dependent. If a reduction of these properties was considered in the impact models, the failure load would be almost certainly lower. However, as experimental measurements for the characterization of the fracture properties under high strain rates were not performed, some differences are to be expected between experimental and numerical impact tests.

While RTV 106 adhesive specimens were simulated with non-strain rate dependent data and this caused large discrepancies between experimental and numerical data, the models seem to be adequate for the validation of the experimental failure loads for some adhesive configurations such as DP 8005, AV 138 and RTV 106 + AV 138. For the remaining combinations, the deviation was more significant, resulting in less accurate failure load predictions. Still, taking in consideration this error factors, a reasonable prediction can still be made with the numerical models.

As performed for the quasi-static results, a few examples of experimental and numerical *P-δ* curves are compared and discussed in the following paragraphs.

An analysis of the model of the joints with DP 8005 adhesive (Fig. 21) shows that both the prediction of the failure load and the stiffness of the model generally follow the experimental results. The deviation encountered can be in part justified by an overestimation of the adhesive properties obtained by the extrapolation function previously explained in numerical simulation procedure section.

In contrast, the model of a SLJ with XNR6852 E-2 (Fig. 22) exhibited a more significant deviation in the failure load, resulting in less accurate load predictions. A justification for the larger deviation could be due to the overestimation of the values obtained from the extrapolation criteria. This might be related with the previously discussed problems encountered with the characterization of this material.

Lastly, the model with DP 8005 and AV 138 is shown in Fig. 23. This model exhibited a significant deviation of the failure load. The results revealed a joint strength increase by combining the adhesive DP 8005 with AV 138, which validates the same conclusion found in experimental tests but also revealed a higher maximum load compared to the application of only DP 8005, something which was not verified in the experimental results. The mechanical properties applied for this mixed adhesive model may not be well determined and thus resulting in higher relative errors. The significant difference between the numerical and experimental failure load can be attributed to the presence of a physical separation barrier (nylon wire) between the two adhesives, which serves as small defect. This barrier is not modelled in the numerical model, which assumes a perfect transition between the two adhesives.

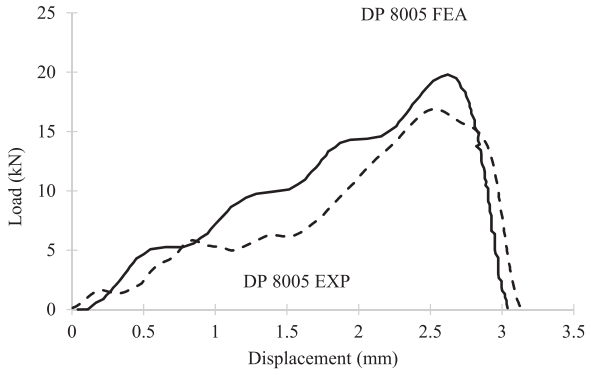

Fig. 21. Numerical and experimental P-δ curves with impact conditions for DP 8005.

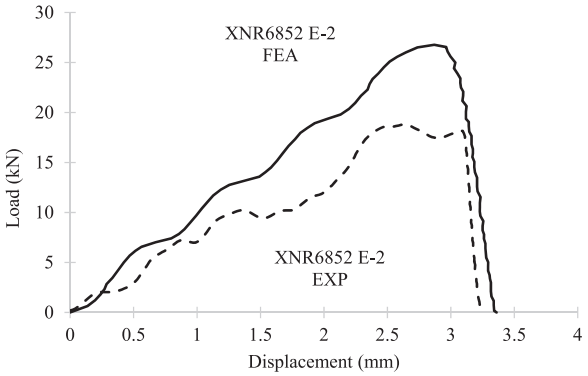

Fig. 22. Numerical and experimental P-δ curves with impact conditions for XNR6852 E-2.

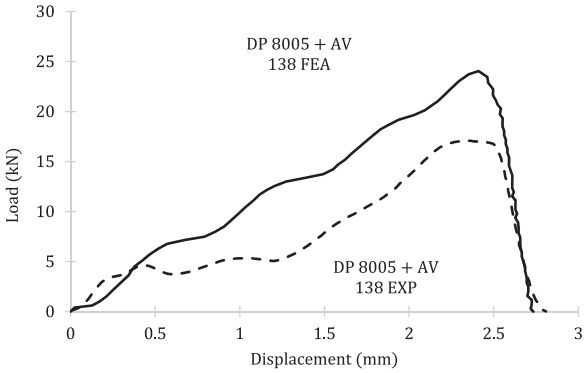

Fig. 23. Numerical and experimental P-δ curves with impact conditions for DP 8005 + AV 138.

4. Conclusions

This work consisted of a numerical study of the mechanical behaviour of various mixed joints configurations under quasi-static and impact conditions. For this purpose, quasi-static and dynamical FEA models were developed, employing boundary conditions and strain rates able to simulate experimental results with mixed adhesive joints. An initial study was performed do determine optimal the model configurations, by studying the difference between 2D and 3D models, the mesh dependency and the use of strain rate dependent properties.

For the complete study, two-dimensional FEA models of SLJs were created, using layers of cohesive elements to simulate adhesive failure. The cohesive zone elements were constructed using mechanical properties derived from experimental testing. For higher strain rates an extrapolation procedure was followed, using a logarithmic law to extrapolate data obtained at lower strain rates.

Most quasi-static models exhibited reasonably accurate results both in stiffness and failure load. However, modelling of the more flexible adhesive was more complex. For example, the ductility of DP 8005 specimens was not captured by the model, even with the use of trapezoidal elements. The dynamical models were also found to be a good tool for predicting the failure load, demonstrating the usefulness of the dynamical cohesive modelling process. The failure load was slightly overestimated it for all cases under study except for RTV 106 (where adhesive failure occurred). This indicates that the extrapolation process is a valid solution, although it might lead to slightly optimistic mechanical properties.

In summary, the use of cohesive numerical models was shown to be a viable technique for modelling mixed adhesive joints subjected to quasi-static and impact loadings and predicting its behaviour. Although some limitations were identified for this approach, such as difficulty in modelling the plastic behaviour, this procedure sets the groundwork for a study of alternative mixed adhesive joint configurations without the

need for extensive experimental testing.

Acknowledgments

The authors gratefully acknowledge the funding of Project NORTE-01-0145-FEDER-000022 – SciTech – Science and Technology for Competitive and Sustainable Industries, co-financed by Programa Operacional Regional do Norte (NORTE2020), through Fundo Europeu de Desenvolvimento Regional (FEDER). The authors would also like to thank NAGASE ChemteX® for the financial support. The authors declare that they have no conflict of interest.

References

[1] da Silva LFM. Handbook of adhesion technology. Berlin, Germany: Springer Science & Business Media; 2011.
[2] Pethrick RA. Design and ageing of adhesives for structural adhesive bonding–a review. Proc Inst Mech Eng Part L: J Mater Des Appl 2014. [1464420714522981], Hoboken, NJ, USA.
[3] Machado J, Marques E, da Silva LFM. Adhesives and adhesive joints under impact loadings: an overview. J Adhes 2017. http://dx.doi.org/10.1080/00218464.2017.1282349.
[4] da Silva LFM, Dillard DA, Blackman B, Adams RD. Testing adhesive joints: best practices. Amsterdam, Netherlands: John Wiley & Sons; 2012.
[5] da Silva LFM, Adams R. Adhesive joints at high and low temperatures using similar and dissimilar adherends and dual adhesives. Int J Adhes Adhes 2007;27(3):216–26.
[6] Adams RD. Adhesive bonding: science, technology and applications. Elsevier; 2005.
[7] Loureiro A, da Silva LFM, Sato C, Figueiredo M. Comparison of the mechanical behaviour between stiff and flexible adhesive joints for the automotive industry. J Adhes 2010;86(7):765–87.
[8] Raphael C. Variable-adhesive bonded joints. Appl Polym Symp 1966:99–108.
[9] Fitton M, Broughton J. Variable modulus adhesives: an approach to optimised joint performance. Int J Adhes Adhes 2005;25(4):329–36.
[10] da Silva LFM, Lopes MJC. Joint strength optimization by the mixed-adhesive technique. Int J Adhes Adhes 2009;29(5):509–14.
[11] Silva M, Marques E, da Silva LFM. Behaviour under impact of mixed adhesive joints for the automotive industry. Lat Am J Solids Struct 2016;13(5):835–53.
[12] Harris J, Adams R. An assessment of the impact performance of bonded joints for use in high energy absorbing structures. Proc Inst Mech Eng Part C: J Mech Eng Sci 1985;199(2):121–31.
[13] Higuchi I, Sawa T, Suga H. Three-dimensional finite element analysis of single-lap adhesive joints under impact loads. J Adhes Sci Technol 2002;16(12):1585–601.
[14] Higuchi I, Sawa T, Suga H. Three-dimensional finite element analysis of single-lap adhesive joints subjected to impact bending moments. J Adhes Sci Technol 2002;16(10):1327–42.
[15] Sawa T, Nagai T, Iwamoto T, Kuramoto H. A study on evaluation of impact strength of adhesive joints subjected to impact shear loadings. In: Proceedings of the ASME 2008 international mechanical engineering congress and exposition. American Society of Mechanical Engineers; 2008. p. 55–61.
[16] Yang X, Xia Y, Zhou Q, Wang P-C, Wang K. Modeling of high strength steel joints bonded with toughened adhesive for vehicle crash simulations. Int J Adhes Adhes 2012;39:21–32.
[17] Wada H, Kubo S, Murase K, Kennedy T. Dynamic tensile strength of PMMA/AL plate butt adhesive joints. ICF10, Honolulu (USA); 2001–2013.
[18] Cavalli MN, Thouless MD. The effect of damage nucleation on the toughness of an adhesive joint. J Adhes 2001;76(1):75–92.
[19] Campilho RDSG, De Moura MFSF, Domingues JJMS. Stress and failure analyses of scarf repaired CFRP laminates using a cohesive damage model. J Adhes Sci Technol 2007;21(9):855–70.
[20] Carlberger T, Stigh U. An explicit FE-model of impact fracture in an adhesive joint. Eng Fract Mech 2007;74(14):2247–62.
[21] Haufe A, Pietsch G, Graf T, Feucht M. Modelling of weld and adhesive connections in crashworthiness applications with LS-DYNA. In: Proceedings of the NAFEMS seminar “simulation of connections and joints in structures”. Wiesbaden, Germany; 2010.
[22] May M, Voß H, Hiermaier S. Predictive modeling of damage and failure in adhesively bonded metallic joints using cohesive interface elements. Int J Adhes Adhes 2014;49:7–17.
[23] Clarke MI, Broughton JG, Hutchinson AR, Buckley M. Application of the design of experiments procedure to the behaviour of adhesively bonded joints with plastically deformable adherends to enable further understanding of strain rate sensitivity. Int J Adhes Adhes 2013;44:226–31.
[24] Avendaño R, Carbas RJC, Chaves FJP, Costa M, da Silva LFM, Fernandes AA. Impact loading of single lap joints of dissimilar lightweight adherends bonded with a crash-resistant epoxy adhesive. J Eng Mater Technol 2016;138(4):041019.
[25] Neumayer J, Kuhn P, Koerber H, Hinterhölzl R. Experimental determination of the tensile and shear behaviour of adhesives under impact loading. J Adhes 2016;92(7–9):503–16.
[26] ASTM D. 1002. Standard test method for apparent shear strength of single-lap-joint adhesively bonded metal specimens by tension loading (metal-to-metal); 15; 200. p. 45–8.
[27] ISO, 4587:2003. Adhesives – determination of tensile lap-shear strength of rigid-to-rigid bonded assemblies. ISO; 2003.
[28] da Silva LFM, da Silva R, Chousal J, Pinto A. Alternative methods to measure the adhesive shear displacement in the thick adherend shear test. J Adhes Sci Technol 2008;22(1):15–29.
[29] Pinto AMG, Magalhães A, Campilho RDSG, de Moura M, Baptista A. Single-lap joints of similar and dissimilar adherends bonded with an acrylic adhesive. J Adhes 2009;85(6):351–76.
[30] da Silva LFM, De Magalhaes F, Chaves F, De Moura M. Mode II fracture toughness of a brittle and a ductile adhesive as a function of the adhesive thickness. J Adhes 2010;86(9):891–905.
[31] Araújo H, Machado J, Marques E, da Silva LFM. Dynamic behaviour of composite adhesive joints for the automotive industry. Compos Struct 2017;171:549–61.
[32] da Silva LFM, Sato C, Marques E, Banea M, Carbas R. Effect of low temperature on tensile strength and mode I fracture energy of a room temperature vulcanizing silicone adhesive. J Test Eval 2015;44(3).
[33] Silva M, Marques E, Silva LFM. Behaviour under impact of mixed adhesive joints for the automotive industry. Lat Am J Solids Struct 2016;13(5):835–53.
[34] Carlberger T, Biel A, Stigh U. Influence of temperature and strain rate on cohesive properties of a structural epoxy adhesive. Int J Fract 2009;155(2):155–66.
[35] Avendaño R, Carbas R, Marques E, da Silva LFM, Fernandes A. Effect of temperature and strain rate on single lap joints with dissimilar lightweight adherends bonded with an acrylic adhesive. Compos Struct 2016;152:34–44.
[36] Blackman B, Kinloch A, Sanchez FR, Teo W, Williams J. The fracture behaviour of structural adhesives under high rates of testing. Eng Fract Mech 2009;76(18):2868–89.
[37] Morin D, Bourel B, Bennani B, Lauro F, Lesueur D. A new cohesive element for structural bonding modelling under dynamic loading. Int J Impact Eng 2013;53:94–105.
[38] Choudhry R, Hassan SF, Li S, Day R. Damage in single lap joints of woven fabric reinforced polymeric composites subjected to transverse impact loading. Int J Impact Eng 2015;80:76–93.
[39] May M, Hesebeck O, Marzi S, Böhme W, Lienhard J, Kilchert S, et al. Rate dependent behavior of crash-optimized adhesives–experimental characterization, model development, and simulation. Eng Fract Mech 2015;133:112–37.
[40] Sauer RA. A survey of computational models for adhesion. J Adhes 2016;92(2):81–120.
[41] da Silva LFM, Campilho RD. Advances in numerical modelling of adhesive joints. Berlin, Germany: Springer; 2012.
[42] Jousset P, Rachik M. Comparison and evaluation of two types of cohesive zone models for the finite element analysis of fracture propagation in industrial bonded structures. Eng Fract Mech 2014;132:48–69.

Paper 13

Content of Paper 13

Abstract

1. Introduction

2. Experimental details

2.1. Mechanical properties of the materials

2.1.1. Adhesives

2.1.2. CFRP

2.2. SLJ geometry and adhesive combinations

3. Numerical simulations procedure

3.1. Quasi-static model

3.2. Dynamic model

4. Numerical results

4.1. Quasi-static simulations

4.2. Dynamic simulations

5. Conclusions

References

Composite Structures 185 (2018) 373–380

Contents lists available at ScienceDirect

Composite Structures

journal homepage: www.elsevier.com/locate/compstruct

Numerical study of the behaviour of composite mixed adhesive joints under impact strength for the automotive industry

J.J.M. Machado[a], P.M-R. Gamarra[b], E.A.S. Marques[a], Lucas F.M. da Silva[b,*]

[a] Instituto de Ciência e Inovação em Engenharia Mecânica e Engenharia Industrial (INEGI), Rua Dr. Roberto Frias, 4200-465 Porto, Portugal
[b] Departamento de Engenharia Mecânica, Faculdade de Engenharia (FEUP), Universidade do Porto, Rua Dr. Roberto Frias, 4200-465 Porto, Portugal

ARTICLE INFO

Keywords:
CFRP
Mixed adhesive joints
Single lap joints, Quasi-static
Impact
Numerical simulation

ABSTRACT

The increasing use of composite structures in the automotive industry is due to strict regulations regarding both fuel efficiency and safety standards, since this kind of structures allow to produce strong yet light vehicles. The main advantage of the use of adhesives is the possibility of joining dissimilar materials, particularly composite materials, representing an optimal method in comparison with more traditional ones such as fastening or welding. This work focused on the development and validation of numerical models able to simulate the performance of previously experimentally tested joints. The experimental tests were performed to assess the improvement of quasi-static and impact strength of composite adhesive joints, and with the focus of avoiding early delamination of the composite substrates. The technique selected for this purpose was the use of mixed adhesive joints. Mixed adhesive joints combine two or more adhesives in a single lap joint and combine these properties to attain mechanical performance superior to that obtained using those adhesives individually. The numerical results demonstrated to be able to simulate the experimental results with reasonable accuracy.

1. Introduction

The automotive industry requires increasingly lighter and stronger structures capable of withstanding an impact load without compromising its integrity. The increasing application of composite materials has the advantage of decreasing the weight of a vehicle, therefore, allowing to meet the strict regulations regarding fuel consumption and emissions. In this industry, one of the most important use of adhesives is in joining dissimilar materials, especially composite materials where other conventional methods are not adequate (bolts, rivets, etc). Nevertheless, several of the materials used in these structures exhibit some form of strain rate sensitivity, which adding to the presence of inertial effects causes the impact behaviour of an adhesive joint to be distinct from its quasi-static behaviour [1,2].

It is a general assumption that by decreasing the strength of an adhesive it is possible to obtain an increase in its ductility. Such compromise is still not clear in terms of optimization of joint strength. The concept of mixed adhesive joints aims to provide the best combination of strength and ductility using two distinct adhesives [3–7]. In the mixed adhesive joint configuration, the stiff and brittle adhesive should be in the centre of the overlap length, while the low-modulus and flexible adhesive is located at the ends of the overlap length, a region prone to high stress concentrations [8–11]. This method aims to delay the beginning of the failure and transfer the stresses from the ends of the overlap length to the centre.

Raphael [4] proposed the use of a more flexible adhesive at the ends of the overlap and a stiffer stronger adhesive in the section corresponding to the centre, attaining a more uniform stress distribution and delaying the occurrence of failure. Later work, by Fitton and Broughton [12] demonstrated that the right combination of adhesives with different modulus can reduce stress concentration in joints using carbon fibre reinforced polymer (CFRP) substrates. Similarly, changes in the mode of failure can be obtained. However, correct selection of adhesives for use in mixed adhesive joints should not only take the mechanical properties into account but also require the adhesives to exhibit a degree of compatibility [13]. The work of Hart-Smith [14] has also demonstrated that the mixed adhesive joint configuration can also be exploited to attain improvements in the strength of joints subjected to large thermal loads. Extensive experimental work on this subjected was performed by da Silva and Adams [15], which found significant improvements in the mechanical behaviour of a joint under a large temperature gradient. Analytical work performed by Neves et al. [16] enabled the assessment of the shear deformation in the substrates as well the nonlinear geometric effect which is characteristic of SLJs, comparing favourably the performance of this model with a finite element analysis. The same authors [17] later performed a parametric

* Corresponding author.
E-mail address: lucas@fe.up.pt (L.F.M. da Silva).

https://doi.org/10.1016/j.compstruct.2017.11.045
Received 31 August 2017; Received in revised form 6 November 2017; Accepted 16 November 2017
Available online 20 November 2017
0263-8223/ © 2017 Elsevier Ltd. All rights reserved.

study of several joint parameters focusing on the stress distribution of mixed adhesive joints.

Further experimental work, performed by da Silva and Lopes [3] on mixed adhesive SLJs, used three different ductile adhesives. It was determined that if the joint strength of the ductile adhesive is lower than of the brittle adhesive, a mixed adhesive joint will lead to a joint strength higher than that of the adhesives used individually. Mixed adhesive SLJs using aluminium substrates were tested under quasi-static and impact conditions by Silva et al. [18]. The main conclusion of this work is that in configurations using a stiff epoxy with a room temperature vulcanizing silicone adhesive the results are not good, while, for the mixed adhesive SLJ combination using a stiff epoxy and an acrylic adhesive the results were superior to the individual use of both adhesives.

The performance of joints with composite substrates under impact was studied by Harding and West [19] and Taniguchi et al. [20], which have determined that while the tensile properties of unidirectional CFRP are not influenced by the strain rate, in the transverse direction the composite properties do have strong dependence of strain rate. This is because in the transverse direction the mechanical properties of the CFRP are governed by the resin.

The ability to simulate impact processes is fundamental for the design of crashworthy structures, minimizing the need for expensive experimental testing. A very powerful tool for simulating the behaviour of adhesive joints, including mixed adhesive joints, are cohesive zone models (CZM). Authors such as Needleman [21], Tvergaard et al. [22] and Camacho et al. [23] were among the first to adapt this technique to determine the failure load of adhesive joints. These elements have also been extensively used for modelling composite delamination [24,25]. The CZMs proposed by these authors completely model the fracture process, determining the crack location and advance, something which is not possible to achieve using classical continuum mechanics. The cohesive elements introduced in these models use both strength and energy parameters to simulate the nucleation and advance of a fracture crack [26,27], with the relationship between stresses and displacements being governed by a traction separation law. More recently, CZMs have also been combined with extended finite element method (XFEM) models, allowing more freedom in the location of the crack initiation [42].

The work of Carlberger et al., published in 2007 [28], was among the first that demonstrated the use of this approach to predict impact performance. Later, authors such as Haufe et al. [29], May et al. [30], Clarke et al. [31] Avendaño et al. [32] and Neumayer et al. [33] have performed similar analysis employing commercial software packages or custom elements, achieving accurate failure load predictions using complex dynamical cohesive models with strain rate dependent data.

Numerical simulations based on the mixed adhesive joints concept were already performed and proved experimentally. Kong et al. [34] developed a 3-D elastic finite element model to assess the influence in the stress distribution of different sequences and ratios of variable modules adhesives (bi-adhesive joints) in a bond line, in comparison to the use of a single adhesive. A decrease in the maximum stress of the adhesive layer occurred when using a suitable bi-adhesive combination, when meeting appropriate length ratios and bonding sequence of adhesives. From the simulations, it was concluded that the under different modes of loading, the optimization of the bonding parameters of bi-adhesives is required to be able to provide appropriate results. Similar results were obtained by Kumar and Pandey [35] (using also 2-D plane strain analysis) and Pires et al. [36]. Later, Pires at al. [37] performed a numerical study using Drucker-Prager plasticity model for the adhesives. Temiz [38] experimentally and numerically assessed that by using double strap joints subjected to bending moment, the use of two adhesives carried more loads as well higher strength. Akpinar et al. [39] studied experimentally and numerically (using a non-linear 3-D model) the effect of a mixed adhesive T-joint, in terms of normal and shear stress distribution. The finite element model could fit the experimental results, the peal stresses decrease with the use of mixed adhesives being the stresses carried into the inner regions, and the same behaviour was observed regarding shear stress. A numerical study to assess the effect of mixed adhesive joints with and without tapering plate on the interfacial stress in the adhesive layer was performed by Bouchikhi et al. [40] providing accurate results.

The present work focused on the numerical simulation with the aim of developing and validate models able to simulate loadings obtained experimentally in a previous work. The experimental tests were performed to assess the improvement of the static and impact strength of composite adhesive joints, and with the focus of avoiding early delamination of the composite substrates. The techniques selected for this purpose are the use of mixed adhesive joints and the use of crash resistant adhesives. Mixed adhesive joints combine two or more adhesives in a single lap joint and combine these properties to attain mechanical performance superior to that obtained using those adhesives individually. On the other hand, crash resistant adhesives are extremely strong yet ductile adhesives.

2. Experimental details

The mechanical properties of both substrates and adhesives tested experimentally are presented in this section. This data is of extreme importance for the numerical models, being defined for quasi-static and impact testing conditions. The geometry and all the adhesive configurations are also presented once they were used in all the numerical models created.

2.1. Mechanical properties of the materials

2.1.1. Adhesives

A total of five adhesives were tested experimentally in a previous work, two of those being considered as stiff and three being considered as flexible. The identification and type of adhesive is presented in Table 1, as well some of the authors who have determined the mechanical properties of these adhesives. It is also important to mention that the adhesives are ordered from the stiffest to the least stiff.

To perform accurate numerical simulation, it is essential to have the material properties at higher testing speeds, due to its strain rate dependency. The required value of high strain rate (3 m/s) the adhesives were not directly characterized. To determine these values, some of the adhesives were initially tested at 1 and 100 mm/min. An extrapolation process was then used, based in a logarithmic trend function able to estimate the properties at higher speeds [47,48] (Eq. (1)).

$$Property\ to\ determine = A\ln(\dot{\varepsilon}) + B \tag{1}$$

where A and B are constrains attained from experimental data, and $\dot{\varepsilon}$ is the strain rate in s^{-1}.

In Eq. (2), $\dot{\varepsilon}$ (strain) was determined:

$$\dot{\varepsilon} = \frac{v}{L_o} \tag{2}$$

Being v the velocity of the test and L_o the initial calibrated longitudinal deformation length of the specimen section where the strain is measured.

The mechanical properties of the adhesives (for room temperature)

Table 1
Types of adhesives studied.

Adhesive	Type	References
Araldite AV 138	Stiff	Silva et al. [41]
Nagase-Chemtex XNR6852 E-3	Stiff	Araújo et al. [42]
3M DP 8005	Flexible	Silva et al. [43] and Pinto et al. [44]
SikaFast 5211 NT	Flexible	Netusil et al. [45]
Momentive RTV 106	Flexible	Banea et al. [46]

Table 2
Adhesive properties.

Adhesive	Test speed (mm/min)	Young's modulus [MPa]	Shear modulus [MPa]	Tensile strength [MPa]	Shear strength [MPa]	Mode I fracture energy [N/mm]	Mode II fracture energy [N/mm]
AV 138	1	4890	1560	41	30.2	0.35	4.9
	100			49.1	36.2		
	18000*			72.1	45.9		
XNR6852 E-3	1	1728	665	51.5	44.9	6.4	51
	100		645	60.5	44	7.1	58.2
	180000*		603	77.7	42.9	8	64.1
DP 8005	1	590	159	6.3	8.4	1.1	6
	100			13	17.4		
	180000*			32	32		
SikaFast 5211NT	1	260	n/a	5.06	n/a	n/a	n/a
	100	n/a					
	180000*	n/a					
RTV 106	1	1.6	0.86	2.3	1.97	2.73	5
	100						
	180000*						

* Mechanical properties extrapolated considering an impact velocity of 3 m/s.

which were used in the numerical models are presented in (Table 2). The values presented range from quasi-static (1 mm/min) to impact (180,000 mm/min or an equivalent impact speed of 3 m/s).

In the literature, it is possible to find some studies of the mechanical properties of the selected adhesives. Some adhesives have their strain rate characterized, such as XNR6852 E-3, and others only have properties represented as strain rate dependent, namely DP 8005 and AV 138. For the case of the RTV 106 adhesive, once this adhesive is very difficult to test, for this work it was considered strain rate independent in the model. For the adhesive SikaFast 5211NT the information concerning mechanical properties is scarce and only regarding quasi-static loadings.

2.1.2. CFRP

The CFRP used in the experimental work previously performed (SEAL® Texipreg HS 160 RM) was in the configuration of 0° lay-up plies. The elastic properties of the CFRP used in the same configuration were determined in the work of Campilho [49] in 2009. Youngs modulus (E), the shear modulus (G), and the Poissońs ratio (v), in the three axis direction (x, y, z), are presented in Table 3, being E_1 the normal direction, E_2 the transverse direction and E_3 the out plane direction. The tensile properties of CFRP are known not to vary significantly with the strain rate.

The cohesive mechanical properties of CFRP were previously experimentally determined for 1 mm/min and 100 mm/min by the authors [50,51]. For high speed (3 m/s), the properties were determined using the same extrapolation process described for the adhesives [42]. Table 4 presents the cohesive properties of CFRP for three testing speeds.

2.2. SLJ geometry and adhesive combinations

A geometry representative of automotive industry applications was selected for the study (Fig. 1). The overlap length was of 25 mm for all SLJs made of both single and mixed adhesives combinations. The thickness of CFRP substrates was also selected in accordance with the general value used in real applications being of 2.1 mm.

Table 3
Properties of CFRP elastic orthotropic [49].

Elastic Modulus (MPa)	Poissońs Ratio	Shear Modulus (MPa)
E_1 = 1.09E5	ν_{12} = 0.342	G_{12} = 4315
E_2 = 8819	ν_{13} = 0.342	G_{13} = 4315
E_3 = 8819	ν_{23} = 0.380	G_{23} = 3200

Table 4
Cohesive properties of CFRP under quasi-static and impact conditions.

Properties	1 mm/min	100 mm/min	180,000 mm/min
Young's modulus, E [MPa]	109000	109000	109000*
Shear modulus, G [MPa]	4315	4315	4315*
Tensile strength, σ_n [MPa]	40	40	40*
Shear strength, t_s [MPa]	35	35	35*
Fracture energy (mode I), G_{IC} [N/mm]	0.59	0.53	0.39*
Fracture energy (mode II), G_{IIC} [N/mm]	1.17	1.04	0.82*

* Mechanical properties extrapolated considering an impact velocity of 3 m/s.

The total number of combinations possible to perform using the two stiff and three flexible adhesives was eleven. Due to compatibility problems experienced in previous experimental works [52], one of the mixed adhesive combination (DP 8005 + XNR6852 E-3) was discarded.

All the adhesive combinations tested experimentally are listed in Table 5.

The mixed adhesive joints configuration is divided in three distinct section: a stiff adhesive (positioned in the centre of the overlap) and a flexible adhesive at both overlap ends. The schematic representation of the adhesive section along the overlap length is presented in Fig. 2. Considering the overlap length of 25 mm, the ratio between the stiff and flexible adhesives was found to be optimal at a proportion of 16.6 mm for the stiff adhesive and, respectively, of 4.2 mm for both sections at the end of overlap length using the flexible adhesive. This ratio was chosen based on a previous work [18] performed with the same adhesives, although using steel substrates.

3. Numerical simulation procedure

A finite element analysis was performed using the software ABAQUS® with the objective of reproducing the experimental results. The use of this software provides the possibility of determining force-displacement curves (P-δ) curves as well as obtaining a prediction of the failure load. The model employed cohesive elements with a triangular (bilinear) traction-separation law, based on the mechanical and cohesive properties of both CFRP and adhesives. It was assumed that the structure of the SLJs was in perfect condition and no defects were present at the interface and within the adhesive layer.

Fig. 3 shows the pure-mode (traction or shear) and mixed-mode traction separation laws, where t_n^0 and t_s^0 are the cohesive strengths in tension and shear, respectively, and δ_n^0 and δ_s^0 are the respective displacements, and δ_n^f and δ_s^f are the tensile and shear displacements at

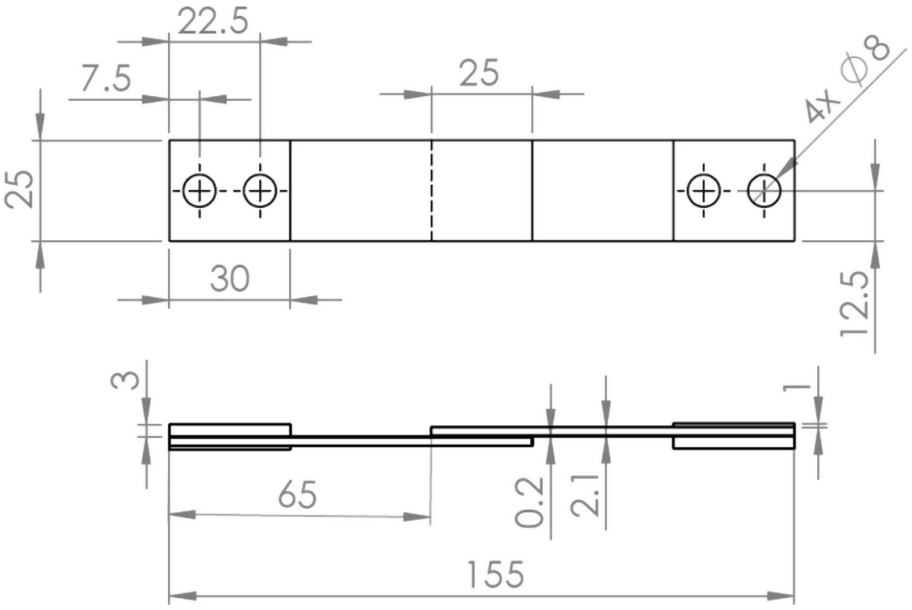

Fig. 1. Geometry of SLJ specimens (dimensions in mm).

Table 5
Adhesive combinations used (single and mixed adhesives).

Combination	Adhesives
Single adhesive	**AV 138** (full overlap) – stiff adhesive
	XNR6852 E-3 (full overlap) – stiff adhesive
	SikaFast 5211NT (full overlap) – flexible adhesive
	DP 8005 (full overlap) – flexible adhesive
	RTV 106 (full overlap) – flexible adhesive
Mixed adhesive	**AV 138** (centre) – stiff adhesive + **SikaFast 5211NT** (edges) – flexible adhesive
	AV 138 (centre) – stiff adhesive + **DP 8005** (edges) – flexible adhesive
	AV 138 (centre) – stiff adhesive + **RTV 106** (edges) – flexible adhesive
	XNR6852 E-3 (centre) – stiff adhesive + **SikaFast 5211NT** (edges) – flexible adhesive
	XNR6852 E-3 (centre) – stiff adhesive + **RTV 106** (edges) – flexible adhesive

failure, respectively.

The shape of this law can be changed to more adequately fit the mechanical behaviour of the simulated material. The initial elastic portion is always kept linear, defined by a constitutive matrix (**K**), containing the stiffness parameters and relating current stresses (**t**) and strains (ε) in the three loading modes across the interface.

$$\mathbf{t} = \begin{Bmatrix} t_n \\ t_{s1} \\ t_{s2} \end{Bmatrix} = \begin{bmatrix} K_{nn} & K_{ns1} & K_{ns2} \\ K_{ns1} & K_{s1s1} & K_{s1s2} \\ K_{ns2} & K_{s1s2} & K_{s2s2} \end{bmatrix} \cdot \begin{Bmatrix} \varepsilon_n \\ \varepsilon_{s1} \\ \varepsilon_{s2} \end{Bmatrix} = \mathbf{K}\boldsymbol{\varepsilon} \tag{3}$$

After the mixed-mode cohesive strength is attained (t_m^0 in Fig. 3) the material stiffness is degraded. Complete separation is predicted by a linear power law form of the required energies for failure in the pure modes (Eq. (6)).

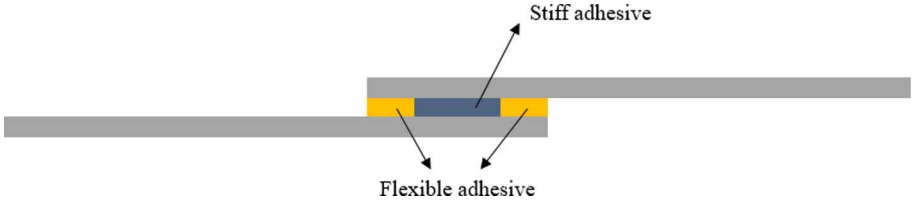

Fig. 2. Schematic representation of the mixed-adhesive SLJ configuration.

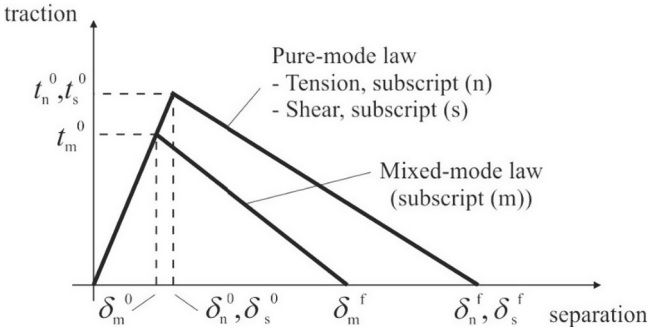

Fig. 3. Triangular traction-separation law with linear softening: pure and mixed-mode models.

$$\frac{G_n}{G_n^c} + \frac{G_{s1}}{G_{s1}^c} + \frac{G_{s2}}{G_{s2}^c} = 1. \tag{4}$$

G_n and G_s are the current strain energy release rates in each loading mode, while G_n^c and G_s^c are the respective critical values. Various shapes for the softening portion of the curve can be found, such as polynomial [22], exponential [25], trapezoidal [23] or triangular. [28]. It has been demonstrated that triangular laws are well suited for stiff, brittle adhesives, while more ductile adhesives are more correctly modelled by trapezoidal cohesive laws [53].

3.1. Quasi-static model

The quasi-static model employed in this work includes cohesive elements to fully simulate the failure of the joint either by cohesive failure of the adhesive or delamination of the CFRP. For this purpose, the complete adhesive layer was considered as having a cohesive behaviour and a cohesive law was also attributed to a thin layer of the CFRP adherend close to the adhesive area. The thickness of this layer

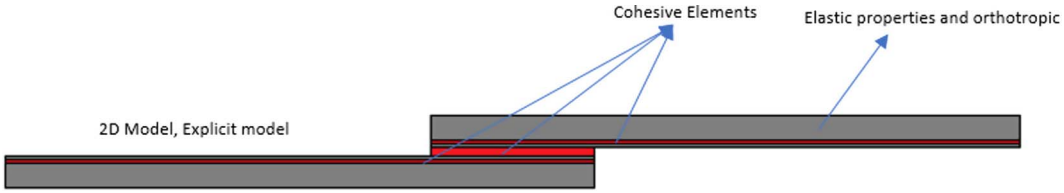

Fig. 4. Elements introduced in FE software for the static analysis.

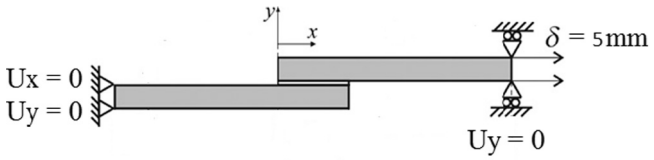

Fig. 5. Boundary conditions applied for the static model.

was 0.1 mm and it was located 0.1 mm away from the interface between adhesive and CFRP. A 2D model was used due to the simple geometry of the SLJ (Fig. 4).

A mixed mode formulation was considered, using the quadratic stress criterion for damage initiation and the linear energetic criterion for damage propagation.

The quasi-static mechanical properties of the adhesives used were previously presented in Table 2. The CFRP adherend was modelled using elastic engineering constants and fracture properties (Tables 3 and 4).

Subsequently, the boundary conditions were added to the model. In the left side, the impossibility of movement was considered. In the opposite side, displacement in the vertical axis was restricted, and a displacement of 5 mm was considered. Fig. 5 shows a schematic drawing of the boundary conditions.

For the visualization of the CZM degradation, scalar stiffness degradation (SDEG) was requested in the field outputs, enabling monitoring of the crack propagation.

The meshes of the adhesive layer and substrates near the overlap region were refined to satisfy the simulation accuracy. Most of the mesh used 0.2 mm long elements, however, further mesh refinement was performed in the overlap ends. For this purpose, seeds were defined using biased elements. Regarding to the element types, the bondline area was defined as a 4-node-two-dimensional cohesive element (COH2D4) and substrates were defined as a 4-node bilinear plane strain quadrilateral, reduced integration, hourglass control (CPE4R). For each specimen arm, six elements were used through-thickness [54,55].

3.2. Dynamic model

For simulating the impact tests, an explicit model was used. This model uses an explicit formulation, optimal for simulating high-speeds impact problems. The geometry is close to that of the static model but includes a mass in one end of the specimen (Fig. 6), representing an impact block. By varying the mass parameters, namely, the length of the sides and/or the density, it is possible to adjust the impact energy.

The boundary conditions used the same restrictions of the quasi-static model but also included a velocity field of 3000 mm/s applied to the impact block (Fig. 7).

The volume of the impact block is of 1250 mm^3, and to simulate the 117 J of energy and the velocity of 3000 mm/s the density was set to 3.8 kg/m^3. The impact simulation was performed using a dynamical explicit calculation with a period of 0.02 s and considering non-linear geometries in the step. A predefined velocity field was applied to the initial step with a value of 3000 mm/s in the mass. The SDEG field output was added with the same purpose of the static simulation. The mesh for the dynamic models was created following the same premises described for the static simulation, but varying the mesh elements to explicit elements.

4. Numerical results

The assessment and validation of the simulations performed was possible by making a contrast between the previously experimental results obtained using the same mixed adhesive SLJ configurations, and considering the values of the failure loads and displacement. In this section, the numerical results are displayed and a critical analysis is performed to discuss the results and problems occurred in both quasi-static and impact models.

4.1. Quasi-static simulations

Fig. 8 shows a comparison between the experimental failure loads and the numerical failure loads.

The model provides results which are reasonably close to experimental results in most cases under study. However, the numerical results tend to be below the experimental results which may be due to the mechanical properties introduced in the model. For example, the model for XNR6852 E-3 exhibits delamination failure, but is not able to reach the experimental failure load which might mean that the CFRP properties could also be slightly higher than the ones used in the model.

The following paragraphs describe two specific cases that were selected to demonstrate the capabilities and limitations of the developed model. Fig. 9 depicts the numerical and experimental P-δ curves for AV 138 adhesive.

The model shows good results, with reasonable agreement of the numerical and experimental curves. The experimental failure load is slightly higher than the numerical failure load. Again, this might be due to some slight difference in the mechanical properties of the composite due to manufacturing variations

Fig. 10 exhibits the comparison between the numerical and experimental curves of the static tests of mixed joints containing the XNR6852 E-3 and the RTV 106 adhesives.

In this case, the numerical model predicts very high failure loads,

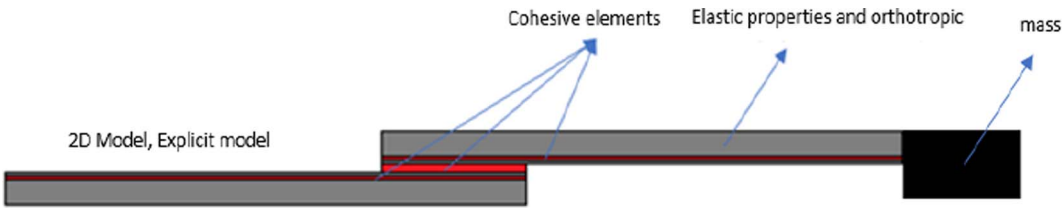

Fig. 6. Elements types introduced in FE software for the dynamic analysis.

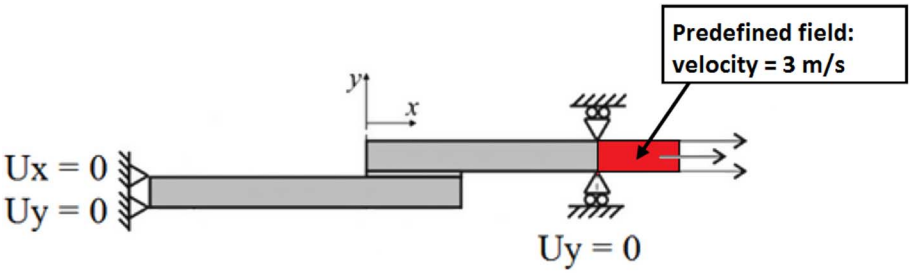

Fig. 7. Boundary conditions applied for the dynamic model.

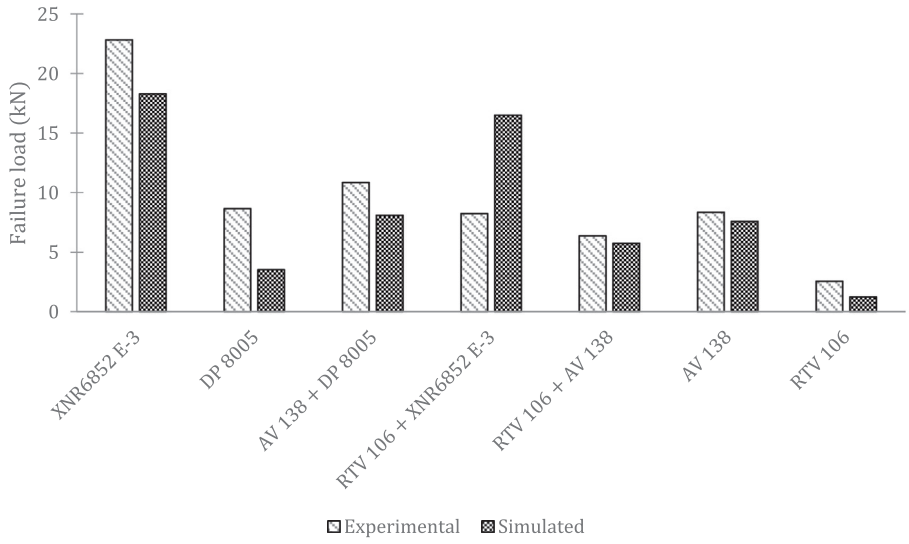

Fig. 8. Comparison experimental and numerical failure loads.

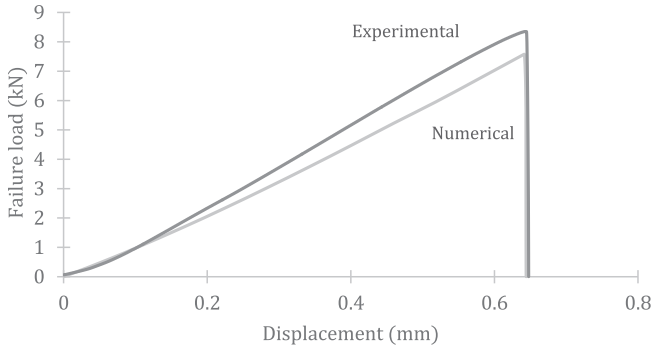

Fig. 9. Comparison between experimental and numerical P-δ curves of AV 138 under quasi-static conditions.

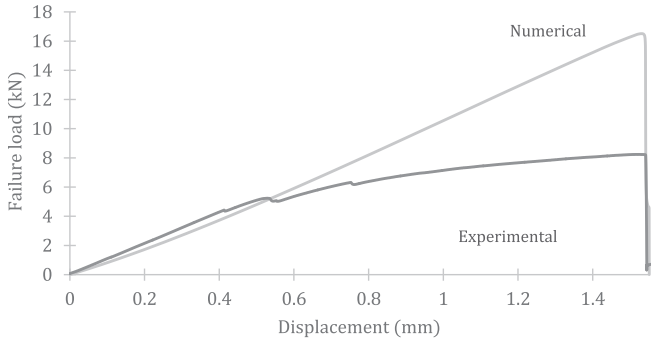

Fig. 10. Comparison between experimental and numerical P-δ curves of XNR6852 E-3 + RTV 106 under quasi-static conditions.

far from those experimentally obtained. This can be mainly explained by a degree of contamination of the central section by RTV 106, which occurred due to manufacturing difficulties in the experimental phase. It is also compounded by the low adhesion of RTV 106 to the CFRP substrate. Another important factor is the fact that very flexible adhesives, such as RTV106 and DP-8005 cannot be easily modelled using triangular cohesive laws. A trapezoidal cohesive law should be more suitable for modelling theses adhesives.

4.2. Dynamic simulations

As for the static results, a comparison between the forces in the different adhesives between numerical and simulated results was made and is shown in Fig. 11.

For all cases under study, the experimental and numerical values are quite close, except for RTV 106 and DP 8005 single adhesive configurations. The low numerical result for RTV106 is mainly due to the fact that no strain rate dependent properties were available for this material.

As presented in the static simulation results, the following paragraphs include comparisons between numerical and experimental *P-δ* curves for two configurations.

Fig. 12 shows the comparison between the experimental and numerical *P-δ* curves of impact tested SLJs with XNR6852 E-3 adhesive.

In this case, the numerical simulation is quite accurate, with the experimental and numerical data having good agreement. This is due to the precise mechanical properties available, which have been extensively studied under higher strain rates in previous works.

Fig. 13 shows another example of numerical and experimental *P-δ* curves, this time for the combination of AV 138 with RTV 106.

This configuration shows similar numerical and experimental failure loads but the numerical model predicts a larger displacement which does not occur for the experimental results. This can be

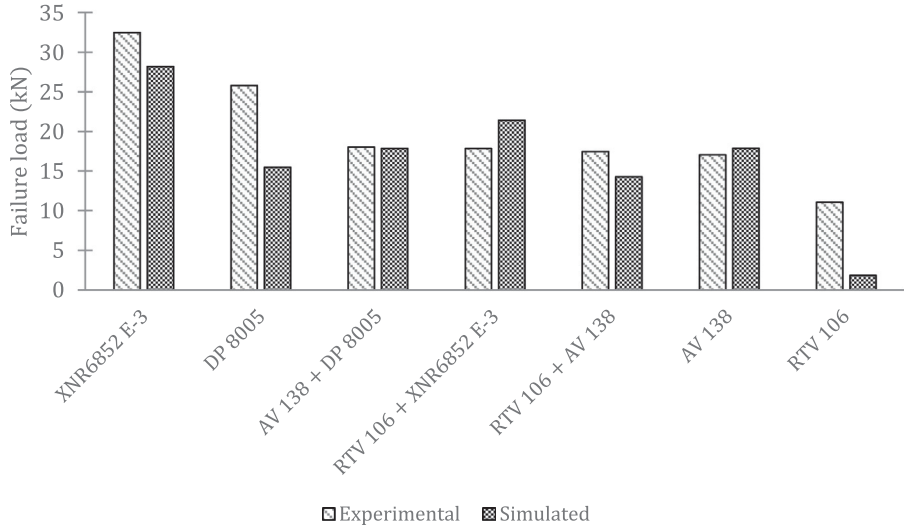

Fig. 11. Comparison of impact failure loads obtained experimentally and with the numerical model.

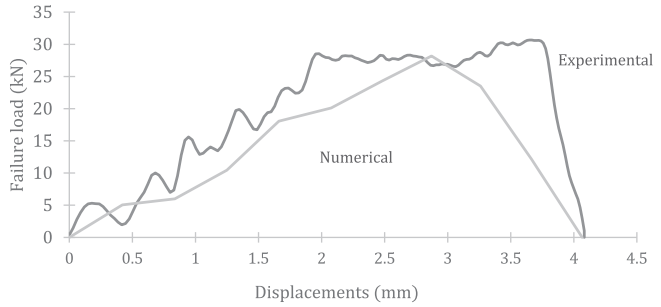

Fig. 12. Comparison between experimental and numerical P-δ curves of XNR6852 E-3 under impact conditions.

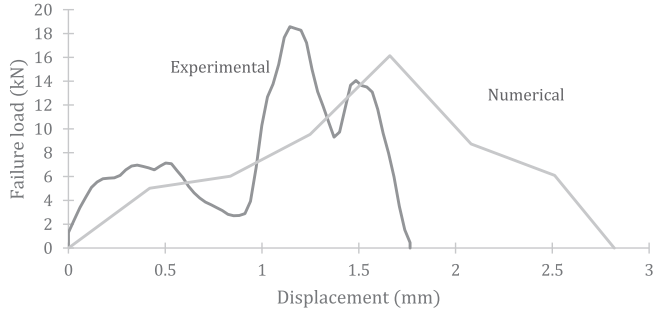

Fig. 13. Comparison between experimental and numerical P-δ curves of AV 138 + RTV 106 under impact conditions.

attributed to two main factors. The first factor is the early adhesive failure of RTV 106, not allowing the joint to deform more before failure. The second factor is the lack of strain rate dependent properties, which, due to the adhesive failure, do not influence greatly the result of this model.

5. Conclusions

The main goal of this work was the development of numerical models to predict the mechanical behaviour of composite adhesive joints under quasi-static and impact loads, aiming to serve as a tool to avoid early delamination of the composite substrates. The joint configurations under study employ the mixed adhesive technique and use high performance crash resistant adhesive, which were experimentally tested in a previous work and were numerically simulated. The main conclusions drawn from this work are presented below:

- The quasi-static models developed using ABAQUS® could simulate reasonably well most of the configurations under study. However, models of the single adhesive joints with very flexible adhesives (DP 8005 and RTV 106) exhibited poor results, mainly due to triangular cohesive zone model inability to model very flexible adhesives effectively.
- The numerical models for the impact tests were also able to model most of the experimental results. Again, the most inaccurate models were those containing the flexible DP 8005 and RTV 106 adhesives. In this case, not only the use of a triangular cohesive zone law contributes to the poor results but also the difficulty in establishing the correct strain rate dependent properties.

Acknowledgments

The authors gratefully acknowledge the funding of Project NORTE-01-0145-FEDER-000022 – SciTech – Science and Technology for Competitive and Sustainable Industries, co-financed by Programa Operacional Regional do Norte (NORTE2020), through Fundo Europeu de Desenvolvimento Regional (FEDER). The authors would also like to thank NAGASE ChemteX® for the financial support provided.

References

[1] Machado J, Marques E, da Silva L. Adhesives and adhesive joints under impact loadings: an overview. J Adhes 2017. http://dx.doi.org/10.1080/00218464.2017.1282349.
[2] Banea M, da Silva L, Campilho R. Effect of temperature on tensile strength and mode I fracture toughness of a high temperature epoxy adhesive. J Adhes Sci Technol 2012;26(7):939–53.
[3] da Silva L, Lopes MJC. Joint strength optimization by the mixed-adhesive technique. Int J Adhes Adhes 2009;29(5):509–14.
[4] Raphael C. Variable-adhesive bonded joints. Appl Polym Symp 1966: 99–108.
[5] Srinivas S. Analysis of Bonded Joints. DTIC Document; 1975.
[6] Semerdzhiev SG. Metal-to-metal adhesive bonding: random house. Business 1970.
[7] Patrick RL. Treatise on adhesion and adhesives: structural adhesives with emphasis on aerospace applications: Dekker; 1976.
[8] Carver D, Wooley G. Stress concentration factors for bonded lap joints. J Aircr 1971;8(10):817–20.
[9] Volkersen O. Die Nietkraftverteilung in zugbeanspruchten Nietverbindungen mit konstanten Laschenquerschnitten. Luftfahrtforschung 1938;15(1/2):41–7.
[10] Goland M, Reissner E. The stresses in cemented joints. J Appl Mech 1944;11(1):A17–27.
[11] Adams RD, Comyn J, Wake WC. Structural adhesive joints in engineering: Springer Science & Business Media; 1997.
[12] Fitton M, Broughton J. Variable modulus adhesives: an approach to optimised joint performance. Int J Adhes Adhes 2005;25(4):329–36.
[13] Breto R, Chiminelli A, Duvivier E, Lizaranzu M, Jiménez M. Functionally graded

bond-lines for metal/composite joints; 2014.
[14] Hart-Smith LJ. Adhesive-bonded single-lap joints: Langley Research Center Hampton, VA; 1973.
[15] Da Silva LF, Adams R. Techniques to reduce the peel stresses in adhesive joints with composites. Int J Adhes Adhes 2007;27(3):227–35.
[16] das Neves PJ, da Silva LF, Adams R. Analysis of mixed adhesive bonded joints part I: theoretical formulation. J Adhes Sci Technol 2009;23(1):1–34.
[17] das Neves PJ, da Silva LF, Adams R. Analysis of mixed adhesive bonded joints part II: parametric study. J Adhes Sci Technol 2009;23(1):35–61.
[18] Silva M, Marques E, da Silva L. Behaviour under impact of mixed adhesive joints for the automotive industry. Latin Am J Solids Struct 2016;13(5):835–53.
[19] Harding J, Welsh L. A tensile testing technique for fibre-reinforced composites at impact rates of strain. J Mater Sci 1983;18(6):1810–26.
[20] Taniguchi N, Nishiwaki T, Kawada H. Tensile strength of unidirectional CFRP laminate under high strain rate. Adv Compos Mater 2007;16(2):167–80.
[21] Needleman A. A continuum model for void nucleation by inclusion debonding. J Appl Mech 1987;54(3):525–31.
[22] Tvergaard V, Hutchinson JW. The relation between crack growth resistance and fracture process parameters in elastic-plastic solids. J Mech Phys Solids 1992;40(6):1377–97.
[23] Camacho GT, Ortiz M. Computational modelling of impact damage in brittle materials. Int J Solids Struct 1996;33(20):2899–938.
[24] Li X, Hallett SR, Wisnom MR. Predicting the effect of through-thickness compressive stress on delamination using interface elements. Compos A Appl Sci Manuf 2008;39(2):218–30.
[25] Sockalingam S, Dey M, Gillespie JW, Keefe M. Finite element analysis of the microdroplet test method using cohesive zone model of the fiber/matrix interface. Compos A Appl Sci Manuf 2014;56:239–47.
[26] Banea MD, da Silva LF, Campilho R. Effect of temperature on the shear strength of aluminium single lap bonded joints for high temperature applications. J Adhes Sci Technol 2014;28(14–15):1367–81.
[27] Da Silva LF, Campilho RD. Advances in numerical modelling of adhesive joints. Springer; 2012.
[28] Carlberger T, Stigh U. An explicit FE-model of impact fracture in an adhesive joint. Eng Fract Mech 2007;74(14):2247–62.
[29] Haufe A, Pietsch G, Graf T, Feucht M. Modelling of weld and adhesive connections in crashworthiness applications with LS-DYNA. In: Proceedings of the NAFEMS seminar “simulation of connections and joints in structures” Wiesbaden, Germany; 2010.
[30] May M, Voß H, Hiermaier S. Predictive modeling of damage and failure in adhesively bonded metallic joints using cohesive interface elements. Int J Adhes Adhes 2014;49:7–17.
[31] Clarke MI, Broughton JG, Hutchinson AR, Buckley M. Application of the design of experiments procedure to the behaviour of adhesively bonded joints with plastically deformable adherends to enable further understanding of strain rate sensitivity. Int J Adhes Adhes 2013;44:226–31.
[32] Avendaño R, Carbas RJC, Chaves FJP, Costa M, da Silva LFM, Fernandes AA. Impact loading of single lap joints of dissimilar lightweight adherends bonded with a crash-resistant epoxy adhesive. J Eng Mater Technol 2016;138(4):041019.
[33] Neumayer J, Kuhn P, Koerber H, Hinterhölzl R. Experimental determination of the tensile and shear behaviour of adhesives under impact loading. J Adhes 2016;92(7–9):503–16.
[34] Kong F-R, You M, Zheng X-L. Three-dimensional finite element analysis of the stress distribution in bi-adhesive bonded joints. J Adhes 2008;84(2):105–24.
[35] Kumar S, Pandey P. Behaviour of bi-adhesive joints. J Adhes Sci Technol 2010;24(7):1251–81.
[36] Pires I, Quintino L, Durodola J, Beevers A. Performance of bi-adhesive bonded aluminium lap joints. Int J Adhes Adhes 2003;23(3):215–23.
[37] Pires I, Quintino L, Miranda R. Numerical simulation of mono-and bi-adhesive aluminium lap joints. J Adhes Sci Technol 2006;20(1):19–36.
[38] Temiz Ş. Application of bi-adhesive in double-strap joints subjected to bending moment. J Adhes Sci Technol 2006;20(14):1547–60.
[39] Akpinar S, Aydin MD, Özel A. A study on 3-D stress distributions in the bi-adhesively bonded T-joints. Appl Math Model 2013;37(24):10220–30.
[40] Bouchikhi A, Megueni A, Gouasmi S, Boukoulda F. Effect of mixed adhesive joints and tapered plate on stresses in retrofitted beams bonded with a fiber-reinforced polymer plate. Mater Des 2013;50:893–904.
[41] da Silva LF, De Magalhaes F, Chaves F, De Moura M. Mode II fracture toughness of a brittle and a ductile adhesive as a function of the adhesive thickness. J Adhes 2010;86(9):891–905.
[42] Araújo H, Machado J, Marques E, da Silva L. Dynamic behaviour of composite adhesive joints for the automotive industry. Compos Struct 2017.
[43] da Silva LF, da Silva R, Chousal J, Pinto A. Alternative methods to measure the adhesive shear displacement in the thick adherend shear test. J Adhes Sci Technol 2008;22(1):15–29.
[44] Pinto AMG, Magalhães A, Campilho RDSG, De Moura M, Baptista A. Single-lap joints of similar and dissimilar adherends bonded with an acrylic adhesive. J Adhes 2009;85(6):351–76.
[45] Netusil M, Eliasova M. Trends and requirements for adhesives with load bearing role. Proc Challenging Glass 2014;4:369–74.
[46] Banea MD, da Silva L. Mechanical characterization of flexible adhesives. J Adhes 2009;85(4–5):261–85.
[47] Zgoul M, Crocombe A. Numerical modelling of lap joints bonded with a rate-dependent adhesive. Int J Adhes Adhes 2004;24(4):355–66.
[48] Avendaño R, Carbas R, Marques E, da Silva L, Fernandes A. Effect of temperature and strain rate on single lap joints with dissimilar lightweight adherends bonded with an acrylic adhesive. Compos Struct 2016;152:34–44.
[49] Campilho R. Repair of composite and wood structures: Instituto Superior de Engenharia do Porto; 2009.
[50] Machado J, Marques E, Campilho R, da Silva L. Mode I fracture toughness of CFRP as a function of temperature and strain rate. J Compos Mater 2016;0021998316682309.
[51] Machado J, Marques E, Campilho R, da Silva LF. Mode II fracture toughness of CFRP as a function of temperature and strain rate. Compos B Eng 2017;114:311–8.
[52] da Silva MRG. Impact of mixed adhesive joints for the automotive industry [Master thesis]. Faculty of Engineering of the University of Porto; 2015.
[53] Fernandes R, Campilho R. Numerical evaluation of dissimilar cohesive models to predict the behavior of Double-Cantilever Beam specimens. Proc Struct Integrity 2016;1:42–9.
[54] Daghyani HR, Ye L, Mai Y-W. Mixed-mode fracture of adhesively bonded CF/epoxy composite joints. J Compos Mater 1996;30(11):1248–65.
[55] Campilho RDSG, De Moura M, Barreto A, Morais J, Domingues J. Fracture behaviour of damaged wood beams repaired with an adhesively-bonded composite patch. Compos A Appl Sci Manuf 2009;40(6):852–9.

Paper 14

Content of Paper 14

Abstract

1. Introduction

2. Experimental details

2.1. Material and properties

2.1.1. Crash resistant adhesive

2.1.2. Substrates

2.1.2.1. CFRP

2.1.2.2. Aluminium alloys

2.2. Joints geometry and substrates configuration

2.3. Quasi-static and impact testing

3. Numerical simulation details

3.1. Cohesive zone modelling

3.2. Quasi-static model

3.3. Dynamic model

4. Results and discussion

4.1. Quasi-static modelling

4.1.1. SLJs with similar substrates

4.1.2. SLJs with dissimilar substrates

4.2. Impact modelling

4.2.1. SLJs with similar substrates

4.2.2. SLJs with dissimilar substrates

5. Geometrical study

5.1. Adhesive thickness

5.2. Overlap length

5.3. CFRP substrate thickness

6. Conclusions

References

Numerical study of similar and dissimilar single lap joints under quasi-static and impact conditions

J. J. M. Machado[1], P. D. P. Nunes[2], E. A. S. Marques[1], Lucas F. M. da Silva[2*]

[1]Instituto de Ciência e Inovação em Engenharia Mecânica e Engenharia Industrial (INEGI), Rua Dr. Roberto Frias, 4200-465 Porto, Portugal

[2]Departamento de Engenharia Mecânica, Faculdade de Engenharia (FEUP), Universidade do Porto, Rua Dr. Roberto Frias, 4200-465 Porto, Portugal

Abstract

Aiming to achieve the targets of reduction of fuel consumption and emissions, automotive manufacturers are increasingly using lightweight materials in the vehicle structures, namely, carbon fibre composites and aluminium alloys. The construction techniques for vehicle structures using this type of materials differ greatly from the techniques used for the most commonly used steel bodies, with adhesive bonding being extensively used due to its capability to bond dissimilar materials. Nevertheless, the application of adhesive bonding poses several challenges to the automotive industry, as dissimilar bonded joints must be designed to perform well under impact. In this work, numerical models were created and validated against previously determined experimental data in both quasi-static and impact conditions of similar and dissimilar (CFRP and aluminium as substrates) single lap joints bonded using a crash resistant adhesive. Cohesive zone models were used to simulate adhesive failure and composite delamination while damage models were used to simulate plastic deformation and failure of the aluminium alloy, allowing to conclude that it is possible to use dissimilar adhesive joints bonded with a crash resistant adhesive in an automotive structure, not compromising the joints performance.

Keywords

CFRP; Aluminium; Quasi-static; Impact; Finite element analysis

*Corresponding author. Tel: +351225081706. Fax: +351225081445. Email: lucas@fe.up.pt

1. Introduction

The automotive industry has significantly increased the use of adhesives for joining load-bearing components to lower vehicle weight, improve fuel economy and reduce emissions. However, the design process of a bonded structure can be complex, as the properties of adhesives vary widely from brittle to highly deformable adhesives [1]. Adhesives are viscoelastic, and their properties greatly depend on several factors such as temperature, humidity and loading rate. While some design criteria consider these effects, there is still limited information regarding the impact behaviour of bonded joints, especially when used with composite substrates.

Although most structural components used in the automotive industry are still made from steel, it is also true that the aluminium and composite materials are gaining more and more space in the industry. Vehicle bodies, that before were mainly made of steel, now increasingly include assemblies made of aluminium. Additionally, the use of composite materials for bonnets and others body panels is becoming more frequent [1]. Since the loads applied to the distinct parts of a car can vary widely, the use of different materials and geometries is necessary to reduce weight and increase overall structural stiffness. These two parameters are currently the focus of the industry, in order to reduce emissions and increase performance.

The aluminium characteristic properties, like high strength stiffness to weight ratio, excellent formability, good corrosion resistance, and potential for recycling, make it the ideal candidate to replace heavier materials (steel or copper) in vehicle construction to meet the weight reduction requirements of the automotive industry. Although the aluminium density (2700 kg/m^3) is about one third of the steel (7600 kg/m^3), the weight reduction when replacing steel by aluminium in car manufacturing is around 50% as, to ensure structural stiffness equivalent to that of steel, the cross-sectional areas of aluminium elements need to be larger. The use of aluminium in structural parts of vehicles is continually increasing as new alloys and design solutions are developed. The alloys of 5000 and 6000 series are particularly interesting in the automotive industry since they allow the construction of most of the structure of a car body and because of their improved metal corrosion when compared to steel. Aluminium is also suitable for application in energy absorbing structures, as it presents a mass-specific energy absorption capacity

twice of that for mild steels and comparable with the latest high-strength steels (HSS steels).

The most common type of composite used in the automotive industry is the carbon fibre reinforced polymer (CFRP), consisting in a polymer matrix reinforced with carbon fibres. Considering that the strength is provided mainly by the fibres, composite materials are an anisotropic material, stronger in the direction of the fibres and weaker in the perpendicular direction. These types of materials present some disadvantages as well, like high cost when compared with most common materials (steel and aluminium) and possibility of failure by delamination between plies, specially under impact conditions.

Regarding the impact load, the energy that adhesive joints are capable of absorbing is an important factor, since, in case of accident, is important to guarantee the structural integrity of the vehicle structure, but, at the same time, is necessary that the structure absorbs the energy of the collision, otherwise this energy will be transferred to the passengers. Sharon et al. [2], using four adhesives (structural types), analysed the influence of loading rate and temperature parameters on the viscoelastic related properties, observing that there was no influence on the modulus, but when increasing the temperature the yield stress and modulus decreased, as the loading rate greatly influence the effect the yield stress by increasing its value with the increase of loading rate. A similar study was performed by Banea et al. [3] to find the tensile properties of a high temperature epoxy with a glass transition temperature (T_g) of 155 °C. This study shows a clear effect of temperature and loading rate on tensile stress-strain (P-δ) curve of the adhesive. The ultimate tensile stress decreased linearly with temperature while it increased logarithmically with the loading rate. The Young´s modulus presents a behaviour like that of the ultimate tensile stress, increasing as function of loading rate while the decrease as function of temperature is nonlinear. It's also worth mentioning that the effect of temperature on the properties was more significant than that of the strain rate.

Aluminium has traditionally been considered to have low strain rate sensitivity; however, this strongly depends on the alloy. Holt et al. [4] found that pure aluminium reveals moderate sensitivity to strain rate. The flow stress of pure aluminium increases linearly with the logarithm of strain rate at room temperature, and the strain rate sensitivity increases at rates above $1\times10^3\ s^{-1}$. However, with increasing alloy content or processing,

such as heat treating or cold working, the strain rate sensitivity for aluminium alloys decreases.

Chen et al. [5] studied the stress-strain behaviour of four aluminium alloys for a wide range of strain rates. They found that while Al 6060-T6 and Al 6082-T6 exhibit only slight sensitivity to the strain rate and could probably be modelled as rate-insensitive with good accuracy, Al 7003-T6 and Al 7108-T6 show a marked sensitivity to strain rate, which should be included in simulations.

Considering that composite materials are anisotropic and composed of two constituents it is expected that the analysis of behaviour as a function temperature and strain rate isn´t straight forward. While the carbon reinforcements are highly insensitive to temperature variation and loading rate, the matrix is of polymeric nature, as are the adhesives used for joining composites. As described above for adhesives, it is expected that temperature and strain rate have influence on CFRP properties.

Harding and Welsh [6] studied the effect of strain rate in the longitudinal tensile properties of unidirectional CFRP and found no significant strain rate effects. Taniguchi et al. [7] performed a more detailed study of the effect of strain rate also for unidirectional CFRP, since transversal tensile properties and shear properties were also determined as function of strain rate. It is possible to confirm that the longitudinal tensile properties were unaffected by the strain rate but regarding the transversal tensile properties and shear properties the same conclusion cannot be made. While for transverse tensile modulus and transverse strength the increase with strain rate is slight, for shear modulus and shear strength this trend is more pronounced.

Hou and Ruiz [8] also concluded in their study that properties that are dominated by the matrix, such as compression strength, Poisson’s ratio, in-plane shear modulus, shear modulus and shear strength are strain rate dependent. The properties dominated by the fibres like tensile modulus and strength are virtually rate independent. Gómez-del Río et al. [9] studied the effect of low temperature on the dynamic tensile properties of unidirectional and quasi-isotropic CFRP. For unidirectional CFRP they found that the effect of temperature was negligible in the longitudinal direction whereas in the transversal direction the strength increased appreciably.

Strength prediction of single lap joints (SLJs) can be made by an analytical and numerical approach. There are several useful analytical methods available to predict strength of

joints and since dynamic behaviour and non-conventional materials were considered in this study, a numerical approach was used resorting to Finite Elements (FE) methods.

The first authors that used FE models for joints were Wooley and Carver [10] in 1971, followed by Adams and Peppiatt [11] in 1974. Although the work of Wooley and Carver [10] is considered as a big evolution in the prediction of the failure load in SLJs, these models do not consider fracture mechanics. This method has been recently combined with fracture mechanics to create cohesive damage models, which offer the possibility of predicting the crack propagation as a result of simulated degradation of the material.

It was the necessity to create a bridge between stress analysis criteria and classical fracture mechanics that led to the creation of a computational tool called the Cohesive Zone Model (CZM). The combination of the stress criteria with the fracture mechanics data made possible to determine the crack initiation and growth. The CZM was first introduced by Barenblatt [12] based on the Griffith´s theory of fracture, however the first researcher that applied it to the computational frameworks of FEM was Hillerborg et al. [13], who established the relation between traction and the crack opening displacement, and consequently the law of traction-separation.

The aim of this work is to numerically understand and predict the behaviour of dissimilar adhesive joints, using composite and aluminium adherents, under quasi-static and impact loads. Numerical models were validated against previously determined experimentally data, under quasi-static and impact conditions. Cohesive zone models were used to simulate adhesive failure, and composite delamination while damage models were used to simulate plastic deformation and failure of the aluminium alloy.

2. Experimental details

The mechanical properties of the crash resistant epoxy adhesive and the substrates (CFRP and Al 6060-T6), were experimentally tested in a previous work [14] and are presented in this section. This data is fundamental for the construction of the numerical models, being defined for quasi-static (1 mm/min) and impact (3 m/s) testing conditions performed at room temperature (24 °C, achieved and kept constant with the use of air condition). The geometry and all the adhesive configurations are also presented as they were used as a basis for the creation of the numerical models.

To perform accurate numerical simulation, it is essential to have the material properties at higher testing speeds, due to its strain rate dependency. The required value of high strain rate (3 m/s) the adhesives were not directly characterized. To determine these values, some of the adhesives were initially tested at 1 and 100 mm/min. An extrapolation process was then used, based in a logarithmic trend function able to estimate the properties at higher speeds [15, 16] (Equation 1).

$$Property\ to\ determine = A\ln(\dot{\varepsilon}) + B \quad (1)$$

Where A and B are constants determined from a linear fitting the experimental data, where A corresponds to the slope, B corresponds to the intercept, and $\dot{\varepsilon}$ is the strain rate in s^{-1}.

2.1. Material and properties

2.1.1. Crash resistant adhesive

A crash resistant adhesive (epoxy-based) from Japanese company Nagase ChemteX® offering the mechanical properties suitable for application in the automotive industry, such as being able to undergo high plastic deformation prior to failure (absorbing impact energy), was used in this work. The adhesive is designated by XNR6852 E-3 and was experimentally characterized under quasi-static (1 mm/min) and impact (3 m/s, extrapolated) loads (Table 1) [17].

Table 1 – Mechanical properties of Nagase ChemteX® XNR6852 E-3 epoxy adhesive under quasi-static (1 mm/min) and impact (3 m/s - extrapolated) conditions (average values) [17].

Mechanical Properties	1 mm/min	3 m/s*
Young's modulus, E [MPa]	1800	2147
Shear modulus, G [MPa]	665	603
Tensile strength, σ_n [MPa]	48.5	71.7
Shear strength, t_s [MPa]	44.9	42.9
Fracture energy (mode I), G_{IC}[N/mm]	9.2	13.3
Fracture energy (mode II), G_{IIC}[N/mm]	51	64.1

* Extrapolated properties considering an initial impact velocity of 3 m/s.

2.1.2. Substrates

2.1.2.1. CFRP

The CFRP (SEAL® Texipreg HS 160 RM) substrates previously experimentally tested consisted of a 0° lay-up plies configuration, and this material was characterized by Campilho [18] in 2009. CFRP substrates thickness was selected in accordance with the average value used in real automotive applications being of 2.1 mm.

Table 2 presents the Young´s modulus (E), the shear modulus (G), and the Poisson´s ratio (v), in the three axis direction (x,y,z). Being E_1 the normal direction, E_2 the transverse direction and E_3 the out-plane direction.

Table 2 – Mechanical properties of an unidirectional ply of CFRP(elastic orthotropic) aligned in direction 1; 2 is the transverse direction and 3 is the out-of-plane direction [18].

Elastic Modulus (MPa)	Poisson´s Ratio	Shear Modulus (MPa)
E_1 = 1.09E5	v_{12} = 0.342	G_{12} = 4315
E_2 = 8819	v_{13} = 0.342	G_{13} = 4315
E_3 = 8819	v_{23} = 0.380	G_{23} = 3200

The author [19] previously characterized the CFRP under quasi-static conditions, and for the case of an impact load (3 m/s), extrapolation process was considered [17]. Table 3 presents the cohesive properties of CFRP under quasi-static (1 mm/min) and impact (3 m/s) conditions. As an important note, strain rate values for this material are not experimentally available, the Young´s modulus, shear modulus and tensile strength were not considered to be strain rate dependent in this model.

Table 3 – Mechanical properties used to simulate (cohesively) CFRP substrates subjected to quasi-static (1 mm/min) and impact (3 m/s) conditions.

Properties	1 mm/min	3 m/s*
Young's modulus, E [MPa]	109000	109000
Shear modulus, G [MPa]	4315	4315
Tensile strength, σ_n [MPa]	40	40
Shear strength, t_s [MPa]	35	35
Fracture energy (mode I), G_{IC}[N/mm]	0.59	0.39
Fracture energy (mode II), G_{IIC}[N/mm]	1.17	0.82

* Extrapolated properties considering an initial impact velocity of 3 m/s.

2.1.2.2. Aluminium alloys

An aluminium alloy commonly applied in the automotive industry was selected for this work, namely the Al 6060-T6. The thickness of the aluminium alloy used (2 mm) is representative of the average value of the different thicknesses used in the automotive industry. The 6060-T6 aluminium was provided with an anodization surface treatment, required for corrosion resistance and to improve the adhesion process. The mechanical elastic properties of the Al 6060-T6 used are the following: elastic modulus, *E*, of 69 GPa and Poisson´s ratio of 0.33.

A curve plotting the true stress versus true strain of the 6060-T6 aluminium alloy can be observed in Figure 1.

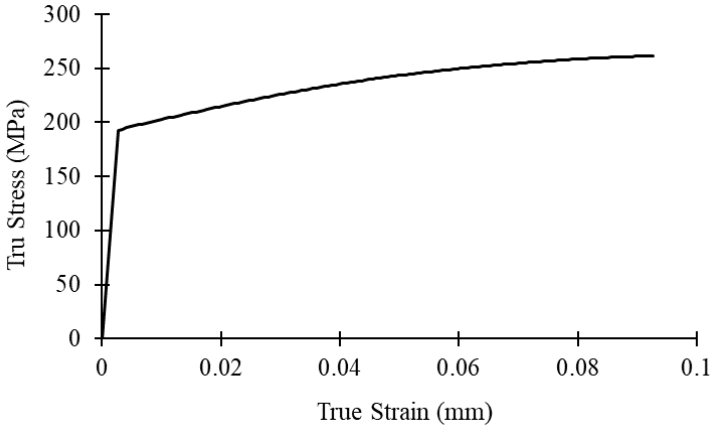

Figure 1 – Curve of 6060-T6 aluminium alloy plotting true stress versus true strain.

2.2. Joint geometry and substrates configuration

A geometry representative of automotive industry applications was selected for the study (Figure 2). The overlap length was set at 25 mm for all SLJs manufactured.

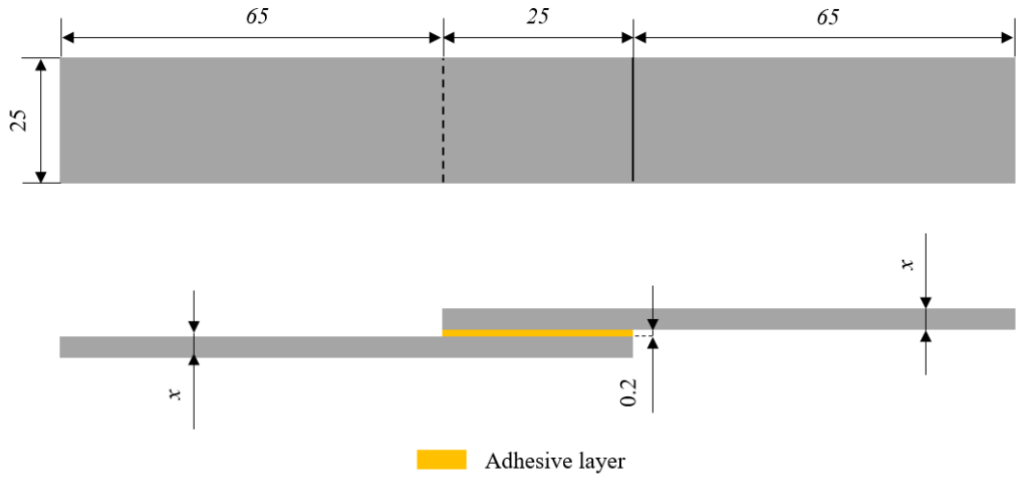

x corresponds to the different SLJs substrates thickness: 2.1 mm for CFRP and 2.0 mm for Al 6060-T6.

Figure 2 – Geometry of SLJ specimens considering similar (CFRP + CFRP and Al 6060-T6 + Al 6060-T6) and dissimilar (CFRP + Al 6060-T6) substrates combinations (dimensions in mm).

Considering the two types of substrate materials under study (CFRP and Al 6060 T6), it is possible to create SLJs with three distinct combinations of substrates, using similar (CFRP + CFRP and Al 6060-T6 + Al 6060-T6) and dissimilar (CFRP + Al 6060-T6) materials. A total of six specimens were tested for each substrate type and test speed. Load displacement (P-δ) curves were registered for all the SLJs tested, namely, for quasi-static (1 mm/min) and impact (3 m/s) conditions.

To ensure a constant thickness of the adhesive layer, a mould was used, an tabs were positioned at the end of each substrate not only to ensure the adhesive thickness but also the correct alignment. A problem when manufacturing SLJs is the finishing quality of the bond line, due to the presence of fillets which causes a significant change in the joint strength. The presence of a fillet in the specimens would create the need to simulate its presence, what would introduce more unnecessary variables to the numerical simulation. A special care was given to solve this problem, as during the SLJs manufacturing metal spacers were positioned on both sides at the end of the overlap, not only to ensure the

correct adhesive thickness layer, but at the same time to prevent the adhesive to flow to the overlap edges.

2.3. Quasi-static and impact testing

Using a universal testing machine, tests under quasi-static (constant crosshead displacement of 1 mm/min) conditions were performed at room temperature of 24 °C. The temperature was measured using a thermometer and kept constant since the tests were performed in a closed room with an air conditioner set to the desired temperature.

The impact test with an initial impact velocity of 3 m/s was performed using a drop weight equipment. A special care was taken to align both the SLJs and the impact load, and the clamping area was reinforced. Testing conditions were of 117 J of initial impact energy (26 kg of weight associated to the high strength steel impactor). More details regarding the geometry of the impact and its geometry can be found in [14].

3. Numerical simulation details

3.1. Cohesive zone modelling

A numerical analysis study was carried out to predict the SLJ strength under quasi-static and impact conditions. For this purpose, Abaqus® (Dassault Systèmes, Suresnes, France) was the Finite Element Method (FEM) software used.

The numerical model was created using a triangular (bilinear) traction-separation law, considering the mechanical and cohesive properties of the XNR6852 E-3 adhesive and substrates (CFRP and Al6060-T6), and considering the absence of any SLJ defect (interface and within the adhesive layer). The adhesive layer was modelled following the 0.2 mm thick cohesive elements (same thickness of the adhesive layer), aiming to control the zone of crack initiation.

For pure-mode (both in traction or shear solicitations) and mixed-mode traction separation laws, it can be defined that t_n^0 and t_s^0 are the cohesive strengths in tension and shear), δ_n^0 and δ_s^0 correspond to the respective displacements, and δ_n^f and δ_s^f refer to the tensile and shear displacements at failure (Figure 3).

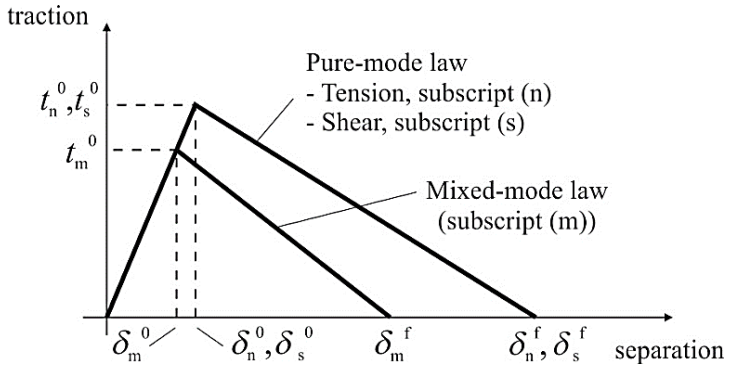

Figure 3 – Triangular traction-separation law with linear softening: pure and mixed-mode models available in Abaqus®.

The shape of the triangular law can be altered to satisfactorily fit the mechanical performance of the simulated adhesive and substrate. The initial elastic portion is constantly maintained linear, defined by a constitutive matrix (K), containing the stiffness parameters and relating current stresses (t) and strains (ε) in three loading modes across the interface, as represented by Equation 1.

$$t = \begin{Bmatrix} t_n \\ t_{s1} \\ t_{s2} \end{Bmatrix} = \begin{bmatrix} K_{nn} & K_{ns1} & K_{ns2} \\ K_{ns1} & K_{s1s1} & K_{s1s2} \\ K_{ns2} & K_{s1s2} & K_{s2s2} \end{bmatrix} . \begin{Bmatrix} \varepsilon_n \\ \varepsilon_{s1} \\ \varepsilon_{s2} \end{Bmatrix} = K\varepsilon \quad (1)$$

The materials stiffness is degraded after the mixed-mode cohesive strength is reached (t_m^0 in Figure 2), and the linear power law predicts the required energies for failure in the pure modes (Equation 2).

$$\frac{G_n}{{G_n}^c} + \frac{G_{s1}}{{G_{s1}}^c} + \frac{G_{s2}}{{G_{s2}}^c} = 1 \quad (2)$$

From Equation 2 it is possible to characterize G_n and G_s as the parameters referring to strain energy release rates in each loading mode, and G_n^c and G_s^c as being the respective critical values. Other shapes able to simulate the softening portion of the curve can be used accordingly to the type of material properties, namely the polynomial [22], exponential [25], trapezoidal [23] or triangular [28] types. It is well known that triangular laws are the most suitable type of law for stiff and brittle adhesives, while for ductile adhesives the trapezoidal cohesive laws are the most reliable [20].

A bulk viscosity parameter of 1E-5 was used for the cohesive element during the explicit simulation. This value was found not to alter the results significantly and improve the convergency of the model significantly.

P-δ curves were determined and the prediction of the failure load was recorded. The software also allows to extract information regarding crack initiation and propagation and state of plasticity from cohesive elements.

3.2. Quasi-static model

For the numerical simulation a few conditions were taken into account with the objective of making the models as reliable as possible. Since three distinct types of materials were used during this work, the elements used to simulate them need to be chosen according to their physical behaviour. Figure 4 shows the model of a dissimilar joint with aluminium and CFRP adherends where all the different types of elements used in all the possible configurations are presented. As mentioned before for the adhesive, a 0.2 mm layer was modelled with cohesive elements. For CFRP adherends, elastic orthotropic properties (engineering constants) were used, being also necessary to resort to cohesive elements to predict a possible failure by delamination. For the simulation, a 0.15 mm thick layer was added considering a distance of 0.15 mm from the interface between the adhesive and CFRP. Each ply of the prepreg used to manufacture the CFRF adherend as a thickness of 0.15 mm. Aluminium substrates were simulated with elastic isotropic and plastic properties to account for the plastic deformation of the substrates.

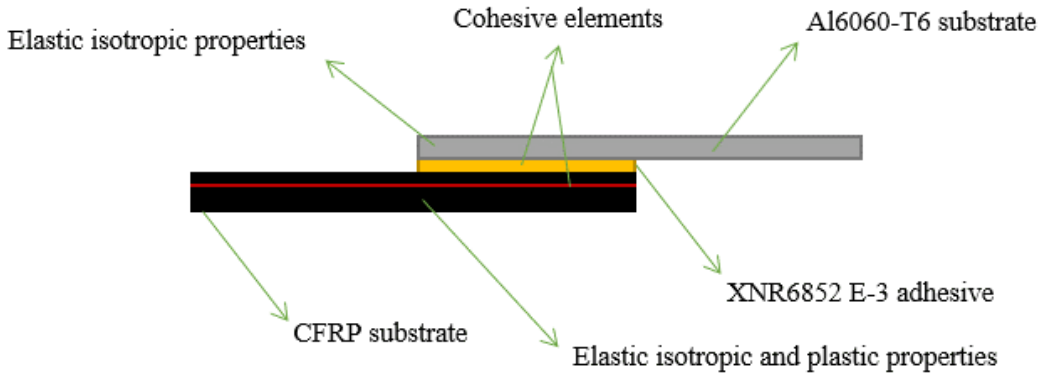

Figure 4 – Schematic representation of the FE elements considered for the quasi- static (1 mm/min) simulations for the case of dissimilar substrates combination (CFRP + Al6060-T6).

The elastic properties used for aluminium and CFRP were previously introduced. Triangular laws for adhesive (Figure 5) and for cohesive layer of CFRP (Figure 6) were performed for both loading modes. The adhesive tensile properties, Young's modulus (*E*)

and normal cohesive stress (t_{n0}), were obtained from bulk tensile tests. Fracture toughness in pure mode I (G_{IC}) was obtained from DCB tests. The other properties, shear modulus (G), shear cohesive stress (t_{s0}) and fracture toughness in pure mode II (G_{IIC}), needed to complete the triangular law was obtained from a previous works [21, 22], as well the cohesive and elastic properties for the CFRP.

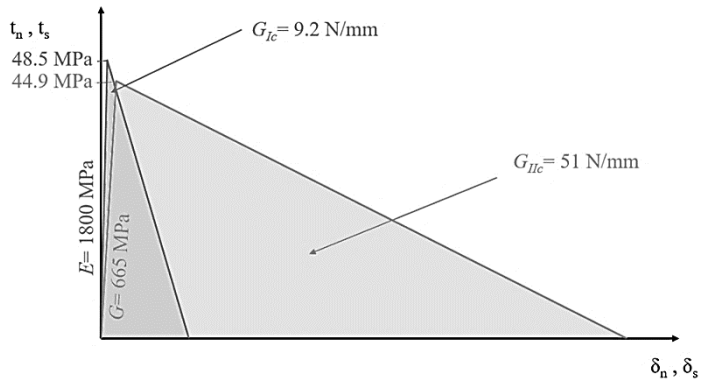

Figure 5 – Triangular law for the adhesive (XNR6852 E-3) at quasi-static conditions.

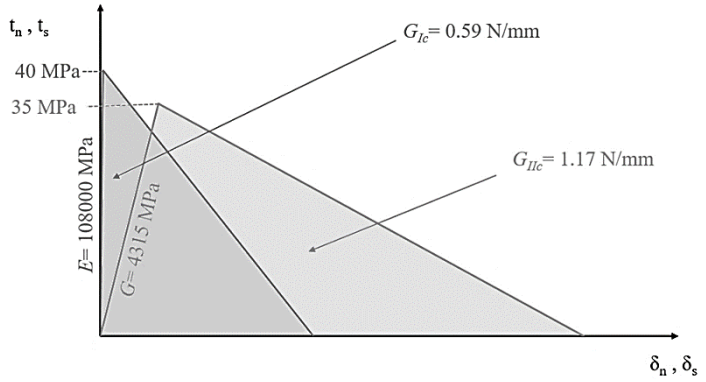

Figure 6 – Triangular law for CFRP at quasi-static conditions.

The boundary conditions were defined as indicated in Figure 7. In one end, on the left side, a clamped condition was added in order to simulate the static grip of tensile machine while in the other end a longitudinal displacement was applied, restrained in the perpendicular direction of the displacement, simulating the gripping fixture that applies the load during the test.

Figure 7 – Schematic representation of the applied constraints and forces for the quasi-static (1 mm/min) model.

The mesh was created using elements with different sizes, resorting to biasing (Figure 8). For cohesive elements, for CFRP adherends and for adhesive, elements with 0.15 mm and 0.2 mm length was used, respectively. To reduce computational loads, the size of elements was increased in zones away from the ends of the overlap, as the stress gradients are less severe.

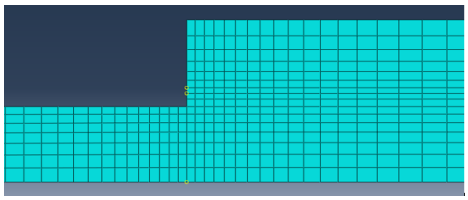

Figure 8 – Representative mesh in the overlap area.

To visualize the CZM degradation, it was used in the field outputs a scalar stiffness degradation (SDEG). The crack propagation can also be visually monitored using this approach. As for the element types, it was used a 4-node-two-dimensional cohesive element (COH2D4) to define the bondline area, and a 4-node bilinear plane stress quadrilateral, reduced integration, hourglass control (CPS4R) for the substrates.

3.3. Dynamic model

To recreate the impact conditions of the drop weight test, a two-dimensional model was created resorting to Abaqus/Explicit. The model was geometrically similar to that used quasi-static simulations save for one modification, the addition of a block to the non-clamped edge that represents the impact mass in the experimental tests.

The boundary conditions were also similar to those used in the quasi-static model but, instead of a longitudinal displacement in the non-clamped end of the joint, a velocity field of 3 m/s was applied to the mass that was added to the model (Figure 9). In order to simulate the 117 Joules of impact energy with 3 m/s of initial impact velocity of the mass,

its density was defined in order to guarantee that the impact mass was 26 kg. The mesh geometry used was the same that was used in the quasi-static model, being the SDEG field output was also requested.

Figure 9 – Boundary conditions applied for the impact model.

For adhesive properties, Young's modulus (E), normal cohesive stress (t_{n0}) and fracture toughness in pure mode I (G_{n0}) were extrapolated from experimental results resorting to a logarithmic trend line as described in the results chapter. Shear modulus (G), shear cohesive stress (t_{s0}) and fracture toughness in pure mode II (G_{s0}) was obtained from a previous work [21, 22]. Again, a new triangular cohesive law was made for the adhesive under impact (Figure 10).

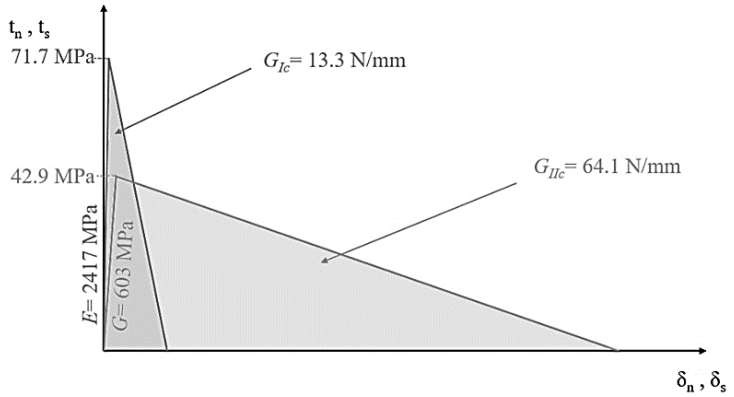

Figure 10 – Triangular law for the adhesive (XNR6852 E-3) at impact conditions.

As previously stated, aluminium alloys are generally insensitive to the strain rate (Al 6060-T6), and the properties used for the static model could be used for the dynamic model as well. The CFRP behaves differently, as while it is strain rate insensitive in the tensile direction the same does not occurs in the other ones. For the purposes of this model, and because the CFRP properties, namely the same specific material used in this study, were determined in previous works, the properties from the elastic domain were kept constant and those from the plastic domain, critical for modelling the crack onset

and propagation, were considered to be strain rate dependent. A new triangular cohesive law was therefore created for CFRP under impact (Figure 11).

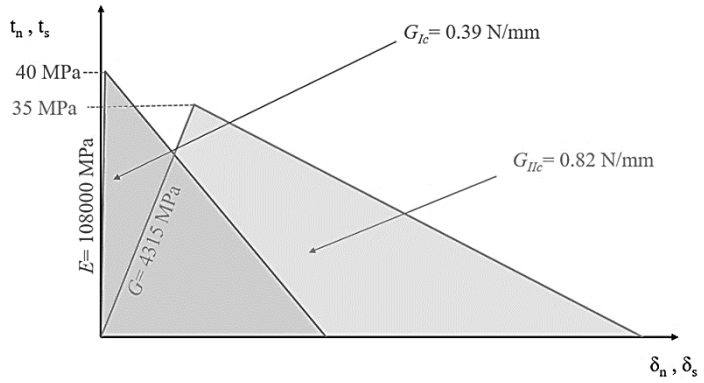

Figure 11 – Triangular law for CFRP at impact conditions.

4. Results and discussion

4.1. Quasi-static modelling

4.1.1. SLJs with similar substrates

Figure 12 shows the *P-δ* curves for the experimental results and the numerical simulations of SLJs with similar substrates of CFRP under quasi-static conditions.

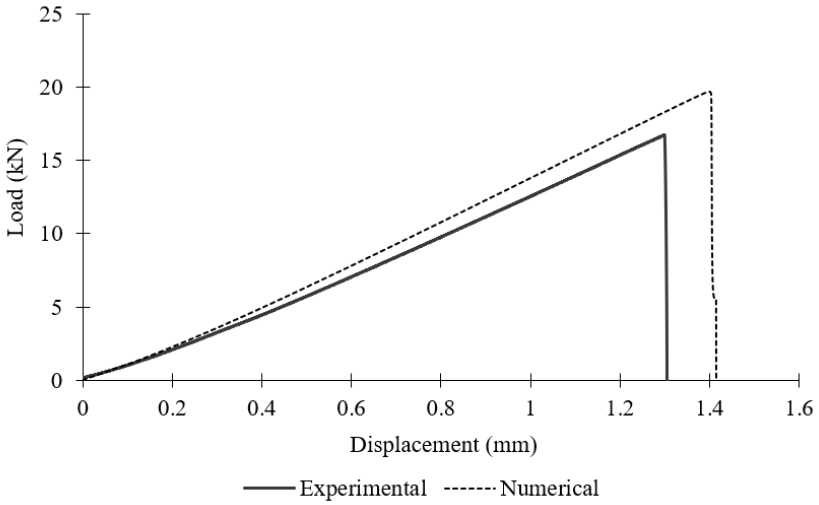

Figure 12 – Comparison between experimental and numerical *P-δ* curves of SLJs manufactured with similar substrates, namely, CFRP + CFRP under quasi-static conditions.

In this case, the numerically obtained failure load, which correspond to the initiation of the failure identified using the SDEG parameter, is higher than the experimental results, which is expected, given that the experimental failure load is expected to be affected by the presence of micro defects in the CFRP lay-up, which are not considered in the model. The stiffness of both curves is comparable, however.

Figure 13 shows the *P-δ* curves for the experimental results and the numerical simulations of SLJs with similar substrates of Al 6060-T6 under quasi-static conditions.

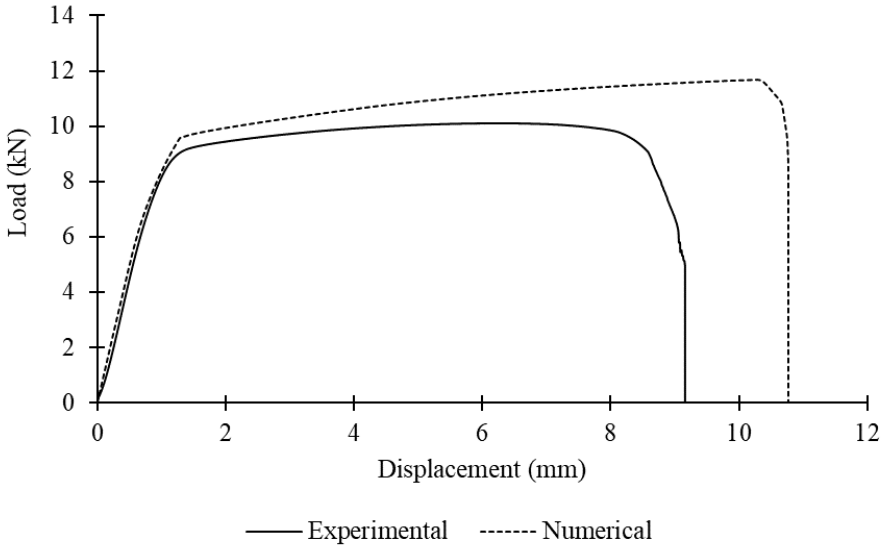

Figure 13 – Comparison between experimental and numerical *P-δ* curves of SLJs manufactured with similar substrates, namely, Al 6060-T6 + Al 6060-T6 under quasi-static conditions.

The shape of the curves is similar, although, the transition from elastic to plastic behaviour is more abrupt in the numerical simulation. The failure load and the displacement are higher in the numerical simulation than the experimental results. The difference could also be explained by several aspects, such as the fact that the local strain rates are not being modelled at the element level with this type of simulation, as well as the presence of defects on the experimental joints which are not reproduced in the numerical model. Analysing Figure 13, it is possible to notice that, in the numerical simulation, the increase in the maximum load in the plastic domain is higher than that observed for experimental results, which is usually attributed to defects which lead to early failure of the joint.

The failure point is determined by using the SDEG parameter of the cohesive element, which will clearly allow to identify the initiation of failure.

4.1.2. SLJs with dissimilar substrates

Figure 14 shows the *P-δ* curves for the experimental results and the numerical simulations of SLJs manufactured with dissimilar (CFRP + Al 6060-T6) substrates under quasi-static conditions.

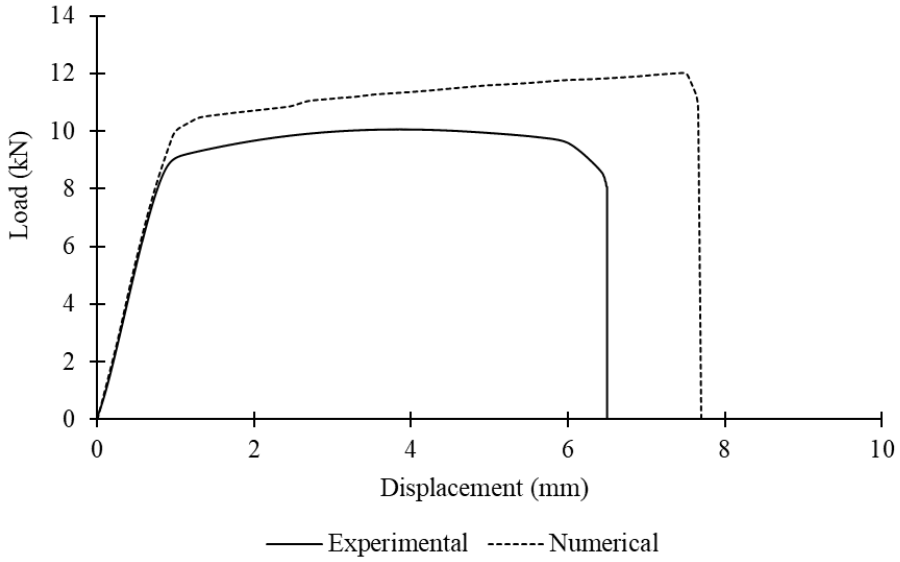

Figure 14 – Comparison between experimental and numerical *P-δ* curves of SLJs with dissimilar substrates (CFRP + Al 6060-T6) under quasi-static conditions.

As previously observed using other configurations, the shape of the plots is similar between experimental and numerical results. The maximum load and the displacement are higher in the numerical simulation. The reason of such behaviour is the same than the one presented in the case of SLJs with similar substrates of Al 6060-T6.

4.2. Impact modelling

4.2.1. SLJs with similar substrates

Figure 15 shows the *P-δ* curves for the experimental results and the numerical simulations of SLJs with similar substrates of CFRP under impact conditions.

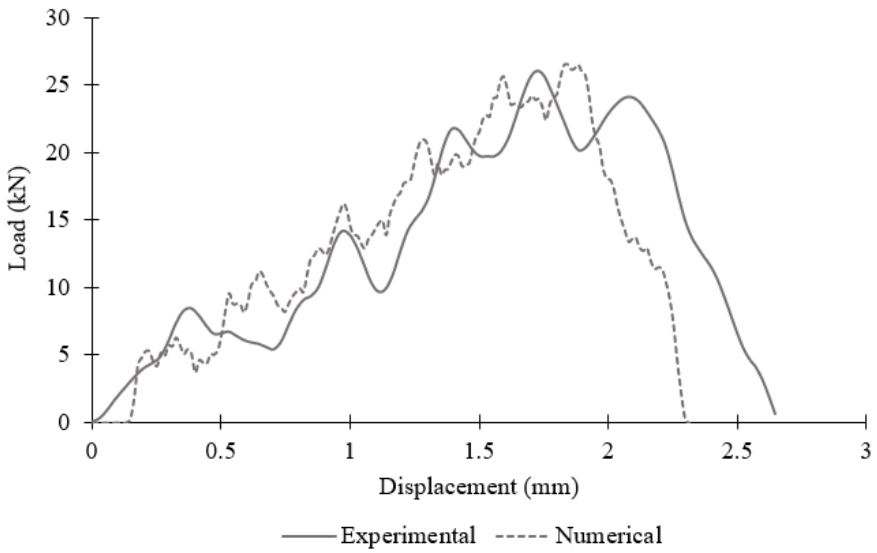

Figure 15 – Comparison between experimental and numerical *P-δ* curves of SLJs with similar substrates, namely, CFRP + CFRP under impact conditions.

The shape of the *P-δ* curves are very similar. The results are very close except a difference in the displacement with the numerical simulation presenting a slightly lower value that the experimental results. The numerical curves shown delay in the initiation of load, this is because on the model, the load is measured on one end of the overlap, while the displacement is applied to the opposite end. There is a delay between the displacement and the load build-up as the stress waves propagate along the substrates during the simulation of the impact test.

Figure 16 shows the *P-δ* curves for the experimental results and the numerical simulations of SLJs with similar substrates of Al 6060-T6 under impact conditions.

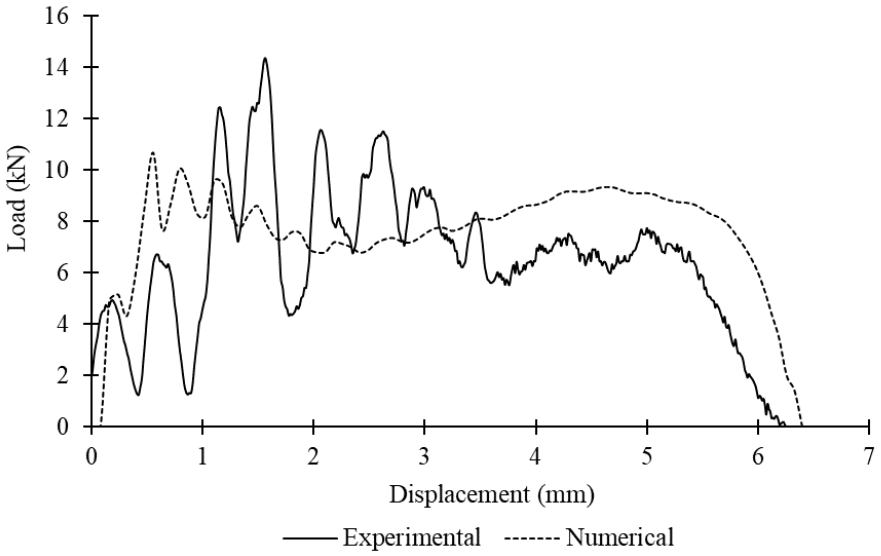

Figure 16 – Comparison between experimental and numerical *P-δ* curves of SLJs with similar substrates, namely, Al 6060-T6 + Al 6060-T6 under impact conditions.

For this case, although the model exhibits a behaviour which is generally consistent with that of the experiment, the predicted failure load is below the experimental result, with smaller peaks. This can be attributed to a limitation of the current model because it only includes data for the plasticity of the aluminium substrates and does not feature a more complex and strain rate dependent failure criterion, one including nucleation and damage propagation. The model created therefore is shown to be of limited use when the failure does not occur in the composite or the adhesive layer, only allowing a rough prediction of the joint strength under impact.

4.2.2. SLJs with dissimilar substrates

Figure 17 shows the *P-δ* curves for the experimental results and the numerical simulations of SLJs with dissimilar substrates of CFRP + Al 6060-T6 under impact conditions.

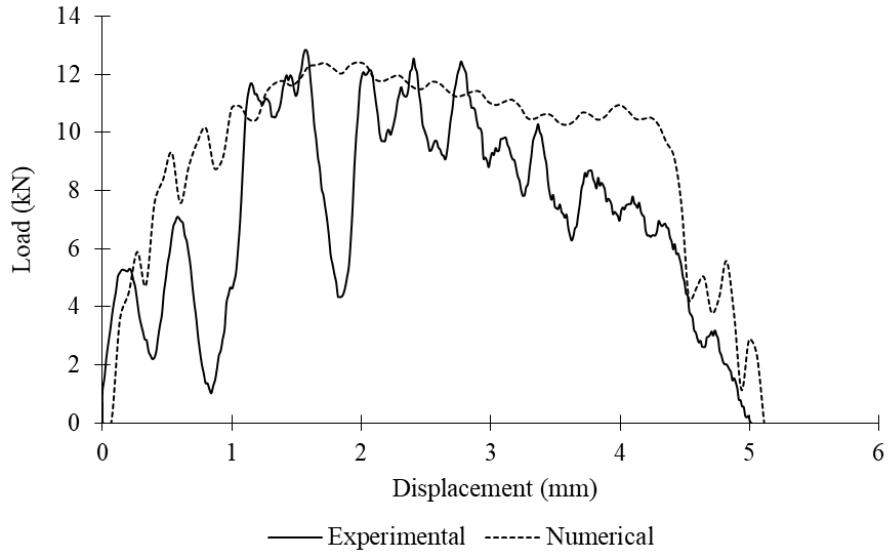

Figure 17 – Comparison between experimental and numerical *P-δ* curves of SLJs with dissimilar substrates (CFRP + Al 6060-T6) under impact conditions.

The performance of the model was similar to that obtained with the model for SLJs manufactured with similar substrates of Al 6060-T6, as the experimental failure also occurs in the aluminium substrate. The prediction of the failure load was more satisfactory but still not perfect, as under impact tests, the peak load is always difficult to exactly define. This is due to the fact that it occurs for very short time periods and is very sensitive to the data acquisition rate. As such, especially in cases where there are strong load oscillation, it is very difficult to reliably obtain failure loads similar to those under impact conditions, especially when taking into account that the local strain rates can have significant variations which are not accounted for in this model, which is intended to propose a simple design approach that does not require the use of a complete strain rate dependent material data and local calculations of the strain rate at the element level. Nonetheless, the performance of the joint was fully captured throughout the impact test, allowing, for example to estimate the absorbed energy accurately.

For all the cases studied, the average value of scatter experimentally obtained was very similar, being of around 0.8%.

5. Geometrical study

In automotive applications, due to practical considerations, the joint and substrate geometry cannot be as tightly controlled as in laboratorial tests, with adhesive layer thicknesses thicker than 1 mm being common. To ensure that the joints studied in this work can perform consistently in practical usage, it is important to understand the influence of geometrical parameters such as the adhesive layer thickness, overlap length and the CFRP substrate thickness. To this effect, a numerical analysis was performed for the case of joints using similar substrates, namely, CFRP + CFRP, and for both quasi-static and impact conditions. The adhesive thicknesses under study were 0.1, 0.2, 0.4, 0.8 and 1.5 mm, while the CFRP substrate thicknesses under study were 1.05 (7 plies), 1.5 (10 plies) and 2.1 mm (14 plies). The three overlap lengths under study were 12.5, 25 and 50 mm. To isolate the effect of each parameter, the CFRP thickness was kept constant at 2.1 mm for the adhesive thickness study, and the adhesive layer thickness was kept at 0.2 mm for the substrate thickness study. In the overlap length study, the thickness of the CFRP and the adhesive were 2.1 and 0.2 mm respectively.

5.1. Adhesive thickness

From Figure 18 it is possible to observe that, for both quasi-static and impact conditions, the highest failure loads are attained with lower adhesive layer thickness, in the range of 0.1 to 0.4 mm.

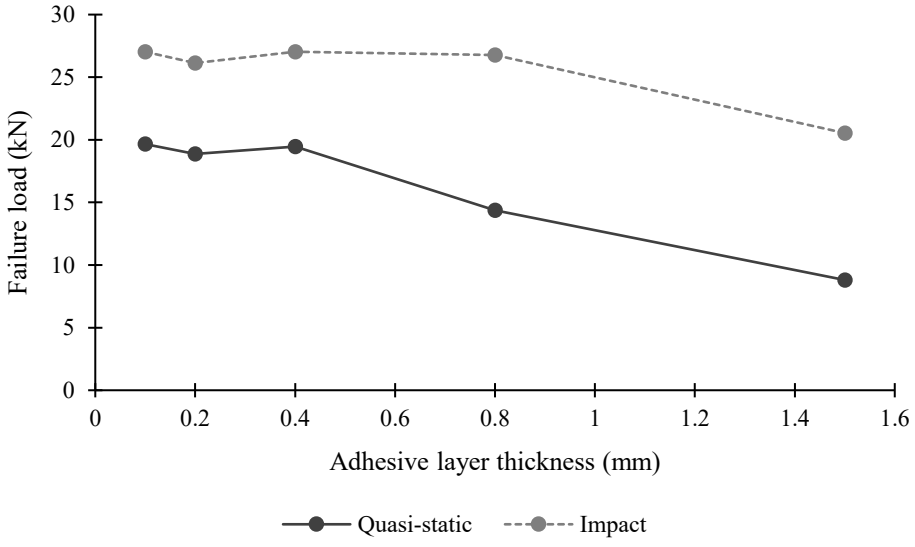

Figure 18 – Numerical comparison of the failure load of joints with similar substrates (CFRP + CFRP) after varying the XNR6852 E-3 adhesive thickness under quasi-static and impact conditions.

It is interesting to notice that there is a small dip in the failure load for the 0.2 mm thick adhesive case. This is perhaps caused by the fact that the model considers the very thin 0.1 mm adhesive layer thickness case to be the optimal, with minimal substrate misalignment and consequently lower peel loads. However, it is widely reported that experimental testing does not corroborate this assumption due to the practical concerns associated with very thin adhesive layers.

The quasi-static and impact data both follow a similar trend, with the impact strength being noticeably higher for all cases under study due to the changed stress distribution and improved material properties at higher strain rates.

The displacement at failure, which can be considered as representative of the energy absorption capabilities is shown in Figure 19. The displacement at failure under quasi-static conditions follows a behaviour similar to that encountered to the failure load for quasi-static loads, but under impact it appears to be almost insensitive to the adhesive layer thickness.

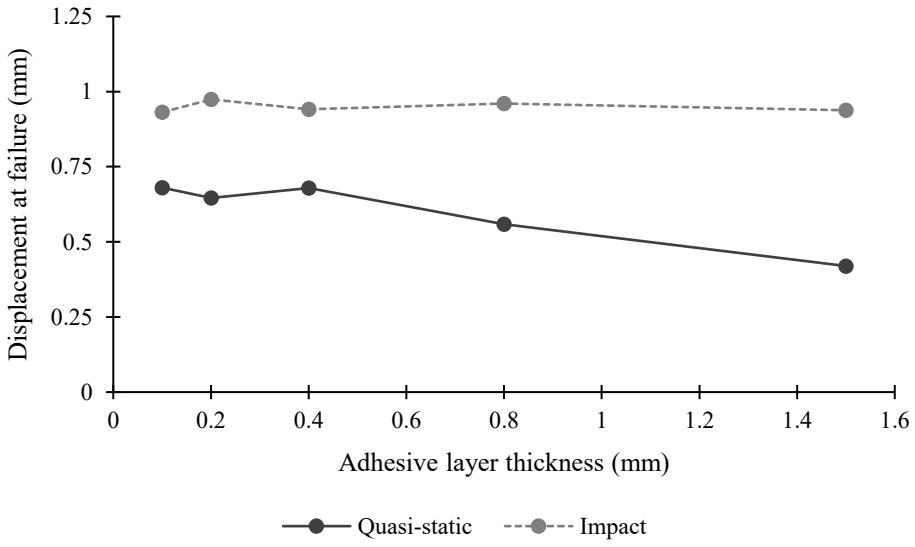

Figure 19 – Numerical comparison of the displacement at failure of joints with similar substrates (CFRP + CFRP) under quasi-static and impact conditions, varying the XNR6852 E-3 adhesive thickness.

Overall, the results indicate that the use of thicker adhesive layers will result in slightly lower joint performance. Although the drop is not drastic, the change associated with the increased adhesive thickness must be considered when designing structures. This is important as in practical applications this type of joint can only be manufactured with thick adhesive layers due to limitations in component tolerances.

5.1. Overlap length

Figure 20 shows that for both conditions under study (quasi-static and impact), the overlap length has a linear effect on joint strength. It is also evident that as the overlap length increases, the strength improvement from static to impact conditions also increases consistently. Considering the results as percentage of strength improvement, such increase is practically constant (varying between 35 and 38%).

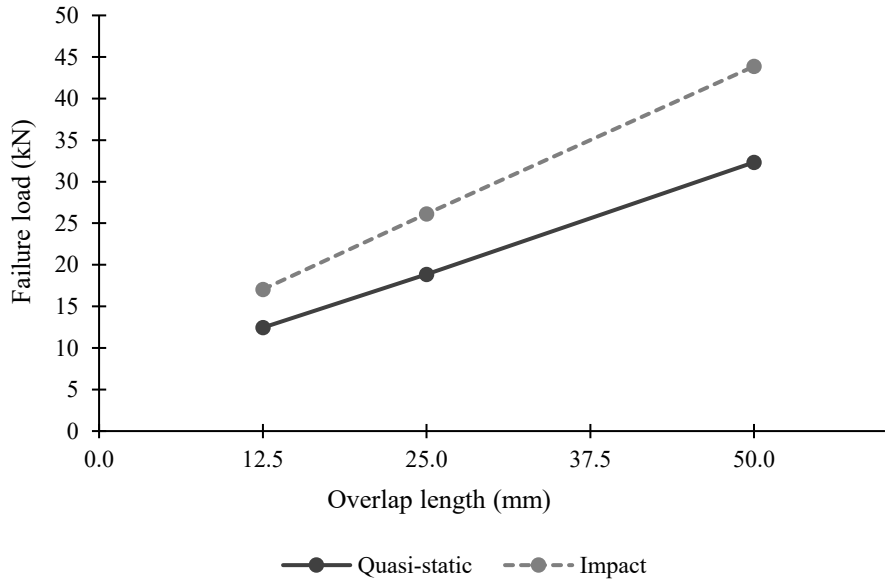

Figure 20 – Numerical comparison of the failure load of joints with similar substrates (CFRP + CFRP) after varying the overlap length under quasi-static and impact conditions.

The model predicts failure by delamination for the three overlap lengths under study, which would be expected to lead to a plateau in the joint strength, limited by the transverse strength of composite. However, this does not occur within the modelled range of overlaps. This can be explained by the fact that the three overlaps where modelled by keeping the substrate length constant, which means that the free arm of the substrate will reduce as the overlap length increases, which will have a strong effect on the reduction of the bending moments and, consequently, of the peel stresses. The reduction of the peel stresses will have a significant effect, delaying the delamination failure, which is translated into a higher overall joint strength.

Figure 21 shows the behaviour for the displacement at failure, which also shows a nearly linear trend until the 50 mm overlap length is reached.

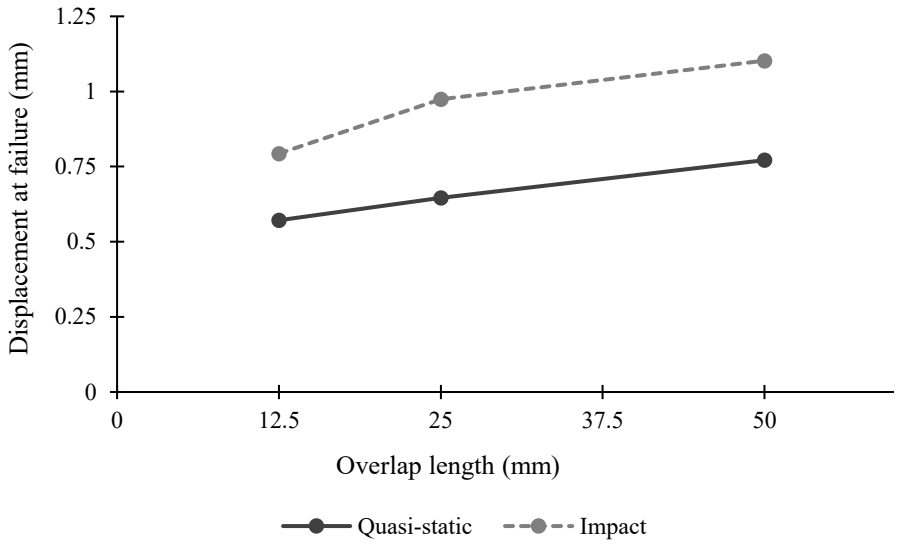

Figure 21 – Numerical comparison of the displacement at failure with similar substrates (CFRP + CFRP) after varying the overlap length under quasi-static and impact conditions.

Overall the results indicate that for the configuration under study, the overlap length will have a strong effect on the joint stiffness and will be directly related to the joint strength and displacement at failure. This effect can easily be exploited in the design phase of adhesively bonded joints with composite substrates, allowing for improved mechanical performance and energy absorption.

5.2. CFRP substrate thickness

Currently, due to the advances in composite materials, the use of thin CFRP substrates in structural construction is of great practical interest, making it relevant to understand how the adhesive joint performance is affected by the thinner substrates. Figure 22 and Figure 23 show the numerically determined failure load and displacement at failure for three different CFRP substrates thicknesses, under quasi-static and impact conditions. The XNR6852 E-3 adhesive layer has been kept constant at the optimal 0.2 mm.

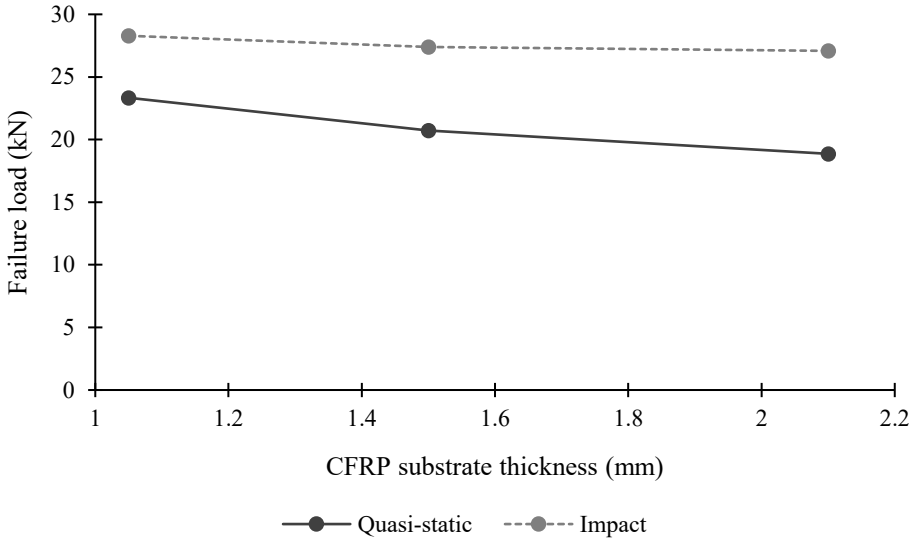

Figure 22 – Numerical comparison of the failure load of joints with similar substrates (CFRP + CFRP) under quasi-static and impact conditions, varying the CFRP substrate thickness.

The numerical model shows that the use of thinner composites slightly increases both the failure load and the displacement at failure for the case of simulations representative of quasi-static conditions.

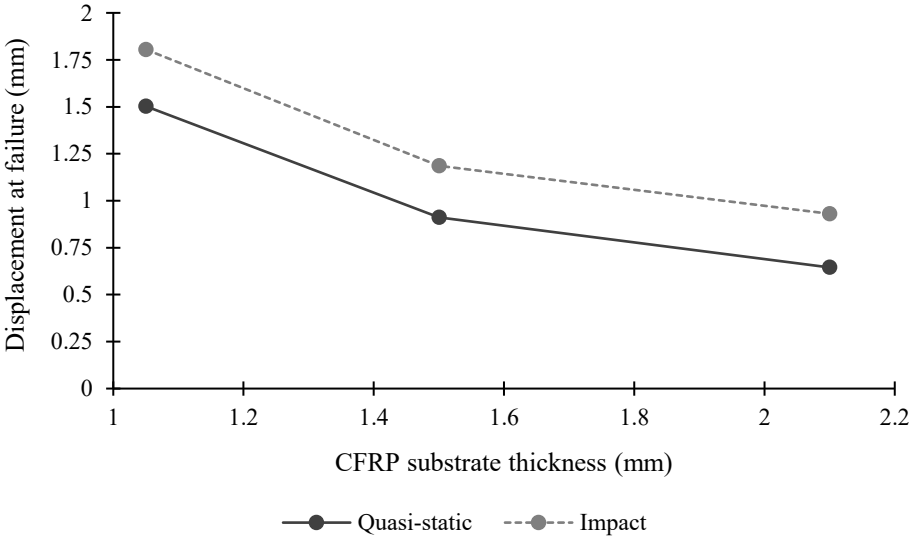

Figure 23 – Numerical comparison of the displacement at failure of joints with similar substrates (CFRP + CFRP) under quasi-static and impact conditions, varying the CFRP substrate thickness.

Although no significant changes in the failure load are suggested, a significant increase is found for the displacement at failure as a function of the substrate thickness. The reason

behind this significant increase of the displacement at failure is related to an improved alignment of the load path, which generates lower peel stresses that are highly damaging to the composite substrates, which have low transverse strength. Therefore, it is possible to state that the drive to thinner and stronger composite substrates has evident benefits for adhesive joining.

6. Conclusions

The focus of this work is to the creation of numerical models capable of predicting the behaviour of similar and dissimilar adhesively joints, manufactured with composite and aluminium substrate and subjected to quasi-static and impact loads. The main conclusions drawn from this work are presented below:

- The quasi-static models using cohesive zone modelling were able to simulate reasonably well the mechanical behaviour of most of the configurations under study, especially when predicting the failure of CFRP substrates. However, given the limitations of the model with regards to metal failure, complete modelling of the aluminium failure process was not possible.
- The impact models developed during this work were also able to simulate reasonably well the mechanical behaviour of most of the configurations under study. Again, the failure process of CFRP materials was found to be more accurately modelled that then the failure process of aluminium.
- A numerical study of the adhesive and substrate thicknesses as well as the overlap length was performed for the CFRP-CFRP joint. This study indicates that the use of thinner adhesive layers and substrates will generally yield better performance under quasi-static and impact loads, although the behaviour with thicker adhesive layers can still be considered as satisfactory for all cases under study. It was also found that, for the joint configuration under study there is a linear relationship between joint performance and overlap length, valid for a range of overlaps between 12.5 and 50 mm.

It was possible to state that the use of dissimilar adhesive joints, using a modern crash resistant adhesive, can be effectively used in automotive structures, without significant sacrifices in joint performance, such as energy absorption under impact. and increased the failure loads over the use of single adhesives. Moreover, their performance can also

be simulated using advanced cohesive zone models minimizing the need to perform extensive experimental testing.

Acknowledgments

The authors gratefully acknowledge the funding provided by PhD grant SFRH/BD/139341/2018 “Impact strength optimization with cohesive zone elements of multi-material bonded structures used in the automotive industry”, Project Nº 028473 POCI-01-0145-FEDER-028473 “Design methodology for impact resistant bonded multi-material automotive structures (ImpactBondDesign)”, Project NORTE-01-0145-FEDER-000022 – “SciTech - Science and Technology for Competitive and Sustainable Industries”, co-financed by Programa Operacional Regional do Norte (NORTE2020), through Fundo Europeu de Desenvolvimento Regional (FEDER). The authors would also like to thank NAGASE ChemteX® for the financial support provided.

References

1. da Silva, L.F.M., A. Öchsner, and R.D. Adams, *Handbook of Adhesion Technology*. 2011: Springer Berlin Heidelberg.
2. Sharon, G., H. Dodiuk, and S. Kenig, *Effects of loading rate and temperature on the mechanical properties of structural adhesives containing a carrier.* The Journal of Adhesion, 1989. **31**(1): p. 21-31.
3. Banea, M., et al., *Effects of temperature and loading rate on the mechanical properties of a high temperature epoxy adhesive.* Journal of Adhesion Science and Technology, 2011. **25**(18): p. 2461-2474.
4. Holt, D., *The strain-rate dependence of the flow stress in some aluminum alloys.* Trans. ASM, 1967. **60**: p. 152-159.
5. Chen, Y., et al., *Stress–strain behaviour of aluminium alloys at a wide range of strain rates.* International Journal of Solids and Structures, 2009. **46**(21): p. 3825-3835.
6. Harding, J. and L.M. Welsh, *A tensile testing technique for fibre-reinforced composites at impact rates of strain.* Journal of Materials Science, 1983. **18**(6): p. 1810-1826.

7. Taniguchi, N., T. Nishiwaki, and H. Kawada, *Tensile strength of unidirectional CFRP laminate under high strain rate.* Advanced Composite Materials, 2007. **16**(2): p. 167-180.
8. Hou, J. and C. Ruiz, *Measurement of the properties of woven CFRP T300/914 at different strain rates.* Composites Science and Technology, 2000. **60**(15): p. 2829-2834.
9. Gomez-del Rio, T., et al., *Dynamic tensile behaviour at low temperature of CFRP using a split Hopkinson pressure bar.* Composites Science and Technology, 2005. **65**(1): p. 61-71.
10. Wooley, G.R. and D.R. Carver, *Stress concentration factors for bonded lap joints*. 1971: Louisiana State University and Agricultural and Mechanical College. Division of Engineering Research.
11. Adams, R. and N. Peppiatt, *Stress analysis of adhesive-bonded lap joints.* Journal of strain analysis, 1974. **9**(3): p. 185-196.
12. Barenblatt, G., *Equilibrium cracks formed on a brittle fracture.* Doklady Akademii Nauk Sssr, 1959. **127**(1): p. 47-50.
13. Hillerborg, A., M. Modéer, and P.-E. Petersson, *Analysis of crack formation and crack growth in concrete by means of fracture mechanics and finite elements.* Cement and concrete research, 1976. **6**(6): p. 773-781.
14. Machado, J., et al., *Adhesive joints using aluminium and CFRP substrates tested at low and high temperatures under quasi-static and impact conditions for the automotive industry.* Composites Part B: Engineering, 2019. **158**: p. 102-116.
15. Zgoul, M. and A. Crocombe, *Numerical modelling of lap joints bonded with a rate-dependent adhesive.* International journal of adhesion and adhesives, 2004. Volume 24, Issue 4, August 2004, Pages 355-366.
16. Avendaño, R., et al., *Effect of temperature and strain rate on single lap joints with dissimilar lightweight adherends bonded with an acrylic adhesive.* Composite Structures, 2016. **152**: p. 34-44.
17. Araújo, H.A.M., et al., *Dynamic behaviour of composite adhesive joints for the automotive industry.* Composite Structures, 2017.
18. Campilho, R.D.S.G., *Repair of composite and wood structures*. 2009, Instituto Superior de Engenharia do Porto.

19. Machado, J., et al., *Mode I fracture toughness of CFRP as a function of temperature and strain rate.* Journal of Composite Materials, 2016: p. 0021998316682309.
20. Fernandes, R. and R. Campilho, *Numerical evaluation of dissimilar cohesive models to predict the behavior of Double-Cantilever Beam specimens.* Procedia Structural Integrity, 2016. **1**: p. 42-49.
21. Araújo, H.A.M., *Impact and Damping Behaviour of Composite Adhesive Joints.* 2016.
22. Machado, J., et al., *Mode I fracture toughness of CFRP as a function of temperature and strain rate.* Journal of Composite Materials, 2017. **51**(23): p. 3315-3326.

Paper 15

Content of Paper 15

Abstract

1. Introduction

2. Experimental details

2.1. Material and properties

2.1.1. CFRP

2.1.2. Crash resistant adhesive

2.2. Specimen fabrication

2.2.1. CFRP specimens

2.2.2. Adhesive bulk plates

2.2.3. Single lap joints

2.3. Testing procedures

2.3.1. Hygrothermal aging process of bulk adhesives and CFRP

2.3.1.1. Gravimetric and swelling measurements

2.3.1.2. Diffusion analysis

2.3.1.3. Fourier transform infrared spectroscopy (FTIR)

2.3.2. Measurement of the glass transition temperature (T_g)

3. Results and discussion

3.1. Moisture diffusion of the bulk adhesive and the CFRP substrates

3.2. Measurement of T_g

3.3. XNR6852 E-3 adhesive bulk tensile properties

3.4. Fourier transform infrared spectroscopy (FTIR)

3.5. Quasi-static tests of aged and unaged single lap joints

3.5.1. Fracture surface

3.5.2. Failure load

3.5.3. Energy absorbed

4. Numerical analysis of water ingress in SLJs

4.1. Simulation of water ingress in the XNR6852 E-3 adhesive

4.2. Simulation of water ingress in XNR6852 E-3 adhesive layer in SLJs

4.3. Discretization of adhesive and CFRP properties along the overlap as a function of water intake

4.4. Simulation of single lap joints in the unaged and hygrothermally aged conditions

5. Conclusion

References

Composite Structures 214 (2019) 451–462

Contents lists available at ScienceDirect

Composite Structures

journal homepage: www.elsevier.com/locate/compstruct

Effect of hygrothermal aging on the quasi-static behaviour of CFRP joints varying the overlap length

J.J.M. Machado[a], E.A.S. Marques[a], A.Q. Barbosa[a], Lucas F.M. da Silva[b,*]

[a] Instituto de Ciência e Inovação em Engenharia Mecânica e Engenharia Industrial (INEGI), Rua Dr. Roberto Frias, 4200-465 Porto, Portugal
[b] Departamento de Engenharia Mecânica, Faculdade de Engenharia (FEUP), Universidade do Porto, Rua Dr. Roberto Frias, 4200-465 Porto, Portugal

ARTICLE INFO

Keywords:
Hygrothermal aging
CFRP
Quasi-static
Numerical simulation
Overlap length

ABSTRACT

Adhesively bonded joints with composite substrates are crucial for the manufacture of lightweight structural components for the automotive industry. However, the safety of the vehicles must still be ensured after hygrothermal aging of both composite substrates and adhesive, as adverse conditions such as moisture and temperature will be a constant during a vehicle lifecycle. This work studies the influence of hygrothermal aging and temperature on the quasi-static behaviour of adhesive joints made with unidirectional composite substrates and a crash resistant adhesive using different overlap lengths. A complementary numerical simulation was performed to model both the water uptake processes and the failure process of moisture affected materials. Both the simulation and the experimental data showed increased susceptibility to delamination failure induced by water absorption in the composite and changes in the adhesive properties.

1. Introduction

The wide use of fibre reinforced composite materials, namely carbon fibre reinforced polymer (CFRP), in the automotive industry can offer several advantages, such as lower structural weight, high strength and excellent stiffness to weight ratios [1]. While initially the use of carbon fibre in the automotive industry was restricted to non-structural components, nowadays these materials are starting to be used in crash absorbing structures. To achieve the technical requirements necessary for ensuring safety, the structures designed in the automotive industry must be able to undergo a variety of load conditions, deforming and absorbing energy but at the same time being capable to maintain their integrity. When in use, these structures can be subjected to wide ranges of temperature and strain rates (including impact loads), and therefore a complete knowledge of the behaviour of CFRP when operating under those circumstances is necessary [2], especially considering that during their life cycle the structures will experience aging due to temperature and the presence of water [3].

Epoxy resins, such as the resin matrix used in composites materials, absorb moisture from humid environments. This moisture absorption can be attributed largely to the moisture affinity of specific functional groups of a highly polar nature in the cured epoxy resin [4]. The water is hydrogen-bonded to the resin, its mobility in epoxy resins occurs between the values in the solid and free water states. Since moisture cannot penetrate fibres, the behaviour of diffusing moisture in composites is usually affected by the resin properties. Moisture absorption in the fibre is negligible [5]. Apicella et al. [6] proposed three distinct sorption methods: bulk dissolution of water in the polymer network; moisture absorption onto the surface of vacuoles which define the excess free volume of the glassy structure; and hydrogen bonding between polymer hydrophilic groups and water. If the two first modes occur consecutively, a dual sorption behaviour can be detected [7,8].

The absorbed water usually depresses the glass transition temperature (T_g) by plasticizing the polymer network and affects mechanical performance and long-term durability of high-performance applications [6,9–12]. Several authors [13,14] tested composite materials after hygrothermal aging and observed that the T_g decreases with the increment of moisture absorption. Adamson [15] assumed that the moisture transport below the T_g is a process which can be divided in three distinct stages, in which the absorbed water first occupies the free volume present in the form of voids. In the second stage, water become bound to network sites causing swelling. Finally, it enters the densely crosslinked regions. Mechanisms based on free volume neglect the existence of specific interaction between the water and hydrophilic sites of the network. It has been proposed that the water equilibrium concentration is mainly governed by the available free volume [16,17] or that water molecules occupy essentially micro voids and other morphological defects.

* Corresponding author.
E-mail address: lucas@fe.up.pt (L.F.M. da Silva).

https://doi.org/10.1016/j.compstruct.2019.02.035
Received 12 November 2018; Received in revised form 4 January 2019; Accepted 8 February 2019
Available online 10 February 2019
0263-8223/ © 2019 Elsevier Ltd. All rights reserved.

Several mathematical models can be used to predict moisture transport in epoxy resin and epoxy composites using concentration and stress dependent diffusion coefficients [18,19]. Moisture absorption or cyclic absorption and desorption at high temperatures and relative humidity can cause voids and/or microcracks in epoxy resins. If these effects are extensive, conditions for non-Fickian transport can be induced. Thus, it is possible to expect non-Fickian transport as well as Fickian diffusion, according to the resin properties and environmental conditions [20]. In some cases, the moisture transport in composites can be described by a Fickian diffusion model with a constant diffusion coefficient [21–24], a concentration-dependent diffusion coefficient [25], or a stress-dependent diffusion coefficient [26]. Shen and Springer [21] developed a model with direction-dependent diffusion coefficients in a unidirectional fibre composite. Several studies [22,23] revealed a two-staged sorption behaviour. Carter and Kibler [7] suggested a Langmuir-type model to predict two-stage sorption behaviour for composite resins. The model could fit anomalous moisture uptake curves for resin exposed to several relative humidity levels. From the fact that the same parameters give equally good fits to the data at all humidity, they suggest that the absorption anomalies do not result from non-linear effects (e.g. concentration-dependent diffusivity).

When an epoxy resin absorbs water, the local degree of swelling depends on the local water concentration. As a result, the more swollen regions experience a compressive force, whereas less swollen regions experience tensile forces [27]. The tensile stress can enhance the water transport rate. Such a self-induced stress can cause a non-Fickian behaviour.

Kumar et al. [28] assessed the influence of humid environment (23 ± 2 °C at 100% relative humidity) on high strength structural carbon fibre composites and found that the longitudinal tensile strength dropped by 25–30% during the first month of the exposure and remained constant within the experimental scatter during the rest of the exposure time. The transverse tensile strength showed decreasing trend during the exposure period. Longitudinal tensile modulus decreases during first two months of exposure time and remained constant during the rest of the exposure time. Transverse tensile modulus, in-plane shear modulus and Poisson's ratio remained constant during the exposure period.

Numerical simulations tools can help in the prediction of the behaviour of the mechanical behaviour of joints subjected to hygrothermal aging. Hua et al. [29] was able to numerically simulate the mechanical behaviour of SLJs after environmental degradation. Mubashar et al. [30] conducted a numerical study modelling cyclic moisture uptake in an epoxy adhesive using SLJs made with aluminium substrates, concluding that the diffusion rates in absorption and desorption were different and dependent on the moisture history. More recently, Viana et al. [31] assessed numerically the water diffusion in double cantilever beam (DCB) adhesive joints made with aluminium substrates, hygrothermally aged in deionized and salt water taking into account the diffusion through the interface and the adhesive. This approach demonstrated good correlation between experimental and numerical results.

To the best of the authors knowledge, published studies do not assess how the water ingress changes the mechanical behaviour of composite SLJs bonded with modern crash resistant adhesives. It is therefore the aim of this work to produce experimental and numerical data to support the design of joints intended to operate after severe hygrothermal aging (immersed in water at 50 °C for 2000 h). To be representative of real-world automotive applications, the adhesive joints under study were manufactured with unidirectional composite substrates and a crash resistant adhesive, bonded with different overlap lengths. The aging process of the substrate (CFRP) and adhesive (crash resistant XNR56852E-3 adhesive from Nagase ChemteX® - Japan) was studied and the existence of changes on the chemical structure of these materials. A comparison between unaged joints and joints subjected to hygrothermal aging was performed, demonstrating a decrease in strength for hygrothermal aged, joints which was more pronounced with the increase of the overlap length. A numerical simulation was also performed, to model the water ingress on the joints and to simulate the failure load and the failure mechanism associated with each overlap length and hygrothermal aging condition.

2. Experimental details

This section presents the mechanical properties of the unidirectional (0°) CFRP substrates, as well as those of the crash resistant epoxy adhesive used in this work. The SLJs manufactured with these materials were experimentally tested at quasi-static conditions (1 mm/min), prior and after hygrothermal aging (immersed in deionised water at 50 °C for 2000 h). Different overlap lengths were considered (12.5, 25 and 50 mm) to assess the influence of this parameter. The detailed manufacturing process and joint configuration, as well the hygrothermal aging procedure are therefore described.

2.1. Materials and properties

2.1.1. CFRP

The CFRP specimens used in this work were made of plies of carbon/epoxy pre-preg (SEAL® Texipreg HS 160 RM), with a fibre orientation of 0°, aiming to obtain better properties in the loading direction of the specimens.

The elastic mechanical properties of this material, at room temperature, were previously determined in the work of Campilho [32]. In Table 1 it is possible to observe the Young's modulus (E), the shear modulus (G), and the Poisson's ratio (ν), for the three axis directions (x,y,z), E_1 corresponding to the normal direction, E_2 to the transverse direction and E_3 to the out plane direction.

The fracture toughness in both mode I (G_{IC}) and II (G_{IIC}) has been previously experimentally determined by the authors [33,34] at quasi-static conditions (1 mm/min).

The cohesive properties of CFRP when unaged at quasi-static (1 mm/min) conditions are presented in Table 2.

2.1.2. Crash-resistant adhesive

The adhesive investigated in this work was supplied by the company Nagase ChemteX® (Osaka, Japan). The tough epoxy adhesive is a crash resistant designated XNR6852 E-3, which is a one-part component, developed for the automotive industry. This type of adhesive is particularly relevant for bonding vehicle structures due to the combination of its high strength, ductility and resistance to impact. This material can deform significantly without breaking, allowing the bonded structure to deform plastically and absorb the impact energy. The cure cycle of XNR6852 E-3 adhesive requires a stage of four hours at 150 °C. Table 3 lists the experimentally measured mechanical properties (average values) for the adhesive under quasi-static conditions [35].

Saldanha et al. [37] and Avendaño et al. [38] have studied previous versions of XNR6852 E-3 adhesive and in their works the G_{IIC} determined experimentally was 6 to 10 times higher than G_{IC}. Considering this previous data, and due to the high ductility of the adhesive, the value for G_{IIC} was therefore assumed to be 8 times higher than the fracture toughness in mode I, being therefore of 70.72 N/mm.

Table 1
Properties of CFRP elastic orthotropic [32].

Elastic Modulus (MPa)	Poisson's Ratio	Shear Modulus (MPa)
E_1 = 1.09E5	ν_{12} = 0.342	G_{12} = 4315
E_2 = 8819	ν_{13} = 0.342	G_{13} = 4315
E_3 = 8819	ν_{23} = 0.380	G_{23} = 3200

Table 2
Cohesive properties of CFRP under quasi-static(measured) [33–36].

Properties	1 mm/min
Young's modulus, E [MPa]	108,000
Shear modulus, G [MPa]	4315
Tensile strength, σ_n [MPa]	40
Shear strength, t_s [MPa]	35
Fracture energy (mode I), G_{IC} [N/mm]	0.59
Fracture energy (mode II), G_{IIC} [N/mm]	1.17

Table 3
Mechanical properties of Nagase ChemteX® XNR6852E-3 epoxy adhesive under quasi-static conditions (average values) [35].

Properties	1 mm/min
Young's modulus, E [MPa]	1874
Tensile strength, σ_n [MPa]	48.44
Fracture energy (mode I), G_{IC} [N/mm]	8.84

2.2. Specimen fabrication

2.2.1. CFRP specimens

Two distinct types of CFRP specimens were used in this work, namely, in SLJs as substrates (95 × 25 mm) and as bulk plates (60 × 60 mm) for the assessment of the hygrothermal aging.

The specimens were composed of unidirectional (0°) laminates of CFRP cut from bulk laminates, produced by hand lay-up and cured using a hot plate press with the use of a metallic mould with spacers to attain the correct plate thickness. The laminates where built from carbon/epoxy pre-preg material (SEAL® Texipreg HS 160 RM). Each ply used was 0.015 mm thick.

Laminates with two different thicknesses were manufactured. A set 2.1 mm thick (a total of 14 plies) for the SLJs substrates; and another 1 mm thick (a total of 7 plies) in the case of the plates used to study the hygrothermal aging (dimensions of 60x60 mm, based on ISO/DIS 294-3 [39]). The cure cycle applied for this material was of 130 °C for 1 h.

The region of the overlap length, in the case of the substrates for the SLJs, as well as the exposed surface of the plates for hygrothermal aging were sanded by hand using a 90-grit sandpaper, firstly to remove any silicon film or release agent from the surface of the mould used, as well to improve the adhesion in the case of the SLJs. This procedure also allows for better absorption by removing the glossy resin on the laminate surface.

2.2.2. Adhesive bulk plates

Two distinct bulk plates of XNR6852 E-3 adhesive were manufactured for the assessment of the hygrothermal aging and the influence of hygrothermal aging process in its mechanical properties. Following the French standard NF T 76-142 [47], the 1 and 2 mm thick XNR6852 E-3 adhesive plates were produced, using a mould lined with a silicone rubber frame to ensure hydrostatic pressure. A hot plate press was used to apply the necessary pressure and temperature to follow the curing cycle of each adhesive.

The 1 mm thick adhesive plates were then machined to the final dimensions of 60 × 60 mm (based on ISO/DIS 294-3 [39]) to assess the influence of water ingress, and the 2 mm thick plates were machined according the "dogbone" geometry presented in Fig. 1, which follows the BS 2782 standard [40]. These specimens were manufactured to be tested under quasi-static (1 mm/min) conditions.

2.2.3. Single lap joints

The geometry used for the quasi-static tests (1 mm/min) was chosen as this configuration is representative of the joints used in an automotive structure (Fig. 2), with a CFRP substrate thickness of 2.1 mm, overlap lengths of 12.5, 25 and 50 mm and adhesive XNR6852 E-3 layer

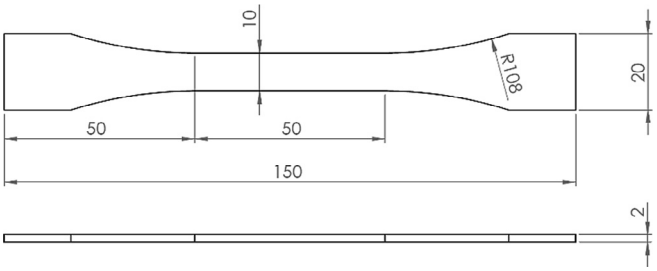

Fig. 1. Geometry of the tensile specimen ("dogbone") accordingly to BS 2782 (dimensions in mm) [40].

thickness (0.2 mm), based on the ASTM D1002-99 [41] and ISO 4587:1995 [42] standards.

The free length of each SLJ was kept constant (at 65 mm), to allow a direct comparison between the results of the different overlap lengths and better understand the trade-off between additional bonding area and the increase in peel stress. A total of six specimens were tested at quasi-static (1 mm/min) conditions for each overlap length configuration, regarding the unaged and hygrothermally aged joints (immersed in deionised water at 50 °C for 2000 h).

2.3. Testing procedures

2.3.1. Hygrothermal aging process of bulk adhesive and CFRP

The process of moisture diffusion was performed using the bulk plate specimens of XNR6852 E-3 adhesive and the CFRP. A total of six plates were considered for the absorption study for each material being studied. Using the same value of thickness (1 mm) allows to compare the absorption rate between both materials and ensures that the diffusion is one dimensional.

After being fabricated, all specimens were kept in a container with silica, to remove any moisture that might have been absorbed from the environment during its preparation. In addition, prior to the initiation of the absorption tests, the specimens were placed in an oven and dried at a temperature of 50 ± 2 °C with 10% of moisture, until a constant mass was attained. All the specimens were weighed using a microbalance with 1 mg of accuracy (Kern-Toledo, Balingen, Germany). The specimens were then immersed in deionized water and kept at a constant temperature of 50 ± 2 °C, following standard ISO 62:2008 [43]. The period of immersion was of 2000 h. The selected aging temperature is significantly lower than the T_g of the materials under study, ensuring that only physical processes ensue, and no chemical changes on both materials occur [2,10].

All the specimens were kept immersed until the moisture absorption mass stabilized (designated as infinite mass (M_∞)). In the case of XNR6852 E-3 adhesive, a constant value of the maximum moisture absorption was observed. In the case of the CFRP, it was not possible to fully saturate this material, and the maximum water uptake considered corresponds to the last measurement.

2.3.1.1. Gravimetric and swelling measurement. All XNR6852 E-3 adhesive plate specimens had its weight regularly measured until saturation was achieved, although for the case of the CFRP plates, an aging period of 2000 h was not enough to reach saturation. The process of weighing was performed in such a way as to avoid drying, which has a significant impact on the absorbed moisture.

The moisture uptake M_t was determined using Eq. (1):

$$M_t = \frac{w_t - w_0}{w_0} \times 100\% \quad (1)$$

where, w_t corresponds to the mass of the specimen at any point in time while immersed in deionised water, and w_0 is the initial constant mass. The saturation mass uptake can be defined when the weight gain from three consecutive measurements varies less than 1% of the overall

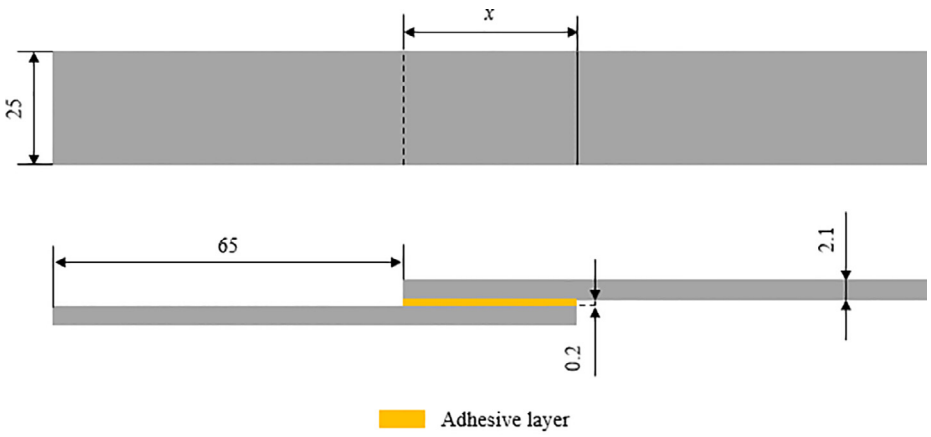

x corresponds to the different SLJs overlap length used: 12.5, 25 and 50 mm.

Fig. 2. Schematic representation of the geometry of SLJ specimens (dimensions in mm).

weight gain.

The effect of swelling was also assessed by measuring the specimens periodically (three times a day) with a micrometre (Mitutoyo, Mizonokuchi Japan), and the relative dimensional increase can be determined by using Eq. (2).

$$\frac{\Delta V}{V_0} = \frac{V_f - V_0}{V_0} \tag{2}$$

Being, V_f the volume of XNR6852 E-3 adhesive or CFRP plates after aging, and V_0 the initial volume of XNR6852 E-3 adhesive or CFRP plates in the final stage of considered aging.

2.3.1.2. Diffusion analysis. Using the diffusion coefficient (D) it is possible to quantify the absorption behaviour of XNR6852 E-3 adhesive and the CFRP. The most common approach to model moisture sorption is the Fick's law, which assumes that the moisture flux is directly proportional to the concentration gradient in a material. In a situation of moisture uptake, the absorbed mass of water increases linearly with the square root of time, thereafter, slowly decreasing until an equilibrium plateau is achieved (M_∞). In general, the moisture absorption of adhesives and some composite materials (accordingly to the resin properties and environmental conditions, as experimentally assessed by some authors [5,18,28,44–46]) under hygrothermal conditions can be described by Fick's law (considered a one-dimensional diffusion through an infinite plate of thickness, represented by the variable h [47,48]) and presented by Eq. (3).

$$\frac{\partial c}{\partial t} = D\frac{\partial^2 c}{\partial x^2} \tag{3}$$

where, D is the coefficient of diffusion, c is the concentration of water and t is time of the process. Crank [47] suggests a simplification of Eq. (3), revealing that for the initial stage of the process, where $\frac{M_t}{M_\infty} < 6$, the resulting relationship can be applied as follows:

$$\frac{M_t}{M_\infty} = \frac{4}{\sqrt{\pi h}}\sqrt{Dt} \tag{4}$$

For several materials, due to its chemical properties, it is necessary to consider the dual Fickian models [49–51], and two distinct diffusion mechanisms working simultaneous can be considered, where the fractional mass uptake increases continuously until M_∞ is reached, such models are commonly designated as "parallel dual Fickian" (PDF). By assuming a pseudo-equilibrium state at intermediate exposure times prior to reaching the final saturation, Ameli et al. [52] developed the "sequential dual Fickian" (SDF) model (Eq. (5)), specifically for highly toughened epoxy adhesives, as in the case of XNR6852 E-3 adhesive being used in this work.

$$M_t = \left(1 - \frac{8}{\pi^2}\sum_{n=0}^{\infty}\frac{1}{(2n+1)^2}e^{\left(\frac{-D_1(2n+1)^2\pi^2 t}{4h^2}\right)}\right) \times M_{1\infty} + \varnothing(t - t_d) * \left(1 - \frac{8}{\pi^2}\sum_{n=0}^{\infty}\frac{1}{(2n+1)^2}e^{\left(\frac{-D_2(2n+1)^2\pi^2 t}{4h^2}\right)}\right) \times M_{2\infty} \tag{5}$$

Being $M_{1\infty}$ and $M_{2\infty}$ the first and second uptakes, and $M_{1\infty} + M_{2\infty} = M_\infty$.

Rearranging both Eqs. (4) and (5), the relationship for D is given by:

$$D = \pi\left(\frac{h}{4M_\infty}\right)^2\left(\frac{M_t}{\sqrt{t}}\right)^2 \tag{6}$$

2.3.1.3. Fourier transform infrared spectroscopy (FTIR). The evaluation of the Fourier transform infrared spectroscopy (FTIR) can be of great interest to evaluate and understand the effects of hygrothermal aging, since in the presence of irreversible damage, the intensity of the absorption bands for some relevant chemical groups will increase or even decrease [53]. The measurements were carried out in a Bruker Vertex 70 (Billerica, MA, USA). The tests were performed using a wave length of 4000–500 cm^{-1} and 0.2 cm^{-1} of scanning velocity. A $LiTaO_3$ detector (15,500–370 cm^{-1}) and a KBr window were used. A total of six tests were performed for each material, namely, three for each condition (unaged and hygrothermally aged).

2.3.2. Measurements of the glass transition temperature (Tg)

An important property to characterize the XNR6852 E-3 adhesive and the CFRP resin is the glass transition temperature, T_g. This property can be related to the strength of a polymer at a given temperature, therefore it is important to understand where the glass transition zone is located [54,55]. An in-house developed apparatus (based on the device proposed by Zhang *et al.* [56]) was used, working on the principle that at the T_g there is a corresponding peak in the damping value of a polymer. For measuring the T_g using this apparatus, the specimen (an aluminium beam with a portion of adhesive bonded to it) is subjected to a constant vibrational movement at the beam's resonance frequency. The temperature at which the specimen displacement is lower, and damping is maximum (corresponding to the T_g) can be identified by varying the temperature in a chamber containing the specimen and registering the amplitude of its movement.

2.3.3. Quasi-static conditions

The quasi-static tests were performed using an INSTRON® 3367 (Norwood, Massachusetts, USA) universal testing machine, with a load

cell with a capacity of 30 kN. All quasi-static tests (XNR6852 E-3 adhesive bulk "dogbone" and SLJs) were performed at room temperature and with a constant cross head displacement rate of 1 mm/min.

In the case of XNR6852 E-3 adhesive bulk "dogbone" specimens, the displacement could not be directly recorded using an extensometer (due to the large values of strain), and an optical method, using high resolution digital images was selected. After the test, the photos were analysed by a Matlab® subroutine in which the strain of each specimen was computed, considering an input file with the values measured during the test from the tensile equipment. Each specimen had two horizontal parallel lines drawn to mark the computational area.

Six specimens were tested for each condition, unaged and hygrothermally aged (immersed in deionised water at 50 °C for 2000 h), and for each specimen a stress–strain (P-δ) curve was obtained.

3. Results and discussion

This section presents the mechanical and chemical changes resultant from the hygrothermal aging process (immersed in deionised water at 50 °C for 2000 h) for both XNR6852 E-3 adhesive and the CFRP substrates. The mechanical performance of SLJs tested under quasi-static conditions (1 mm/min) is also presented, shown as a function of the overlap length (12.5, 25 and 50 mm), and hygrothermal aging state.

3.1. Moisture diffusion of the bulk adhesive and the CFRP substrates

Water saturation occurred in the case of adhesive XNR6852 E-3, and due to its chemical properties, it was possible to observe that the most suitable mathematical model of diffusion was the "sequential dual Fickian" (SDF) (Fig. 3).

The maximum gain of water mass registered by XNR6852 E-3 adhesive was of approximately 1.56%. The general properties of absorption of water by the adhesive (XNR6852 E-3) are presented in Table 4.

As for the CFRP, it was not possible to determine the Fick's law as there was no plateau in the gain percentage, which means that maximum water absorption was not reached by the end of the measurements (Fig. 4).

The maximum water uptake of the CFRP was 3.3%, a larger value than the maximum obtained for XNR6852 E-3 adhesive. Another parameter evaluated was the swelling of both XNR6852 E-3 adhesive and the CFRP. The swelling of both materials was found not to be significant.

3.2. Measurement of T_g

The measurement of T_g (Fig. 5) revealed a decrease of its value with the hygrothermal aging (immersed in deionized water at 50 °C for 2000 h) for both XNR6852 E-3 adhesive and CFRP. In the case of the CFRP, the carbon fibres were not considered and solely its resin was studied, as the T_g of this material is controlled by the resin. Although

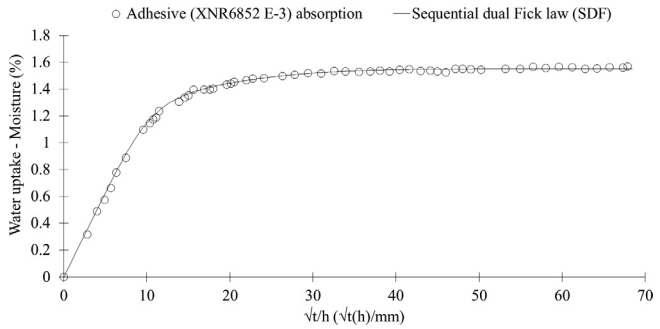

Fig. 3. Moisture absorption of XNR6852 E-3 adhesive (immersed in deionised water at 50 °C), as well the SDF fit curve – results presented as a function of hours for better display of the results.

Table 4
General properties of absorption of water by the adhesive XNR6852 E-3.

Stage	Property	
Absorption	$M_{1\infty}$ (%)	0.012
	D^I (m^2s^{-1})	19E−13
	$M_{2\infty}$ (%)	0.0035
	D_2 (m^2s^{-1})	28E−14

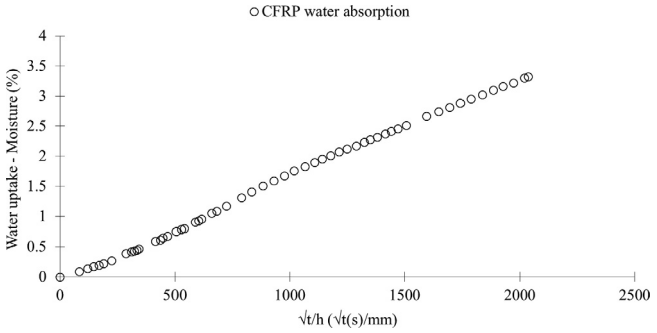

Fig. 4. Moisture absorption of the CFRP (immersed in deionised water at 50 °C) – results presented as a function of seconds for better display of the results.

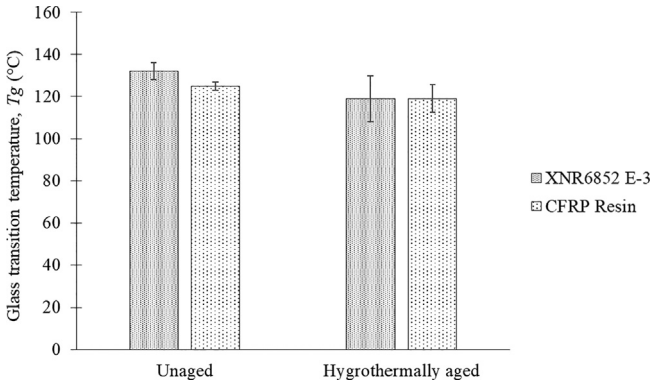

Fig. 5. Comparison between the glass transition temperatures (T_g) values of both XNR6852 E-3 adhesive and CFRP resin at unaged and hygrothermally aged conditions.

the decrease of T_g was not severe, it can be explained by the plasticization of the polymer network with the moisture absorption.

3.3. XNR6852 E-3 adhesive bulk tensile properties

The tensile results of XNR6852 E-3 adhesive bulk specimens are presented in Fig. 6 (representative P-δ curves shown).

A comparison between the mechanical properties obtained from XNR6852 E-3 adhesive bulk "dogbone" specimens tested at quasi-static load, and at the unaged and hygrothermally aged conditions is shown in Table 5.

It is possible to conclude that there was a slight increase of the Young's modulus after hygrothermal aging. In terms of tensile strength, there was a decrease of about 4 MPa. The most affected parameter under after the aging process was the strain to failure, which revealed an increment of 50%, and could be explained by the relaxation of the polymeric chains.

3.4. Fourier transform infrared spectroscopy (FTIR)

Analysing the previous results, it can be observed that the presence of water can alter the properties of the adhesive and the CFRP.

In this way, to fully understand all the phenomena inherent in

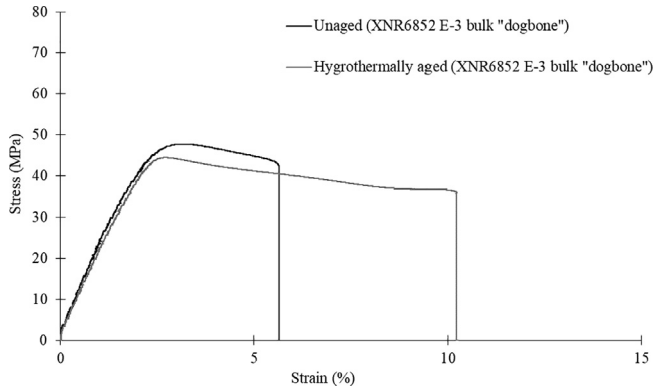

Fig. 6. Representative stress-strain (P-δ) curves obtained from XNR6852 E-3 adhesive bulk "dogbone" specimens tested at room temperature and at quasi-static (1 mm/min), for the unaged and hygrothermally aged conditions.

Table 5
Comparison between the mechanical properties measured from XNR6852 E-3 adhesive bulk "dogbone" tested under quasi-static in the unaged, and hygrothermally aged ("Aged") conditions.

Properties	Unaged	Aged
Tensile strength, σ_n [MPa]	48.44 ± 1.12	43.75 ± 1.57
Young's modulus, E [MPa]	1873.98 ± 180.15	2262.85 ± 38.85
Strain to failure [%]	5.34 ± 0.72	11.65 ± 1.04

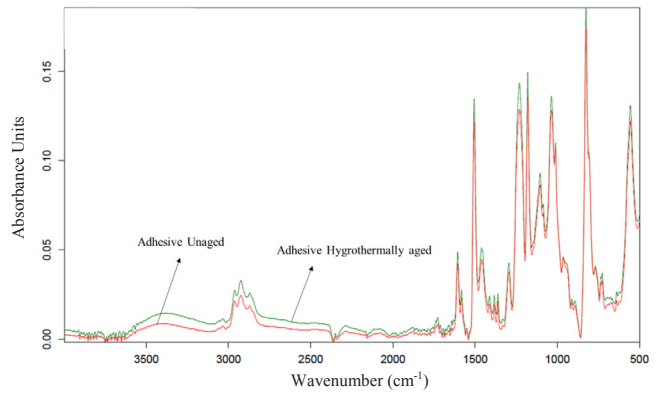

Fig. 7. FTIR spectrum, in the 4000–500 cm^{-1} wavenumber range of XNR6852 E-3 adhesive for different conditions (unaged and hygrothermally aged).

hygrothermal aging it was necessary to analyse whether these differences are also visible at the level of the chemical structure. For this purpose, the unaged and hygrothermally aged (immersed in deionised water at 50 °C for 2000 h) XNR6852 E-3 adhesive and CFRP were analysed by FTIR. Fig. 7 shows the spectrum in the 4000–500 cm^{-1} wavenumber range of adhesive, the two states of moisture studied in this research, unaged, and maximum water absorption. A general analysis of the data also allows to conclude that the spectra are quite similar, indicating that there are no permanent changes in the chemical structure of XNR6852 E-3 adhesive due to the hygrothermal aging process. However, the following changes between aging stages should be considered. After hygrothermal aging, there is an increase of the –OH, as this absorption is due to O—H and N—H stretching and intermolecular hydrogen bonds; this can be explained by the fact that water absorption induces hydroxyl and amine groups into the epoxy chain. It is also observed that C—H stretching vibrations (3100–2800 cm^{-1}) increase, arising from aliphatic hydrocarbons, which also changes with the water absorption. Furthermore, changes are observed in C=C stretching of the benzene ring (1505 cm^{-1}) and the out-of-plane bending of aromatic rings (824 cm^{-1}). The aromatic band (1230 cm^{-1}) increases when bonded water is present [16,57].

Samples of CFRP were also analysed using FTIR but no major changes were identified. The results can be considered as somewhat inconclusive since the material since did not reach full water saturation at the time of testing.

3.5. Quasi-static tests of aged and unaged single lap joints

3.5.1. Fracture surface

Representative images of the fracture surface regarding each overlap length used (12.5, 25 and 50 mm) for unaged and hygrothermally aged SLJs are presented in Table 6.

It was possible to observe that delamination of CFRP substrate occurred for all cases. In the case of unaged SLJs with an overlap length of 12.5 mm the type of failure was partially cohesive in the adhesive, which can be explained by the fact that the maximum load required for the failure of the SLJs, although higher than XNR6852 E-3 adhesive resistance, was not high enough to induce more significant damage on the CFRP substrate.

From a visual inspection it was possible to determine that, for the cases of hygrothermally aged SLJs, the fracture surface revealed to be glossy and with fibres free from the CFRP resin, which indicated some degree of plasticization of the CFRP substrates, therefore conducting to a lower and less severe failure of the joints by delamination, being the XNR6852 E-3 adhesive strength superior to that of the CFRP substrates.

For the cases of hygrothermally aged SLJs with overlap length of 25 and 50 mm, although delamination of CFRP substrates occurred, it was possible to observe that such mechanism was not so severe as for SLJs unaged. The surfaces were found to be shiny and more homogeneous, with less fibre damage after the failure of the joints, an indicator of the plasticization of the adhesive and the CFRP after the hygrothermal aging process.

In the case of hygrothermally aged SLJs with an overlap length of 12.5 mm, the SLJs failed with more severe delamination of CFRP substrates than observed for other overlap lengths (respectively 25 and 50 mm), indicating that XNR6852 E-3 adhesive strength was sufficiently high to cause such failure as the CFRP substrate suffered higher plasticization due to the aging process. In comparison with the unaged SLJs under the same conditions, the hygrothermally SLJ revealed that XNR6852 E-3 adhesive strength overcame the load necessary to fail the joint due to plasticization of the CFRP substrates.

3.5.2. Failure load

The failure load of unaged and hygrothermally aged SLJs, as a function of the overlap length (12.5, 25 and 50 mm) is shown in Fig. 8.

Although delamination is the major failure mechanism in play, an almost linear behaviour can be found for both unaged and hygrothermally aged SLJs as a function of the overlap length. Also, for both cases, with the increase of the overlap length there was associated an increase of the failure load of the SLJs. A combined degradation process of the adhesive and the CFRP substrates is occurring, leading to increased susceptibility to water uptake.

The failure load values of the hygrothermally aged SLJs were lower than those found for the unaged SLJs, independently of the overlap length considered. With the increase of the overlap length, there was a noticeable increase of the difference in the failure load between the unaged and hygrothermally aged SLJs, with lower failure loads being always exhibited by the hygrothermally aged SLJs, a trend which is reinforced with the increase of the overlap length considered. A correspondence can also be observed in terms of maximum failure load versus the overlap length between the unaged and hygrothermally aged conditions, namely, the values obtained for the case of 12.5 and 25 mm of overlap length of joints unaged were similar to those obtained for the case 25 and 50 mm of overlap length after hygrothermal aging, respectively. From the FTIR results it was possible to conclude that no

Table 6
Representative failure surfaces of CFRP SLJs specimens tested under quasi-static conditions (1 mm/min) as a function of the overlap length (12.5, 25 and 50 mm), and in the unaged and hygrothermally aged conditions.

Overlap length	Unaged	Hygrothermally aged
12.5 mm	Delamination of CFRP*	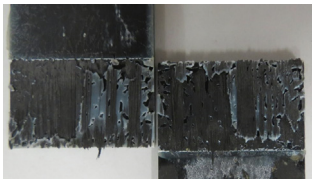 Delamination of CFRP
25 mm	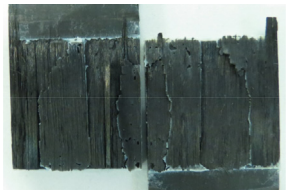 Delamination of CFRP	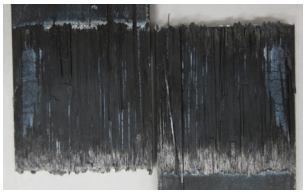 Delamination of CFRP
50 mm	Delamination of CFRP	Delamination of CFRP

* Partially cohesive in the adhesive.

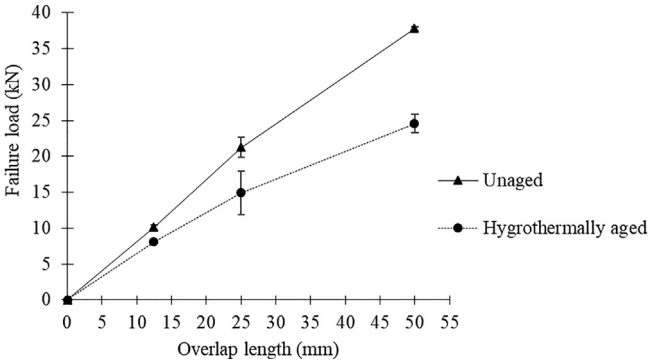

Fig. 8. Comparison between the failure load of unaged and hygrothermally aged SLJs as a function of the overlap length, and in the unaged and hygrothermally aged conditions.

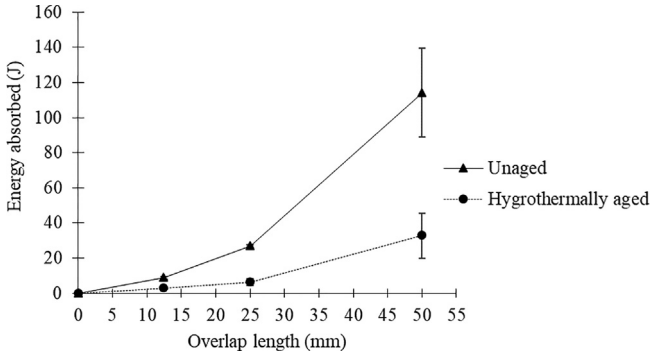

Fig. 9. Comparison between the energy absorbed by unaged and hygrothermally aged SLJs as a function of the overlap length, and in the unaged and hygrothermally aged conditions.

major chemical changes occurred for both materials, being the lower joint strength in the case of hygrothermally aged joints also partially explained by the plasticization and increased toughness of XNR6852 E-3 adhesive, supported by the bulk "dogbone" results, where a significant increase of strain to failure was observed.

3.5.3. Energy absorbed

The energy absorbed by unaged and hygrothermally aged (immersed in deionized water at 50 °C for 2000 h) SLJs, as a function of the overlap length (12.5, 25 and 50 mm) is shown in Fig. 9. The energy absorbed is calculated by integrating the area underneath the *P-δ* curve of each experimental test.

With the increase of the overlap length an increase of the energy absorbed by the SLJs was registered, for both unaged and hygrothermally aged cases. Also, in both cases a significant increase of the energy absorbed from SLJs was registered when increasing the overlap length from 25 to 50 mm.

The lowest values of energy absorption were achieved for the hygrothermally aged SLJs, such fact was due to the plasticization of the CFRP substrates which decreased the joints strength (as previously stated regarding the decrease of failure load).

4. Numerical analysis of water ingress in SLJs

A numerical simulation procedure was performed with the objective of replicating the experimental results and to provide further insights on the influence of water uptake on the mechanical performance of SLJs with three different overlap lengths. The numerical procedure comprised of several steps aiming at a comparison of the joint's strength with both the unaged and hygrothermally aged conditions

experimentally determined. The first step was the simulation of water ingress in the adhesive and the substrates, which enabled the assessment of the saturation level along the adhesive layer for all three overlap lengths (12.5, 25 and 50 mm). This data was combined with aged and unaged mechanical properties of the adhesives and CFRP to create a discretized model of the adhesive and substrate mechanical properties along the overlap length. Due to limited data on the effect of water on the mechanical properties of CFRP, some assumptions based on the literature were made. Finally, a complete model of the SLJs was created, using cohesive elements to model adhesive failure and CFRP delamination. All the numerical models were developed using Abaqus® software.

4.1. Simulation of water ingress in the XNR6852 E-3 adhesive

The simulation of water ingress in XNR6852 E-3 adhesive was performed considering a bulk plate under the effect of the hygrothermal aging, following the experimental process already described (in Section 2.3.1.1.). In this phase, an inverse method was used to numerically determine an average diffusion coefficient (D) of XNR6852 E-3 adhesive and to compare it with the real values obtained. This approach was followed to simplify the modelling process, as the modelling of an SDF process, with two coefficients of diffusion, significantly increases model complexity.

The diffusion process was numerically modelled as a two-dimensional heat transfer problem, with the thermal conductivity, thermal diffusivity and the heat capacity being equivalent to the permeability coefficient, diffusion coefficient and solubility coefficient, respectively, while nodal temperature values correspond to the humidity level. The elements used were the DC2D4 heat transfer type present in the Abaqus® library. Due to the symmetry of the specimens, only a two-dimensional section of the specimen needed to be simulated, reducing the computational effort and increasing the speed of the analysis. A convergence analysis was performed and indicated that optimal element size had uniform width and height of 0.05 mm, resulting in a total number of 37,500 elements. Fig. 10 schematically shows the modelled section of the specimen and the water uptake direction. The numerical analysis considered the hygrothermal aging process of specimens immersed in deionized water at 50 °C for 2000 h.

From Fig. 11 it was possible to observe a comparison between the real and the numerical evolution of the water uptake of XNR6852 E-3 adhesive, after an iterative process for fitting the D value.

The best fitting value of D (2.8E-11) is in between the D_1 and D_2 values, determined using the SDF model, which is expected for type of simplification.

4.2. Simulation of water ingress in XNR6852 E-3 adhesive layer in SLJs

The aim of this numerical simulation was the comparison of the absorbed moisture (%) of the SLJs, as function of time, between the three overlap lengths studied. The moisture uptake was assessed using finite element analysis, through the thin bondline and considering the average value of D determined in the previous subsection. Diffusion is again only considered to occur in two-dimensions, through the sides and the edges of the bonded area (shown in Fig. 12). The element type and size of this model were the same as used in the bulk model described in the previous subsection.

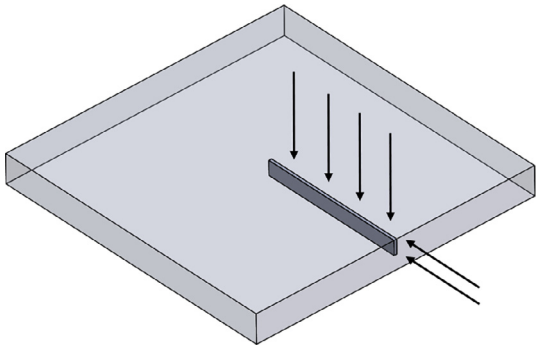

Fig. 10. Schematic representation of the 2D model used for determining water uptake in XNR6852 E-3 bulk plate. Arrows indicate the water uptake directions.

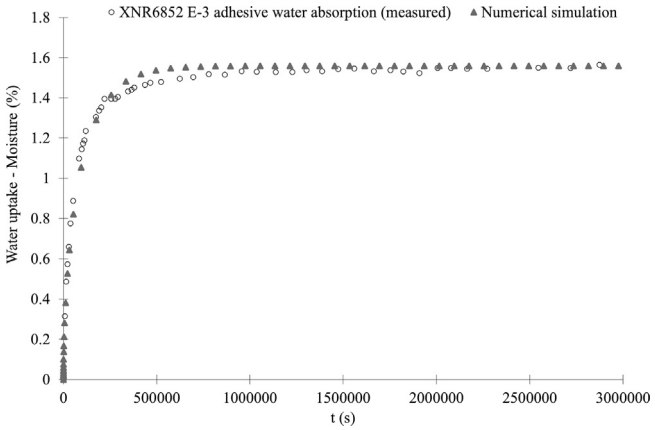

Fig. 11. Comparison of measured and numerical simulation of water absorption of XNR6852 E-3 adhesive bulk plates.

In Fig. 13 it is possible to observe the numerically predicted moisture level (%) of the adhesive layer of the SLJs as a function of the normalized overlap position. It was possible to verify that with the increase of the overlap length there was a decrease of the average water uptake level, which is in accordance with the previous results obtained.

Using this two-dimensional model, it is also possible to graphically visualize the water uptake in the adhesive layer (Fig. 14).

The numerical results were in accordance with the previously obtained data, being the water ingress higher for the lower values of overlap length. Another conclusion was that for all of the three cases of overlap length studied, the SLJs were not fully saturated after the hygrothermal aging process, although, in the region of the end of the overlap length full saturation was observed, which largely contributes to explain the experimental results due to great importance of this regions on the joint strength (peak of stress concentration that cause peel load and compromises the joints integrity).

4.3. Discretization of adhesive and CFRP properties along the overlap as a function of water intake

The saturation curves obtained for each overlap were used to discretize the adhesive layers into ten sections, each one corresponding to a specific value of water saturation. The mechanical properties, such as the stiffness, yield stresses and fracture toughness, were then locally determined by the calculation of the degradation of its mechanical properties due to water ingress, creating a gradient effect. A linear relationship was assumed between the dry and saturated mechanical

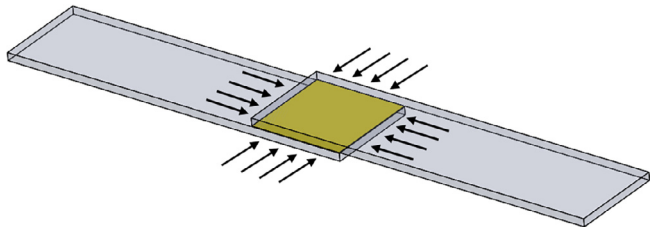

Fig. 12. Schematic representation of the 2D model used for determining water uptake in the hygrothermally aged SLJ specimens. Arrows indicate the water uptake directions.

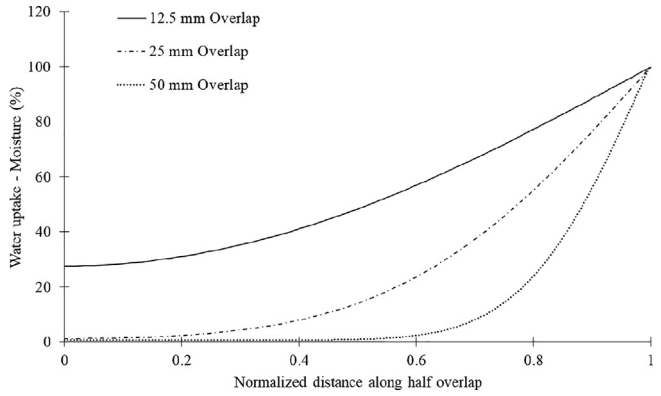

Fig. 13. Numerical results comparing the total absorbed moisture along the different overlap lengths studied (12.5, 25 and 50 mm).

Table 7
Estimated cohesive properties of CFRP after hygrothermal aging.

Properties	1 mm/min
Young's modulus, E [MPa]	108,000
Shear modulus, G [MPa]	3883
Tensile strength, σ_n [MPa]	32
Shear strength, t_s [MPa]	28
Fracture energy (mode I), G_{IC} [N/mm]	0.67
Fracture energy (mode II), G_{IIC} [N/mm]	0.99

properties.

The procedure employed for modelling the CFRP as a function of the hygrothermal aging was necessarily distinct, as the CFRP plates did not achieve full saturation (for 2000 h at 50 °C). For simulation purposes, it was decided instead to consider that at this stage, the whole joint would be at the maximum value of moisture level achieved during the experimental tests (3.3%). From the literature, it was found that CFRP matrixes with moisture levels between 2 and 3% exhibit a drop of around 20% in the yield stresses, 15% drop in terms of fracture

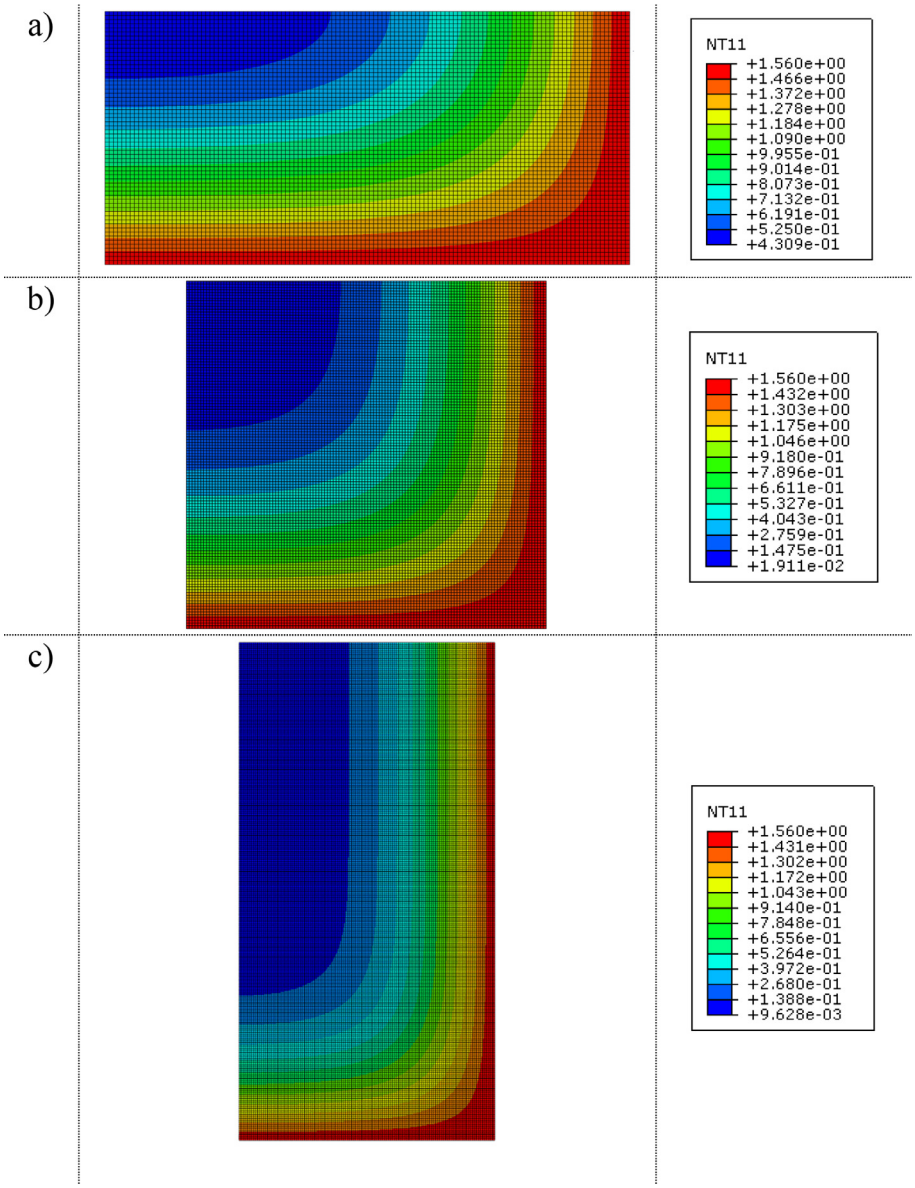

Fig. 14. Numerical simulation of the evolution of the water ingress in the adhesive layer of a SLJ immersed in water at 50 for 2000 h, as a function of the three overlap lengths studied: a) 12.5, b) 25 and c) 50 mm.

toughness in mode I (G_{IC}), and an increase of 15% in mode II (G_{IIC}). Stiffness is assumed constant in the fibre direction with only a 10% reduction considered in the transverse stiffness. These assumptions, are based on data presented by Zafar et al. [14] and Selzer and Friedrich [58]. The estimated cohesive properties are shown in Table 7, modifying the data previously shown in Table 2.

4.4. Simulation of single lap joints in the unaged and hygrothermally aged conditions

A two-dimensional model, able to reproduce the performance and failure mode of the unaged and hygrothermally aged SLJs was created using cohesive zone modelling. The use of strategically placed cohesive elements enables the simulation of joint performance by allowing both cohesive failure on the adhesive and delamination of the CFRP substrate to occur.

The cohesive elements (4-node-two-dimensional, COH2D4 elements) used in this work employed a triangular cohesive law. This model is available in Abaqus® and enables the use of mixed mode loading. The adhesive layer was modelled with 0.2 mm thick cohesive elements, the same thickness of the adhesive layer to control the zone of crack initiation. For the CFRP substrates, elastic orthotropic properties (as engineering constants) were considered in the zones not susceptible to delamination (with 4-node bilinear plane stress quadrilateral, reduced integration, hourglass control, CPS4R elements) but it was also necessary to resort to cohesive elements to enable possible failure by delamination. To simulate this type of failure, a 0.15 mm thick layer was added at 0.15 mm from the interface between adhesive and CFRP. The thickness of 0.15 mm corresponds to one ply of the prepreg used to manufacture the CFRP substrate, close to the adhesive/substrate interface. The cohesive element used for modelling the adhesive are 0.4 mm wide and 0.2 mm high, while those used for modelling the delamination of the CFRP are only 0.15 mm high. The remaining elements (the CPS4R elements) used for this model are uniformly sized, 0.4 mm wide and 0.4 mm high. These element sizes were selected to ensure convergence in the result and minimize calculation time. The total element size depended on the overlap length under study. The model with 12.5 mm of overlap used a total of 2718 element, the 25 mm overlap model was constructed with 2730 elements, while the larger 50 mm overlap required 2848 elements. The generic model configuration is shown schematically in Fig. 15.

The boundary conditions employed in the model construction are shown in Fig. 16.

To enable the use of the property gradients proposed in Section 4.3, the adhesive layer was discretized into ten distinct regions, allowing for five different levels of adhesive properties on each side of overlap.

The model was then used to return a numerically determined failure load as well as the failure mode of the unaged and hygrothermally aged SLJ. To support the model validation process, Figs. 17 and 18 compare representative *P-δ* curves obtained experimentally for the different overlap lengths, with those obtained numerically, for the unaged and the hygrothermally aged ("Aged") cases, respectively.

Considering the different overlap lengths, a comparison between the numerical and experimental failure loads is shown in Fig. 19 (for both unaged and hygrothermally aged conditions).

Analysing both the representative *P-δ* curves and the failure loads, it can be stated that a good agreement between the experimental and numerical results exists, with the model being generally able to

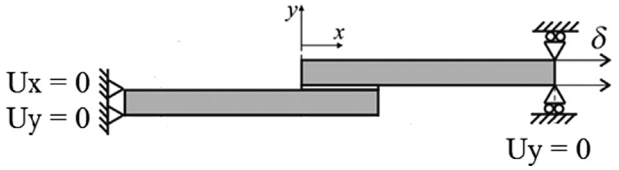

Fig. 16. Boundary conditions for the SLJ joint numerical model.

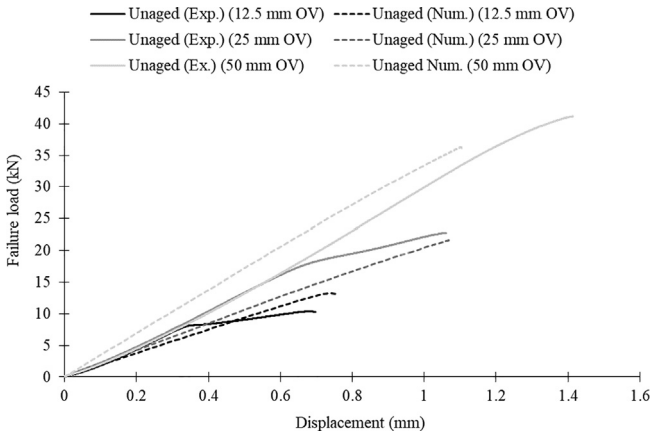

Fig. 17. Comparison between representative experimental and numerical P-δ obtained with unaged specimens for different overlap lengths.

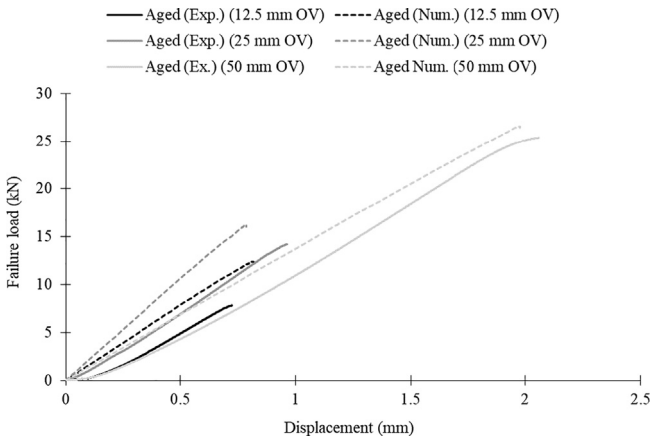

Fig. 18. Comparison between representative experimental and numerical P-δ obtained with hygrothermally unaged ("Aged") specimens for different overlap lengths.

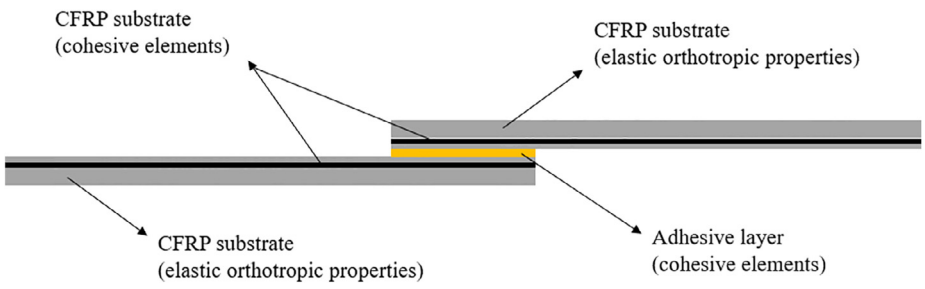

Fig. 15. Location of the cohesive layers on the SLJ numerical model.

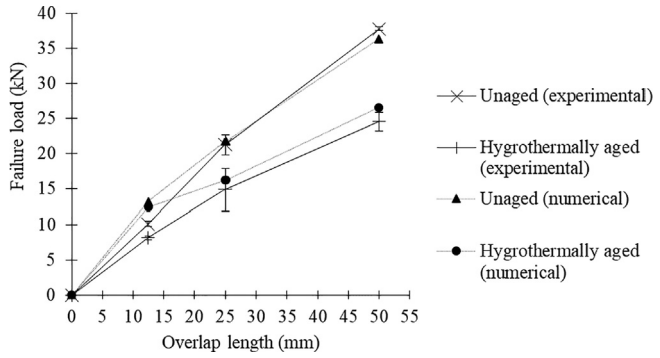

Fig. 19. Numerical comparison of SLJ tested under quasi-static load with an overlap length of 25 mm, considering the unaged and hygrothermally aged conditions.

accurately match the behaviour of a joint in its unaged and hygrothermally aged conditions, as a function of the overlap length. The largest discrepancies appear to occur for the short overlap length (12.5 mm), there is a more complex failure mode, especially for the unaged condition. Nonetheless, the numerical results indicate a trend similar to that found to the experimental results, with slight differences in overall joint stiffness.

The types of failure obtained numerically of SLJs under quasi-static conditions, as function of overlap length, considering the unaged and hygrothermally aged conditions are presented in Table 8.

It is possible to state that the numerical results in terms of type of failure mode were in accordance with the experimental results obtained in this work. Failure by delamination occurred for all cases under study, except for the case of SLJ in the unaged condition and overlap length of 12.5 mm. The analysis of *P-δ* curves reinforces that the numerical simulation was in good accordance with the experimental results.

5. Conclusions

This work focused on the influence on the quasi-static behaviour, of hygrothermal aging with temperature on adhesive joints made with unidirectional composite substrates and a crash resistant adhesive using different overlap lengths.

The main conclusion drawn from this work were the following:

- The water uptake of XNR6852E-3 crash resistant adhesive and CFRP substrates was experimentally assessed for a period of 2000 h at 50 °C. Using data from this experiment, the parameters of a SDF model were adjusted to accurately model the water uptake of the adhesive.
- The existence of changes in the T_g and the chemical composition of the adhesive and the CFRP after hygrothermal aging was also studied. A small reduction in the T_g was identified, explained by the plasticization of the polymer network with the moisture absorption.
- The chemical analysis also indicated that no permanent changes in the chemical structure of XNR6852 E-3 adhesive occurred due to the hygrothermal aging process.
- The mechanical performance of unaged joints and after hygrothermal aging (immersed in deionized water at 50 °C for 2000 h) was performed demonstrating a decrease in strength for hygrothermally aged joints, which was more pronounced with the increase of the overlap length.
- A numerical simulation procedure was first used to successfully

Table 8
Numerical simulation of the type of failure of CFRP SLJs specimens under quasi-static conditions (1 mm/min) as a function of the overlap length (12.5, 25 and 50 mm) and unaged and hygrothermally aged conditions.

Overlap length	Unaged	Hygrothermally aged
12.5 mm	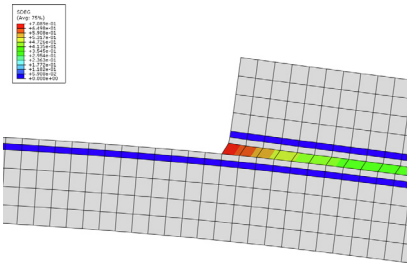 Cohesive in the adhesive	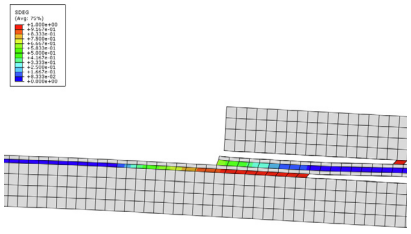 Delamination of CFRP
25 mm	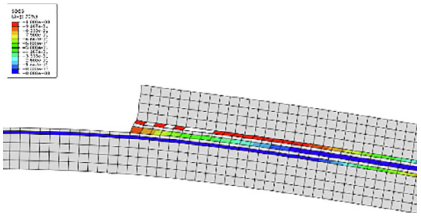 Delamination of CFRP	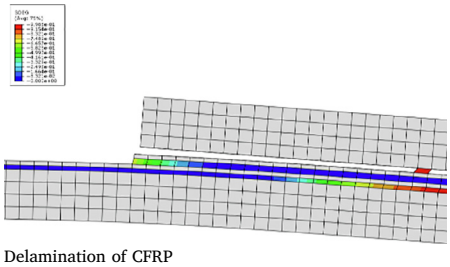 Delamination of CFRP
50 mm	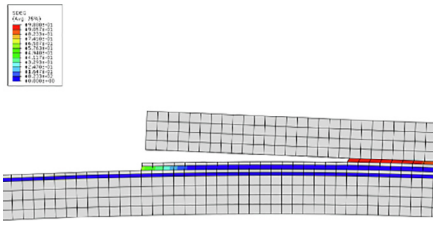 Delamination of CFRP	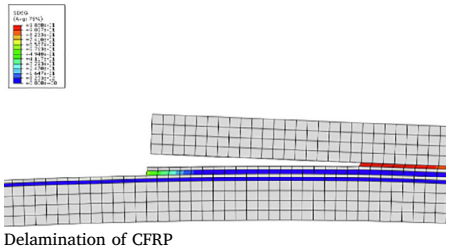 Delamination of CFRP

model the water ingress on the joints and then, using moisture dependent cohesive element properties, predict the failure load and failure mode for different overlap lengths.

- The numerical simulation generally agreed with the experimental results, showing increased susceptibility to delamination failure induced by water absorption in the composite and changes in the adhesive properties.

Acknowledgments

The authors gratefully acknowledge the funding provided by PhD grant SFRH/BD/139341/2018 “Impact strength optimization with cohesive zone elements of multi-material bonded structures used in the automotive industry”, Project N° 028473 POCI-01-0145-FEDER-028473 “Design methodology for impact resistant bonded multi-material automotive structures (ImpactBondDesign)”, Project NORTE-01-0145-FEDER-000022 – “SciTech - Science and Technology for Competitive and Sustainable Industries”, co-financed by Programa Operacional Regional do Norte (NORTE2020), through Fundo Europeu de Desenvolvimento Regional (FEDER). The authors would also like to thank NAGASE ChemteX® for the financial support provided.

References

[1] Campilho R, et al. Tensile behaviour of three-dimensional carbon-epoxy adhesively bonded single-and double-strap repairs. Int J Adhes Adhes 2009;29(6):678–86.
[2] da Silva L. Handbook of adhesion technology. Springer Science & Business Media; 2011.
[3] Hartshorn SR. The durability of structural adhesive joints. Structural adhesives. Springer; 1986. p. 347–406.
[4] Sethi S, Ray BC. Environmental effects on fibre reinforced polymeric composites: evolving reasons and remarks on interfacial strength and stability. Adv Colloid Interface Sci 2015;217:43–67.
[5] Alessi S, Pitarresi G, Spadaro G. Effect of hydrothermal ageing on the thermal and delamination fracture behaviour of CFRP composites. Compos B Eng 2014;67:145–53.
[6] Apicella A, Nicolais L, De Cataldis C. Characterization of the morphological fine structure of commercial thermosetting resins through hygrothermal experiments. Characterization of polymers in the solid state I: Part A: NMR and other spectroscopic methods Part B: mechanical methods. Springer; 1985. p. 189–207.
[7] Carter HG, Kibler KG. Langmuir-type model for anomalous moisture diffusion in composite resins. J Compos Mater 1978;12(2):118–31.
[8] Joliff Y, et al. Study of the moisture/stress effects on glass fibre/epoxy composite and the impact of the interphase area. Compos Struct 2014;108:876–85.
[9] Costa M, et al. Environmental effect on the fatigue degradation of adhesive joints: a review. J Adhes 2017;93(1–2):127–46.
[10] Viana G, et al. A review on the temperature and moisture degradation of adhesive joints. Proc Inst Mech Eng, Part L: J Mater: Des Appl 2017;231(5):488–501.
[11] Viana G, et al. Behaviour of environmentally degraded epoxy adhesives as a function of temperature. J Adhes 2017;93(1–2):95–112.
[12] Barbosa A, da Silva L, Öchsner A. Hygrothermal aging of an adhesive reinforced with microparticles of cork. J Adhes Sci Technol 2015;29(16):1714–32.
[13] Otaluka EP, Arnold C, Alston S. The long term effects of water absorption, desorption and re-absorption in carbon-fibre/epoxy composites. Behaviour 2015;3(6):7.
[14] Zafar A, et al. Investigation of the long term effects of moisture on carbon fibre and epoxy matrix composites. Compos Sci Technol 2012;72(6):656–66.
[15] Adamson MJ. Thermal expansion and swelling of cured epoxy resin used in graphite/epoxy composite materials. J Mater Sci 1980;15(7):1736–45.
[16] Diamant Y, Marom G, Broutman L. The effect of network structure on moisture absorption of epoxy resins. J Appl Polym Sci 1981;26(9):3015–25.
[17] Gupta V, et al. The temperature-dependence of some mechanical properties of a cured epoxy resin system. Polym Eng Sci 1985;25(13):812–23.
[18] Lee MC, Peppas NA. Models of moisture transport and moisture-induced stresses in epoxy composites. J Compos Mater 1993;27(12):1146–71.
[19] Maggana C, Pissis P. Water sorption and diffusion studies in an epoxy resin system. J Polym Sci, Part B: Polym Phys 1999;37(11):1165–82.
[20] Augl JM, Berger AE. The Effect of Moisture on Carbon Fiber Reinforced Epoxy Composites. 1. Diffusion. 1976, naval surface weapons center white oak lab silver spring MD.
[21] Shen C-H, Springer GS. Moisture absorption and desorption of composite materials. J Compos Mater 1976;10(1):2–20.
[22] Loos AC, Springer GS. Moisture absorption of graphite-epoxy composites immersed in liquids and in humid air. J Compos Mater 1979;13(2):131–47.
[23] Illinger JL, Schneider NS. Water vapor transport in an epoxy resin based on TGMDA and DICY. Polym Eng Sci 1980;20(4):310–4.
[24] Boll D, Bascom W, Motiee B. Moisture absorption by structural epoxy-matrix carbon-fiber composites. Compos Sci Technol 1985;24(4):253–73.
[25] Shirrell C, Halpin J. Moisture absorption and desorption in epoxy composite laminates. Composite materials: testing and design (fourth conference). ASTM International; 1977.
[26] Neumann S, Marom G. Prediction of moisture diffusion parameters in composite materials under stress. J Compos Mater 1987;21(1):68–80.
[27] Prolongo S, Gude M, Urena A. Water uptake of epoxy composites reinforced with carbon nanofillers. Compos A Appl Sci Manuf 2012;43(12):2169–75.
[28] Kumar S, Sridhar I, Sivashanker S. Influence of humid environment on the performance of high strength structural carbon fiber composites. Mater Sci Eng, A 2008;498(1–2):174–8.
[29] Hua Y, et al. Modelling environmental degradation in EA9321-bonded joints using a progressive damage failure model. J Adhes 2006;82(2):135–60.
[30] Mubashar A, et al. Modelling cyclic moisture uptake in an epoxy adhesive. J Adhes 2009;85(10):711–35.
[31] Viana G, et al. Water diffusion in double cantilever beam adhesive joints. Latin Am J Solids Struct 2017;14(2):188–201.
[32] Campilho RDSG. Repair of composite and wood structures. Instituto Superior de Engenharia do Porto; 2009.
[33] Machado J, et al. Mode I fracture toughness of CFRP as a function of temperature and strain rate. J Compos Mater 2016. 0021998316682309.
[34] Machado J, et al. Mode II fracture toughness of CFRP as a function of temperature and strain rate. Compos B Eng 2017;114:311–8.
[35] Araújo H, et al. Dynamic behaviour of composite adhesive joints for the automotive industry. Compos Struct 2017;171:549–61.
[36] Machado J, et al. Improvement in impact strength of composite joints for the automotive industry. Compos B Eng 2018;138:243–55.
[37] Saldanha DFS, et al. Mechanical characterization of a high elongation and high toughness epoxy adhesive. Int J Adhes Adhes 2013;47:91–8.
[38] Avendano R, et al. Impact loading of single lap joints of dissimilar lightweight adherends bonded with a crash-resistant epoxy adhesive. J Eng Mater Technol-Trans Asme 2016;138(4).
[39] 294-3, I., Plastics-injection moulding of test specimens of thermoplastic materials, part 3: small plates. 2002: Switzerland.
[40] Standard, B., BS 2782, in Methods of Testing Plastics, Part. 1970.
[41] ASTM D. 1002. Standard Test Method for Apparent Shear Strength of Single-Lap-Joint Adhesively Bonded Metal Specimens by Tension Loading (Metal-to-Metal) 2005;15:45–48.
[42] ISO 4587. Determination of tensile lap-shear strength of rigid-to-rigid bonded assemblies 1995.
[43] ISO E. Plastics. Determination of water absorption. Geneva, Switzerland: EU adoption of International Organization for Standardization; 2008.
[44] Parker B. Some effects of moisture on adhesive-bonded CFRP-CFRP joints. Compos Struct 1986;6(1–3):123–39.
[45] Suh D-W, et al. Equilibrium water uptake of epoxy/carbon fiber composites in hygrothermal environmental conditions. J Compos Mater 2001;35(3):264–78.
[46] Choi H, et al. Hygroscopic aspects of epoxy/carbon fiber composite laminates in aircraft environments. Compos A Appl Sci Manuf 2001;32(5):709–20.
[47] Crank J. The mathematics of diffusion: 2d Ed. Clarendon Press; 1975.
[48] Lin Y, Chen X. Moisture sorption–desorption–resorption characteristics and its effect on the mechanical behavior of the epoxy system. Polymer 2005;46(25):11994–2003.
[49] Mubashar A, et al. Moisture absorption–desorption effects in adhesive joints. Int J Adhes Adhes 2009;29(8):751–60.
[50] Loh W, et al. Modelling anomalous moisture uptake, swelling and thermal characteristics of a rubber toughened epoxy adhesive. Int J Adhes Adhes 2005;25(1):1–12.
[51] Loh W, et al. Modelling interfacial degradation using interfacial rupture elements. J Adhes 2003;79(12):1135–60.
[52] Ameli A, et al. Hygrothermal properties of highly toughened epoxy adhesives. J Adhes 2010;86(7):698–725.
[53] Lin Y, et al. Effects of hygrothermal aging on epoxy-based anisotropic conductive film. Mater Lett 2006;60(24):2958–63.
[54] da Silva L, et al. Effect of low temperature on tensile strength and mode I fracture energy of a room temperature vulcanizing silicone adhesive. J Test Eval 2015;44(3).
[55] Marques E, et al. Adhesive joints for low-and high-temperature use: an overview. J Adhes 2015;91(7):556–85.
[56] Zhang Y, Adams R, da Silva L. A rapid method of measuring the glass transition temperature using a novel dynamic mechanical analysis method. J Adhes 2013;89(10):785–806.
[57] Xiao G, Shanahan M. Irreversible effects of hygrothermal aging on DGEBA/DDA epoxy resin. J Appl Polym Sci 1998;69(2):363–9.
[58] Selzer R, Friedrich K. Inluence of water up-take on interlaminar fracture properties of carbon fibre-reinforced polymer composites. J Mater Sci 1995;30(2):334–8.

Paper 16

Content of Paper 16

Abstract

1. Introduction

2. Experimental details

2.1. Material and properties

2.1.1. CFRP

2.1.2. Aluminium alloy

2.1.3. Crash resistant adhesive

2.2. Specimens fabrication

2.2.1. CFRP specimens

2.2.2. Adhesive bulk plates

2.2.3. Single lap joints

2.3. Testing procedures

2.3.1. Hygrothermal aging and desorption process of bulk adhesive and CFRP

2.3.1.1. Gravimetric analysis

2.3.1.2. Diffusion analysis

2.3.1.3. Fourier transform infrared spectroscopy (FTIR)

2.3.2. Measurement of the glass transition temperature (T_g)

2.3.3. Quasi-static testing procedure

2.3.4. Impact testing procedure

3. Results and discussion

3.1. Moisture diffusion of the bulk adhesive and the CFRP substrates

3.2. Measurement of T_g

3.3. Bulk tensile tests of XNR6852 E-3 adhesive

3.4. Fourier transform infrared spectroscopy (FTIR)

3.5. Quasi-static conditions

3.5.1. Fracture surfaces

3.5.2. Failure loads

3.5.3. Energy absorbed

3.6. Impact conditions

3.6.1. Fracture surfaces

3.6.2. Failure load

3.6.3. Energy absorbed

3.7. Comparison between quasi-static and impact results

3.7.1. Failure load

3.7.2. Energy absorbed

4. Conclusions

References

Influence of hygrothermal aging on the quasi-static and impact behaviour of single lap joints using CFRP and aluminium substrates

J. J. M. Machado[1], E. A. S. Marques[1], A. Q. Barbosa[1], Lucas F. M. da Silva[2*]

[1]Instituto de Ciência e Inovação em Engenharia Mecânica e Engenharia Industrial (INEGI), Rua Dr. Roberto Frias, 4200-465 Porto, Portugal

[2]Departamento de Engenharia Mecânica, Faculdade de Engenharia (FEUP), Universidade do Porto, Rua Dr. Roberto Frias, 4200-465 Porto, Portugal

Abstract

The use of adhesive to bond composites in vehicles continues to increase. Due to hygrothermal conditions, both adhesive and composite properties can be altered, making the mechanical behaviour of a joint unpredictable. The novelty of this work is the assessment of the behaviour of joints manufactured using composite and aluminium substrates tested under quasi-static and impact conditions in the following states: unaged, hygrothermally aged, and dried after hygrothermal aging. A significant reduction of failure load was registered for composite joints (quasi-static and impact) after hygrothermal aging. Joints dried after aging achieved a recovery in the failure load of quasi-static tests.

*Corresponding author. Tel: +351225081706. Fax: +351225081445. Email: lucas@fe.up.pt

Keywords

CFRP; Aluminium; Quasi-static; Impact; Hygrothermal aging; Moisture; Joints

1. Introduction

The automotive industry is major user of fibre reinforced composite materials in vehicle construction. Materials such as carbon fibre reinforced plastic (CFRP) offer several advantages, such as lower structural weight, high strength and excellent stiffness to weight ratios. While in an initial phase the automotive industry restricted the use of CFRP to non-structural components, nowadays these materials are being used to manufacture more complex assemblies, such as crash absorbing structures. To reach the highest safety levels, automotive structures must be able to withstand a very wide range of load conditions. These structures must be able to plastically deform and absorb energy but at the same time they must be capable of maintaining their integrity. When in use, these structures can be simultaneously subjected to temperatures (that can range from -40 to 80ºC) and impact loads, which demands full knowledge of the behaviour of CFRP when operating under those circumstances [1, 2], especially considering that during their life cycle these structures will experience aging.

Epoxy resins, such as the resin matrix used in composites materials, absorb moisture from humid environments. This moisture absorption can be attributed largely to the moisture affinity of specific functional groups of a highly polar nature in the cured epoxy resin [3]. As the fibres are not susceptible to water ingress, the behaviour of diffusing moisture in composites is usually affected by the resin properties. The work of Apicella et al. [4] lists three distinct methods through which water ingress in polymers occurs. The first method is the bulk dissolution of water, through the polymer network. The second method is the creation of hydrogen bonds between suitable polymers groups and the polar water molecules. Finally, another process is described by which water occupies the vacuoles caused by the free space on the glassy structure. A combination of two of these modes might lead to a dual behaviour in the water absorption process [5, 6]. When these water absorption processes reach their limit, the polymer will swell [7], with the local degree of swelling depends on the local water concentration. As a result, the most swollen regions experience a compressive force, whereas less swollen regions experience tensile forces

[8]. The tensile stress can enhance the water transport rate. Such a self-induced stress can cause a non-Fickian behaviour.

Several mathematical models can be used to predict moisture transport in epoxy resin and epoxy composites using concentration and stress dependent diffusion coefficients [9]. Moisture absorption or cyclic absorption and desorption at high temperatures and relative humidity can cause voids and/or microcracks in epoxy resins. If these effects are extensive, conditions for non-Fickian transport can be induced. Thus, it is possible to expect non-Fickian transport as well as Fickian diffusion, according to the resin properties and environmental conditions [10]. Fickian diffusion model with a constant diffusion coefficient can be effectively used to model the moisture absorption process in composites [11].The presence of absorbed water is known to lower the glass transition temperature (T_g), as it plasticizes polymer chains, with consequences to the thermal and long term performance of the materials [12]. Several authors [13, 14], tested composite materials after hygrothermal aging and observed that the T_g decreases with the increment of moisture absorption.

Ashcroft et al. [15] investigated the effects of humidity and temperature on the strength of composite bonded joints and indicated that the bonding strength can increase depending on the matrix material. Zhong et al. [16] manufactured three groups of unidirectional CFRP laminates, one group was immersed in water until saturation, while another group was subjected to 78 days of hygrothermal cycling. After absorbing around 1.7% of moisture (by weight), both the impact energy absorbed through elastic deformation and the incipient damage load or load corresponding to incipient damage point, increased by 21 and 39.1%, respectively. Ahmad et al. [17] assessed the hygrothermal effects (aged at 80°C and using deionized water) on the low-velocity impact (3.71 m/s corresponding to 23.62 J) behaviour of unidirectional composite plates for aircraft applications. The experimental results showed that the moisture content played a negative role by decreasing the impact resistance of composite plates.

The literature demonstrates that the ingress of water in adhesive joints can be accurately modelled with a variety of different models, allowing to correctly predict the state of hygrothermal aging. These studies agree that water greatly influences the mechanical behaviour of composite substrates and adhesives. The influence of moisture is almost always detrimental and that plasticization of the adhesive (and the matrix of the composite) due to water ingress and this plays a key role on the joint strength.

This work aims to assess the behaviour of SLJs manufactured using CFRP and aluminium substrates subjected to the following environmental conditions: unaged, hygrothermally aged (immersed in deionized water at 50°C for 2000 hours) and dried after hygrothermal aging (at 50°C). The behaviour of the joints was assessed under quasi-static and impact conditions. To help interpret the results of the SLJ testing, complementary tests were performed to assess the moisture diffusion on the bulk adhesive and CFRP substrates, determine the influence of the moisture on the glass transition temperature of the adhesive and identify any changes in the chemistry of the materials induced by the moisture. Bulk tensile testing was also carried out on the adhesive to assess its mechanical properties as a function of the hygrothermal aging state.

2. Experimental details

2.1. Materials

2.1.1. Substrates

Two different materials were used as substrates for this work: unidirectional CFRP plates and an aluminium alloy. The CFRP plates used in this work are manufactured from SEAL® Texipreg HS 160 RM prepregs, laminated at 0º of orientation. The mechanical elastic properties of this material, at room temperature, were already previously described in previous works [18-20]. The 5754-H22 alloy, which is typically employed in the automotive industry, was used in this work. The 1.5 mm thickness of the 5754-H22 aluminium alloy substrates was selected as it closely matches the typical thicknesses used in vehicle body construction. To avoid interfacial failures, the 5754-H22 aluminium alloy is used in an anodized state. The 5754-H22 aluminium alloy used has an elastic modulus of 69 GPa, with a Poisson´s ratio of 0.33.

2.1.2. Crash-resistant adhesive

The adhesive used in this work is a crash resistant epoxy-based adhesive, commercially designated as XNR6852 E-3 and is manufactured by Nagase ChemteX® (Osaka, Japan). This adhesive, formulated for the automotive industry, is extremely tough and excels under impact loads, with a very significant energy absorption capability. This epoxy adhesive was previously experimentally characterized by the authors [21, 22] and the

main mechanical properties are presented in Table 1. The curing process of the XNR6852 E-3 adhesive consists on a three-hour stage at 150°C.

Table 1 – Cohesive properties of Nagase ChemteX® XNR6852E-3 epoxy adhesive under quasi-static and impact conditions [21, 22].

Mechanical Properties	1 mm/min	3 m/s
Young's modulus, E [MPa]	1874	3667
Shear modulus, G [MPa]	665	603
Tensile strength, σ_n [MPa]	48	72
Shear strength, t_s [MPa]	45	43
Fracture energy (mode I), G_{IC}[N/mm]	9	13
Fracture energy (mode II), G_{IIC}[N/mm]	72	104

2.2. Specimens fabrication

2.2.1. CFRP specimens

Two distinct types of specimens manufactured with CFRP were used in this work, namely, in SLJs as substrates and as bulk plates for the assessment of the hygrothermal aging. CFRP plates with a thickness of 2.1 mm (a total of 14 prepreg plies) were used for the SLJs substrates and 1 mm thick plates (a total of 7 plies) were produced to suit the specimens used in the hygrothermal aging (dimensions of 60x60 mm, based on ISO/DIS 294-3 [23]). This material was cured following a one-hour stage at 130°C.

The overlap areas (in the SLJs), as well as the exposed surface the hygrothermal aging specimens were lightly sanded manually using a 90-grit sandpaper. This was performed with the objective of removing any silicone film or release agent that might have been picked up from the surface of the mould used, as well as improving the surface roughness and adhesion (in the case of the SLJs). This surface treatment also allows for better water absorption through the removal of the glossy resin on the surface of the hygrothermal aging specimens.

2.2.2. Adhesive bulk plates

Bulk plates of the XNR6852 E-3 adhesive were manufactured for the assessment of the hygrothermal aging and drying processes, as well as determining the influence of those

processes in the mechanical properties of the material, following the French NF T 76-142 standard [24]. The 1 mm thick adhesive plates (for hygrothermal aging) were then machined to the final dimensions of 60x60 mm (based on ISO/DIS 294-3 [23]) and the 2 mm thick plates (for determination of tensile properties) were machined according the "dogbone" geometry presented in Figure 1, which follows the BS 2782 standard [25]. These specimens were manufactured to be tested under quasi-static (1 mm/min) conditions.

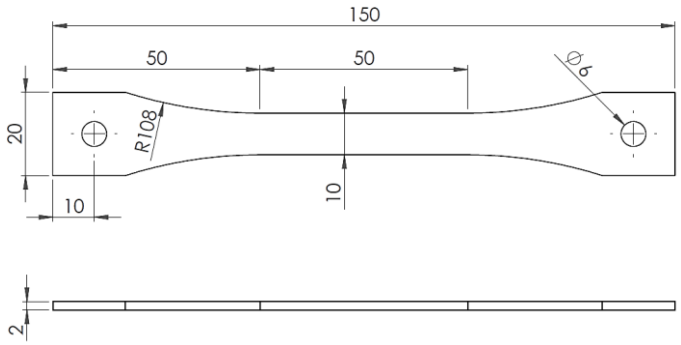

Figure 1 – Geometry of the tensile specimen ("dogbone") accordingly to BS 2782 (dimensions in mm) [25].

2.2.3. Single lap joints

SLJs were manufactured with an overlap length of 25 mm (Figure 2). The substrates thickness was representative of automotive applications, being 2.1 mm for the CFRP substrates and 1.5 mm for the Al5754-H22. The adhesive layer thickness used was 0.2 mm, which ensures optimal performance of the adhesive. The SLJ specimen geometry is based on the ASTM D1002-99 [26] and ISO 4587:1995 [27] standards. The overlap length of 25 is very typical for this type of studies [28, 29].

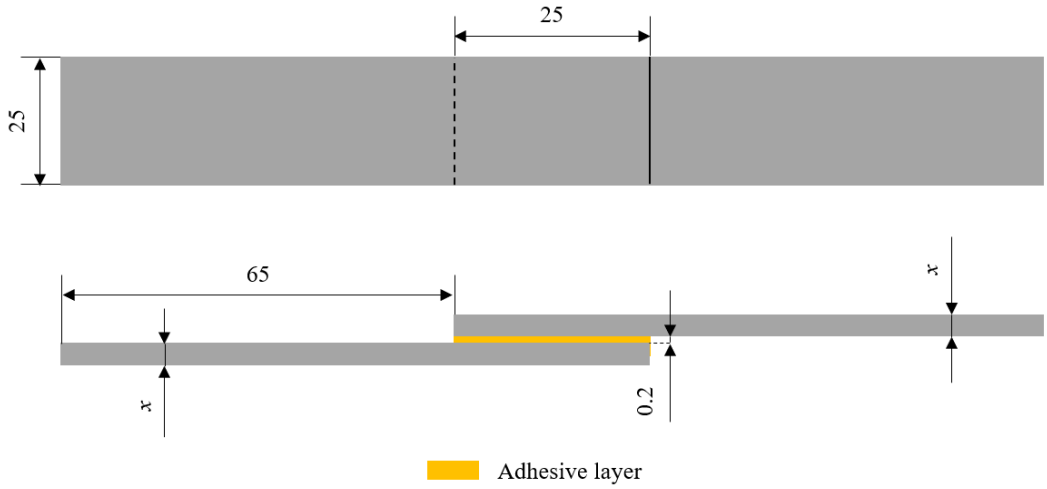

X corresponds to the substrate thickness: 2.1 mm for the CFRP and 1.5 mm for the aluminum alloy 5754-H22.

Figure 2 – Schematic representation of the geometry of SLJ specimens (dimensions in mm).

Considering the two distinct substrates under study (CFRP and 5754-H22 aluminium alloy), it is possible to manufacture two combinations of SLJs, one with similar substrates (CFRP + CFRP) and another with dissimilar substrates (CFRP + Al5754-H22).

A total of six specimens were tested for each condition: quasi-static (1 mm/min), and impact (3 m/s), repeated for each of the three different hygrothermal aging states (unaged, hygrothermally aged and dried after hygrothermal aging).

2.3. Testing procedures

2.3.1. Hygrothermal aging and desorption process of bulk adhesive and CFRP

The determination of the moisture diffusion was performed using the bulk plate specimens of the XNR6852 E-3 adhesive and the CFRP. A total of six plates were considered for the absorption study for each material being studied. Using the same value of thickness (1 mm) allows to compare the absorption rate between both materials and ensures that diffusion is one dimensional.

After being manufactured, all specimens were kept in a container with silica desiccant, to remove any moisture that might have been absorbed from the environment during their preparation. In addition, prior to the initiation of the absorption tests, the specimens were placed in an oven and dried at 50ºC and 10% of moisture. Measurements were carried out until a constant mass was attained.

The specimens were weighed using a microbalance with 1 mg of accuracy (Kern-Toledo, Balingen, Germany). After weight stabilization, the specimens were immersed in deionized water (in a closed glass container, each specimen being positioned in the middle of the liquid medium using a nylon wire, exposing the entire surfaces) and kept at a constant temperature of 50 ± 2°C, selected according to the ISO 62:2008 [30] standard. The period of immersion was 2000 hours. The selected temperature is significantly lower than the T_g of the materials under study, ensuring that only physical processes ensue, and no chemical changes on both materials would occur [1, 31].

All the specimens were kept immersed in deionized water until the moisture absorption mass stabilized (designated as infinite mass (M_∞)). In the case of the XNR6852 E-3 adhesive a constant value of the maximum moisture absorption was observed. In the case of the CFRP it was not possible to fully saturate this material, and the maximum water uptake considered corresponds to the last measurement.

After a time period of 2000 hours immersed in deionized water was completed, the specimens were manually dried (water removed from the surface using paper), and thereafter stored inside a glass container full of silica desiccant in the same climatic chamber at 50°C. The drying process was performed until no water was present in the adhesive, assessed by regular mass measurements performed as previously described for the absorption process.

2.3.1.1. Gravimetric analysis

All the XNR6852 E-3 adhesive plate specimens had their weight regularly measured until saturation was achieved. The maximum aging period was set to reduce the probability of interfacial failure of the SLJs. In the case of the CFRP plates, this aging period was not enough to reach saturation. The process of weighing the specimens started with the removal of the water of the surface with a dry cloth, the specimens being handled with gloves to prevent the contamination of the surface.

The moisture uptake M_t was determined using the following equation:

$$M_t = \frac{w_t - w_0}{w_0} \times 100\% \quad (3)$$

Where, w_t corresponds to the mass of the specimen while immersed in deionised water, and w_0 is the initial constant mass. The saturation of the mass uptake in considered to occur when the overall weight gain increases less than 1% after three consecutive measurements.

2.3.1.2. Diffusion analysis

Using the diffusion coefficient (D) it is possible to quantify the absorption behaviour of the XNR6852 E-3 adhesive and the CFRP. The most common approach to model moisture sorption is the Fick´s law, which can forecast the mass of water absorbed. The simple Fickian diffusion assumes that the moisture flux is directly proportional to the concentration gradient in a material. When moisture uptake occurs, the absorbed mass of water follows a linear increase with the square root of time, thereafter, slowly decreasing until equilibrium is achieved (M_∞). In general, the moisture absorption of adhesives and some composite materials (accordingly to the resin properties and environmental conditions, as experimentally assessed by some authors [9, 32]) under hygrothermal conditions can be described by Fick´s law [33] and presented by Equation 4.

$$\frac{\partial c}{\partial t} = D\frac{\partial^2 c}{\partial x^2} \tag{4}$$

Where, D is the coefficient of diffusion, c is the concentration of water and t is time of the process. Crank [34] suggests a simplification of Equation 3, stating that for the initial stage of the process, where $\frac{M_t}{M_\infty} < 6$, the resulting relationship can be applied as follows:

$$\frac{M_t}{M_\infty} = \frac{4}{\sqrt{\pi h}}\sqrt{Dt} \tag{5}$$

For several materials, due to their chemical properties, it is necessary to consider the dual Fickian models [35], and two distinct diffusion mechanisms working simultaneous occur, where the fractional mass uptake increases continuously until M_∞ is reached. Such models are commonly designated as “parallel dual Fickian” (PDF). By assuming a pseudo-equilibrium state at intermediate exposure times prior to reaching the final saturation, Ameli et al. [36] developed the “sequential dual Fickian” (SDF) model

(Equation 7), specifically for highly toughened epoxy adhesives, as in the case of the XNR6852 E-3 adhesive being used in this work.

$$M_t = \left(1 - \frac{8}{\pi^2}\sum_{n=0}^{\infty}\frac{1}{(2n+1)^2}exp\left(\frac{-D_1(2n+1)^2\pi^2 t}{4h^2}\right)\right) \times M_{1\infty} + \emptyset(t - t_d) \times \left(1 - \frac{8}{\pi^2}\sum_{n=0}^{\infty}\frac{1}{(2n+1)^2}exp\left(\frac{-D_2(2n+1)^2\pi^2 t}{4h^2}\right)\right) \times M_{2\infty} \quad (6)$$

Being $M_{1\infty}$ and $M_{2\infty}$ the first and second uptakes, and $M_{1\infty} + M_{2\infty} = M_{\infty}$.

Rearranging both Equation 6 and Equation 7, the relationship for D is given by:

$$D = \pi\left(\frac{h}{4M_{\infty}}\right)^2\left(\frac{M_t}{\sqrt{t}}\right)^2 \quad (7)$$

2.3.1.3. Fourier transform infrared spectroscopy (FTIR)

The FTIR measurements were carried in a Bruker Vertex 70 (Billerica, MA, USA) spectrometer. The tests were performed using a wavelength of 4000-500 cm^{-1} and 0.2 cm^{-1} of scanning velocity. A $LiTaO_3$ detector (15,500-370 cm^{-1}) and a KBr window were used. A total of nine tests were performed for each material, namely, three for each condition (unaged, hygrothermally aged and dried after hygrothermal aging).

2.3.2. Measurements of the glass transition temperature (T_g)

The glass transition temperature, T_g, relates the mechanical behaviour of the materials with the temperature, and it is critical to understand where the glass transition zone is located for materials that will operate under wide temperature ranges [37]. An in-house developed apparatus (constructed according to the principles described by Zhang *et al*. [38]) was used for this purpose.

2.3.3. Quasi-static testing procedure

The quasi-static tests were performed using an INSTRON® 3367 (Norwood, Massachusetts, USA) universal testing machine, equipped with a 30 kN load cell. An optical extensometry method was used for the XNR6852 E-3 adhesive tensile bulk specimens. Digital images were recorded every five seconds using a digital camera and

after the test was concluded, a Matlab® subroutine was used to process the images, enabling the determination of the strains present in the specimen via image correlation. Stress-strain (P-δ) curves were obtained for each test. Nine specimens were tested per condition (unaged, hygrothermally aged and dried after hygrothermal aging).

2.3.4. Impact testing procedure

Impact testing was carried out using a Rosand® instrumented falling weight impact tester, type 5 H.V. (Stourbridge, West Midlands, U.K). equipped with of 60 kN load cell. The perform each test, a weighted mass was released from a pre-set height (which defines impact and energy), falling until it hits a specially designed clamp, bolted to the lower substrate of the SLJ specimen. The drop height was set to reach an impact speed of 3 m/s, which, given the specimen geometry, corresponds to a strain rate of 15000 s^{-1}. The impactor used has a total mass of 26 kg, which results in an impact energy of 117 J, enough to break all specimen configurations under study. Due to the wide dispersion inherent to this type of test, six specimens were experimentally tested per configuration.

3. Results and discussion

3.1. Moisture diffusion of the bulk adhesive and the CFRP substrates

The XNR6852 E-3 adhesive samples achieved complete water saturation during the aging process. The most suitable mathematical model of diffusion (for both the absorption and desorption phases) was found to be the Sequential Dual Fickian (SDF) model. The model fitted to the experimental data is shown in Figure 3.

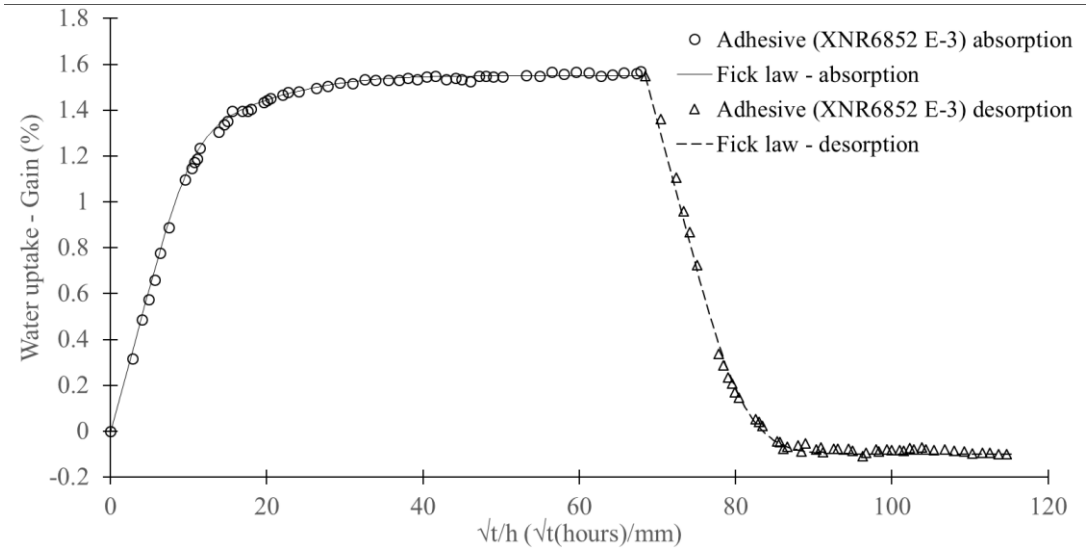

Figure 3 – Moisture absorption and desorption of the XNR6852 E-3 adhesive, as well the SDF fit curve – results presented as a function of hours for better display of the results.

The maximum gain of water registered by the XNR6852 E-3 adhesive was of approximately 1.6%. By proceeding with the drying process after hygrothermal aging it was observed that a small percentage of water (approximately 0.1%) was removed, in comparison with the initial average valued measured in the unaged condition. Such phenomena might be explained by the relaxation of the molecular chains of the XNR6852 E-3 epoxy adhesive, enabling a rearrangement of the structure and creating enough space for the internally trapped water to be released. These results also show that the desorption process was faster than the absorption process.

The general properties of absorption and desorption of water of the XNR6852 E-3 adhesive are presented in Table 2.

Table 2 – General properties of absorption and desorption of water by the XNR6852 E-3 adhesive.

Stage	Property	
Absorption	$M1_\infty$ (%)	0.012
	$D1$ (m^2s^{-1})	19E-13
	$M2_\infty$ (%)	0.0035
	$D2$ (m^2s^{-1})	28E-14
Desorption	$M1_\infty$ (%)	0.013
	$D1$ (m^2s^{-1})	14E-13
	$M2_\infty$ (%)	0.0035
	$D2$ (m^2s^{-1})	10E-13

As for the CFRP, it was not possible to determine the Fick´s law as the material did not reach the maximum water absorption after 2000 hours (Figure 4).

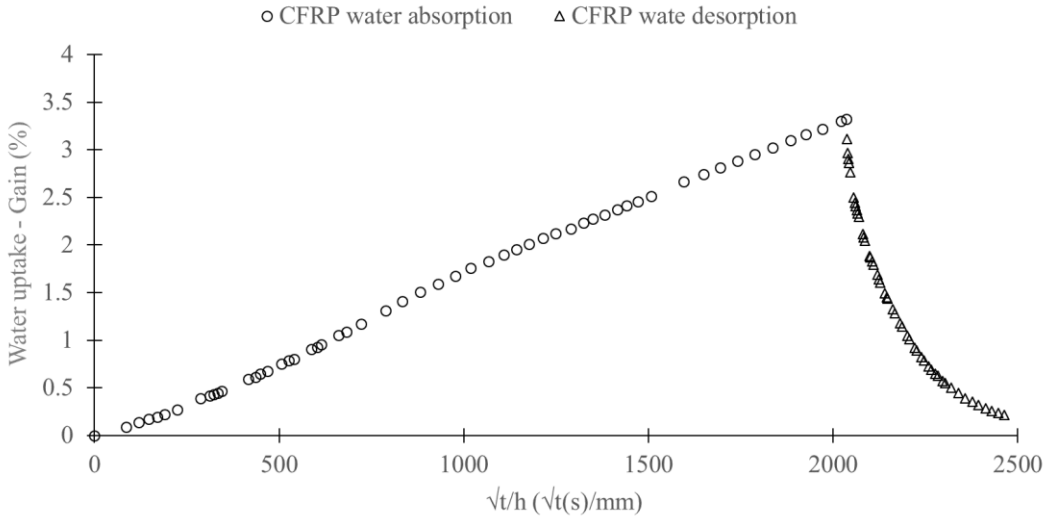

Figure 4 – Moisture absorption and desorption of the CFRP results presented as a function of seconds for better display of the results.

The maximum water uptake registered for the CFRP was of 3.3%, a value greater than that of the XNR6852 E-3 adhesive. It is possible to observe that, similarly to the XNR6852 E-3 adhesive, the water ingress followed a linear behaviour. It is therefore reasonable to expect that, after a long aging period (up to several years) the moisture diffusion of CFRP would fit a Fickian law [39].

When performing the drying process that followed the hygrothermal aging, a high rate of water desorption in the CFRP was observed, although 0.23% of water remained locked in the CFRP after the drying process was completed. This is in contrast with the behaviour of the XNR6852 E-3 adhesive, which completely lost its absorbed water in the same time period. This type of behaviour was observed by Arnold et al. [40], and after excluding likely causes such as microcracks and chemical changes, the most plausible intervening mechanism might be the slow molecular relaxation, allowing for additional pockets of free volume for the water molecules to occupy. The authors also found that such process will not depend of the presence or absence of carbon fibres. The presence of water when drying the specimens after hygrothermal aging could be explained by the relaxation process which caused some liquid molecules to become trapped in molecular cavities.

3.2. Measurement of T_g

The T_g of the adhesive and the composite pre-preg resin was measured to determine the influence of hygrothermal aging on its value. The variation of the T_g of the XNR6852 E-3 adhesive and the resin of the CFRP substrates is shown in Figure 5.

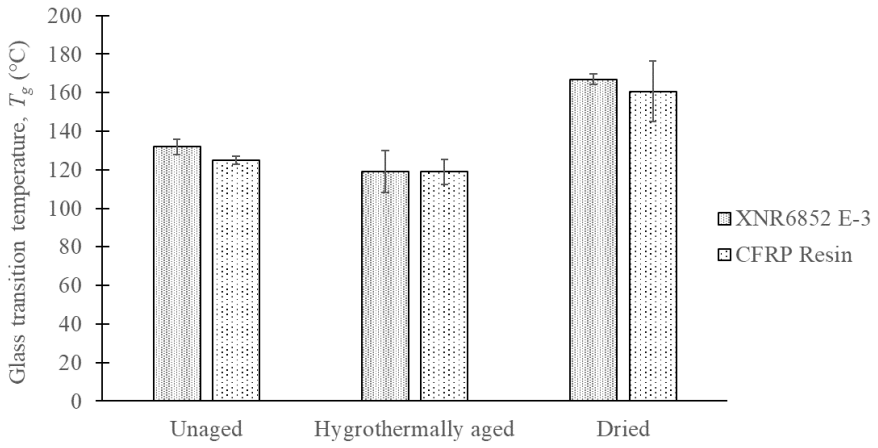

Figure 5 – Glass transition temperature T_g of adhesive XNR6852 E-3 and CFRP resin in the following conditions: unaged, hygrothermally aged and dried.

A similar trend was found for both the XNR6852 E-3 adhesive and the resin of the CFRP substrates under the three conditions under study (unaged, hygrothermally aged and dried after aging). A slight drop in the T_g value was observed when the samples were hygrothermally aged, which might be explained by the phenomena of plasticization of the polymer network due to the ingress of water, which was initially faster due to the voids present in the materials polymer networks. The value of T_g increased for both materials after drying, reaching values higher than those obtained prior to the hygrothermal aging. Such result might be due to the softening of the polymer network due to rearrangements of chains. The drying process is thought to have led to an increase in crosslinking between some polymeric chains, affecting the material properties as well as inducing a post-curing effect. It is also likely that, as a consequence of the water desorption, larger voids appeared between the molecular chains, representing free space that was previously occupied by water. All these factors led to noticeable changes of the material behaviour, reflected in changes in the T_g.

3.3. Bulk tensile tests of XNR6852 E-3 adhesive

The results obtained after room temperature tensile testing of the XNR6852 E-3 adhesive bulk specimens are presented in Figure 6 (examples of *P-δ* curves obtained).

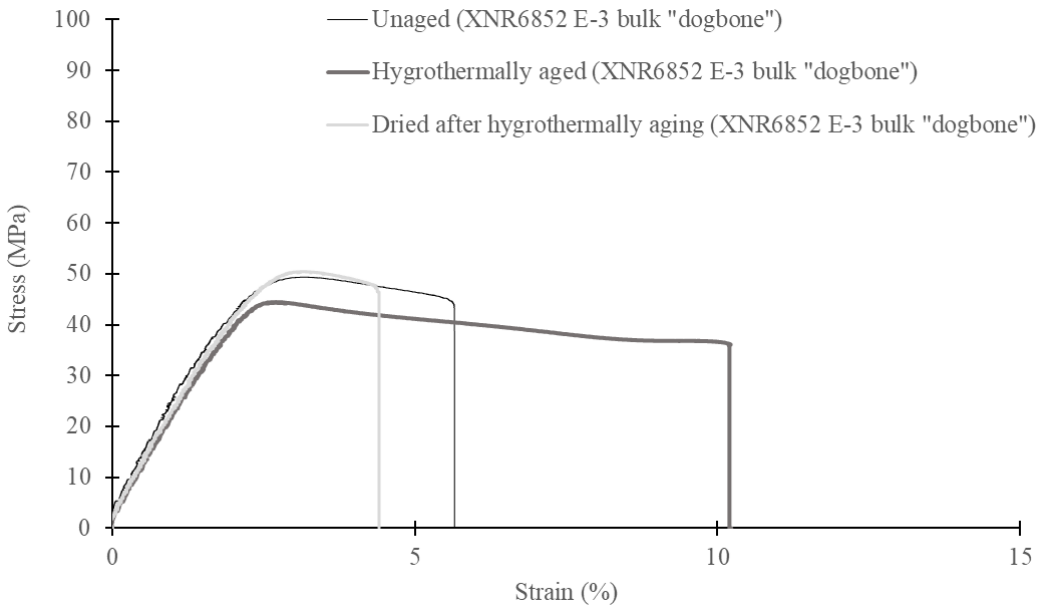

Figure 6 – Example of stress-strain (P-δ) curves obtained from XNR6852 E-3 adhesive bulk "dogbone" specimens tested at room temperature and at quasi-static (1 mm/min) conditions in the three distinct states: unaged, hygrothermally aged and dried after hygrothermal aging.

It is possible to conclude that the value of Young´s modulus does not change substantially with the hygrothermal aging processes. In terms of tensile strength, there was a decrease of about 10%. The most affected parameter after the hygrothermal aging process was the strain to failure, which increased around 50% and could be explained by the relaxation of the polymeric chains and its rearrangement.

A slight increase of the tensile strength was observed after the drying process, with a value very close to that obtained for the unaged condition. It is therefore possible to conclude that this mechanical parameter was fully recovered. Concerning the strain to failure, a significant reduction was recorded after drying, with the average value being lower than that obtained for the unaged condition.

3.4. Fourier transform infrared spectroscopy (FTIR)

Unaged and hygrothermally aged XNR6852 E-3 adhesive samples were analysed by FTIR. Figure 7 shows the spectrum in the 4000–500 cm^{-1} wavenumber range of adhesive,

for the two states of moisture level under study: unaged, and at maximum water absorption.

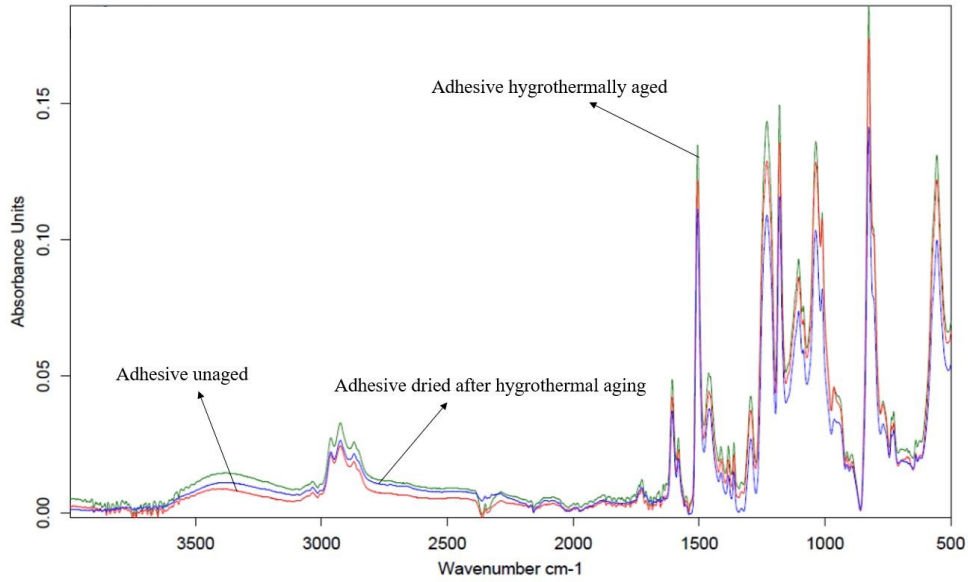

Figure 7 – FTIR spectrum, in the 4000-500 cm^{-1} wavenumber range of XNR6852 E-3 adhesive for different conditions (unaged, hygrothermally aged and dried after hygrothermal aging).

Analysis of the spectra allows to conclude that the spectra are quite similar, indicating that there are no significant and permanent changes in the chemical structure of the XNR6852 E-3 adhesive due to the hygrothermal aging process. Following the process of water desorption, it was again observed that the spectrum remains similar to the unaged condition. There are no significant changes to the peaks of the oxirane and benzene rings, which leads to the conclusion that no permanent chemical changes have occurred for the XNR6852 E-3 adhesive. It was only possible to observe that, for the dry after hygrothermal aging condition, there was a decrease of the absorbance of –OH, comparatively to the spectrum obtained in the hygrothermally aged condition. The FTIR analysis therefore corroborates the results obtained after tensile testing of the XNR6852 E-3 adhesive bulk specimens.

3.5. Quasi-static conditions

3.5.1. Fracture surfaces

Representative fracture surfaces of joints with similar and dissimilar substrates combinations, tested under quasi-static conditions are presented in Table 3, considering unaged, hygrothermally aged and dried conditions.

Table 3 – Representative failure surfaces of similar and dissimilar SLJs configuration tested under quasi-static conditions (1 mm/min) as a function of different testing conditions (unaged, hygrothermally aged and dried after hygrothermal aging).

Condition	**Joint configuration**	
	CFRP + CFRP	CFRP + Al5754-H22
Unaged	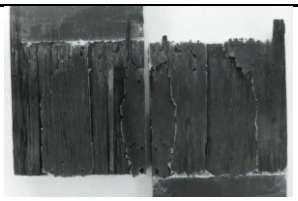	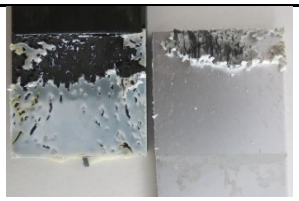
	Delamination of CFRP	Delamination of CFRP
Hygrothermally aged	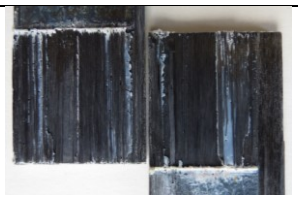	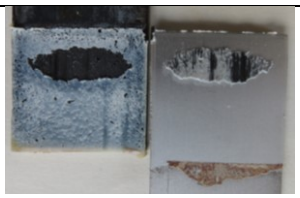
	Delamination of CFRP	Delamination of CFRP
Dried	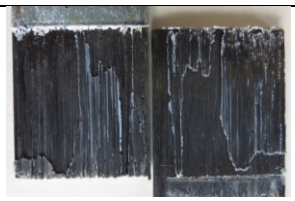	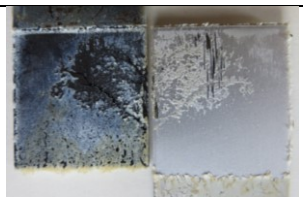
	Delamination of CFRP	Delamination of CFRP

In the case of joints manufactured with a similar combination of CFRP substrates, it was possible to observe that for the three stages (unaged, hygrothermally aged and dried after hygrothermal aging) the dominant type of failure was delamination of the CFRP substrate. When subjected to hygrothermal aging, the joints manufactured with similar CFRP substrates exhibited less severe delamination of the CFRP, possibly due to the large level of plasticization of both the CFRP substrate and the XNR6852 E-3 adhesive, as evidenced by the previously described adhesive bulk tensile tests and FTIR results, corroborated by the visible discolorations on the plasticized regions of the overlap length.

The fracture surface obtained when drying the SLJs after hygrothermal aging was considered as representative of a behaviour between that exhibited by the unaged and hygrothermally aged conditions. Although severe delamination occurred, a change of the surface colour (due to water ingress) was found. This discoloration was also found for specimens tested after the hygrothermal aging process.

The failure surfaces of joints manufactured with dissimilar substrates combination (CFRP + Al5754-H22) evidence bending and plastic deformation of the 5754-H22 aluminium substrate (less thick than the CFRP substrate, leading to unbalanced joint stiffness), which caused a large increase of peel forces and therefore led to premature failure of the joint by adhesive failure. This can be demonstrated by the portion of the XNR6852 E-3 adhesive present on the surface of the 5754-H22 aluminium, near the end of the overlap length – a region less affected by the peel forces. The failure surface of joints with dissimilar substrates combination also revealed a slightly lower degree of XNR6852 E-3 adhesive layer plasticization due to the water ingress being limited in one of the surfaces (5754-H22 aluminium bonded section).

3.5.2. Failure load

The failure load values of joints tested under quasi-static load, considering the three distinct aging conditions are shown in Figure 8.

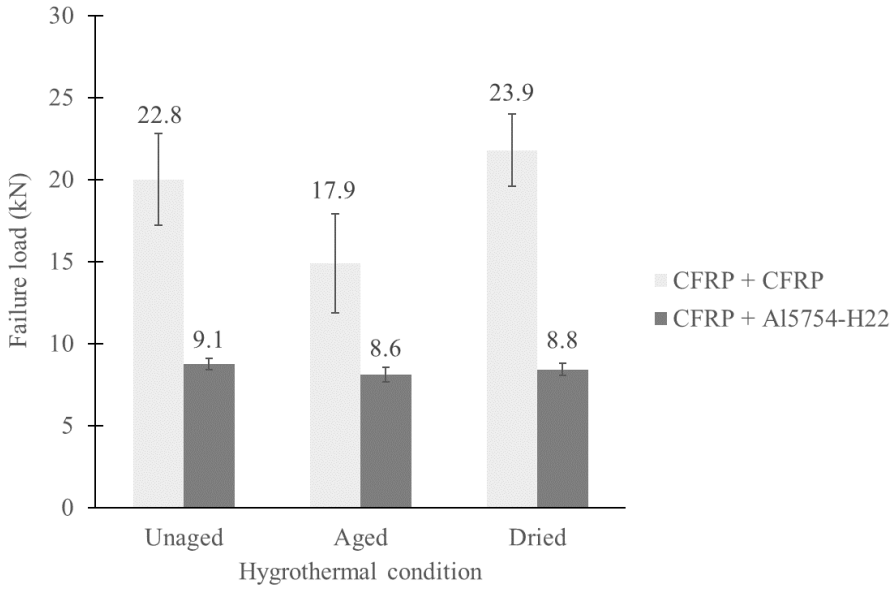

Figure 8 – Failure load results of joints manufactured with similar and dissimilar combination of substrates (CFRP and Al 5754-H22) tested under quasi-static (1 mm/min) load, as a function of unaged, hygrothermally aged ("Aged") and dried after hygrothermal aging ("Dried") conditions (maximum values presented).

In the case of joints manufactured using similar substrates of CFRP, where the failure mode was delamination of CFRP, it was possible to verify that with hygrothermal aging of the joints there was a significant decrease of the failure load, due to the plasticization of the CFRP substrates and the XNR6852 E-3 adhesive and, as observed from the bulk adhesive tensile testing there was a decrease of its tensile strength. Drying after hygrothermal aging revealed that the joints were able to fully recover their strength to failure (also in accordance with the bulk adhesive tensile testing behaviour), with the average values of failure load being higher than those obtained for unaged joints, In this case, the plasticization of CFRP substrates allowed for improved joint flexibility, compensating the reduction of strain to failure of the XNR6852 E-3 adhesive. It was also observed that the failure load of the dissimilar joints (CFRP + Al5754-H22) was almost identical, independently of the aging state of the joint. Such fact, associated to the similar failure surfaces and the plastic deformation of the 5754-H22 aluminium, is a clear indicator that the potential strength of the adhesive was never fully achieved, with the joint strength being limited by the early occurrence of large peel forces.

Therefore, the failure load at which the joints with dissimilar substrates (CFRP + Al5754-H22) failed was below that necessary to cause the failure by delamination of the CFRP substrates. The results also show that the influence of hygrothermal aging and drying is not felt.

3.5.3. Energy absorbed

The values of failure energy absorbed by the joints tested under quasi-static load, considering the three distinct aging conditions are shown in Figure 9.

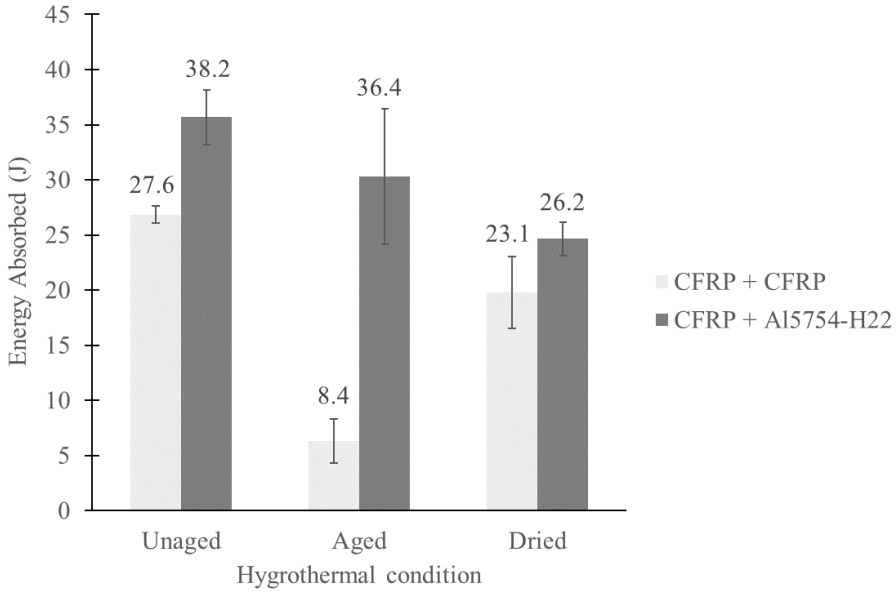

Figure 9 – Energy absorbed results of joints manufactured with similar and dissimilar combination of substrates (CFRP and Al 5754-H22) tested under quasi-static (1 mm/min) load, as a function of unaged, hygrothermally aged ("Aged") and dried after hygrothermal aging ("Dried") conditions (maximum values presented).

The energy absorbed by joints manufactured with similar combinations of CFRP substrates followed to same trend as the failure load, namely, decreasing after being hygrothermally aged and increasing when dried after hygrothermal aging. In this last condition the values were lower than those registered for joints tested in unaged condition. This might be explained by the by the presence of small cracks or increase of voids in the CFRP polymeric matrix.

For the case of joints manufactured with dissimilar substrates (CFRP + Al5754-H22) combinations, the trend is inverse of that observed for the joint failure load, as the energy absorbed significantly decreases after hygrothermal aging. Although the energy absorbed increased after the joints were dried, such value was still inferior to the one obtained for unaged joints.

3.6. Impact conditions

3.6.1. Fracture surface

Representative fracture surfaces of the joints (with similar and dissimilar substrates combinations) tested under impact load are presented in Table 4, considering the three aging conditions.

Table 4 – Representative failure surfaces of similar and dissimilar SLJs configuration tested under impact conditions (3 m/s) as a function of different testing conditions (unaged, hygrothermally aged and dried after hygrothermal aging).

Condition	**Joint configuration**	
	CFRP + CFRP	CFRP + Al5754-H22
Unaged	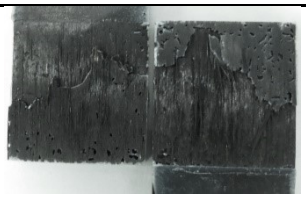	
	Delamination of CFRP	Delamination of CFRP
Hygrothermally aged		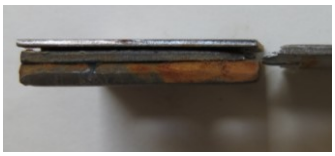
	Delamination of CFRP	Delamination of CFRP
Dried	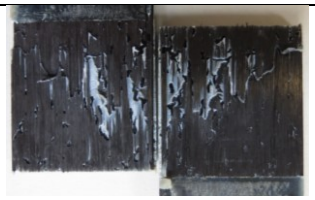	
	Delamination of CFRP	Delamination of CFRP

The fracture surface of joints manufactured using similar combination of CFRP substrates are indicative of delamination failure for all the three aging conditions tested. Due to the plasticization of the CFRP substrate after hygrothermally aging (evidenced by the large value of strain to failure exhibited by this condition during tensile testing), the fracture surface is indicative of a more severe failure of the joint by delamination of the CFRP substrates, and a similar failure surface was found when the joints were dried (specimens showed some discoloration on region of the overlap length).

When considering joints manufactured with dissimilar substrates (CFRP + Al5754-H22), independently of the joint condition (unaged, hygrothermally aged and dried), the failure of the joint always occurred in the grip area. As was the case for the quasi-static tests, the 5754-H22 aluminium substrates were significantly bent and plastically deformed during the impact tests, creating large peeling forces which strongly limit the maximum joint strength.

3.6.2. Failure load

The failure load values of joints (with similar and dissimilar substrates combinations) tested under impact, considering the three aging conditions are shown in Figure 10.

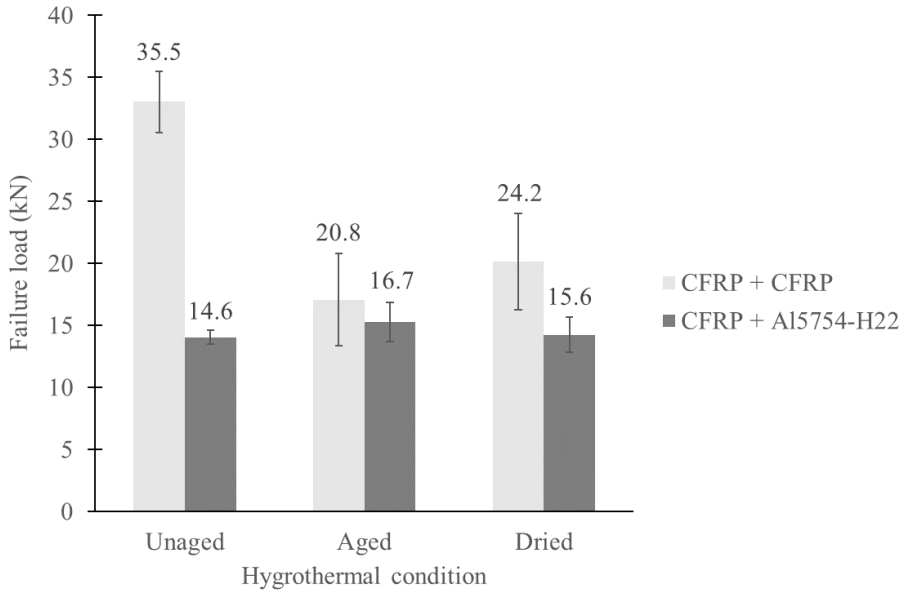

Figure 10 – Failure load results of joints manufactured with similar and dissimilar combination of substrates (CFRP and Al 5754-H22) tested under impact (3 m/s) load, as a function of unaged, hygrothermally aged ("Aged") and dried after hygrothermal aging ("Dried") conditions (maximum values presented).

All joints manufactured with dissimilar substrates (CFRP + Al5754-H22) presented almost identical average values of failure load, allowing to infer that this type of joint is insensitive to hygrothermal aging and drying under impact conditions. This behaviour is consistent with the previously described static tests.

A considerable drop of failure load occurred when testing joints manufactured only with CFRP substrates after hygrothermal aging. After drying, these joints were able to recover only a small amount of their strength, with the failure load values being closer to those of the hygrothermally aged joints than those of the unaged joints.

3.6.3. Energy absorbed

The values of energy absorbed by the joints (with similar and dissimilar substrates combinations) tested under impact load and considering the three distinct aging conditions are shown in Figure 11.

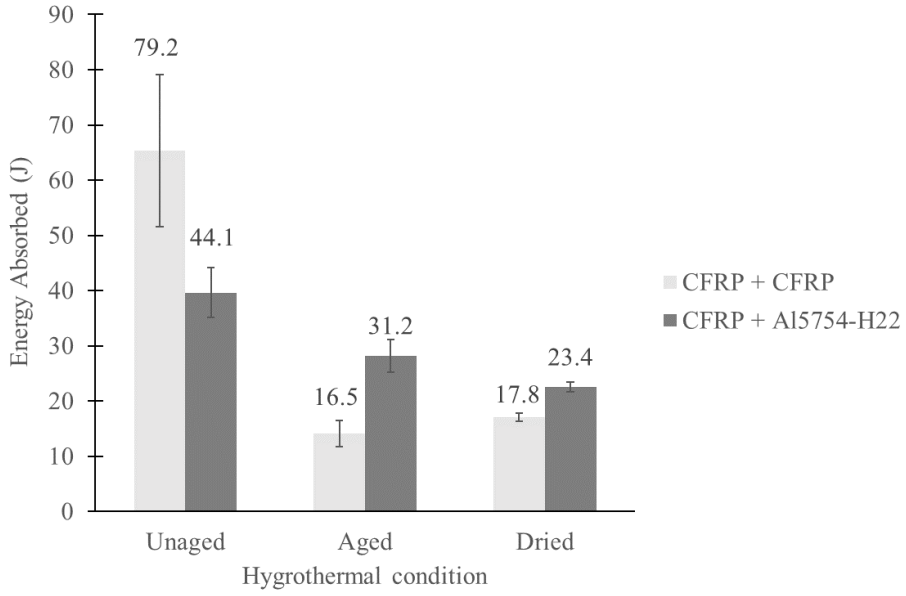

Figure 11 – Energy absorbed results of joints manufactured with similar and dissimilar combination of substrates (CFRP and Al 5754-H22) tested under impact (3 m/s) load, as a function of unaged, hygrothermally aged ("Aged") and dried after hygrothermal aging ("Dried") conditions (maximum values presented).

For both the joints manufactured with similar (CFRP + CFRP) and dissimilar (CFRP + Al5754-H22) substrates, there was a drop of energy absorbed under impact conditions, which was significantly higher for the case of similar joints using CFRP substrates (due to plasticization of the CFRP substrates). After drying the joints, only a small recovery of the energy absorbed by the joints using CFRP substrates was observed. As for the case of joints manufactured with dissimilar substrates (CFRP + Al5754-H22) there was a decrease of the energy absorption.

4. Conclusions

This work aims to assess the behaviour of adhesive joints manufactured with substrates typical of the automotive industry (CFRP and aluminium) when subjected to quasi-static and impact conditions in the following states: unaged, hygrothermally aged, and dried after hygrothermal aging. The main conclusion possible to be drawn from this work were:

- The moisture diffusion test show that the SDF model was able to satisfactorily model the absorption process of XNR6852 E-3 adhesive. As for the CFRP, a 2000-hour period at 50°C was not adequate to achieve full saturation, precluding the use of model to characterize water ingress.

- For joints manufactured with CFRP substrates, a significant decrease of the failure load was observed for both quasi-static and impact conditions after hygrothermal aging, even though a recovery in the failure load value was obtained for joints dried only under quasi-static conditions. Plasticization of the CFRP substrates was the cause for this behaviour.
- The experimental results have shown that in the case of joints manufactured using CFRP + Al5754-H22 substrates, for both quasi-static and impact conditions there was no significant change of the failure load, although a decrease on the energy absorbed by the joints was observed. The behaviour of these joints was controlled by the plastic deformation of the aluminium substrate.

Acknowledgments

The authors gratefully acknowledge the funding provided by PhD grant SFRH/BD/139341/2018 "Impact strength optimization with cohesive zone elements of multi-material bonded structures used in the automotive industry", Project Nº 028473 POCI-01-0145-FEDER-028473 "Design methodology for impact resistant bonded multi-material automotive structures (ImpactBondDesign)", Project NORTE-01-0145-FEDER-000022 – "SciTech - Science and Technology for Competitive and Sustainable Industries", co-financed by Programa Operacional Regional do Norte (NORTE2020), through Fundo Europeu de Desenvolvimento Regional (FEDER). The authors would also like to thank NAGASE ChemteX® for the financial support provided.

References

1. da Silva, L., *Handbook of adhesion technology*. 2011: Springer Science & Business Media.
2. Soykok, I.F., *Degradation of single lap adhesively bonded composite joints due to hot water ageing.* The Journal of Adhesion, 2017. **93**(5): p. 357-374.
3. Sethi, S. and B.C. Ray, *Environmental effects on fibre reinforced polymeric composites: Evolving reasons and remarks on interfacial strength and stability.* Advances in colloid and interface science, 2015. **217**: p. 43-67.
4. Apicella, A., R. Tessieri, and C. De Cataldis, *Sorption modes of water in glassy epoxies.* Journal of Membrane Science, 1984. **18**: p. 211-225.

5. Kaelble, D., P. Dynes, and E. Cirlin, *Interfacial bonding and environmental stability of polymer matrix composites.* The Journal of Adhesion, 1974. **6**(1-2): p. 23-48.
6. Joliff, Y., L. Belec, and J. Chailan, *Modified water diffusion kinetics in an unidirectional glass/fibre composite due to the interphase area: Experimental, analytical and numerical approach.* Composite Structures, 2013. **97**: p. 296-303.
7. Adamson, M.J., *Thermal expansion and swelling of cured epoxy resin used in graphite/epoxy composite materials.* Journal of materials science, 1980. **15**(7): p. 1736-1745.
8. Zhou, J. and J.P. Lucas, *The effects of a water environment on anomalous absorption behavior in graphite/epoxy composites.* Composites Science and Technology, 1995. **53**(1): p. 57-64.
9. Lee, M.C. and N.A. Peppas, *Models of moisture transport and moisture-induced stresses in epoxy composites.* Journal of Composite Materials, 1993. **27**(12): p. 1146-1171.
10. Augl, J.M. and A.E. Berger, *The Effect of Moisture on Carbon Fiber Reinforced Epoxy Composites. 1. Diffusion*. 1976, NAVAL SURFACE WEAPONS CENTER WHITE OAK LAB SILVER SPRING MD.
11. Shen, C.-H. and G.S. Springer, *Moisture absorption and desorption of composite materials.* Journal of composite materials, 1976. **10**(1): p. 2-20.
12. Viana, G., et al., *Water diffusion in double cantilever beam adhesive joints.* Latin American Journal of Solids and Structures, 2017. **14**(2): p. 188-201.
13. Choi, H., et al., *Hygroscopic aspects of epoxy/carbon fiber composite laminates in aircraft environments.* Composites Part A: applied science and manufacturing, 2001. **32**(5): p. 709-720.
14. Barbosa, A., L. da Silva, and A. Öchsner, *Hygrothermal aging of an adhesive reinforced with microparticles of cork.* Journal of Adhesion Science and Technology, 2015. **29**(16): p. 1714-1732.
15. Ashcroft, I., D. Hughes, and S. Shaw, *Adhesive bonding of fibre reinforced polymer composite materials.* Assembly Automation, 2000. **20**(2): p. 150-161.
16. Zhong, Y. and S.C. Joshi, *Impact behavior and damage characteristics of hygrothermally conditioned carbon epoxy composite laminates.* Materials & Design (1980-2015), 2015. **65**: p. 254-264.

17. Ahmad, F., et al., *Hygro effects on the low-velocity impact behavior of unidirectional CFRP composite plates for aircraft applications.* Composite Structures, 2016. **135**: p. 276-285.
18. Campilho, R.D.S.G., *Repair of composite and wood structures*. 2009, Instituto Superior de Engenharia do Porto.
19. Machado, J., et al., *Mode I fracture toughness of CFRP as a function of temperature and strain rate.* Journal of Composite Materials, 2016: p. 0021998316682309.
20. Machado, J., et al., *Mode II fracture toughness of CFRP as a function of temperature and strain rate.* Composites Part B: Engineering, 2017. **114**: p. 311-318.
21. Araújo, H., et al., *Dynamic behaviour of composite adhesive joints for the automotive industry.* Composite Structures, 2017. **171**: p. 549-561.
22. Machado, J., et al., *Strain rate dependence of a crash resistant adhesive as a function of temperature for the automotive industry.* Proceedings of the Institution of Mechanical Engineers, Part L: Journal of Materials: Design and Applications, 2019: p. 1464420719836914.
23. 294-3, I., *Plastics-injection moulding of test specimens of thermoplastic materials, part 3: small plates.* 2002: Switzerland.
24. 76-142, N.T., *Méthode de préparation de plaques d'adhésifs structuraux pour la réalisation d'éprouvettes d'essai de caractérisation*. 1998.
25. Standard, B., *BS 2782*, in *Methods of Testing Plastics, Part*. 1970.
26. ASTM, D., *1002.* Standard Test Method for Apparent Shear Strength of Single-Lap-Joint Adhesively Bonded Metal Specimens by Tension Loading (Metal-to-Metal), 2005. **15**: p. 45-48.
27. *ISO 4587: Determination of tensile lap-shear strength of rigid-to-rigid bonded assemblies.* 1995.
28. Fitton, M.D. and J.G. Broughton, *Variable modulus adhesives: an approach to optimised joint performance.* International Journal of Adhesion and Adhesives, 2005. **25**(4): p. 329-336.
29. da Silva, L.F.M. and R.D. Adams, *Adhesive joints at high and low temperatures using similar and dissimilar adherends and dual adhesives.* International Journal of Adhesion and Adhesives, 2007. **27**(3): p. 216-226.

30. ISO, E., *62 (2008).".* Plastics. Determination of water absorption," EU adoption of International Organization for Standardization, Geneva, Switzerland.
31. Viana, G., et al., *A review on the temperature and moisture degradation of adhesive joints.* Proceedings of the Institution of Mechanical Engineers, Part L: Journal of Materials: Design and Applications, 2017. **231**(5): p. 488-501.
32. Parker, B., *Some effects of moisture on adhesive-bonded CFRP-CFRP joints.* Composite structures, 1986. **6**(1-3): p. 123-139.
33. Lin, Y. and X. Chen, *Moisture sorption–desorption–resorption characteristics and its effect on the mechanical behavior of the epoxy system.* Polymer, 2005. **46**(25): p. 11994-12003.
34. Crank, J., *The Mathematics of Diffusion: 2d Ed*. 1975: Clarendon Press.
35. Loh, W., et al., *Modelling anomalous moisture uptake, swelling and thermal characteristics of a rubber toughened epoxy adhesive.* International journal of adhesion and adhesives, 2005. **25**(1): p. 1-12.
36. Ameli, A., et al., *Hygrothermal properties of highly toughened epoxy adhesives.* The Journal of Adhesion, 2010. **86**(7): p. 698-725.
37. da Silva, L., et al., *Effect of Low Temperature on Tensile Strength and Mode I Fracture Energy of a Room Temperature Vulcanizing Silicone Adhesive.* Journal of Testing and Evaluation, 2015. **44**(3).
38. Zhang, Y., R. Adams, and L. da Silva, *A rapid method of measuring the glass transition temperature using a novel dynamic mechanical analysis method.* The Journal of Adhesion, 2013. **89**(10): p. 785-806.
39. Arnold, J., S. Alston, and F. Korkees, *An assessment of methods to determine the directional moisture diffusion coefficients of composite materials.* Composites Part A: Applied Science and Manufacturing, 2013. **55**: p. 120-128.
40. Arnold, C., F. Korkees, and S. Alston. *The Long-Term Water Absorption and Desorption Behaviour of Carbon-Fibre/Epoxy Composites*. in *Proceeding of ECCM*. 2012.

Paper 17

Content of Paper 17

Abstract

1. Introduction

2. Experimental details

2.1. Material and properties

2.1.1. CFRP

2.1.2. Aluminium alloy

2.1.3. Crash resistant adhesive

2.2. Specimens fabrication

2.2.1. CFRP specimens

2.2.2. Adhesive bulk plates

2.2.3. Single lap joints

2.3. Testing procedures

2.3.1. Hygrothermal aging and desorption process of bulk adhesive and CFRP

2.3.2. Quasi-static testing procedures

2.3.3. Fatigue testing procedure

3. Results

3.1. Moisture diffusion of the bulk adhesive and the CFRP substrates

3.2. XNR6852 E-3 adhesive bulk “dogbone”

3.3. Quasi-static tests of single lap joints

3.3.1. Fracture surface

3.3.2. Failure load

3.4. Fatigue tests

3.4.1. SLJs with similar substrates

3.4.1.1. Failure surface

3.4.1.2. Stress versus the number of cycles at failure

3.4.2. SLJs with dissimilar substrates

3.4.2.1. Failure surface

3.4.2.2. Stress versus the number of cycles to failure

3.4.3. Fatigue life comparison

3.4.4. Residual strength of SLJs

4. Conclusions

References

Received: 2 April 2019 | Revised: 14 May 2019 | Accepted: 16 May 2019

DOI: 10.1111/ffe.13067

ORIGINAL CONTRIBUTION

WILEY FFEMS Fatigue & Fracture of Engineering Materials & Structures

Fatigue performance of single lap joints with CFRP and aluminium substrates prior and after hygrothermal aging

J. J. M. Machado[1] | E. A. S. Marques[1] | A. Q. Barbosa[1] | L. F. M. da Silva[2]

[1]UCVE, Instituto de Ciência e Inovação em Engenharia Mecânica e Engenharia Industrial (INEGI), Rua Dr. Roberto Frias, Porto 4200-465, Portugal

[2]Departamento de Engenharia Mecânica, Faculdade de Engenharia (FEUP), Universidade do Porto, Rua Dr. Roberto Frias, Porto 4200-465, Portugal

Correspondence
Lucas F. M. da Silva, Departamento de Engenharia Mecânica, Faculdade de Engenharia (FEUP), Universidade do Porto, Rua Dr. Roberto Frias, Porto 4200-465, Portugal.
Email: lucas@fe.up.pt

Abstract

Adhesive bonding has been extensively used to join composites and aluminium alloys in the automotive industry, but a deeper understanding of its fatigue behaviour is still required. This work presents a novel evaluation of the combined performance of joints manufactured with carbon fibre reinforced plastic (CFRP) and aluminium substrates subjected to fatigue loads in the unaged, hygrothermally aged, and dried after hygrothermal aging states. The experimental results allowed to conclude that the fatigue performance of joints can be affected by changes induced by the drying process or losses in the interface strength and that dissimilar combination of substrates sustains higher number of cycles to failure. The fatigue performance of joints with dissimilar substrates was found to be better than that of joints with similar substrates, which can be attributed to the lower stresses acting on the adhesive layer. The presence of water has also noticeably changed the fatigue performance of joints with dissimilar substrates.

KEYWORDS

CFRP, fatigue, hygrothermal aging, moisture, quasi-static

1 | INTRODUCTION

The wider application of composite materials in the automotive industry (such as carbon fibre reinforced plastic [CFRP]) offers several benefits, namely, inferior structural weight, high strength, and excellent stiffness-to-weight ratios.[1] Although the main use of carbon fibre within the automotive industry was first limited to components with nonstructural applications, its usage has expanded significantly and even comprehends crash absorbing structures. During its life cycle, automotive structures are subjected to a wide range of temperature and loading modes, and to design a durable structure, it is first necessary to understand the CFRP response when loaded under those circumstances.[2-5] This is particularly important when considering the combination of the aging process and fatigue loads.[6,7]

The epoxy resin of composite materials can absorb moisture when in the presence of humid environments, which can be determined by the affinity of functional groups with a very polar nature obtained from the curing process of the epoxy resin.[8-10] Three distinct sorption methods were proposed by Apicella et al.[11,12] The first is the dissolution of water in the polymer network in bulk, the second refers to moisture absorption onto the vacuoles' surface corresponding to the excess free volume of

Nomenclature: CFRP, carbon fibre reinforced polymer; SLJ, single lap joints; ADCB, asymmetric double cantilever beam; Gth, fatigue threshold strain rate energy release; E, Young modulus; G, shear modulus; E_1, normal direction; E_2, transverse direction; E_3, out-of-plane direction; M_∞, infinite mass; M_t, moisture uptake; w_t, specimen mass; w_0, initial constant mass

 © 2019 Wiley Publishing Ltd.

the glassy structure, and the third considers the hydrogen bonding between polymer hydrophilic groups and water. A dual sorption behaviour can be detected if the two first modes occur consecutively.[13-17] Tsenoglou et al[18] explained the penetration of water in composite materials of different interfacial strength as being the outcome of two processes occurring at the same time, as diffusion through the matrix and through a network of microchannels was formed along the bonded polymer-fibre interface, which presented imperfections. Channels along the exterior of the loose fibre may contribute to a mesoscopic "free volume" to the composite, which is conductive to diffusion.

The increase of volume of the epoxy resin caused by swelling is known to be lower than the volume of the absorbed water. Adamson[19] stated that when water is absorbed by an epoxy material, the comparatively small water molecules either occupy the free volume of the epoxy or swell the epoxy. Moisture absorption in the fibre is negligible.[20]

Aiming to predict the process of moisture transport in epoxy resin and composites, several mathematical models have been presented, focusing on the use of concentration- and stress-dependent diffusion coefficients.[21-23] Some authors consider that a Fickian diffusion model with a constant diffusion coefficient can define the following: the main moisture transport in composites,[24-27] a concentration-dependent diffusion coefficient,[28] or a stress-dependent diffusion coefficient.[29] Fujita[30] assessed that if the penetrant liquid is a good swelling agent for the polymer, the dependence of diffusion coefficient upon the penetrant concentration can be described by an exponential equation. Several studies[10,25,26] revealed a two-staged sorption behaviour. In the work of Augl,[31] a reduction of strength (ranging from 10% to 40%) was observed because of moisture absorption and is dependent on the temperature, although the strength reduction levelled out when an equilibrium was reached with the surrounding environment. For unidirectional composites, longitudinal properties are not expected to have a noticeable decrease, although some properties (compression strength or intralaminar/interlaminar shear strength)[32] can be significantly affected by the absorbed moisture, especially at high temperatures.[33,34] An important characteristic of adhesive joints is the resistance to fatigue and corrosion.[35] It is therefore important to understand the behaviour of composites under fatigue loads.

The failure assessment of double strap joints made with steel and CFRP was performed by Majidi et al,[36] and by using a proposed approach (point stress method), the authors were able to predict the failure load under quasi-static conditions, a method found to be in good agreement with experimental tests. More recently, Razavi et al[37] presented a strain-based criterion to predict the failure load of the same type of joints (based on a two-dimensional linear elastic finite element analysis), being able to present a good consistency in its predictions and comparing well with experimental results found in the literature.

Also important is the fatigue behaviour of adhesive joints after hygrothermal aging on the fatigue behaviour. Datla et al[38] aged open-faced asymmetric double cantilever beam (ADCB) specimens manufactured with two distinct rubber-toughened epoxy adhesives, being therefore subjected to cyclic loading under mixed-mode conditions. The results have shown that the fatigue threshold strain rate energy release, G_{th}, of the one adhesive decreased in an initial stage, therefore achieving a minimum value that was constant for a considerable time. Likewise, fatigue crack growth rates firstly increased with the aging time until reaching a limiting greater value. However, G_{th} reached the lowest value sooner than observed for the crack growth rate. In contrast, G_{th} of a second adhesive significantly decreased with aging time whereas the crack growth rates remained unchanged, even after prolonged aging. From the analysed literature, it is possible to conclude that both adhesives and CFRP substrates are greatly influenced by hygrothermal aging, with substantial changes in the mechanical properties. The combined behaviour of hygrothermal aging and fatigue is a field of great importance, which is still relatively unexplored.

The novelty of this work is the assessment and understanding of the behaviour of similar and dissimilar single lap joints (SLJs) subjected to combined aging and fatigue effects. The joints were manufactured using CFRP and aluminium substrates (in similar and dissimilar joint configurations) under different fatigue loads in the following conditions: unaged, hygrothermally aged (immersed in deionized water at 50°C for 2000 h), and dried (at 50°C) after hygrothermal aging. The experimental results allowed to conclude that for both SLJs combinations (similar and dissimilar), hygrothermally aged SLJs revealed a decrease in the number of cycles to failure, with a partial recovery in the maximum number of cycles to failure being observed for both cases after drying the specimens. For low values of stress, it was possible to achieve one million of cycles to failure for several conditions, a value which can be considered as infinite life for practical purposes.

2 | EXPERIMENTAL DETAILS

This section describes the two distinct substrates (CFRP and aluminium alloy 5754-H22) used in the manufacture of the SLJs, as well as XNR6852 E-3 epoxy crash resistant adhesive. The SLJs were manufactured in similar and

dissimilar substrate combinations using materials suitable for vehicle frame construction.

2.1 | Material and properties

2.1.1 | Carbon fibre reinforced plastic

CFRP specimens were manufactured with a carbon/epoxy pre-preg (SEAL Texipreg HS 160 RM), with 0° of fibre orientation. The elastic mechanical properties of the used material were previously determined in the work of Campilho.[39] Also, the complete cohesive properties of the CFRP, determined at quasi-static conditions (1 and 100 mm/min), were previously determined by the authors.[40-43]

2.1.2 | Aluminium alloy

An aluminium alloy (5754-H22) typically used in the automotive industry was used in this work, with 1.5-mm-thick substrates (a nominal thickness in frame manufacture). The substrates were supplied in an anodized state, required to improve the adhesion process.

2.1.3 | Crash-resistant adhesive

XNR6852 E-3 adhesive from Nagase ChemteX (Osaka, Japan) was used in this work. Due to its mechanical properties, combining high strength and ductility under impact loads, it is suitable for bonding vehicle structures. The mechanical characterization under quasi-static loads (1 and 100 mm/min) was previously performed by the authors.[42] The curing process consists of a stage of 3 hours at 150°C.

2.2 | Specimens fabrication

2.2.1 | CFRP specimens

Two CFRP specimen configurations were manufactured, namely, SLJs substrates and bulk plates (hygrothermal aging assessment). These plates used to study the hygrothermal aging are based on the ISO/DIS 294-3 standard.[44] The specimens were manufactured by stacking unidirectional 0° lay-up sheets, using a carbon/epoxy pre-preg material (with the commercial reference SEAL Texipreg HS 160 RM). Each ply has a thickness of 0.015 mm. Two different thicknesses were used according to the type of specimen. The SLJs substrates were 2.1 mm thick (a total of 14 plies) and the bulk plates were 1 mm thick (a total of seven plies). The cure cycle applied to the CFRP included a 1-hour stage at 130°C.

2.2.2 | Adhesive bulk plates

Bulk plates configurations (with thickness of 1 and 2 mm) of XNR6852 E-3 adhesive were manufactured to determine the hygrothermal aging and drying processes, as well for studying the influence of these processes in its mechanical properties (French standard NF T 76-142 [46]).

Adhesive plates (1 mm thick) were machined with the dimensions of 60 × 60 mm (ISO/DIS 294-3)[44] aiming to determine the evolution of ingress of water.

Other adhesive plates, with 2 mm of thickness and intended to be used for tensile testing, were machined following the BS 2782 standard.[45] These adhesive bulk specimens were tested under quasi-static (1 mm/min) conditions in all the aging conditions mentioned.

2.2.3 | Single lap joints

The 5754-H22 alloy was delivered in an anodized state; therefore, it was only cleaned by heating it to 190°C for 30 minutes followed by the application of isopropanol alcohol to eliminate any impurities from the surface.

SLJs were manufactured with an overlap length of 25 mm (Figure 1), since this geometry is representative of automotive industry applications. The adhesive layer thickness (0.2 mm) was defined to be as close as possible to that used in the final application and based on the ASTM D1002-99[46] and ISO 4587:1995[47] standards.

Considering the two distinct substrates (CFRP and aluminium alloys 5754-H22), it was possible to manufacture two combinations of SLJs manufactured of similar (CFRP [2.1 mm] + CFRP [2.1 mm]) and dissimilar (CFRP [2.1 mm] + Al 5754-H22 [1.5 mm]) combinations.

2.3 | Testing procedures

2.3.1 | Hygrothermal aging and desorption process of bulk adhesive and CFRP

The bulk plate specimens of CFRP and XNR6852 E-3 adhesive (six units per each material) were used to determine the moisture diffusion process (absorption capacity) of the substrate materials. The use of a thickness of 1 mm for both materials allows for a comparison of the absorption rate between them as well to ensure that the diffusion is solely one dimensional.

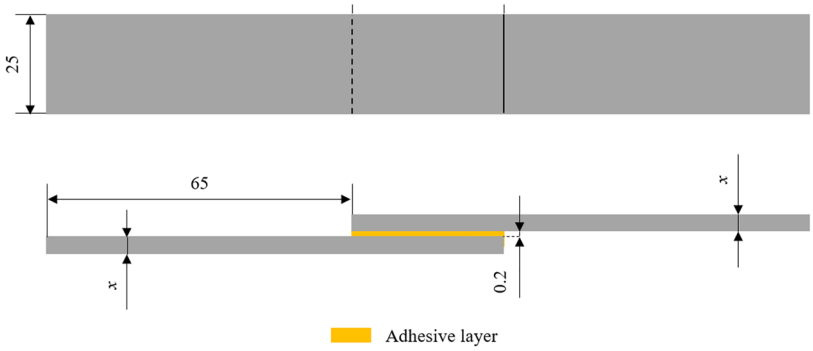

X corresponds to the substrate thickness: 2.1 mm for the CFRP and 1.5 mm for the aluminum alloy 5754-H22.

FIGURE 1 Scheme of the single lap joints (SLJs) specimens manufactured (with dimensions in millimetre) [Colour figure can be viewed at wileyonlinelibrary.com]

To remove any water that might have been absorbed from the manufacturing process or in contact with environment, the specimens were kept in a container with a silica-based desiccant product. Initially, the specimens were dried in an oven (50 ± 2°C) with 10% of moisture, until a constant mass was reached. After weight stabilization occurred, the specimens were fully immersed in deionized water, at a constant temperature of 50 ± 2°C, selected according to the ISO 62:2008 standard.[48] The immersion period was 2000 hours. The aging temperature was set to be significantly below the T_g of each material, to ensure the only physical processes occur, avoiding any chemical changes.[49,50]

Specimens were kept immersed in deionized water until the stabilization of the moisture absorption mass (also named of infinite mass [M_∞]). A constant value in terms of maximum moisture absorption was observed for XNR6852 E-3 adhesive; as for the CFRP, it was not possible to achieve a full saturation; therefore, the maximum water uptake considered corresponds to the value of the final measurement.

After 2000 hours of immersion, the specimens were dried manually, removing any water droplets from the surface. The specimens were subsequently stored inside a glass container with silica desiccant and placed inside the climatic chamber at 50°C. This dried the material until no water was present, with mass measurements being performed as previously described for the absorption process.

The moisture uptake M_t was determined using the following equation:

$$M_t = \frac{w_t - w_0}{w_0} * 100\%, \quad (1)$$

where w_t refers to the specimen mass and w_0 to the initial constant mass. Mass uptake saturation is considered to have occurred when the gain values from three successive measurements differ less than 1% of the overall weight gain.

The diffusion analysis can be described by a Fick law, which, for these materials, was previously determined by the authors in another work.[51]

2.3.2 | Quasi-static testing procedure

The quasi-static (constant crosshead displacement of 1 mm/min) tests were performed at room temperature using a universal testing machine model INSTRON 3367 (Norwood, Massachusetts), with a load cell with of 30 kN.

While testing XNR6852 E-3 adhesive bulk "dogbone" specimens, it was not possible to directly measure displacement using an extensometer, with an optical method being selected. Nine specimens were tested for each condition (unaged, hygrothermally aged, and dried after hygrothermal aging), and for each specimen, a stress-strain (P-δ) curve was determined.

2.3.3 | Fatigue testing procedure

The fatigue behaviour of the SLJs bonded with XNR6852 E-3 adhesive was assessed by testing in an MTS 810 servo-hydraulic testing machine. The test was performed in force control with a sinusoidal waveform, load ratio (minimum to maximum load) of $R = 0.1$, and different values of frequency. The fatigue experiments were conducted at three different load values (60%, 40%, and 20%) of the average values of quasi-static (1 mm/min) failure load of each specimen combination: similar (CFRP + CFRP) and dissimilar (CFRP + Al5754-H22) substrates at unaged, hygrothermally aged (immersed in deionized water at 50°C), and dried (at 50°C) after hygrothermally aging. A total of six specimens were tested for each condition. The tests were performed in ambient laboratory conditions and were conducted up to failure of the specimen or until infinite life was achieved (considered to be maximum of one million load cycles). Table 1 present the experimental values considered to test experimentally

TABLE 1 Experimental data used to test under fatigue loads SLJs manufactured with similar substrates (CFRP + CFRP) and dissimilar substrates (CFRP + Al5754-H22), in the following conditions: unaged, hygrothermally aged ("Aged"), and dried after hygrothermal aging ("Dried")

Condition	Quasi-static Failure Load, kN	Fatigue Load		Average Value of Load, kN	Amplitude, kN	Frequency, Hz
		%	kN			
Similar substrates (CFRP + CFRP)						
Unaged	20	60	12	6.6	5.4	6
		40	8	4.4	3.6	8
		20	4	2.2	1.8	12
Aged	14.9	60	8.9	4.9	4.0	6
		40	5.9	3.3	2.6	8
		20	2.9	1.6	1.3	12
Dried	20.2	60	12.1	6.7	5.4	6
		40	8.1	4.5	3.6	8
		20	4.0	2.2	1.8	12
Dissimilar substrates (CFRP + Al5754-H22)						
Unaged	8.7	60	5.2	2.8	2.4	8
		40	3.4	1.9	1.6	8
		20	1.7	0.9	0.7	12
Aged	8.1	60	5.0	2.7	2.3	8
		40	3.3	1.8	1.5	8
		20	1.6	0.9	0.7	12
Dried	8.7	60	5.0	2.7	2.3	8
		40	3.3	1.8	1.5	8
		20	1.6	0.9	0.7	12

Abbreviations: CFRP, carbon fibre reinforced plastic; SLJs, single lap joints.

the SLJs under fatigue loads, in similar and dissimilar substrates combinations.

3 | RESULTS

Experimental outputs from the hygrothermal aging and drying process of both the XNR6852 E-3 adhesive and the CFRP substrates are presented in the following section. Shown are the SLJs results (similar and dissimilar substrates combination) tested under quasi-static conditions in the following states: unaged, hygrothermally aged ("Aged") (immersed in distilled water for 2000 h at 50°C), and dried (at 50°C) after hygrothermal aging ("Dried"). Finally, a thorough analysis of the fatigue tests results is made.

3.1 | Moisture diffusion of the bulk adhesive and the CFRP substrates

XNR6852 E-3 adhesive was found to achieve full saturation, and it was concluded that the mathematical model to be used for diffusion (for both cases of water absorption and desorption) was the "sequential dual Fickian" (SDF) (Figure 2), which is based on the work of Ameli et al,[52] and it is represented by Equation (2).

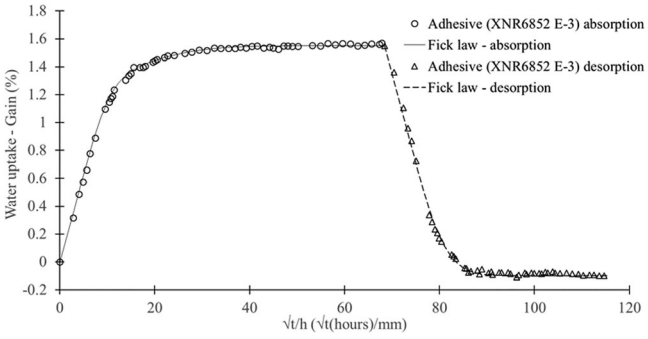

FIGURE 2 Moisture absorption and desorption of XNR6852 E-3 adhesive, with the sequential dual Fickian (SDF) fit curve (data presented as a function of hours)

$$M_t = \left(1 - \frac{8}{\pi^2}\sum_{n=0}^{\infty}\frac{1}{(2n+1)^2}\exp\left(\frac{-D_1(2n+1)^2\pi^2 t}{4h^2}\right)\right) \times M_{1\infty} + \varnothing(t - t_d) \times \left(1 - \frac{8}{\pi^2}\sum_{n=0}^{\infty}\frac{1}{(2n+1)^2} \exp\left(\frac{-D_2(2n+1)^2\pi^2 t}{4h^2}\right)\right) \times M_{2\infty}. \quad (2)$$

The maximum gain of water by adhesive was 1.6%. By proceeding with the drying process after hygrothermal aging ("Dried" state), it was possible to observe that the moisture level was 0.1% lower than the initial, unaged level. This might be explained by the relaxation of the molecular chain of the XNR6852 E-3 epoxy adhesive, which allowed for a new rearrangement of the structure, creating enough space for the internally trapped water to be released. The data also enable to conclude that the desorption process was faster than the absorption process.

TABLE 2 General properties of absorption and desorption of water by XNR6852 E-3 adhesive

Stage	Property	
Absorption	$M1_\infty$ (%)	0.012
	D1 ($m^2\ s^{-1}$)	19E-13
	$M2_\infty$ (%)	0.0035
	D2 ($m^2\ s^{-1}$)	28E-14
Desorption	$M1_\infty$ (%)	0.013
	D1 ($m^2\ s^{-1}$)	14E-13
	$M2_\infty$ (%)	0.0035
	D2 ($m^2\ s^{-1}$)	10E-13

The general properties of absorption and desorption of water by XNR6852 E-3 adhesive are presented in Table 2.

Regarding the CFRP, it was not possible to determine the Fick law as the material did not reach the maximum water absorption by the end of the measurement period (Figure 3).

The maximum water uptake of the CFRP was 3.3%, greater than the maximum obtained for XNR6852 E-3 adhesive. It was possible to observe that in the same way of XNR6852 E-3 adhesive that the water ingress was linear; therefore, after a long period of time (up to several years), a Fickian law would fit the moisture diffusion of CFRP.[20,53,54]

When performing the drying process after hygrothermal aging ("Dried"), a very high water desorption rate was observed, although the water percentage that remained locked in the CFRP after drying was 0.23%, when for the

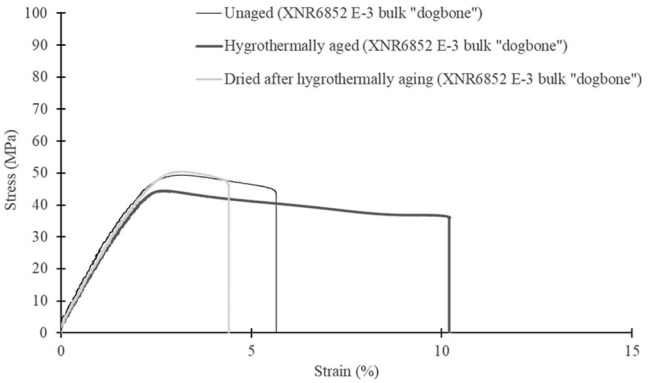

FIGURE 4 Example of *P-δ* curves obtained from XNR6852 E-3 adhesive bulk "dogbone" specimens tested at quasi-static (1 mm/min) conditions in the three distinct states: unaged, hygrothermally aged ("Aged"), and dried after hygrothermal aging ("Dried")

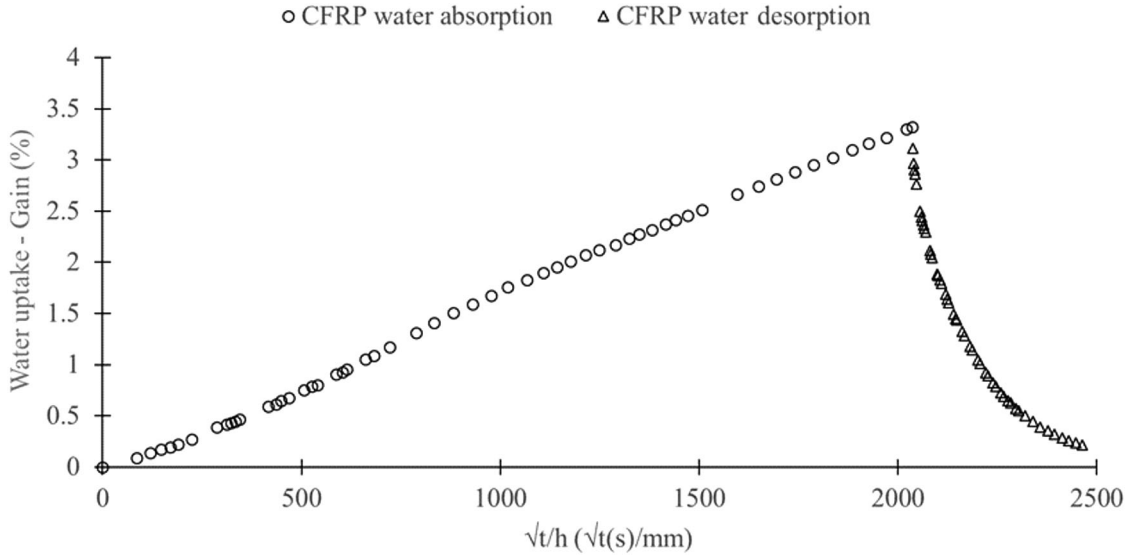

FIGURE 3 Moisture absorption and desorption of the carbon fibre reinforced plastic (CFRP) results (in seconds)

case of XNR6852 E-3 adhesive, the removal of all water was already long achieved. Arnold et al[53] found the same behaviour, and discarding causes such as microcracks or chemical changes, the authors infer that the mechanism responsible is the slow molecular relaxation, which allows for additional pockets of free volume for the water molecules to occupy, and are independent from the presence of carbon fibres. The presence of water when drying the specimens after hygrothermal aging ("Dried") could be explained by the relaxation process that caused some liquid molecules to become trapped in molecular cavities.

3.2 | XNR6852 E-3 adhesive bulk "dogbone"

Figure 4 presents the tensile test results of XNR6852 E-3 adhesive bulk "dogbone" (examples of P-δ curves obtained).

The value of Young modulus measured after hygrothermal aging ("Aged") was similar to that obtained for the unaged condition. The tensile strength experienced a decrease of about 10%. The most affected parameter after the hygrothermal aging ("Aged") process was the strain to failure, which exhibited an increase of 50%, likely related to the relaxation of the polymeric chains and its rearrangement. After the drying process ("Dried"), it was observed that there was a slight increase of the tensile strength, with the average value being close to that of the unaged condition specimens, leading to the conclusion that this mechanical parameter was fully recovered. A similar behaviour was identified for the Young modulus. Concerning the strain to failure, a significant reduction was noticeable, with the average value being lower than that obtained for the case of the unaged condition, indicating that the material loses some toughness after the drying process is completed.

3.3 | Quasi-static tests of single lap joints

3.3.1 | Fracture surface

Representative fracture surfaces of SLJs in similar and dissimilar substrates combinations tested under quasi-static conditions are presented in Table 3.

In the case of the SLJs manufactured with a similar combination of CFRP substrates, it was possible to

TABLE 3 Representative failure surfaces of similar and dissimilar SLJs configuration tested under quasi-static conditions (1 mm/min) as a function of different testing conditions: unaged, hygrothermally aged ("Aged"), and dried after hygrothermal aging ("Dried")

	Joint Configuration	
Condition	**CFRP + CFRP**	**CFRP + Al 5754-H22**
Unaged	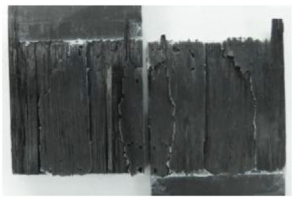	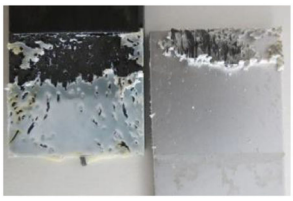
	CFRP delamination	CFRP delamination
Aged	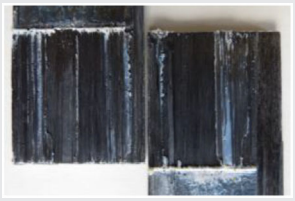	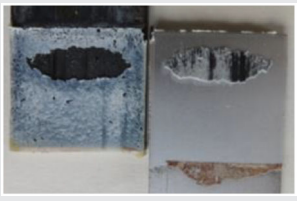
	CFRP delamination	CFRP delamination
Dried	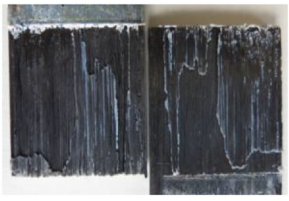	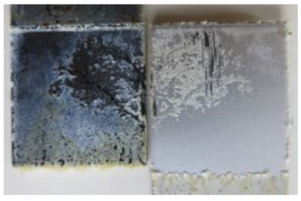
	CFRP delamination	CFRP delamination

Abbreviations: CFRP, carbon fibre reinforced plastic; SLJs, single lap joints.

observe that for the three stages (unaged, hygrothermally aged, and dried after hygrothermal aging), the type of failure load present was delamination of the CFRP substrate. When subjected to hygrothermal aging ("Aged"), the SLJs manufactured with similar CFRP substrates revealed a less severe failure by delamination of the CFRP, although this might be due to the high level of plasticization of both the CFRP substrate and XNR6852 E-3 adhesive (and assumption that is supported by some evidence of discoloration of the adhesive layer). The fracture surface of the SLJs dried after hygrothermal aging ("Dried") has characteristics in between those of the unaged and hygrothermally aged ("Aged") conditions as severe delamination occurred. A colour change of the surface is noticeable due to water ingress.

The failure surface of SLJs manufactured with dissimilar substrates combination (CFRP + Al5754-H22) was dominated by the plastic deformation of the aluminium substrate. The aluminium substrate is significantly less thick than the CFRP substrate, with highly unbalanced substrate stiffness. This caused an increase of peel forces and therefore led to premature failure of the joint. The failure surface of SLJs with dissimilar substrates combination also evidences a slightly lower degree of XNR6852 E-3 adhesive layer plasticization due to the water ingress being limited to one of the surfaces (CFRP substrate).

3.3.2 | Failure load

The values of failure load of SLJs tested under quasi-static load, considering the three distinct aging conditions, are shown in Figure 5.

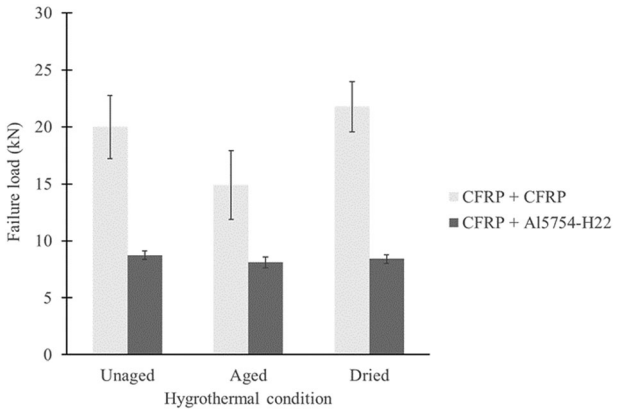

FIGURE 5 Failure load results of single lap joints (SLJs) manufactured with similar and dissimilar combination of substrates (carbon fibre reinforced plastic [CFRP] and Al 5754-H22) tested under quasi-static (1 mm/min) load, as a function of unaged, hygrothermally aged ("Aged"), and dried after hygrothermal aging ("Dried") conditions

In the case of SLJs manufactured using similar substrates of CFRP, failure was controlled by delamination of CFRP, and it was possible to verify that with hygrothermal aging ("Aged") of the SLJs, a significant decrease of the failure load occurred, because of the plasticization of the CFRP substrates and loss of strength of XNR6852 E-3 adhesive. Drying after hygrothermal aging ("Dried") revealed that the SLJs were able to fully recover their strength to failure (in accordance with the bulk adhesive tensile behaviour), with average failure load values being higher than those obtained for unaged SLJs. The plasticization of CFRP substrates is thought to reduce overall joint stiffness, reducing stress concentration on the adhesive layer. It was possible to observe that the failure load of the dissimilar SLJs (CFRP + Al5754-H22) was almost identical, independently of the state of the joint in terms of being tested. Such fact, associated to the similar failure surfaces and bending of the 5754-H22 aluminium, revealed that the full potential of the adhesive layer was never achieved, being limited by the large peel stresses. Therefore, the failure load at which the SLJs with dissimilar substrates (CFRP + Al5754-H22) failed was lower than that necessary to cause the failure by delamination of the CFRP substrates. An important observation was that the failure of the Al5754-H22 substrates occurs mainly because of its cohesive mechanical properties rather than adhesive failure due to the provided surface treatment.[55]

3.4 | Fatigue tests

3.4.1 | SLJs with similar substrates

Failure surface

The representative failure surfaces of SLJs manufactured with similar substrates (CFRP + CFRP) tested under three different fatigue loads (60%, 40%, and 20% of the quasi-static failure loads) are presented in Table 4.

It was possible to observe that for all fatigue load cases, the type of failure was always delamination of CFRP substrates. Two distinct failure mechanisms can be introduced, being the first associated to the dried after hygrothermal aging ("Dried") under 60% of failure load presenting pure delamination of CFRP, and the second (corresponding to the other tested conditions) to an additional failure mechanism of delamination near the surface, which can be defined as a combination of delamination of CFRP and adhesion failure.

However, the severity of delamination varied, ranging from highly severe (occurring for higher failure load percentage and for the unaged and dried after hygrothermal aging ["Dried"] conditions) to less severe (occurring for

TABLE 4 Representative failure surfaces of similar SLJs configuration tested under quasi-static loads and different conditions: unaged, hygrothermally aged ("Aged"), and dried after hygrothermal aging ("Dried")

CFRP + CFRP	60% of Load	40% of Load	20% of Load
Unaged	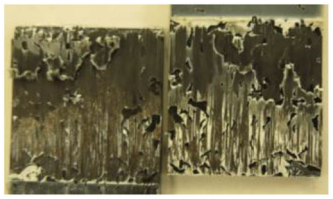		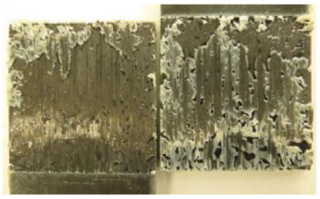
	CFRP delamination[a]	CFRP delamination[a]	CFRP delamination[a,b]
Aged	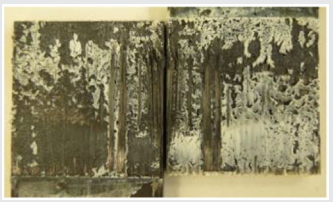	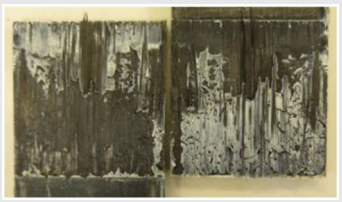	
	CFRP delamination[a]	CFRP delamination[a]	CFRP delamination[a,b]
Dried	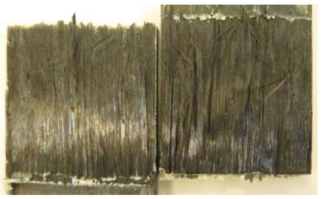		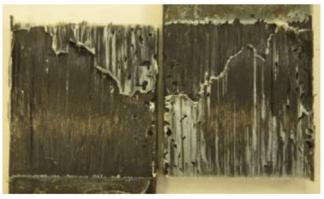
	CFRP delamination	CFRP delamination[a]	CFRP delamination[a]

Abbreviations: CFRP, carbon fibre reinforced plastic; SLJs, single lap joints.

[a]Near surface delamination.

[b]Failure surface of SLJs tested under quasi-static (1 mm/min) conditions as the SLJs were able to sustain one million of cycles.

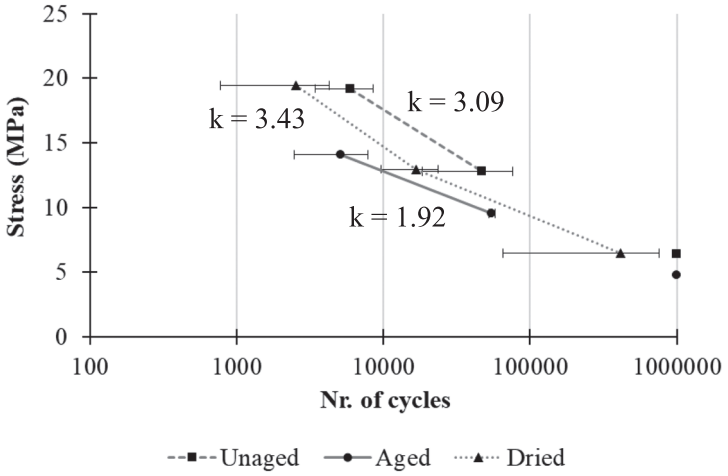

FIGURE 6 Comparison of the stress versus the number of cycles to failure of single lap joints (SLJs) manufactured with similar substrates (CFRP + CFRP) under different conditions: unaged, hygrothermally aged ("Aged") and dried after hygrothermal aging ("Dried"), and respective values of inverse slope (k)

the case of lower load percentages and hygrothermally aged ["Aged"] conditions). The fracture surfaces of hygrothermally aged ("Aged") specimens were found to be less affected by the delamination process of CFRP in comparison with the other conditions. This fact can be attributed to the plasticization of both XNR6852 E-3 adhesive and the CFRP. As previously stated for XNR6852 E-3 "bulk" adhesive tests, when undergoing hygrothermal aging ("Aged"), the adhesive plasticizes and its strain to failure increases 50%. The inverse effect

was observed for the specimens dried after hygrothermal aging ("Dried").

Stress versus the number of cycles to failure

A comparison of the stress versus the number of cycles to failure of SLJs manufactured with similar substrates (CFRP + CFRP) for the three aging conditions studied is presented in Figure 6.

The results show that the fatigue life of the hygrothermally aged ("Aged") specimens was reduced when compared with that of those in the unaged state. This was found to occur for stress levels around 20 and 15 MPa. Dried specimens exhibit a good degree of recovery in fatigue behaviour but do not fully return to the performance of the unaged joint. It can be noted that the fatigue life, as a function of the stress levels, follows a nearly logarithmic trend as time progresses. The only specimens that did not achieve the target of one million of cycles at the lowest load level were those dried after hygrothermal condition ("Dried"). This can be explained by the analysis of the bulk tensile test results, which indicates that although the dried condition does recover its strength, it does so with a noticeable loss of ductility, which is reflected on the long-term fatigue performance. The values of inverse slope, k, were found to be higher for dried after hygrothermal condition ("Dried") conditions and lower for the hygrothermally aged (Aged") conditions.

3.4.2 | SLJs with dissimilar substrates

Failure surface

The representative failure surfaces of SLJs manufactured with similar substrates (CFRP + Al5754-H22) tested under three different fatigue loads (60%, 40%, and 20% of the quasi-static failure loads) and at three distinct conditions (unaged, hygrothermally aging, and dried after hygrothermal aging) are presented in Table 5.

The main failure mode was cohesive failure of the aluminium substrate, except for the case of hygrothermally aged SLJs tested in fatigue with 60% of failure load. Such result might be not only due to the drop of mechanical properties of both XNR6852 E-3 adhesive and CFRP but also to some degree of degradation of the metal-adhesive interface due to water ingress. The higher peel loads

TABLE 5 Representative failure surfaces of similar and dissimilar SLJs configuration tested under quasi-static conditions (1 mm/min) as a function of different testing conditions: unaged, hygrothermally aged ("Aged"), and dried after hygrothermal aging ("Dried")

CFRP + Al5754-H22	60% of Load	40% of Load	20% of Load
Unaged			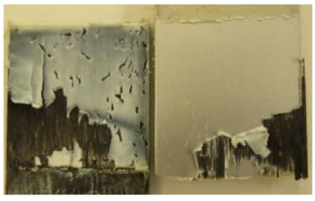
	Failure in Al substrate[a]	Failure in Al substrate[a]	Delamination of CFRP[b,c]
Aged	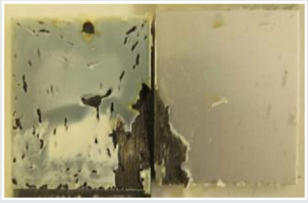	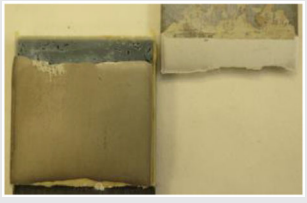	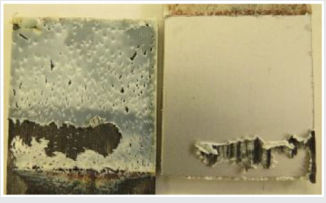
	Delamination of CFRP[b]	Failure in Al substrate[a]	Delamination of CFRP[b,c]
Dried	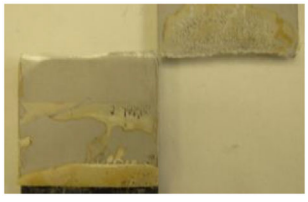	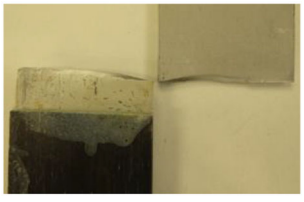	
	Failure in Al substrate[a]	Failure in Al substrate[a]	Delamination of CFRP[b,c]

Abbreviations: CFRP, carbon fibre reinforced plastic; SLJs, single lap joints.

[a]Failure of the joints occurred within the aluminium substrates; therefore, the bonded area was kept unchanged.

[b]Partial delamination of CFRP (peel forces induced by bending of Al5754-H22 substrates).

[c]Failure surface of SLJs tested under quasi-static (1 mm/min) conditions once the SLJs were able to sustain one million of cycles.

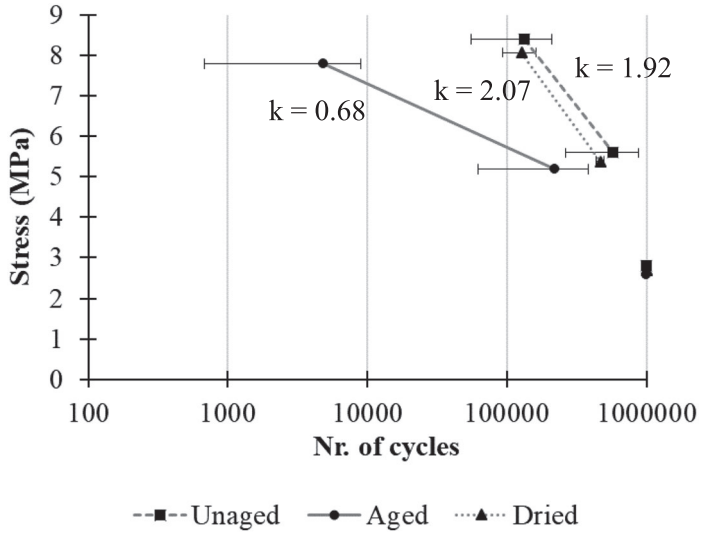

FIGURE 7 Comparison of the stress versus the number of cycles to failure of single lap joints (SLJs) manufactured with dissimilar substrates (CFRP + Al5754-H22) under different conditions: unaged, hygrothermally aged ("Aged"), and dried after hygrothermal aging ("Dried"), and respective values of inverse slope (k)

created during the 60% load level tests will create higher demands on the interface and expose this degradation.

It was possible to observe that the fatigue tests performed for 20% of failure load, the type of failure load was delamination of CFRP, independently of the aging condition. As previously stated for the quasi-static tests, there was a noticeable bending of the Al5754-H22 substrates, leading to higher peel forces and therefore increasing the probability of failure, especially when coupled with moisture-induced degradation of the CFRP-adhesive and adhesive-aluminium interfaces.

Stress versus the number of cycles to failure

A comparison of the stress versus the number of cycles to failure of SLJs manufactured with similar substrates (CFRP + CFRP) for the three aging conditions studied is presented in Figure 7.

According to these data, under fatigue loads, the best performing joints are in those in the unaged state, achieving the higher number of cycles to failure for all stress levels under testing. The aged joints exhibit a noticeably worse behaviour, especially for the highest stress level under consideration. In contrast, the joints that were dried after aging are quite close in behaviour to those in the unaged stated, indicating there an almost complete performance restitution. Infinite life (greater than one million cycles) was achieved for all the joint conditions when fatigue is tested at the lowest stress level (3 MPa). The values of inverse slope (k)[56,57] were found to be higher for the dried after hygrothermal condition ("Dried") conditions and lower for the hygrothermally aged (Aged") conditions.

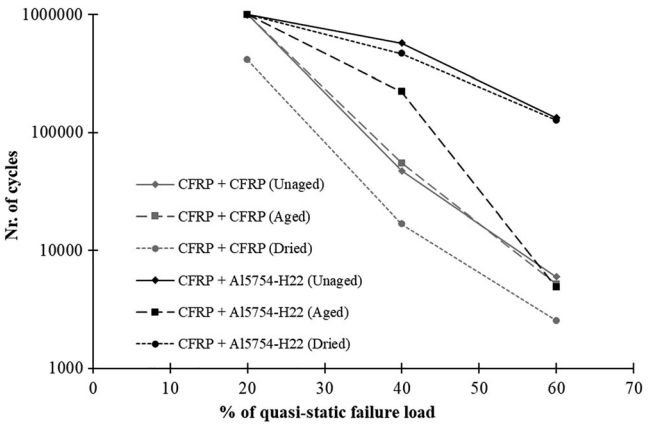

FIGURE 8 Fatigue life as a function of the number of cycles for all tested single lap joint (SLJ) configuration

3.4.3 | Fatigue life comparison

An analysis of the number of cycles to failure as a function of the percentage of quasi-static load used to test under fatigue is presented in Figure 8 for all substrates under study in this work.

Overall, the results indicate that, given the geometry under study, the dissimilar SLJs (CFRP + Al5754-H22) have the best fatigue performance achieving higher life for the same load level. The dissimilar joints exhibited higher flexibility, and as such, the adhesive layer is less stressed during the cyclic loadings. In fact, as seen in Table 5, most of the failures for this configuration occur on the metal substrate itself, which is itself susceptible to fatigue loads.

Comparing the aging state, the behaviour is highly dependent on the SLJ configuration. The SLJs with dissimilar substrates exhibit a consistent behaviour for the unaged and dried substrates, with the aged joint exhibiting a drastically lower fatigue life. The presence of moisture in these joints appears to have degraded

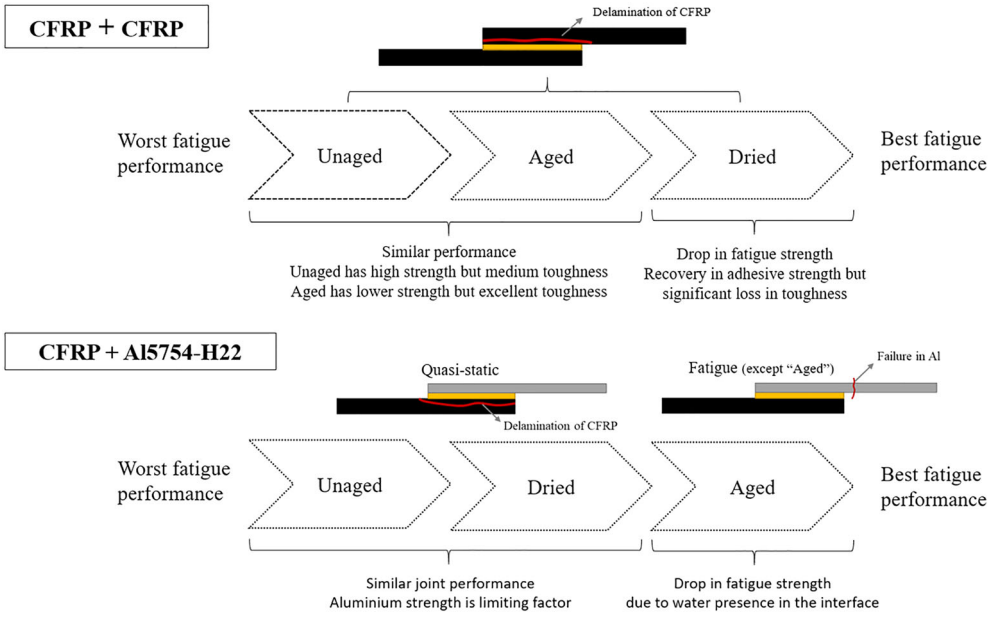

FIGURE 9 Schematic representation of the fatigue performance of the similar and dissimilar single lap joints (SLJs) [Colour figure can be viewed at wileyonlinelibrary.com]

performance, possibly because of some degree of failure at the adhesive-aluminium interface, which shifts the locus of failure from the metallic substrate to the interface area. In the SLJs with similar substrates, the aged and unaged states performed very closely, with the dried joints exhibiting a noticeable loss of performance. As previously explained, this might be due to the loss in joint ductility that was identified in bulk testing dried adhesive samples. These results appear to indicate that while joints with moisture do not suffer a reduction in their fatigue behaviour, those that undergo drying processes can in fact suffer a degradation process. Figure 9 shows a schematic representation of the behaviour of the SLJs under study, describing the key parameters that determine the fatigue life.

3.4.4 | Residual strength of SLJs

A comparison between the failure load of SLJs tested under quasi-static loads, prior and after undergoing one million cycles of fatigue loads, was performed in this section for both cases of SLJs manufactured with similar

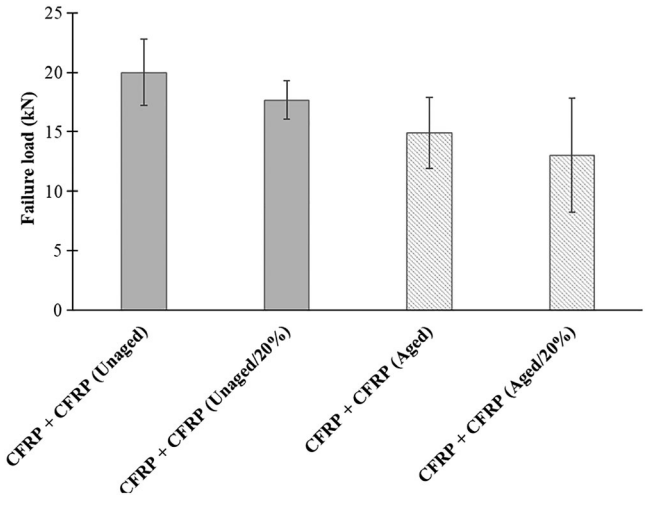

FIGURE 10 Comparison of the residual joint strength of single lap joints (SLJs) tested until one million cycles of fatigue—manufactured with similar substrates (CFRP + CFRP) at the unaged and hygrothermally aged ("Aged") conditions

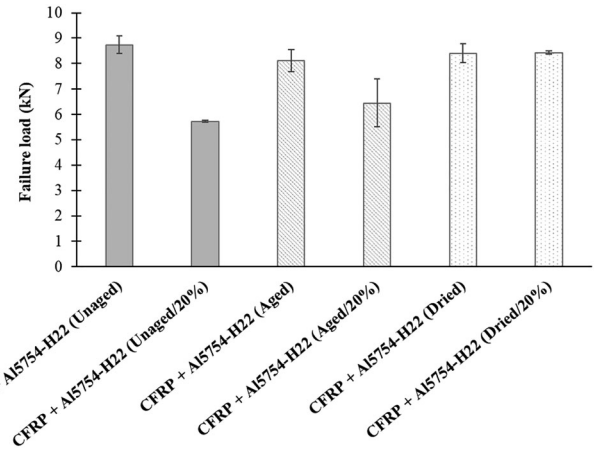

FIGURE 11 Comparison of the residual joint strength of single lap joints (SLJs) tested until one million cycles of fatigue—manufactured with similar substrates (CFRP + CFRP) at the unaged, hygrothermally aged ("Aged"), and dried after hygrothermal aging ("Dried") conditions

(CFRP + CFRP) and dissimilar (CFRP + Al5754-H22) substrates.

Most of the joints tested at 20% of failure load achieved infinite life. Of the SLJs manufactured with similar substrates, only those dried after hygrothermal aging did not achieve one million cycles. The results of failure load for SLJs manufactured with similar substrates are presented in Figure 10.

It can be observed that for both aging conditions, there was a decrease of the average values of failure load after the SLJs were subjected to fatigue (at 20% of the quasi-static failure loads), although the results can be considered as comparable when taking into account the standard deviation. Another conclusion is that there was a decrease of the failure load when the SLJs were hygrothermally aged ("Aged"). The comparison of the failure load prior and after fatigue load (after achieving the target of one million cycles) of SLJs manufactured with dissimilar substrates is presented in Figure 11.

Although it was stated in Section 3.3.2 that there was no change in terms of the SLJs failure load varying the aging condition, it is possible to observe that in the case of unaged SLJs, a large drop of the failure load was identified after the fatigue tests. As for the case of SLJs dried after hygrothermal aging ("Dried"), the value of failure load was the same, indicating that the SLJ strength was fully recovered after this aging condition.

In the unaged and hygrothermally aged ("Aged") conditions, the average value of failure load was higher in the unaged state than in the hygrothermally aged ("Aged") condition, but considering the standard deviation, both values are similar, which is in accordance with the values obtained for the SLJs tested under quasi-static conditions prior to the fatigue tests.

4 | CONCLUSIONS

This work focused on the assessment and understanding of the behaviour of SLJs manufactured using CFRP and aluminium substrates (in similar and dissimilar joint configurations) under different fatigue loads in the unaged, hygrothermally aged (immersed in deionized water at 50°C for 2000 h), and dried (at 50°C) after hygrothermal aging conditions. The main conclusions that can be drawn from this work are as follows:

- Failure loads at quasi-static conditions for dissimilar SLJs (CFRP + Al5754-H22) were almost identical, independent of the state of the joint in terms of being tested as unaged, hygrothermally aged, or dried after hygrothermal aging. For the case of SLJs with similar substrates (CFRP + CFRP), there was a decrease of failure load when hygrothermally aged fully recovered after drying.
- The fatigue performance of the SLJs with dissimilar substrates was always better than that of SLJs with similar substrates, a fact that can be attributed to the lower level of stress being applied to the adhesive layer.
- The presence of moisture was found to not change the fatigue performance of the similar SLJ configurations, while dried joints were found to have suffered a loss in performance due to changes in the adhesive behaviour. These considerations were however not true for the case of the dissimilar substrates. The failure was either controlled by the substrate (which is not sensitive to moisture) or instead occurred near the interface in the aged joints, which offered much lower strength against peel stresses.

ACKNOWLEDGEMENTS

The authors gratefully acknowledge the funding provided by PhD grant SFRH/BD/139341/2018 "Impact strength optimization with cohesive zone elements of multi-material bonded structures used in the automotive industry", project no. 028473 POCI-01-0145-FEDER-028473 "Design methodology for impact resistant bonded multi-material automotive structures (ImpactBondDesign)." The authors also acknowledge of NAGASE ChemteX in respect to the financial support provided.

ORCID

J. J. M. Machado https://orcid.org/0000-0002-1094-0114
E. A. S. Marques https://orcid.org/0000-0002-2750-8184
A. Q. Barbosa http://orcid.org/0000-0002-1661-9989
L. F. M. da Silva https://orcid.org/0000-0003-3272-4591

REFERENCES

1. Campilho R, de Moura M, Ramantani D, Morais J, Domingues J. Tensile behaviour of three-dimensional carbon-epoxy adhesively bonded single-and double-strap repairs. *Int J Adhes Adhes*. 2009;29(6):678-686.
2. Harding J, Welsh LM. A tensile testing technique for fibre-reinforced composites at impact rates of strain. *J Mater Sci*. 1983;18(6):1810-1826.
3. da Silva L, Öchsner A, Adams RD. *Handbook of adhesion technology*. Second edition ed. Berlin, Germany: Springer Science & Business Media; 2018.
4. Papanikos P, Tserpes K, Pantelakis S. Modelling of fatigue damage progression and life of CFRP laminates. *Fatigue Fract Eng Mater Struct*. 2003;26(1):37-47.

5. Venkatachalam S, Khaja Mohiddin S, Murthy H. Determination of damage evolution in CFRP subjected to cyclic loading using DIC. *Fatigue Fract Eng Mater Struct*. 2018;41(6):1412-1425.
6. Malinowski PH, Ostachowicz WM, Brune K, Schlag M. Study of electromechanical impedance changes caused by modifications of CFRP adhesive bonds. *Fatigue Fract Eng Mater Struct*. 2017;40(10):1592-1600.
7. Li D, Huang P, Guo X, Zheng X, Lin J, Chen Z. Fatigue crack propagation behavior of RC beams strengthened with CFRP under cyclic bending loads. *Fatigue Fract Eng Mater Struct*. 2018;41(1):212-222.
8. Lee MC, Peppas NA. Water transport in epoxy resins. *Prog Polym Sci*. 1993;18(5):947-961.
9. Sethi S, Ray BC. Environmental effects on fibre reinforced polymeric composites: evolving reasons and remarks on interfacial strength and stability. *Adv Colloid Interface Sci*. 2015;217:43-67.
10. Wright W. The effect of diffusion of water into epoxy resins and their carbon-fibre reinforced composites. *Composites*. 1981;12(3):201-205.
11. Apicella A, Tessieri R, De Cataldis C. Sorption modes of water in glassy epoxies. *J Membr Sci*. 1984;18:211-225.
12. Apicella A, Nicolais L, De Cataldis C. Characterization of the morphological fine structure of commercial thermosetting resins through hygrothermal experiments. In: *Characterization of Polymers in the Solid State I: Part A: NMR and Other Spectroscopic Methods Part B: Mechanical Methods*. Amsterdam, Netherlands: Springer; 1985:189-207.
13. Kaelble D, Dynes P, Cirlin E. Interfacial bonding and environmental stability of polymer matrix composites. *J Adhes*. 1974;6(1–2):23-48.
14. Kaelble D. A relationship between the fracture mechanics and surface energetics failure criteria. *J Appl Polym Sci*. 1974;18(6):1869-1889.
15. Carter HG, Kibler KG. Langmuir-type model for anomalous moisture diffusion in composite resins. *J Compos Mater*. 1978;12(2):118-131.
16. Joliff Y, Belec L, Chailan J. Modified water diffusion kinetics in an unidirectional glass/fibre composite due to the interphase area: experimental, analytical and numerical approach. *Compos Struct*. 2013;97:296-303.
17. Joliff Y, Rekik W, Belec L, Chailan J. Study of the moisture/stress effects on glass fibre/epoxy composite and the impact of the interphase area. *Compos Struct*. 2014;108:876-885.
18. Tsenoglou CJ, Pavlidou S, Papaspyrides CD. Evaluation of interfacial relaxation due to water absorption in fiber-polymer composites. *Compos Sci Technol*. 2006;66(15):2855-2864.
19. Adamson MJ. Thermal expansion and swelling of cured epoxy resin used in graphite/epoxy composite materials. *J Mater Sci*. 1980;15(7):1736-1745.
20. Alessi S, Pitarresi G, Spadaro G. Effect of hydrothermal ageing on the thermal and delamination fracture behaviour of CFRP composites. *Compos Part B Eng*. 2014;67:145-153.
21. Lee MC, Peppas NA. Models of moisture transport and moisture-induced stresses in epoxy composites. *J Compos Mater*. 1993;27(12):1146-1171.
22. Maggana C, Pissis P. Water sorption and diffusion studies in an epoxy resin system. *J Polym Sci B*. 1999;37(11):1165-1182.
23. Costa M, Viana G, Da Silva L, Campilho R. Environmental effect on the fatigue degradation of adhesive joints: a review. *J Adhes*. 2017;93(1–2):127-146.
24. Shen C-H, Springer GS. Moisture absorption and desorption of composite materials. *J Compos Mater*. 1976;10(1):2-20.
25. Loos AC, Springer GS. Moisture absorption of graphite-epoxy composites immersed in liquids and in humid air. *J Compos Mater*. 1979;13(2):131-147.
26. Illinger JL, Schneider NS. Water vapor transport in an epoxy resin based on TGMDA and DICY. *Polym Eng Science*. 1980;20(4):310-314.
27. Boll D, Bascom W, Motiee B. Moisture absorption by structural epoxy-matrix carbon-fiber composites. *Compos Sci Technol*. 1985;24(4):253-273.
28. Shirrell C, Halpin J. Moisture absorption and desorption in epoxy composite laminates. Paper presented at: Composite Materials: Testing and Design (Fourth Conference) 1977.
29. Neumann S, Marom G. Prediction of moisture diffusion parameters in composite materials under stress. *J Compos Mater*. 1987;21(1):68-80.
30. Fujita H. Diffusion in polymer-diluent systems. In: *Fortschritte Der Hochpolymeren-Forschung*. Berlin, Heidelberg: Springer; 1961:1-47.
31. Augl JM. *The Effect of Moisture on Carbon Fiber REinforced Epoxy Composites. II. Mechanical Property Changes*. Virginia, USA: NAVAL SURFACE WEAPONS CENTER WHITE OAK LAB SILVER SPRING MD; 1977.
32. Kumar S, Sridhar I, Sivashanker S. Influence of humid environment on the performance of high strength structural carbon fiber composites. *Mater Sci Eng A*. 2008;498(1–2):174-178.
33. Choi H, Ahn K, Nam J-D, Chun H. Hygroscopic aspects of epoxy/carbon fiber composite laminates in aircraft environments. *Compos A: Appl Sci Manuf*. 2001;32(5):709-720.
34. Bellenger V, Decelle J, Huet N. Ageing of a carbon epoxy composite for aeronautic applications. *Compos Part B Eng*. 2005;36(3):189-194.
35. De Barros S, Kenedi P, Ferreira S, Budhe S, Bernardino A, Souza L. Influence of mechanical surface treatment on fatigue life of bonded joints. *The Journal of Adhesion*. 2017;93(8):599-612.
36. Majidi H, Razavi S, Berto F. Failure assessment of steel/CFRP double strap joints. *Metals*. 2017;7(7):255.
37. Razavi SMJ, Ayatollahi MR, Majidi HR, Berto F. A strain-based criterion for failure load prediction of steel/CFRP double strap joints. *Compos Struct*. 2018;206:116-123.
38. Datla N, Ameli A, Azari S, Papini M, Spelt J. Effects of hygrothermal aging on the fatigue behavior of two toughened epoxy adhesives. *Eng Fract Mech*. 2012;79:61-77.
39. Campilho RDSG. *Repair of Composite and Wood Structures*. Amsterdam, Netherlands: Instituto Superior de Engenharia do Porto; 2009.
40. Machado J, Marques E, Campilho R, da Silva L. Mode I fracture toughness of CFRP as a function of temperature and strain rate. *J Compos Mater*. 2017;51(23):3315-3326. https://doi.org/10.1177/0021998316682309

41. Machado J, Marques E, Campilho R, da Silva LF. Mode II fracture toughness of CFRP as a function of temperature and strain rate. *Compos Part B Eng*. 2017;114:311-318.
42. Araújo H, Machado J, Marques E, da Silva L. Dynamic behaviour of composite adhesive joints for the automotive industry. *Compos Struct*. 2017;171:549-561.
43. Machado J, Gamarra P-R, Marques E, da Silva LF. Improvement in impact strength of composite joints for the automotive industry. *Compos Part B Eng*. 2018;138:243-255.
44. 294–3 I. Plastics-injection moulding of test specimens of thermoplastic materials, part 3: small plates. In. Switzerland2002.
45. Standard B. BS 2782. In. *Methods of Testing Plastics, Part*. Vol 31970.
46. ASTM D. 1002. Standard test method for apparent shear strength of single-lap-joint adhesively bonded metal specimens by tension loading (metal-to-metal). 2005;15:45-48.
47. ISO 4587: Determination of tensile lap-shear strength of rigid-to-rigid bonded assemblies. In: 1995.
48. ISO E. 62. *Plastics Determination of Water Absorption*. Geneva, Switzerland: EU adoption of International Organization for Standardization; 2008.
49. da Silva LFM. *Handbook of Adhesion Technology*. Amsterdam, Netherlands: Springer Science & Business Media; 2011.
50. Viana G, Costa M, Banea M, da Silva L. A review on the temperature and moisture degradation of adhesive joints. *Proc Inst Mech Eng, Part L: J Mater Des Appl*. 2017;231(5):488-501.
51. Machado J, Marques E, Barbosa A, da Silva LF. Effect of hygrothermal aging on the quasi-static behaviour of CFRP joints varying the overlap length. *Compos Struct*. 2019;214:451-462.
52. Ameli A, Datla N, Papini M, Spelt J. Hygrothermal properties of highly toughened epoxy adhesives. *J Adhes*. 2010;86(7):698-725.
53. Arnold C, Korkees F, Alston S. The long-term water absorption and desorption behaviour of carbon-fibre/epoxy composites. Paper presented at: Proceeding of ECCM2012.
54. Arnold J, Alston S, Korkees F. An assessment of methods to determine the directional moisture diffusion coefficients of composite materials. *Compos A: Appl Sci Manuf*. 2013;55:120-128.
55. Machado J, Nunes P, Marques E, da Silva LF. Adhesive joints using aluminium and CFRP substrates tested at low and high temperatures under quasi-static and impact conditions for the automotive industry. *Compos Part B Eng*. 2019;158:102-116.
56. Berto F, Lazzarin P. Fatigue strength of structural components under multi-axial loading in terms of local energy density averaged on a control volume. *Int J Fatigue*. 2011;33(8):1055-1065.
57. Lazzarin P, Livieri P, Berto F, Zappalorto M. Local strain energy density and fatigue strength of welded joints under uniaxial and multiaxial loading. *Eng Fract Mech*. 2008;75(7):1875-1889.

How to cite this article: Machado JJM, Marques EAS, Barbosa AQ, da Silva LFM. Fatigue performance of single lap joints with CFRP and aluminium substrates prior and after hygrothermal aging. *Fatigue Fract Eng Mater Struct*. 2019;1–15. https://doi.org/10.1111/ffe.13067

Paper 18

Content of Paper 18

Abstract

1. Introduction

2. Experimental details

2.1. SLJ

2.1.1. Material and properties

2.1.1.1. Aluminium

2.1.1.2. Adhesive

2.1.2. Fabrication and testing

2.2. Automotive structure (front header)

2.2.1. Material and properties

2.2.1.1. Aluminium

2.2.1.2. Adhesive

2.2.2. Fabrication and testing

3. Numerical details

3.1. SLJs

3.1.1. Quasi-static modelling

3.1.2. 0.1 m/s modelling

3.2. Automotive structure (front header)

4. Results and discussion

4.1. SLJs: experimental and numerical analysis

4.1.1. Quasi-static testing

4.1.2. 0.1 m/s testing

4.1.3. Displacement rate dependence

4.2. Automotive structure (front header): experimental and numerical analysis

4.3. Influence of the adhesive system on the automotive structure response

5. Conclusions

References

Experimental and numerical study of the quasi-static response of an adhesively bonded automotive structure

N.D.D. Silva[1], J.J.M. Machado[1], E.A.S. Marques[1], M. Parente[2], L.F.M. da Silva[2,*]

[1]Instituto de Ciência e Inovação em Engenharia Mecânica e Engenharia Industrial (INEGI), Rua Dr. Roberto Frias, 4200-465 Porto, Portugal

[2]Departamento de Engenharia Mecânica, Faculdade de Engenharia (FEUP), Universidade do Porto, Rua Dr. Roberto Frias, 4200-465 Porto, Portugal

Abstract

The constant demand for fuel saving in the automotive industry requires the design of lighter structures, which encourage the application of low-density materials together with structural adhesives to bond the automotive frames. Still, it is fundamental to ensure that weight reduction does not compromise mechanical resistance, making it possible to obtain lighter yet strong structures, able to fulfil the requirements of this sector. The aim of this work is to analyse the quasi-static behaviour of a component-scale automotive frame bonded with a crash-resistant epoxy adhesive, representative of the use of adhesives in real-life automotive structures. The tests were performed at room temperature (24 ºC), characteristic of normal service conditions. A numerical simulation of the structure was also conducted, allowing the comparison of the finite element model predictions with the experimental data. The results showed that the adhesive did not compromise the integrity of the automotive structure, as the failure was caused by fracture in the lower aluminium substrate. The numerical analysis revealed good accuracy in the failure load prediction of the joint. Considering the experimental observations, a more flexible polyurethane adhesive was considered to join the component, avoiding the previous fracture.

Keywords

High-performance crash-resistant adhesive; Adhesively bonded automotive structure; Quasi-static; Displacement rate; Single lap joints

[*] Corresponding author. Tel.: +351 22 508 17 06; fax: +351 22 508 14 45. *E-mail address:* lucas@fe.up.pt (L.F.M. da Silva)

1. Introduction

Reduction in both fuel consumption and CO_2 emissions is one of the most challenging concerns for automotive manufacturers. A solution to achieve this goal is the manufacture of lighter structures, encouraging the use of materials such as aluminium and composites in opposition to traditional steel in the body structure of vehicles [1]. Despite the excellent strength and stiffness to weight ratios of composites, their use in high volume structural automotive applications is still limited, mainly due to high material and manufacturing process costs as well as some uncertainty related to its functionality and long term durability [2, 3]. On the other hand, aluminium is a well-studied material and its low density in comparison to steel, associated to high corrosion resistance and good formability [4, 5], makes it attractive for body frame construction.

These lightweight concepts are also leading to innovations and new paradigms in the field of joining techniques. Fasteners and rivets represent a common solution in worldwide applications, but imply discontinuity of the materials, increase in total weight and local stress concentration that reduces structures' integrity [6]. Welding processes often cause heat distortions and residual stresses in the heat affected zone (HAZ), leading to deterioration of material properties [7]. Premature failure due to corrosion is another frequent problem, demanding more regular inspections [8]. Furthermore, it is difficult to weld aluminium properly as it tends to react with oxygen, forming an oxide layer in the surface that, although protecting against corrosion, has a higher melting point than aluminium [9]. Welding composites is also difficult and a matter of intense research, as existing processes and technologies cannot be directly transferred to these materials [10]. For these reasons, the automotive industry (as well as others like the aerospace and naval sectors) have searched for alternative joining methods and increased the use of adhesive bonding. This technique allows the manufacture of structures that would be impossible otherwise and is readily automated [9], leading to an equal stress distribution along the bonded length and reduction of stress concentrations [11], thus enhancing fatigue resistance [9, 12]. Additionally, the use of adhesives leads to a reduction of noise and vibrations [1, 9], improved damage tolerance and lower fabrication costs [13].

Adhesives, which are usually polymeric materials, are known to be highly sensitive to strain rate [12-14]. Several studies were conducted in the last decade about the effect of this parameter on the properties of the adhesives. For instance, Banea et al. [13] investigated the effect of test speed on the tensile properties of an epoxy and concluded

that both ultimate tensile stress and Young's modulus increased with strain rate. Machado et al. [12] tested a crash-resistant epoxy adhesive at different strain rates and similar conclusions were drawn. Of all types of adhesives, epoxies are one of the most used in automotive structural applications due to their high strength [15]. Borsellino et al. [9] analysed the joint resistance of an aluminium alloy sheet with several adhesives (orthophtalic polyester, vinylester and epoxy resins) and concluded that the epoxy resin joint was the most resistant, due to the intrinsic strength of the adhesive, the enhanced stability of aluminium oxide in alkaline environment and the effect of mixing with catalyst. Besides epoxy systems, the use of structural polyurethanes in the automotive industry is also common, mainly due to their high durability, good fatigue behaviour and peel strength [16].

Despite offering accurate results, experimental testing is not always desired, as it often requires time-consuming manufacturing processes, material spending and specific testing equipments and procedures. Therefore, numerical simulation through finite element (FE) models has become a powerful tool for design, as it allows a reduction in the number of experimental tests that must be conducted. When designing bonded joints, a damage mechanics approach based in cohesive zone modelling (CZM) has been widely used in the strength prediction of adhesive joints, using energy-based principles to model damage growth [17]. The validation of the FE models with experimental data is necessary in a first stage, so that model calibration can be performed and reliable results achieved. Numerical modelling using CZM has already been extensively applied in the prediction of the mechanical behaviour of adhesive joints with simple configurations, such as single lap joints (SLJs). Mixed adhesive SLJs under quasi-static conditions were numerically analysed by Machado et al. [18] and the results were compared to the experimental data obtained in a previous work. Cohesive numerical models were concluded to be a viable tool to predict the behaviour of mixed joints. A numerical approach was also used in [17] with the goal of predicting the behaviour of adhesive corner joints, previously tested in [19]. The FE analysis was considered to present a good agreement with the data obtained in the experiments, showing that cohesive damage models provide good results for these configurations. However, for the static response of real, full-scale automotive structures, the information available is still limited and few examples can be found where comparisons are made between experimental and numerical results. Lahaye et al. [20] focused on the development of an aluminium bonnet for the Saab 9-3 model in replacement of the steel version. The new prototype underwent a series of tests to evaluate

its performance during the lifetime of a vehicle and allowed a 50% weight reduction while satisfying the performance tests required by Saab®. Cheon et al. [21] investigated the use of a glass-fibre-reinforced epoxy composite in alternative to steel in the side-door impact beams of passenger cars. The energy absorption behaviour of the composite beams was found to be worse when the beams were subjected to static conditions. The FE results obtained in ABAQUS® showed good agreement with experimental data.

The present work aims to experimentally analyse the mechanical behaviour of a real, adhesively bonded automotive structure under quasi-static (1 mm/min) conditions. Using the data collected in previous works [12, 22], the mechanical properties of the epoxy system will allow the definition of cohesive laws that can be applied to predict the behaviour of the joint through a finite element method (FEM) simulation using CZM in the adhesive. The numerical results can then be compared to the experimental data obtained at room temperature (RT) to validate the model. Since the adhesive layer thickness used to bond the automotive structure is considerably high (1.6 mm), the quasi-static (1 mm/min) and 0.1 m/s response of SLJs bonded with different thicknesses of the same adhesive is also studied, so that the influence of this parameter in the behaviour of the joint can be properly evaluated. As a complement, a polyurethane adhesive was also used to bond the automotive structure under the same loading conditions.

2. Experimental details

2.1. SLJ

2.1.1. Material and properties

The SLJ specimens used in the present work were manufactured with aluminium substrates, bonded with a highly ductile, crash-resistant epoxy adhesive, with the reference XNR6852 E-3, supplied by Nagase ChemteX®.

2.1.1.1. Aluminium

Since the substrates of the automotive structure are made of the AA6016-T4 aluminium alloy, the research plan for SLJ tests entailed use the same material. However, this was not possible because the aluminium manufacturers that were contacted only provide the AA6016-T4 alloy in large quantities, compatible with industrial production

but not with scientific research. Furthermore, the storage of this alloy is not common in T4 (naturally aged) temper, as prolonged exposure to environmental agents leads to the deterioration of this heat treatment. For these reasons, the AA6082-T6 alloy was selected for this step instead due to its similar mechanical properties, shown in Table 1, and greater availability in the market.

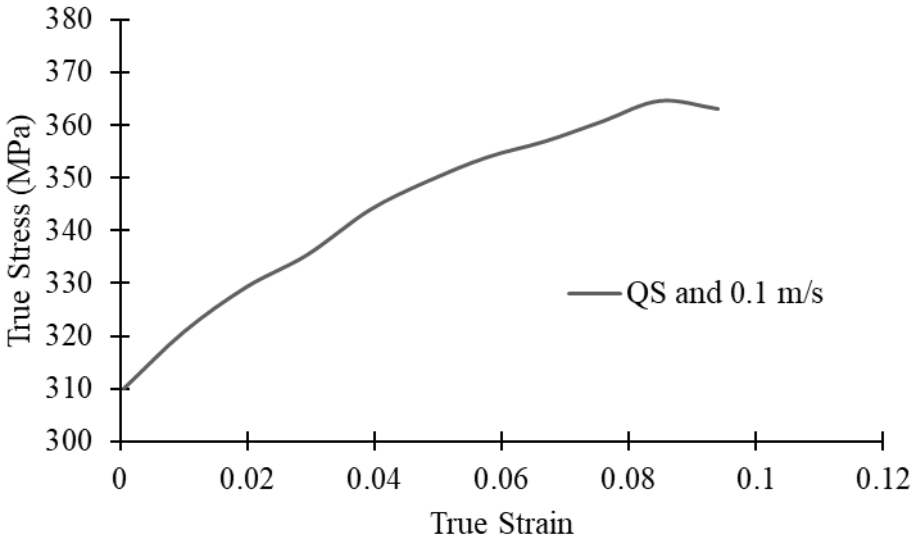

Fig. 1. Plastic behaviour of AA6082-T6 for the tested conditions (adapted from [23]).

The influence of strain rate on the mechanical properties of this alloy was studied by several authors [23-26], all reporting that AA6082-T6 presents low strain rate sensitivity at RT. Its plastic behaviour was adapted from [23] and is represented in Fig. 1.

Table 1. General mechanical properties of the AA6082-T6 aluminium alloy.

Properties	
Density, ρ [kg/m^3]	2700
Young's modulus, E [MPa]	69000
Shear modulus, G [MPa]	26000
Poisson's ratio, ν	0.33
Tensile strength, σ_n [MPa]	360
Yield strength, σ_y [MPa]	310
Shear strength, τ [MPa]	220
Elongation at break, ε [%]	9.8

2.1.1.2. Adhesive

The adhesive chosen to bond the aluminium substrates in the SLJs is the same that was initially applied in the automotive structure, namely a crash-resistant epoxy system.

The mechanical properties of this adhesive at RT have already been obtained in previous works for quasi-static (1 mm/min) conditions. The tensile strength and Young's modulus were determined by Machado et al. [12] performing tensile tests over bulk specimens. DCB specimens tested at 1, 10 and 100 mm/min allowed the assessment of the fracture toughness in mode I (G_{IC}). The remaining properties of the adhesive for this two conditions, as the fracture toughness in mode II (G_{IIC}) and the shear strength and modulus, were studied by Araújo et al. [22].

The properties of XNR6852 E-3 for a displacement rate of 0.1 m/s were found using the logarithmic laws proposed in [12]. These laws are generically given by Eq. (1).

$$\text{Property to determine} = A\ln(x) + B \tag{1}$$

where A and B are constants obtained from experimental data. When determining tensile strength, Young's modulus and G_{IC}, the value of x should be the displacement rate, in mm/min, while for shear strength the x variable stands for the strain rate, in s^{-1}. A displacement rate of 0.1 m/s is equivalent to 6000 mm/min and the conversion to strain rate can be achieved by using Eq. (2).

$$\dot{\varepsilon}(t) = \left(\frac{L(t) - L_0}{L_0}\right) = \frac{v(t)}{L_0} \tag{2}$$

where $v(t)$ corresponds to the displacement rate, in mm/s, and L_0 to the value of length of the adhesive bulk tensile specimen used to determine the shear properties, which acquired the value of 120 mm. Therefore, a displacement rate of 0.1 m/s leads to a strain rate of 0.83 s^{-1}. Logarithmic laws were not proposed for the shear modulus and G_{IIC} in [12]. For these parameters, similar laws were constructed using the values at 1 mm/min (quasi-static) and 180000 mm/min (3 m/s, impact condition), the last presented as well in [22]. The properties at 0.1 m/s were then calculated using the same procedure. Table 2 summarizes the properties of the adhesive for quasi-static and 0.1 m/s conditions. The glass transition temperature, T_g, was also determined to be 132 ± 4.51°C [12] and its density 1550 kg/m^3.

Table 2. Mechanical properties of XNR6852 E-3 adhesive for quasi-static and 0.1 m/s loadings.

Properties	**QS (1 mm/min)**	**0.1 m/s**
Cohesive tensile strength, t_n^0 [MPa]	48	65
Young's modulus, E [MPa]	1874	1717
Cohesive shear strength, t_s^0 [MPa]	45	46
Shear modulus, G [MPa]	665	620
Fracture toughness in mode I, G_{IC} [N/mm^2]	9.2	12.2
Fracture toughness in mode II, G_{IIC} [N/mm^2]	51	60

2.1.2. Fabrication and testing

The SLJs specimens used aluminium adherends with a thickness of 2 mm, as this value is close to the substrates thickness in the automotive structure. Due to the high ductility of the adhesive, an overlap length of 12.5 mm was chosen in an effort to ensure that failure was ruled only by the adhesive's behaviour and not by the plasticity of aluminium. Two adhesive layer thicknesses were tested, namely 0.2 and 1.6 mm, allowing to analyse the influence of this parameter on the failure load. The last is the approximate thickness of the adhesive in the automotive frame, while the first is well known as a typical optimum thickness that provides the highest static strength in most joint configurations. However, in many practical applications, including in the automotive industry, non-optimal configurations are often used, as very thin layers are difficult to manufacture and control in a typical production line [27]. At least three specimens (which dimensions are shown in Fig. 2) were tested for each configuration and loading condition.

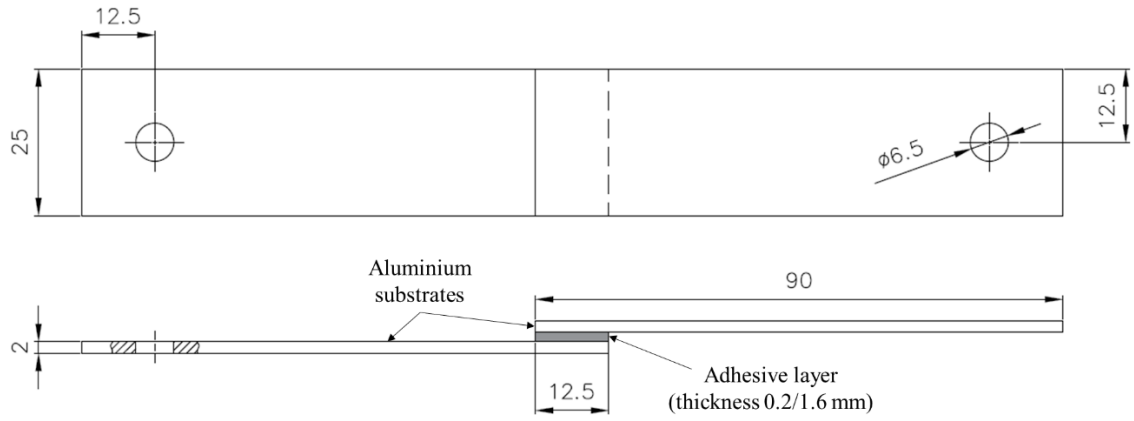

Fig. 2. Configuration and dimensions of the tested SLJs.

The first step in the fabrication of the SLJs was to drill and anodise the adherends using phosphoric acid anodizing. This superficial treatment is recommended for adhesive joints with aluminium substrates, creating a surface which offers a good level of adhesion and avoids interfacial failure. The joints were manufactured using an aluminium mould, with pins being used to ensure the correct alignment of the joint. Spacers with a length of 77.5 mm were inserted in the mould assembly, ensuring that the desired overlap length is attained. Aluminium was chosen as the mould material to avoid large differentials in thermal expansion between the mould and the joints. For a bond thickness of 0.2 mm, the adhesive was manually spread with a spatula, while a pressure gun was used for a thickness of 1.6 mm so that voids in the adhesive layer could be avoided. The manufacturing process was completed by placing the mould in a hot plate press, under pressure and temperature, allowing the fulfilment of the curing cycle of this epoxy system, defined by the manufacturer as 4h at 165 °C.

The quasi-static tests of the joints were performed in an INSTRON® universal testing machine, model 3367 (Norwood, Massachusetts, USA), with a loading capacity of 30 kN. The tests were performed at a constant cross-head displacement rate of 1 mm/min. For 0.1 m/s condition, a Material Test System® 8801 servo-hydraulic testing machine with a capacity of 100 kN was used. This machine was necessary to perform tests at this condition as the first equipment, which uses electrical drive, does not have capacity to apply such a large displacement rate.

2.2. Automotive structure (front header)

Fig. 3 shows the analysed automotive component in the body structure of the vehicle.

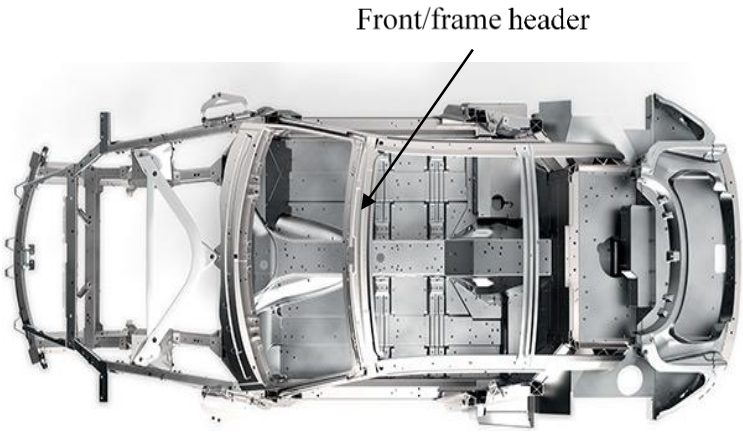

Fig. 3. Location of the front header in the structure of the Aston Martin's DB11 model.

2.2.1. Material and properties

2.2.1.1. Aluminium

The automotive structure, often called front header of a vehicle, uses AA6016-T4 alloy substrates, and were supplied in an already anodised state. After being submitted to the curing cycle of the adhesive, the properties of this alloy become similar to those of the AA6016-T6. The mechanical properties of both alloys are shown in Table 3, while the plastic behaviour of the substrates after curing is represented in Fig. 4.

Table 3. General mechanical properties of the AA6016-T4 and AA6016-T6 alloys.

Properties	**AA6016-T4**	**AA6016-T6**
Density, ρ [kg/m^3]	2700	2700
Young's modulus, E [MPa]	69000	69000
Shear modulus, G [MPa]	26000	26000
Poisson's ratio, ν	0.33	0.33
Tensile strength, σ_n [MPa]	200	280
Yield strength, σ_y [MPa]	110	210
Shear strength, τ [MPa]	130	170
Elongation at break, ε [%]	27	11

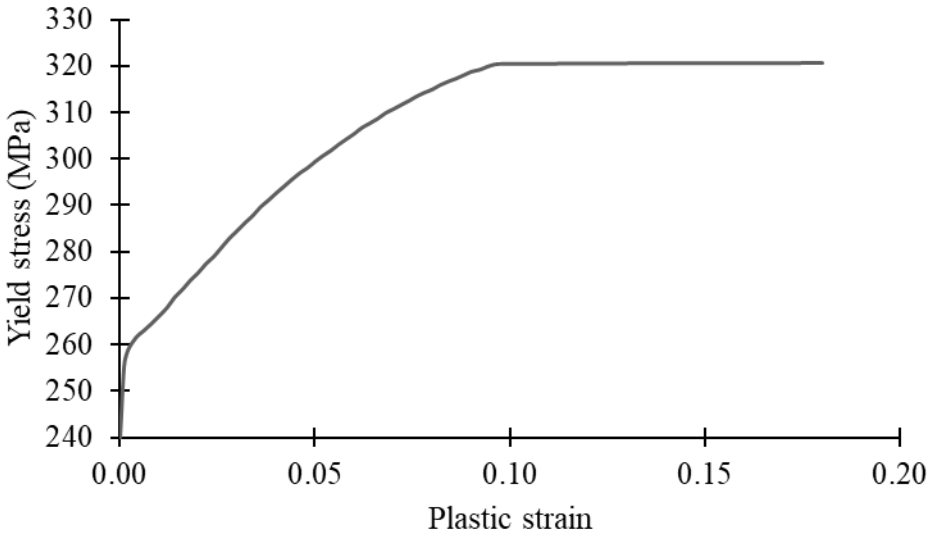

Fig. 4. Plastic behaviour of the AA6016-T6 aluminium alloy, used in the substrates of the automotive structure.

2.2.1.2. Adhesive

The lower and upper substrates of the structure were initially bonded with the XNR6852 E-3 adhesive, which properties at quasi-static conditions were already described in Table 2.

2.2.2. Fabrication and testing

Before the actual bonding procedure was carried out, the lower and upper substrates were cleaned with isopropanol alcohol in order to clean and degrease the surfaces and ensure a good adhesion. The adhesive bead was adjusted to ensure that the final adhesive layer was approximately 17 mm wide and 1.6 mm thick, with constant dimensions throughout all the bondline. To guarantee this thickness, a total of 14 spacers consisting of overlapped calibrated tape layers were assembled in the edges of the lower substrate, in order to minimize the interference with the adhesive bead. The XNR6852 E-3 was applied at both sides of the lower substrate using an applicator gun (approximately 70 g of adhesive were deposited for each specimen) and the upper substrate was then assembled on its top. Clamps were positioned in the spacers' locations to fix the substrates together and apply pressure along the bondlines. Finally, the structure was placed in an oven to perform the curing cycle of the adhesive and any excess was removed from the joint after this process. The steps of the manufacturing procedure are resumed in Fig. 5.

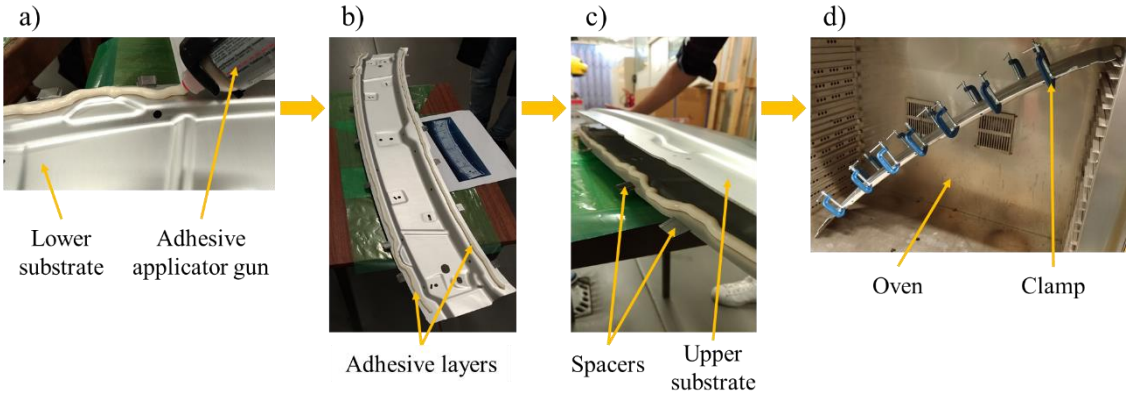

Fig. 5. Manufacturing sequence of the "front header": a) adhesive application; b) adhesive layers on the lower substrate; c) assembling of the upper substrate; d) introduction in the oven of the clamped structure to perform the curing cycle.

The tests were performed in a Material Test System® 8801 servo-hydraulic testing machine with a capacity of 100 kN, with a constant cross-head displacement rate of 1 mm/min being applied. The contact with the structure was made by an "impactor",

designed with a round bottom shape to apply the load uniformly throughout the contact area. A total of eight screw-nut connections were used to fix the automotive structure on its ends. The applied load and vertical displacement, necessary to construct the load-displacement curves, were directly measured by the machine. The assembly of the test is shown in Fig. 6 and two specimens were tested.

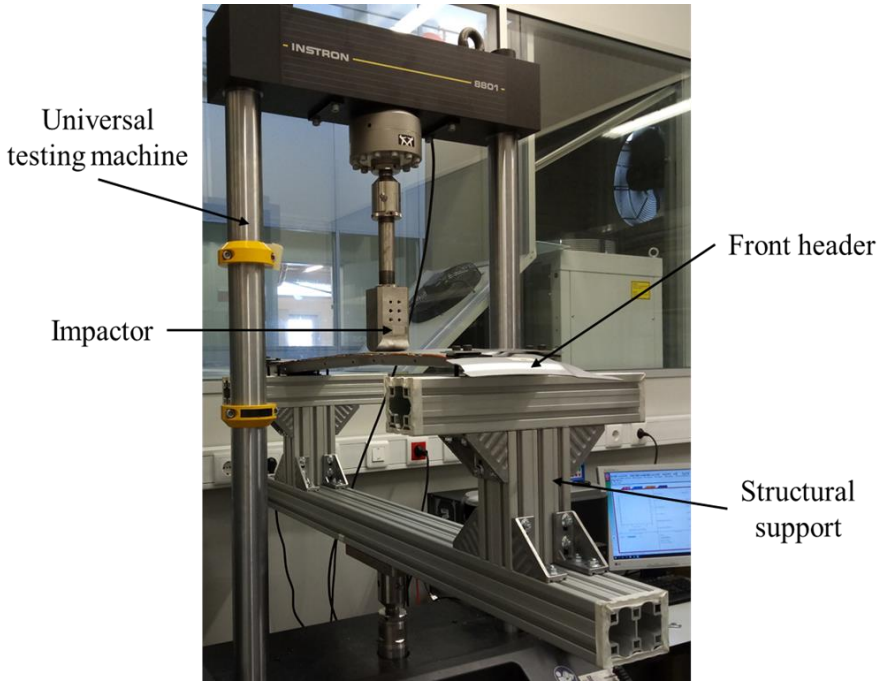

Fig. 6. Configuration of the performed tests under quasi-static conditions.

3. Numerical details

As mentioned before, numerical modelling using CZM is a powerful and accurate tool for failure load prediction of adhesive joints. This technique, originally applied by Hillerborg [28], is able to model the fracture process through the combination of concepts from elasticity and classical fracture mechanics. Cohesive elements, which make use of strength and energetic parameters, are used to simulate crack growth and traction-separation laws are responsible for establishing a relation between stresses and displacements along the process [22]. The most commonly used laws in adhesive bonding are the triangular, trapezoidal and exponential laws and, within these three, the triangular shape (Fig. 7) is often the first choice due to its simplicity, standard implementation in FEM packages as ABAQUS® and lowered susceptibility to convergence problems [29]. The application of these laws requires the knowledge of several adhesive properties and

can be constructed for tensile (mode I) and shear (mode II) loading conditions. When the law is built for mode I, the cohesive tensile strength (σ_n), the Young's modulus (E) and the critical fracture toughness in mode I (G_{IC}) are needed, while the cohesive shear strength (τ_s), the shear modulus (G) and the critical fracture toughness in mode II (G_{IIC}) are required for mode II.

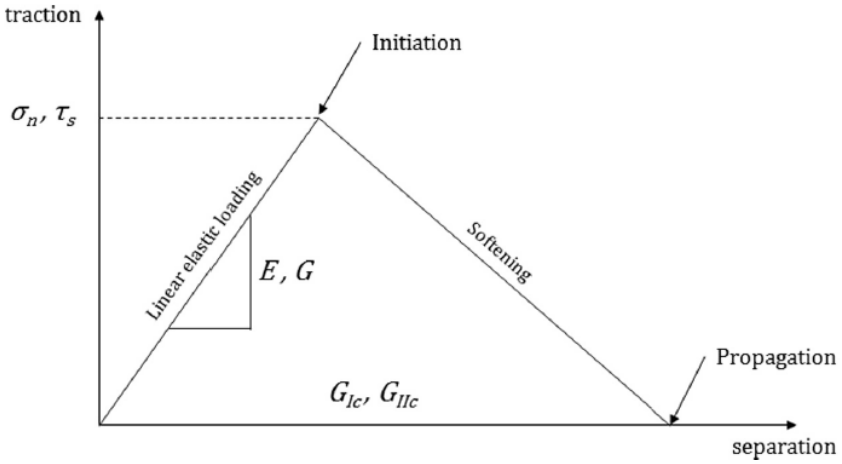

Fig. 7. Triangular traction-separation law for mode I, mode II [22].

3.1. SLJ

3.1.1. Quasi-static modelling

All FE analysis were conducted with the ABAQUS® software package, with two-dimensional (2D) meshes being used to model the SLJs due to its simple geometry. For an adhesive thickness of 0.2 mm, 4-node bilinear plain strain quadrilateral elements (CPE4 in ABAQUS® nomenclature) were assigned to the aluminium adherends, while a unique layer of 4-node two-dimensional cohesive elements (COH2D4 in ABAQUS® nomenclature) was used in the adhesive region. In the case of the SLJs with an adhesive thickness of 1.6 mm, the only difference was located on the bonded area, which was modelled using intercalated layers of plain strain and cohesive elements (Fig. 8). Within this region, the elastic properties of the adhesive were attributed to the plain strain elements. This new design was considered for the higher adhesive thickness as it reproduces the failure mechanism more accurately, leading to better results in the failure load prediction of the joints. For both thicknesses, the cohesive elements were modelled through a triangular law (Fig. 10a), built with the quasi-static properties mentioned before (Table 2). A mesh refinement was made in the most stressed areas, namely the overlap

region, using the bias functionality (Fig. 9). This technique allows a good compromise between accuracy in the results and computational time. A static, general step was chosen to solve the model and as boundary conditions, one end of the joint was prevented to move in the two in-plane directions, while on the other end of the specimen, an horizontal displacement was directly imposed, with a restriction in vertical movement being made, simulating the displacement imposed by the universal testing machine (Fig. 11). Finally, the SDEG parameter (that allows to check the degradation of the cohesive elements representing the adhesive), the reaction forces on the bi-restrained end and the displacement on the single-restrained end were requested as outputs to construct the load-displacement curves.

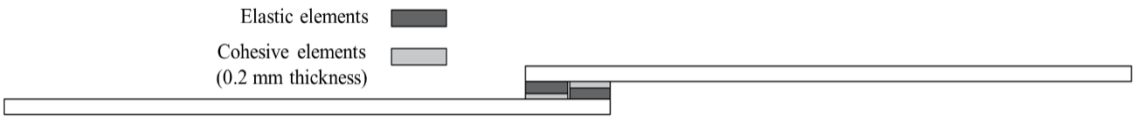

Fig. 8. Joint design used to model the behaviour of the SLJs with an adhesive thickness of 1.6 mm, with plain strain and cohesive elements being applied in the bonded region.

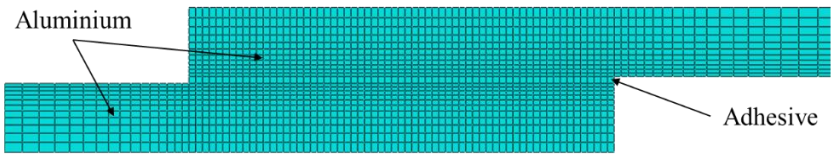

Fig. 9. Mesh refinement on the overlapped area, using the bias functionality.

3.1.2. 0.1 m/s modelling

The geometry, element types and concepts applied at the numerical model for the 0.1 m/s condition were similar to those presented for quasi-static. The only change applied focused on the triangular law used, which was now constructed with the properties corresponding to 0.1 m/s (Fig. 10b).

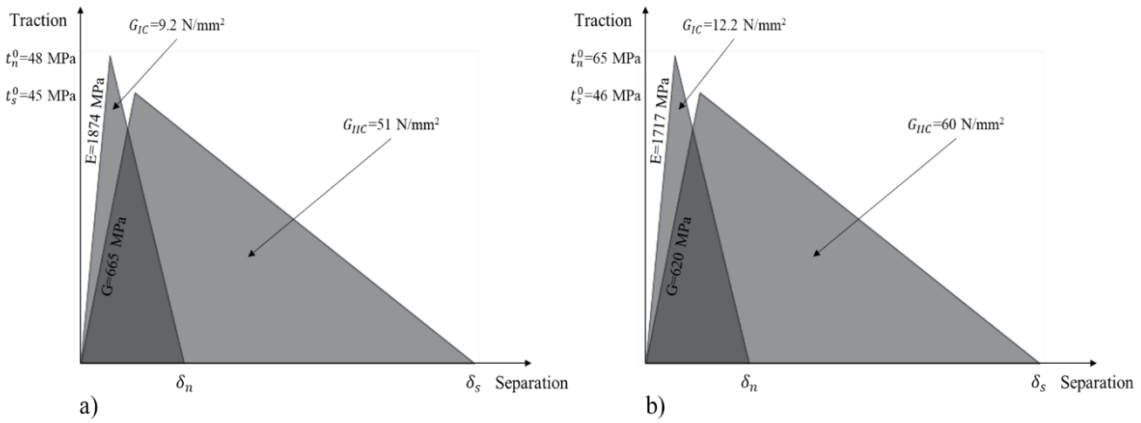

Fig. 10. CZM's traction-separation law for a) quasi-static and b) 0.1 m/s models.

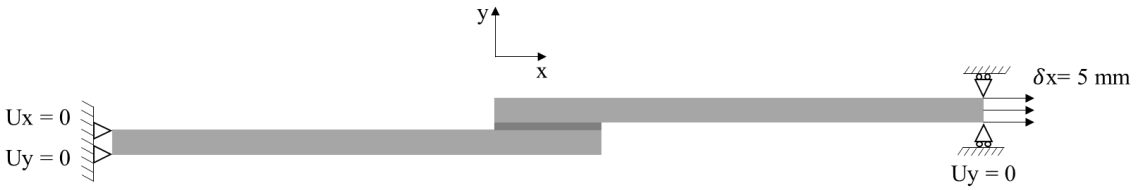

Fig. 11. Representation of the boundary conditions for quasi-static and 0.1 m/s conditions.

3.2. Automotive structure (front header)

The quasi-static numerical simulations of the front header were also carried out in ABAQUS®, with the mesh being imported from a model created in the HYPERMESH® software package. Shell elements with thicknesses of 1.7 and 1.2 mm were used to model the upper and lower aluminium substrates, respectively. The majority of these were linear quadrilateral elements (S4 in ABAQUS® nomenclature), but linear triangular elements (S3 in ABAQUS® nomenclature) were also employed due to the complex geometry of the structure. For modelling the adhesive bondlines, a single layer of linear, 8-node three-dimensional (3D) cohesive elements (COH3D8 in ABAQUS® nomenclature) was assigned and the properties at quasi-static conditions were used. Since the deformation and stress states on the impactor are negligible and not of interest, the same was modelled as a rigid body. To avoid penetration of the structure by the impactor, an interaction between the two was given, with a normal behaviour of the type “Hard contact” and a tangential behaviour with a friction coefficient of 0.61. As boundary conditions, the ends of the front header were encastred at both sides, simulating the service conditions (Fig. 12), and the impactor was allowed to move only in the vertical direction. A static, general

step was used to simulate the process and the SDEG parameter, the reaction forces at the encastre zones and the impactor's displacement were requested as outputs.

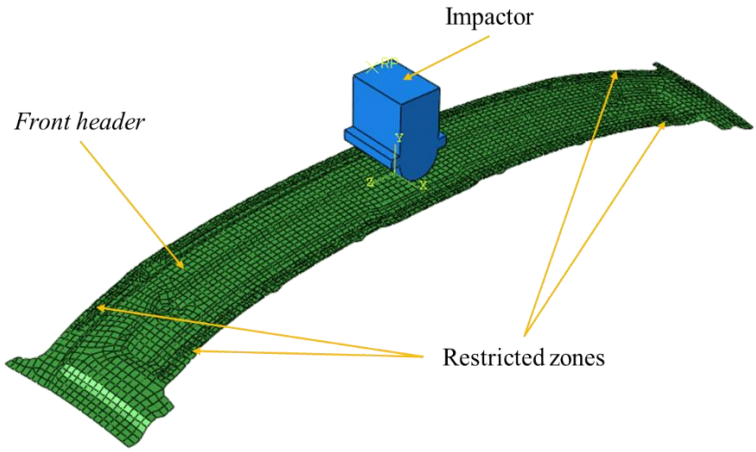

Fig. 12. Boundary conditions applied to the structure at static conditions.

4. Results and discussion

4.1. SLJ: experimental and numerical analysis

4.1.1. Quasi-static testing

The tests under quasi-static conditions for an adhesive thickness of 0.2 and 1.6 mm were found to lead to cohesive failure in the adhesive, as shown in Fig. 13.

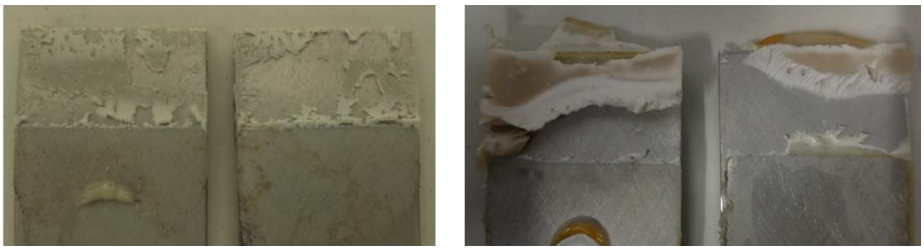

a) b)

Fig. 13. Cohesive failure in the adhesive for SLJs with a) 0.2 and b) 1.6 mm of adhesive layer thickness.

The SDEG parameter obtained in the numerical analysis, showing the degradation of the adhesive layer during the process, is displayed in Fig. 14 for the case of an adhesive thickness of 0.2 mm. The degradation was found to begin in the boundaries of the adhesive layer, continuously propagating until cohesive failure was reached. Similar results were obtained for a thickness of 1.6 mm.

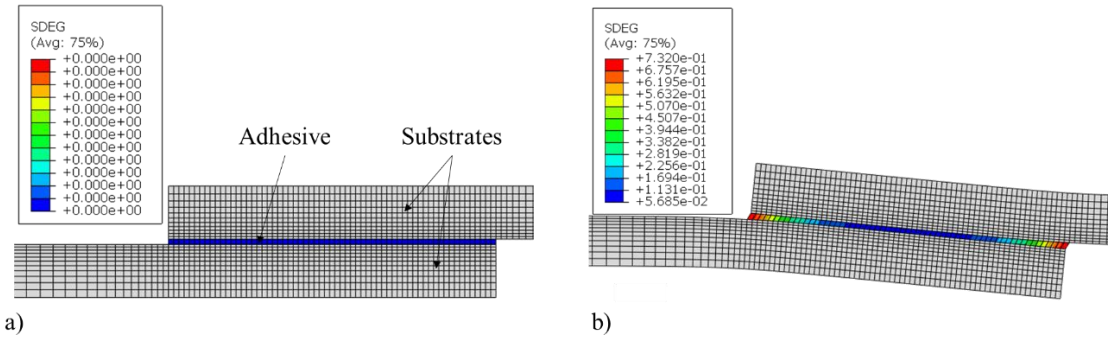

Fig. 14. Adhesive's numerical degradation for a thickness of 0.2 mm at a) the initial and b) an intermediate stage of the quasi-static loading process.

Comparisons between representative experimental load-displacement curves and the numerical results, for both thicknesses, are represented in Fig. 15.

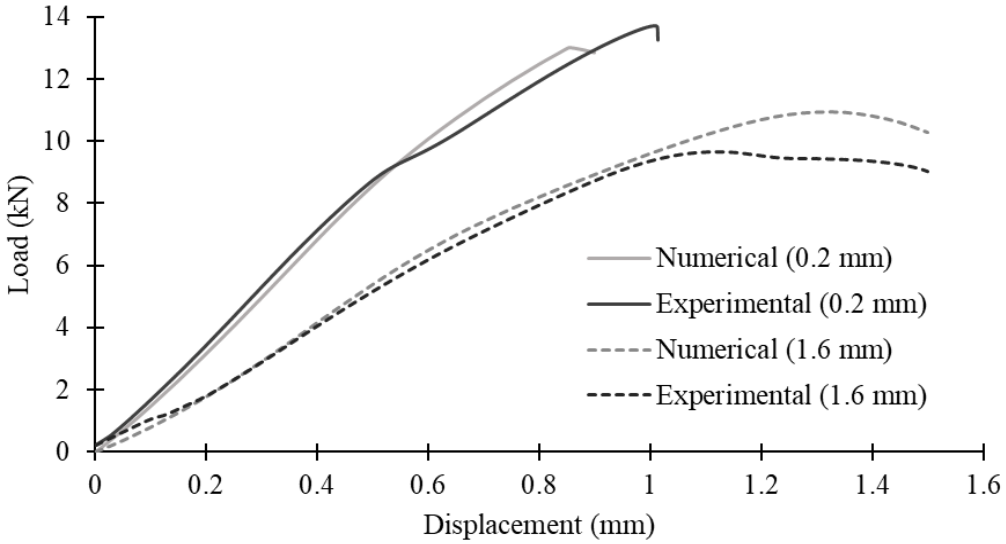

Fig. 15. Typical experimental and numerical load-displacement curves for the two tested adhesive thicknesses under quasi-static conditions.

The numerical curves can be considered to be in good agreement with the experimental data regarding the failure load, especially for a thickness of 0.2 mm. Concerning the 1.6 mm thickness, the prediction is not so accurate, but still reasonably good. This phenomenon can be explained by the higher susceptibility of the much thicker 1.6 mm joints to manufacturing defects, such as voids, leading to experimental failure loads lower than those expected by the FE models, where perfect material is assumed to exist. For a thickness of 0.2 mm, the experimental results show a slightly higher failure load than that predicted by the numerical analysis, which may be due to the intrinsic variation associated with the adhesive properties introduced in the model. The results

revealed that an increase in the adhesive thickness lead to a decrease in the failure load of the joint, as a better value was found for 0.2 mm. This observation is in accordance with the results obtained by Goglio et al. [30], when testing lap shear steel joints with an epoxy adhesive thickness of 0.5 and 1 mm, and by Banea et al. [31], when analysing SLJs with hard steel substrates bonded with a structural polyurethane adhesive with thicknesses ranging from 0.2 to 2 mm.

The complete results for the quasi-static loading can be found in Table 4, with the total absorbed energy being calculated as the area below the curves. Although they present worse results regarding the failure load, the joints with an adhesive thickness of 1.6 mm provide better energy absorption capabilities when compared to a thickness of 0.2 mm. Although larger bondline thicknesses are preferred in adhesively bonded automotive structures due to their better capability to deal with geometrical deviations in the substrates, they are also able to provide benefits to the mechanical behaviour. The strength, the energy absorption or a compromise between both can be the most important factor according to the application, being the adhesive thickness adjusted to fulfil the desired requirements.

Table 4. Failure load and energy absorption results for an adhesive thickness of 0.2 and 1.6 mm.

	0.2 mm		**1.6 mm**	
	Experimental	**Numerical**	**Experimental**	**Numerical**
Failure load (kN)	13.39 ± 0.36	13.03	9.20 ± 0.49	10.94
Absorbed energy (J)	8.64 ± 0.55	5.98	12.19 ± 3.02	13.14

4.1.2. 0.1 m/s testing

The failure surfaces for the 0.1 m/s condition are shown in Fig. 16, where it is possible to conclude that cohesive failure in the adhesive occurred also for this case. Regardless the thickness, the degradation process of the adhesive layer, obtained numerically, was found once again to initiate on its ends. Fig. 17 presents the SDEG parameter, now for the thickness of 1.6 mm.

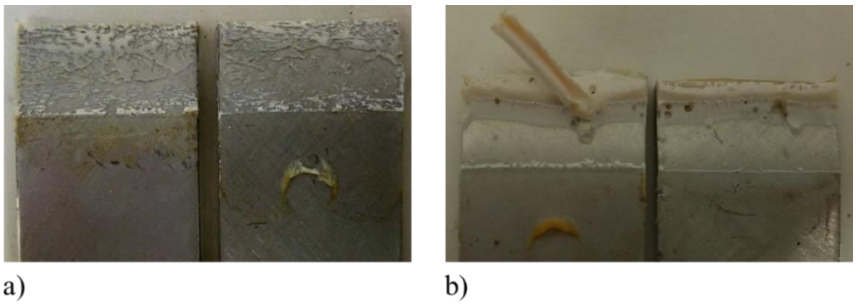

Fig. 16. Cohesive failure in the adhesive verified at 0.1 m/s: a) 0.2 mm and b) 1.6 mm adhesive thickness.

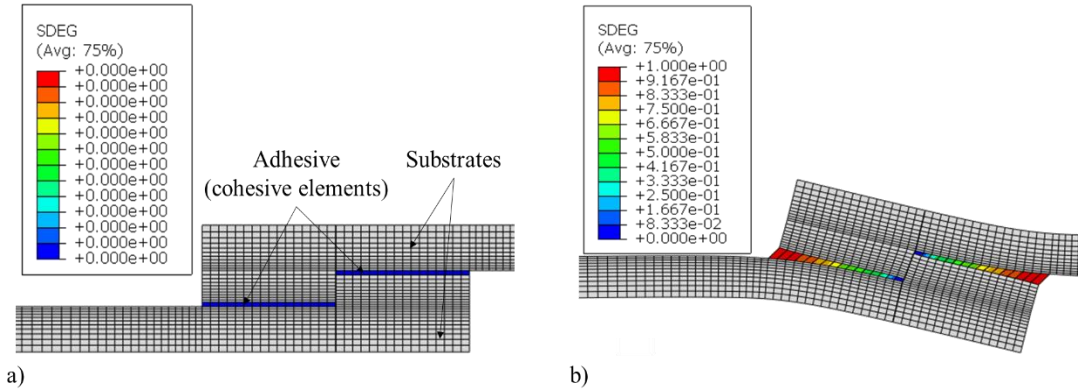

Fig. 17. Adhesive's numerical degradation for an adhesive thickness of 1.6 mm, at 0.1 m/s: a) initial and b) failure-imminent moments.

Fig. 18 shows the load-displacement evolutions (with representative experimental curves), where it is possible to conclude that the numerical results accurately predict the experimental data for both thicknesses.

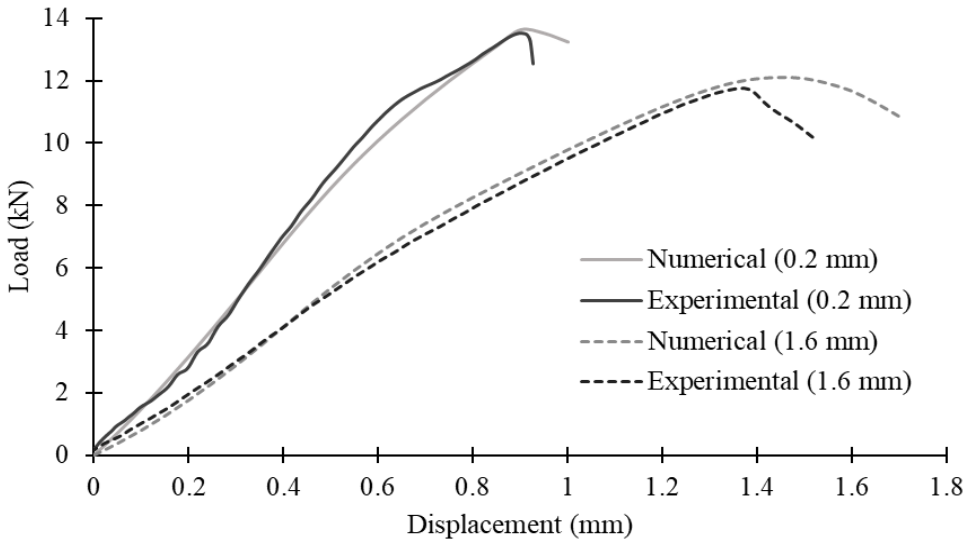

Fig. 18. Experimental and numerical load-displacement evolutions for both thicknesses at 0.1 m/s.

Also, for a displacement rate of 0.1 m/s, and in accordance with the quasi-static results, a higher joint strength and energy absorption were found for the lowest and highest thickness, respectively (Table 5).

Table 5. Summary of the failure load and energy absorption results obtained at 0.1 m/s.

	0.2 mm		**1.6 mm**	
	Experimental	**Numerical**	**Experimental**	**Numerical**
Failure load (kN)	13.99 ± 0.75	13.62	11.10 ± 0.86	12.12
Absorbed energy (J)	8.93 ± 3.13	6.58	14.60 ± 3.03	14.78

4.1.4. Displacement rate dependence

The SLJs strength appears to increase with the displacement rate for both adhesive layer thicknesses (Fig. 19), being the rise more pronounced for 1.6 mm. A similar conclusion was reached by Machado et al. [6] and [32] when testing joints composed of carbon-fibre reinforced plastic (CFRP) and AA6060-T6 alloy substrates, respectively, bonded with the same crash-resistant adhesive at RT.

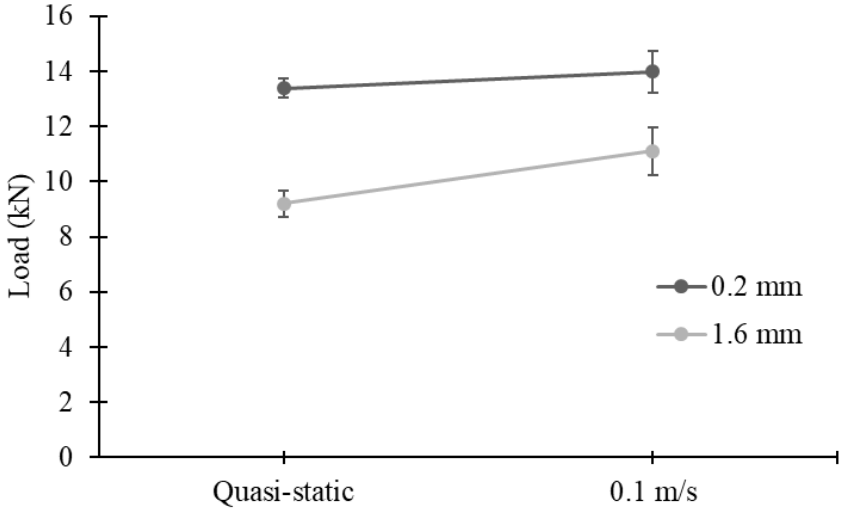

Fig. 19. Comparison of the average values and standard deviation of the failure load results for both adhesive thicknesses tested at quasi-static (1 mm/min) and 0.1 m/s conditions.

4.2. Automotive structure (front header): experimental and numerical analysis

When subjected to the quasi-static load, the two automotive specimens failed due to the high stress concentration around the central holes, which led to the initiation and propagation of a crack (Fig. 20). For this reason, it can be concluded that the behaviour

of the structure was ruled by the aluminium substrates, and that the adhesive used to bond them did not compromise structure's integrity. This can be observed by the shape of the representative experimental and numerical load-displacement curves (Fig. 21), which follow a typical elastic-plastic behaviour of aluminium. From the crack initiation moment forward, the load capacity of the front header abruptly decreases, being its total strength considerably low.

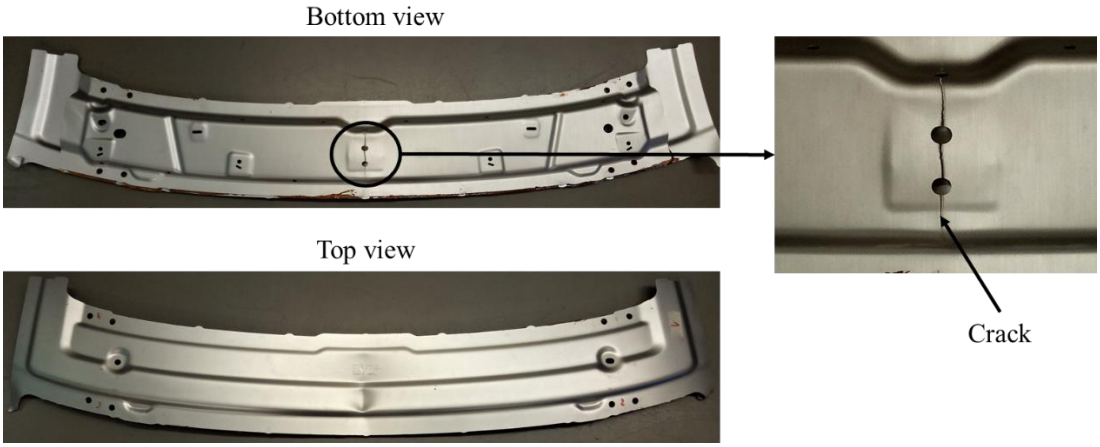

Fig. 20. Failure verified in both specimens at quasi-static conditions.

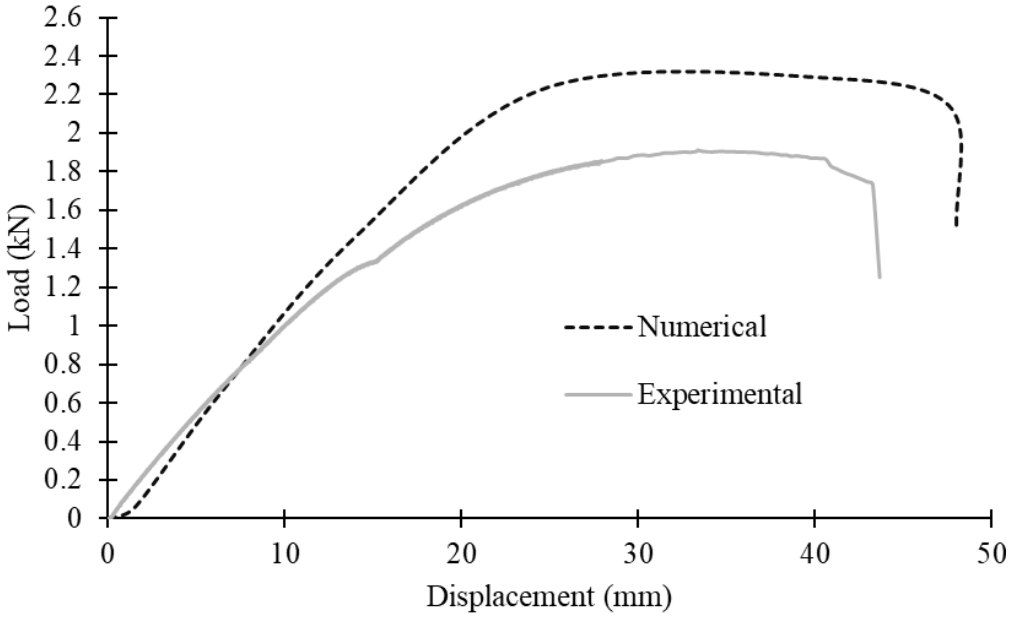

Fig. 21. Experimental and numerical results obtained for the quasi-static loading.

Since no information regarding the damage evolution of the aluminium substrates was available, the numerical analysis results were only considered until the moment when the ultimate stress of the aluminium was reached (shown in Fig. 4). The numerical model

shows relatively good results regarding the failure load prediction, but the displacement values are not as satisfactory, which can be due to the boundary conditions imposed to the structure. As mentioned before, encastre boundary conditions were applied to the ends of the component in the numerical analysis, something that is not exactly replied in the experimental procedures. Therefore, the specimens mounted in the assembly are less stiff than the model and can slightly move during the tests, leading to higher displacements. So that this effect could be compensated, the stiffness of the model in Fig. 21 was adjusted to the observations to better compare the results.

The numerical and experimental results regarding the failure load and the absorbed energy are shown in Table 6. The failure load predicted by the numerical model is slightly higher than the one observed in the experiments, which is usual as eventual manufacturing deviations and defects in both adhesive and aluminium substrates are not considered in the FE analysis.

Table 6. Failure load and absorbed energy of the automotive structure at quasi-static conditions.

	Experimental	**Numerical**
Failure load (kN)	1.78 ± 0.19	2.28
Absorbed energy (J)	60.23 ± 2.55	81.74

4.3. Influence of the adhesive system on the automotive structure response

Considering the failure mechanism observed in the automotive structure bonded with the crash-resistant epoxy, a new adhesive system was considered to join the aluminium substrates, namely a two-component, high-performance structural polyurethane with the reference SikaForce®-7818 L7, supplied by Sika®. The aim of this study was to determine the influence of the type of adhesive on the behaviour of the component. The general mechanical properties of this adhesive, given by the manufacturer, are shown in Table 7. For this case, only one specimen was manufactured and tested. The manufacturing process was the same as the one previously presented, excepting for the curing cycle. In opposition to the epoxy system that requires high curing temperatures, the polyurethane cures at RT by chemical reaction of the two components.

Table 7. General properties of the structural polyurethane adhesive.

Properties	
Density [kg/m^3]	1230
Tensile strength [MPa]	35
Young's modulus [MPa]	2500
Tensile lap-shear strength [MPa]	20
Elongation at break [%]	2.5
Glass transition temperature [°C]	45

Fig. 22 represents the experimental load-displacement curves for the specimens bonded with both adhesives, with a representative curve being used for the crash-resistant epoxy.

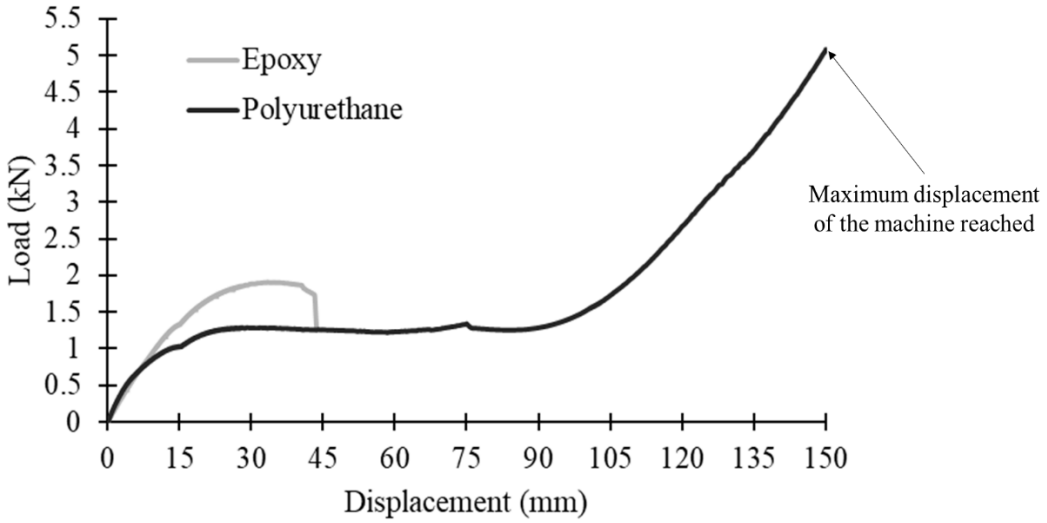

Fig. 22. Load-displacement curves for the automotive structure bonded with a crash-resistant epoxy and a high-performance polyurethane for quasi-static conditions.

When the automotive specimen was bonded with the structural polyurethane, no crack was found in the lower substrate (Fig. 23). The total strength of the component for this case was not found, as the maximum displacement that the universal testing machine is able to provide was reached before the failure load was verified. Although being weaker, the polyurethane is more flexible than the crash-resistant adhesive, absorbing more energy and transferring less load to the lower substrate, preventing its fracture. Therefore, in the context of a joint, the polyurethane adhesive seems to be more advantageous. Table 8 resumes the results of the specimens bonded with the two adhesives under quasi-static conditions.

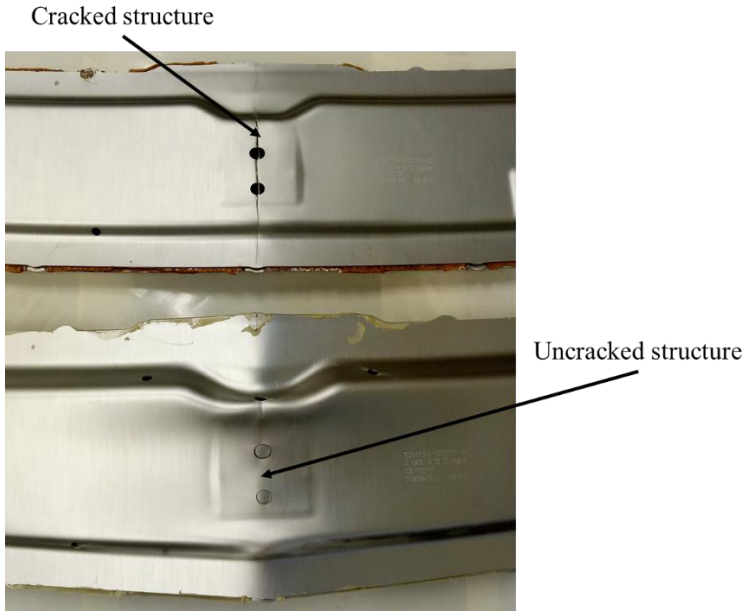

Fig. 23. Cracked and uncracked specimens, bonded with the crash-resistant epoxy and the structural polyurethane adhesive, respectively.

Table 8. Results of the automotive structure bonded with the two adhesive systems.

	Epoxy	**Polyurethane**
Failure load (kN)	1.78 ± 0.19	Not reached
Absorbed energy (J)	60.23 ± 2.55	(271.95)*

*Until the moment when the maximum displacement was reached and the test stopped

5. Conclusions

The main purpose of this work was to study the behaviour of an adhesively bonded automotive structure under quasi-static conditions, showing the applicability of adhesive bonding in real automotive applications. The tests, conducted at RT, revealed premature failure of the structure due to a crack initiation and propagation around the middle holes of the lower substrate, proving that the integrity of the component is ruled by the behaviour of the aluminium substrates. Therefore, it can be concluded that the crash-resistant adhesive was successfully capable of bonding the structure and transfer the loads to the aluminium adherends, being suited for automotive applications. The numerical simulation carried out in ABAQUS® was able to correctly predict the failure load of the structure, but the obtained displacement was not as precise. This can be explained by difficulty in accurately reproducing the boundary conditions experimentally applied to the specimens. While in the numerical model, where perfect conditions are considered,

the specimens were guaranteed not to move on their ends, in the experimental tests this was not exactly accomplished, leading to higher displacements. In order to verify if the aluminium fracture could be avoided, a high-performance polyurethane was used to bond the automotive structure as an alternative to the epoxy system. The specimen bonded with the polyurethane behaved better than those bonded with the epoxy, as the former adhesive is more ductile than the last, transferring less energy to the lower substrate and preventing its fracture.

The analysis of the SLJs, composed by similar aluminium substrates bonded with two different thicknesses of the same epoxy adhesive, showed that an increase in the adhesive thickness is followed by a decrease in the joint strength for the two tested conditions. However, the higher thickness led to an increase in the energy absorption capabilities. Additionally, as the displacement rate applied to the joints increased, the failure load was found to present higher values, for both thicknesses. The FE analysis carried out in ABAQUS® showed good accordance with the experimental data for the two loading conditions.

Acknowledgments

The authors gratefully acknowledge the funding provided by Project NORTE-01-0145-FEDER-000022 - SciTech - Science and Technology for Competitive and Sustainable Industries, co-financed by Programa Operacional Regional do Norte (NORTE2020), through Fundo Europeu de Desenvolvimento Regional (FEDER), and by PhD grant SFRH/BD/139341/2018 “Impact strength optimization with cohesive zone elements of multi-material bonded structures used in the automotive industry”, Project Nº 028473 POCI-01-0145-FEDER-028473 “Design methodology for impact resistant bonded multi-material automotive structures (ImpactBondDesign)”. The authors would also like to thank Nagase ChemteX® for the financial support provided, as well to Aston Martin Lagonda Limited® for supplying the aluminium substrates.

References

1. Barnes, T.A. and I.R. Pashby, *Joining techniques for aluminium spaceframes used in automobiles: Part II — adhesive bonding and mechanical fasteners.* Journal of Materials Processing Technology, 2000. **99**(1): p. 72-79.
2. Brooks, R., S.M. Shanmuga Ramanan, and S. Arun, *Composites in Automotive Applications: Design*, in *Reference Module in Materials Science and Materials Engineering*. 2017, Elsevier.
3. Beardmore, P. and C.F. Johnson, *The potential for composites in structural automotive applications.* Composites Science and Technology, 1986. **26**(4): p. 251-281.
4. Miller, W.S., et al., *Recent development in aluminium alloys for the automotive industry.* Materials Science and Engineering: A, 2000. **280**(1): p. 37-49.
5. Hirsch, J., *Recent development in aluminium for automotive applications.* Transactions of Nonferrous Metals Society of China, 2014. **24**(7): p. 1995-2002.
6. Machado, J.J.M., et al., *Adhesive joints using aluminium and CFRP substrates tested at low and high temperatures under quasi-static and impact conditions for the automotive industry.* Composites Part B: Engineering, 2019. **158**: p. 102-116.
7. C England, J., et al., *Design of Automotive Metal and Composite Chassis Structures.* Recent Patents on Mechanical Engineering, 2010. **3**(3): p. 211-225.
8. Galvez, P., et al., *Study of the behaviour of adhesive joints of steel with CFRP for its application in bus structures.* Composites Part B: Engineering, 2017. **129**: p. 41-46.
9. Borsellino, C., G. Di Bella, and V. Ruisi, *Adhesive joining of aluminium AA6082: The effects of resin and surface treatment.* International Journal of Adhesion and Adhesives, 2009. **29**(1): p. 36-44.
10. Costa, A.P.d., et al., *A Review of Welding Technologies for Thermoplastic Composites in Aerospace Applications.* Journal of Aerospace Technology and Management, 2012. **4**: p. 255-265.
11. Grujicic, M., et al., *An overview of the polymer-to-metal direct-adhesion hybrid technologies for load-bearing automotive components.* Journal of Materials Processing Technology, 2008. **197**(1-3): p. 363-373.

12. J. J. M. Machado, A.H., P. D. P. Nunes, E. A. S. Marques, R. J. C. Carbas, C. Sato, L. F. M. da Silva, *Strain rate dependence of a crash resistant adhesive as a function of temperature for the automotive industry.* 2018.
13. Banea, M.D., et al., *Effects of Temperature and Loading Rate on the Mechanical Properties of a High Temperature Epoxy Adhesive.* Journal of Adhesion Science and Technology, 2011. **25**(18): p. 2461-2474.
14. Bezemer, A.A., C.B. Guyt, and A. Vlot, *New impact specimen for adhesives: optimization of high-speed-loaded adhesive joints.* International Journal of Adhesion and Adhesives, 1998. **18**(4): p. 255-260.
15. Saldanha, D.F.S., et al., *Mechanical characterization of a high elongation and high toughness epoxy adhesive.* International Journal of Adhesion and Adhesives, 2013. **47**: p. 91-98.
16. Silva, L.F.M., A. Öchsner, and R. Adams, *Handbook of Adhesion Technology*. 2011. p. 1-7.
17. Neto, R.C., E. Sampaio, and J. Assis, *Numerical and experimental analysis of bonded joints with combined loading.* International Journal of Adhesion and Adhesives, 2019. **90**: p. 61-70.
18. Machado, J.J.M., et al., *Numerical study of impact behaviour of mixed adhesive single lap joints for the automotive industry.* International Journal of Adhesion and Adhesives, 2018. **84**: p. 92-100.
19. da Costa Mattos, H.S., E.M. Sampaio, and A.H. Monteiro, *Static failure analysis of adhesive corner joints.* International Journal of Adhesion and Adhesives, 2013. **47**: p. 110-116.
20. Lahaye, C., et al., *Development of an aluminium prototype bonnet for Saab 9-3*. 1998, SAE Technical Paper.
21. Cheon, S.S., D.G. Lee, and K.S. Jeong, *Composite side-door impact beams for passenger cars.* Composite Structures, 1997. **38**(1): p. 229-239.
22. Araújo, H., et al., *Dynamic behaviour of composite adhesive joints for the automotive industry.* Composite Structures, 2017. **171**: p. 549-561.
23. Yibo, P., et al., *Dynamic Mechanical Behaviors of 6082-T6 Aluminum Alloy.* Advances in Mechanical Engineering, 2013. **5**: p. 878016.
24. Oosterkamp, L.D., A. Ivankovic, and G. Venizelos, *High strain rate properties of selected aluminium alloys.* Materials Science and Engineering: A, 2000. **278**(1-2): p. 225-235.

25. Torca, I., et al., *Tensile Behaviour of 6082 Aluminium Alloy Sheet under Different Conditions of Heat Treatment, Temperature and Strain Rate*. Vol. 423. 2009. 105-112.
26. Chen, Y., et al., *Stress–strain behaviour of aluminium alloys at a wide range of strain rates.* International Journal of Solids and Structures, 2009. **46**(21): p. 3825-3835.
27. Gleich, D.M., M.J.L. Van Tooren, and A. Beukers, *Analysis and evaluation of bondline thickness effects on failure load in adhesively bonded structures.* Journal of Adhesion Science and Technology, 2001. **15**(9): p. 1091-1101.
28. Hillerborg, A., M. Modéer, and P.-E. Petersson, *Analysis of crack formation and crack growth in concrete by means of fracture mechanics and finite elements.* Cement and concrete research, 1976. **6**(6): p. 773-781.
29. Campilho, R.D.S.G., et al., *Modelling adhesive joints with cohesive zone models: effect of the cohesive law shape of the adhesive layer.* International Journal of Adhesion and Adhesives, 2013. **44**: p. 48-56.
30. Goglio, L. and M. Rossetto, *Impact rupture of structural adhesive joints under different stress combinations.* International Journal of Impact Engineering, 2008. **35**(7): p. 635-643.
31. Banea, M., L.F.M. Silva, and R. Campilho, *The Effect of Adhesive Thickness on the Mechanical Behavior of a Structural Polyurethane Adhesive*. Vol. 91. 2014. 331-346.
32. Machado, J., E. Marques, and L. da Silva, *Mechanical behaviour of adhesively bonded composite single lap joints under quasi-static and impact conditions with variation of temperature and overlap.* Journal of Composite Materials, 2018. **52**(26): p. 3621-3635.

Paper 19

Content of Paper 19

Abstract

1. Introduction

2. Experimental details

2.1. SLJs

2.1.1. Material and properties

2.1.1.1. Aluminium

2.1.1.2. Adhesive

2.1.2. Fabrication and testing

2.2. Automotive structure (front header)

2.2.1. Material and properties

2.2.1.1. Aluminium

2.2.1.2. Adhesive

2.2.2. Fabrication and testing

3. Numerical details

3.1. SLJs

3.2. Automotive structure (front header)

4. Results and discussion

4.1. SLJs: experimental and numerical analysis

4.2. Automotive structure (front header): experimental and numerical analysis

4.3. Influence of adhesive type on the dynamic response of the automotive structure

5. Conclusions

References

Experimental and numerical study of the dynamic response of an adhesively bonded automotive structure

N.D.D. Silva[1], J.J.M. Machado[1], E.A.S. Marques[1], P.M.G.P. Moreira[1], L.F.M. da Silva[2,*]

[1]Instituto de Ciência e Inovação em Engenharia Mecânica e Engenharia Industrial (INEGI), Rua Dr. Roberto Frias, 4200-465 Porto, Portugal

[2]Departamento de Engenharia Mecânica, Faculdade de Engenharia (FEUP), Universidade do Porto, Rua Dr. Roberto Frias, 4200-465 Porto, Portugal

Abstract

Based on economic and environmental factors related to energy efficiency, the automotive industry is being increasingly encouraged to design lighter structures, making use of adhesive bonding in vehicle body frames. To meet the standards of the automotive sector, adhesive joints must provide high strength and stiffness, low cost and good energy absorption at a component level, therefore ensuring good impact strength and passenger safety. This work aims to study, at room temperature (24 ºC), the impact response of a real scale automotive structure bonded with a crash-resistant epoxy, allowing to access the suitability of adhesives for automotive structural purposes. The same component was also analysed through a finite element model, so that the numerical predictions could be compared with experimental data. The epoxy adhesive was found to successfully transfer the loads to the substrates and not to compromise the integrity of the structure, as its failure was dominated by the behaviour of the aluminium. Furthermore, the simulation showed good accordance with the experimental failure load, revealing that numerical analysis can be a viable tool to predict structure's behaviour. Additionally, a polyurethane was used as an alternative to the epoxy system to bond the structure, proving that the joint behaves better in the presence of a more flexible adhesive.

Keywords

Adhesively bonded automotive structure; High-performance crash-resistance adhesive; Aluminium; Impact; Single lap joints

* Corresponding author. Tel.: +351 22 508 17 06; fax: +351 22 508 14 45. *E-mail address:* lucas@fe.up.pt (L.F.M. da Silva)

1. Introduction

In an attempt to develop energy-efficient vehicles, the automotive industry has been encouraged to design lightweight structures, making use of low-density materials such as aluminium alloys and composites. Although offering a good compromise between weight and strength, the application of composite materials in large production structural automotive components is still facing some drawbacks. These are mainly caused by some uncertainty related to their long-term performance and by their high material and manufacturing costs [1, 2], which can be prohibitive for some applications. Aluminium alloys represent an economically advantageous solution and its excellent formability and corrosion resistance [3], allied with low weight, turns it particularly suitable for vehicle body frames. The lower strength and stiffness can be successfully compensated with the design of the spaceframe and the use of thicker cross-sections [4], with high strength aluminium alloys being able to satisfy the torsional stiffness requirements of an automotive component [5]. The aluminium alloys most commonly used in vehicle construction belong to the 5xxx and 6xxx series [6]. The former, highly deformable, are mostly used for inner panel applications, while the latter, heat-treatable, are preferred for outer panels [7]. Within the 6xxx series, the AA6016 (Europe) and AA6111 (USA) alloys are frequently used for body structures. The AA6016 alloy is preferred in Europe because it shows a superior formability and corrosion resistance compared to AA6111 [5, 8].

Lighter body frames, however, should not compromise mechanical strength, ensuring the simultaneous fulfilment of the requirements regarding fuel consumption and safety. Load bearing automotive structures must perform well under complex loading situations such as impact, which often leads to an increase in the complexity and manufacturing difficulties [9]. Such factors encouraged the expansion of adhesive bonding in this industry, as this technique is able to tolerate damage, presents low manufacturing costs, allows the reduction of vibrations [10] and lead to an uniform stress distribution in the bonded area, reducing the stress concentration [11] and improving the fatigue behaviour [12, 13]. Several vehicle manufacturers have shown the benefits of adhesive bonding with the production of several concept cars [8, 10]. The 2002 Aston Martin's V12 Vanquish, one of the most technically advanced cars of its time, had a space-frame made of extruded aluminium and adhesive bonding was chosen to join the entire vehicle together [14].

Structural polyurethanes and epoxies represent the most common adhesive systems in the automotive industry. The first are often chosen due to their peel strength, good

fatigue behaviour and high durability [15], while the last are often selected to bond structural automotive components due to their capability to guarantee a strong and stiff bond, as well as joint stability. These epoxy characteristics allowed their application, for instance, in the load carrying components of the Lamborghini's Murcièlago model [16] and in the extruded aluminium sections that shape the chassis of Lotus' Elise and Evora models [2]. However, conventional epoxy adhesives are very brittle and therefore have insufficient energy-absorption properties, leading to reduced shear strength and peel resistance under impact [17, 18]. Toughened, crash-resistant epoxy adhesives have been recently introduced in the market, possessing superior energy absorption capabilities and good strength at high strain rates [19]. The toughening process is usually achieved with the addiction of flexible polymer or rubber particles to epoxy-based formulations. Crash-resistant epoxy adhesives are able to combine high ductility with high strength and stiffness, allowing the absorption of significant amounts of energy in comparison to standard adhesives [12].

Over the years, finite element (FE) analysis has become a viable and accurate tool for prediction the behaviour of structures subjected to a large variety of loading conditions, including impact. This method stands as a complement or even an alternative to experimental procedures, which are sometimes undesirable or impossible to perform. Within the field of adhesive bonding, cohesive zone modelling (CZM) has been used as an add-in to FE to model the behaviour of the adhesive using cohesive elements. This damage mechanics technique, based in energetic concepts, has already been successfully applied to simple joint configurations, such as single lap joints (SLJs) [20] and corner joints [21], providing good results when compared to experimental data.

The test and analysis of real-scale automotive structures, especially of bonded construction, under impact loads is not common in the literature and few examples can be found regarding this matter. Golzar et al. [22] manufactured a prototype of a composite body cover structure to replace steel in an automobile model and a FE study was carried out in ABAQUS® to analyse its behaviour under impact. Although no experimental tests were conducted, a composite body cover with 1.6 mm thickness was found to have higher energy absorption performance in comparison to steel, while allowing a 42% weight saving. The crash behaviour of thin-walled aluminium extrusions, which represent the base of the aluminium space-frame concept, was studied by Langseth et al. [23]. The extrusions were subjected to axial loading conditions and three different configurations were tested, namely non-filled extrusions and aluminium foam-filled extrusions with and

without an epoxy adhesive between the foam and the walls of the extrusion. Results suggested that the presence of the foam filler drastically changes the energy absorption behaviour, with the use of adhesive increasing the mass specific energy absorption. The non-linear finite element simulations conducted in the computer code LS-DYNA® over the AA6060 alloy non-filled extrusions (the only numerical simulations presented) were in accordance with the experimental results. The response of a composite side-door impact beam was studied by Cheon et al. [24], as an alternative to the traditional steel version. The new beam showed higher energy absorption capabilities when subjected to the dynamic load. A similar automotive component was analysed by Li et al. [25] exclusively using a numerical approach with the software LS-DYNA®. The goal was to optimize the design of the beam so that energy absorption could be maximized in a lateral crash accident. The results of the new beam design showed improvements of 18% in the impact energy absorption and 14% in the impact load peak.

The work developed in this article aims to analyse the impact behaviour of a full-scale, adhesively bonded automotive structure, by numerical and experimental approaches. The behaviour of the joint was predicted using a FE model with CZM being applied in the crash-resistant epoxy adhesive. The mechanical properties of the epoxy that allowed the construction of the cohesive law were determined in previous works [26, 27]. The experimental tests were conducted at room temperature (RT) and with an impact velocity of 3 m/s. Furthermore, a polyurethane adhesive was also considered to bond the component, so that the influence of the adhesive type on the behaviour of the structure could be analysed. As a complement, the dynamic response (at 3 m/s) of SLJs bonded with two adhesive layer thicknesses, namely 0.2 and 1.6 mm, was studied to evaluate the effect of this parameter on the behaviour of the joints.

2. Experimental details

2.1. SLJ

2.1.1. Material and properties

The SLJ specimens tested in the context of this work consisted of similar substrates of an aluminium alloy bonded with a crash-resistant, highly ductile one-component epoxy adhesive, well suited for impact loads.

2.1.1.1. Aluminium

The initial research plan was to use the AA6016-T4 aluminium alloy for the substrates of the SLJs, as this represents the material used in the substrates of the automotive structure. Unfortunately, this was not possible due to difficulty in obtaining this specific alloy. The contacted aluminium manufacturers only supply this material in industrial quantities, not compatible with those desired for this project. Additionally, its storage in a naturally aged temper (T4) is not common, as prolonged exposure to environmental agents often leads to the degradation of this treatment.

In the presence of this information, the AA6082-T6 aluminium alloy was selected for this purpose as alternative, due to its reasonably identical general mechanical properties (Table 1) and easier obtainment in the market.

The strain rate sensitivity of AA6082-T6 was reported in the literature to be low at RT [28-31]. Yibo et al. [31] studied its plastic behaviour for quasi-static to moderate strain rates (0.001-100 s^{-1}) and noticed a slightly increase in yield and tensile strengths within this range. Therefore, the considered plastic behaviour of AA6082-T6 under impact was adapted from his work and is represented Fig. 1.

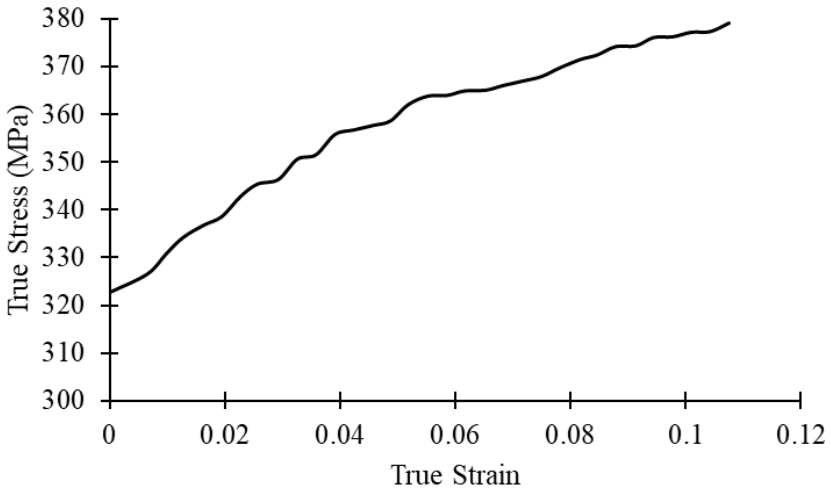

Fig. 1. Plastic behaviour of AA6082-T6 under impact (adapted from [31]).

Table 1. General mechanical properties of the AA6082-T6 aluminium alloy.

Properties	
Density, ρ [kg/m^3]	2700
Young's modulus, E [MPa]	69000
Shear modulus, G [MPa]	26000
Poisson's ratio, v	0.33
Tensile strength, σ_n [MPa]	360
Yield strength, σ_y [MPa]	310
Shear strength, τ [MPa]	220
Elongation at break, ε [%]	9.8

2.1.1.2. Adhesive

The aluminium substrates in the SLJs specimens were bonded with the same crash-resistant epoxy adhesive applied in the automotive component, with the reference XNR6852 E-3, supplied by Nagase ChemteX®. Aside from high mechanical strength, a crash-resistant adhesive should also support significant plastic deformation before failure, allowing the structure to remain bonded and transferring the load to the metallic substrates, leading to large absorption of energy and ensuring the safety of the structure in a crash situation.

The mechanical properties of this adhesive at RT under impact condition (3 m/s) were already determined by Machado et al. [26] and Araújo et al. [27], being summarized in Table 2. Its density was considered to be 1550 kg/m^3.

Table 2. Mechanical properties of XNR6852 E-3 adhesive.

Properties	**Impact (3 m/s)**
Glass transition temperature, T_g [°C]	132
Cohesive tensile strength, t_n^0 [MPa]	72
Young's modulus, E [MPa]	3667
Cohesive shear strength, t_s^0 [MPa]	43
Shear modulus, G [MPa]	603
Critical strain energy release rate in mode I, G_{IC} [N/mm]	13.3
Critical strain energy release rate in mode II, G_{IIC} [N/mm]	64

The glass transition temperature was measured by dynamically exciting a test specimen during cycles of heating and cooling and recording the corresponding amplitude of the vibration. The T_g was reached when a peak in the damping value was observed.

The cohesive tensile strength and Young's modulus were determined by performing tensile tests over "dogbone" bulk specimens in a drop-weight testing machine [26]. Thick adherend shear tests (TAST) were conducted to obtain the shear properties of the adhesive, namely the cohesive shear strength and shear modulus, for two displacement rates (1 and 100 mm/min). The value for impact was then extrapolated using this data [27]. Similarly, a direct measurement of the critical strain energy release rate in mode I was not performed for the impact condition. Double Cantilever Beam (DCB) tests were performed to obtain the values of this parameter for three displacement rates, which results allowed the construction of a logarithmic law and the extrapolation for the impact condition [26]. The critical strain energy release rate in mode II of this adhesive is difficult to obtain experimentally, since plastic deformation of the metallic substrates were observed in the conducted End-Notched Flexure (ENF) tests. Therefore, due to the high ductility of XNR6852 E-3, Araújo et al. [27] considered this parameter to be approximately 8 times higher than the value of the critical strain energy release rate in mode I obtained in his work.

2.1.2. Fabrication and testing

Aluminium adherends with a thickness of 2 mm were used in the SLJs, due to the proximity of this value with the thickness of the automotive structure substrates. An overlap length of 12.5 mm was applied to avoid plasticity of aluminium and ensure failure in the bonded region, as the adhesive presents high ductility. With the goal of analysing the influence of the adhesive layer thickness on the response of the joints, two configurations were produced, with thicknesses of 0.2 and 1.6 mm. The last value was chosen because it corresponds to the approximate thickness of the adhesive in the automotive component, while the first is commonly used in the study of SLJs [32].

The specimens were initially drilled and the adherends anodised using phosphoric acid anodizing. The purpose of this superficial treatment was to improve the adhesion between the aluminium and the adhesive, in an attempt to avoid interfacial failure. So that thermal expansion differentials between the joints and the mould could be minimized, an aluminium mould was used to manufacture the joints. Pins were applied to ensure the correct alignments of the joints and spacers, with a length of 77.5 mm, were positioned into the mould assembly to obtain the desired overlap length of 12.5 mm. Tapes with calibrated thicknesses were selected to ensure the correct thickness of the adhesive. Its

application was achieved using a spatula for an adhesive thickness of 0.2 mm and using a pressure gun for the 1.6 mm thickness, so that voids inside the adhesive layer could be avoided. Finally, the mould assembly was introduced in a hot plate press to perform the curing cycle of this epoxy, set as 4h at 165 °C by the manufacturer.

An in-house developed drop-weight testing machine was used to perform the impact tests. In this device, the specimen is assembled in a grip and a mass is dropped from a certain height, impacting the lower section of the grip and loading the specimen in tension-shear (Fig. 2).

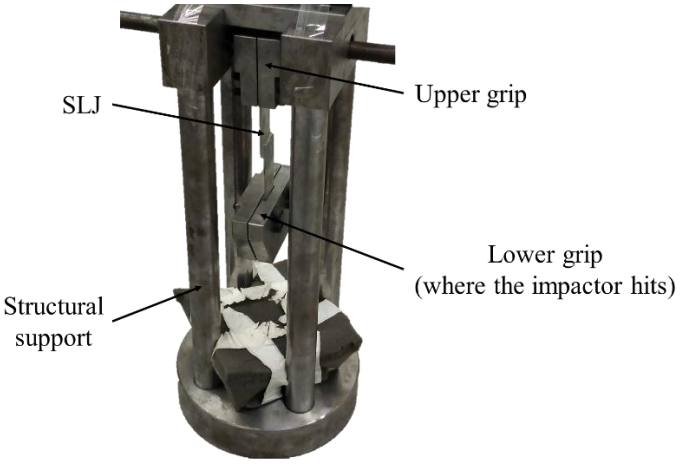

Fig. 2. Apparatus used to perform SLJ impact tests.

The impact velocity (V) is controlled by the drop height (H), making use of the energy conservation principle:

$$V = \sqrt{2gH} \tag{1}$$

where g is the acceleration of gravity. For these impact tests, a mass of 26 kg and an impact velocity of 3 m/s were defined, providing an impact energy of 117 J. The evolution of the impact load with time was recorded by a load cell present in the drop-weight testing machine. The integration of the load vs time curve, divided by the impact mass, allowed the assessment of the velocity vs time evolution. This information was finally used to calculate, by integration, the displacement of the joints during the tests. At least three specimens (which dimensions are shown in Fig. 3) were tested for each configuration.

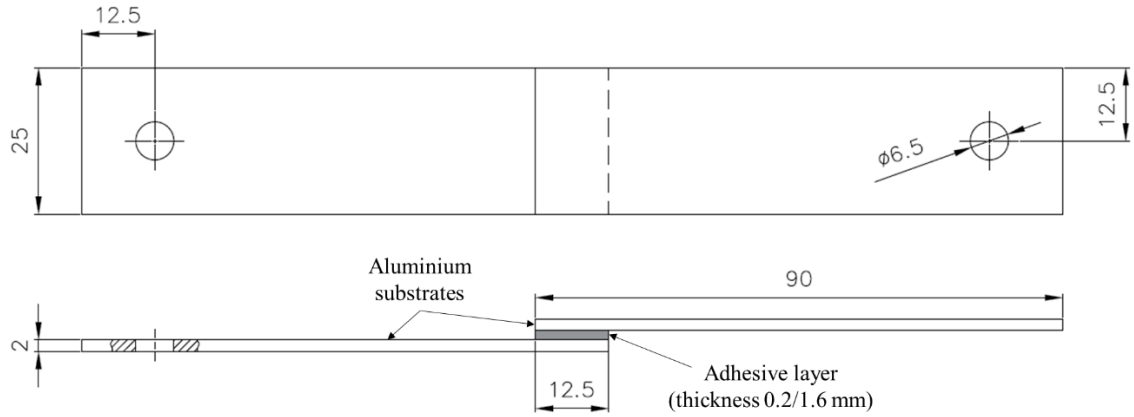

Fig. 3. Configuration and dimensions of the manufactured SLJs.

2.2. Automotive structure (front header)

The location of the adhesively bonded automotive component in the body structure of the vehicle is shown in Fig. 4.

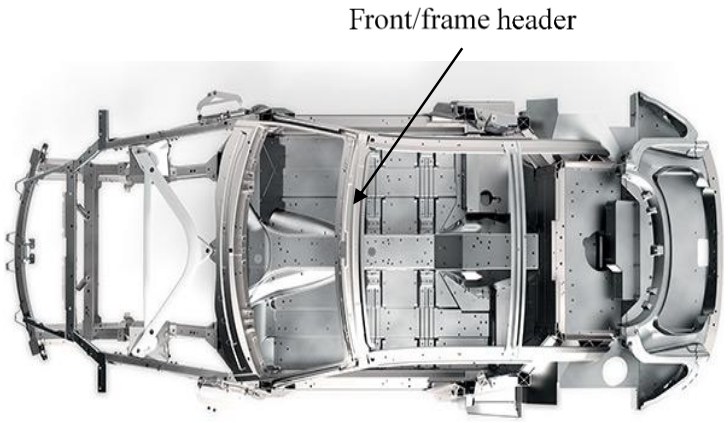

Fig. 4. Automotive front header in the body frame of the Aston Martin's DB11.

2.2.1. Material and properties

2.2.1.1. Aluminium

The adhesively bonded automotive structure, often named as front header, was manufactured with AA6016-T4 substrates, which were already provided in an anodised state. In terms of mechanical behaviour, this alloy was referred by the supplier to become close to the AA6016-T6 alloy after the structure being subjected to the curing cycle of the adhesive. Therefore, the properties of both alloys are represented in Table 3, being the plastic behaviour of the substrates in the final stage of manufacture shown in Fig. 5.

Table 3. General mechanical properties of the AA6016-T4 and AA6016-T6 aluminium alloys.

Properties	**AA6016-T4**	**AA6016-T6**
Density, ρ [kg/m^3]	2700	2700
Young's modulus, E [MPa]	69000	69000
Shear modulus, G [MPa]	26000	26000
Poisson's ratio, ν	0.33	0.33
Tensile strength, σ_n [MPa]	200	280
Yield strength, σ_y [MPa]	110	210
Shear strength, τ [MPa]	130	170
Elongation at break, ε [%]	27	11

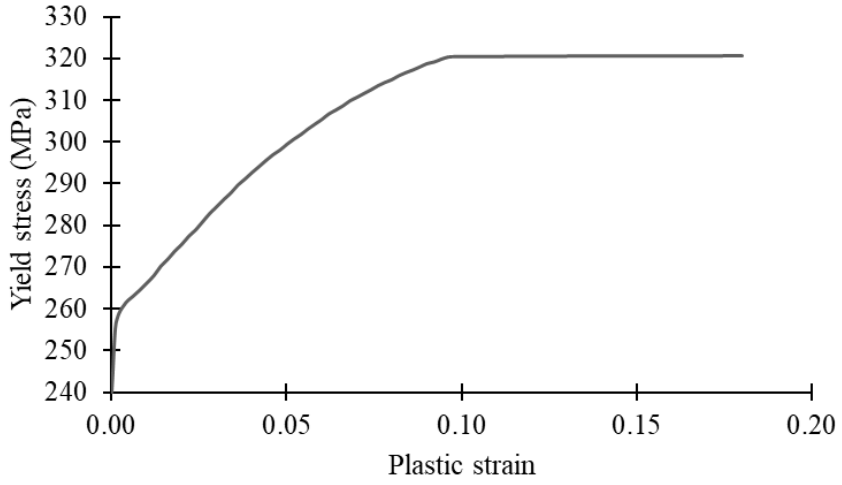

Fig. 5. Plastic behaviour of AA6016-T6, used as substrates in the automotive structure.

2.2.1.2. Adhesive

The XNR6852 E-3 adhesive was initially chosen to bond the structure, due to its crash resistance and high energy absorption capabilities. Its properties under impact were already introduced in Table 2.

2.2.2. Fabrication and testing

To ensure a good adhesion with the adhesive and remove undesirable particles on its surfaces, the aluminium substrates were initially cleaned with isopropanol alcohol. A total of 14 spacers, constructed by assembling layers of calibrated tape, were joined to the edges of the lower substrate to guarantee the thickness of the adhesive bead, which dimensions were set as approximately 17 mm wide and 1.6 mm thick throughout the

bondlines. The locations of these spacers were chosen in order to disturb the adhesive the least as possible. For each specimen, about 70 g of adhesive were applied in both sides of the lower substrate, using a pressure gun. The next steps consisted in assembling the upper substrate on the top of the lower substrate and positioning clamps in the locations of the spacers to restrain the structure and apply pressure. The manufacturing process was completed by placing the whole structure in an oven to perform the curing cycle of the adhesive. A resume of all the described steps is represented in Fig. 6.

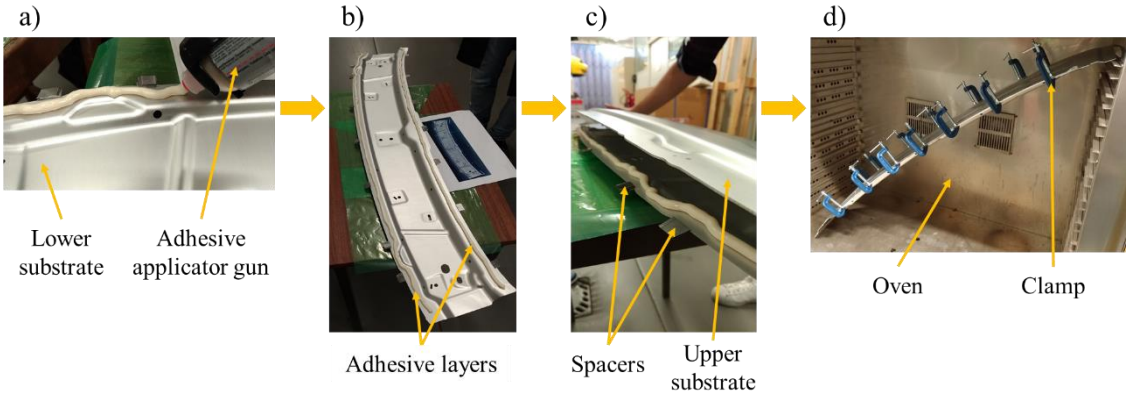

Fig. 6. Steps in the manufacturing of the automotive structure: a) adhesive application using a pressure gun; b) adhesive layers on the top of the lower substrate; c) assembling of the upper substrate; d) structure with clamps inside the oven, to perform the curing cycle of the adhesive.

A drop-weight testing machine was used to conduct the impact tests, with an impact mass and velocity of 30 kg and 3 m/s, respectively, providing an impact energy of 135 J. The contact with the structure was made by an impactor, as presented in the configuration of Fig. 7. The fixation of the automotive component in the structural support, designed for this purpose, was accomplished by a total of eight typical screw-nut connections. The impact load was recorded by the machine, while the vertical displacement was measured with a high-speed video camera. Two automotive structures were tested at this condition.

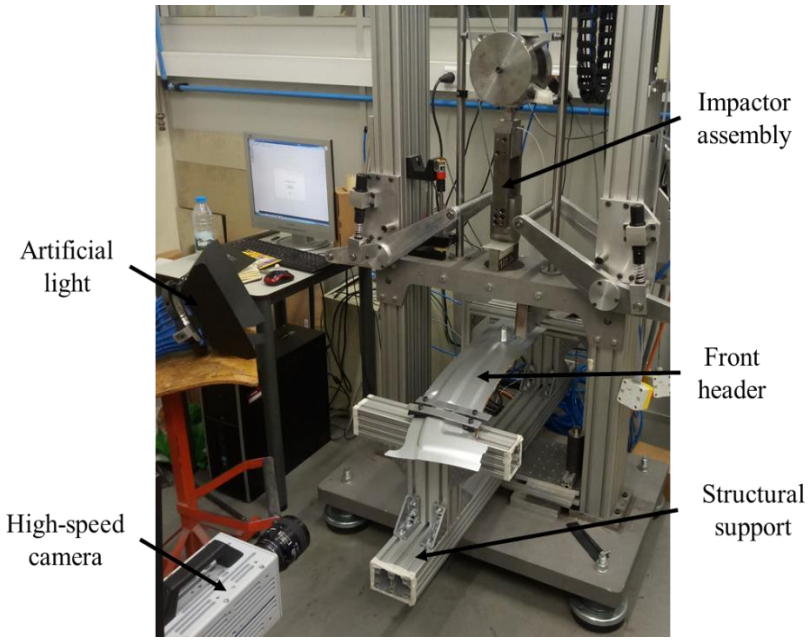

Fig. 7. Testing configuration for the impact load.

3. Numerical details

The numerical models using CZM have been increasingly used in the prediction of adhesive joints behaviour, as they represent an accurate tool and serve as an alternative or complement to experimental procedures. This method is able to simulate damage growth, and therefore determine the strength of a joint, by using energetic principles and parameters, combining concepts of elasticity and fracture mechanics.

Traction-separation laws are constructed to model the behaviour of the cohesive elements that simulate the adhesive, by establishing a relation between stresses and displacements throughout the process [27]. Of all common shapes of these laws (triangular, trapezoidal and exponential), the triangular shape (Fig. 8) is often preferred, as it is the simplest, tends to present less convergence problems and is readily implemented in most FE software [33].

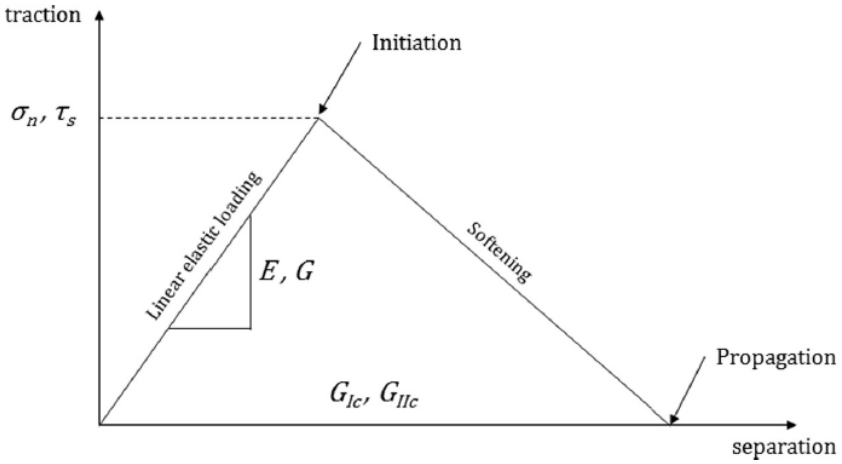

Fig. 8. Traction-separation law with a triangular shape for mode I, mode II [27].

For the construction and implementation of these laws, the mechanical properties of the adhesive in study are needed, according to the type of the loading condition. Thus, the values of the cohesive tensile strength (σ_n)/cohesive shear strength (τ_s), Young's modulus (E)/shear modulus (G) and critical strain energy release rate in mode I (G_{IC})/critical strain energy release rate in mode II (G_{IIC}) are required for mode I/mode II loading conditions, respectively.

3.1. SLJ

The numerical analysis of the SLJs under impact was carried out in ABAQUS® software package. A two-dimensional (2D) geometry was considered due to the simplicity of the joint configuration and reduced computational time, without prejudice of the results. The properties of the adhesive and aluminium at this condition were used, as well as material densities. For the case of the aluminium substrates, their plastic behaviour (Fig. 1) was introduced in the material definition. A movement restriction in both in-plane directions was applied to one end of the joint, while in the opposite end a restriction was made regarding the vertical movement only. To model the dropped mass and the impact velocity, a new geometrical feature with a mass of 26 kg was added to the SLJ configuration and subjected to a boundary condition that specified its initial velocity as 3 m/s (Fig. 9).

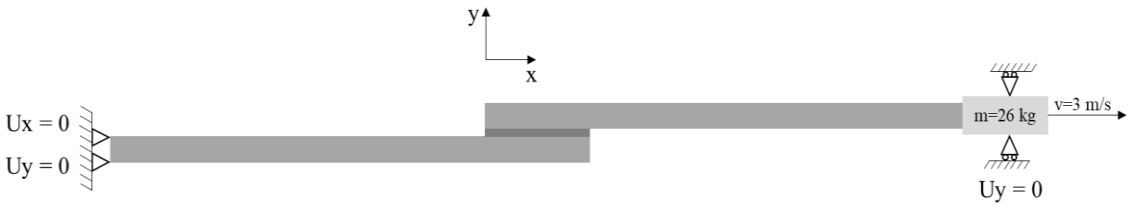

Fig. 9. Boundary conditions applied to the SLJs model.

So that a good compromise between the accuracy of the results and computational time could be achieved, different mesh refinements were created in the most critical regions using the bias functionality, with explicit, 4-node bilinear plain strain quadrilateral elements (CPE4R in ABAQUS® nomenclature) being applied to the adherends and explicit, 4-node two-dimensional cohesive elements (COH2D4 in ABAQUS® nomenclature) being used in the adhesive. A triangular law, shown in Fig. 10 and constructed with the properties of the adhesive (Table 2), was directly implemented in the software to model the cohesive elements.

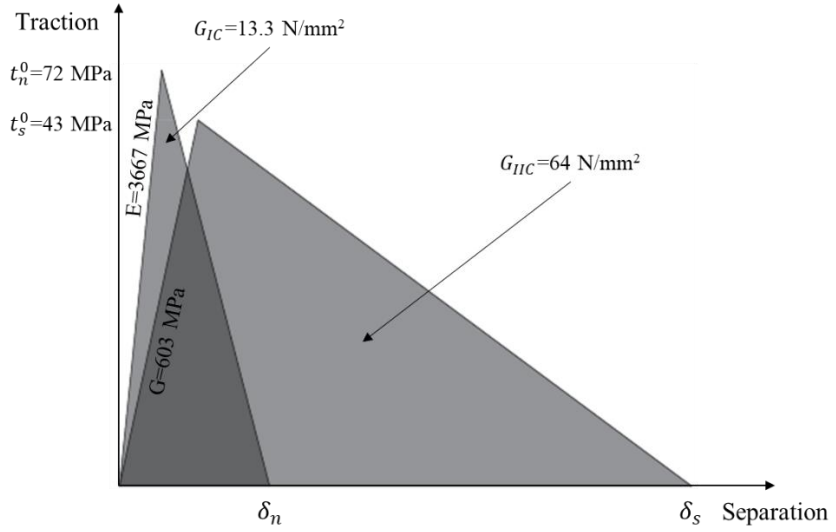

Fig. 10. CZM's traction-separation law for impact conditions.

While a single layer of cohesive elements was applied to model the adhesive region for a thickness of 0.2 mm, a different design was considered for the 1.6 mm thickness (Fig. 11). For this case, intercalated layers of cohesive and plain strain elements were used, with the elastic properties of the adhesive being attributed to the elastic areas. This new configuration was applied instead because better results were achieved regarding the failure load prediction, as the failure process is replicated more accurately. A dynamic, explicit step was selected to solve the model and the SDEG parameter, that shows the

adhesive degradation along the process, the reaction forces in the bi-restrained end and the displacement in the end where the solicitation was applied were requested as outputs, in order to construct the load-displacement curve.

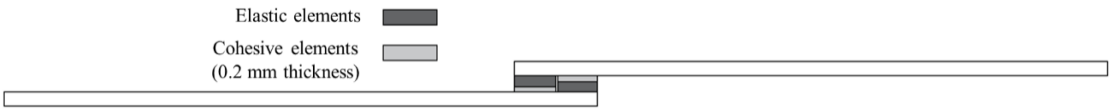

Fig. 11. Adhesive layer configuration used to model the behaviour of the SLJ with an adhesive thickness of 1.6 mm, with cohesive and plain strain elements being applied.

3.2. Automotive structure (front header)

The FE analysis of the front header was also conducted in ABAQUS®, with the mesh and geometry being imported from the HYPERMESH® software package. The properties under impact and material densities were applied and solid elements were assigned to both substrates and adhesive. In the case of the substrates, the plastic behaviour of the aluminium (Fig. 5) was also introduced. Explicit, 8-node 3D cohesive elements (COH3D8 in ABAQUS® nomenclature) were assigned to the adhesive layers, while explicit, 8-node linear 3D stress elements (C3D8R in ABAQUS® nomenclature) were applied to the upper and lower aluminium substrates, with a thickness of 1.7 and 1.2 mm, respectively. Due to the complex geometry of the frame, explicit, 6-node linear triangular 3D stress elements (C3D6 in ABAQUS® nomenclature) were used to complement the mesh in the adherends. Encastre boundary conditions were given to the ends of the automotive structure to simulate the experimental procedure (Fig. 12) and the impactor, which was only allowed to move vertically, was modelled as a rigid body, since its stress state was not of interest. As the total mass and impact velocity of the dropping structure in the experimental tests were 30 kg and 3 m/s, respectively, these mass parameters were attributed to the impactor body. An interaction between the impactor and the structure was created to avoid penetration and ensure the correct contact between the two bodies, with a normal behaviour of the type “Hard contact” and a tangential behaviour with friction coefficient of 0.61. A dynamic, explicit step was used to run the model and the SDEG, the reaction forces at the restricted zones and the impactor’s displacement were requested as outputs.

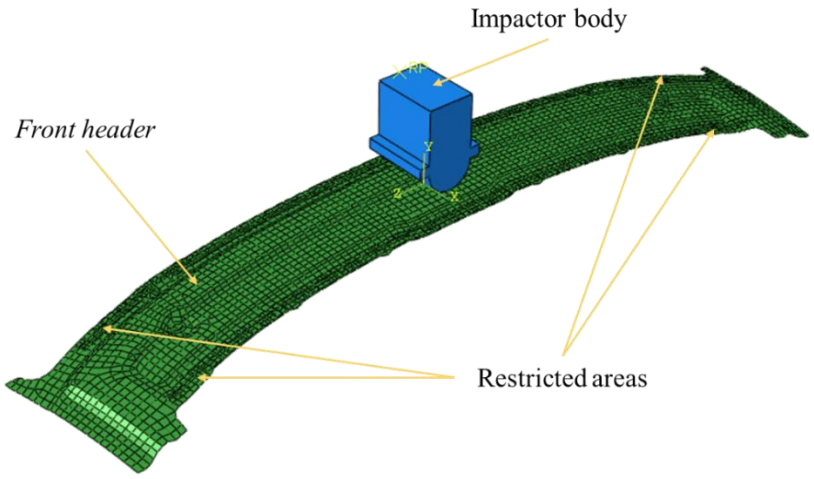

Fig. 12. Configuration of the numerical model used to simulate the behaviour of the automotive structure under impact.

4. Results and discussion

4.1. SLJ: experimental and numerical analysis

Fig. 13 shows a representative experimental load-displacement curve for both thicknesses, together with the numerical evolutions.

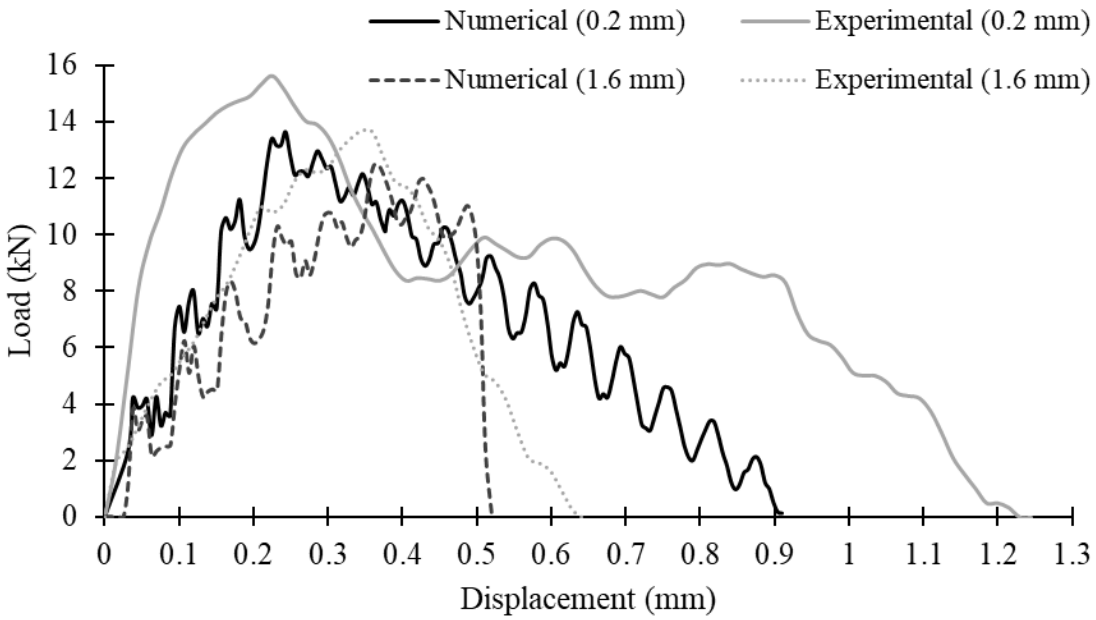

Fig. 13. Comparison between the experimental and numerical curves at impact conditions for an adhesive thickness of 0.2 and 1.6 mm.

As the impactor hits the fixture where the joints are assembled during the tests, high load peaks were observed in the initial stages of the raw experimental data. These are induced by acceleration peaks that occur due to the first contact between the impactor and the lower metal grip and do not correspond to the real strength of the joint. The information provided by the load cell was therefore manually treated and filtered to remove this undesirable initial noise, resulting in the true experimental data presented in Fig. 13. The failure loads predicted by the numerical models show relatively good accuracy with the experimental ones. The deviations can be explained by the fact that some adhesive properties were extrapolated for impact in [26] and [27]. The stiffness of the numerical models was slightly adjusted to compensate possible errors induced by clearances in the fixtures.

The SDEG parameter given by the numerical analysis is shown in Fig. 14 for both adhesive thicknesses, where it is possible to state that the degradation of the adhesive started in the edges and propagated to the middle of the adhesive layer, until cohesive failure was reached in the two configurations.

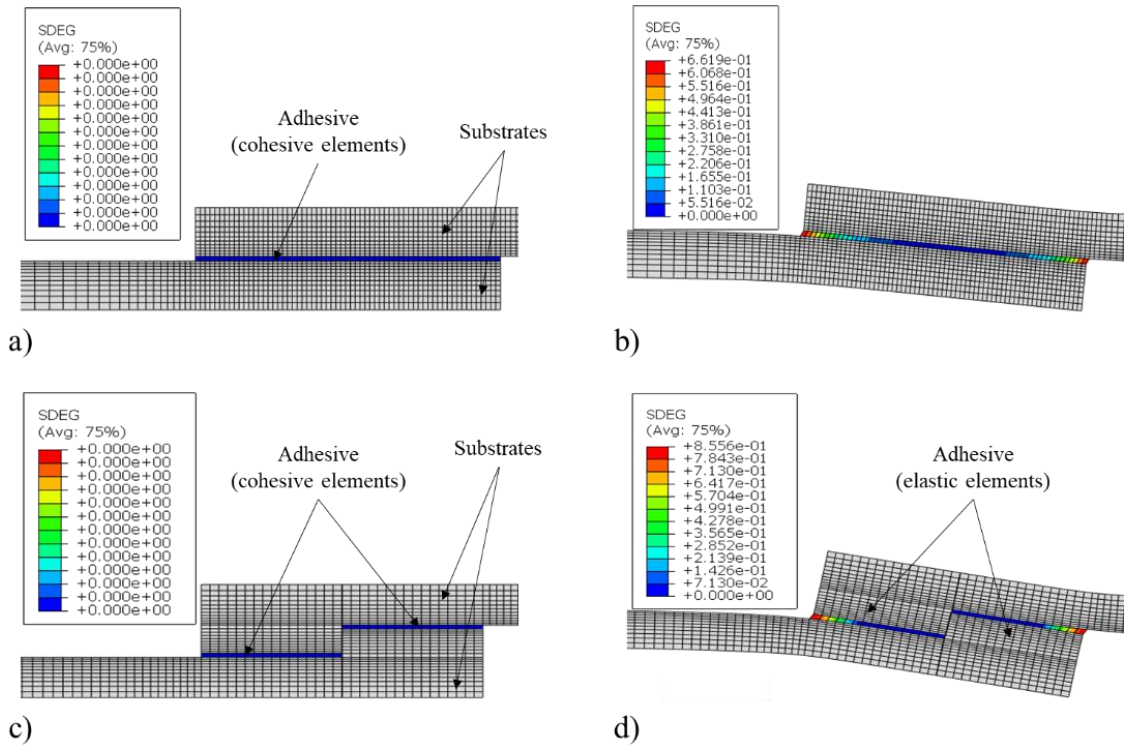

Fig. 14. Adhesive's degradation for a thickness of 0.2 mm (a) initial and b) intermediate stages) and 1.6 mm (c)initial and d) intermediate stages).

The results for impact are summarized in Table 4. A decrease in the joint strength was found with the increase of the adhesive thickness. Some general theories have been

proposed to explain the reduction of strength for higher thicknesses. Gleich et al. [32] proposed, using a FE analysis, that the peel and shear stresses at the interface increase as the bondline gets thicker, leading to lower failure loads. Adams and Peppiatt [34] stated that thicker bondlines have tendency to contain more voids and microcracks, which cause premature failure of the joints. However, FE simulations conducted by Liao et al. [35] on SLJs subjected to impact tensile loads revealed that the maximum principal stress in the joint interface increases as the adhesive layer thickness decreases, suggesting lower failure loads for thinner thicknesses. These results appear to be in opposition to what was mentioned above and with the numerical and experimental results found in this work. Thus, the effect of bondline thickness on the strength of SLJs under impact conditions is still an open issue.

Table 4. Failure load results for the impact load.

	0.2 mm		**1.6 mm**	
	Experimental	**Numerical**	**Experimental**	**Numerical**
Failure load (kN)	17.18 ± 1.51	13.65	13.58 ± 1.46	12.50

4.2. Automotive structure (front header): experimental and numerical analysis

During the impact tests, the automotive structure specimens were found to fail due to high stress concentration around the middle holes present in the lower substrate. Such phenomenon led to the initiation and propagation of a crack (Fig. 15), which caused the decreasing of the load carrying capacity of the component. The response of the structure can therefore be said to be highly dependent of the behaviour of the aluminium substrates, with the adhesive being responsible by transferring the loads between the substrates. The load-displacement curves for the numerical analysis and a representative experimental specimen are shown in Fig. 16. Due to the failure mechanism described above, it can be concluded that the load the automotive structure is able to withstand is relatively low. Due to the lack of information regarding the damage evolution of the aluminium substrates, no damage and failure criterion was introduced in the FE analysis, which did not allow to replicate in the numerical model the fracture verified during the experimental tests. Therefore, to overcome this difficulty and for comparation purposes, the numerical simulation data was only considered until the moment when the equivalent von Mises stress in the lower substrate reached the ultimate stress, defined by the plastic behaviour of the aluminium (Fig. 5). From this moment forward, the numerical structure was

considered to fail and no further information was used. In these circumstances, the numerical model was able to correctly predict the maximum load of the front header, but the displacement was not so accurate. This was due to the boundary conditions assigned to the numerical analysis and the ones verified in the experimental procedure: while in the FE analysis perfect conditions were considered, truly restraining the ends of the component from moving, such condition was not exactly replied during the tests. In fact, the structure and its assembly during the impact load were less stiff than the numerical model, allowing small movements and therefore leading to higher displacements in the load-displacement curve. In order to compensate these observations, the stiffness of the FE model was slightly corrected to allow a more realistic comparison with the experimental data.

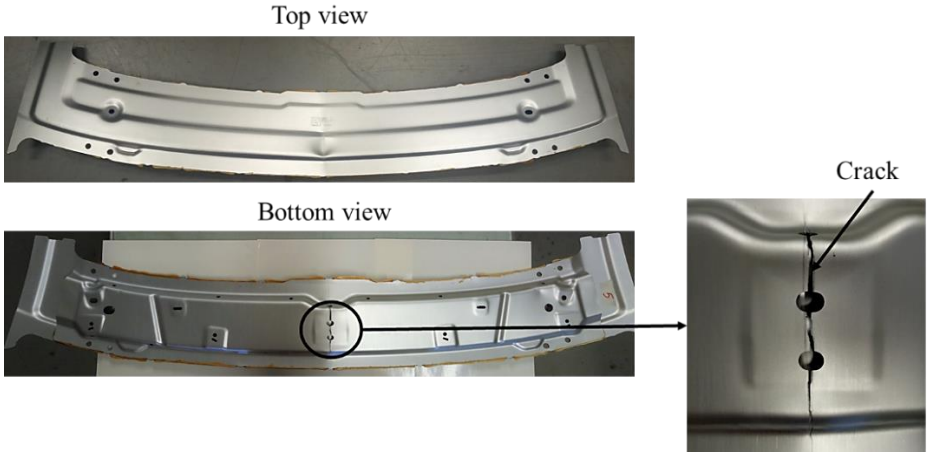

Fig. 15. Failure mechanism observed in the specimens during the impact tests.

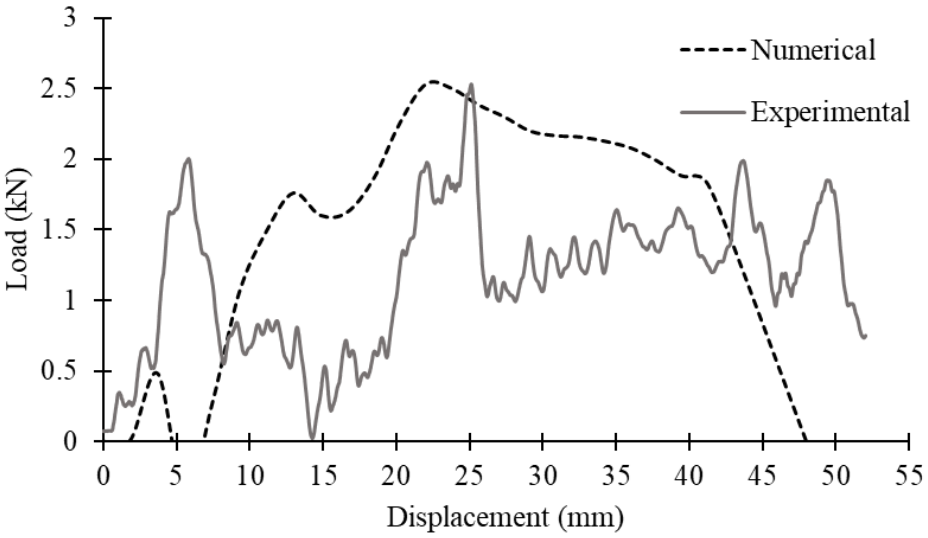

Fig. 16. Load-displacement curves for the impact loading.

Table 5 summarizes the results obtained for the dynamic testing, in terms of failure load and absorbed energy, the last calculated as the area below the curves. The values of the simulation are slightly higher than those measured experimentally as ideal conditions are considered in the software, something that is practically impossible to obtain during the tests.

Table 5. Failure load and absorbed energy of the automotive structure under impact conditions.

	Experimental	**Numerical**
Failure load (kN)	2.32 ± 0.30	2.53
Absorbed energy (J)	60.22 ± 0.06	72.30

4.3. Influence of adhesive type on the dynamic response of the automotive structure

Since fracture was observed in the front header specimens bonded with the crash-resistant epoxy system, another adhesive was selected to verify if this phenomenon could be avoided. Therefore, a high-performance structural polyurethane was chosen, supplied by Sika® and with the reference SikaForce®-7818 L7 (Table 6). The manufacturing process previously described for the epoxy remains valid for the polyurethane-bonded specimens, excepting for the curing cycle. This adhesive cures at RT by chemical reaction of two components, dispensing the use of the oven.

Table 6. General properties of the SikaForce®-7818 L7 polyurethane adhesive.

Properties	
Density [kg/m^3]	1230
Tensile strength [MPa]	35
Young's modulus [MPa]	2500
Tensile lap-shear strength [MPa]	20
Elongation at break [%]	2.5
Glass transition temperature [°C]	45

For the case of the automotive structure bonded with the polyurethane, no failure was found in the component, in opposition to what was verified with the specimens bonded with the crash-resistant adhesive (Fig. 17).

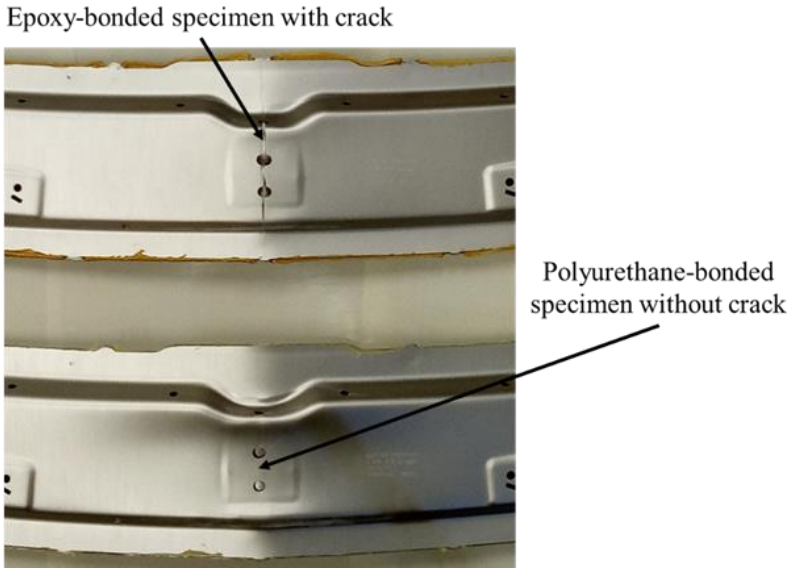

Fig. 17. Front header specimens tested under impact condition, showing that aluminium fracture does not occur when polyurethane is used.

Fig. 18 represents the evolutions of the load in the structure and the displacement of the impactor with time. Its analysis allows to conclude that the load in the structure increases as the impact moves downwards (its displacement is considered positive in this direction) and starts to decrease from the moment when the impactor starts to rebound (its displacement evolves in the opposite direction). This is, the maximum load in Fig. 18 do not correspond to the strength of the joint. This value was not possible to find because the impact conditions (30 kg and 3 m/s) were insufficient to cause the failure of the new specimen. The same impact conditions were considered for both epoxy and polyurethane so that comparisons between the results could be made.

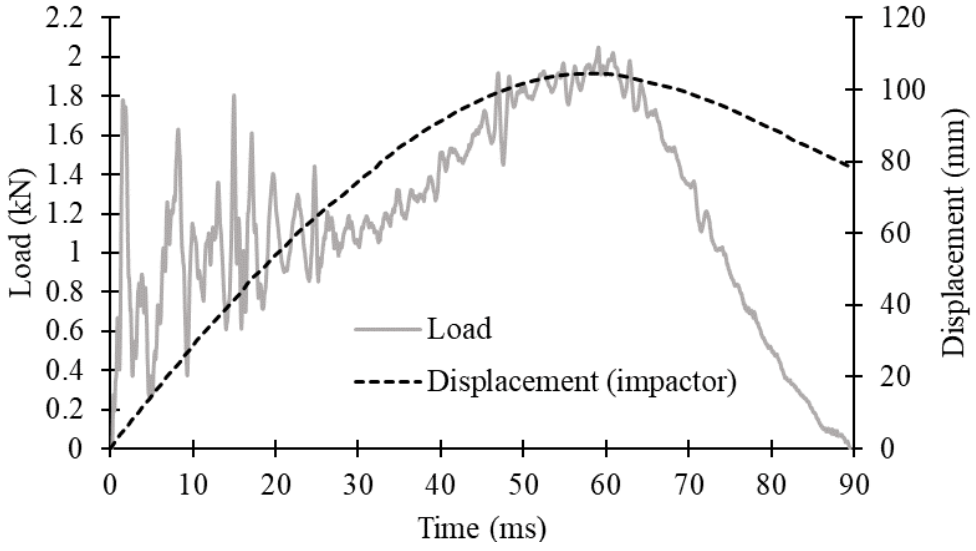

Fig. 18. Evolutions of the load in the structure and the displacement on the impactor for the polyurethane-bonded automotive structure.

The load-displacement evolutions for the automotive structures bonded with the two adhesives are shown in Fig. 19. As two epoxy-bonded specimens were tested, a representative experimental curve is presented for this case. Only one structure bonded with polyurethane was tested due to specimens' availability.

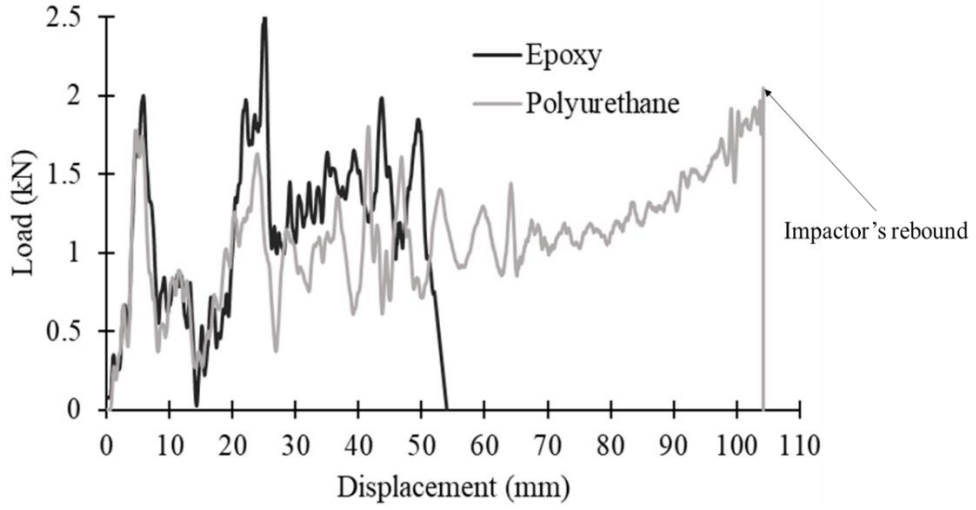

Fig. 19. Load-displacement curves for the automotive structure bonded with the two adhesives.

The curves present a similar shape until the moment when the specimen bonded with the epoxy adhesive starts to fail due to the initiation of the crack. The structural polyurethane seems to be more suited than the crash-resistant epoxy in the context of the joint, as it leads to higher energy-absorption capabilities (Table 7) and no failure for the

same boundary conditions. Such observation can be explained by the fact that the polyurethane, although weaker, is more flexible than the epoxy. This means higher absorption energy in the adhesive and less transmitted load to the lower substrate, avoiding the appearance of the high stress concentrations in the middle holes that caused the crack.

Table 7. Failure load and absorbed energy for the specimens bonded with the two adhesives.

	Epoxy	**Polyurethane**
Failure load (kN)	2.32 ± 0.30	Not reached
Absorbed energy (J)	60.22 ± 0.06	(113.75)*

*Until impactor's rebounding moment

5. Conclusions

In this work, a real, adhesively bonded automotive structure was tested under impact condition (3 m/s), with the main goal of showing that adhesive bonding behaves well during crash situations. The analysis conducted at RT, corresponding to the temperature verified in most service situations, allowed to conclude that failure in the specimens bonded with the crash-resistant epoxy adhesive occurred due to the formation and further propagation of a crack in the middle of the lower substrate, caused by the presence of holes which led to high stress concentrations. Therefore, the adhesive can be concluded to successfully transfer the loads between the adherends and not to compromise the response of the structure, as its behaviour is predominantly ruled by the aluminium substrates. The simulation carried out in ABAQUS® software package correctly predicted the maximum load of the front header, while its displacement was not as accurate. This was attributed to the boundary conditions applied to the model and to the specimens, as the assembly of the last was less stiff and allowed some movement, leading to higher displacements than those obtained numerically. When a more flexible adhesive was used instead, namely a high-performance structural polyurethane, the joint performance was found to improve under the same conditions. This is due to the higher ductility of the polyurethane, which is responsible for absorbing higher amounts of energy and transferring less of it to the lower substrate, avoiding its fracture. Still, even in the presence of a crack, the adhesion capabilities of the epoxy system were not affected, as the structure remained perfectly bonded (but with its load carrying capabilities lost). Thus,

it is possible to state that the behaviour of the adhesive influences the response of the structure, but in neither case the adhesive bonding compromised the integrity of the joint, being therefore a trustworthy solution to join real automotive components subjected to impact loads.

As a complement, SLJs with aluminium adherends similar to those used in the automotive structure were bonded with the same crash-resistant epoxy adhesive, in an attempt to study the influence of the adhesive layer thickness on the behaviour of the joints. Two thicknesses were tested at RT, namely 0.2 and 1.6 mm, allowing to conclude that the joint strength decreases with increasing thickness for impact. The numerical results, also conducted in ABAQUS®, showed relatively good accordance with the experimental observations. The considerably difference regarding the 0.2 mm thickness can be explained by possible variations in the properties used to model the adhesive under impact, as some of them were obtained by extrapolation.

Acknowledgments

The authors gratefully acknowledge the funding provided by Project NORTE-01-0145-FEDER-000022 - SciTech - Science and Technology for Competitive and Sustainable Industries, co-financed by Programa Operacional Regional do Norte (NORTE2020), through Fundo Europeu de Desenvolvimento Regional (FEDER), and by PhD grant SFRH/BD/139341/2018 "Impact strength optimization with cohesive zone elements of multi-material bonded structures used in the automotive industry", Project Nº 028473 POCI-01-0145-FEDER-028473 "Design methodology for impact resistant bonded multi-material automotive structures (ImpactBondDesign)". The authors would also like to thank Nagase ChemteX® for the financial support provided, as well to Aston Martin Lagonda Limited® for supplying the aluminium substrates.

Declaration of interest

The authors declare that there is no conflict of interests regarding this work.

References

1. Thornton, P. and R. Jeryan, *Crash energy management in composite automotive structures.* International Journal of Impact Engineering, 1988. **7**(2): p. 167-180.

2. C England, J., et al., *Design of Automotive Metal and Composite Chassis Structures.* Recent Patents on Mechanical Engineering, 2010. **3**(3): p. 211-225.
3. Khan, A.S. and H. Liu, *Variable strain rate sensitivity in an aluminum alloy: Response and constitutive modeling.* International Journal of Plasticity, 2012. **36**: p. 1-14.
4. Barnes, T.A. and I.R. Pashby, *Joining techniques for aluminium spaceframes used in automobiles: Part II — adhesive bonding and mechanical fasteners.* Journal of Materials Processing Technology, 2000. **99**(1): p. 72-79.
5. Tisza, M. and I. Czinege, *Comparative study of the application of steels and aluminium in lightweight production of automotive parts.* International Journal of Lightweight Materials and Manufacture, 2018. **1**(4): p. 229-238.
6. Hirsch, J., *Aluminium Alloys for Automotive Application*. Vol. 242. 1997. 33-50.
7. Miller, W.S., et al., *Recent development in aluminium alloys for the automotive industry*. Materials Science and Engineering: A, 2000. **280**(1): p. 37-49.
8. Hirsch, J., *Recent development in aluminium for automotive applications.* Transactions of Nonferrous Metals Society of China, 2014. **24**(7): p. 1995-2002.
9. Henning, F., et al., *Fast processing and continuous simulation of automotive structural composite components.* Composites Science and Technology, 2019. **171**: p. 261-279.
10. Borsellino, C., G. Di Bella, and V. Ruisi, *Adhesive joining of aluminium AA6082: The effects of resin and surface treatment.* International Journal of Adhesion and Adhesives, 2009. **29**(1): p. 36-44.
11. Galvez, P., et al., *Study of the behaviour of adhesive joints of steel with CFRP for its application in bus structures.* Composites Part B: Engineering, 2017. **129**: p. 41-46.
12. Machado, J.J.M., E.A.S. Marques, and L.F.M. da Silva, *Adhesives and adhesive joints under impact loadings: An overview*. The Journal of Adhesion, 2018. **94**(6): p. 421-452.
13. He, X., *A review of finite element analysis of adhesively bonded joints.* International Journal of Adhesion and Adhesives, 2011. **31**(4): p. 248-264.
14. Hill, J., *Adhesively Bonded Structural Composites for Aston Martin Vehicles.* Ford Motor Company Research and Advanced Engineering, 2003.
15. Silva, L.F.M., A. Öchsner, and R. Adams, *Handbook of Adhesion Technology*. 2011. p. 1-7.

16. Feraboli, P. and A. Masini, *Development of carbon/epoxy structural components for a high performance vehicle.* Composites Part B: Engineering, 2004. **35**(4): p. 323-330.
17. Silva, M.R.G., E.A.S. Marques, and L.F.M.d. Silva, *Behaviour under Impact of Mixed Adhesive Joints for the Automotive Industry.* Latin American Journal of Solids and Structures, 2016. **13**: p. 835-853.
18. Saldanha, D.F.S., et al., *Mechanical characterization of a high elongation and high toughness epoxy adhesive.* International Journal of Adhesion and Adhesives, 2013. **47**: p. 91-98.
19. Adams, R.D., *Adhesive bonding: science, technology and applications*. 2005: Elsevier.
20. Machado, J.J.M., et al., *Numerical study of impact behaviour of mixed adhesive single lap joints for the automotive industry.* International Journal of Adhesion and Adhesives, 2018. **84**: p. 92-100.
21. Neto, R.C., E. Sampaio, and J. Assis, *Numerical and experimental analysis of bonded joints with combined loading.* International Journal of Adhesion and Adhesives, 2019. **90**: p. 61-70.
22. Golzar, M. and M. Poorzeinolabedin, *Prototype fabrication of a composite automobile body based on integrated structure.* The International Journal of Advanced Manufacturing Technology, 2010. **49**(9-12): p. 1037-1045.
23. Langseth, M., O.S. Hopperstad, and A.G. Hanssen, *Crash behaviour of thin-walled aluminium members.* Thin-Walled Structures, 1998. **32**(1): p. 127-150.
24. Cheon, S.S., D.G. Lee, and K.S. Jeong, *Composite side-door impact beams for passenger cars.* Composite Structures, 1997. **38**(1): p. 229-239.
25. Li, Q.F., et al., *Optimum Design and Numerical Simulation of Automotive Front Side-Door Impact Beam.* Key Engineering Materials, 2011. **452-453**: p. 169-172.
26. J. J. M. Machado, A.H., P. D. P. Nunes, E. A. S. Marques, R. J. C. Carbas, C. Sato, L. F. M. da Silva, *Strain rate dependence of a crash resistant adhesive as a function of temperature for the automotive industry.* 2018.
27. Araújo, H., et al., *Dynamic behaviour of composite adhesive joints for the automotive industry*. Composite Structures, 2017. **171**: p. 549-561.
28. Oosterkamp, L.D., A. Ivankovic, and G. Venizelos, *High strain rate properties of selected aluminium alloys.* Materials Science and Engineering: A, 2000. **278**(1-2): p. 225-235.

29. Torca, I., et al., *Tensile Behaviour of 6082 Aluminium Alloy Sheet under Different Conditions of Heat Treatment, Temperature and Strain Rate*. Vol. 423. 2009. 105-112.
30. Chen, Y., et al., *Stress–strain behaviour of aluminium alloys at a wide range of strain rates.* International Journal of Solids and Structures, 2009. **46**(21): p. 3825-3835.
31. Yibo, P., et al., *Dynamic Mechanical Behaviors of 6082-T6 Aluminum Alloy.* Advances in Mechanical Engineering, 2013. **5**: p. 878016.
32. Gleich, D.M., M.J.L. Van Tooren, and A. Beukers, *Analysis and evaluation of bondline thickness effects on failure load in adhesively bonded structures.* Journal of Adhesion Science and Technology, 2001. **15**(9): p. 1091-1101.
33. Campilho, R.D.S.G., et al., *Modelling adhesive joints with cohesive zone models: effect of the cohesive law shape of the adhesive layer.* International Journal of Adhesion and Adhesives, 2013. **44**: p. 48-56.
34. Adams, R.D. and N.A. Peppiatt, *Stress analysis of adhesive-bonded lap joints.* Journal of Strain Analysis, 1974. **9**(3): p. 185-196.
35. Liao, L., et al., *3-D FEM stress analysis and strength evaluation of single-lap adhesive joints subjected to impact tensile loads.* International Journal of Adhesion and Adhesives, 2011. **31**(7): p. 612-619.